

NASA SP-3

NASA

SP

335

c.1

LOAN COPY: RET
AFWL TECHNICAL
KIRTLAND AFB,

0063408

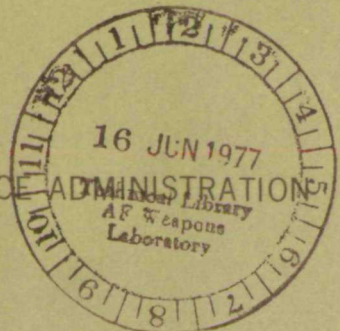
TECH LIBRARY KAFB, NM

ADVANCED SCANNERS AND IMAGING SYSTEMS FOR EARTH OBSERVATIONS

Report of a working group meeting at
COCOA BEACH, FLORIDA
December 11-15, 1972



NATIONAL AERONAUTICS AND SPACE ADMINISTRATION





ADVANCED SCANNERS AND IMAGING SYSTEMS FOR EARTH OBSERVATIONS

The report of a working group
sponsored by Goddard Space Flight Center
on behalf of the
National Aeronautics and Space Administration
which met at Cocoa Beach, Florida,
December 11-15, 1972

Prepared by Goddard Space Flight Center



Scientific and Technical Information Office

NATIONAL AERONAUTICS AND SPACE ADMINISTRATION
Washington, D.C.

1973

For sale by the Superintendent of Documents, U.S. Government Printing Office, Washington, D.C. 20402

FOREWORD

The Ad Hoc Advanced Imagers and Scanners Working Group met at Cocoa Beach, Florida from December 11 to 15, 1972 in a meeting sponsored by NASA-Goddard Space Flight Center on behalf of the National Aeronautics and Space Administration.

The meeting addressed sensors, sensors systems and user applications for remote monitoring of the earth from orbiting satellites. The Working Group limited itself to consideration of electromechanical scanners and electronic imaging systems for the spectral region including the visible through the thermal infrared. The use of photographic cameras and film is addressed only briefly, and microwave imaging is excluded. In addressing remote sensing technology and its applications, the Working Group was asked to consider the present and then project into a period both four and eight years hence, the growth of technical capability and the expansion of requirements in terms of performance specifications.

The Working Group was divided into five panels, which are listed here together with their chairmen:

1. Electromechanical Scanners - D. Lowe
2. Self-Scanned Solid State Sensors - J. Early
3. Electron-Beam Imagers - G. Barna
4. Sensor Related Technology - M. Maxwell
5. User Applications - W. Fischer

The first three panels addressed and forecasted the capabilities and limitations of the specific technologies within their areas of interest respectively. Panel four covered topics which include the scene-atmosphere-sensor interface, platform stability, data processing, and output products for the users. The fifth panel included representatives from the user community. Their function was to generate a current list of requirements for use by the technology panels, to work with each of these panels to familiarize these panels with the user needs, and in addition to gain a better insight themselves into sensor technology.

This report provides both broad assessments of present and future sensors and sensor related technology, as well as, a description of user needs and applications. Although these statements of needs and assessments of technology are

to an extent subjective, they were generated by a group of people considered to be among the leaders in their respective fields, and thus the judgements presented are believed to be substantive and worthy of use by the appropriate decision makers.

Prior to the meeting the four technology panels submitted preliminary material which was compiled into a working document and distributed to all participants. The present report has evolved from that initial document.

During the meeting an essentially non-structured format was used to facilitate and encourage people of mutual interests and concerns to share ideas and information with each other. The goal was to consolidate and correct the initial material and to develop a set of recommendations and conclusions by the end of the week's meeting.

This report has been structured for both the non-technical reader as well as the reader who wants more detailed technological information. For the non-technical reader each chapter is preceded by a summary. For easy reference, a condensed summary of the overall report is placed at the beginning of the document and provides an overview of the results of the Working Group.

It may be noted that there is a certain unevenness in the technical treatment of many of the topics. This results from a conscious effort to avoid extensive editorial changes and the associated delays. It appears also that in the effort to get to publication, some references have been separated out and lost for some individual work. For that, we apologize to any authors whose work has not been properly acknowledged.

In an effort of this sort, there have been many contributors and unfortunately it is not possible to acknowledge all of them. Special thanks are due the panel chairmen and the technical director, Dr. George Zissis, for their hard work, and to the working group members for their support and contributions. Acknowledgement is due the work of Mr. Roamer Predmore and Mr. Les Thompson of Goddard Space Flight Center who were responsible for the details of organizing the meeting and for providing coordination between the panel chairmen and the panels. In addition, Mr. Thompson has guided the report of the working group to its final form as editor-in-chief. Acknowledgement should also be made of the continuing support and encouragement given to this effort by Mr. M. I. Schneebaum, Mr. J. R. Schulman and Mr. H. Ostrow of NASA-GSFC.

With the publication of this report, work will come to a close on an effort that began in March 1972, when planning first began for the Ad Hoc Advanced Imager and Scanner Working Group.

Goddard Space Flight Center
July, 1973

NASA ADVANCED IMAGERS AND SCANNERS WORKING GROUP

L. Jaffe - Chairman

A. Park - Assistant Chairman

J. Lehmann - Assistant Chairman

G. Zissis - Technical Coordinator

User Applications Panel

W. Fischer -
Chairman

J. Clifton
S. Q. Duntley
J. Glover
H. M. Gurk
R. C. Heller
R. McEwen
E. Risley
C. Robinove
L. Shaefer
J. Sherman
J. W. Sherman III

Electromechanical Scanner Panel

D. S. Lowe -
Chairman

J. R. Biard
F. Gabron
R. Hummer
R. B. MacDonald
L. Mundie
C. T. Paludan
R. Predmore -
Assoc. Chairman
R. L. Sendall
W. Wolfe

Electron Beam Imagers Panel

G. Barna -
Chairman

K. J. Ando
F. Cook
O. Graham
M. Green
E. Koenig
F. Leccese
J. Lowrance
E. D. Savoye
M. St. John
O. Weinstein -
Assoc. Chairman

Solid State Imagers Panel

J. M. Early -
Chairman

D. E. Bode
R. Ennulat
F. Huck
A. Koso
N. Lavery
J. Mudar
B. Rubin
P. N. Slater
G. Strull
L. L. Thompson -
Assoc. Chairman
P. K. Weimer

Sensor Related Technology Panel

M. Maxwell -
Chairman

F. C. Billingsley
J. Edmond
R. Fenn
A. Guha
D. Landgrebe
B. Steiner

Ex Officio Members

I. L. Goldberg H. Ostrow
J. Harnage J. R. Schulman
B. Kerne

CONTENTS

	<u>Page</u>
FOREWORD	iii
THE SUMMARY OF THE REPORT OF THE ADVANCED IMAGERS AND SCANNERS WORKING GROUP	1
CHAPTER 1—USER APPLICATIONS	13
PANEL RECOMMENDATIONS	13
Near Term Requirements	14
Long Term Needs	15
Data Attributes	15
PERSPECTIVE	16
Purpose of User Requirements Panel	17
Constraints Applied to User Panel Study	17
Panel Guidelines	18
Selection of Applications	18
Applications Groupings	19
Definition of Terms and Validity of Estimates	20
SUMMARY CHARTS	21
Repeat Coverage Needs (Figure 1-1)	21
Sensor Geometry (Table 1-1)	21
Spectral Requirements (Figure 1-2)	21
Sensitivity Requirements (Figure 1-3)	23
General Comments	24
DESIGN AND TECHNIQUES EVALUATION	25
Digital and Analog Data Processing	25
Data Transmission	26
Photographic Processing	26
Stereo Coverage	26
Night-Time Imaging	27
Imaging of Luminescence	28
Measurement of Atmospheric Aerosol Content by Polarization	28
APPLICATIONS IN VARIOUS DISCIPLINE CATEGORIES	28
Agriculture-Statistical Design for Multi-Stage Sampling of Crop Acreages and Production Predictions	28
<i>First Level of Information — ERTS-1 Imagery</i>	29
<i>First Stage — Medium Altitude CIR (Color Infrared)</i> <i>Photography</i>	29

CONTENTS (Continued)

	<u>Page</u>
<i>Second Stage — Low Altitude 70mm CIR (or Normal Color) Photography</i>	29
<i>Third Stage — Ground Sample</i>	30
<i>Statistical Analysis of Data</i>	30
<i>Subsequent ERTS Coverage</i>	30
<i>Other Considerations</i>	30
Monitoring Environmental Quality Parameters	31
<i>General</i>	31
<i>Development Needs for Monitoring of Chlorophyll</i>	32
<i>Wildlife Research</i>	32
Marine and Ocean Applications	33
<i>Currents</i>	33
<i>Sea-Ice Surveillance</i>	34
<i>Biological Processes</i>	34
<i>Coastal Zone-Geological Processes</i>	34
Meteorology	35
<i>Expanded Observations</i>	35
<i>Prediction and Assessment of Natural Disasters</i>	35
Geography — Cartography	36
<i>Mapping</i>	36
<i>Earth Resources Location</i>	37
<i>Cartographic Example</i>	37
USER VIEWPOINTS	39
BIBLIOGRAPHY	40
ATTACHMENT A—AGRICULTURE/FORESTRY/GEOGRAPHY REQUIREMENTS	43
ATTACHMENT B—GEOLOGY REQUIREMENTS	51
ATTACHMENT C—HYDROLOGIC APPLICATIONS	57
ATTACHMENT D—METEOROLOGY REQUIREMENTS	61
ATTACHMENT E—MARINE AND OCEAN APPLICATIONS	65
CHAPTER 2—ELECTROMECHANICAL SCANNERS	71
PANEL SUMMATION AND RECOMMENDATIONS.	71
ELECTROMECHANICAL SYSTEMS DESIGN	72
PHOTODETECTORS	73
CRYOGENIC SYSTEMS	73
<i>Optical Systems</i>	74
<i>Hadamard System</i>	75

CONTENTS (Continued)

	<u>Page</u>
INTRODUCTION	77
Scope	77
Approach	78
SCANNER SYSTEM DESIGN	79
Past Trends in Mechanical Scanner Design	80
Performance Theory	86
<i>Scanners Employing Photomultiplier Tubes</i>	86
<i>Scanners Employing Photodiode Detectors</i>	88
<i>Scanners Employing Photoconductive Detectors</i>	89
Resolution Improvement Considerations	89
<i>Impact of Decreasing α on Required Values of D and n</i>	90
<i>Effect of Increased Resolution on Required</i>	
<i>Scan Frequency</i>	94
<i>Effect of Increased Resolution on Dwell Time</i>	97
<i>Impact of Increasing Resolution on Scanner Weight</i>	97
<i>Impact of Increasing Resolution on Data Rate</i>	99
<i>Optical Design Problems Associated with</i>	
<i>Increasing Resolution</i>	99
Other Tradeoff Considerations	102
Image Plane vs Object Plane Scanners	104
Resolution and Sample Data	104
<i>Definitions Pertaining to Resolution and Sample Data</i>	105
Summary of Design Considerations	109
PHOTODETECTORS	110
Detector Performance	113
<i>Quantum Efficiency/Responsivity</i>	113
<i>Photoconductive Gain</i>	115
<i>Noise Sources</i>	116
<i>Noise Equivalent Power</i>	123
<i>Detectivity</i>	124
<i>Speed of Response</i>	127
DETECTOR COOLING SYSTEMS	129
Cooling System Design Criteria	131
Description of Cooling Systems	131
<i>System Types</i>	131
<i>Passive Radiators</i>	132
<i>Open-Cycle Systems</i>	136
<i>Closed-Cycle Refrigerators</i>	140
Current Status and Future Trends	143

CONTENTS (Continued)

	<u>Page</u>
OPTICAL SYSTEMS	148
Scanning Systems	149
<i>45-Degree Folding Flat</i>	150
<i>Split Field Optical System</i>	152
<i>Reverse Polygons</i>	155
<i>Refractive Polygons</i>	155
<i>Refractive Wedges</i>	156
Optical Materials	160
<i>Mirror Blank Materials</i>	163
<i>Mirror Reflective Coatings</i>	165
<i>Construction and Fabrication</i>	166
<i>Lightweight Solids</i>	167
HADAMARD SCANNING	169
Some Instrument Considerations	171
Signal and Noise	172
Some Hadamard Codes	174
BIBLIOGRAPHY	176
ATTACHMENT A—SYSTEMS THAT HAVE PROGRESSED BEYOND THE PROTOTYPE STAGE	177
CHAPTER 3—ELECTRON BEAM IMAGERS	183
PANEL SUMMATION AND RECOMMENDED TECHNICAL APPROACHES	183
Summary of Performance Characteristics	183
Recommendations	183
<i>RBV Improvements</i>	186
<i>Higher Signal-to-Noise Sensors</i>	186
<i>Larger Format Vidicons</i>	186
<i>Large Silicon Target Vidicons</i>	187
<i>High-Sensitivity, High-Resolution, Fast-Erase Tube</i>	187
<i>Optics</i>	187
<i>Cold Cathode Development</i>	187
INTRODUCTION	189
Direct Beam Readout Vidicon	191
Focus Projection and Scanning (FPS) Vidicon	191
Return Beam Vidicon (RBV)	191
Image Dissectors	191
Dielectric Tape Cameras	193
Secondary Electron Conduction (SEC) and Electron Bombarded Silicon (EBS/SIT) Tubes	193

CONTENTS (Continued)

	<u>Page</u>
APPLICATIONS OF ELECTRON BEAM SENSORS	193
CURRENT DEVICES	195
Return-Beam Vidicons	195
<i>Vidicon Operation</i>	195
<i>Silicon Return Beam Vidicon</i>	198
<i>Performance Considerations</i>	199
<i>Multispectral Line Scan Sensor</i>	207
Focus Projection and Scanning Technology	210
<i>Description of Technique</i>	210
<i>Current Status</i>	214
<i>Growth Action Requirements</i>	215
Direct Beam Readout Vidicons with Silicon Diode Targets	217
<i>Silicon Target Vidicons</i>	217
<i>State of the Art and Future Potentials of Silicon</i> <i>Vidicon Technology</i>	224
Direct Beam Readout Vidicons with Large Formats	225
Infrared Vidicons	228
Image Dissector Cameras	230
<i>Description</i>	230
<i>The Image Dissector Tube</i>	231
<i>Signal Characteristics of the Image Dissector</i>	233
<i>Intensified Image Dissector</i>	235
<i>Correlation Techniques in Earth Sensing</i>	238
<i>Present and Future Characteristics of Image Dissector</i> <i>Systems</i>	240
<i>Actions Suggested</i>	243
<i>Benefits and Applications</i>	244
Dielectric Tape Cameras	244
<i>Photoconductive-Dielectric Tape Camera</i>	246
<i>Grating-Target-Tape Camera</i>	248
<i>Electrostatic Storage Camera</i>	250
Secondary Electron Conduction and Electron Bombarded Silicon Camera Tubes	256
<i>Principles of Operation</i>	257
<i>Performance Characteristics</i>	260
ADVANCED TECHNOLOGY	269
Negative Electron Affinity	269
Photoemitters	270
Electron Bombarded CCD	275
<i>Cold Cathode Emitter</i>	276

CONTENTS (Continued)

	<u>Page</u>
SYSTEMS AND ACCESSORIES	279
<i>Wide Area Image Detection</i>	279
Techniques for Multispectral Separated Signals	281
<i>Alternative Possibilities</i>	281
<i>Striped Filters</i>	282
<i>Widerange Image Spectrophotometer (WISP)</i>	289
Forward Motion Compensation	294
TECHNOLOGY OPTIONS REACHED BY PANEL	296
RBV Improvements	296
Higher Signal-to-Noise Sensors	296
Large Format Vidicons	298
Large Silicon Target Vidicons	298
High Sensitivity, High Resolution, Fast-Erase Camera Tube	299
Optics	299
Cold Cathodes (Negative Electron Affinity Materials)	300
Dielectric Tape Camera	300
BIBLIOGRAPHY	301
 CHAPTER 4—SOLID-STATE SENSOR ARRAYS FOR MULTISPECTRAL IMAGING FROM EARTH ORBIT	 305
PANEL SUMMATION OF SOLID-STATE SENSOR TECHNOLOGY	 305
Silicon Detector Arrays	305
<i>Status and Outlook</i>	306
Infrared Detector Arrays	307
<i>Current Status of IR Solid State Imaging</i>	307
<i>Near-Term Prospects of IR Solid-State Imaging Devices (Four Years)</i>	307
<i>Long-Term Prospects of IR Solid-State Imaging Devices (Eight Years)</i>	307
INTRODUCTION	309
Scope	309
Overview	309
General Performance Criteria	310
Calibration Requirements	311
SILICON DETECTOR ARRAYS	311
Photodiode Technology	313
<i>Photodiode Array Design Considerations</i>	314
<i>Array Performance</i>	318

CONTENTS (Continued)

	<u>Page</u>
Phototransistors	322
<i>Characteristics of Phototransistor Arrays</i>	323
<i>Performance Characteristics</i>	326
Charge-Coupled Devices	329
<i>Technical Considerations</i>	329
<i>CCD Image Sensors Basic Technology</i>	350
<i>Variable Exchange of Resolution and S/N Ratio</i> <i>in CCD Sensors</i>	359
<i>Performance of Charge-Coupled Imaging Devices</i> <i>(Through December 1972)</i>	360
INFRARED DETECTOR ARRAYS	364
IR System Considerations	364
Current Status of IR Solid-State Imaging and Readout	364
Near Future Prospects of IR-CCD Devices (4 years hence)	365
Long Term Prospects (8 years hence)	365
Technical Considerations	366
<i>Cooling Requirements</i>	366
<i>Background Generation of Charge</i>	366
<i>Power Considerations</i>	368
<i>Element and Array Fabrication</i>	368
IR System Summary	369
SYSTEM CONSIDERATIONS	369
Optical Design	369
<i>Primary Optics Design</i>	372
Performance Considerations	373
<i>Spectral Separation and Registration</i>	375
<i>Spectral Image Separation</i>	375
<i>Spectral Image Registration</i>	376
Environmental Considerations	377
<i>Temperature</i>	378
<i>Shock and Vibration</i>	379
<i>Other Environmental Factors</i>	379
MULTISPECTRAL IMAGING SYSTEMS FOR EARTH	
RESOURCE SURVEY	379
Characteristics of High Resolution Photodiode Self-Scanned	
Solid-State Systems	381
<i>Image Detection Electronic Subsystem</i>	384
<i>Readout Approaches</i>	385
<i>Digital Processor</i>	385
<i>Noise and Compensation</i>	386

CONTENTS (Continued)

	<u>Page</u>
Characteristics of Phototransistor Solid-State Systems	387
<i>Imaging System Configurations and Performance</i>	394
<i>Preliminary Design Configuration</i>	395
<i>Laboratory Test Results</i>	401
BIBLIOGRAPHY	405
ATTACHMENT A—SPECTRORADIOMETRIC ACCURACY— ATMOSPHERE AND INTERNAL AND EXTERNAL CALIBRATION	407
CHAPTER 5—SENSOR RELATED TECHNOLOGY	413
PANEL CONCLUSIONS AND RECOMMENDATIONS	413
Atmospheric Effects	413
<i>Conclusions</i>	413
<i>Recommendations for Future Efforts in Atmospheric Transmission Studies</i>	414
Radiometric Calibration	415
<i>Present Situation</i>	415
<i>Recommendations</i>	415
Platform Effects	416
<i>State-of-the-Art Survey</i>	416
<i>Recommendations</i>	417
Sensor Data Systems Concepts	418
<i>State-of-the-Art</i>	418
<i>Conclusions</i>	418
Data Correction and Image Generation	418
<i>Conclusions and Recommendations</i>	418
Image Processing	419
<i>Conclusions</i>	419
<i>Recommendations</i>	420
Sensor Related Aspects of User Data Analysis	421
INTRODUCTION	423
Scope of Chapter	425
ATMOSPHERIC EFFECTS	427
Object Scene Irradiance Levels	427
<i>Directional Solar and Lunar Radiation</i>	428
<i>Diffuse Sky Radiation and Global Radiation</i>	428
<i>Effect of Haze and Clouds on Irradiance</i>	430
Atmospheric Attenuation Effects	430
<i>Description of Atmospheric Effects</i>	430
<i>Magnitude of Atmospheric Effects</i>	433

CONTENTS (Continued)

	<u>Page</u>
<i>Present Prediction Capabilities for Atmospheric Effects</i>	438
<i>Present Capabilities for Real Time Atmospheric</i>	
<i>Data Collection</i>	440
Recommendations for Future Efforts in Atmospheric	
Transmission Studies for Remote Sensing	441
RADIOMETRIC CALIBRATION	443
Types of Radiometric Requirements	444
<i>Amplifier Gain Setting Adjustment</i>	444
<i>Verification of Radiometer Operation</i>	445
<i>Channel Gain-Match</i>	445
<i>Inter- and Intra-Orbit Comparison of Data</i>	445
<i>Spectral Bandpass Shape</i>	446
<i>Spectral Signatures</i>	446
<i>Benchmark Data</i>	447
Quality of Radiometric Measurement Required	447
<i>Visible and Near Infrared</i>	447
<i>Thermal Infrared</i>	448
Present State of Radiometry	449
New Technical Constraints	450
<i>Time Behavior</i>	450
<i>Environment</i>	450
<i>Aperture</i>	450
<i>Spectral Regions of Greatest Importance</i>	451
Systems Currently Operating or Being Planned	451
<i>Multispectral Data System (MSDS)</i>	451
<i>Earth Resources Technology Satellite (ERTS)</i>	452
<i>SkyLab</i>	452
<i>Visible-Infrared Spin-Scan Radiometer (VISSR)</i>	453
Recommendations	453
<i>Timing of Design</i>	453
<i>Evaluation of Basic Approaches to Calibration</i>	453
<i>Specification Detail</i>	453
<i>Fulfillment of Specifications</i>	454
<i>Establishment of Calibration Capability on the Ground</i>	454
<i>Detectors</i>	454
<i>Visible Sources of Radiation</i>	454
<i>Blackbody Theory</i>	454
<i>Stability of Surfaces</i>	455
<i>Cryogenic Factors in Infrared Measurements</i>	455
<i>On-Going Program—Skylab</i>	455
PLATFORM EFFECTS	455

CONTENTS (Continued)

	<u>Page</u>
Orbit Requirements and State-of-the-Art	459
Attitude Requirements and State-of-the-Art	460
Spacecraft Error Sources and Attitude Motions	464
<i>Mathematical Model</i>	465
Future Developments and Recommendations	468
SENSOR DATA SYSTEMS	471
High Speed Multiplexers	471
On-Board Storage	474
<i>Spacecraft Tape Recorders—Present</i>	474
<i>Spacecraft Tape Recorders—Future</i>	475
<i>Ground Recorders (See Table 5-8)</i>	477
DATA CORRECTION AND IMAGE GENERATION	478
Radiometric Requirements	479
Geometric Requirements	480
<i>Spatial Registration</i>	480
<i>Positioning</i>	481
<i>Temporal Registration</i>	481
Image Geometry	482
<i>Sensor Geometry</i>	482
<i>Sensor Geometry Calibration</i>	487
<i>External Geometric Effects</i>	489
Basic Processing Operations	491
<i>Sensor Radiometric Correction</i>	492
<i>Atmospheric Radiometric Correction</i>	493
<i>Image Recording</i>	494
<i>Image Resolution, Scale and Format Size</i>	495
<i>Data Interpolation</i>	497
<i>Sensor-Geometry Correction</i>	497
<i>Conical-Scan Conversion</i>	498
<i>Correction of Platform Effects</i>	501
Present ERTS Ground Data Processing System Operations	503
Discussion of the Summary of the Conclusions	505
IMAGE PROCESSING CONSIDERATIONS	506
Image Processing Software Considerations	507
System Hardware Considerations	509
<i>Data Recording and Dissemination</i>	510
<i>Black-and-White Films</i>	511
<i>Color Film Outputs</i>	513
<i>Volatile Display</i>	514

CONTENTS (Continued)

Page

<i>Advanced Hardware Development</i>	515
<i>GSFC Program to Develop "Real Time"</i>	517
<i>Image Processing Systems</i>	517
<i>Data Processing</i>	518
Rationale for On-Board Image Processing Computer	519
General Philosophical Considerations	520
<i>Spacecraft Data Techniques</i>	520
<i>Ground Data Processing</i>	521
Image Processing Recommendations	522
<i>Short Term Payoff</i>	522
<i>Long Term Payoff</i>	523
SENSOR-RELATED ASPECTS OF USER DATA	
ANALYSIS	524
Sample Identification	524
Spatial, Spectral Resolution and S/N Interdependencies	524
Conclusions	526
REPRESENTATIVE SYSTEM DESCRIPTIONS	527
General	527
ERTS-1-MSS	527
<i>Sensor Subsystems</i>	527
<i>Transmission and Receiving Equipment</i>	532
<i>Ground Data Recorder</i>	534
<i>Checkout Display System</i>	537
SMS-VISSR	540
<i>Sensor</i>	540
<i>Multiplexer</i>	544
<i>Spacecraft to Ground Communication</i>	550
<i>Demultiplexer</i>	551
<i>Synchronizer/Data Buffer</i>	552
<i>Direct Readout Ground Station (DRGS)</i>	555
<i>Recorder/Processor</i>	560
ATTACHMENT A—ATMOSPHERIC EFFECTS IMPACTING	
SENSOR TECHNOLOGY	563
ATTACHMENT B—MSS CALIBRATION	565
ATTACHMENT C—VISSR CALIBRATION	567
ATTACHMENT D	569
ATTACHMENT E	577
REFERENCES	585

THE SUMMARY OF THE REPORT OF THE ADVANCED IMAGERS AND SCANNERS WORKING GROUP

OVERVIEW

The following is a summary of the conclusions and recommendations contained in the individual reports generated by each of the five panels involved in the Ad Hoc Working Group on Advanced Imagers and Scanners.

The report of the panel on User Applications describes the type of data needed by the users of remotely-sensed earth resources images, and indicates the general directions for further sensor development. The three panels on imaging instruments described the state-of-the-art of instruments falling within their cognizance, and pointed out areas where improvement is desired in these sensors.

In addition to the sensors, other important elements of remote sensing systems were discussed by the panel on Related Technological Constraints. It considered the limitations placed upon imaging system design by system elements, such as the atmosphere between the scene and the sensor, the platform (spacecraft or aircraft), the communications links, and the image processing facility. Figure 1 depicts the major elements of an earth-viewing imaging system.

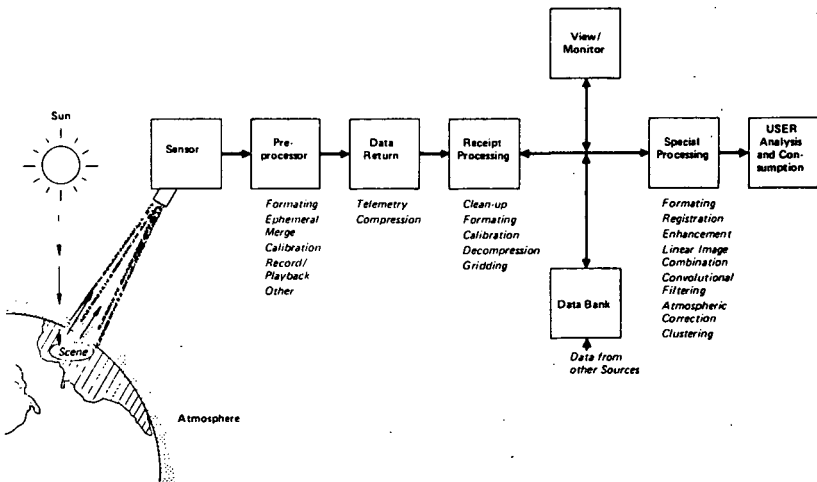


Figure 1. An Example of a System Functional Block Diagram

Spectral Distinctions

This report deals exclusively with imagers and scanners operating in the visible and infrared (IR) spectrum (0.4–16 μm). In the shorter wavelength part of this band (0.4–4 μm), reflected radiation from the sun is primarily observed by a remote sensor. In the longer wavelength portion (6–16 μm), the earth and its features absorb the incoming solar energy and emit energy in proportion to their temperature. Thus, observations in the reflective band are functions of input energy and the object's reflectance, while in the thermal band they are indicative of the feature's temperature and its emittance. This distinction permits the use of instruments which are sensitive to different portions of the band, to be used separately or in conjunction with one another depending upon the nature of the object being observed.

Effective Instantaneous Field of View

An important performance parameter for all imagers and scanners is the spatial resolution. The Working Group found that the term "spatial resolution" has no unique definition and may lead to technical misunderstandings. To overcome this potential difficulty, a parameter called Effective Instantaneous Field of View (EIFOV) was defined as the resolution of the 50% response point on the modulation transfer function (MTF) for non-sample data limited systems. A modification of the EIFOV is required for systems in which the duration of the interval between the times at which the sensor signal is sampled significantly affects the system spatial response. Although approximated for the purposes of this report, proper specification requires additional research as is discussed in detail in Chapter II. This parameter should permit a reasonable comparison between different kinds of instruments in the sense that equal values of EIFOV imply equal ground resolution capability. For the purposes of this report, the term resolution will be taken to mean the EIFOV, unless otherwise stated.

Other System Considerations

The Working Group investigated the impact of the Space Shuttle on the development of advanced imagers and scanners. The Shuttle system allows the use of "laboratory type" instruments, configured to support "in space" experimentation aimed at optimizing critical sensor performance characteristics.

The Working Group considered the use of orbits other than the sun-synchronous, medium altitude orbit of Earth Resources Technology Satellite (ERTS), for earth resources applications. The geostationary orbit was chosen as the most likely candidate, since it gives the opportunity for continuous coverage of a given area.

The Working Group, also, considered that imagery for small scale photogrammetric applications can presently be achieved with minimum system complexity and cost by photographic film.

FINDINGS AND RECOMMENDATIONS

This section contains a synopsis of the findings, conclusions, and recommendations of each of the five panels.

User Applications

The User Applications Panel considered the results of previous applications studies to aid in identifying and evaluating potential applications in terms of importance and benefit. These studies, updated by experience with ERTS data, recent and proposed legislation, and international trade developments, were examined to provide a framework of data characteristics considered desirable for incorporating into future systems. Figure 2 is a summary of the spatial resolution and coverage frequencies desired by panel members. Figure 3 shows the spectral bands of interest to the users.

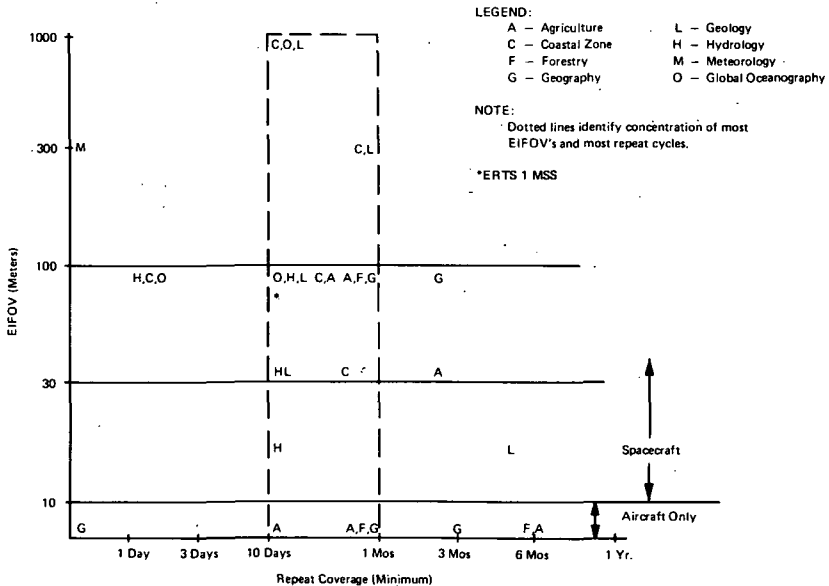


Figure 2. Repeat Coverage Needs

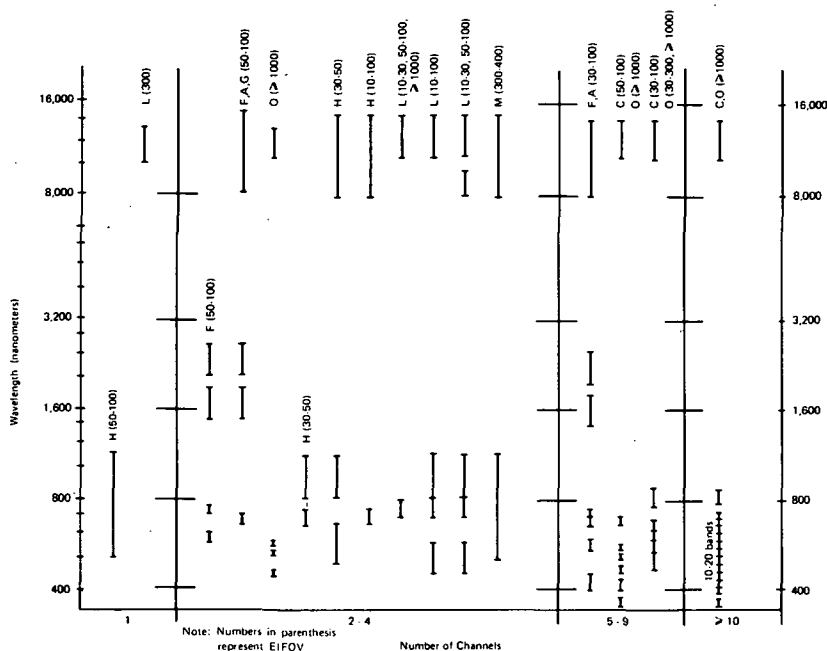


Figure 3. Spectral Requirements Summary

Conclusions for the Near Term (Four Years)

The panel concluded that for the near term:

- If an improvement is required over the current ERTS sensors, it is only by a factor of 2-3 in resolution to meet most applications needs for "broad scale" coverage.
- Some applications require a high frequency of observation, perhaps daily or even hourly, thus requiring development of a geostationary observation capability.
- A multiband, high sensitivity low resolution imager will be needed to perform highly important ocean color measurements. Ocean color is indicative of the existence of phytoplankton which perform 3/4 of the photosynthesis occurring on the earth.
- "Broad coverage" must be supplemented by higher resolution "sample" data acquired from aircraft or spacecraft.
- Experiments should be undertaken to determine the utility of nighttime images for assessment of cultural patterns.

Needs Over the Longer Term (Eight Years)

In considering the longer term needs of the user community, the panel noted that environmental monitoring needs will become larger and of greater importance. This is also the area most in need of instrument R&D. In this respect:

- Water (including oceans) and air quality assessments are sorely needed. Remote sensor research and development in these areas must progress at a faster rate and should be given a high priority.
- It can be expected that active remote sensor systems, employed from aircraft, will be required for solution of some resource and environmental problems; a state-of-the-art survey would be in order.
- The panel recognized the need for continuing data processing research aimed at reducing the human involvement in the interpretation process, thus speeding the derived information to the ultimate user.

Data Attributes

The panel identified certain general data attributes that should be given strong consideration in the design of post ERTS systems. These are:

- Geometry suitable for detection of change between sequential images. Image registration within one picture element (pixel) is optimum, but image registration within 3 pixels is usable.
- Pixel by pixel registration of multispectral bands.
- Data processed for reference to the figure of the earth with accuracy related to map scale and projection.
- Orbital parameters and attitude knowledge to a level commensurate with map scale and projection.
- "Sample" data collected concurrently with broad-scale coverage.

Electromechanical Scanners*Technical Background*

Electromechanical scanners are capable of producing geometrically registered, multispectral images in spectral channels extending from the visible to the thermal infrared. In addition, accurate radiometric measurements can be made. As implied, image formation is accomplished by mechanical scanning.

Typically, mechanical motion causes the scene to be sampled in the across-track direction by a detector or array of detectors while satellite motion provides the orthogonal scan component. Many electromechanical scanners have flown, a typical example being the multispectral scanner (MSS) on ERTS-1.

Conclusions and Recommendations

The conclusions and recommendations of the panel on Electromechanical Scanners were as follows:

- E-M scanners in the reflective bands can achieve increases by a factor of 2-3 in spatial and spectral resolution and in signal-to-noise over that currently achieved, using existing technology. This will require a large number of detectors and/or an increase in the size of the collecting optics.
- E-M scanners in the thermal-IR band require cooled detectors. Cryogenic development is one of the limiting factors in resolution and signal-to-noise improvement.
- E-M scanners can possibly be used for photogrammetric applications if a greater spacecraft stability and/or compensating processing capability can be achieved.
- For visible and near-IR wavelengths, solid state self-scanning arrays may be incorporated into mechanical scanners, to help improve signal-to-noise performance.

Electron Beam Imagers

Technical Background

Electron-Beam Imagers are those devices which, by means of a shutter or similar mechanism, put an image, fixed in time, of an entire scene on a photosensitive surface, and then read out the photosensitive surface by means of a beam of electrons after the shutter has closed. The common television camera and the ERTS Return-Beam Vidicon (RBV) are two examples of electron-beam imagers. Differences among electron-beam imagers generally are based upon either the method of reading the image on the photosensitive surface or on the material used as the surface.

In considering future space missions, the main argument for developing improved electron beam readout image sensors is based on the advantages of framing cameras over other imagers for some purposes.

Recommendations

The Electron Beam Panel has recommended a number of technology options which offer the most promising performance for future applications, as follows:

- RBV Improvements—Striped filters should be developed to provide registered images from a single camera at the same resolution offered by the ERTS-1 RBV multispectral system.
- Larger Format Sensors—Some of the problems experienced in current systems (e.g., ERTS) where “multiple-camera” cameras are used, are solvable using larger single sensors. It is expected that larger format electron beam sensors may have reduced resolution per mm, but that overall data packing density, which allows simplified optics and reduced electronics, will prove most beneficial. Target formats as large as 100 mm x 100 mm should be studied.
- Large Silicon Target Vidicons—The high quantum efficiency afforded by silicon in the visible and near IR gives it greater sensitivity than other vidicon photosensitive targets. A program to make large silicon diode array targets would be valuable.
- High sensitivity, high resolution, fast-erase tube—Development of a camera tube, having high sensitivity and resolution with fast erase properties, is required for practical application of the Wide-range Image Spectrophotometer (WISP) technique.
- Optics—The current state-of-the-art in refractive optics needs to be improved to use the resolution available in the present electron-beam sensors. Large reflective and catadioptric optical systems should be studied as a means of improving the optical performance.
- Cold cathode development—Gun designs incorporating cold cathodes should be included in studies relating to development of new tubes. The cold cathode will provide solid state reliability and significantly higher current density capabilities, thus permitting reductions in beam cross-section and correspondingly increasing the sensor spatial resolution.

Self-Scanned Solid State Imaging Systems

Technical Background

Solid state sensor technology provides a new tool for future satellite remote sensing applications. It is now feasible to build solid state imaging systems that provide geometrically registered multispectral images, and with proper

calibration, permit accurate relative radiometric measurements to be made. The inherent advantage of the solid state approach lies in the fact that no mechanical scanning motion is required; the detector arrays are scanned electronically.

The solid state system approach, currently most useful for remote sensing applications, uses line arrays of many thousand elements in what is called a "pushbroom" scan mode. The across track scene is imaged on the line array which electronically samples the image, while the satellite motion provides the orthogonal scan component.

Self-scanned solid state sensors, in general, comprise arrays of discrete photo-sensitive elements which are scanned by means of electronic circuits that are integrated on the same semiconductor wafer with the detector elements. At the present time, electronically self-scanned detector array technology is practical only in silicon.

Conclusions

- Solid state imaging sensor systems are feasible. These systems can be designed and built for use on advanced earth resources missions anticipated for the late 1970's and early 1980's. Photodiode and phototransistor arrays are in an advanced stage of development. A sensor using them could probably be developed for space flight in a period of three to four years. Charge-coupled devices are in the early developmental stage. A sensor system using them could probably be developed for space flight in about six years.
- Silicon photodetector elements can be assembled into arrays of thousands of elements with a center-to-center element spacing of 15 micrometers (0.6 mil) for high resolution pushbroom mode scan systems.
- The fixed geometry, spatially quantized nature of the arrays make possible accurate geometric relationships in the imaged scene in the across-track direction.
- Registered multispectral data can be obtained by using careful alignment techniques for the arrays in each spectral band.
- At this time calibration information must be stored for each detector element. This has significant impact when it is considered that there are thousands of elements in the typical multispectral solid state imaging system.
- It is presently possible to make high density arrays of infrared detectors (photoconductive and photovoltaic) out of infrared semiconductor

materials. However, it is not yet possible to integrate these detectors with associated electronics on one chip. As an alternative, it is possible to consider hybrid devices consisting of infrared detector arrays cemented to a silicon chip containing the necessary readout circuitry.

- Another form of hybrid device consisting of conventional infrared detector arrays connected to silicon charge coupled devices via appropriate interfacing electronics integrated on the same silicon chip could possibly be developed within six years.

Related Technological Constraints

Calibration, atmospheric effects, platform attitude, data processing and transmission, and other factors all affect the ability of imagers and scanners to produce the information desired by users. In some cases, these constrain the sensor performance, while in others they afford opportunities for image manipulation and data management. Recommendations were made as follows:

Atmospheric Effects

The current understanding of the atmosphere makes it very difficult to estimate the absolute surface reflectance of elements in a scene. However, atmospheric effects can be estimated with sufficient accuracy to allow meaningful information on reflectance ratios between near elements (both spatially and spectrally) to be extracted from the data. Future NASA programs should include auxiliary sensors, flown with imagers, to locate and allow the automatic identification of regions where the data is significantly disturbed by haze or thin cirrus clouds.

Calibration

Both absolute and relative (band-to-band) radiometric calibration is presently limited by knowledge of the characteristics of standards currently available for use with flight instruments. For example, it is barely possible to meet the 5% values required for the ERTS Multispectral Scanner (MSS). If calibration to a few percent will be required in the future, an effort to provide the proper facilities is called for.

Spacecraft Stability

Precision attitude and attitude rate sensing and control in all 3-axes is essential to allow the easy generation of geometrically corrected images. The spacecraft

technology to do this is feasible, but much work remains to incorporate it into earth resources satellites.

Data Handling

Multiplexing and Storage. Data rates under 280 million bits per second (MB/S) and 7 bit accuracy can be multiplexed at the present time. Onboard storage systems can be developed to store from 30 to 60 MB/S. Ground data recorders currently can accept data at 30 MB/S, with 60 MB/S a reasonable improvement. Rates of 100 to 200 MB/S are within reach, but will require considerable development.

Transmission. Communication of broad-band data up to 200 MB/S to a regional receiving site with a cost of about 2 million dollars per station is feasible. A small directional antenna is required on the spacecraft to offer this service.

Direct broadcast ("APT") to local users will be limited to about 2 MB/S or 100 kHz analog data allowing production of a 4,000 line picture at a ground station which costs about 200 thousand dollars.

Ground Data Processing. The present ERTS Ground Data Facility can probably support sensors with up to 6,000 elements per line with only minor modifications. A conical image space electromechanical scanner would require modification of the Electron Beam Recorder or significant modification of the format of the output product.

Different types of sensors have a varying impact on ground system design. The line array scanners or pushbroom sensors will require the development of a specialized high speed digital system to radiometrically calibrate the data from many thousands of detectors at very high rates. The built-in geometric accuracy of these arrays will, however, simplify the geometric correction problems.

Distribution. The distribution of large quantities of digital data to the users will require the development of a new high density digital interchange tape. The design and development of this system must be such that many copies can be economically made with the same data, and a low cost reader must be available for data input to the user's computer.

Film products offering more flexible and economical false color display also will be required to use the data from the new multiband sensors.

CHAPTER 1

USER APPLICATIONS

PANEL MEMBERS

W. Fischer — *Chairman*

J. Clifton

S. Q. Duntley

J. Glover

H. M. Gurk

R. C. Heller

R. McEwen

E. Risley

C. Robinove

L. Schaefer

J. Sherman

J. W. Sherman III

CHAPTER 1

USER APPLICATIONS

PANEL RECOMMENDATIONS

The user community agreed that current ERTS-1 data has proven valuable but that higher spatial resolution, narrower spectral bands, wider spectral coverage, better radiometric accuracy, improved geometric precision, etc., would contribute greatly toward their informational data requirements.

Present scheduling for the 1970's and 1980's offers a limited number of earth resources survey systems into which advanced visible and IR imagers and scanners will be integrated. Considering the ERTS RBV and 4-channel MSS and associated processing equipments as a baseline, efforts should be made to achieve greater total benefits for the nation through qualitative improvement in sensors. The improvements sought should be aimed at increasing the types and values of data obtained and the achievement of greater efficiency and economy in operation.

The economic stringencies limiting the number of spacecraft which could be available in the near term (6-10 years) at a time when earth resource data needs are expanding rapidly, must be recognized. The largest possible number of user groups should be accommodated in design considerations, while the higher payoff areas must be the focus of attention. Facility type sensors, capable of satisfying requirements of diverse users should be developed to provide the greatest benefits for the moneys expended. Figure 1-1 is a summary of user needs as now recognized in terms of spatial resolution and coverage frequency (see Summary Charts for discussion).

The User Applications Panel considered the results of previous applications studies (e.g., EOS study, Space Council Study) to aid in identifying and evaluating potential applications in terms of importance and benefit. These selections as updated by experience with ERTS data, recent and proposed legislation, and international trade developments, were examined to provide a framework of data characteristics considered desirable for incorporating into post-ERTS systems. In addition, the user members of the panel, brought to the discussion their own particular experience in the various disciplines, and thus provided an overview of the potential and requirements for sensor data applications. The user panel also benefited greatly from the exchange of information with the instrumentation panels. The new insights, thus gained, into technical developments and opportunities in the use of remote sensors

- Experiments should be undertaken to test the usefulness of nighttime images for assessment of cultural patterns, and polarization observations for measuring aerosol distributions in the atmosphere.
- A high sensitivity, multiband sensor will be needed to perform highly important ocean color measurements. Ocean color is indicative of the existence of phytoplankton which performs 3/4 of the photosynthesis occurring on the earth. There are indications that the chlorophyll content of the oceans is getting smaller. Since CO₂ can be absorbed only as long as sufficient phytoplankton are present, it is imperative that a baseline be established promptly by which to measure these changes affecting the ocean release of life-sustaining oxygen.

Long Term Needs

In considering the longer term (8 years) needs of the user community, the panel noted that environmental monitoring needs will become larger and of greater import. This is also the area most in need of R&D. In this respect:

- Water (including oceans) and air quality assessments are sorely needed. Remote sensor research and development in these areas must progress at a faster rate and should be given a high priority.
- There are promising developments in the field of luminescence mapping which may have great significance in water quality measurement and oil pollution monitoring. These new instruments make measurements within single Fraunhofer lines and may push the "state-of-the-art" sensor development.
- It can be expected that the support of active remote sensors from aircraft as part of total systems will assist the solution of some resource and environmental problems; a state-of-the-art survey is in order.
- Additional research is needed in the use of remote sensors for public health and wildlife management purposes.
- The science and applications research experience that is required for definition of user needs has not kept pace with evolving technology. There is a need to evaluate more fully the current technology and user activities.

Data Attributes

The panel identified certain general data attributes that should be given strong consideration in the design of post-ERTS systems:

- Geometry suitable for detection of change between sequential images is required. Image registration within one picture element (pixel) is considered optimum; but image registration within 3 pixels is usable. Also, time comparisons with ERTS data may be facilitated if improvements in EIFOV are made in integral multiples of ERTS capability.
- Pixel-by-pixel registration of multispectral bands is essential. To accomplish this with systems having varying resolution, degradation of the finer resolution channels must be provided for by the data processing system on the ground.
- Data processed for reference to the figure of the earth must have accuracy related to map scale and projection.
- "Sample" data must be collected concurrently with broad-scale coverage.
- Orbital parameters and attitude knowledge must be obtainable to a level commensurate with map scale and projection.

PERSPECTIVE

That part of the world landscape whose characteristics can be determined through the use of remote sensing techniques is primarily in the 0.4 to 16 micron spectral range. This range, therefore, was the specific concern of the user applications panel of the Advanced Imagers and Scanners Working Group.

Since the static and temporal landscape data needs are so tightly interrelated, the panel attempted to emphasize the commonalities within the temporal, spectral, sensitivity, resolution and spatial geometric requirements that need to be fulfilled by imaging, scanning and data processing capabilities. Special needs were also identified, particularly those related to meteorology (atmospheric science), oceanography, and hydrology, but the panel did not develop similarly detailed recommendations for the study of air and water quality parameters, since there is at present insufficient scientific research to draw upon.

The panel's members came from both federal agencies and private institutions. Representing Agriculture/Forestry/Geography disciplines were L. Schaefer (USDA) and J. Clifton (now retired from USDA); R. C. Heller (Pacific S.W. Forest and Range Experiment Station); and J. Sherman (University of Washington), and E. Risley (USGS), respectively. Representing the oceanographic disciplines were S. Q. Duntley (Scripts Inst.) and J. W. Sherman, III (NOAA-Spacecraft Oceanography Project). J. Glover (NESS) represented meteorology. R. McEwen (USGS) and C. Robinove (USGS) represented cartographic and hydrologic disciplines, respectively. H. Gurk (RCA) provided

coordination between user needs and technology constraints and opportunities. W. Fischer (USGS-EROS Program) chaired the User Applications Panel.

Purpose of User Requirements Panel

The prime purpose of the user requirements panel was to serve as advisors to the instrumentation panels and to set boundaries on technical requirements based on user needs.

To accomplish this purpose, it was found desirable to review past applications studies, in light of recent developments and better understandings of terminology.

The user panel benefited greatly by the exchange of information with the instrumentation panels and its new insight into technical developments and opportunities will be valuable in considering future applications and in developing estimates of data quality needs.

Constraints Applied to User Panel Study

The User Requirements Panel limited its considerations in several areas because of the known limitations of certain technology and also the limitations of some present and planned applications. The constraints imposed were as follows:

- Only the spectral range of 0.4 - 16 microns was considered.
- Limited consideration was given to further meteorological programs because of the already well-developed and parallel efforts in NASA and NOAA.
- Atmospheric effects on spectral response were not evaluated.
- Limited experience with ERTS-1 and NOAA-2 precluded definition of a number of applications (for example, snow cover).
- There was limited consideration of air and water quality because of the minimum of research and valid data in these application fields at this time.

Panel Guidelines

The following guidelines were followed in the deliberations of the user applications panel:

- Commonality in Needs – The entire study was conducted so as to search out and document common data requirements from the variety of applications considered.
- Time Frame – At the request of the study organizers, conclusions were related to the 4 and 8-year time frames.
- Existing Reception/Processing Systems – Consideration was given to the investment already made in existing reception and processing systems. This consideration was tempered by uncertainties surrounding future transmission bands.
- Transmission/Processing Requirements – Recommendations and needs were expressed in light of transmission and processing requirements. This consideration was also hampered by future transmission band uncertainties. The impact of transmitting both “broad-coverage” data and “sample” data simultaneously, or alternately, was not considered.
- Economics of Data Collection – Expressions of need for improved EIFOV were developed in consideration of the square relationship by which costs of data acquisition and processing increase with respect to improved (finer) EIFOV. Consideration was not given to the comparative cost of collecting data from aircraft or spacecraft nor to the economics related to shuttle launch.

Selection of Applications

Applications within the earth resource disciplines were selected on the basis of the following criteria and information sources. In general, these considerations helped determine for each application, its value, attainability, and viability. The technical specifications discussed herein were developed in this way.

- Applications studies reviewed. Documents such as the Woods Hole Summer Study reports, the National Aeronautics and Space Council Study, the EOS Study and others were used as a basis for selection of applications.
- Experience with ERTS-1. Although limited at this time, ERTS-1 data demonstrated the feasibility of some applications such as geohydrology, mapping of geologic structure, and gross land use mapping.

- Experience of the experts. In the working group the presence of users from almost every application interest allowed a critical selection and ranking of the applications.
- Newly-developed sciences. Mesometeorology, and weather modification, for example, provided clarification regarding additional requirements that have not heretofore been stated.
- Demonstrated data processing capabilities. Capabilities for increased throughput of data and new cartographic products made many applications more feasible than in the past.
- Better understanding of terms. The sensor engineering terminology such as "resolution" and "calibration" was defined to provide a more definitive knowledge of the technical capability needed for a given application.
- Federal and State legislation (recent and pending). In fields such as land use, coastal zone management, clean air and water, and environmental input statements, critical data needs were identified.
- Newly-recognized interests and markets. Such new international developments as the need for global wheat information, in light of recent wheat sales to the USSR and other commodity exports, have spurred the development of applications to meet the needs for information.

Applications Groupings

Eight disciplines were established as the major categories for applications of the data generated through remote measurement with imagers and scanners. Obviously areas of need in different categories overlap and results of analyses impinge on different areas. However, the broadly defined categories were:

Agriculture	Geology
Coastal Zone Studies	Hydrology
Forestry	Meteorology
Geography	Oceanography-Global

Agriculture, forestry and geography were studied as one group because of many similarities in their needs. Most of the conclusions of this users part of the study show this grouping, although a few separate needs are identified.

The coastal zone includes both surrounding inland water terrain and those ocean applications along the coast. The extent to which the group entered either area is somewhat variable. It can usually be distinguished where the land greatly affects the water and vice versa. Similarly, there is some

overlap between an arbitrary demonstration of water boundaries of the coastal zone and the near shore ocean boundaries of the global oceanography categories. In general, these overlapping considerations caused no problems; rather, they demonstrated a common need for both fields.

Other categories or disciplines were found more obvious in their definitive needs and applications. For meteorology, stated needs are small since the working group did not evaluate items already being planned in the existing space programs for this field. Many of these items, or applications, were well defined; this discipline appeared to have been developed well in advance of the needs in the other areas.

Definition of Terms and Validity of Estimates

The most troublesome term for the user group (and indeed for the workshop as a whole) was "Effective Instantaneous Field of View" (EIFOV). The sensor technology panels defined it very quantitatively as "the 50 percent response point on the MTF curve." While the user panel would have liked to affirm the same definition, it could not in fact do so. Such a definition was not sufficiently meaningful of itself to suit the user needs.

The definition of EIFOV used by this panel was "the minimum linear dimension on the surface (at nadir) at which user specified characteristics can be discerned." The most significant characteristic within the EIFOV was sensitivity which is defined below.

Other terms used in the study analysis are defined as follows:

- Repeat Coverage – The minimum time between the repeat passes over a given location in order to satisfy coverage needs (e.g., only during the growing season for agriculture).
- Field of Coverage – Swath width for a nadir pointing sensor.
- Maximum Oblique Pointing Angle – Angle to the edge of the picture if tilting the camera is acceptable.
- Sample Coverage – Image selected portions of a large area only in a sampling technique.
- Sensitivity – Smallest change in temperature or reflectivity which a user wishes to detect.

SUMMARY CHARTS

The following section describes the chart presentations of Figures 1-1 through 1-3 and Table 1-1. These diagrams and table represent the consolidation of individual parameters for each discipline and should be broadly interpretable by themselves. They relate to each other by discipline, EIFOV, and spectral band and should serve as guides for sensor developers and designers. However, some brief comments are provided here for each of the referenced figures.

Repeat Coverage Needs (Figure 1-1)

As can be seen within the dotted lines, most of the needs for EIFOV fall in the 30-100 meter range which includes ERTS and improvements of a factor of two or slightly more. Likewise, most repeat needs are similar to ERTS, or a factor of two improvement (10-30 days). (Repeat coverage consideration here has allowed for cloud cover.) There are some obvious groupings of needs and these suggest the possibility of flight on the same spacecraft of sensors with different missions, or on spacecraft with similar orbits. We suggest geostationary satellites for daily, even hourly, repeat coverage needs. Film return satellites may be desirable for the very long term needs, especially for small EIFOVs. No consideration of aircraft applications appears on the other charts.

Sensor Geometry (Table 1-1)

Most of the needs seem to be for ERTS type swaths (about 200 km) and for contiguous coverage for a very large mid-range (30-300 m) of EIFOVs. To a certain extent this may be the result of some familiarity already achieved by the users with such a situation on ERTS. Off angle pointing is also often a multiple of the ERTS swath (e.g., 12 degrees). "Nadir" refers to a vertical picture with no pointing. From the table, it would appear that a high resolution "sample" data sensor is not necessary. However, most of the panel felt that it should be considered because of its great reduction in data volume, if used for sampled rather than contiguous coverage at a given EIFOV. Time really did not permit the detailed examination of this concept during the study. It seems desirable to suggest that user agencies identify the utility of statistical processing of sampled coverage data from space.

Spectral Requirements (Figure 1-2)

This chart illustrates most vividly the differences in needs among the disciplines. Only in the thermal IR (i.e., 8 to 14 μm) does there seem to be a real

Table 1-1

Scanner Geometrical Needs Summary

EIFOV (Meter-Ground)	Field of Coverage (Km-Ground)	Maximum Oblique Pointing Angle	Sample (S) or Continental (C) Coverage
<u>10</u>			
C	40	Nadir	(C)
A,F,G (5-10)	15-30	6°	(S)
<u>10-30</u>			
H	50	15°	(S)
L (10-20)	13	45°	(S)
<u>30-50</u>			
H,C	200	Nadir	(C)
C	200	45°	(C)
G,A,F	200	12°	(C) or (S)
L	200	12°	(C)
<u>50-100</u>			
H,C	200	Nadir	(C)
C,O	200	30°	(C)
C	200	45°	(C)
G,A,F	200	12°	(C) or (S)
L	200	12°	(C)
<u>100-300</u>			
C	200	45°	(C)
<u>300-</u>			
L (300)	400	20°	(C)
M (300-400)	1000 x 400	8°	(S) (2-3 minute repeat)
C,O (1000-10,000)	400	20°	(C)
L (1000-2000)	1300	45°	(C)

LEGEND:

A - Agriculture F - Forestry L - Geology M - Meteorology
 C - Coastal Zone G - Geography H - Hydrology O - Global Oceanography

consistency of needs. The multichannel sensor bandwidths are shown in the same column. The EIFOVs in parentheses represent the smallest requirement for any sensor. Generally this is for the visible or near IR channels; some relaxation may be acceptable in the thermal IR, even a factor of 3-5.

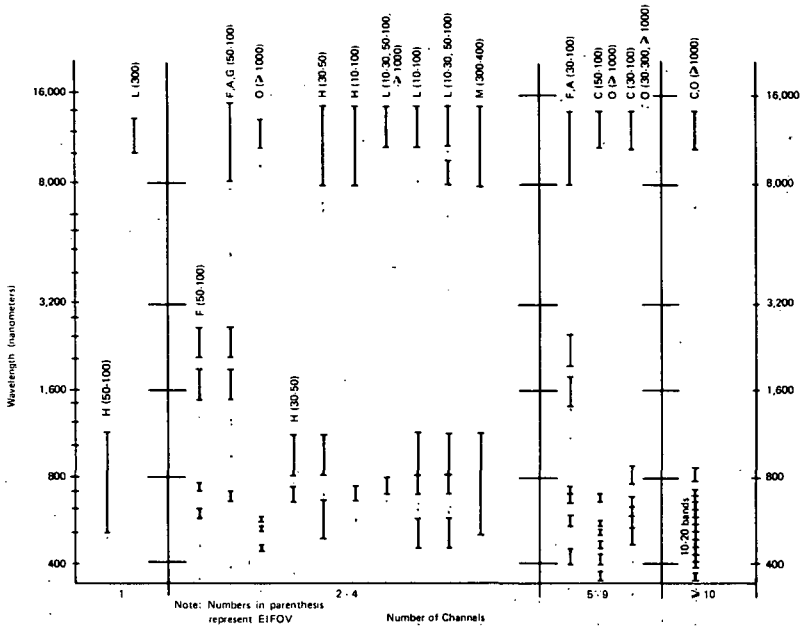
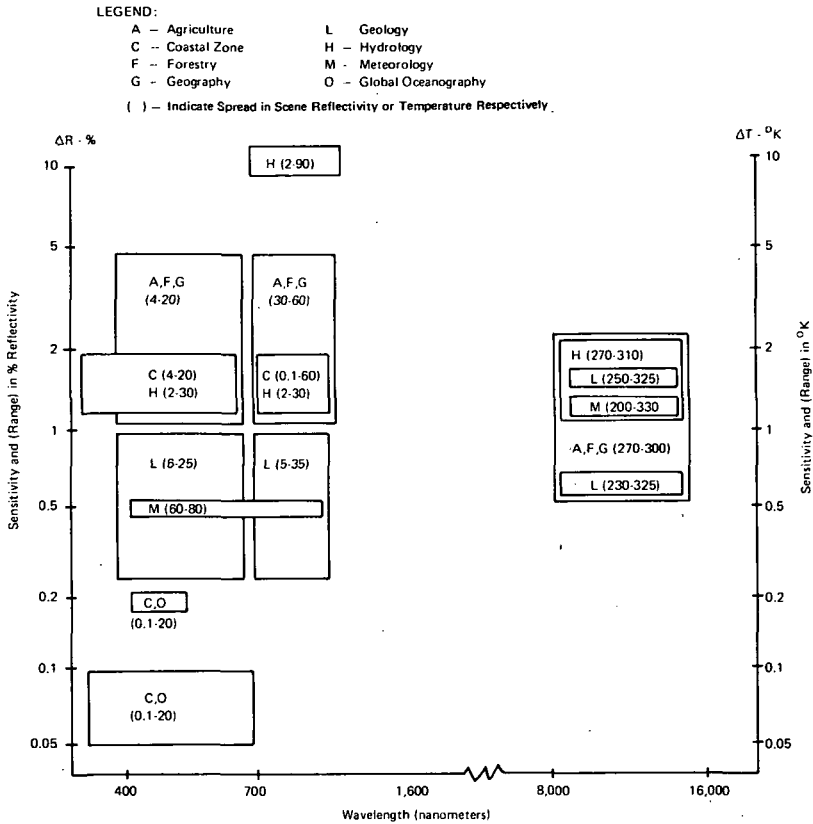


Figure 1-2. Spectral Requirements Summary

It would appear from the chart that many different sensors may be needed, each tailored to its special characteristics. Several alternatives should be considered. First, some variation of requirements – spectral or spatial – may permit some consolidation. Second, it might be possible to consider some groupings of classes so that several different “standard” sensor system concepts might be designed and relatively easy adaptations of each standard could be planned to meet the parameters of any member of the class. Finally, a variable band, multichannel sensor could be designed and flown experimentally to determine if some of the differences in the listed needs could be eliminated.

Sensitivity Requirements (Figure 1-3)

This chart represents the users way of identifying by spectral band what sensitivity is of interest. The specific values do require further interpretation in order to consider atmospheric effects, sun angle changes, and the fact that in many cases the techniques of analysis are new, such as the use of spectral signatures. Experimentation in this area would be helpful to determine if the predicted sensitivities can be relaxed or are valid.



General Comments

The parameters represented in the figures and table represent a good consolidation of users estimates of their needs. There is some uncertainty in the specifications shown, however, and experimentation, especially spaceflight experimentation, would be most helpful. It would generally appear that the ERTS type sensors should be improved by perhaps a factor of two spatially and that more bands would assist the user needs. Most of the users would prefer narrower bands than used with ERTS, e.g., 50 nanometers rather than 100 nanometers. It is conceivable that some tradeoff of bandwidth might be made with sensitivity, but obviously such sensor effects as a change in signal-noise ratio must be considered in this tradeoff.

Besides the recommendations made previously, the working group felt that a base map for reference should also be generated from space-acquired data. This map need not be updated more frequently than 3 years, but such a reference would be very helpful. It would appear that the required base map should be developed from visible panchromatic data and should be in the 1:250,000 scale range at least.

In addition, the group felt that some consideration should be given to the "mixed high" principle in order to reduce data volume. This technique uses one wide band at small EIFOV to determine the boundaries and edges of images accurately and several bands at larger EIFOV to get multispectral data to identify surface materials. Investigations should be made by the users to verify the usefulness of this technique and by the sensor technologists to determine its implementation feasibility.

DESIGN AND TECHNIQUES EVALUATION

Digital and Analog Data Processing

Within the time period from 1973-1980, there will be a continuing requirement for high quality images and a selective demand for digital computer-compatible tapes. As the number of users increases, the demand for images may increase more rapidly than the demand for digital data. All users desire reference images even with some digital processing. Therefore, an exclusive development of one type of data processing to the neglect of the others, must not take place.

Digital processing is compatible with serial processing, sequential comparisons and mathematical modeling. The natural applications are in spectral analysis and change detection, if the geometric register of data is maintained. Digital processing appears weak for all types of pattern recognition at this time; breakthroughs may be far off. The reliance on human interpretation and analysis will probably continue for some time.

However, considerable improvement in equipment and techniques for manipulating the image and assisting the interpreter are needed. These should be made widely available. One needed device is a high quality color-additive viewer using preregistered B&W (black & white) images. This would reduce the requirements at the central facility for many options of color images.

A serious problem already exists in the dynamic range limitation of films. Film cannot record all the data available from the sensors. This may be solved by selective expansion of parts of the data into the film range with attendant loss

of some data. Serious consideration should be given to allocating this data processing step to the user through development of less expensive drum printers. The central facility could prepare a standard image and a digital tape that is system corrected and registered. The digital tape would then drive the drum printer. Consideration should also be given to the increased use of other high density digital storage mediums.

Data Transmission

The availability of earth images and data to users with a very short time lapse after its collection is a key factor in its input for resources and environmental management decisions. For this reason, automatic picture transmission from the Earth Resource Satellites to users both domestic and foreign is highly desirable.

However, these images must be of high quality (spatially and spectrally), and must suffer the least possible degradation during transmission, reception, and processing, commensurate with economic constraints. At the present time, the panel is able to identify only a few applications which may justify local receipt of limited or degraded data. Such applications include sea and lake ice monitoring, offshore oil production monitoring and possibly fisheries monitoring.

Photographic Processing

There is a serious problem in all image data processing using photographic film. The quality of control in the film processing, enlargement register, color balance, density range, gamma, and spectral fidelity is extremely difficult even with a centralized facility. The average user with modest equipment finds the task almost impossible.

Since it is unreasonable for the central processing facility to selectively respond to every user, this facility must standardize on a few products. At the same time, those users whose needs are inconsistent with the standard products of the centralized facility, present urgent needs for developing simple reliable, and inexpensive image equipment and processes that they can operate.

Stereo Coverage

Panchromatic frame-format imaging systems can be designed in a stereo configuration which will be a valuable supplement to many users. One image is a

nominal vertical and the second covers the same ground area from an exposure station further along the orbit. The tilted image can be rectified during data processing into a vertical format. A minimum angle of 15 degrees should be maintained between sensor axes to detect elevation differences of 400 meters from altitudes of 1,000 kilometers. Convergence angles of 25 degrees would allow most individuals to detect elevation differences of 250 meters.

The shape of many landforms of lesser elevation change could also be determined. Absolute elevation contours could not be compiled in most cases, but relative contour intervals of 500-1,000 meters could be obtained and these would have value in poorly mapped areas. The EIFOV should be at least 30 meters to provide satisfactory image detail and compatibility with map scales of 1:100,000 for general interpretation and 1:250,000 for orthophotoimage preparation.

Night-Time Imaging

A potentially meaningful experiment could utilize a presently unassigned capacity of the ERTS satellite for imaging the earth's surface in the visible part of the spectrum at night. Darkness becomes a filter in this situation, and is presumed that only areas and patterns of artificial illumination would be recorded. The spectral character and low intensity of such light would probably require application of image intensification at least, in order to achieve a visual image.

The purpose of such an experiment would be to determine whether night-time imaging could enhance our ability to determine:

1. Settlement patterns:

- Patterns of disbursed settlement
- Urban agglomerations – systems of cities
- Gross functional differentiations between cities and possibly within cities
- Gross measurement of the connectivity of urban places

2. Gross estimates of energy consumption on a national and international scale:

- As a surrogate for determining technological levels
- As a measure of regional concentration within larger units

3. Detection of volcanic activity on a global scale
4. Detection of bioluminescence at sea and along coastal margins for identification of highly productive waters and potential applications to monitoring fish schools at night. (This is discussed in more detail under "Oceanography".)

Imaging of Luminescence

As stated in the summary, luminescence imaging is little used due to the lack of instruments although it is known that much needed data can be obtained through luminescence sensing. Requirements are for high sensitivity, and/or narrow spectral bandwidth, and ability to change bands in a single instrument. An excellent example of a viable instrument is the Fraunhofer Line Discriminator which is designed for water pollution detection, but which could be used for measurement of chlorophyll in plants.

Measurement of Atmospheric Aerosol Content by Polarization

Remote sensing technology has devoted great effort to refinements in sensing certain space and time variations of areas of interest through the measurement of radiation intensity from those areas in spectral bands defined by sharp-edged spectral filters. Relatively little effort has been expended on measuring the polarization of the radiation. Recent research indicates promise for the use of the measurement of the polarization of radiation for determining soil moisture, atmospheric aerosol content, and cloud particle size. There appear to be other similar application possibilities.

APPLICATIONS IN VARIOUS DISCIPLINE CATEGORIES

Agriculture-Statistical Design for Multi-Stage Sampling of Crop Acreages and Production Predictions

A combination of satellite imagery supported by one or more stages of aircraft and ground monitoring may be the most feasible method to efficiently sample and estimate croplands statistically. It is estimated that one level of satellite imagery and three stages of sampling (two aircraft and one ground) would be needed to acquire the data and estimate the crop acreages in order to generate accurate production predictions. The following is a description of how such a system might be designed.

First Level of Information – ERTS-1 Imagery

Three or more ERTS-1 images would be selected from each major crop area which embraces major crop types. Each 9-1/2-inch color composite bulk image would furnish the gross information for sampling croplands versus non-croplands. A template could be overlaid on the image showing a 185 km area so that it divided the total area into 200 rectangles each representing 9.25 km (5 n.m.) by 18.5 km (10 n.m.).

The image and attached template should be enlarged for viewing using available viewing or projection equipment (Variscan, B&L microscope, etc.). Each rectangle is then systematically viewed and a rating given to the nearest 5 percent for the presence of cropland (row, cereal, orchards, etc.). These ratings are then listed and their values accumulated. From a set of random numbers which range from zero to the accumulated total, five sample rectangles are chosen. (It is probable that rectangles with large percentages of croplands will be chosen over those with low percentages.) These same five rectangles will be defined on each subsequent ERTS-1 image (three additional periods selected for crops) to develop the yearly survey estimate.

First Stage – Medium Altitude CIR (Color Infrared) Photography

Photographic stereo coverage (1:40,000 for crop type discrimination) will be obtained for each rectangle representing 9.25 km by 18.5 km at each time period required to determine the crop type. The same area outlined on the ERTS-1 image will be delineated on the CIR, 1:40,000 transparencies. Allowance must be made for attitude errors in order to align the photographs. Approximately five to seven CIR photos will be needed at this scale for each rectangle. Templates for areas 9.25 km wide will be divided into ten strips 0.925 km wide and the major crop types (such as row crops, cereals, orchards, or the predominant crop type for the area) will be identified by stereo inspection within each strip. The measurement in mm will be summarized quickly for each crop type by strip. Two strips of the ten will be selected based on the probability of the major crop type occurring on all strips. For example, if cereal grains occur over more of strip length than other crop types, cereal grain distance will be used as the representative crop for the rectangle. Here the selection of two strips would be based on the percentage of cereal grain occurrence on each strip. A total of 25 to 35 CIR photos will be required at this stage of photography.

Second Stage – Low Altitude 70 mm CIR (or Normal Color) Photography

Simultaneous 70 mm color transparencies will be taken of the two selected strips in order that continuous stereo coverage will be obtained at the smaller

scale (1:16,000), and sample stereo coverage (triplets every 10 seconds) be obtained at the larger scale (1:2,000) to positively identify crop species and identify plant stress areas. The center photo of each triplet will be examined completely and the crop identified in each quarter of the photo according to the crop percentage in that quarter photo. These percentages will be accumulated and summed by each quarter, and two samples will be drawn at random from each line based on the probability of their occurrence. One quarter of the large scale photo covers about 0.8 acre (0.32 hectare). About 80 photos will be taken at the smaller scale and 180 photos at the larger scale per rectangle. Five times that many 70 mm photos will be needed per ERTS image.

Third Stage - Ground Sample

The two samples per line will be surveyed on the ground. The corners of the quarter photo which was selected above will be identified on the ground. The triplets can be protected and carried in the field for identification of the crop and a quick template made of the crop boundaries. Conventional yield sampling measurements can also be made at this time (survival, stress, forage, cereal and grain yields, etc.).

Statistical Analysis of Data

The formulas developed by Langley and Norick for multistage sampling with probability proportional to prediction will be applied to the ground data and to each successive stage developed for the area covered by the ERTS image.

Subsequent ERTS Coverage

On subsequent dates, when ERTS images become available for the selected areas, the identical rectangles and flight strips can be used at each stage. Thus, the photography can be planned so that the aircraft and field data will very nearly coincide with ERTS imagery.

Other Considerations

Multispectral data collected by aircraft and by digital and analog processing techniques, such as those developed at LARS and the Willow Run Laboratories, can be interposed instead of the aerial photography, wherever it would appear advantageous. However, the first level of information achieved by visual inspection of the rectangles which were established from the ERTS images can probably be analyzed more rapidly and just as effectively as the multispectral processing of those ERTS images.

Crop species identification by an aircraft Model Shape Survey might be possible at the second sampling stage, after the crop type strips are selected from the medium scale CIR photos. Computer printouts, should be useful in the field, if the front stage CIR transparencies are used in conjunction with them for location of ground samples.

Monitoring Environmental Quality Parameters

General

The ability to detect and measure environmental parameters depends to some extent on the availability of sensors and platforms, but to a greater extent on a better understanding of the environment itself (through modeling efforts) and upon improved methods of data processing. An excellent reference on the subject is the report sponsored by the National Aeronautics and Space Administration: Remote Measurement of Pollution (NASA SP-285).

Using airborne sensors, the environment can be monitored in terms of both gross and highly quantitative measurements. The following two examples will illustrate the kinds of parameters which should be determined:

- a. Urban and suburban growth, decay, and associated environmental modification can be monitored by repetitive viewing of urbanized areas to delineate areas of new construction (high albedo) and areas of vegetation stress and decline (change in color response).
- b. Water quality (the concentrations of specific substances in water) is a prime indicator of environmental conditions. Precise determinations of the types of substances, their concentration, their source, movement and rate are required.

Measurements of additional environmental parameters are also needed, such as the identification of constituents and their concentrations in the stratosphere, a task which might be accomplished by limb spectroscopy from a satellite.

Another reasonable requirement would be the capability to measure salinity (total dissolved solids) with a 2 percent accuracy in the range from 1,000 to 35,000 mg/l. This would cover the range required to assess salinity of water from the heads of estuaries to the open ocean as well as brackish inland water bodies. Preservation of water quality in the global oceans depends on the capability to monitor the ocean chlorophyll concentration at very low levels

(0.02 mg/cu. m or greater). Such a capability would allow observation of any environmental features which affect photosynthesis on a global scale. This need is discussed in detail in the paragraphs that follow.

Development Needs for Monitoring of Chlorophyll

Ocean color outside the immediate coastal region is primarily determined by the presence or absence of chlorophyll. Three basic roles may be delegated to the application of color sensing to global ocean analysis. First ocean circulation could be determined during the next four years by qualitative water mass identification using a relatively simple 4 or 5-channel system. Second, biological environmental assessment of the more productive waters (greater than 0.2 mg/m³) of the world could be accomplished during the eight-year time period. Measurement of chlorophyll concentration to within a factor of two is needed. Additional channels are needed for the 4 or 5-channel system area to handle atmospheric and ocean surface "noise".

Lastly, environmental technology needs to address the impact of natural and cultural stress on the basic life cycle of the earth. A system for global ecosystem which addresses the problem of measurement of basic ocean productivity from the most sterile water to the most fertile. A system which quantitatively measures chlorophyll concentration in productive waters must be extended in capability to measure not only chlorophyll concentration but productivity from approximately 0.02 mg/m³ of chlorophyll or greater. It is presently estimated that 5×10^{13} to 400×10^{13} kg per year of carbon are fixed by ocean photosynthesis. Carbon fixation in terrestrial plants is about 5×10^{13} kg each year. As a result, the oceans may be considered as completely dominating the fundamental CO₂ and O₂ cycles on a global scale.

Since an effective means of monitoring global stress will require the ocean productivity measurement also, the global monitoring effort is estimated at requiring eight to ten years for development.

Wildlife Research

During the next four years it should be possible to develop a technology which would combine on the same spacecraft the capability to monitor the habitat of wild animals, including marine animals, and to locate a particular marked animal with an accuracy of 1 km. (This would be supported by aircraft sensors.) During the next eight years, the technology should have advanced to include the implantation of physiological sensors monitored by the spacecraft (or supporting aircraft). This will permit combining physiological response

with habitat conditions. The goal is to understand the behavior of animals under normal and abnormal environmental conditions, so that controls can protect and conserve both the animal and the habitat.

In addition to providing information on wildlife habitat conditions as a function of location, such monitoring would act as a sentinel of disease, especially those diseases that are contagious to domestic animals or man, and provide new knowledge on the physiological and behavioral response to stimuli in a completely unconfined and unrestrained situation.

Marine and Ocean Applications

The needs of the ocean community for synoptic environmental data are naturally divided into two broad categories: one of which requires contiguous samples from areas on the order of 1 to 1000 km², and a second from 10 to 10,000 m². The former relates to the general global oceans and the latter to the coastal environment.

For purposes of aerospace observations, the coastal environment is defined to include all major inland bodies of water; bays, estuaries and deltas; and those regions of the ocean under the influence of tidal phenomena. The global ocean encompasses the vast open ocean as well as the large scale features in the coastal realm.

The EIFOVs for the optical and infrared observation of the ocean are on the order of 1 to 10 km in the global ocean and 3 to 300 meters in the coastal environment. The categories for aerospace application broadly fall into four general areas: currents, sea ice, biological processes and coastal geological processes. A national priority exists to emphasize techniques which will permit the observation, monitoring and forecasting of environmental phenomena in the coastal area. This national priority should serve to guide the development of aerospace technology over the next four-year period.

Currents

The observation of currents in the coastal environment include mapping, measurement and transport studies. The most demanding sensor requirement arises in doing surface current measurement. Such measurement requires 3 to 10 meter EIFOVs observation over areas on the order of 40 x 40 km, every 15 to 30 minutes during peak ebb and flood tide on a seasonal basis. Such observations require the use of dyes in the water that must then be mapped in such a manner as to permit current velocity determination to ± 2.5 cm/sec.

Currents on a global scale can be mapped with relatively low EIFOVs. Spatial dimensions of 10km in extent would be meaningful for ocean applications. However, higher EIFOVs may be desired to permit sampling between cumulus clouds. In general, the use of ocean color to monitor currents, and biological and ecological features requires high sun elevation angles and a scan which looks away from the sunside of the spacecraft. A sensor system capable of observing the oceans at a 10 to 20 degree angle away from nadir enhances the contrast of ocean features at space altitudes.

Sea-Ice Surveillance

Space techniques have demonstrated an immediate sensor application for observation of the polar environment. EIFOVs as large as 10 km may be used to delineate major boundaries and ice movements. However, the most pressing problem is to define, monitor and forecast the amount and location of open water in polar regions, in particular, the Arctic. EIFOVs on the order of 30-100 meters are needed, with a preference for infrared over optical observations because of the nonavailability of solar illumination during the long winter months.

Biological Processes

Assessment of features of biological significance in the more productive waters of the global oceans (approximately 10 percent of the total global area) require EIFOVs on the order of 1 km and remotely acquired signatures of such a quality as to permit the determination of chlorophyll to within a factor of two for concentrations of 0.2 mg/m^3 or greater. Observations of chlorophyll in the open oceans for concentrations as low as 0.02 mg/m^3 are important for global ecosystem analysis. Pollution detection and environmental impact are particularly important in monitoring the natural and cultural stress induced in the coastal region.

Coastal Zone-Geological Processes

The monitoring of the physical as well as the biological environment in the coastal-zone regions is of great importance in preserving the quality of life in this region. Specifically, the mapping of shorelines and shoals, wetlands, bathymetry and bottom topography and mean high/low water lines can be accomplished by aerospace observations. The sensor requirements for these observations are quite similar and compatible with terrestrial requirements, with the exception of a need to add spectral coverage into the blue region of the visible spectrum.

Meteorology

Expanded Observations

Scanner/imager sensors have been providing meteorological observations for more than a decade. The scanner/imager sensors already specified for TIROS N and SMS/GOES (the AVHRR and the VISSR, respectively) will satisfy the bulk of the needs of meteorology for this type of sensor with one important exception. That exception is the "area scanner" recommended in the following paragraphs. Because of the guideline limits placed on this Working Group—sensors in the 0.4 - 16.0 micron spectral range—the "area scanner" is the only specific meteorological recommendation.

However, the panel recognizes strong meteorological needs for other types of sensors. Examples include sounders from geostationary attitude, microwave scanners and sounders to observe through clouds, clouds physics radiometers, etc. Such sensor needs have already been expressed in the Earth Observatory Satellite (EOS) Mission which sanctioned the recommendations of other reports, documents and AAFE experiments. In connection with meteorological sensing, a specific area of civil need is discussed in the next few paragraphs. While the technology exists currently, this needed application has not been pursued, and the panel made special note of the requirement for immediate programs in this area.

Prediction and Assessment of Natural Disasters

Disasters resulting from hurricanes, tornadoes, flash floods, etc., could be predicted more accurately and damage assessed more quickly by employing remote-sensing technology. A new insight into the behavior of severe weather has been gained from the analysis of ATS satellite time-lapse photography, radar, and motion picture photography of tornado cloud tops taken from aircraft about 15 km. A telltale "cloud turret" rises from the cirrus cloud shield, punctures the tropopause, and collapses and falls back into the smooth top of the cirrus shield. Then, another turret pops up. This tornado associated phenomena is shortlived, lasting 8 to 20 minutes.

These new scientific findings point the way to use existing technology for the observation of severe weather. An area scanner capability to view the whole earth every 20 minutes needs to be added to a geostationary satellite. This area scanner would be pointed toward an active weather area (approximately 800 x 1000 km) and view that specific area every 2 or 3 minutes. Targets of 200 to 400 meters should be distinguishable. Such data would allow the

meteorologists to observe the turret cloud phenomena and refine his severe weather warnings both in time and space.

However, pin-pointing the occurrence of severe weather more accurately still cannot prevent the disaster. Once it has occurred, other remote-sensing technology can be used for damage assessment. Side-looking aircraft radar (SLAR) is an example. The geostationary "area scanner," which is recommended previously for predicting the severe weather, might also be used for this purpose. With another set of optics, smaller areas (consequently having higher resolution) might be viewed for damage assessment itself after the clouds have cleared. In an area measuring approximately 80 x 100 km, those features approximating 80 to 100 meters in size could be imaged as a first gross assessment of the destruction.

Damage assessment data can be used for many purposes: emergency routing of traffic – especially rescue vehicles, evacuation steps, for estimates of emergency housing needs, location of emergency feeding stations, and even in verifying damage claims by IRS. (In the recorded case of Lubbock, Texas, the evidence of the energy path of the tornado, combined with the evidence of the storm force as indicated by the dispersal of debris, permitted the National Bureau of Standards to calculate new standards for similar housing in the tornado-prone areas.)

The application of sensor technology to the disaster problem is a matter of timeliness or speed in acquiring the observational data in usable form. Imagery from the spacecraft through an "area scanner" is required in realtime, i.e., instantaneously. The SLAR data also should be telemetered in realtime from the aircraft to mobile receiver/processor stations.

Geography – Cartography

Mapping

There are two separate approaches to cartography as related to imaging sensors on earth resource satellites. The first is the traditional view of map preparation – base maps, topographic maps, aeronautical and navigational charts, orthophotomaps, and others. The requirements are well defined and need not be repeated here. Generally high resolution and geometric accuracy are necessary. For scales of 1:250,000 to about 1:50,000, a film return camera system has been specified in previous studies and that concept can be endorsed. Desired frequency of observation is between five to ten years with selective coverage of most of the land areas of the earth.

The present capability of electronic imaging systems is suitable for orthophoto-image map preparation at scales of 1:500,000 and 1:1,000,000. Approximately two-times improvements will permit scales of 1:250,000 from selected images. The geometric quality of some frame-format image systems is presently adequate. Cartographic reference is provided by ground control points but could be accomplished with orbit and attitude telemetry of accuracy commensurate with map scale.

Earth Resources Location

The second cartographic approach is the implicit requirement for reliability in the location of earth resources data. The individual user cannot manage large amounts of data which lack cartographic reference to the earth. There are three general concepts of mutual consideration between sensor designers, data processors, and data users: First, the resolution and geometric quality limits the scale at which data can be processed with cartographic reliability. Enlargement to a larger scale may be desirable for selective users but the inherent accuracy will not be improved.

Second, the Universal Transverse Mercator (UTM) and polar stereographic projections are in use for satellite-acquired earth resource data. This should be continued for scales between 1:100,000 and 1:1,000,000 to provide a common base. Third, a satisfactory error distribution will result in 90 percent of well-defined points falling within 1 mm of their correct coordinate position on the image at the defined scale. This is twice National Map Accuracy Standards and is satisfactory for thematic resource data.

These concepts are summarized on Table 1-2 with suggested numerical values. This table presents the tolerance limits for positional reference of the thematic data. Sensor and data processing equipment must be calibrated to deliver image data of the suggested accuracy.

Cartographic Example

This discussion presents an example of such sensor application to the fields of Cartography/Geography. At the present, several of the states have assembled earth resource data banks which lists a large number of characteristics for land parcels. The parcel size has been set by one state as a 1 km square grid based on UTM coordinates. The original data was interpreted from aerial photographs, census data, and field inspection. Parcel characteristics such as housing density, forest cover, soil type, water area, crop type, transportation facilities, and others have been computer coded and stored. Individual characteristics

Table 1-2

Error Budgets for Satellite Acquired Thematic Data

EIFOV (Meters)	Scale	Ground Values		
		Image Relative Geometry (Meters) (rms)	Image Absolute Geometry (Meters) (rms)	Sensor Calibration Geometry (Meters) (rms)
10-30	1: 50,000	20	25	10
30-50	1: 100,000	40	50	25
50-100	1: 250,000	100	125	50
100-300	1: 500,000	200	250	100
300-1000	1: 1,000,000	400	500	300

Notes:

1. Scale is for design purposes and may be enlarged or reduced for selective users.
2. Relative geometry is the internal accuracy of a single image.
3. Absolute geometry is the accuracy of fitting the image to a defined map projection (UTM) or Polar Stereographic). The above rms values will generally result in 90% of the well-defined points falling within one millimeter of their correct position on the map base (double the error specified in the National Map Accuracy Standards).
4. Calibration geometry is a suggested guideline for determining the systematic characteristics of a sensor.

can, therefore, be queried, combined, and analyzed. The results can be economically printed in a map-like output that becomes an extremely flexible and powerful source of information for studying geographic data distribution.

Satellite sensors can contribute large amounts of information to such data banks if the sensor image has cartographic reliability. Similarly, the particular data bank provides a good source of ground truth information. All the information should be computer compatible and register with the different sensors, platforms and sequential times of observation. Change detection is then practical for a large number of users and applications in this example.

USER VIEWPOINTS

The users comprising this applications panel, as a result of their discussions and interaction with the different panel experts in the sensors technology, concluded that their current applications capabilities for sensor data lag behind the sensor technology. This is to say that these representative users acknowledged that their particular communities must for the most part improve their capability (in both numbers and sophistication) to assimilate, process, interpret, and apply the relevant sensor data which is essential to their programs.

It follows therefore that users, for the near term, must develop their own applications capability. This is necessary before they can specify incremental additions to existing systems or the development of entirely new systems based on the applications needs. This does not imply, as a corollary, that research and development in the sensors field can mark time until the users catch up, but rather that additional R&D efforts for the near term must be directed toward enhancing existing systems and improving the present quality of data reduction and processing.

BIBLIOGRAPHY

- Earth Observatory Satellite Mission Review Group (EOSMRG) Final Report*
National Aeronautics and Space Administration, Washington, D. C.,
November 1971.
- Remote Measurement of Pollution*, NASA Report SP-285, NASA Langley
Research Center, August 1971.
- Proceedings of the Princeton University Conference on Aerospace Methods
for Revealing and Evaluating Earth's Resources*, Edited by J. Preston
Layton, The Princeton University Conference, Princeton, N. J.,
June 1970.
- Report of the Interagency Ad Hoc Study Group on the Earth Resources
Survey Program*, National Aeronautics and Space Council, Executive
Office of the President, Washington, D. C., March 10, 1971.
- Langley Working Paper: A Summary of Advanced Studies for Coastal Zone
Oceanographic Requirements for EOS A and B*, Limited Distribution
NASA Report, LWP-1072, National Aeronautics and Space Admin-
istration, September 5, 1972.

CHAPTER 1 - ATTACHMENTS

The following five attachments present in graphical form overview material for the five subgroups that were formed within the User Panel. These subgroups were: (A) Agriculture/Forestry/Geography, (B) Geology, (C) Hydrology, (D) Meteorology, and (E) Marine and Ocean Applications. The tables and figures represent a consolidation of the salient data needs for those applications ranked most important in each of the five groups. These data provided the basic input for the summary charts.

ATTACHMENT A

AGRICULTURE/FORESTRY/GEOGRAPHY REQUIREMENTS

The following Table A-1 provides an overview of the more obvious Agriculture/Forestry/Geography applications – with as much guidance relative to desired EIFOV, acquisition frequency, coverage, scale and probable platform as is possible from a combination of past experience and “best estimates” for the future. It is emphasized that these data do not represent hard parameters but should be regarded only as logical starting points for investigation of the various applications.

Four categories have been designated as top priorities: (1) Land-Use Change, in the conventional application; and three categories involving multistage sampling; (2) Forest Inventory; (3) Crop Acreage and Production Predictions; and (4) Range Inventory. Many of the other categories, listed as needing accomplishment are clearly related to the development of a land-use data base against which change may be determined and which would assist in sampling techniques. Other categories listed have no necessary relevance to the top priority categories but stand alone as desirable, and these are therefore assigned a lesser priority.

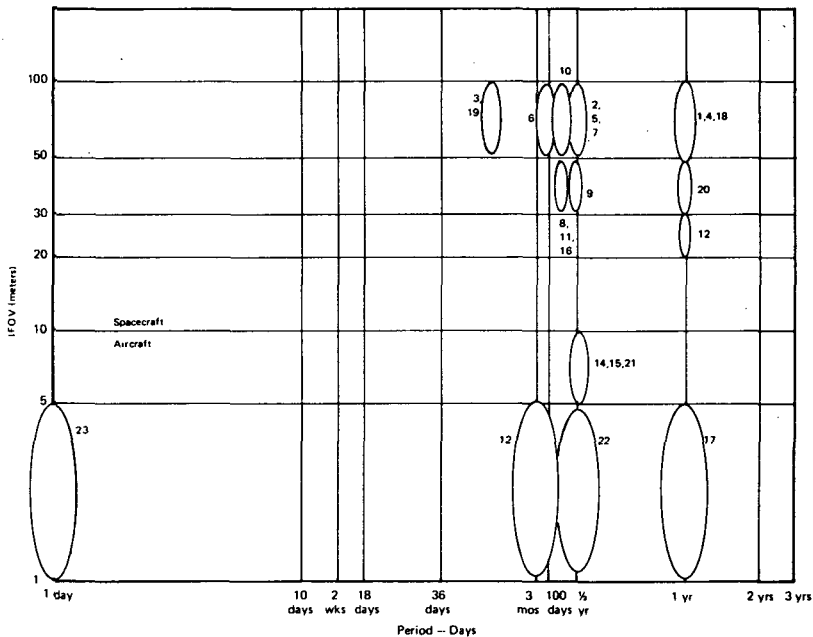


Figure A-1. Land-Use Change Relating to Agriculture/Forestry/Geography
(See Table A-1 for Time of the Year and Number Keys)

Table A-1

Agriculture/Forestry/Geography Requirements

	Specific Application and Parameters to be Measured	Desired Time of Acquisition	E/FOV (Meters)	Sequential Coverage (Yes or No) (1) Indicates Probable Coverage Required	Estimated Working Scale	Frequency for Determination of Application	Probable Platform
Multistage Sampling Photography or Imagery	<u>General Guide Lines:</u>						
	1st level, Information	—	50-100	—	1:1,000,000	—	S/C
	2nd level, (As in Forest Typing)	—	5-10	—	1:50,000	—	A/C
	3rd level, (Individual Species Identif.)	—	< 1-2	—	1:2,000 to 1:4,000	—	A/C
	<u>Forest Inventory</u>						
	1. 1st level, Forest-Nonforest	Winter, Early Spring	50-100	Yes (2)	1:250,000	5 yrs.	S/C
	2. 2nd level, Forest Typing	Spring & Winter	2-5	Yes (2)	1:50,000	5 yrs.	A/C
	3. 3rd level, Tree Counts	Summer	< 1	No (1)	1:2,000 to 1:4,000	5 yrs.	A/C
	Crown diam., Individual Species Identification						
	4. 4th level, Ground						
Continental Data Needs	<u>Crop Acreage and Production Predictions</u>						
	1. 1st level, Crop-Noncrop	Growing Season	50-100	Yes (continuous)	1:250,000	Annual	S/C
	2. 2nd level, Crop Types, Crop, Pasture, Orchard	Growing Season	5-10	Yes (4 flights per yr.)	1:100,000	Annual	A/C
	3. 3rd level, Crop Identification and Stress	Growing Season	< 1	Yes (4 flights)	1:2,000	Annual	A/C
	4. 4th level, Ground						
	<u>Range Inventory</u>						
	1. 1st level, Range-Nonrange		50-100	Yes	1:250,000	5 yrs.	S/C
	2. 2nd level, Range Types		2-5	Yes (twice a yr.)	1:50,000	5 yrs.	A/C
	3. 3rd level, Range Identif. and Trend		< 1	No (once a yr.)	1:600	5 yrs.	A/C
	4. 4th level, Ground						
	1. Timberline	Early Summer	50-100	No (1)	1:500,000	5 yrs.	S/C
	2. Waterline	Various	50-100	Yes (2)	1:500,000	Annual	S/C
	3. Snowline	Winter	50-100	Yes (6)	1:500,000	Biweekly	S/C
	4. Desertline	Various	50-100	No (1)	1:500,000	5 yrs.	S/C
	5. Grassland - Brushland Interface	Spring & Fall	50-100	Yes (2)	1:500,000	5 yrs.	S/C
	6. Bushland - Timberland Interface	Spring	50-100	Yes (3)	1:500,000	5 yrs.	S/C
	7. Grassland - Timberland Interface	Spring & Fall	50-100	Yes (2)	1:500,000	5 yrs.	S/C
	8. Bare Soil vs. Vegetated Areas	Spring & Summer	30-50	Yes (3)	1:100,000	Annual	S/C
	9. Major Roads, Railroads and Waterways	Summer & Winter	30-50	Yes (2)	1:100,000	Annual	S/C
	10. Cropland vs. Non-Cropland	Growing Season	50-100	Yes (4)	1:250,000	Annual	S/C
	11. Plant Stress Detection	Growing Season	2-5/30-50	Yes (4)	1:10,000	Weekly	A/C
	12. Farmsteads	Growing Season	20-30	No (1)	1:100,000	5 yrs.	S/C
	13. Mature Orchard Trees	Growing Season	2-5	Yes (4)	1:50,000	Annual	A/C
	14. Forest Engineering	Winter & Summer	5-10	Yes (2)	1:100,000	Annual	A/C
	15. Areal Extent of Water Surfaces	Summer	5-10	Yes (2)	1:50,000	Annual	A/C
	16. Crop Species Iden. in Fields	Growing Season	2-5/30-50	Yes (4)	1:50,000	Annual	S/C, A/C
	17. Areal Meas. of Fields on Farms	Growing Season	2-5	No (1)	1:50,000	Annual	A/C
	18. Urbanized Areas	Various	50-100	No (1)	1:250,000	Annual	S/C
	19. Land Use Change	Various	30-50	Yes (6)	1:250,000	Annual	S/C
	20. Areal Extent of Single City	Various	30-50	No (1)	1:250,000	Annual	S/C
	21. Functional Morphology	Winter & Summer	5-10	Yes (2)	1:100,000	Annual	A/C
	22. Detailed Urban Struc.	Winter & Summer	1-5	Yes (2)	1:25,000	Annual	A/C
	23. Emergency or Disaster	On Command	1-5	Yes (4)	1:50,000	As Needed	A/C

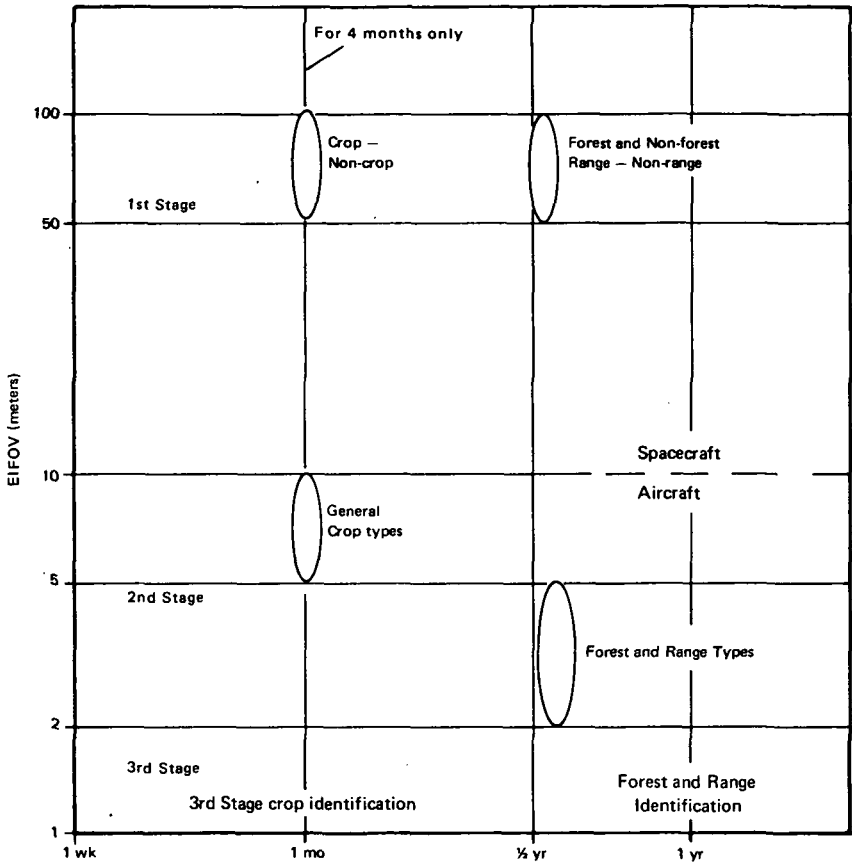


Figure A-2. Multistage Sampling - Agriculture/Forestry

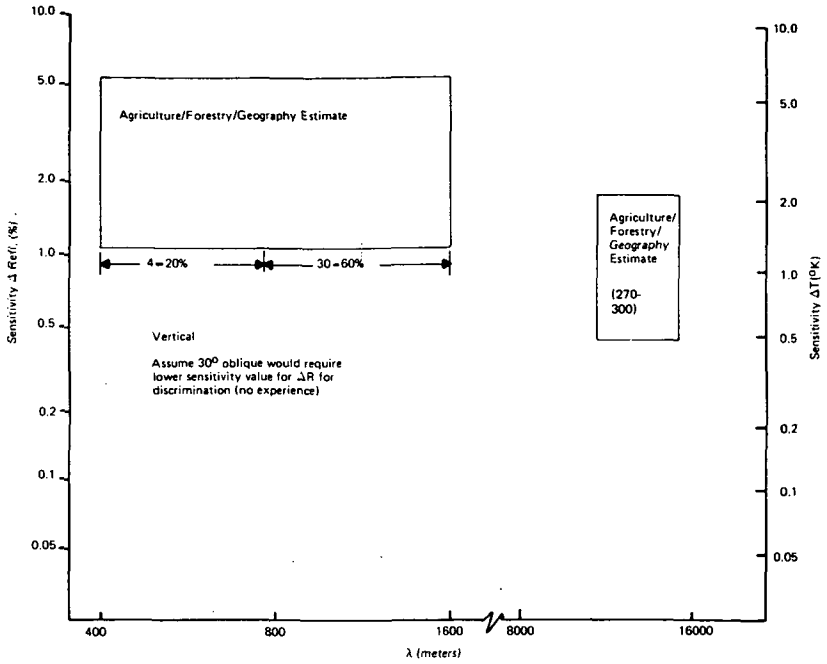


Figure A-4. Sensitivity Requirements for 0 to 30° Solar Zenith
(Similar to 30° - 60° Night)

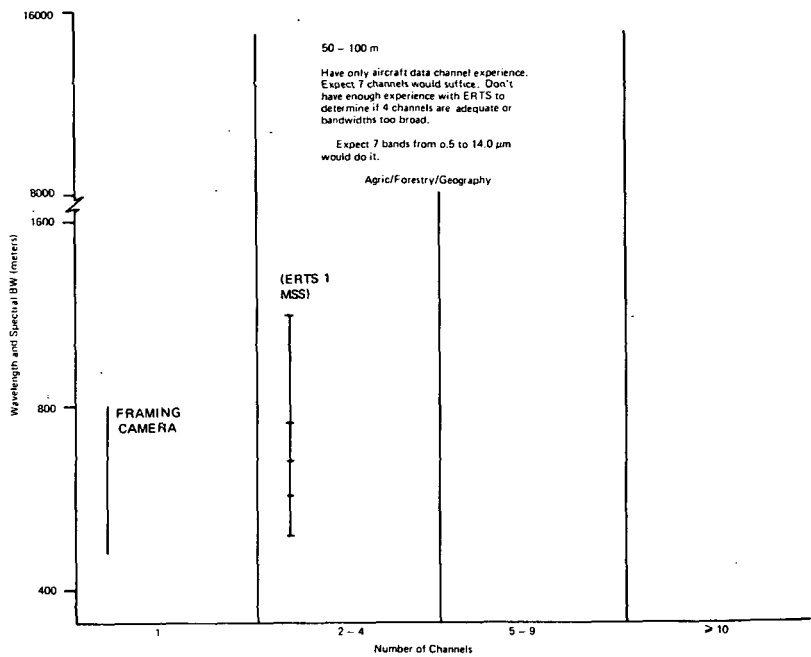


Figure A-5. Spectral Requirements Per Channel for 30 to 100 m Min EIFOV

Table A-2
Agriculture/Forestry/Geography

EIFOV (Meters on Ground)	Field of Coverage (km)	Max Oblique Pointing Angle (Degrees)	Sample or Contiguous (S or C)
50-100	185 km	$\pm 12^\circ$ (one swath to right or left if nadir clouded in)	C or S (on disasters)
30-50	185 km	$\pm 12^\circ$ (two swath widths right or left) same as above	C or S depending on clouds at nadir
5-10	15-30 km	Keep within 185 km vertical image $\pm 6^\circ$	S

ATTACHMENT B

GEOLOGY REQUIREMENTS

Table B-1 lists the important geologic applications and some of the data attributes needed for these applications. The figures that follow are keyed to the number designation in Table B-1.

Table B-1

Specific Applications	Application Designation	ElFOV (meters)	Sequential Coverage*	Estimated Scale	Frequency for determination and Application	Platform	Multispectral
Structural geology Faults, folds, lineaments	1						
	2	50-80	Yes S/A & V	1:250,000-1:1,000,000	Varies with development of science ~5	S/C	Yes
		10-20	Yes S/A & V	1:24,000		A/C	Yes
Geomorphology (landform classification)	3	50-80	Yes S/A	1:250,000-1:1,000,000	As above	S/C	No
	4	10-20	No	1:24,000		A/C	No
Lithologic mapping	5	50-80	Yes V	1:1,000,000-1:250,000	Once	S/C	Yes
	6	10-20	?	1:24,000		A/C	Yes
Geologic Hazards Faults	7						
	8	50-80	Yes S/A V	1:1,000,000-1:250,000	Once/decade	S/C	Yes
		10-20	Yes S/A V	1:24,000		A/C	Yes
Landslides Volcanos	9	10-20	Yes V	1:24,000	Once/year		Yes
	10	100-200	Yes ΔT *	1:1,000,000		S/C	No
†** (Possibly also SO ₂)							
Shoreline changes	11	30-50	Yes, varies with location	1:250,000	Varies	S/C	Yes
	12	5-10	PC	1:24,000	Varies	A/C	Yes
Geochemical (plant stress)	13	50-80	Yes V	1:250,000	Once	S/C	Yes
	14	10-20	Yes, V†	1:24,000	Once	A/C	Yes
†† (Possibly also luminescence)							
Gross physical Properties	15	1000-2000	Yes S/A	1:1,000,000	Once	S/C	Yes
	to						
	17	50-80	Yes S/A	1:250,000	Once	S/C	Yes
		10-20	No	1:24,000	Once	A/C	Yes

*Reason for sequential coverage

A/C, Aircraft

S/A, changing sun angle

PC, physical change

ΔT , change in temperature

V, vegetation change

S/C, Spacecraft

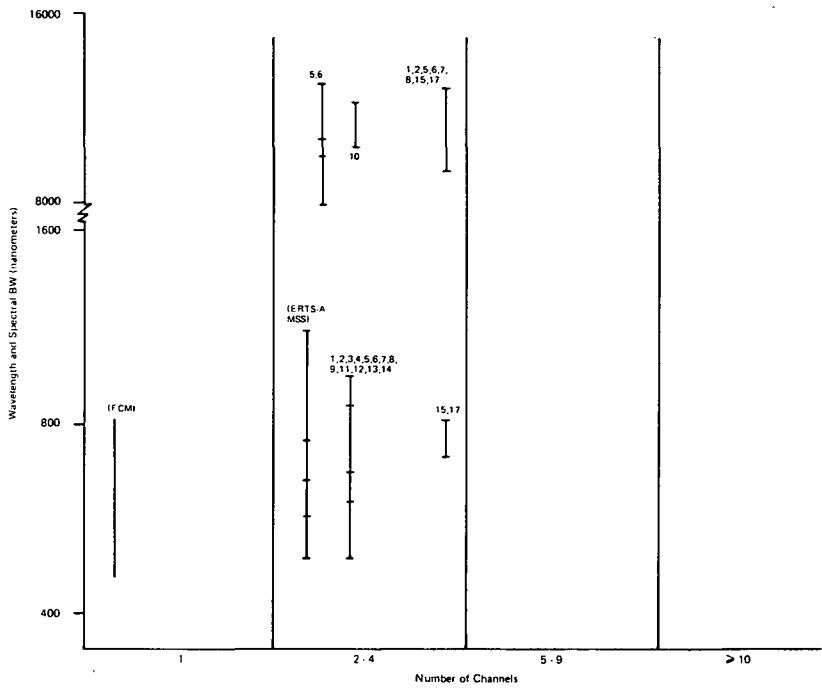
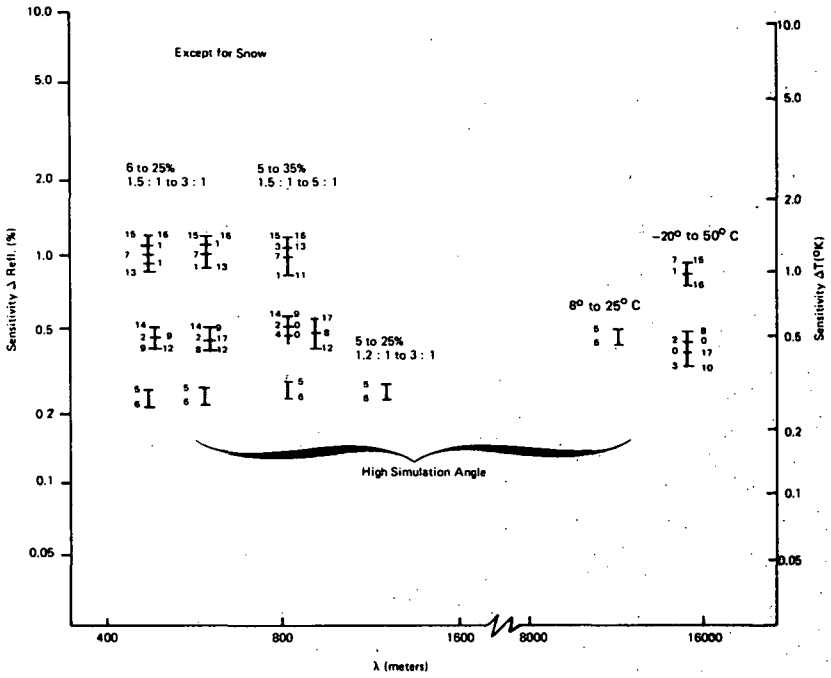


Figure B-1. Spectral Requirements Per Channel for 30-100 m Min EIFOV



**Figure B-2. Sensitivity Requirements for 0°-30° Solar Zenith
(Similar to 30 to 60° Night)**

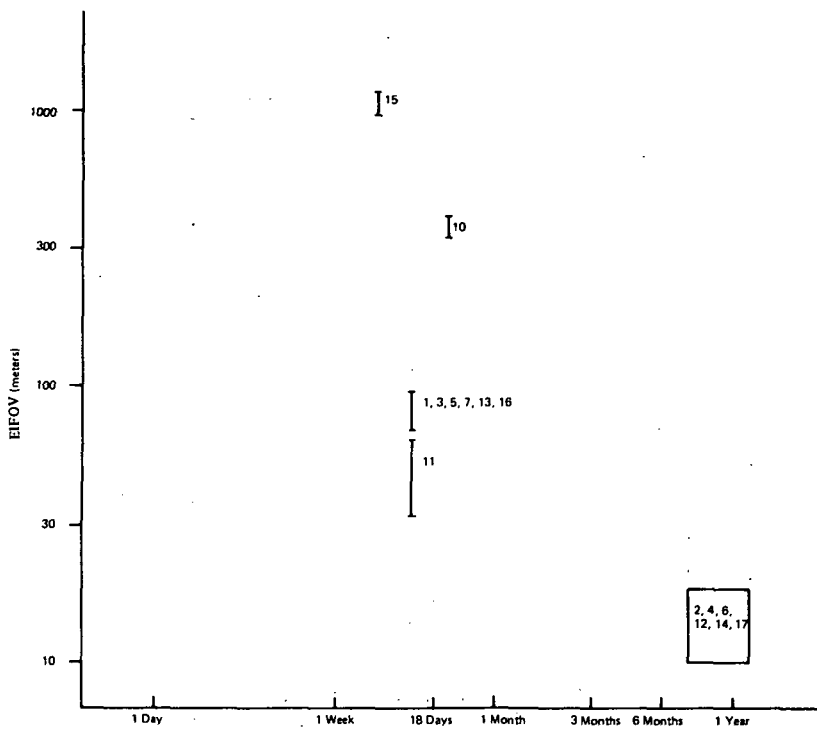


Figure B-3. Repeat Coverage Needs (Spacecraft Only)

Table B-2

Geology Sensor Geometrical Needs

EIFOV (Meters on Ground)	Field of Coverage (km)	Max Oblique Pointing Angle (Degrees)	Sample or Contiguous (S or C)
<u>300-400</u> (10)	400	20°	C
<u>50-100</u> (1,3,7,13,16)	185	10°	C
<u>1000</u> (15)	1300	45°	C
<u>10-20</u> (4,6,8,9, 12,14,17)	13	45°	S
<u>30-50</u> (11)	~185	10°	C

ATTACHMENT C

HYDROLOGIC APPLICATIONS

The following list gives the high priority hydrologic applications, and the figures that follow give the data requirements for these applications. These figures are keyed to the applications as numbered here and in Table C-1.

1. Delineation of land-water boundaries can be accomplished with ERTS (improved) with a spatial location and "resolution" accuracy sufficient for global, continental, large nation and state coverage. Smaller area coverage with height accuracy can be provided from aircraft. Small water bodies (≥ 1 hectare) can be located, the area measured, and the perimeter can either be measured or calculated from the shoreline development ratio. Statistical sampling is satisfactory for large areas, but not for small.
2. Delineation of hydrologically related terrain hectares requires cartographic image positional accuracy and geometry. Spatial "resolution" should be 1/3 to 1/2 that of ERTS. Spectral bands in green, red, solar infrared, and thermal infrared are required. Temporal resolution should occur up to 20 times per year during first two years; annually thereafter. Knowledge of the exact location is required; this includes wetland mapping.
3. Hydrodynamics, including floods, reservoirs, and estuaries. Large water bodies can be surveyed with reasonable accuracy from ERTS. Delineation of flood boundaries requires 10 m positional accuracy and 10 m resolution. Solar infrared is adequate for delineation of most land-water boundaries; spectral combinations in blue-green and red are usable for sediment/water, algae/water, and individual effluent/water boundaries. Additional spectral bands are desirable to delineate boundaries and extent of discrete water masses. Statistical sampling is satisfactory for large areas.
4. Water quality evaluation. Accuracy requirements for delineation of chemical and biological quality of water are not within the state-of-the-art at present and methods for such measurement are, at best, in their infancy. Sediment distribution can be mapped in whole bands.
5. Snow cover and runoff evaluation. ERTS "resolution" is satisfactory for these analyses. Higher temporal resolution (daily) is needed during melt and runoff periods. Spectral resolution in any visible band is adequate for snow, but solar infrared band is needed for snow/runoff delineation. The exact location is required in this evaluation.

Table C-1

Hydrology Requirements

Applications	EIFOV Coverage	Sequential Coverage	Estimated Scale	Frequency Determination	Platform
1. Delineation of land-water boundaries	40-60	Yes	1:100,000	weekly,	S/C
	1-10	Yes	1:10,000-1:100,000	as required	A/C
2. Delineation of hydrologically related terrain features	30-50	Yes	1:100,000	bi-weekly	S/C
	1-10	Yes	1:10,000-1:100,000	as required	A/C
3. Hydrodynamics, including floods, and estuaries	10-30	Yes	1:100,000	weekly, on command for cloud coverage	S/C
	1-10	Yes	1:10,000-1:100,000	as required	A/C
4. Water quality-evaluation	30-70	Yes	1:100,000	weekly	S/C
	1/3	Yes	1:10,000-1:100,000	as required	A/C
5. Snow cover and runoff	50-80	Yes	1:250,000	daily	S/C
	10-50	Yes	1:100,000	Daily in season	A/C

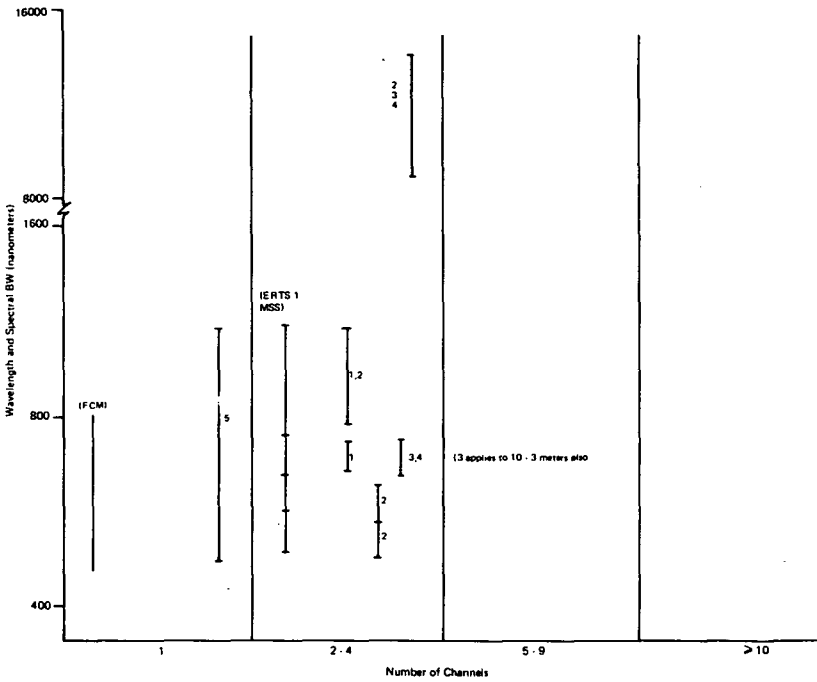


Figure C-1. Hydrology Spectral Requirements Per Channel for 30 to 100 m Min EIFOV

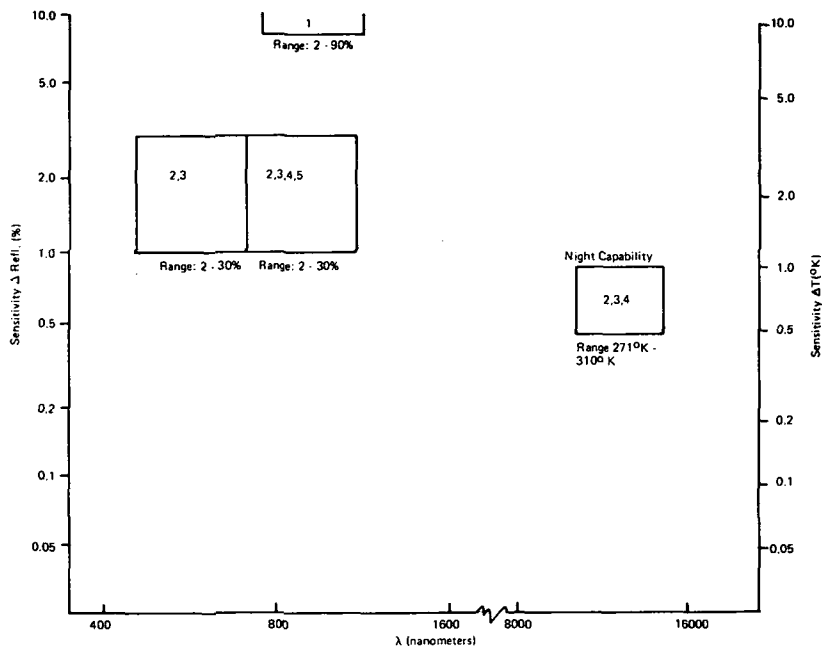


Figure C-2. Hydrology Sensitivity Requirements for 0 to 30° Solar Zenith (Similar to 30 to 60° Night)

Table C-2

Hydrology Sensor Geometrical Needs

EIFOV (Meters on Ground)	Field of Coverage (km)	Max Oblique Pointing Angle (Degrees)	Sample or Contiguous (S or C)
1. 40-60	200	Nadir	Area
2. 30-50	200	Nadir	Area
3. 10-30	50	15°	Sample
4. 30-70	200	Nadir	Area
5. 50-80	200	Nadir	Area

ATTACHMENT D

METEOROLOGY REQUIREMENTS

The meteorologic application considered most important by the panel (within the limits set for the panel's deliberations) was the prediction and assessment of severe weather conditions and the damage that results from these conditions. The following data needs address this application.

Table D-1

Meteorology Sensor Geometrical Needs

EIFOV (Meters on Ground)	Field of Coverage (km)	Max Oblique Pointing Angle (Degrees)	Sample or Contiguous Coverage
200-400 m	1000 km x 800 km (800,000 sq km)	8°	scan 1000 x 800 km one each 2 to 3 minutes from Geosynchronous altitude

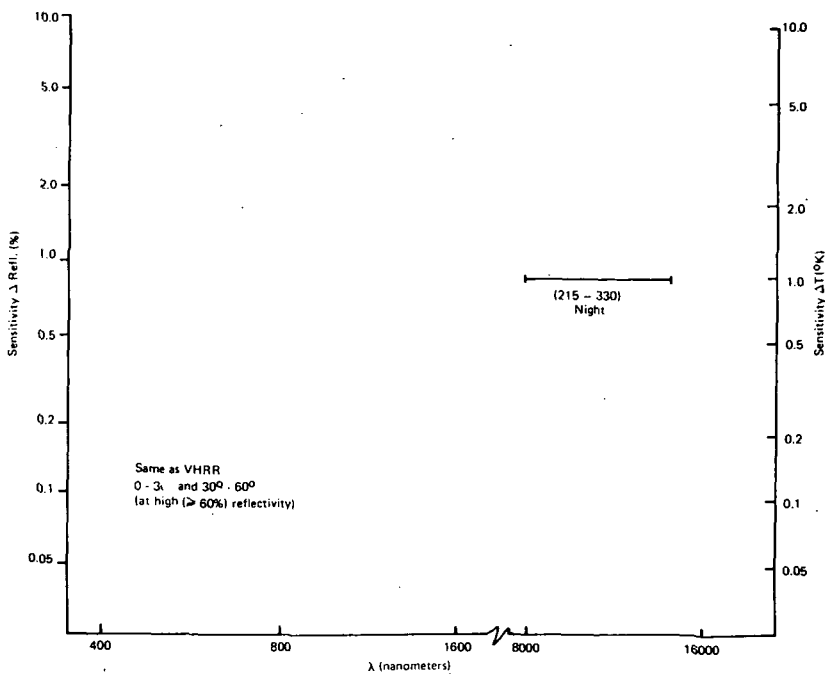


Figure D-1. Sensitivity Requirements for 0 to 30° Solar Zenith
(Similar to 30 to 60° Night)

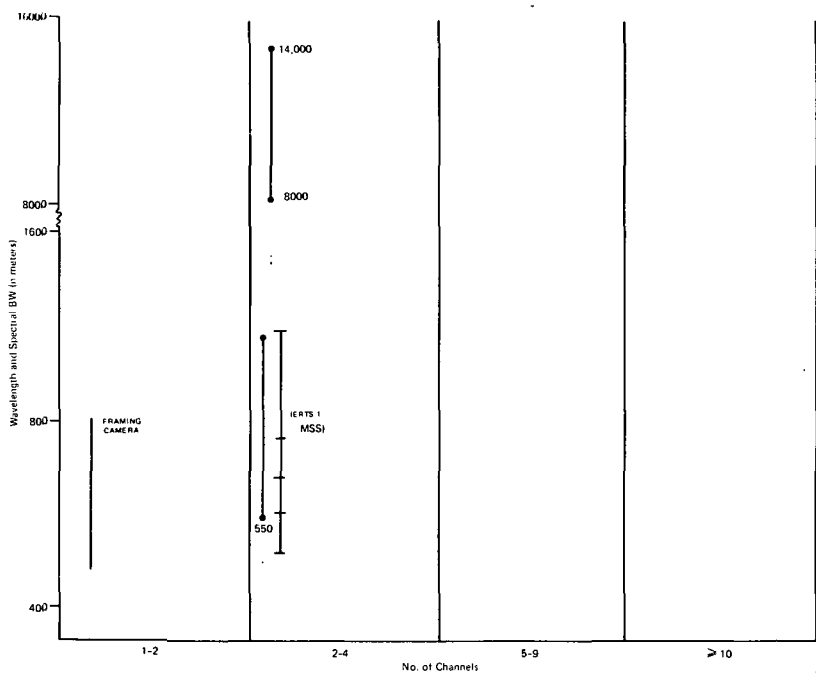


Figure D-2. Spectral Requirements Per Channel for 30 - 100 m Min EIFOV

ATTACHMENT E

MARINE AND OCEAN APPLICATIONS

Table E-1 presents the important applications in marine and ocean science. The figures that follow are keyed to the number/letter designation indicated for each application in Table E-1

Table E-1

Sensor Geometrical Needs for Marine and Ocean Applications

Marine and Ocean Applications*	EIFOV (Meters on Ground Unless Otherwise Specified)	Field of Coverage (km) (Minimum Swathwidth)	Max Oblique Pointing Angle (Degrees)	Sample or Contiguous Coverage (S or C)
(1) Currents				
(a) Coastal Current Mapping	0-100	200 km	30°	C
(b) Coastal Current Measurement	3-10	40 km	nadir	C
(c) Turbidity and Transport	50-100	200 km	30°	C
(d) Global Mapping	1-10 km	400 km	20° **	C
(2) Sea Ice Surveillance	30-100	200 km	30°	C
(3) Biological Processes				
(a) Assessment	1-2 km	400 km	20° **	C
(b) Coastal Pollution Detection	30-50	200 km	45°	C
(c) Pollution Environmental Impact	30-300	200 km	45°	C
(d) Global Ecosystem Analysis	1-10 km	400 km	20° **	C
(4) Coastal Geological Processes				
(a) Shoreline Mapping & Shoals	30-50	200 km	nadir	C
(b) Wetlands Inventory	30-50	200 km	nadir	C
(c) Bathymetry & Bottom Topography	50-100	200 km	nadir	C
(d) Mean High/Low Water	3-10	40 km	nadir	C

*Identifying number and alphabetical designations are referred to by Figures E-1 and E-2.

**10-20 degree angle away from nadir is desired to look away from the sun side of the spacecraft.

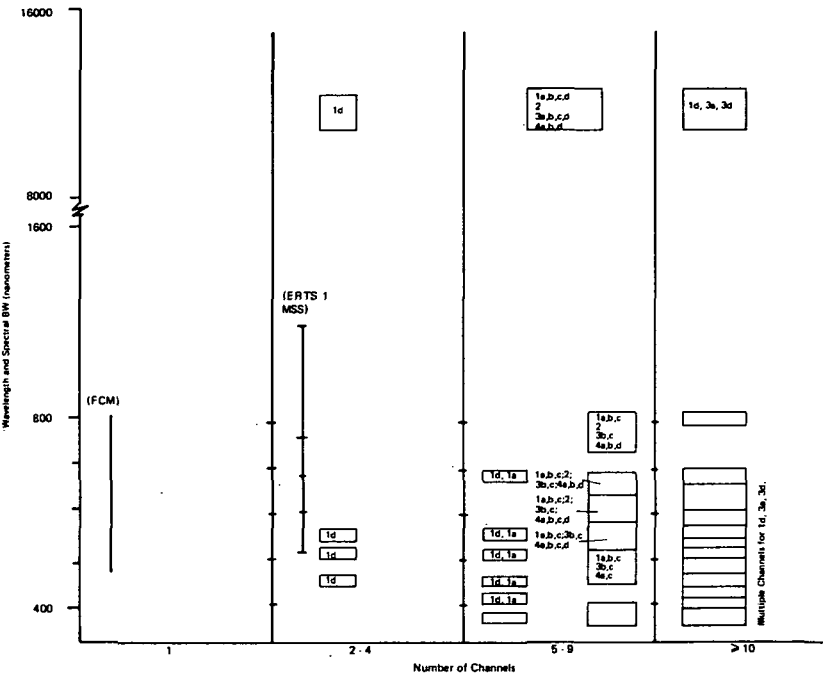
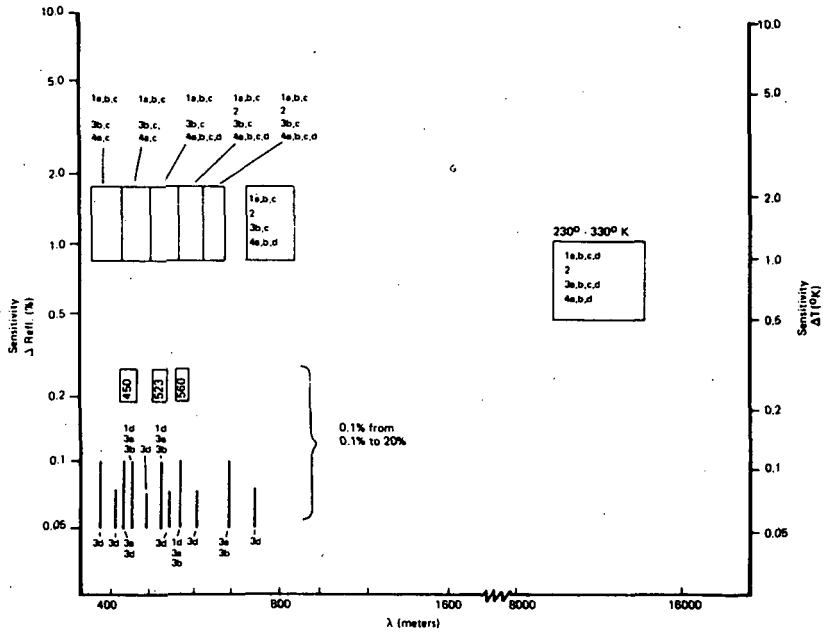


Figure E-1. Spectral Requirements Per Channel for 30 to 100 m Min EIFOV



CHAPTER 2
ELECTROMECHANICAL SCANNERS

PANEL MEMBERS

D. Lowe — *Chairman*
R. Predmore — *Associate Chairman*

R. Biard
F. Gabron
R. Hummer
R. MacDonald
L. Mundie
T. Paluden
R. Sendall
W. Wolfe

ELECTROMECHANICAL SCANNERS

PANEL SUMMATION AND RECOMMENDATIONS

The electromechanical scanners panel analyzed the state-of-the-art for those electromechanical devices and techniques having potential as advanced imagers for earth observation. Problems considered were the interrelation between scanner parameters, the need for higher resolution and its impact on basic scanner design, the acquisition of increased angular resolution by the employment of detector arrays with large numbers of elements, the tradeoffs between optimal design and operating parameters applied to existing sensors, and between detector and cooling system parameters. Consideration of current optical scanning and of Hadamard scanning techniques, in particular, concluded the study.

The panel found that electromechanical scanners are capable of producing geometrically registered, multispectral images in spectral channels extending from the visible to the thermal infrared. In addition, accurate radiometric measurements can be made. As implied, image formation is accomplished by mechanical scanning. Typically, mechanical motion causes the scene to be sampled in the across-track direction by a detector or array of detectors while satellite motion provides the orthogonal scan component. Many electromechanical scanners have already flown, a typical example being the multispectral scanner (MSS) on ERTS-1.

The panel made a clear differentiation between needs of current technology and projected technology; however, it recommended present and future use of a large number of elements in detector arrays, and that design studies include simultaneous development of the cryogenic cooling system for a well-balanced system.

A summary of the panel recommendations is as follows:

- Scanners in the reflective bands can achieve increases by a factor of 2-3 in spatial and spectral resolution and in signal-to-noise over that currently achieved, using existing technology. However, such improvement will require a larger number of detectors and/or an increase in the size of the collecting optics.

- Scanners in the thermal-IR band require cooled detectors. Cryogenic development is one of the limiting factors in resolution and signal-to-noise improvement for such detectors.
- Scanners may be used for photogrammetric applications if a greater spacecraft stability and/or compensating processing capability can be achieved. This is the limiting factor for this application.
- For visible and near-IR wavelengths, solid state self-scanning arrays may be incorporated into mechanical scanners, improving the performance.

Investigation of electromechanical scanner problems was limited by the panel to:

- System design
- Photodetectors
- Cryogenic systems for earth orbiting sensors
- Optical systems
- Hadamard systems.

ELECTROMECHANICAL SYSTEMS DESIGN

As indicated, the primary key to the acquisition of increased angular resolution of electromechanical earth-mapping scanners is the employment of detector arrays with large numbers of elements. If this quantity is increased to 100-200, the resolution of scanners [similar to MSS (ERTS-A) and VISSR] can be doubled in the 0.5 to 1.2 μm spectral region with only a modest increase (doubling or less) in aperture diameter. A tenfold increase in resolution would require, for example, 1000-2000 elements and aperture diameters of 1 to 2 meters.

Present optical technology enables acquisition of this two- or tenfold increase in resolution near the optical axis. However, since aberrations increase rapidly with increasing off-axis angle, the employment of object-plane scanning is indicated.

In addition to keeping down the required aperture size, employment of detector arrays with large numbers of elements counters the requirement

for unrealistically fast detectors and excessive scan frequency at high resolution. The latter consideration keeps those optical systems employing object-plane scan in design contention.

PHOTODETECTORS

Photomultiplier tubes are currently used in multispectral scanner systems for the short wavelength channels. For high resolution, such devices are used for wavelengths shorter than approximately 800 nm; in lower resolution systems, silicon detectors are preferred at wavelengths longer than 500 nm.

Silicon planar p-n junction photodetectors represent the most advanced semiconductor technology at this time providing good resolution and parameter control in wavelength regions out to 1.1 μm . These units also show good high frequency response, high quantum efficiency, low noise, and require no special cooling for most applications.

Photoconductive detectors are most useful at infrared wavelengths longer than 3 μm . Intrinsic photoconductors are narrowband gap semiconductors that absorb long wavelength photons by the generation of hole-electron pairs. Thus, the infrared absorption is an inherent or intrinsic property of the particular semiconductor. Extrinsic photoconductors are wideband gap devices that absorb long wavelength photons by the excitation of impurity levels added to the material. Both types show photoconductive gain.

CRYOGENIC SYSTEMS

Passive radiators for cooling loads of 10 milliwatts or less to temperatures in the 85-120 K region have been tested to flight acceptance levels. These systems have been designed for use in either near-earth sun-synchronous or geostationary orbits. Although orbital thermal performance is available for only two passive coolers operating in the 105 K region, a relatively large number of systems will be flown in the 1972-1976 time period. Very little is now known about the long-term degradation of passive coolers in the space environment.

Larger radiators will be required to handle the increased power dissipation in detector arrays and the additional heat leaks associated with the focal plane structural supports required to provide more accurate detector

alignment. The last requirement will result from the need for improved spatial resolution in advanced imagers and scanners.

Open-cycle cryogenic cooling systems employing supercritical helium and solid cryogens are currently being tested for space applications. Such systems have limited application for NASA advanced imagers and scanners because of the weight penalties associated with long-term cooling requirements.

Stirling cycle refrigerators for spaceborne use have been developed and are available for missions in which the total operational time is 300-500 hours. They are efficient and lightweight for operation in the 77 K region with heat loads up to one watt.

Vuilleumier cycle refrigerators for spaceborne use are in the advanced development status. Systems presently in development will probably achieve a useful operating life that is an order of magnitude greater than Stirling cycle systems.

For future NASA imagers and scanners, it is anticipated that the detector cooling requirements for airborne and spaceborne systems will generally fall in the 50-120 K region. Cooling capacities will range from a few milliwatts to perhaps one watt.

Limited applications for open-cycle cooling systems are anticipated. This type of cooling system may not be applicable for the one- to two-year missions with focal plane heat loads which are expected to exceed 100 milliwatts. Technology development in this area should not be high-priority.

Closed-cycle spaceborne refrigerators require additional developmental work to demonstrate their potential for missions of one to two years' duration.

The costs of developing spaceborne refrigerators are high; therefore, continued developments should be highly focused on one or two major programs. It is recommended that NASA developmental work on refrigerators be continued with greater emphasis than at present, to develop coolers having a capacity of approximately 1 watt in the 50-80 K region.

Optical Systems

Both narrow-field and wide-field optical systems can be used. It is difficult to evaluate the different systems because so many possibilities exist.

Narrow-field systems usually include simple spheres, parabolas, Cassegrain, Newtonian, Ritchey Chretien and Dall-Kirkham systems. Using the most expensive system, the Ritchey Chretien, a resolution of 0.02 mr for about 1 degree full field (17 mr) can be obtained.

Wide-field systems, 10 degrees or more, are much more difficult to design and build. They have scanning mechanisms that are simpler to implement, however, and are therefore of considerable interest. The two main candidates for such wide angle optical systems are the Schmidt and the Bouwers-Maksutov system. Both provide resolutions on the order of 0.1 mr out to angles of about 15 degrees.

Hadamard System

A newer optical technique that makes use of the multiplex advantages in spectroscopy is called the Hadamard. Where the normal spectrometer uses one exit slit and rotates a prism for multiple imaging, the Hadamard uses a mask that provides multiple exit slits. The system is of great advantage for sampling a scene with a few bright spots. Scanning noise, however, will present a problem.

CHAPTER 2

ELECTROMECHANICAL SCANNERS

INTRODUCTION

The objective of the panel on electromechanical scanners was to review all of NASA's state-of-the-art of scanner systems and sensor technology with the idea of recommending future research and systems development programs. The objective was too ambitious to be accomplished in the time allowed for the work of the panel. Moreover, it was felt that a wide data base was necessary before a definitive review could be made. This chapter contains the results of the work of the panel and, although it is only a first step, it is felt that this material will be a worthwhile contribution to NASA's earth resources program.

This report represents the deliberation of the panel as a group. To make more effective use of our one week study period, written material was prepared for consideration by the panel. The discussion on Sensor Systems was prepared by L. Mundie, R. Sendall, and R. Hummer. The Cryogenic Section was prepared by F. Gabron, the Detectors Section by R. Biard, and the Optics Section by W. Wolfe. As background material on current state-of-the-art technology, T. Paludan, R. MacDonald, and R. Predmore supplied the panel with summary material on NASA imaging sensor development and programs.

Scope

For this investigation, electromechanical scanners were considered to be any imaging device in which individual detectors or detector arrays scan the object or image plane in a manner that permits reconstruction of the scene radiance. Attention was directed to advanced imagers for earth observation, with high resolution, although it is acknowledged that many low resolution imaging systems can be both complex and advanced. Consideration was limited to earth-looking sensors, although much of the technology is similar

to that required for nonearth-looking sensors. As a result, planetary fly-by scanners or earth orbiting, astronomical sensors were not considered.

Approach

The information extracted from scanner data is in the spatial, spectral, and temporal distribution of radiation from a scene. For the most part, sensor advancement means improving the spatial resolution for a given operating distance. More recently, attention has been given to spectral distribution and automatic classification based on the spectral information from the scene. Since the spectra of vegetative features vary with their growth cycle or season, the spectral classification task becomes easier when temporal variations are included. Thus, the advanced imager may be viewed as a high resolution, multispectral scanner with the ability to observe a scene periodically.

Due to time constraints, work on this investigation was limited to a review of the state-of-the-art of electromechanical scanner technology and sensor performance and an examination of the feasibility of increasing spatial resolution by factors of two and ten over existing state-of-the-art mechanical scanning systems. The relative importance of spatial, spectral, and temporal resolution was then examined in collaboration with the user panel.

Three classes of scanners were considered: airborne, low altitude orbiters (forward motion of the vehicle provides one-scan direction), and geo-stationary.

Component technology, as well as systems design, is discussed in this chapter. The following specific topics are discussed: detector state-of-the-art technology for the spectral range of useful atmospheric transmission ($0.32\ \mu\text{m}$ to $13.5\ \mu\text{m}$), cryogenic systems for airborne and earth orbiting sensors as the longer wavelength detectors require cooling, electromechanical imaging systems design, and optical systems and materials. Tradeoff relationships between design and operating parameters are presented in graphical form. These relationships are applied to existing sensors to show the burden (in sensor complexity) of improving resolution.

Although the overall recommendations of the panel for electromechanical scanners are given ahead of this chapter, pertinent recommendations for

component technology and systems design are given with each particular discussion. In addition, Attachment 1, at the end of this chapter, contains a set of tables comparing the specifications for various NASA spaceborne electromechanical imaging systems. These specifications were evaluated by the panel members and are included with this report as a basis for the discussion of advanced imagers.

SCANNER SYSTEM DESIGN

Electromechanical scanners, as defined for this study and evaluation, are imaging devices in which the image of the scene to be mapped is physically scanned by a detector or detector array by means of mechanical motion. The detailed characteristics both of suitable optical systems needed to form the image, and appropriate detector arrays are presented later in this chapter. It is noted that the scanner arrays may be of the self-scanned variety (CCDs or photodiodes with integral shift registers); use of this type of detector array would facilitate achievement of greatly improved sensitivity through increased effective dwell time.

Panel attention was directed toward an analysis of the interrelation between such scanner parameters as angular resolution, coverage rate, scanner size, number and sensitivity of detectors, and the various efficiency factors involved. In order to focus the discussion, emphasis was placed on an examination of the feasibility (assuming desirability) of pushing to ever higher spatial and spectral resolution.

In order to put this system design discussion in proper historical perspective, past trends in the resolution, weight per channel, and packing density of spaceborne scanners are presented first. Then, the impact of an effort to achieve still higher resolution on other system parameters and on basic scanner design, and the limitations on achieving higher resolution as imposed by present-day optical technology, are examined.

As bench-marks in future development, the prospects for increasing scanner resolution by factors of 2 and 10 above that employed by two representative scanners — the MSS (ERTS-1) and VISSR (SMS) — are specifically examined.

Past Trends in Mechanical Scanner Design

Before examining possible future improvements in scanner designs, the characteristics of a number of past and presently planned scanners will be surveyed with a view to observing trends in design and improvements in performance and in efficiency. Any conclusions based solely on temporal trends observed in such a survey must, of course, be treated with great caution, because each scanner design is usually the result of complex and often unique requirements and boundary conditions.

Table 2-1 presents pertinent information concerning 15 representative scanners. Attachment 1 shows additional unclassified imaging systems. In Table 2-1, the spacecraft carrying the scanners are represented by the following acronyms:

ATS Applications Technology Satellite

SMS Synchronous Meteorological Satellite

EOS Earth Observatory Satellite*

SEOS Synchronous EOS*

ITOS Improved TIROS Operational System

ERTS Earth Resources Technology Satellite.

Data extracted from this table is plotted in Figures 2-1 through 2-3. Figures 2-1 and 2-2 present angular resolution as a function of launch date for scanners operating in the 0.5 to 1.1 μm wavelength regions, respectively. Figure 2-3 presents weight per channel and density, again as a function of launch date. In this figure the numbers in parentheses refer to the number of channels employed. The points identified as "Pioneer Imager" in this figure refer to the imaging photopolarimeter carried on Pioneer-10. "Viking" is a 32-channel thermopile radiometer. "A" and "B" refer to scanners employing focal plane arrays built for the U.S. Air Force by the Hughes Aircraft Company. It is noted that all of the scanners indicated in

*These missions are being studied as possible future advanced, earth oriented, remote sensing satellites.

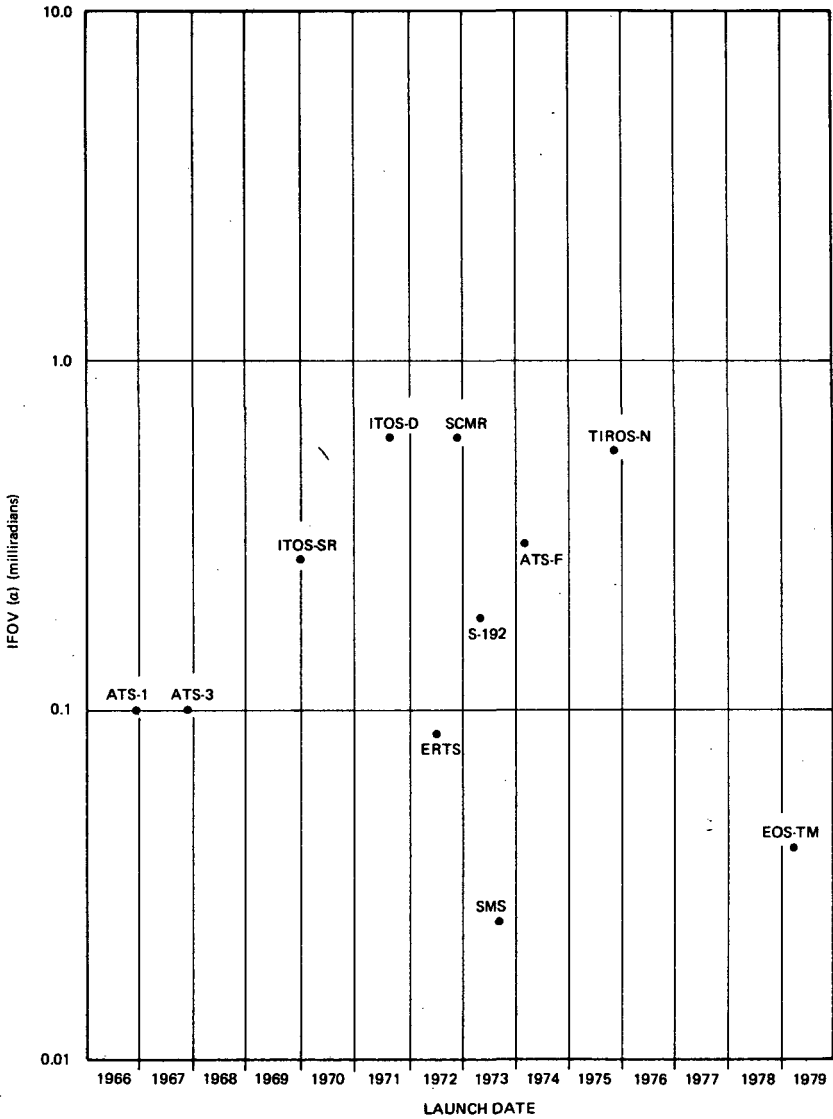


Figure 2-1. Resolution of scanners operating in the visible-to-near IR vs launch date

Table 2-1
Characteristics of Fifteen Electromechanical Scanners

Scanner Spacecraft	First Launch	Altitude KM (n.m.)	Spectral Vis & Near IR (μ m)	IFOV Vis & Near IR (mrad)	Nadir Resolution	Spectral IR (μ m)	IFOV IR (mrad)	Nadir Resolution
High Resolution IR Radiometer (HRIR) NIMBUS	4/69	1,100 (600)	0.7-1.1	7.9	8.7 km (28,600 ft)	3.4-4.2	7.9	8.7 km (28,600 ft)
Scanning Radiometer (SR) ITOS	1/70	1,460 (790)	0.55-0.73	2.7	4.0 km (13,100 ft)	10.5-12.5	5.6	8.2 km (26,900 ft)
Temperature Humidity IR Radiom. (THIR) NIMBUS	4/70	1,100 (600)				6.7 10.5-12.5	21 7	23.2 km 7.7 km (25,200 ft)
Very High Resolution Radiometer (VHRR) ITOS-D	9/72	1,460 (790)	0.55-0.73	0.6	0.88 km (2,880 ft)	10.5-12.5	0.6	0.88 km (2,880 ft)
Multispectral Scanner (MSS) ERTS-1	7/72	920 (496)	0.5-0.6 0.6-0.7 0.7-0.8 0.8-1.1	0.086	0.079 km (259 ft)	(B) 10.4-12.6	0.258	0.237 km (776 ft)
Surface Composition Mapping Radiometer (SCMR) NIMBUS	11/72	1,100 (600)	0.8-1.1	0.6	0.66 km (2,160 ft)	8.3-9.3 10.2-11.2	0.6	0.66 km (2,160 ft)
EREP Multispectral Scanner (S-192) SKYLAB	5/73	435 (235)	(9) 0.41-1.2	0.182	0.08 km (262 ft)	(3) 1.2-2.35 (1) 10.2-12.5	0.182	0.08 km (262 ft)

Advanced Very High Resolution Radiometer (AVHRR) TIROS-N	4/75	1,475 (906)	0.5-0.7 0.75-1.0	0.55	0.81 km (2,680 ft)	(10) 6.5-7.0 10.5-12.5	2.65 0.81 km (2,680 ft) 0.55	3.9 km (12,800 ft) 0.81 km (2,680 ft)
Thematic Mapper (TM) EOS	1/79 ?	1,000 (540)	0.5-0.6 0.6-0.7 0.7-0.8 0.8-1.1	0.040	0.04 km (131 ft)	1.55-1.75 2.08-2.35 10.4-12.6	0.040 0.120	0.04 km (131 ft) 0.12 km (394 ft)
Spin-Scan Cloud Camera (SSC) ATS-I	12/66	35,870 (19,400)	0.47-0.6	0.1	3.6 km (11,800 ft)			
Multicolor Spin-Scan Cloud Camera (MSSC) ATS-III	11/67	35,870 (19,400)	0.38-0.48 0.48-0.58 0.55-0.63	0.1	3.6 km (11,800 ft)			
Visible-IR Spin Scan Radiometer (VISSR) SMS	10/73	35,870 (19,400)	0.55-0.75	0.025	0.9 km (2,950)	10.5-12.6	0.250	9.0 km (29,500 ft)
Very High Resolution Radiometer (VHRR) ATS-F	1/74 ?	35,870 (19,400)	0.55-0.7	0.3	1.1 km (3,600 ft)	10.5-12.5	0.3	1.1 km (3,600 ft)
Very High Resolution Scanner SEOS	1/81 ?	35,870 (19,400)	0.5-0.7 0.8-1.2 0.8-1.2	0.006 0.014	0.2 km (656 ft) 0.5 km (1,640 ft)	3.4-4.1 10.5-12.5 6.3-6.7	0.042 0.140	1.5 km (4,920 ft) 5.0 km (16,400 ft)
Multispectral Scanner (MSS) Airborne		$V_h = 0.02-0.18$	(10) .37-1.1	2.0		(14) 1.2-13.0	2.0	

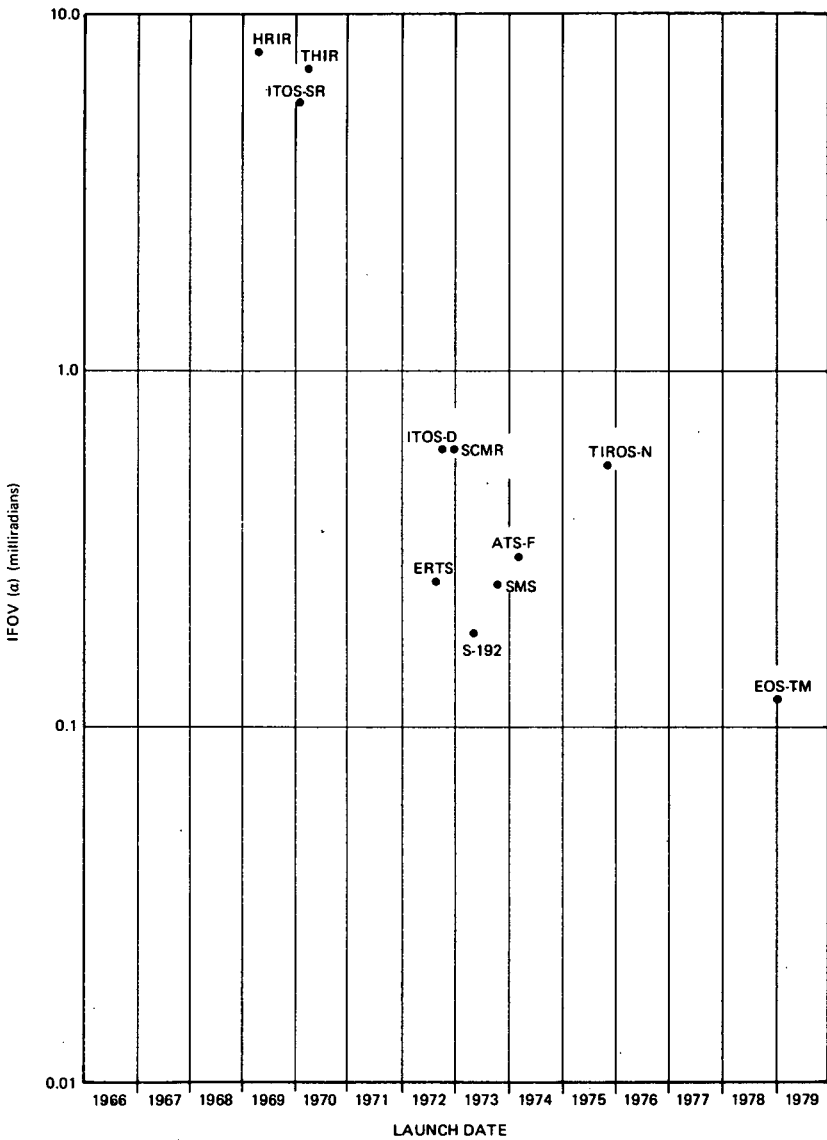


Figure 2-2. Resolution of scanners operating in the thermal window channel vs launch date

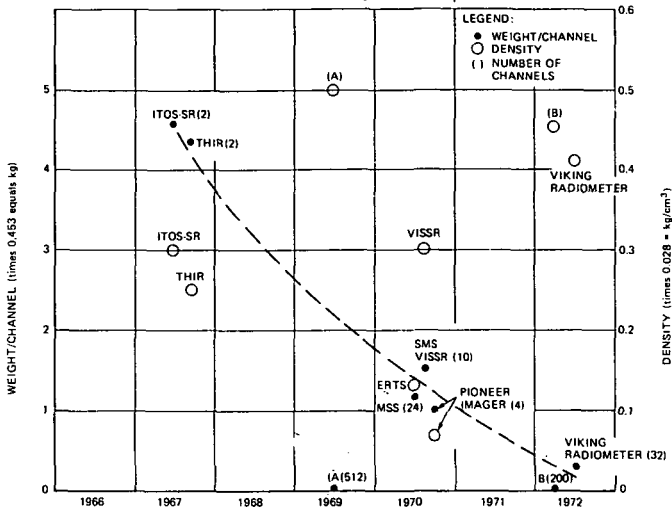


Figure 2-3. Weight and packaging density of spaceborne scanner electronics including module structure vs year of design

Figure 2-3 except A, B, and Viking have discrete components; A and B are all hybrid, while Viking is a partial hybrid.

The scanners operating in the thermal window (10 to 14 μm) are seen in Figure 2-2 to exhibit a fairly consistent (and rapid) improvement in resolution with time. The visible and near-infrared scanners (Figure 2-1) exhibit much greater spread in the data, although again the general trend is toward increased resolution with time. Of great importance is the dramatic decrease in weight per channel with time shown in Figure 2-3 (dashed line), reflecting improvements in detector and electronic technology. The scanners denoted A, B, and Viking are outstanding examples of the improvement associated with modern design. The density plot has more scatter of data points, but reveals a general increase with time.

The remainder of this section is devoted to an examination of the problems associated with achieving still higher resolution in electromechanical scanners.

Performance Theory

Scanners employing three detector types—photomultipliers, photodiodes, and photoconductors—are considered. In each case an expression for the signal-to-noise ratio as a function of scanner parameters is first derived. This expression may be used to deduce the variation of sensitivity with any scanner parameter. To illustrate its use, the increase in aperture size and/or number of detectors, which would be required in order to increase resolution (other parameters being held constant), is calculated. To this end an expression for the resolution in terms of the telescope aperture diameter, D , the number of detectors, n , and a constant combining all other pertinent parameters is derived. This constant is evaluated for representative contemporary scanners (MSS and VISSR) employing detectors of these three types, permitting determination of the impact on D and n of increasing spatial and spectral resolution while maintaining the performance and all other parameters at a constant value.

Scanners Employing Photomultiplier Tubes

When photomultiplier detectors are employed, the internal gain is assumed to be sufficiently high that amplifier noise can be neglected in comparison with photoelectron (shot) noise. In this case the limiting noise can be expressed as the square root of the number of photoelectrons released during an integration period from a resolved elemental area of background while the signal is the difference between the corresponding numbers of photoelectrons associated with target and background. The corresponding photoelectric currents, I_s and I_n , may be written:

$$I_s = (N'_2 - N'_1)F(x, \alpha)\alpha^2 A_o \tau_o \bar{R} \quad (1)$$

and

$$I_n = [2N'_2 \alpha^2 A_o \tau_o \bar{R} k_o \epsilon \Delta f_n]^{1/2} \quad (2)$$

where

N'_1 and N'_2 = apparent radiance in the optical passband employed of the bars in a test pattern as seen from space ($\text{W cm}^{-2} \text{sr}^{-1}$)

$F(x, \alpha)$ = spatial frequency response, expressed as a function of the test pattern bar width, x and IFOV, α

α = angular width of field stop (IFOV), assumed square (radians)

A_o = entrance aperture area (cm^2)

τ_o = optical efficiency, including obscuration

\bar{R} = mean detector responsivity over spectral band (amps W^{-1})

k_o = electron multiplier relative noise multiplication factor

e = electronic charge, 1.6×10^{-19} coulomb

Δf_n = effective noise bandwidth (Hz)

The bandwidth can be expressed as a function of the coverage rate by the expression:

$$\Delta f_n = \frac{k_f(v/h)\theta}{2k_s n \alpha^2} \quad (3)$$

where

k_f = ratio of filter effective noise bandwidth to information bandwidth

v, h = satellite velocity and altitude, respectively

θ = cross-track swath width, radians

k_s = scanning efficiency-factor

n = number of detectors in parallel in each channel.

The signal-to-noise ratio is then

$$\frac{I_s}{I_n} = \frac{(N'_2 - N'_1)F(x, \alpha)\alpha^2 D}{2(N'_2)^{1/2}} \left[\frac{\pi \tau_o \bar{R} k_s n}{e k_o k_f (v/h) \theta} \right]^{1/2} \quad (4)$$

In order to facilitate an examination of the interrelation between α , D , and n , it is useful to rewrite this equation as:

$$\alpha D^{1/2} n^{1/4} = K_{\text{PMT}} \left(\frac{I_s}{I_n}, N'_2, N'_1, F, \tau_o, \bar{R}, k_s, k_o, k_f, v, h, \theta \right) \quad (5)$$

where K_{PMT} is a function of the quantities in brackets, all of which will be held constant during the present discussion.

Scanners Employing Photodiode Detectors

With photodiode detectors the signal current is the same as that given by Equation (1). The noise current, however, is more complex than that of a photomultiplier tube, and may be represented by:

$$I_n = \left[\left(i_{ns}^2 + i_{n\alpha}^2 + i_{np}^2 + \frac{4kT}{R_L} \right) \Delta f_n \right]^{1/2} \quad (6)$$

where

$$\begin{aligned} i_{ns} &= \text{signal shot current noise (amps Hz}^{-1/2}\text{)} \\ i_{n\alpha} &= \text{dark current noise (amps Hz}^{-1/2}\text{)} \\ i_{np} &= \text{preamp noise current (amps Hz}^{-1/2}\text{)} \\ 4kT/R_L &= \text{load resistor thermal noise current (amps Hz}^{-1/2}\text{)} . \end{aligned}$$

Since R_L is fixed at a low value by the scanner bandwidth requirements, the thermal noise is appreciable. This and the preamplifier noise are found to dominate in Equation (6) for low signal values. Accordingly, in order to simplify the comparison of scanner designs at low signal currents it is assumed that the signal shot noise and dark current noise terms can be neglected. The thermal noise and preamplifier noise terms are frequency dependent, but the dependency is of low order and can also be neglected for the purposes of this analysis. Therefore, Equation (6) can be rewritten as:

$$I_n = i_n \Delta f_n^{1/2} \quad (7)$$

where i_n is the root sum square of the contributing noise currents. Combining with Equation (1) and substituting for Δf_n :

$$\frac{I_s}{I_n} = \frac{\pi(N'_2 - N'_1)F(x, \alpha)\alpha^3 D^2 \tau_o \bar{R}}{4i_n} \left[\frac{2k_s n}{k_f(v/h)\theta} \right]^{1/2} \quad (8)$$

In this case we can write:

$$\alpha D^{2/3} n^{1/6} = K_{PD}(N'_1, N'_2, F(x, \alpha), \tau_o, \bar{R}, k_s, i_n, k_f, v, h, \theta, I_s/I_n) \quad (9)$$

where K_{PD} will be held constant in the discussion below.

Scanners Employing Photoconductive Detectors

With photoconductive detectors the signal power, P , incident on the detector, is given by the equation:

$$P = (N'_2 - N'_1)F(x, \alpha)\alpha^2 A_o \tau_o. \quad (10)$$

The noise equivalent power (NEP) is given by

$$NEP = NEP_1 \Delta f_n^{1/2} NF \quad (11)$$

where NF is the preamplifier noise factor, and NEP_1 the specific noise equivalent power that is related to the detectivity (averaged over the spectral band) \bar{D}^* by

$$NEP_1 \equiv A_\alpha^{1/2} / \bar{D}^* \quad (12)$$

where A_α , the detector area, is given by

$$A_\alpha = \alpha^2 D^2 (f/no)^2. \quad (13)$$

The S/N is now given by

$$\frac{S}{N} = \frac{P}{NEP} = \frac{(N'_2 - N'_1)F(x, \alpha)\alpha^2 A_o \tau_o}{D(f/no)NF} \bar{D}^* \sqrt{\frac{2k_s n}{k_f(v/h)\theta}}. \quad (14)$$

In this case we see that

$$\alpha D^{1/2} n^{1/4} = K_{PC}(N'_1, N'_2, F(x, \alpha), \tau_o, \bar{D}^*, k_s, f/no, NF, k_f, v/h, \theta, S/N) \quad (15)$$

where again K_{PC} will for the moment be held constant.

Resolution Improvement Considerations

The capability of scanners to perform many functions improves with increasing resolution. Accordingly, it may be useful to examine the feasibility of increasing resolution to values well beyond those presently realized.

The impact of decreasing α , the angular width of field stop (IFOV), on other scanner parameters is shown in the following subsection. It should be pointed out, that a decrease in α impacts strongly on many other

system parameters besides the scanner characteristics. The data handling problem, for example, becomes rapidly aggravated as the resolution increases; similarly the data processing, calibration, vehicle stabilization, telemetry, cryogenics and vehicle payload requirements all increase rapidly with resolution. Since these properties are treated in a later section, the present discussion will be restricted to the impact of increased resolution on the required values of scanner design parameters.

Impact of Decreasing α on Required Values of D and n

Equations (5), (9), and (15) permit calculation of combinations of values of D and n which are required to achieve resolution values increased by any specified amount above the resolution of a "nominal" scanner. The remaining scanner parameters (enclosed in brackets in these three equations) are held constant—that is, unchanged from the values they possess in the "nominal" scanner.

Both the ERTS-1 Multispectral Scanner (MSS) and the Visible-Infrared Spin Scan Radiometer (VISSR) may be considered as "nominal" scanners or "take-off points" for scanners employing photomultiplier tubes. For the MSS scanner:

$$\alpha = 0.086 \text{ mrad}$$

$$D = 22.86 \text{ cm}$$

$$n = 6$$

then from Equation (5),

$$K_{\text{PMT}}(\text{MSS}) = (0.086) \times (22.86)^{1/2} \times (6)^{1/4} = 0.643 \text{ cm}^{1/2}. \quad (16)$$

Knowing K_{PMT} , Equation (5) can now be used to plot the required value of D as a function of α for any value of n. Figure 2-4 presents the results of this procedure for a number of values of n ranging from 1 to 2000; these curves permit an estimation of the feasibility of increasing the resolution of a MSS-type scanner above its present value (indicated by the arrow in Fig. 2-4). The dashed curves in this and Figures 2-5 to 2-7 represent the limitation imposed on α by diffraction and other aberrations to be expected with state-of-the-art optical technology. The basis for this curve is discussed in a later section.

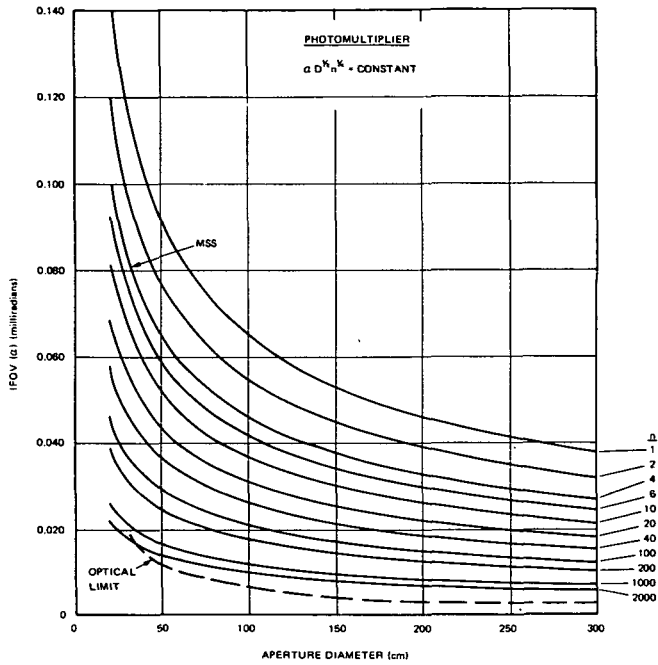


Figure 2-4. Aperture diameter required to achieve increased resolution with scanners employing photomultiplier tubes (relative to ERTS-1 MSS)

In the case of the VISSR scanner,

$$\alpha = 0.025 \text{ mrad}$$

$$D = 40.6 \text{ cm}$$

$$n = 8,$$

so that

$$K_{PMT}(\text{VISSR}) = (0.025) \times (40.6)^{1/2} \times (8)^{1/4} = 0.268 \text{ cm}^{1/2}. \quad (17)$$

Using this value of K_{PMT} , α is plotted as a function of D for various values of n in Figure 2-5.

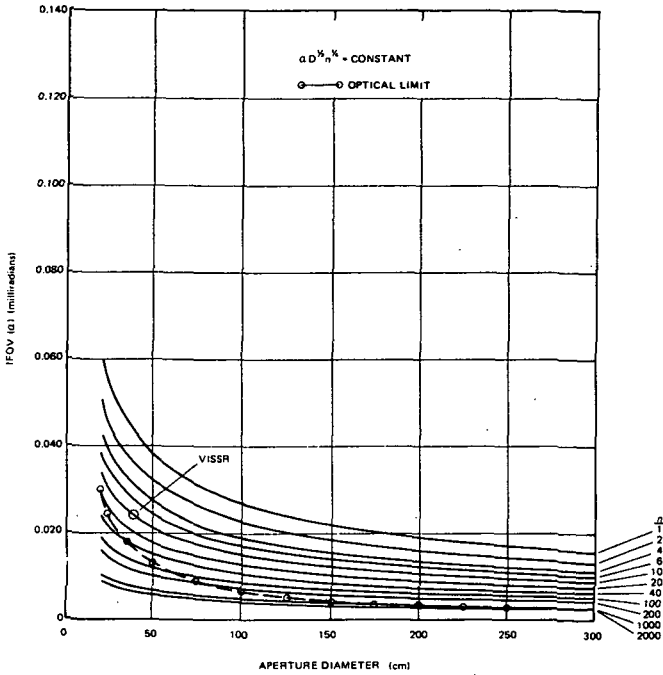


Figure 2-5. Aperture diameter required to achieve increased resolution with scanners employing photomultiplier tubes (relative to VISSR)

The MSS scanner may also be taken as a "nominal" scanner employing photodiodes. In this case, Equation (9) yields:

$$K_{PD}(MSS) = (0.086) \times (22.86)^{2/3} \times (6)^{1/6} = 0.934 \text{ cm}^{2/3}. \quad (18)$$

Using this value of K_{PD} , α is, with the aid of Equation (9), plotted as a function of D for various values of n in Figure 2-6.

The MSS may be treated as a "nominal" scanner employing photoconductors. In this case:

$$\alpha = 0.258 \text{ mrad}$$

$$D = 22.86 \text{ cm}$$

$$n = 2.$$

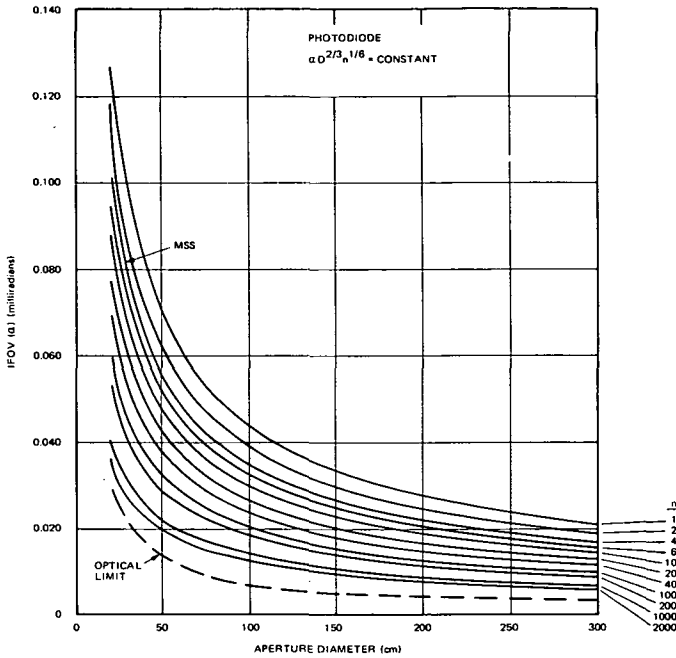


Figure 2-6. Aperture diameter vs resolution for scanners employing photodiode detectors (relative to MSS)

Equation (15) then yields:

$$K_{PC}(MSS) = (0.258) \times (22.86)^{1/2} \times (2)^{1/4} = 1.47 \text{ cm}^{1/2}. \quad (19)$$

Figure 2-7 presents D as a function of α for various values of n assuming this value of K_{PC} .

Figures 2-4 through 2-7 indicate that significant increases in resolution above that employed in the MSS and VISSR scanners can be achieved only at the cost of sizable increases in n and/or D . (The associated increase in weight is discussed later.) Thus Table 2-2 lists the present values of n and D for the MSS and VISSR scanners, together with values which might be selected to (a) double and (b) increase by a factor of 10 the angular resolution, maintaining other parameters constant. In choosing these values, increases in n were favored over increases in D , in the

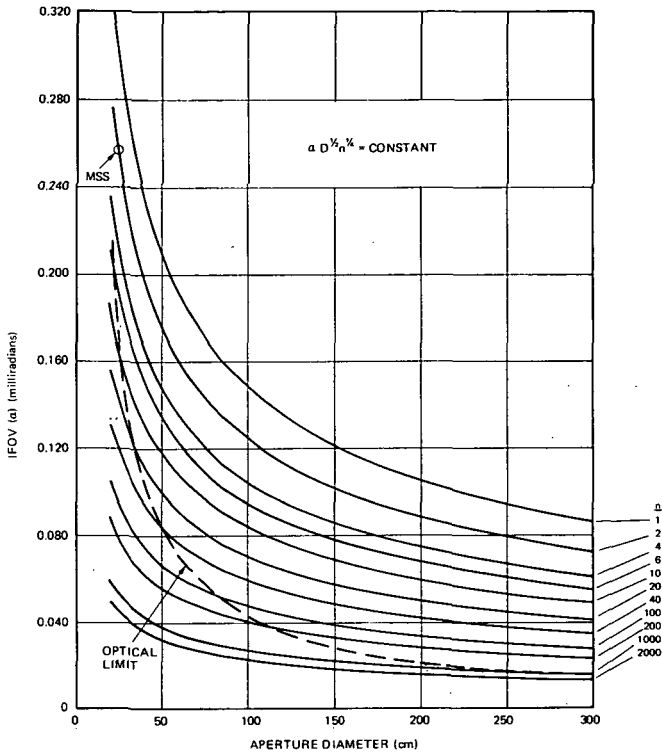


Figure 2-7. Aperture diameter vs resolution for scanners employing photoconductive detectors (relative to MSS)

interest of minimizing the required increase in weight, cost, scan speed, and detector speed. It is seen that a twofold increase in α can be achieved largely through increasing n , while the tenfold increase requires very large increases in both n and D .

Effect of Increased Resolution on Required Scan Frequency

The scan frequency, f_s , required to just avoid gaps in coverage with a unidirectional scan, is given by:

$$f_s = \frac{v/h}{n\alpha} \quad (20)$$

With the aid of this equation, f_s is plotted as a function of $n\alpha$ in Figure 2-8. Appropriate data points are indicated on this graph corresponding to:

1. S-192 (Skylab MSS) scanner, for which $n = 1$ and $\alpha = 0.182$ mr
2. ERTS MSS scanner, for which $\alpha = 0.086$ mr and $n = 6$
3. Advanced image space scanner (called Thematic Mapper), for which $\alpha = 0.040$ mr and $n = 9$
4. Hypothetical upgraded MSS, i.e., photomultiplier, scanner whose resolution was doubled by increasing n to 100 (Table 2-2)
5. Hypothetical MSS photomultiplier scanner whose resolution was increased tenfold by increasing n to 2000 (Table 2-2).

This graph shows that when resolution increases are achieved by increasing n rather than D , the scan speed need not be increased excessively.

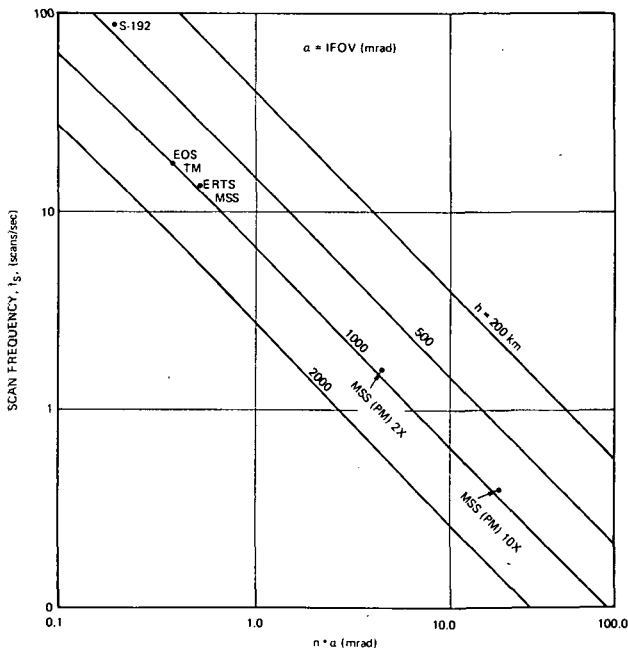


Figure 2-8. Scan frequency required with n detectors along ground track (contiguous unidirectional scans)

Table 2-2
Present Values of D and n For The MSS and VISSR Scanners, and Representative Values
Required to Increase Resolution By Factors of 2 and 10

Scanner	Detector Type	Present Parameter Values			Required Parameter Values					
					Resolution Increase			10X		
		α (mr)	D (cm)	n	α (mr)	D (cm)	n	α (mr)	D (cm)	n
MSS	Photomultiplier	0.086	22.86	6	0.043	23	100	0.0086	125	2000
VISSR	Photomultiplier	0.025	40.6	8	0.125	75	40	0.0025	250	1000
MSS	Photodiode	0.086	22.86	6	0.043	23	200	0.0086	175	2000
MSS	Photoconductor	0.258	22.86	2	0.129	40	10	0.0258	240	200

(In the illustration given, it actually decreases.) In particular, the scan frequency may be kept low enough that object-space scanning may remain feasible as resolution is increased. This is important since image-space scanning may be precluded at high resolution because of inability to achieve the desired resolution off-axis.

Effect of Increased Resolution on Dwell Time

One hazard associated with increasing angular resolution is that t_d , the dwell time of the detectors on a resolution element, may become less than the detector time constant, resulting in a decreased responsivity. For a satellite in polar orbit mapping swaths that provide contiguous coverage without overlap at the equator it can easily be shown that t_d is given by

$$t_d = \frac{k_s n h^2 \alpha^2 T_m}{4\pi^2 R^2} \quad (21)$$

where T_m is the time required to map the earth, and R is the radius of the latter.

It is seen that as α is decreased, n must be increased in proportion to $1/\alpha^2$ in order to avoid a decrease in t_d , unless performance (S/N or coverage rate) is sacrificed.

This analysis for resolution improvement can also be performed for advanced airborne scanners. Because of air drag, however, there is a limit in the size of scan mirrors. Consider the 24-channel scanner of the Multi-spectral Data System used in NASA Earth Resource Aircraft program. In this scanner, which uses a 9-inch aperture scan mirror, increased aperture is very difficult because of surface distortions and drive power requirements. Increasing the resolution by a factor of two by changing the number of detector elements would require increasing the photomultiplier and photoconductive detectors a factor of 16, and the photodiodes a factor of 64.

Impact of Increasing Resolution on Scanner Weight

The increase in both the aperture diameter and the number of detectors, as discussed previously and required to achieve increased resolution, translates directly into increased scanner weight. Figure 2-9 represents an effort to extrapolate the weight of a VISSR-type scanner to larger aperture values, with no regard to changes in n . The weight indicated refers to an

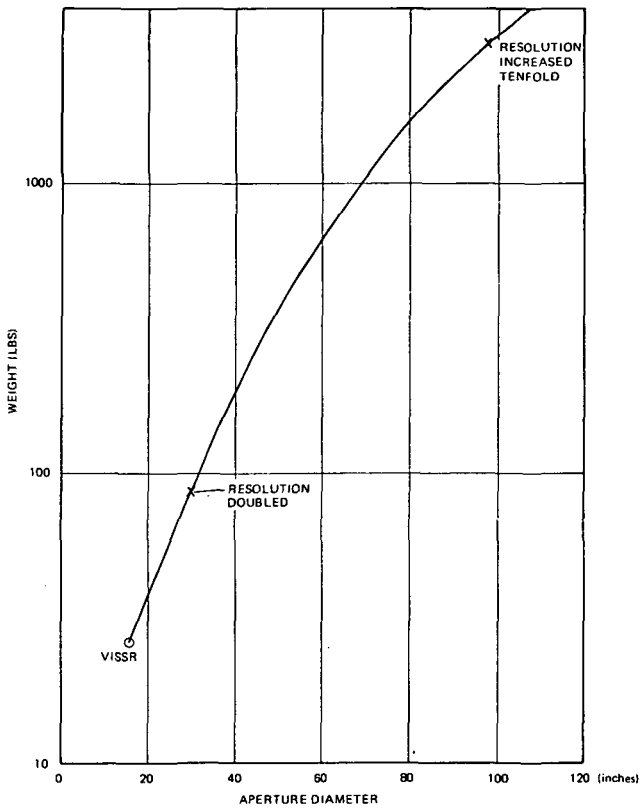


Figure 2-9. Telescope weight for all beryllium system—vs aperture diameter

all-beryllium system, and includes only the primary and secondary mirrors, support assemblies, and tube. In this figure the present weight of the VISSR scanner is indicated by a circle, while the improved-resolution values listed in Table 2-2 are represented by crosses. For a tenfold increase in resolution (always maintaining the same coverage, S/N, etc.), it is seen that the weight of the telescope alone would have to be increased to more than 3000 lbs, to which the weight associated with the 1000 required detectors must be added.

Impact of Increasing Resolution on Data Rate

The data rate B from a multichannel scanner (assuming contiguous scans) is given by

$$B = \frac{v/h}{k_s \alpha^2} \theta \text{ sgb bits sec}^{-1} \quad (22)$$

where

s = number of samples per IFOV

g = gray scale (bits per sample)

b = number of spectral bands.

Note that B is independent of n , the number of detectors per spectral band.

For the ERTS-1 MSS the total bit rate is approximately 15 megabit/sec. Doubling the effective resolution raises the bit rate to 60 megabit/sec, while a tenfold increase in resolution would result in a bit rate of 1500 megabit/sec.

More efficient scan techniques now under development will reduce these bit rates by almost a factor of two.

Optical Design Problems Associated with Increasing Resolution

Axial Imagery. It is interesting to examine the possible increase in telescope resolution as a function of aperture, as limited by diffraction and by the present state of the optical design art. The angular diameter θ of the blur circle is given by

$$\theta = [\theta_D^2 + \theta_F^2 + \theta_A^2]^{1/2} \quad (23)$$

where the subscripts, D, F, and A refer to contributions arising from diffraction, figure imperfections, and misalignment of optical elements, respectively.

The value of θ_D for a cone which will contain 80 percent of the radiant power of a telescope with a central obscuration having a radius equal to 40 percent of the aperture radius is given by Goldberg and McCulloch (1969).

$$\theta_D = 3.69\lambda/D. \tag{24}$$

This contribution to θ is indicated by the dashed lines in Figure 2-10.

The angular diameter, θ_F , of the blur circle associated with a figure imperfection x , again with an obscuration factor of 0.4, is given by

$$\theta_F = 16x/D. \tag{25}$$

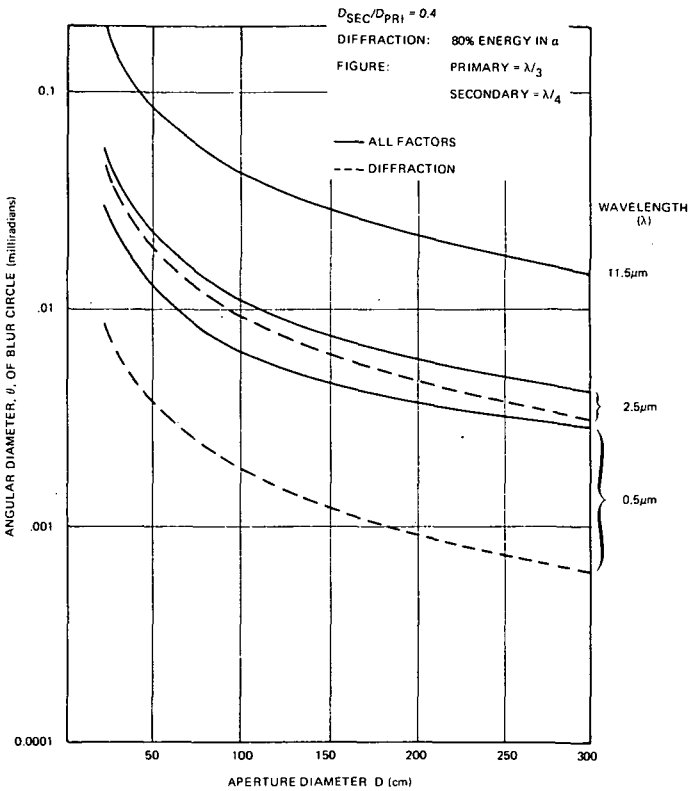


Figure 2-10. Diffraction, figure, and alignment effects on blur circle

A nominal value for figure imperfection (that achieved axially, for example, with the beryllium-substrate VISSR mirrors) is $\lambda/3$ (a third of a wavelength in the visible) on the primary and $\lambda/4$ on the secondary.

The contribution to blur by lateral misalignment, θ_A , is given by the relation

$$\theta_A \approx \frac{m\Delta}{k_1 \text{EFL}^2}, \quad (26)$$

where

m = magnification

Δ = lateral misalignment

k_1 = a constant

EFL = effective focal length.

Remembering that

$$m = \frac{\text{EFL}}{f_{\text{pri}}} = \frac{(f/\text{no.})_{\text{system}}}{(f/\text{no.})_{\text{primary}}}, \quad (27)$$

and that

$$\text{EFL} = (f/\text{no.})_{\text{system}} \times D, \quad (28)$$

it is seen that

$$\theta_A \approx k_2 \frac{\Delta}{D}, \quad (29)$$

where k_2 is a constant involving k_1 and the various f/nos . With the VISSR scanner, Δ was 0.002 in. and θ_A , from ray traces, was found to be 0.002 milliradian. If, as this telescope is scaled up in size, it is assumed that Δ increases in direct proportion to D , θ_A will take on a constant value of 0.002 milliradian.

Figure 2-10 presents, as a function of D , the value of θ calculated from Equation (23), using the value of θ_D , θ_f , and θ_A discussed in the preceding paragraphs. This value of θ is also shown as a dashed line in Figures 2-4 through 2-7. These figures reveal that the present state of the optical art is adequate to achieve the two- and tenfold increase in resolution discussed above.

Off-Axis Aberrations. In choosing between object- and image-space scanning, it must be remembered that the latter requires an optical system with a considerably wider field of view. That this consideration may seriously limit improvement in resolution with image-space scanners is clear from Figure 2-11, in which the blur circle diameter is plotted as a function of the off-axis angle for a number of two-mirror optical systems.

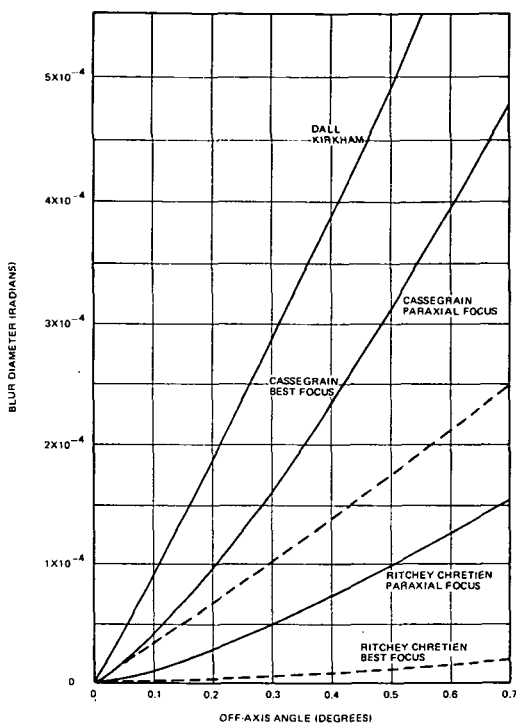


Figure 2-11. Comparison of off-axis image blur for two-mirror optical systems

In all cases the blur circle diameter is seen to increase rapidly with departure from the axis.

Other Tradeoff Considerations

Equations (4), (8), and (14) can be rewritten to facilitate an examination of the interrelation between any set of parameters. For example, the relationships among signal-to-noise ratio, spectral bandpass, and number of detector elements for the three types of detectors previously considered are:

$$\frac{I_S}{I_N} = \Delta\lambda^{1/2} n^{1/2} C_{PMT} \quad (30)$$

$$\frac{I_S}{I_n} = \Delta\lambda n^{1/2} C_{PD} \quad (31)$$

$$\frac{I_S}{I_N} = \Delta\lambda^{1/2} n^{1/2} C_{PC} \quad (32)$$

where the three C-terms represent constants combining the other parameters, as before.

Figure 2-12 plots Equation (30) for the band (1) of the ERTS MSS. This figure shows, for example, that 5 Å resolution could be achieved in this band with an S/N value of 57 through employment of 484 detectors, other parameters remaining unchanged from their values in the MSS scanner.

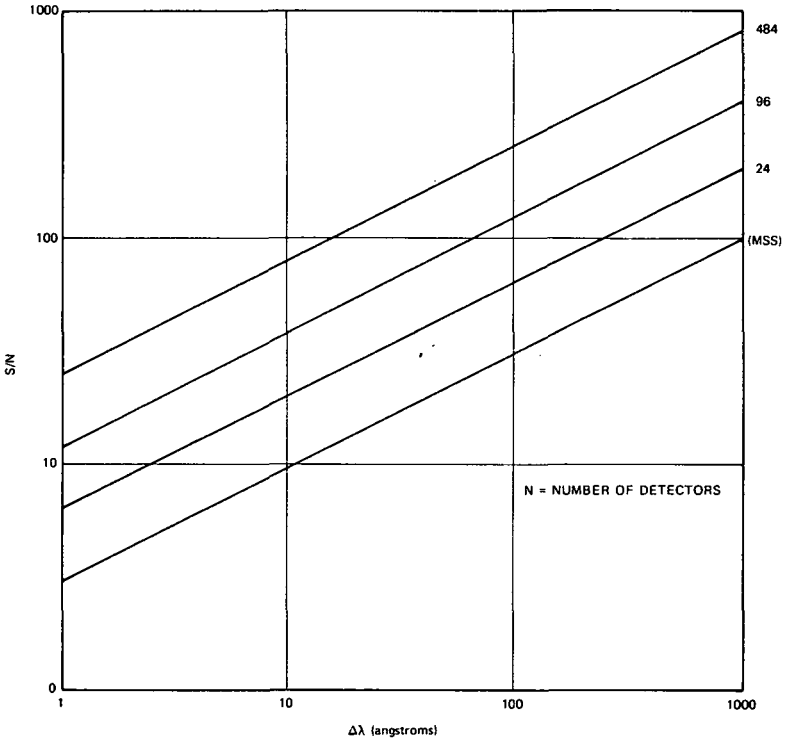


Figure 2-12. Calculated S/N versus $\Delta\lambda$ for various values of n with MSS-type scanner using photomultiplier tubes

Image Plane vs Object Plane Scanners

It is important that electromechanical scanners have the design option of being either object plane or image plane scanners. Designing optics (especially fast optics) with a large number of resolution elements per field of view is a difficult problem placing practical and sometimes theoretical (diffraction) limits on the maximum number of EIFOVs per picture width. For systems requiring the large number of elements per picture width (e.g., ERTS); the only practical design is to object plane scan in order to reduce the optical design requirement by orders of magnitude and bring it into the realm of practicality. (This is especially true for the IR channels.) On the other hand, for snapshot modes (i.e., frame scanning systems) where relatively few EIFOVs are required across the diagonal, image plane scanning can significantly reduce the size of the scan elements and therefore the complexity of the scanner.

Resolution and Sample Data

The usefulness of an imaging system for examining small area details is limited by the size of an area of confusion (blur circle). This area is intuitively defined as the minimum area (diameter) across which meaningful radiance variations can be detected. This ill defined and somewhat arbitrary area is what is often referred to as "resolution" by a practical user of such a system; this procedure is followed in the preceding chapter. Throughout the history of imagery the concept of resolution has been poorly defined, misused, and confused. Recently raster (sample data) systems have added further confusion. Accordingly, a closer look at the concept of resolution is in order.

With scanning systems, resolution has often been equated with the size of the instantaneous field of view (IFOV)—an intuitive but misleading concept. In television systems, the concept of limiting resolution is used. It is defined as the size of the smallest black-and-white bars that can be observed (2 to 5 percent response). This concept has proven to be a useful and easily accepted one being similar to the circle of confusion of purely optical systems. For point impulse inputs, the smallest blur output of an optical mechanical scanner is set by the scanning aperture, and any two points must be farther apart than the scanning aperture (IFOV) or they cannot be resolved. For early low-performance systems, the detector was the dominating factor for determining the size of the scanning aperture of a system, but as systems became more and more sophisticated, design compromises allowed other components to become more important. As a

result, it is necessary to consider the total system blur if a meaningful number is to be discussed.

In the analysis of scanning systems it is convenient to introduce the concept of sinewave response. By using the Fourier transform, the impulse response can be uniquely defined by a frequency response—the modulation transfer function (MTF). This method permits discussing the blur or resolution of systems equally by the line spread or by a filter function (MTF). It is convenient because the MTF of the complete system can be determined by the product of the MTFs of the individual components. The total system spatial response function can then be derived by taking the inverse Fourier transform.

It is also important that the MTF of each component, and for that matter the complete system, be measurable. Because of this requirement, the response of the system to a bar chart may be used to define the resolution of the system and the process of inverse transformation becomes unnecessary.

Definitions Pertaining to Resolution and Sample Data

Definition 1: Effective IFOV—No Raster. For uniformity between systems comparisons through a convenient tie to the past, and in order to have a single number to represent resolution, the panel has somewhat arbitrarily defined the equivalent IFOV or the system IFOV for a rasterless system as the spacing between the half cycles which correspond to the 50 percent MTF point. If expressed as a number of lines per distance in the image or object plane, the resolution also corresponds to the 50 percent MTF point. For systems where the equivalent IFOV is not equal in the along track and cross-track directions, the arithmetic mean will be used for the system IFOV.

If the only limiting aperture of the system were the detector, the MTF would have a value of 64 percent per half cycle at the frequency corresponding to the detector width. However, for any practical system the optics, electronics, and display will degrade this MTF considerably and a value of 50 percent would be difficult to obtain. It was felt that past experience with detector IFOVs could be intuitively extrapolated to future systems, if this definition were used. In addition, while it implies a poorer resolution for vidicon systems (the 50 percent frequency being significantly lower than 5 percent), it permits the various systems to be discussed on a common basis.

The fact that this new uniform definition would make some system types look better, but most look worse, it was of sufficient concern to force the 50 percent definition as an optimistic compromise from the equivalent aperture concept proposed for the National Bureau of Standards by O. Shade. Shade's definition was the reciprocal of the integral of the MTF squared (in units of lines). This corresponded to a 60 to 70 percent point on an MTF curve (similar to bandwidth) and was equal to the detector aperture for a detector limited system.

Definition 2: Effective IFOV—Raster. The effective IFOV for a raster (sample data) system will be defined as the RMS sum of the IFOV of the nonsampled system and the distance between samples. For the typical system using an array of contiguous detectors (or scanning contiguous line), the effective IFOV must account for the raster line spacing in one direction and the multiplexing or digitizing spacing in the other direction; the mean between the equivalent IFOVs for the two directions will be called the equivalent IFOV of the system.

Many systems are sample data (or raster) rather than resolution limited. That is, the smallest details that can be honestly observed and evaluated are determined more by the raster (observed lines or squares) than by the MTF of the system. Somehow the errors introduced must be considered. To accurately analyze such a system, it is necessary to recognize that a sample data system consists of an analyzing aperture, the sampling, and a synthesizing aperture. In the nomenclature of information theory or electrical engineering: a prefilter, a sampler and a postfilter. For a system to be unaffected by the sampling it must satisfy the often quoted and misunderstood Nyquist or Shannon criteria.

These criteria state that to avoid losses due to sampling, necessary and sufficient conditions are that the prefilter must limit the signal to the sampler so that no signal is sampled that is of a frequency greater than one-half of the sampling frequency, and that the postfilter must again provide zero response at a frequency beyond one-half the sampling frequency. While this criterion will get rid of all visible effects of sampling, it may not be economically feasible.

Since the sampling results in the system being no longer spatially invariant (a requirement for Fourier analysis) the frequency domain analysis can be completed but no method for unique inverse transformation exists. That is while the response for any input frequency and phase can be indicated, the impulse or step response, etc., for the system cannot be determined

from the results of the spatial frequency analyses. An impression of the degree of interference, etc., can be determined, however, by a simple analysis in the frequency domain.

Consider the system to consist of an analyzing aperture or prefilter, a sampler of frequency f_s (equal to the reciprocal of the sample spacing, e.g., the raster spacing), and a synthesizing aperture or postfilter A_s . If the input signal is s , then the output O_1 (conceptual maybe) of the analyzing aperture would be the convolution of s and a_a ,

$$O_1 = s * a_a, \quad (33)$$

or, if the capital letter indicates Fourier transform,

$$O_1 = S A_a. \quad (34)$$

The sampling is a comb of delta functions equal spacings apart. Therefore, the output of the sampler is

$$O_2 = [O_1] [\text{Comb}(1/f_s)]. \quad (35)$$

In the frequency domain, since the Fourier transform of a comb of spacing $1/f_s$ is a comb of spacing $f_{(s)}$,

$$O_2 = O_1 * \text{Comb}(f_s). \quad (36)$$

This frequency signal is then filtered by the postfilter A_s , or the final output O_3 is given by:

$$O_3 = [O_1 * \text{Comb}(f_s)] A_s. \quad (37)$$

Considering the case of an impulse input, the frequency response of the complete system, which normally would be considered an MTF, is given by:

$$O_3 = [A_a * \text{Comb}(f_s)] A_s. \quad (37)$$

This is best visualized through the graphs of Figure 2-13.

From this figure, it can be seen that the input spectrum of the sampler is the transform of the analyzing aperture. After sampling, the spectrum becomes a family of spectra around the sampling frequency and its articles. Finally, it can be seen that the synthesizing aperture (display spot) filters this spectrum reducing it ideally only to the original

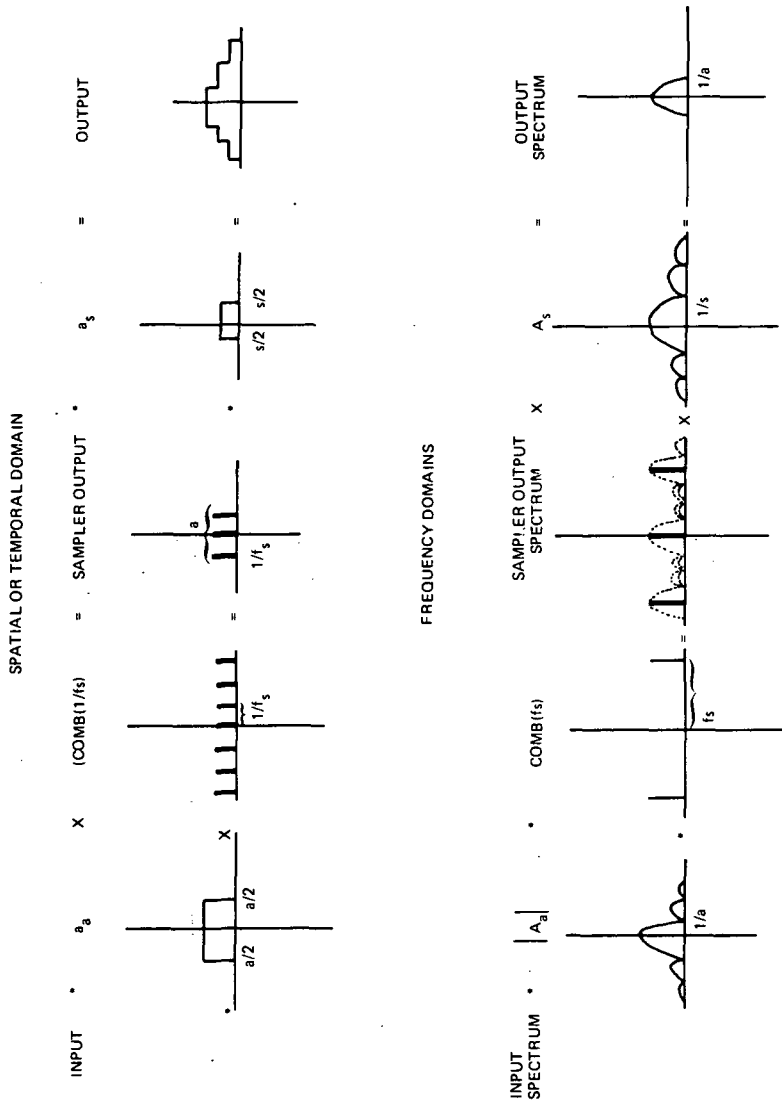


Figure 2-13. The sampling situation

spectrum. For such an ideal case to occur, it is mandatory that the sampling occur at a rate twice this frequency, and that the spectrum of the synthesizing aperture be of such a nature as to filter out all frequencies beyond the reference frequency.

Summary of Design Considerations

A primary key to the acquisition of increased angular resolution in electromechanical earth-mapping scanners is the employment of detector arrays with large numbers of elements. As seen from Table 2-2, if this quantity is increased to 100-200, the resolution of scanners similar to MSS (ERTS-1) and VISSR can be doubled in the 0.5 to 1.2 μm spectral region with only a modest increase (doubling or less) in aperture diameter. A tenfold increase in resolution would require, for example, 1000-2000 elements and aperture diameters of 1 to 2 meters.

In the 8 to 12 μm region a doubling in resolution could be achieved, for example, with 10 detector elements and a 40-cm aperture while a tenfold increase might require 200 detector elements and a 240-cm aperture, assuming in all cases no compromise in S/N or coverage rate. Rapid advances in technology observed during the past decade lead to an optimistic out-look for achieving such an improvement in scanner resolution. Severe burdens would, however, then be placed on such other subsystems as data processing, data handling, telemetry, calibration, and vehicle stabilization. These considerations are discussed in detail in other chapters.

Present optical technology enables acquisition of this two- or tenfold increase in resolution near the optical axis (Figure 2-10). Aberrations increase rapidly with increasing off-axis angle (Figure 2-11) a factor which favors the use of object-plane scanning in wide angle systems.

In addition to keeping down the required aperture size, employment of detector arrays with large numbers of elements relieves the requirement for unrealistically fast detectors (Equation (21)) and excessive scan frequency at high resolution (Figure 2-8); the latter consideration keeps optical systems employing object-plane scan in contention as candidates.

In order to facilitate comparison of sensor types, a common definition of effective instantaneous field of view (EIFOV) was adopted. The EIFOV was defined as the RMS sum of the IFOV of a non-sampled system and the distance between samples where the IFOV is defined as the spacing between the half cycle which corresponds to the 50% MTF point.

PHOTODETECTORS

Photodetectors in three broad categories were considered in the panel evaluations:

- Photomultiplier tubes (PMT)
- P-N junction photodetectors
- Photoconductive devices.

Photomultipliers employ the photoemissive properties of a low work function photocathode with subsequent low noise multiplication of the resulting electron beam by secondary emission. The electron multiplication gain can be accomplished with a series of biased dynodes, or by a channel multiplier. These devices have good signal bandwidth, and at short wavelength have high quantum efficiency and low dark current. Photomultiplier tubes are currently used in multispectral scanner systems for the short wavelength channels. For high resolution systems, PMTs are used for wavelengths shorter than about 800 nm; in lower resolution systems, PMTs may not be used at all or only at wavelengths shorter than 500 nm.

Silicon planar p-n junction photodetectors represent the most advanced semiconductor technology available at this time, and provide good resolution and parameter control. Optical signal detection in these devices is accomplished when hole-electron pairs are generated in the bulk semiconductor by the absorption of incident optical radiation. The resulting increase in minority carrier density causes a signal current to flow at the terminals of the p-n junction. The short circuit signal current of a silicon photodiode is linear over many decades. These units also show good high frequency response, high quantum efficiency, low noise, and require no special cooling for most applications. Because the photodiode has no internal signal gain, high performance channels are usually limited by the noise of the first amplifier stage. Gain can be included in the detector structure by use of transistor action and/or avalanche multiplication. However, in both cases, improved S/N performance is realized only at the cost of reduced dynamic range, degraded linearity, and increased sensitivity to ambient temperature variation.

Silicon photodiodes are normally used in multispectral scanning systems for wavelengths between about 0.4 μm and 1.1 μm . Other semiconductor

materials are used in the fabrication of p-n junction photodetectors for wavelengths longer than $1.1\text{ }\mu\text{m}$. Table 2-3 presents a list of the most common detectors with their useful wavelength ranges and operating temperatures. Several of the materials used in the detectors shown are ternary systems that allow the wavelength of peak response to be shifted over a considerable range by adjusting the composition of the material when it is grown. In general, infrared photodiodes must be operated at low temperature to achieve optimum performance, with the longer wavelength detectors requiring the lower operating temperature.

Table 2-3

Photodiode Detector

Material	Long Wavelength Cutoff	Normal Operating Temperature
Si	$1.1\text{ }\mu\text{m}$	300 K
Ge	$1.5\text{ }\mu\text{m}$	200-300 K
InAs	$3.6\text{ }\mu\text{m}$	150 K
InSb	$5.6\text{ }\mu\text{m}$	77-140 K
PbSnTe	$5.0\text{ }\mu\text{m}$	180 K
	$15.0\text{ }\mu\text{m}$	80 K
HgCdTe	$5.0\text{ }\mu\text{m}$	125 K
	$15.0\text{ }\mu\text{m}$	77 K

Photoconductive detectors are most useful at infrared wavelengths longer than $3\text{ }\mu\text{m}$. These devices are essentially variable resistors in which the conductivity of the bulk material increases monotonically with the magnitude of optical power absorbed in the active volume of the units. A bias signal (usually dc) must be applied to the detector in order to obtain a useful output signal that is proportional to the optical input. The properties of some materials make it possible to achieve significant photoconductive gain. Photoconductive gain occurs when each absorbed photon delivers more than one electron at the terminals of the detector.

Photoconductive detectors are listed in Table 2-4, showing some of the most useful materials. The intrinsic photoconductors are narrowband gap

Table 2-4
Infrared Photoconductive Detectors

Material	Maximum Temperature for Background Limited Operation	Long Wave-length Cutoff (μm)	Peak Wave-length (μm)	Absorption Coefficient (cm^{-1})	Quantum Efficiency	Resistance (Ω)	D* peak ($\text{cm-Hz}^{1/2}/\text{W}$)	Approximate Response Time (seconds)
InAs		3.6	3.3	$\sim 3 \times 10^3$			3×10^{11}	5×10^{-7}
InSb	110	5.6	5.3	$\sim 3 \times 10^3$	0.5-0.8	10^3 - 10^4	6×10^{10} -1×10^{11}	5×10^{-6}
Ge: Au	60	9	6	~ 2	0.2-0.3	4×10^5	3×10^9 - 10^{10}	3×10^{-8}
Ge: Au(Sb)	60	9	6			10^4	6×10^9	1.6×10^{-9}
Ge: Hg	35	14 14	11 10.5	~ 3 ~ 4	0.2-0.6 0.62	1.4×10^4 1.2×10^5	7×10^9 4×10^{10} 4×10^{10}	3×10^{-8} -10^{-9}
Ge: Hg(Sb)	35	14	11			5×10^9	1.8×10^{10}	3×10^{-10} - 2×10^{-9} 3×10^{-10} - 3×10^{-9}
Ge: Cu	17	27	23	~ 4	0.2-0.6	2×10^4	2.4×10^{10}	3×10^{-4} - 10^{-8} 4×10^{-9} - 1.3×10^{-7}
Ge: Cu(Sb)	17	27	23			2×10^5	2×10^{10}	$< 2.2 \times 10^{-9}$
Hg: Cd, Te X = 0.2		14	12	$\sim 10^3$	0.05-0.3	60-400 20-200	10^{10} 6×10^{10}	$< 10^{-8}$ $< 4 \times 10^{-4}$
Pb: Sn, Te X = 0.17-0.2		11 15	10 14	$\sim 10^4$		42 52	3×10^8 1.7×10^{10}	1.5×10^{-8} 1.2×10^{-4}

semiconductors that absorb long wavelength photons by the generation of hole-electron pairs—thus, the infrared absorption is an inherent or intrinsic property of the semiconductor. Extrinsic photoconductors are wide-band gap semiconductors that absorb long wavelength photons by the excitation of impurity levels that have been added to the material—the infrared absorption is an added or extrinsic property of the semiconductor. Both types of materials can show photoconductive gain.

Detector Performance

Quantum Efficiency/Responsivity

Most useful photodetectors are quantum devices in which one electron is generated for each photon absorbed in the active volume, independent of the energy of that photon. Thus, one of the fundamental performance characteristics of photodetectors is the quantum efficiency. The notable exceptions to this general statement are energy detectors such as bolometers and pyroelectric devices.

The presence of wavelength dependent loss mechanisms for both photons and carriers results in quantum efficiency values that are wavelength dependent and less than 1.0 at all wavelengths. In this section the term quantum efficiency is used only in reference to the basic excitation process in the detector. For detectors with internal amplification, the gain is treated separately from the quantum efficiency.

Even though most photodetectors are quantum devices, they are by convention characterized by their measurable terminal response to optical-input power. The optical power response is called responsivity (R), and is given in units of amperes/watt (A/W) or volts/watt (V/W). For photon detectors, the current responsivity is the most fundamental performance characteristic and will be intended whenever the term responsivity is used. For a photon detector, the responsivity is given by

$$R(\lambda) = \frac{\eta(\lambda)}{E_p} G \quad \text{units (A/W)} \quad (39)$$

where

$\eta(\lambda)$ is the quantum efficiency of the excitation process as a function of wavelength

E_p is the photon energy in eV

G is the gain in the detector.

Figure 2-14 shows the responsivity and quantum efficiency for several photoemissive surfaces that are commonly used in photomultiplier tubes. The cesiated III-V semiconductors are a relatively recent development that could have considerable performance impact in future multispectral scanners because of their high quantum efficiencies. The highest quantum efficiencies shown in Figure 2-14 are about 40 percent. The quantum efficiency of PMTs can be increased by use of antireflection coatings and multiple pass optical techniques.

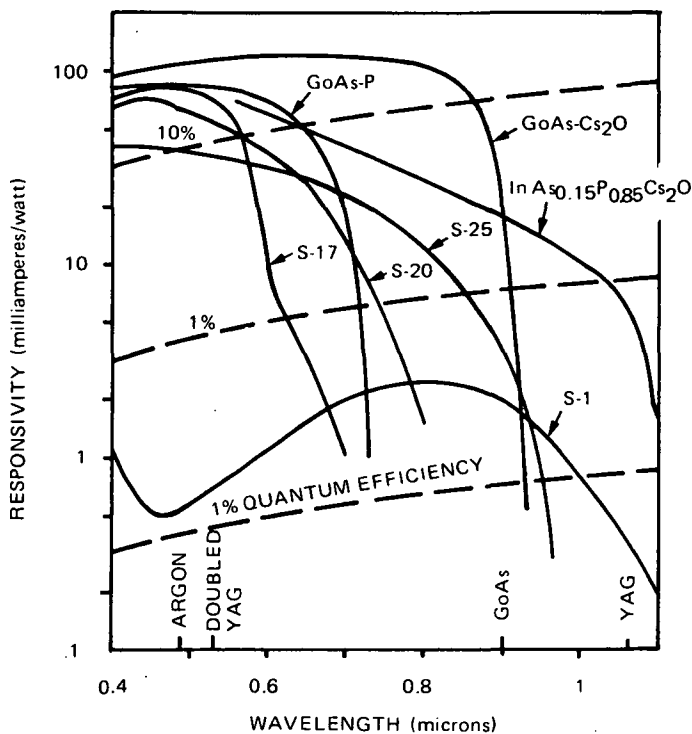


Figure 2-14. Wavelength dependence of responsivity and quantum efficiency for several high efficiency photosurfaces

Figure 2-14 shows typical quantum efficiency and responsivity characteristics for various uncoated photodiodes and photoconductive devices. All detectors are arbitrarily shown for $G = 1$; the general trend to higher responsivities at longer wavelengths is a result of the decrease in photon energy in the denominator of Equation (30). For the detector materials

shown, the technology is efficiently advanced to achieve peak internal quantum efficiencies of about 80 percent. The difference between that value and the curves shown in Figure 2-15 is the front surface reflection loss due to the high refractive index of the semiconductors. The reflection loss can be substantially reduced by use of antireflection coatings.

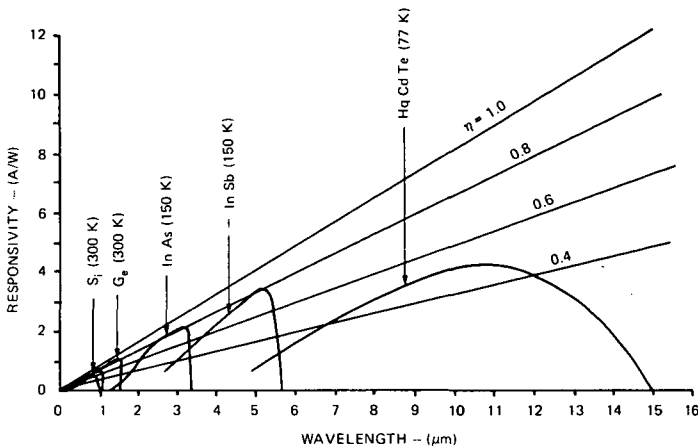


Figure 2-15. Quantum efficiency and responsivity characteristics for uncoated photodiodes and photoconductive devices

Photoconductive Gain

In a photoconductive detector, the conductivity of the element is determined by the incident optical power, whereas the signal current is determined by both the conductivity and the applied bias voltage. Under certain conditions this leads to photoconductive gain which is characterized by more than one electron delivered at the detector terminals for each photon absorbed in the detector.

In the case of extrinsic photoconductors such as Ge:Hg the photoconductive process involves one free carrier and an ionized impurity level. The photoconductive gain is given by the ratio of the lifetime and transit time of the free carrier. Gain increases with bias voltage due to the decrease in transit time with increasing electric field.

Intrinsic photoconductors such as HgCdTe show two-carrier photoconductivity. In this case, both holes and electrons are swept out of the

detector by the applied bias, and the photoconductive gain is limited by the ratio of the transit times of the two carriers. Thus, HgCdTe, which has a high mobility ratio, is useful as a photoconductor, whereas PbSnTe, which has equal hole and electron mobilities, is used primarily in p-n junction photodetectors.

Noise Sources

Each of the detector types discussed in this report has unwanted noise sources that are peculiar to its structure and mode of operation. In addition, all photodetectors produce noise in response to a steady background irradiance. A photodetector is said to be background limited when noise due to the background irradiance is the dominant noise source in the detector. Background limited noise represents the best noise performance that can be achieved with a given system configuration. In multispectral scanner systems, the common use of extensive cold shielding and narrow-band cold filters on the long wavelength channels reduces the background irradiance at the photodetector and makes it difficult to obtain background limited noise performance. Thus, multispectral imaging systems may present a greater challenge to infrared photodetector technology than do the more common terrestrial IR viewing and mapping systems.

Shot Noise. P-N junction photodetectors and photoemissive surfaces produce full shot noise on the background photocurrent. The mean square noise current can be expressed by

$$i_n^2 = 2q\Delta f I_B \text{ units (A}^2\text{)}, \quad (40)$$

where

q is the electronic charge

Δf is the noise bandwidth

I_B is the background photocurrent.

The background photocurrent is produced by the absorbed background photon rate and is given by

$$I_B = qQ_{\Delta\lambda}\eta_{\Delta\lambda}A_D \text{ units (A)}, \quad (41)$$

where

q is the electronic charge

$Q_{\Delta\lambda}$ is the background photon flux rate in the wavelength interval $\Delta\lambda$

$\eta_{\Delta\lambda}$ is the average quantum efficiency in the wavelength interval $\Delta\lambda$

A_D is the optically active area of the detector.

Photomultiplier tubes are normally used in applications where most of the irradiance falling on the photoemissive surface is due to sunlight reflected from the earth's surface and the atmospheric backscatter produces an appreciable unwanted background photon flux that results in background limited noise performance in the PMT channels.

In fluorescence spectroscopy where very narrow spectral bands are used ($\Delta\lambda = 3\text{-}5$ Angstroms) the background photocurrent may become negligible. Under these conditions the dominant noise source in a PMT is shot noise on the dark leakage current, I_D , given by

$$i_n^2 = 2q\Delta f I_D \quad \text{units (A}^2\text{)}. \quad (42)$$

In this case I_D is produced by thermionic emission of electrons from the low-work function photocathode. Dark current can be reduced to an extremely low value by cooling the photoemissive surface. In many PMT systems, it is possible to count individual electrons emitted from the photocathode.

Reverse biased p-n junction photodetectors also produce full shot noise on the dark leakage current as shown in Equation (42). For most p-n junctions at or below their normal operating temperature, the dark leakage is due to the presence of recombination centers in the depletion region at the surface of the junction. This causes the dark leakage to be proportional to the junction perimeter and to have a temperature dependence associated with the band gap.

Since the dark leakage current of most p-n junctions is a function of bias voltage, there is usually an optimum bias voltage for minimum noise.

Generation-Recombination Noise. Photoconductive detectors produce generation-recombination (G-R) noise in response to a steady background irradiance. Hole-electron pairs are generated randomly by the absorption of incident photons and in extrinsic photoconductors recombine

randomly by a statistically unrelated process. Thus, full G-R noise corresponds to twice shot noise on the absorbed background photon rate expressed as a primary photocurrent. The mean square noise current at the terminals of an extrinsic photoconductive detector is

$$i_n^2 = 4q\Delta f I_B G^2 \text{ units (A}^2\text{)}. \quad (43)$$

where G is the photoconductive gain, and the other symbols have been previously defined.

The dc response at the detector terminals, I_ϕ , produced by $Q_{\Delta\lambda}$ is

$$I_\phi = I_B G \text{ units (A)}. \quad (44)$$

Thus, the mean square noise current in Equation (43) becomes

$$i_n^2 = 4q\Delta f I_\phi G \text{ units (A}^2\text{)}, \quad (45)$$

which is $2G$ times greater than shot noise on the current response at the detector terminals, I_ϕ .

For intrinsic photoconductors such as HgCdTe, the noise current at low bias voltages is given by Equations (43) and (45). As the dc bias is increased, a voltage is reached at which the minority carrier (hole) transit time is less than the lifetime. At this bias, the carriers are swept out of the device before they recombine and the G-R noise approaches shot noise on the primary photocurrent given by

$$i_n^2 = 2q\Delta f I_B G^2 \text{ units (A}^2\text{)}. \quad (46)$$

In terms of the dc response at the detector terminals given in Equation (44), this becomes

$$i_n^2 = 2q\Delta f I_\phi G \text{ units (A}^2\text{)}, \quad (47)$$

which is G times greater than shot noise on the current response at the detector terminals, I_ϕ . The bias voltage that gives carrier sweep-out also results in the saturation of the photoconductive gain at the limiting value determined by the mobility ratio. Signal and noise currents as a function of the dc bias field are shown in Figure 2-16 for a HgCdTe photoconductive detector with a cutoff wavelength of $4.8 \mu\text{m}$ operated at a temperature of 150 K.

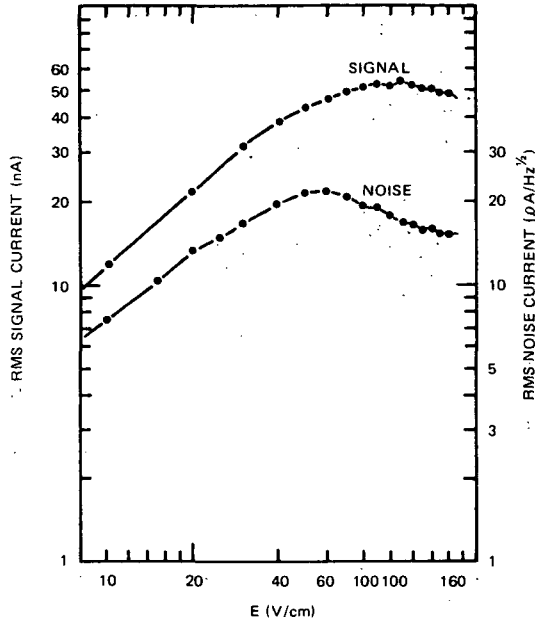


Figure 2-16. Blackbody response at 900 Hz and noise at 10 kHz vs electric field. Noise bandwidth ≈ 3 Hz. Sweep out leads to saturation of both quantities and increases the signal-to-noise ratio by ≈ 2 over the low-field value

When a biased photoconductor is completely cold shielded, there is a thermal G-R noise term which remains. This thermal G-R noise current results from conductivity changes (under bias) produced by the random generation and recombination associated with maintaining the thermal equilibrium carrier densities at the detector temperature. Thermal G-R noise also depends on the lifetime of the detector material and an analytical expression requires detailed knowledge of the recombination mechanisms. For a given detector the mean square value of thermal G-R current is proportional to G^2 .

When extensive cold shielding and/or cold filtering is used on present HgCdTe photoconductors, thermal G-R noise can be the limiting noise source. It can be reduced technologically by eliminating recombination

centers from the detector material or by cooling the detector to a lower operating temperature.

Thermal Noise. Johnson-Nyquist noise or thermal noise is frequently present in photodetectors, and in some cases can be the dominant noise source. However, great care must be used in the assignment of thermal noise sources.

In properly biased PMTs, thermal noise sources can usually be ignored.

Reverse biased silicon photodiodes exhibit an incremental shunt resistance due to the dependence of the dark current on bias voltage. However, this reverse bias shunt resistance should always be treated as noiseless because the total noise is already accounted for by the shot noise on the dark leakage current. Since many photodiodes show an increase in responsivity with reverse bias, a steady background irradiance will give rise to an incremental shunt resistance. The value of this resistance should be treated as noiseless since the total noise is accounted for by the shot noise on the background photocurrent I_B .

Some p-n junction photodetectors have surface inversion layers which give rise to a true "ohmic" conduction path in parallel with the diode. In this case the inversion layer resistance, R_I , exhibits full thermal noise given by

$$i_n^2 = \frac{4kT_D \Delta f}{R_I} \quad \text{units (A}^2\text{)}, \quad (48)$$

where

k is Boltzmann's constant

T_D is the detector temperature.

This undesirable inversion layer resistance is most often encountered in long wavelength photodiodes, and this resistance has been essentially eliminated by recent technological advances.

At zero bias, the dark leakage current of a photodiode is exactly cancelled by an equal and opposite diffusion current. Because of this, a perfectly cold shielded (thermal equilibrium) p-n junction has zero current at zero voltage. Since the dark leakage current and diffusion current

are statistically unrelated, both components contribute full shot noise; the total noise at zero bias is therefore given by

$$i_n^2 = 4q\Delta f I_D \quad \text{units (A}^2\text{)}. \quad (49)$$

The exponential shape of the diffusion current gives a zero bias diode resistance, R_D , of

$$R_D = \frac{kT_D}{qI_D} \quad \text{units } (\Omega), \quad (50)$$

combining Equations (49) and (50) gives

$$i_n^2 = \frac{4kT_D \Delta f}{R_D} \quad \text{units (A}^2\text{)}, \quad (51)$$

which is full thermal noise on the zero bias diode resistance at thermal equilibrium. Many infrared photodiodes show a background sensitive incremental resistance due to the voltage dependence of the responsivity discussed above. Thermal noise should only be attributed to the dark or thermal equilibrium value of the diode resistance; the noise of the background dependent resistance is completely accounted for in the shot noise expression in Equation (41).

For an ideal photodiode, the mean square noise current due to I_D is reduced by a factor of two by reverse biasing the diode; compare Equations (42) and (49). However, many practical photodiodes show a rapid increase in I_D with reverse bias. Because of this, the best infrared photodiode signal-to-noise ratio (S/N) is usually obtained at zero bias or at a small reverse bias.

In the past some infrared photodiodes have shown a tunneling breakdown at zero bias due to the presence of strong surface inversion. This tunneling resistance shows full thermal noise at zero bias. However, in this case the best S/N can occur at a small forward bias where the tunneling current is near zero. This tunneling noise should not be a significant problem in the future because improved detector technology will offer better control of the surface inversion layers.

In extrinsic photoconductors, the major portion of the conductance of the detector is produced by the background response of the detector. This portion of the detector conductance produces full thermal noise in addition to the G-R noise.

Intrinsic photoconductors, such as HgCdTe, show an appreciable conductance at thermal equilibrium. Full thermal noise on this conductance is present but is not normally one of the major unwanted noise sources in these detectors. Present HgCdTe purification techniques leave the basic material n-type with a typical sheet resistance of 20-25 Ω /square for 8-14 μ m material at 77 K. Future advances in the technology of this material system will result in lower free-carrier concentrations, and higher detector resistance. This direction of advance is desirable because it will reduce the problems at the detector/pre-amp interface.

1/f Noise. The term 1/f noise is the name given to a wide range of phenomena that produce a noise power spectral density that varies approximately as 1/f. Thus, the 1/f mean square noise current per Hz bandwidth has the general form

$$\frac{i_n^2}{\Delta f} = K \frac{I_o^a}{f^b}, \quad (52)$$

where

k is a proportionality factor

I_o is the current associated with the noise

a is a constant (often $a \approx 2$)

b is a constant ($b \approx 1$).

The factor varies widely for different types of devices, and only slightly less for different devices of the same kind.

In different device types, 1/f noise has been called "flicker" noise, "contact" noise, and "current" noise; all semiconductor devices and many other electronic components generate 1/f noise.

In photodiodes and photoconductive detectors, 1/f noise is most often related to surface state density and trapping at surface states. Because of this, 1/f noise in a given type of semiconductor device tends to decrease and become more predictable with advances in the technology of passivation and stabilization of the surface of that semiconductor. At the present time, silicon surfaces passivated with thermally grown SiO_2 offer the lowest surface state densities and best surface control of any semiconductor. The silicon surface is also the best understood from a theoretical

standpoint. Other semiconductors used in photodetectors employ technologies that rely on exposed surfaces or foreign dielectrics deposited on the surface. Theoretical understanding of these surfaces has developed much more slowly than for silicon and most progress has been of an empirical nature.

The best semiconductor photodetectors typically show $1/f$ noise corner frequencies of 100 to 500 Hz, with the control being better for the more established semiconductors.

Excess noise in PMTs normally results from a different set of phenomena than for semiconductor detectors. Two of the most common causes of nonwhite noise in PMTs are loss of vacuum in the tube and response to spurious light generated by corona discharge on the outside of the tube. These noise sources can be controlled by adequate testing and use of proper design techniques.

Noise Equivalent Power

In satellite multispectral scanner systems, it is customary to characterize the S/N performance of the short wavelength detectors that respond principally to reflected sunlight in terms of noise equivalent power (NEP). NEP is usually defined as the rms value of the fundamental component of periodically modulated optical power that will produce an rms signal current at the detector terminals equal to the rms noise current for a noise bandwidth of 1.0 Hz. The equation for NEP can be written

$$\text{NEP} = \left[\frac{i_n^2}{\Delta f} \right]^{1/2} \frac{1}{GR_\lambda} \quad (53)$$

where the units of NEP are $\text{W} - \text{Hz}^{-1/2}$. The noise current in Equation (53) includes the effect of all background and detector noise sources. By convention NEP is used as a figure of merit to compare detectors. In this context, noise sources in the first amplifier stage are excluded from detector NEP. While Equation (53) contains no explicit area dependence, the NEP is a function of detector area through I_n . For a typical silicon photodiode at room temperature, I_D is proportional to the junction perimeter; thus, NEP varies as $A^{1/4}$. For a PMT at room temperature, I_D is proportional to the area of the photocathode and NEP varies as $A^{1/2}$.

Detectivity

The longer wavelength channels in MSS systems respond principally to the thermal environment and detect differences in the temperature and/or emissivity of the surface being scanned. Because of the large background noise that is typically present in this wavelength region, the S/N performance of detectors is characterized in terms of detectivity, D^* . D^* is related to NEP by

$$D^* = \frac{A_D^{1/2}}{NEP}, \quad (54)$$

where the units of D^* are $\text{cm} - \text{Hz}^{1/2} - \text{W}^{-1}$. From Equation (54) the detectivity at a specific wavelength D_λ^* may be written:

$$D^* = GR \left[\frac{i_n^2}{A_D \Delta f} \right]^{-1/2}, \quad (55)$$

where $i_n^2/\Delta f$ is the noise measured at the detector terminals. When the detector is background limited and for some detector-limited photodiodes, the term in brackets is independent of area. Thus, in many cases of practical significance, the explicit occurrence of A_D in Equations (54) and (55) renders the value of D^* independent of area. When D^* is used to compare detectors, it is customary to include background and detector noise sources, and exclude amplifier noise.

The mean square noise current in Equation (55) is a function of the background irradiance falling on the detector. Thus, when D^* values are given, it is also necessary to define the applicable background temperature, cold shielding, and cold filtering. The presence of $1/f$ noise and other frequency effects also make it necessary to specify the signal frequency with D^* .

Figure 2-17 shows typical measured D^* values for most of the available photodetectors of interest to multispectral scanner system designers. The measurement conditions are:

Frequency:	1000 Hz
Cold shielding:	none
Cold filtering:	none
Background temperature:	300 K

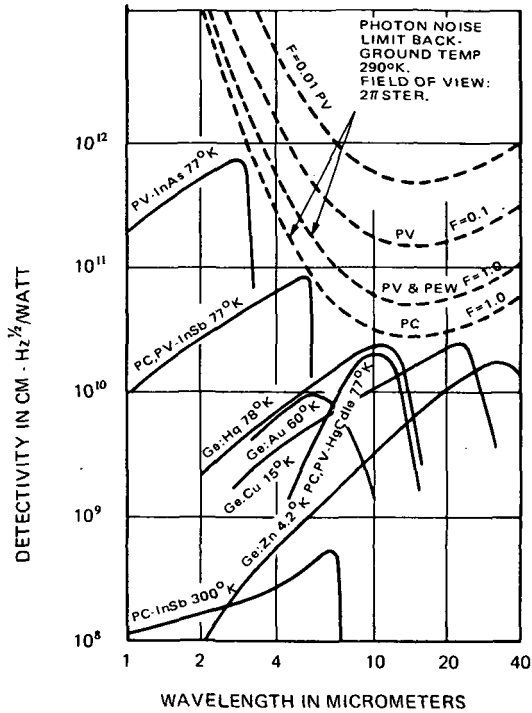


Figure 2-17. Spectral dependence of detectivity for photoconductive and photovoltaic infrared detectors

Theoretical curves of peak D^* for ideal photodiodes and photoconductors are also shown in Figure 2-17. The ideal curves assume 100 percent quantum efficiency and background limited performance for the conditions listed above.

Multispectral scanners typically employ significant cold shielding and cold filtering which reduce the background irradiance falling on the detector. Theoretical curves of background limited peak D^* for ideal photodiodes at reduced background are also shown in Figure 2-17. The parameter F is the fraction of full background irradiance and is given by

$$F = \sin \theta \frac{H_{\Delta\lambda}}{H_T}, \quad (56)$$

where

θ is the half angle of the cold shield

$\frac{H_{\Delta\lambda}}{H_T}$ is the fraction of background irradiance passed through the cold filter.

For cold shielding to be most effective, the cold shield aperture should be as far as possible from the surface of the detector. Some optical systems and scanning techniques are more easily cold shielded than others. Because of this, cold shield considerations can be a major factor in the design of a multispectral scanner system. With discrete detectors, careful cold shielding can yield a value of θ only slightly larger than the half angle of the optical system. Linear detector arrays are more difficult to cold shield; because of the high aspect ratio of long arrays, effective cold shielding is usually possible only in the plane perpendicular to the length of the array. Unless special precautions are used, the detectors near the ends of a long array will have better cold shielding than those near the center of the array and the D^* for each element will be dependent on its location in the array.

The use of cold shields and cold filters on infrared detector channels reduces the background noise current and therefore improves D^* . However, in most cases other noise sources such as thermal noise, thermal G-R noise, $1/f$ noise, and amplifier noise are not dependent on I_B . Thus, a particular detector technology may be capable of producing background limited detectors for the conditions of Figure 2-17 for $F = 1$. However, when F is reduced to the value encountered in a practical system the detectors produced by that technology will fall short of the background limited performance indicated in the figure. Continuing improvement in infrared detector technology will result in detectors which maintain background limited performance with increasing amounts of cold shielding and cold filtering.

A comparison of Equations (39) and (55) shows that D_λ^* is a monotonic function of quantum efficiency. Thus, with quantum efficiency less than 100 percent, it is possible to have a peak D_λ^* that is considerably lower than the appropriate theoretical curve in Figure 2-17 and still have background limited detector performance. In the background limited range, D_λ^* is proportional to $\eta^{1/2}$, while in the detector limited range D_λ^* is proportional to η .

Based on the above discussion, two important parameters that can be used to track progress in infrared detector technology are the value of peak D_{λ}^* , and the limiting value of cold shielding at which background limited performance can be achieved.

Speed of Response

The rise time of photomultiplier tubes is usually limited by velocity spreading and different path lengths for photoelectrons originating at different parts of the photoemissive surface. These effects cause small differences in the time of arrival of the electrons at the anode that result in a Gaussian output current pulse in response to a delta function optical input. The distance traveled by the electrons between the photocathode and anode gives rise to a uniform delay time between the optical input pulse and current output pulse. This fixed delay time is usually much greater than the rise time of the output current pulse. Rise times shorter than 30 ns are readily achieved in PMTs.

The rise time situation in silicon photodiodes is somewhat more complex because of the wide range of phenomena that can come into play at different wavelengths. In diffused-junction silicon photodiodes, there are three regions that must be considered separately:

- Undepleted diffuse layer at the surface
- Depletion Region
- Undepleted bulk material.

Optical energy falling on the surface of a detector is partially reflected due to the miss match in index of refraction. For an uncoated silicon-air interface at $0.9 \mu\text{m}$ and normal incidence, about 32 percent of the light is reflected and 68 percent is transmitted. This surface reflection can be reduced to a few percent by use of an antireflection coating on the silicon surface. The light transmitted into the bulk is absorbed exponentially with an absorption coefficient that is wavelength dependent. For short wavelengths ($\lambda \approx 0.4 \mu\text{m}$) the light tends to be absorbed in the undepleted surface layer.

The minority carriers generated by the photon absorption diffuse to the edge of the depletion region, and then drift across the depletion region under the influence of a high electric field. Typical diffused surface layers

have minority carrier transit times of less than 2 ns. In traversing the depletion region, the minority carriers move at close to the saturated drift velocity of $v_s \approx 10^7$ cm/s. Thus, the transit time is a linear function of the depletion region width. For an 80 μm depletion region, the transit time is about 1.0 ns.

As the wavelength of the input optical energy is increased, the absorption coefficient decreases so that a significant portion of the input photons are absorbed in the undepleted bulk silicon. The minority carriers generated by this process also diffuse to the edge of the depletion region, and then drift across the depletion region under the influence of the high electric field. However, in this case the rise time of the diffusion current is a complex function of the bulk lifetime. Typical rise times of the undepleted bulk portion of the detector response are 1-10 μs ; this is about three decades slower than the rise time of the other two regions. At a wavelength of 0.9 μm , a silicon detector with an 80 μm depletion region will respond to a square optical pulse by rising to 85 percent of the steady output current in less than 3 ns. The final 15 percent change in output current will take about 1 μs . For wavelengths longer than 0.9 μm , the detector structure described above will show a decrease in steady state output and an increase in the fraction of the total output having the slow response time.

Silicon detectors optimized for long wavelength operation ($\lambda \approx 1.06 \mu\text{m}$) use very lightly doped p-type silicon substrates ($\rho = 8,000 - 10,000 \Omega\text{-cm}$) with n-type diffused layers. The junctions are reverse biased to completely deplete the wafer—usually about 400 μm thick. The back of the wafer is normally covered with a mirror to reflect the transmitted light back through the active region of the photodiode. These devices show good quantum efficiency at 1.06 μm , and a rise time of less than 10 ns that is determined by the transit time of the depletion region.

Germanium photodiodes exhibit the full range of transient response phenomena described above for silicon. In the case of germanium photodiodes, the useful wavelength region extends from about 400 μm to 1500 μm . Germanium and silicon are both indirect semiconductors, and show a rather gradual change in absorption coefficient with wavelength.

The detector materials used for wavelengths longer than 1.5 μm are all direct semiconductors, and are characterized by an abrupt change in absorption coefficient with wavelength. The steep absorption edge and relatively short minority carrier lifetime tends to eliminate the occurrence of the slow bulk diffusion response in the direct semiconductors.

For example in InAs and InSb infrared photodiodes, the rise time is determined almost entirely by the response of the undepleted surface p-type layer that is diffused into the n-type substrate. Calculated values of the rise time of the short circuit current are typically less than 2 ns; however, the measured rise times are usually in the range of 0.1-0.5 μ s. The slow response in this case is attributed to the presence of a large density of electron traps in the diffused p-type layers.

HgCdTe photodiodes have been built from starting material with a range of bandgaps that cover the wavelength interval from 3.0 μ m to 15 μ m. These devices have shown good quantum efficiency and rise times of 10-100 ns. The rise time is background dependent.

Different material composition used in PbSnTe photodiodes have covered the wavelength interval from 5.0 μ m to 15 μ m. These diodes have been well behaved and have shown good quantum efficiencies and short circuit current rise times of 10-100 ns.

Another important material parameter that affects the speed of response of a photodiode is the static dielectric constant. With the exception of PbSnTe, all of the materials considered in this section have dielectric constants between 11 and 16.

The dielectric constant is important because it largely determines the junction capacitance at zero bias and therefore determines the high-frequency impedance of the photodiode. PbSnTe with a relative dielectric constant of 400-1200 is seriously handicapped in any application requiring operation above a few kHz.

DETECTOR COOLING SYSTEMS

Future infrared imagers and scanners for NASA applications will utilize cooled quantum or photodetectors. These detectors require cooling to cryogenic temperatures, i.e., below approximately 120 K to achieve background-limited performance.

In general, the long wavelength cutoff and detectivity, as well as other detector parameters, are determined by the operating temperature. Photodetectors operating in the 8-13 μ m atmospheric window require lower operating temperatures than those operating in the 3-5 μ m region. Intrinsic detectors, such as the ternary alloys, mercury cadmium telluride and lead tin telluride, can operate at higher temperatures than the extrinsic

detectors, such as doped germanium. For remote sensing applications, future imagers and scanners particularly those operating in the 8-13 μ m region, will utilize intrinsic photodetectors cooled to 100 K or below to achieve background-limited performance.

Within the next decade, it is anticipated that detector cooling requirements for airborne and spaceborne infrared systems will generally lie in the 50-120 K region with perhaps a few applications requiring temperatures as low as 20 K. The cooling capacity at these temperatures will range from a few milliwatts for a single photovoltaic detector to perhaps a watt for large arrays of photoconductive detectors.

At present, the technology associated with airborne detector cooling systems operating at 20 K and above is well advanced. Low-cost, closed-cycle refrigerators with maintenance intervals of 1,000 hours or more are currently available on an "off-the-shelf" basis. These refrigerator systems were derived from ground-based, cryogenic refrigerators where long system life based on regularly scheduled maintenance and low cost are the most important design parameters. Size, weight, and power consumption are of secondary importance. This existing technology, coupled with future developments being undertaken for advanced airborne reconnaissance missions, should provide an adequate technology base for future NASA airborne infrared imagers and scanners.

The current technology status for spaceborne cryogenic cooling systems is less advanced than in the airborne systems. While airborne systems have been in use for nearly 10 years, the first spaceborne system for providing continuous cryogenic cooling by use of a passive radiator was flown in 1972.

For space application, the important design parameters are system reliability based on maintenance-free operation for periods up to 20,000 hours, electrical power consumption, and system weight and size. The severity of the launch environment and operation at zero "g" conditions impose additional design constraints. These factors preclude the direct use of airborne cryogenic cooling technology in spaceborne systems. There is a technology base for spaceborne cryogenic cooling systems as a result of both NASA and DOD programs; however, considerable additional developmental work will be required to meet the needs of future advanced infrared imagers and scanners for NASA spacecraft.

Cooling System Design Criteria

The basic design parameters for a cryogenic detector cooling system are: the required operating temperature and temperature stability, heat load at the operating temperature, the alignment requirements of the cooled detector(s) relative to the optics, and the reliability and operating life of the system. Usually, the detector parameters (such as detectivity, spectral response, time constant, etc.) determine the operating temperature level. The heat load is mainly determined by the number and size of detectors and leads, total power dissipated at the focal plane, heat leak through the focal plane supports which position the detector(s) and the geometry of cooled baffles which may be used to achieve background-limited performance. Baffles and windows used to prevent contaminant condensation on cryogenically cooled surfaces also influence the heat load.

For spaceborne systems where weight and power are usually limited, the selection of a cooling system involves a detailed tradeoff between the detector and cooling system parameters for a given mission duration. Furthermore, the configuration and orbital parameters of the spacecraft have an influence on the selection of a cooling system.

The reliability and operational lifetime of spaceborne cooling systems are determined by both the degradation or failure of mechanical and electronic parts, by potential long-term degradation from contaminants which may be cryodeposited on critical optical and thermal surfaces, and by the system mass.

Description of Cooling Systems

System Types

Three basic types of cooling systems were considered in the panel efforts:

- Passive radiators for spaceborne system which cool detectors by direct radiation to the low-temperature sink of deep space.
- Open-cycle systems which use fluid or solid cryogens stored in a dewar, or stored high-pressure gas which provides refrigeration by the Joule-Thomson effect. Solid cryogens are only applicable to spaceborne systems.

- Closed-cycle systems employing a mechanical refrigerator using helium gas as the working fluid or closed-cycle Joule-Thomson systems.

Solid-state thermoelectric devices can be used for detector cooling. Multiple-stage thermoelectric coolers are, however, limited in application to systems requiring cooling above 150 K. Because of this inherent limitation, this discussion will be limited to passive radiators, open-cycle and closed-cycle systems.

For airborne application, open-cycle systems, using liquid cryogenics stored in a dewar, or closed-cycle refrigerators are the only logical system choices. Open-cycle systems using liquid nitrogen or liquid helium have been used to cover the temperature range from 4.2 to 70 K. These systems are relatively simple, low in cost, have good temperature stability and do not introduce mechanical vibration or microphonics to the focal plane. They are capable of providing continuous refrigeration for the duration of a single aircraft flight without resupply. Closed-cycle refrigerators eliminate the problem of refilling cryogenic dewars and, therefore, reduce operational complexities. The various closed-cycle systems applicable to airborne systems will be discussed in more detail in the following paragraphs.

System choices for spaceborne application are less obvious. Because of the importance of weight, power and maintenance-free operation, each application must be examined to determine an optimum cooling system. Some of the salient characteristics of passive radiators, open-cycle and closed-cycle systems suitable for spaceborne cooling are summarized in Table 2-5.

Passive Radiators

Conceptually, the simplest way of developing cryogenic temperatures in space is to radiate power to the low-temperature heat sink of space by use of a suitably sized emitting surface. This concept is particularly attractive since such a system is completely passive, requires no continuous electrical power, and is potentially capable of high reliability for extended periods. Considerable effort has been devoted toward the design of passive radiators to maintain the temperature of detectors in electro-optical systems at temperatures in the 70-120 K region, and several such systems have flown.

Table 2-5

Characteristics of Spaceborne
Cooling Systems

Passive Radiators

Characteristics

- Simple and lightweight
- No continuous power requirement
- Limited temperature and heat load capacity
- Require proper orbit orientation and spacecraft location
- Indefinite life possible
- Prone to contamination degradation
- No detector microphonics

Applications

- Temperatures above 50 kelvin
- Geosynchronous or sun-synchronous orbits
- Heat loads <100 mw (present technology)
- Long missions

Open-Cycle Systems

Characteristics

- Wide temperature range (10-150 kelvin)
- Relatively simple
- High weight and volume limited in watt-hours of refrigeration
- No power required
- No detector microphonics
- Systems vent gas continuously
- No attitude control, orbit or location constraints
- Safety must be considered
- Detector alignment dependent on low-conductance supports

Applications

- Low heat loads
- Short to intermediate length missions
- Non-oriented vehicles

Table 2-5 (Continued)

Characteristics of Spaceborne
Cooling Systems

Closed-Cycle Systems

Characteristics

- Complete coverage of temperature and heat load range
- Complex
- Require power and heat-rejection system
- May introduce detector microphonics
- System weight and power strong functions of load temperature

Applications

- Low temperatures with relatively large loads
- Long missions (to 3 years)
- Provide refrigeration at 2 temperature levels

The effective temperature of the star-speckled sky is less than 10 K. A suitably sized cold plate of high emittance to which one or more detectors are mounted can be made to radiate to this sink. It is, of course, necessary to shield the cold plate against heat inputs from the sun, the earth, and the spacecraft. These considerations usually result in a radiator design which is tailored to a particular spacecraft system. The orbit plane, orbit altitude, and the location of the radiator on the spacecraft all significantly influence the design of the radiator.

A typical passive radiator design is shown schematically in Figure 2-18. The assembly consists of a conical outer stage mounted to the optical instrument with low-conductance supports. The outer stage supports a disc-shaped, inner, low-temperature stage, also mounted with low-conductance supports. The cooled detectors are mounted on the low-temperature stage.

As shown in Figure 2-18, the inner stage has a clear-field-of-view to deep space. To achieve low inner-stage temperature, the clear-field-of-view is made as large as possible—usually limited only by geometrical considerations prescribed by the orbit and the location of external appendages on the spacecraft.

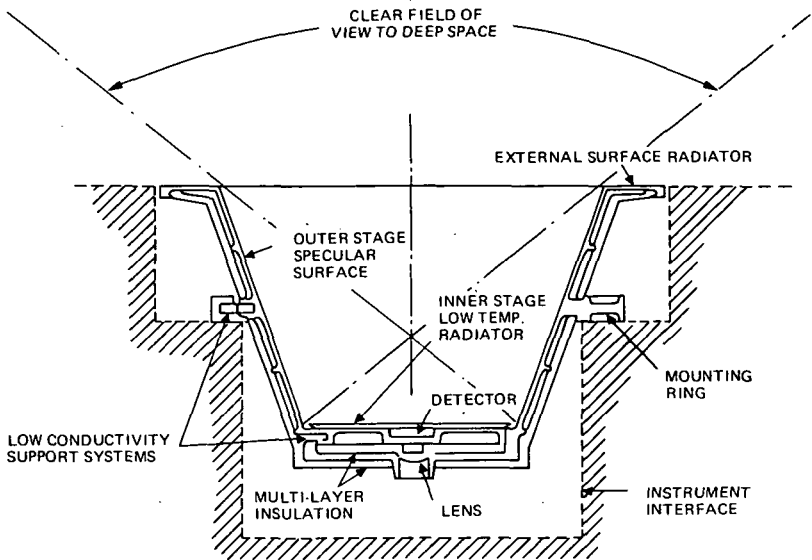


Figure 2-18. Schematic diagram of a passive radiator

Although passive radiators are simple in principle, there are several important design problems associated with the development of flight hardware. The design of the support system is critical since it must support the low temperature stage with an extremely low thermal conductance and must maintain the detector in precise alignment with the room-temperature optical instrument.

Another fundamental design problem is that of preventing contamination of low-temperature optical surfaces, such as detector capsule windows, by outgassing from either the spacecraft or the radiator itself. Contaminants on the low-temperature surfaces can affect the optical signal throughput to detectors, and can also influence the detector operating temperatures by altering the emittance, solar absorptance, or specularity of critical thermal control surfaces. Current design practices are based on using protective covers and heaters to prevent contamination during prelaunch, launch and initial orbital operation.

Several passive radiators have been flown on spacecraft, and approximately 10 additional units of various designs will be flown in the 1972-1975 time period. A single-stage passive radiator designed to operate at 175 K was flown on the Nimbus IV spacecraft (Annable 1970). This cooler attained the design temperature, but the infrared instrument did not operate properly due to contamination on the low-temperature optical surfaces. Flight results have been obtained with a two-stage passive radiator designed to operate in the 100 K region, with detector heat loads up to 10 mw (Gabron 1972). Flight data show that the passive radiator is operating below the design maximum temperature of 107 K after more than 5,000 hours of orbital operation. The data indicate the possibility of initial contamination of critical thermal control surfaces due to spacecraft outgassing.

Three-stage passive radiators are being used to cool infrared detectors on the Very High Resolution Radiometer (VHRR) instruments launched on ITOS-D in a near-polar, 45 degree, 1400 km earth orbit. A passive radiator is used to maintain the temperature of a single HgCdTe detector at approximately 106 K using a proportional control heater on the cold patch of the passive cooler. After initial orbit insertion, the passive radiator was maintained above 200 K for approximately one week to minimize the possibility of forming condensates on critical optical surfaces during the initial outgassing period of the spacecraft. Over the first month of operation no significant changes in thermal performance were observed.

The size and weight of a passive radiator are determined by the desired operating temperature of the detector, the sum of the detector heat load and parasitic heat inputs to the low-temperature stage, and the clear-field-of-view to deep space. Passive radiators designed to maintain detectors in the 85-110 K region, with up to 10 milliwatts of detector heat load, typically weigh 1.5 to 2.5 kg with volumes ranging from 10,000 to 100,000 cm³. Passive radiators currently in the hardware fabrication stage and those which have been flight qualified provide less than 10 mw of refrigeration at temperature levels from 85-120 K depending on the design. Design and preliminary testing of much larger passive radiator loads—up to 5 watts at temperatures in the 100-140 K region—are being undertaken.

Open-Cycle Systems

There are three types of open-cycle systems which can be considered for space cooling: Joule-Thomson (J-T) systems using stored-gas, stored-liquid

systems, and stored-solid systems. These systems are applicable only where the total amount of refrigeration measured in watt-hours is low, since the weight of this type of system precludes its use where large amounts of refrigeration over long periods of time are required. The attractive features of open-cycle systems are simplicity, reliability, and relative economy.

An open-cycle, J-T system consists of a counterflow heat exchanger, an expansion valve (or throttling orifice), and a gas bottle containing high-pressure, gaseous refrigerant. It is one of the simplest systems for cooling detectors, and therein lies its prime virtue. The refrigerant can be stored at ambient temperature for an extended period of time at no loss. Where a relatively small amount of refrigeration is required after an extended inactive period, a J-T system is very attractive. If the gas supply contains no impurities that can freeze out and plug the small passages in the heat exchanger or throttling valve, this system can be very reliable. The optical device can also be mounted at a distance from the gas-storage bottle and articulated with respect to this bottle.

Two-stage J-T coolers using stored gas were flown on two Mariner spacecraft to cool infrared detectors to below 25 K during a Mars fly-by mission. One system worked successfully, and one system failed.

Open-cycle systems using liquid cryogenics stored in conventional dewars have been used to cool infrared optical instruments in aircraft, sounding rockets, and balloons to temperatures below 4 K using liquid helium. Liquid neon and liquid nitrogen systems operating at 27 and 77 K, respectively, have also been successfully utilized. For spaceborne use it appears that stored cryogenics in liquid form will, in the near future, be restricted to missions where the refrigeration is required for short periods of time immediately following launch.

A major design problem with open-cycle liquid systems is to achieve the requisite thermal isolation in a sufficiently rugged dewar package. Extreme care with insulation systems and ingenuity in the design of mechanical supports are required to achieve the required thermal isolation. A further problem area with liquid systems is to determine the location of the vapor phase in the near zero-g environment, since it is necessary to vent only vapor in order to conserve refrigeration. Several schemes have been proposed for circumventing the vapor liquid separation problem, but none have been demonstrated, in a zero-g environment.

With liquid helium systems, a fairly straightforward method of ensuring that only vapor is vented is to increase the pressure in the dewar above the critical pressure so that only one phase exists in the storage vessel. A drawback of this approach is that the refrigeration is not supplied at a constant temperature, but rather the cooling temperature increases gradually with increasing time. Additionally, the cryogen utilization is not as complete as with a system using two-phase liquid helium. With cryogens other than helium, one way to avoid the liquid vapor phase separation problem is to utilize the cryogen in a solid rather than a liquid form.

In a solid-cryogen cooler, the detector is usually mounted on a pedestal which is thermally connected to a vacuum-insulated dewar containing a solidified cryogen. The ullage space above the stored solid is evacuated to maintain the cryogen in its solid state. Heat entering from the detector and the surroundings causes the cryogen to sublime, and the resulting vapor is vented. A solid-cryogen dewar comprises an inner vessel containing the cryogen, an insulation system, and a vacuum shell. A fill and vent tube permits initial filling of the cryogen vessel and venting of a vapor during operation. Auxiliary cooling lines, through which a liquid cryogen is circulated, are used during the filling operation and during prelaunch storage.

Depending on the application, a solid-cryogen cooler can offer several advantages over alternative systems. It offers a lower weight system compared with those using stored-liquid cryogens, since the latent heat of sublimation is greater than the latent heat of vaporization. Additionally, solid systems avoid the problem of location of the vapor phase under conditions of near-zero gravity.

There are several disadvantages to a solid-cryogen cooler in that it imposes restrictions on the detector mounting and, additionally, methane and hydrogen, both of which have excellent properties as solid coolants, are hazardous materials and require special handling.

The design problems for a solid-cryogen cooler are the same as for a liquid-cryogen storage dewar. The art and technology involved in the development of cryogenic dewar. The art and technology involved in the development of cryogenic dewars have application to the design of this cooler. Minimum parasitic heat leak is paramount. A great deal of ingenuity and technical sophistication must be applied to the design of low heat-leak structural supports and mounting arrangements for the inner vessel and the cooled component. Special operational needs, involving

filling procedures, standby requirements, control, and safety are also extremely important to the ultimate design.

The relative mass of stored solid cryogenics is shown in Figure 2-19. It can be seen that as the required cooling temperature decreases the mass of stored solid cryogen for an equal mission length increases rapidly.

The fact that the use of lower temperature cryogenics results in a significantly higher weight, plus the fact that the weight of the cryogen is critically dependent upon the temperature of the external shell of the dewar, has led to the use of dual cryogen systems for applications where low detector temperatures are required. Such a system results in lower cooler weight at the cost of increased complexity. In such a system, a higher temperature cryogen, such as ammonia, is used to cool a thermal shield which completely surrounds a lower temperature cryogen such as methane. A multilayer insulation system is placed between the shield and the outer shell of the cooler.

A solid methane/ammonia cooler, designed to cool a mercury-cadmium-telluride detector array to 65 K, is being developed for the Nimbus F limb-radiance inversion radiometer (Kollodge 1972). This system provides approximately 20 milliwatts of cooling for a one-year design life goal and will weigh approximately 53 pounds.

Due to the complex interaction of cryogenic properties and other design parameters on the weight of the solid-cryogen cooler, it is not possible to make meaningful, quantitative generalizations about the weight of solid-cryogen coolers. One can say, however, that for extended missions (for example, two years) that the weight of solid-cryogen coolers may be measured in hundreds of pounds unless shell temperatures are depressed significantly below approximately 250° K.

Because they require no power and can be built within the framework of present advanced technology, solid-cryogen coolers will probably see service during the next 5 to 10 years in specialized applications. These will include: where the heat loads are low; where detector temperature, orbital conditions, or other constraints preclude the use of radiators; and where mission durations are measured in months rather than years. It will be natural to look for efficient, compact, reliable, closed-cycle refrigerators to displace such coolers in many other applications. Ultimately, the use of solid-cryogen coolers will probably be confined to short- or intermediate-term missions with very low heat loads.

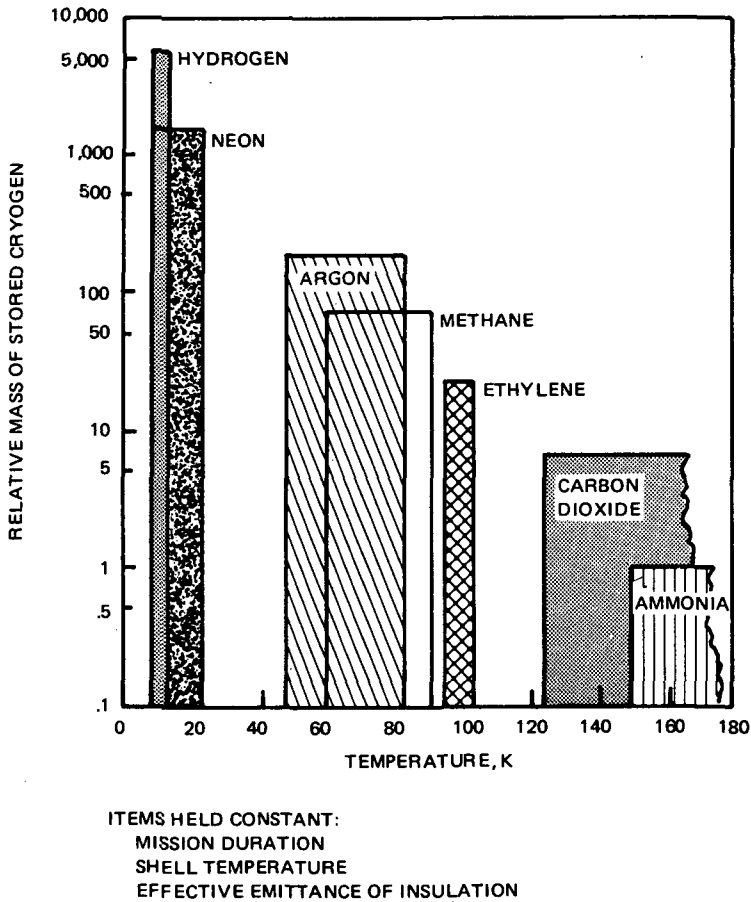


Figure 2-19. Relative mass of cryogen for solid cryogen coolers

Closed-Cycle Refrigerators

At the present time, there are a number of programs underway to develop closed-cycle refrigeration systems suitable for space applications. These systems require significant power and are certainly more complex than either passive radiators or open-cycle systems, but they will be necessary for higher heat load applications.

The basic elements of a closed-cycle refrigeration system are power supply, power-conditioning and control equipment associated with the

refrigerator, the refrigerator itself, and a heat rejection system. For refrigerators designed for electrical power input, the power supply will most likely be solar panels. The refrigerator power-conditioning equipment converts the raw bus power to the voltage and frequency required by the refrigerator, and modulates this power according to the needs of the refrigerator.

The heart of the system is the refrigerator itself, the purpose of which is to pump the heat from the load temperature up to the temperature of the space radiator. The heat load, plus all the energy put into the refrigerator, must be radiated to space by the heat rejection system. This system consists of a heat rejection radiator plus a means of transferring the heat generated in the refrigerator to the radiator. This heat may be transferred by conductive paths, heat pipes, or an active coolant loop in which a heat transfer fluid is circulated by a coolant pump.

There are two general classes of cryogenic refrigerators. The first are the so-called intermittent flow types, which use regenerative heat exchangers. There are three types in this class. Identified by the thermodynamic cycle on which they operate, they are Stirling cycle refrigerators, Gifford-McMahon cycle refrigerators, and Vuilleumier cycle refrigerators. Stirling cycle and Gifford-McMahon cycle refrigerators have been developed for ground-based and airborne applications, where they are presently being used in operational systems. The maintenance intervals of these systems are from 500 hours for the former, up to several thousand hours for the latter. It is doubtful whether these devices, as they are presently constructed for airborne use, can be made reliable enough to satisfy the requirements of space missions having durations of a year or more. At present, no effort is being made to develop a refrigerator utilizing either of these two cycles for extended space missions. However, several Stirling cycle refrigerators for infrared detector cooling will be flown on the SkyLab program where the required operational time is less than 500 hours.

The development of Vuilleumier (VM) cycle refrigerators for groundbased, airborne and spaceborne use has been underway for the past five years. VM cycle refrigerators are heat-driven derivatives of the Stirling cycle refrigerators (Prast 1969). The cycle is attractive for space use because of the potential for using solar or isotope thermal energy to drive the thermal compressor directly, thereby minimizing the electrical power input.

Current developmental programs in VM refrigerators indicate a potential for longer life than the Stirling or Gifford-McMahon systems currently

used in airborne applications. Since VM refrigerators employ bearings and seals, they are wear limited. It is anticipated, however, that continued development will lead to maintenance-free operation exceeding 5,000 hours.

The three systems utilizing regenerative heat exchangers have another limitation involving the minimum temperature which they can achieve with reasonable input power. Due to the characteristics of the heat transfer surfaces (regenerators) used in these refrigerators, refrigeration at temperatures less than approximately 20 K cannot be developed without extremely high power consumption; and temperatures below approximately 10 K may not be possible at all.

The second general class of closed-cycle refrigerators, the continuous-flow type, use counterflow heat exchangers. These units operate on the reversed Brayton thermodynamic cycle or derivatives of it. Refrigerators operating on the reversed Brayton cycle have been used in ground-based equipment for a number of years—mostly in relatively large-scale systems. Recently, efforts have been devoted toward developing reversed Brayton cycle refrigerators suitable for long-term space missions. The effort in these programs has been to scale down the size of existing systems, using an approach to the design of the mechanical elements that is inherently reliable. There are several programs underway to develop refrigerators of this type. One refrigeration system uses rotary-reciprocating machinery (Schulte 1965, Breckenridge 1968); and the other uses turbo-machinery (Gessner 1968, Maddocks 1968).

Extensive effort has been devoted to developing gas-bearing-supported machinery for these refrigerators, resulting in equipment which is inherently capable of extremely long life. The units must be considered developmental at this time, but they appear to be the only ones which are capable of meeting the life requirements of extremely long-term space missions; i.e., up to three years of unattended operation. Therefore, in spite of the rather wide-range cryogenic refrigerators used today, the number of systems which can meet the requirements of a long-term space mission is extremely limited.

The approximate input power requirements for various types of refrigerators are shown in Figure 2-20 for a heat load of 1 watt at various temperature levels. The data show the strong influence of load temperature on input power requirements. Stirling cycle refrigerators are efficient at higher temperature levels. At the 20 K temperature level, the Stirling and VM cycles become inefficient due to regenerator losses. The reversed

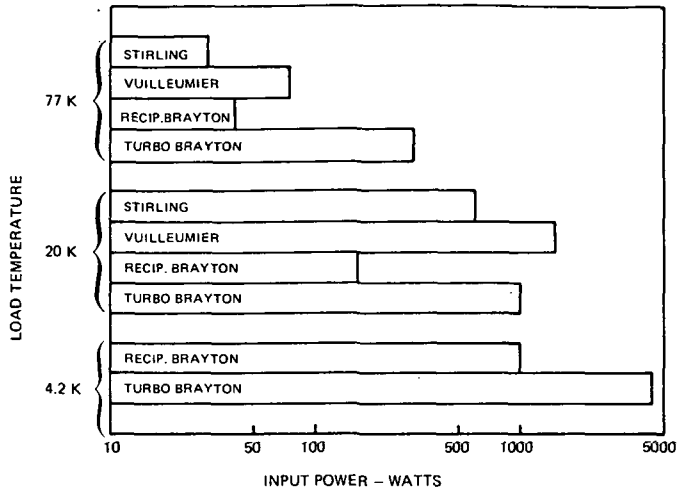


Figure 2-20. Refrigerator power requirements load capacity 1 watt

Brayton cycle systems utilizing high-speed turbomachines are inherently inefficient at the relatively small heat load level of 1 watt.

The weights of typical closed-cycle refrigerators as a function of input power are shown in Figure 2-21. It should be noted that the weights shown in Figure 2-21 do not include the electrical power system or the heat rejection radiator and associated plumbing. It is apparent from Figures 2-20 and 2-21 that, to minimize the weight and power consumption of spaceborne closed-cycle refrigerators, the highest possible temperatures and the lowest possible heat loads consistent with performance requirements should be used.

Current Status and Future Trends

Passive radiators for cooling loads of 10 milliwatts or less to temperatures in the 85-120 K region have been tested to flight acceptance levels. These systems have been designed for use in either near-earth sun-synchronous or geostationary orbits. Although orbital thermal performance is available for only two passive coolers operating in the 105 K region, a relatively large number of systems will be flown in the 1972-1975 time period.

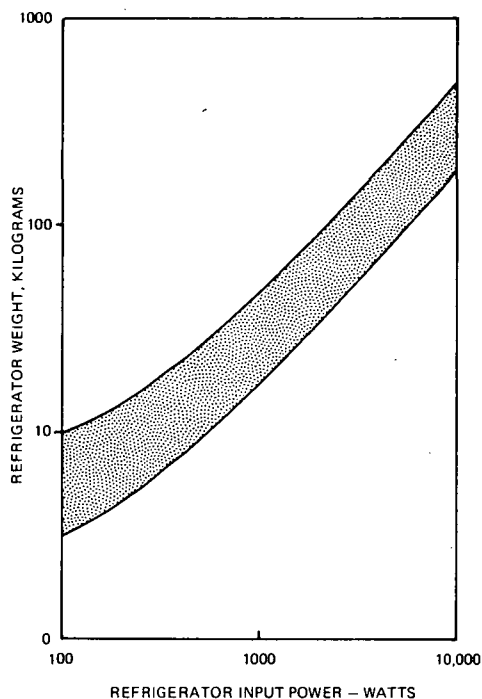


Figure 2-21. Weight of typical spaceborne closed cycle refrigerators

Very little is known about the long-term degradation of passive coolers in the space environment. Simulation tests of contamination of the low-temperature surfaces are difficult to make, and the data are not easily extrapolated to flight conditions. The effects of the space environment on specular coatings used on many passive radiators are not well understood. The efficacy of covers to protect cooler surfaces during launch and heaters which may be periodically used in orbit to "boil-off" contaminants are not known.

The flight experience to be gained in the next five years with a number of passive coolers should provide a reasonable technical base for the design of larger passive coolers having cooling capacities up to one watt. Larger radiators will be required to handle the increased power from detector arrays and the additional heat leaks associated with the focal plane structural supports required to provide more accurate detector alignment.

The last requirement will result from the need for improved spatial resolution in advanced imagers and scanners.

Open-cycle cryogenic cooling systems employing supercritical helium and solid cryogens are currently being tested for space applications. Only a few systems of spaceflight hardware design have been tested, and those have generally not met the design goals for operating life due to the difficulties associated with predicting the heat leaks through multilayer insulation systems and structural supports. It is anticipated that flight data will be available for several open-cycle systems in the 1972-1975 period. Open-cycle systems will have limited application for NASA advanced imagers and scanners because of the weight penalties associated with long-term cooling requirements.

Open-cycle systems using liquid cryogens will continue to be used on airborne systems. The simplicity, low cost, and wide temperature range available make open-cycle systems attractive for airborne systems.

Closed-cycle refrigerators for airborne systems are currently operational in the range of 20 to 77 K. Some improvements in the maintenance of the equipment and cost reductions will be made as a result of DOD programs; however, these factors will have little effect on the utility of the systems for NASA programs.

Stirling cycle refrigerators for spaceborne use have been developed and are available for missions in which the total operational time is 300-500 hours. They are efficient and lightweight for operation in the 77 K region with heat loads up to one watt. No significant improvements in the operational life of these systems are expected due to the design limitations inherent in the cycle.

Vuilleumier cycle refrigerators for spaceborne use are in the advanced development status. Systems presently in development will probably achieve a useful operating life an order of magnitude greater than Stirling cycle systems. Continued development over the next three to five years should result in an operational life of approximately one year. It is anticipated that VM refrigerators of the 1 watt at 77 K class will have application for future NASA programs.

The most probable areas of application of various spaceborne refrigeration systems are summarized in Figure 2-22. Passive radiators are applicable for small heat loads down to their lowest temperature limit. Solid-cryogen

coolers are also applicable for low heat loads, and can be used to reach temperatures below those achievable with radiators. Stirling and Vuilleumier cycle refrigerators are suitable in the important region of moderate heat loads at temperatures down to the point where regenerator inefficiencies limit performance. The upper boundary of this region is limited by machinery size. Reciprocating Brayton cycle refrigerators are applicable for low and intermediate heat loads at temperatures spanning the entire cryogenic region. The upper-capacity boundary of this region is determined by machinery size. Reversed Brayton cycle refrigerators employing turbomachinery will occupy the region of high heat loads over the entire temperature range.

The areas of overlap in Figure 2-22 are due to the developmental nature of the entire technology of spaceborne refrigeration. After systems have been developed further and more have been flown in spacecraft, their capabilities and limitations will be better identified, and the areas of application will become more clearly defined.

For a specific spaceborne instrument, the particular constraints of the instrument and parent spacecraft should be considered in detail before selecting the cryogenic cooler and specifying its interface with the instrument. The cryogenic cooling system must be considered at the outset of a project and its development carried on with the rest of the experiment if a well-balanced system is to result. In all probability, a cooling system will have to be designed specifically for the instrument which means that the cooling system is a major element. It also means that cost, lead time, and technical risk are all greater than for a ground-based or airborne system.

For future NASA imagers and scanners, it is anticipated that the detector cooling requirements for airborne and spaceborne systems will generally fall in the 50-120 K region. Cooling capacities will range from a few milliwatts to perhaps one watt.

The cooling requirements for airborne applications can be met with current technology using open-cycle stored-cryogen systems or mechanical refrigerators.

Many of the cooling requirements for spaceborne applications can probably be met with passive radiators. Current passive radiator systems are not large enough to handle the increased heat loads anticipated for larger detector arrays. Work should be initiated on design studies and engineering

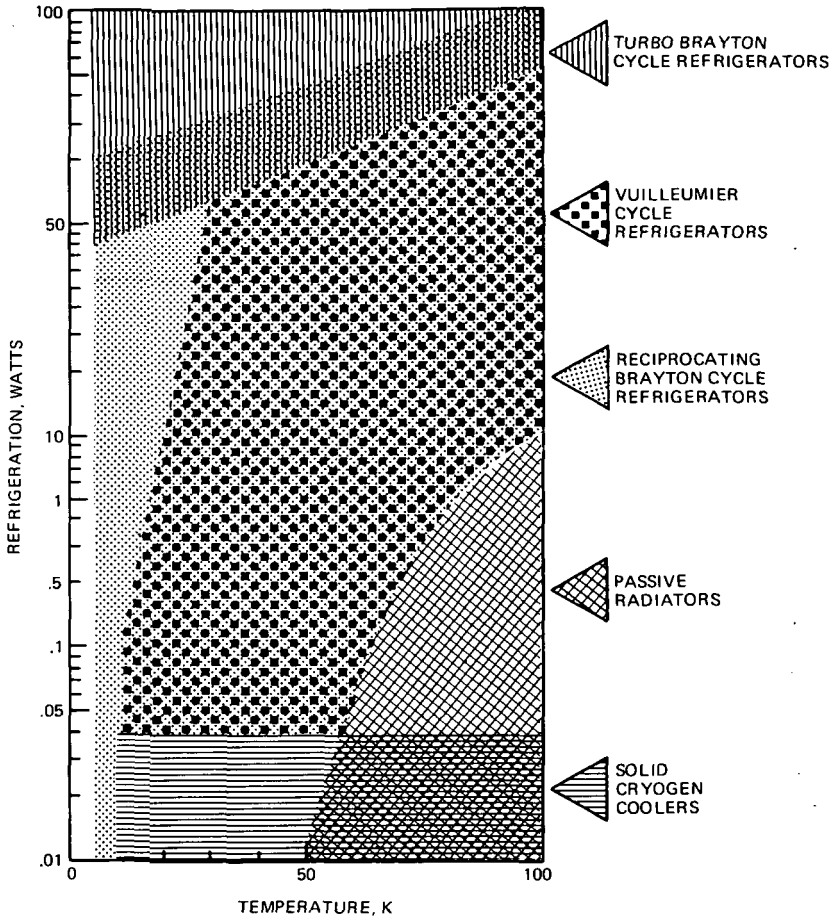


Figure 2-22. Most probable areas of application of various spaceborne refrigeration systems

model fabrication of a large passive radiator having a cooling capacity of approximately 1 watt at the 70-80 K temperature level.

Additional programs related to passive radiators should be initiated to determine the causes and effects of contamination of low-temperature surfaces and to develop appropriate methods to eliminate the problem.

An instrumented passive radiator flown as a separate experiment on a spacecraft should be considered for this purpose.

Limited applications for spaceborne open-cycle cooling systems are anticipated. This technology type of cooling systems may not be applicable for the one to two-year missions with focal plane heat loads which are expected to exceed 100 milliwatts. Technology development in this area should not be carried as a high-priority program.

Closed-cycle spaceborne refrigerators require additional developmental work to demonstrate their potential for missions of one to two years' duration. Because refrigerators can handle relatively large heat loads at any temperature level, they will find application in future cooling systems. The costs of developing spaceborne refrigerators are high; therefore, continued developments should be highly focused on one or two major programs. It is recommended that NASA developmental work on refrigerators be continued with greater emphasis than at present, on coolers having a capacity of approximately 1 watt in the 50-80 K region.

The use of space shuttle could have a significant impact on future cryogenic cooling systems. The maintenance and resupply capability provide opportunities for refilling open-cycle stored cryogen systems, use of on-board cryogen propellants, and in-orbit replaceable mechanical refrigerators.

OPTICAL SYSTEMS

Multispectral electromechanical scanning systems can be classified broadly as image space and object space scanners. The former requires an imaging system that covers the full field of view with the required resolution. The image is then scanned either by reading out each element of a two-dimensional mosaic, using a linear array that is as long as the field of view in one direction (which may be a swath perpendicular to the line of sight or an entire two-dimensional frame) and is scanned optically or mechanically in the other directions, or using a single detector to sequentially cover the whole field element by element. Of course intermediate numbers of detectors can be used. Object plane scanners take the load off the optical system and place it on the scanning system sequencing a narrow optical field of view. (The question of combining the two is considered in the chapter on scanners.) The point here is that both narrow field and wide field optical systems can be used.

Narrow-field optical systems usually include simple spheres, parabolas, Cassegrain, Newtonian, Ritchey Chretien and Dall-Kirkham systems. Their performances are compared in Figure 2-23*. The basic result is that, using the most expensive optical system (the Ritchey Chretien), one can obtain resolution of 0.02 mr for about 1 degree full field (17 mr) \times with $f/3$ optics.

Wide field systems, 10 degrees or more, are much more difficult to design and build. On the other hand, image plane scanning mechanisms are simpler to implement than object plane scanning, and are therefore of considerable interest. The performance of wide angle optical systems can be obtained by plotting the approximations of Warren Smith (Wolfe, 1965) and are summarized in Figure 2-24. Note that they do agree with the curves of Hummer where they can be compared. Also note that the Schmidt and Bouwers systems appear to be ones to use for half fields of view of greater than 6 degrees and resolutions of less than 0.1 mr.

The two main candidates for wide angle optical systems are the Schmidt system and the Bouwers-Maksutov system. The curves shown for their performance are only approximations, and should not be taken literally beyond about 15 degrees. They do provide resolutions on the order of 0.1 mr out to these angles, however. Both require refractive correctors that can be a limitation. The Schmidt plate is relatively thin with a mild aspheric. The Bouwers is generally thick with deep curvature. The front Bouwers shows better performance than the rear but is a less compact system.

In generating a wide-angle, all-reflective, high performance scanning system (which is often desired) one now can work variations on the theme. First of all one can make an all reflective Schmidt system. The idea is to use a 45 degree angle mirror folding flat with the reflecting analog of the Schmidt plate to preshape the wavefront as shown in Figure 2-25. This corrector will still have the off-axis aberrations of a standard Schmidt. One can spread the figure by adding a mirror. The corrector can also be used for scanning, but off-axis errors enter and their calculations are difficult.

Scanning Systems

It is difficult to even start to cover the performance of scanning systems because there are so many possibilities. This section includes some of the major and more interesting ones.

*Provided by R. Hummer, Santa Barbara Research Center.

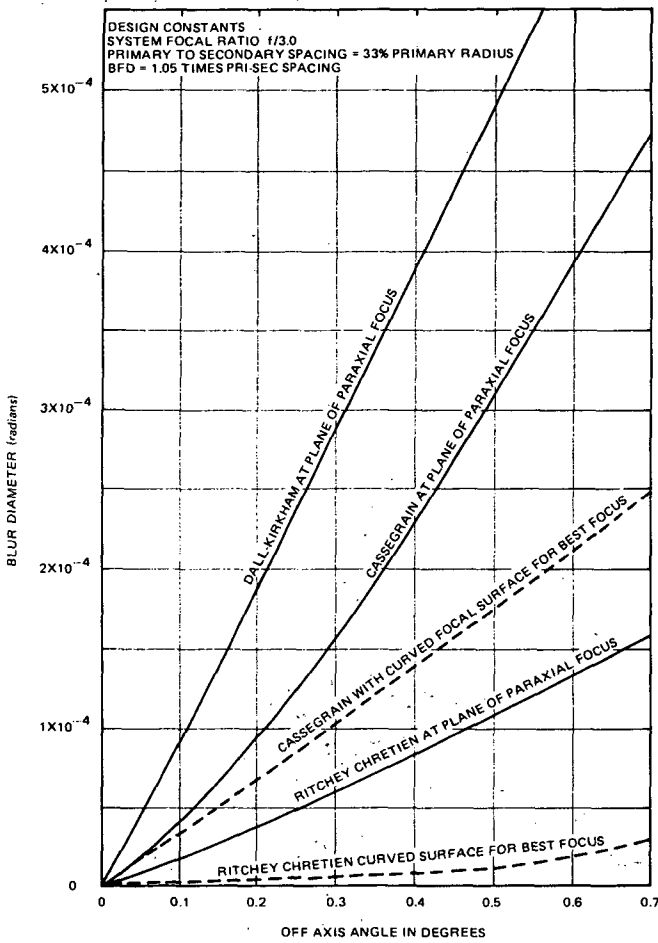


Figure 2-23. Comparison of off-axis image blur for a two-mirror optical configuration

45-Degree Folding Flat

Perhaps the simplest of the scanning mirrors is the 45-degree folding flat that moves the narrow field of a telescope by rotation (Figure 2-26). This type of scanning has been used on Nimbus and Tiros instruments. For near-earth orbits it has about 30 percent scan efficiency. Some of the dead time can be used for calibration purposes. One way to avoid reducing the dead time is to use a second collector and a two channel

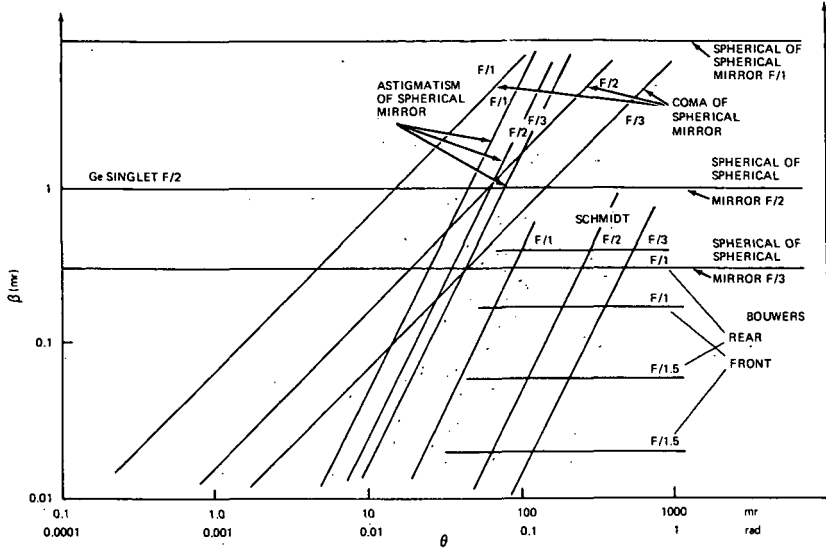


Figure 2-24. Approximate performance of various optical systems by either total blur or individual aberrations

system (Figure 2-27). This of course requires two expensive collecting mirrors. Another alternative is to use a wedge-shaped mirror for scanning (Figure 2-28). Now, however, the collecting mirror must be one-half the size of the scanner as shown, and there is crosstalk for all positions of the mirror except the one shown. Note the projection of the collector onto the flat is shown at the right. The system is designed so that the

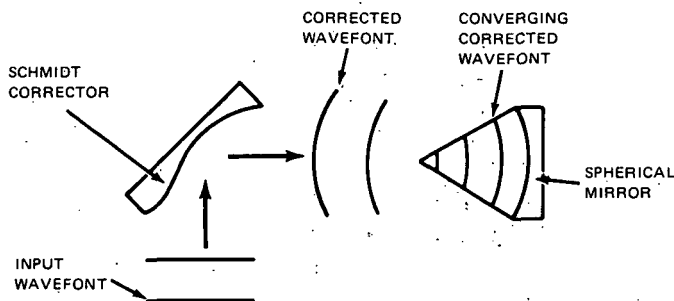


Figure 2-25. Wavefronts of an all reflective Schmidt system

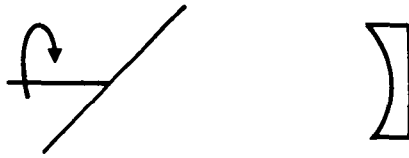


Figure 2-26. Scanning mirror—45° folding flat

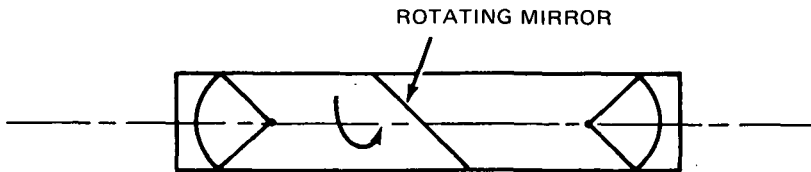


Figure 2-27. Two-channel system

collecting optics receives radiation from only one mirror surface over the desired scan angle. Otherwise, one obtains crosstalk as shown by the dotted projection of the scan optics in Figure 2-28. A four-sided wedge can be visualized for scanning smaller fields. It too gives scanning cross-talk as can be seen in Figure 2-29. Its size compared to the telescope aperture is even smaller.

Split Field Optical System

The Kennedy or split field optical system of Figure 2-30 is a better way. As drawn in Figure 2-30, it would appear that the collecting mirror must work at wide angles, but such is not the case. By carefully tilting and separating the outer mirrors, the system can cover almost 180 degrees with little loss in scan efficiency. There is crosstalk; there are no oscillating motions; and the aperture is almost that of the collecting mirror. Although the entrance pupil size can vary with scan position, this can usually be rectified with masks.

Another way to scan is with a reflecting polygon as shown in Figure 2-31. There is optical crosstalk with such a system. One can use a pair of optical focusing systems or a single one. Unfortunately such a scanning polygon gets large fast as the number of sides increases, as is necessary

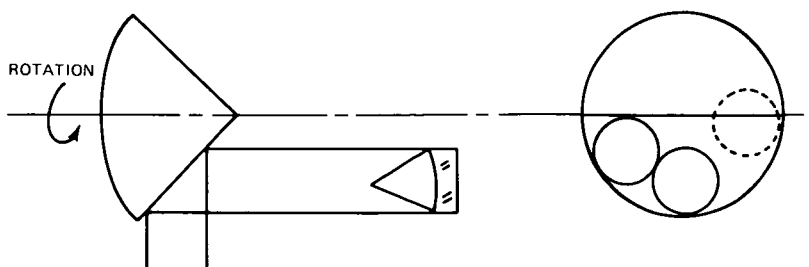


Figure 2-28. Wedge shaped mirror

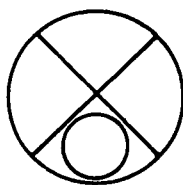


Figure 2-29. Four-sided wedge

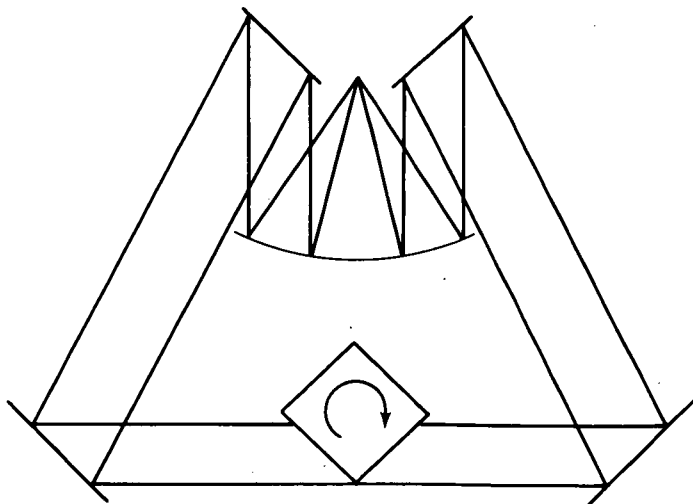


Figure 2-30. Kennedy or split held optical system

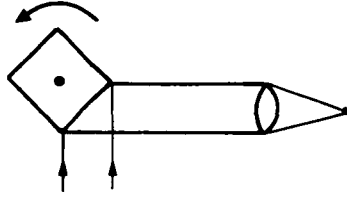


Figure 2-31. Reflecting polygon scanning

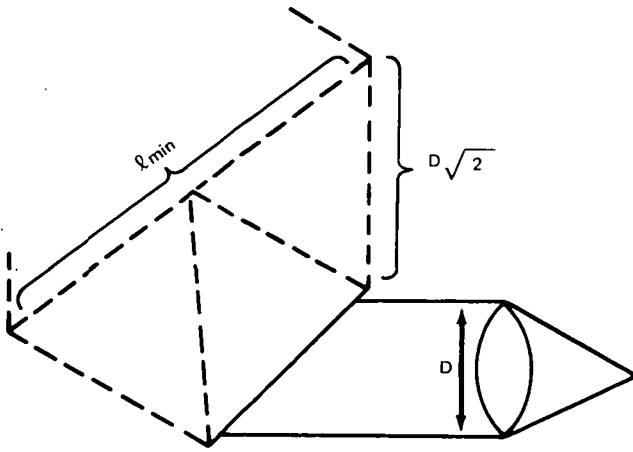


Figure 2-32. Scanning polygon

when one is required to scan small fields of view with high efficiency. If the collecting aperture has a diameter D as shown in Figure 2-32, the side of the polygon for the geometry shown in Figure 2-32 needs to be greater than $D\sqrt{2}$. The minimum point-to-point distance across the polygon (the diameter of the circle in which it is inscribed) is then given by

$$\ell_{\min} = \frac{D\sqrt{2}}{\sin(\pi/n)}$$

where n is the number of sides of the polygon. Therefore for a 180-degree scan ($n=2$), the minimum ℓ is just $D\sqrt{2}$. This is a flat mirror. For

a 90-degree scan ($n=4$), ℓ is 2D. The numbers then get rapidly larger. This type of system is not really adaptable to small, angular fields of view.

Reverse Polygons

These devices might also be called inside-out polygons. The light is brought into them by way of a folding flat and reflected from the insides of the faces of the polygons. The same geometric limits apply to lengths of the arms and the size of the faces of the polygons, but there are times when the geometric relationships of either the inside and or the outside are more favorable.

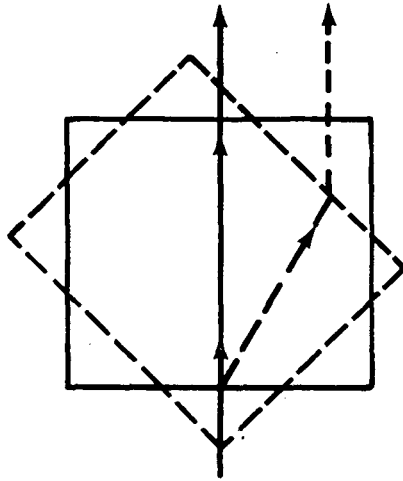


Figure 2-33. AGA thermograph unit

Refractive Polygons

The AGA thermograph unit uses a block of germanium as its scanning device. See Figure 2-33. This scan mechanism uses a rotating plane parallel plate. The ray does not change direction but is displaced with changes in the angle of incidence. The ray will consistently move in one direction as the block rotates, but in parallel light all that will happen is a change of entrance pupil. However, if the refracting polygon is placed in converging light, a scanning action takes place.

Refractive Wedges

One rotating prism will move the chief ray in a circle see Figure 2-34. An added prism rotating in the opposite direction will generate another circle, and the two motions can be added vectorially. Perhaps the most useful result is the effect of counter-rotating prisms at the same velocity. A line is thereby generated. If a second mirror is used, the usual two-dimensional raster can be generated.



Figure 2-34. Refractive wedge with added rotating prism

The deviation of such wedges can be obtained from the usual equations

$$\delta = (n - 1) \sin \alpha , \quad (58)$$

where

δ = deviation angle

α = prism angle

n = prism refractive index.

For a double prism system the prism can be regarded as a split pair. Thus, for synchronous altitude the full field is 22 degrees, the deviation is 11 degrees, and each prism needs a δ of 5.5 degrees. The linear (paraxial) approximation is:

$$\delta = (n - 1) \alpha . \quad (59)$$

Thus,

$$\alpha = \delta / n - 1 . \quad (60)$$

Therefore a small graph can be made for the scan angle vs index for different α . One of the unfortunate things about such an approach is that wedges are refractive and that they tend to be heavy. For a given scan angle the weight is almost invariant of the choice of material; i.e., high index materials are generally dense. The mass of the prism will be

$$M = 1/2 \, bh\ell\rho \quad (61)$$

where $bh\ell$ are the base, height and length of the wedge, and ρ is its density. The mass per unit length and height or unit area can be calculated since these are determined by the entrance aperture of the system. But the side b is given by αh to a good approximation for these small angles. Therefore, the total mass goes linearly as αh , inversely as $n-1$ for a given field angle and aperture size. It also goes linearly as the density ρ . Thus the ratio $\rho/n-1$ is a figure of merit for prism scanning and weight.

The aberrations of such wedges used in collimated light are those of color and astigmatism. The change in angle with respect to color will then be given by

$$\frac{\partial \delta}{\partial \lambda} = \alpha \frac{\partial n}{\partial \lambda} . \quad (62)$$

Probably the oldest of the image scanning devices is the Nipkow scanning wheel. This technique uses a primary optical system which forms an image on a wheel, as shown in Figure 2-35. This wheel has a series of holes in it that scan across the image and allow a small portion of the light to pass through. (See Figure 2-36.) All the light from the primary image is on the scanning wheel; the lens must be in a position to collect all the light from the imaged field and focus it on the detector.

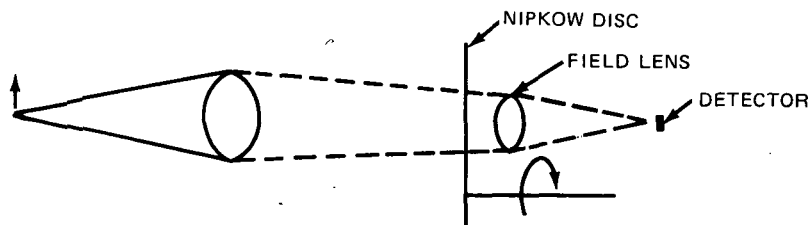


Figure 2-35. Primary optical system

The system is basically inefficient and the optics are a little difficult. Consider the problem of imaging a 1000 line raster. The diameter of each hole in the disc must be 10^{-3} of the total field, for example: 10^{-3} cm ($\approx 10 \mu\text{m}$) for a 1 cm field stop. The effective speed of the optics is 10^3 times the field lens aperture ratio. These holes are difficult to machine and the detector must be 1 cm times the demagnification of the field lens. Detectors do not lend themselves to that size. Nipkow systems are not recommended.

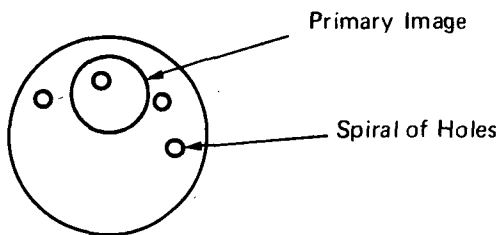


Figure 2-36. Wheel from primary optical system

One variation on this theme is a cylinder of lenses behind an imaging system as shown in Figure 2-37. A device of this nature was built by Perkin Elmer in the 1950's and apparently by the Germans still earlier. In this approach, the field lens f/no is much smaller than the effective f/no of the Nipkow field lens. The problem with this system is that of alignment, uniformity, and more complexity. The detector must still cover the whole field at once and still has all the attendant noise problems.

The S-192 Multispectral Scanner of SKYLAB developed by Honeywell incorporates an interesting scanning method for their device. It uses a

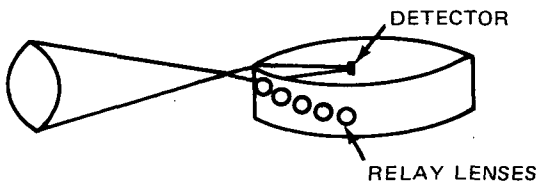


Figure 2-37. Cylinder of Lenses

rotating pair of tilted mirrors, in conjunction with their on-axis all reflective Schmidt system, as shown in Figure 2-38. The small rotating system scans one zone of the spherical aberration. This generates a full circular

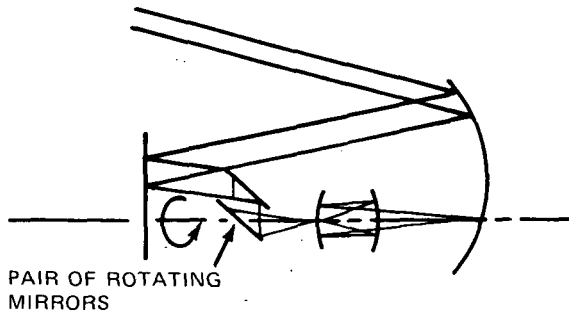


Figure 2-38. Reflective Schmidt system using tilted rotating flat

scan. Using a 120° arc of the circle yields a scan efficiency of 33% with slight overscanning at the edges. It has a constant scan velocity, a uni-directional scan but a low scanning efficiency. One way to improve on the scan efficiency is to use more rotating mirrors; in fact one can use spokes. If there are three spokes, for example, each can cover 120 degrees and be blocked off the rest of the scan.

Texas Instruments has developed a system of scanning secondaries in a different way. This system has the secondaries rotating through a fairly large circle but in some ways is better than moving a primary or flat. (See Figure 2-39.) Another unique system as developed by the Te' Company uses a toothed wheel of corner mirrors (two surfaces) for scanning. The wheel rotates and double reflections are used off the wheel teeth. See Figure 2-40 which illustrates this system.

The University of Arizona has developed another form of scanning secondaries as shown in Figure 2-41. A Pfund-type folding flat is used with a spherical collector. A set of clam shell mirrors are used and each is tilted a little with respect to the preceding one. Each spoke must cover about 1.4 degrees which is reasonable for all reflective systems that are aspheric. Such a system scans without oscillation (at constant velocity in the same direction) and is all reflective. Using brute force engineering and arrays of

detectors can provide 10 arcsec resolution over 22 degrees. Such a system may use as many as 5000 detectors. The data rate would be fantastically large for any reasonable framing time; i.e., there are 80,000 lines or 6.4×10^9 resolution elements. This system is illustrated in detail in Figure 2-42.

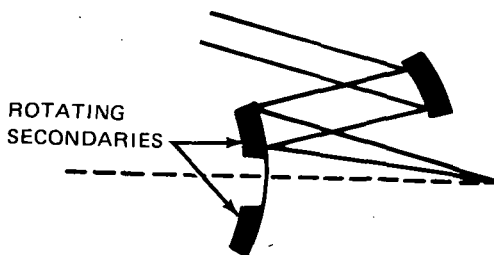


Figure 2-39. An example of rotating scanning secondaries

Optical Materials

Some of the optical systems discussed require corrector plates as large as the entrance pupil, or relay lenses close to the focal plane. Some scanners use refractive elements to scan. In any case these materials must have appropriate transmission, refractive indexes, size and mechanical properties. Great strides have been made in improvements over natural crystals. Nonsilicate and nonoxide glasses, calcium aluminate, germanate, and chalcogenides are now available. Hot pressed versions of many of the useful crystals have also been developed. The most recent work towards developing new materials involves chemical and vapor depositions of various types.

For some of these new materials, there is an extensive list of data; while others have only tentative indications on the limits of their performance. The conclusions that can be drawn regarding these new optical materials are that:

- There is no one material nor any reasonable set of materials that satisfy the desires of the designers of different systems
- There have not been enough measurements made of the different properties of these materials.

This situation has been reviewed in the past. Primarily, for the 8-12 μm region, only the alkali halides have been grown large (12-inch diameter by the Stockbarger technique). There are larger melts in diameter but they are hygroscopic single crystals and expensive. The hot compounds can also be made larger and can be very useful; the only thing that seems to be necessary to accomplish this is experience and larger presses. The same seems to be true for the newly developed chalcogenide glasses. KCl and Zn Se have been made in sizes of about 20 inches by chemical vapor deposition.

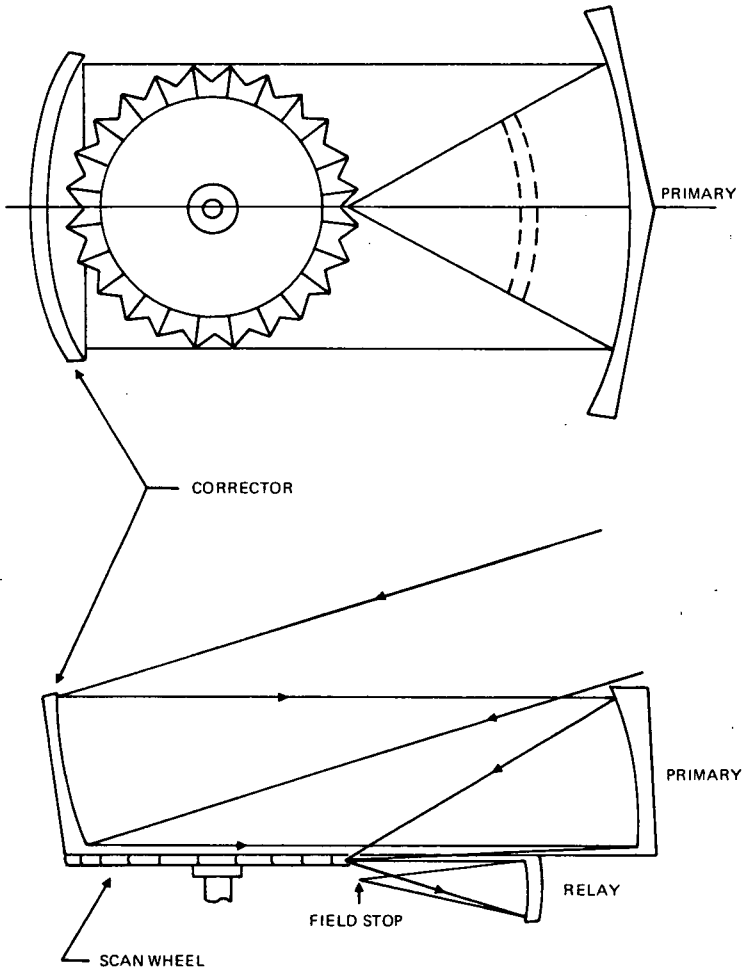


Figure 2-40. Toothed wheel used for scanning

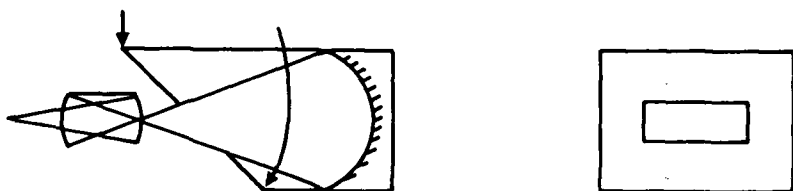


Figure 2-41. Pfund-type folding flat scanner with spherical collector

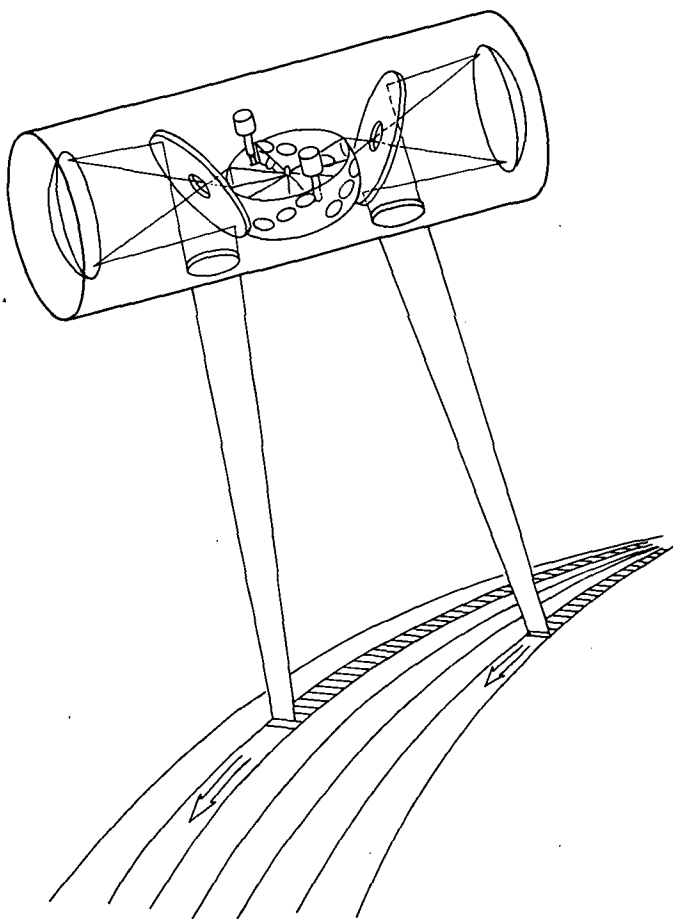


Figure 2-42. Infrared raster scanning telescope

However, in making a balance sheet for measurements, accomplishments are not as great, even on some of the older material. Typical shortcomings include:

- No measured refractive index data on Irtran-6 beyond 10 μm
- Rupture modulus data on Irtran-1 differ by a factor of 2 to 1 due to insufficient statistical testing
- No adequate data on the homogeneity of index of refraction of TI-20 or TI-1173 glass
- Almost no published data on the effects of van Allen belt and other radiations on these materials.

Mirror Blank Materials

Numerous materials have been used as mirror blanks. Their chief properties are strength, lightness, stability, and ability to take a good figure polish and coating. Among the dielectrics the chief materials used are fused silica, Pyrex, BSC glass, Cervit and ULE quartz, among the metals, aluminum and beryllium. The properties of these materials pertinent to their use as mirror blanks are given in Tables 2-6 and 2-7.

In almost every case the blank is ground to the desired figure and polished as well as the surface permits. Then a coating, usually electroless nickel (one trade name is Kanigen), silver, aluminum, or gold is evaporated onto the surface.

It has been well established that Pyrex, fused silica, Cervit and ULE quartz can be coated with electroless nickel and aluminum. These combinations have been used on mirrors at Kitt Peak, Cerro Tololo, Mt. Lemmon and other observatories. Aluminum mirrors can also be stably coated with aluminum, sometimes with a nickel layer. Such systems can be used in all aluminum mountings to maintain focus over wide temperature ranges. The Cervit and ULE materials have very low coefficients of thermal expansion so that they remain stable over broad temperature ranges. In this case the mount must be made of a similar material or partly with Invar.

In theory at least, similar things can be done with beryllium involving less weight since it has a higher strength to weight ratio. However, some

Table 2-6

Density and Young's Modulus Data
For Selected Mirror Blank Materials

	Density (ρ) g cm^{-3}	Modulus (E) $\text{g cm}^{-1} \text{sec}^{-2}$ (10^{-12})	$\frac{\rho}{E}$ $\text{sec}^2 \text{cm}^{-2}$ (10^{12})
Beryllium	1.82	2.8	0.65
Beryllia	3.03		
Alumina	3.85	3.5	1.1
Cer-Vit	2.50	0.92	2.7
Fused Silica (7940)	2.20	0.73	3.0
ULE Fused Silica (7971)	2.21	0.68	3.2
Pyrex (7740)	2.35	0.68	3.5
Aluminum	2.70	0.69	3.9
Magnesium	1.74	0.45	3.9

difficulties have been encountered. Beryllium is usually formed by a directional casting process and is, in a detailed sense, anisotropic. The difference between the coefficient of linear thermal expansion of nickel and that of beryllium, as well as this anisotropy, can cause rippling of the mirror surface. Isostatic casting and other methods of manufacturing the material have been attempted but without success thus far.

The conclusions reached in this analysis are that there are several different mirror substrates that will take a good, stable polish and coating and that can be temperature cycled over reasonable excursions. Some are heavier than others. Whether the well-known ones are too heavy or not depends upon the application and the specific instruments.

Table 2-7

Thermal Expansion and Conductivity For
Selected Mirror Blank Materials

Material	Expansion (α) $K^{-1} \times 10^6$	Conductivity (κ) $cal\ cm^{-1}\ sec^{-1}\ K^{-1}$	a/κ $cm\ sec\ cal^{-1} \times 10^6$
ULE Fused Silica (7971)	0.035	0.0031	11
Cer-Vit	0.05	0.0040	13
Beryllia	9.5	0.42	23
Beryllium	12	0.38	32
Aluminum	24	0.53	45
Magnesium	26	0.38	68
Alumina	6.0	0.041	150
Fused Silica (7940)	0.55	0.0033	170
Pyrex (7740)	3.2	0.0027	1200

Mirror Reflective Coatings

When mirror blanks have been ground and polished to the desired finish, some sort of highly reflective coating is usually evaporated on the surface. The main questions concerning such coatings are how reflective they are and how specular the reflectivity is. The first question can be answered in part by the data shown in Figure 2-43 and in part by the Drude theory. In general all of these metallic surfaces have increasing reflectivity with wavelength, so it is conservative to assume that a reflectivity of 95 percent or better is available of silver, gold, or aluminum for wavelengths greater than $1\ \mu m$. In addition, the reflectivity of these mirrors also increases as their temperature is reduced.

The choice of coating is generally based on whether 0.8 to $0.9\ \mu m$ operation is important and the extent to which the surface can be protected

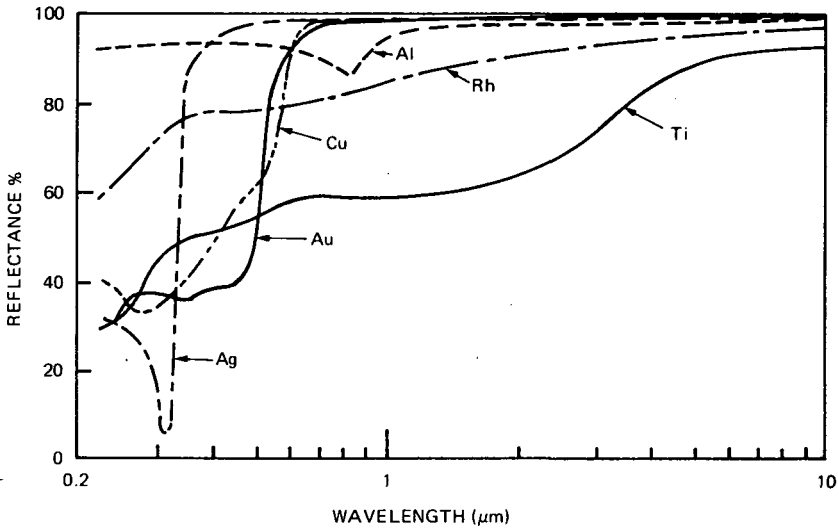


Figure 2-43. Reflectance of various films of silver, gold, aluminum, copper, rhodium, and titanium*

from the atmosphere. Gold and silver are relatively inert but oxides form with aluminum. Sometimes these oxides form an antireflection coating, but generally they decrease the reflectivity and increase the scattering.

A variety of overcoats have been used to protect these surfaces from atmospheric attack. The chief requirements for such overcoating techniques include imperviousness, adhesion, and relatively low absorption. Chief among those tried is MgF_2 , although SiO_2 rates a good second. Some overcoats can be used for spectral selection, but this operation can also be performed later in the system. In fact, most system tradeoffs call for that approach in order to obtain multispectral coverage.

Construction and Fabrication

The fused silica egg-crate mirror was introduced by Corning in the early 1960s. It consisted of two silica disks forming the front and back plates,

*From G. Hass and A.F. Turner, "Coatings for Infrared Optics," *Ergebnisse der Hochvakuumtechnik und der Physik dünner Schichten*, (M. Auwarter, ed.), Wissenschaftliche Verlagsgesellschaft M.B.H., Stuttgart, 1957, p. 143.

separated by a square grid of thin plates fitted together in "egg-crate" manner, wherein one array of rib plates has slots cut halfway through to next with corresponding halfway cuts through the orthogonal array of rib plates. The entire assembly is fused together by heating. Fused silica is very viscous and softens to a point where two pieces in contact under modest pressure will fuse together before the structure collapses under the pressure. In this way the front and back plates were adhered to the ribs. The ribs, however, did not fuse together because manufacturing tolerances did not allow the ribs to be fitted with sufficient precision and because no pressure could be applied in the direction to cause the rib slots to be compressed. These mirrors nevertheless proved to be extremely serviceable in space programs where the low thermal expansion and light weight were necessary.

The monolithic lightweight silica mirror was introduced in the late 1960's. The advancement that made these possible was the development of ULE silica (ULE - ultralow expansion) in which the silica boule was made containing about 8 percent titanium dioxide. This material had a low enough expansion that it could be welded like metal. The rib structure for a mirror was then assembled by welding successive plates together until the entire rib assembly was completed. For convenience each rib was butt-welded to a square column member. The finished assembly was ground to form the mating surfaces of the mirror. Two flat plates of ULE silica were then added to form the front and back surfaces of the finished mirror, and the assembly was placed in an oven for fusing, as with ordinary silica mirrors. Small holes are provided in the rib plates so that the mirror can adjust to changes in atmospheric pressure, since this design is otherwise airtight.

Cervit is generally made into lightweight mirrors by machining techniques. The machining process involves several steps but results in a mirror with only a relatively small hole in the back plate where the tools enter the body of the glass. The ultimate weight of the Cervit lightweight mirror is obtained by subsequently acid-etching the inner rib structure until the desired rib thickness is obtained. This etching step also assures that any machining stresses have been relieved. The degree of weight reduction for Cervit are about equally adequate for all lightweight mirror applications.

Lightweight Solids

The form of lightweight solid mirrors is shown in Figure 2-44. The mirror is solid, and the lightweighting is accomplished by profiling the back. The

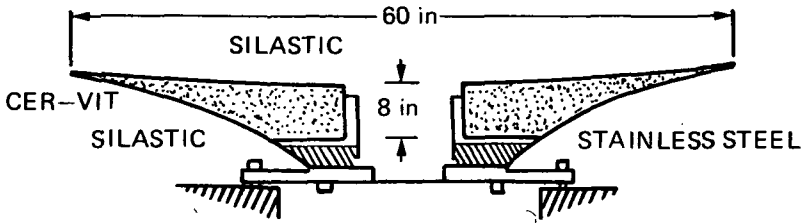


Figure 2-44. Cross section of a lightweight solid mirror and mounting for a 60-inch telescope mirror. The edge thickness is approximately $3/4$ in.

exact shape is determined by the requirement that the change in the shape of the surface be spherical when the mirror is moved from a vertical to a horizontal position. Such a change then requires only a slight refocus of the system using such a mirror. The weight reduction over a solid blank of uniform thickness equal to the central thickness in Figure 2-44 can be between 30 percent and 70 percent, depending on the edge thickness selected by the designer.

In theory this mirror shape has practical advantages; however, in practice some troublesome problems have developed. The basic problem has been the lack of good optical figure; principally there develop astigmatism-like errors. Two factors contribute to these deficiencies:

- Low stiffness of the mirror in processing
- Metal-glas interface forces.

The low stiffness causes two problems. In all optical processing, such as diamond generating, fine grinding, and polishing steps, any initial error in the surface will only slowly be removed by the tool because the mirror deflects away from the tool and low differential forces result from the surface error. Hence, original errors tend to persist. In early processing, such as the generating, machining, or grinding stages, if the mirror has internal stress, removal of material will cause the surface to warp. The thinness of the mirror means that a given force, internal or external, will result in a large dimensional change in the mirror before the restoring force due to the cross section of the mirror equals the perturbing force. This lack of intrinsic rigidity is serious in this design.

HADAMARD SCANNING

One of the newer techniques for obtaining improved throughput and the multiplex advantages in spectroscopy is the encoding technique called Hadamard. It is a system of using masks for the output slit of a spectrometer. The particular scheme uses Hadamard codes, but the concept does not depend directly on that. Imagine that there exists the front end of a monochromator that consists of a slit, a disperser and appropriate optics, as shown in Figure 2-45 schematically. The right-hand side of the diagram is meant to illustrate that several different slit images are formed in several different colors. The figure shows four of these labeled $\lambda_1 \dots \lambda_3$. The normal spectrometer uses one exit slit, rotates the prism so that these images illuminate the detector one at a time. The Hadamard system uses a mask, or a multiple exit slit. Figure 2-46 is a schematic of that scheme. All the light that gets through the mask is focused onto the detector. Whereas the conventional spectrometer uses three positions of the exit slit in sequence (obtained by rotating the prism), the Hadamard uses three positions of the mask. With the conventional spectrometer, the detector "sees" a unit of radiation for each slit position.

Now consider the Hadamard mask as shown in Figure 2-47. For the three positions of the mask, there are three equations. These three equations can be solved for three unknowns, unless the equations are linearly related. The Hadamard scheme allows this to be true and to obtain about 50 percent transmission for any column (of many elements). Then one obtains one column of three for radiation units for the conventional system and $3 \times 3/2 = 9/2$ for the Hadamard system. Thus there is a gain of a factor of $3/2$. In general the gain is about $n/2$.

This is really a space scanning system, and in this example one is scanning the different colors that have been distributed in space. To apply this to space scanning, imagine an image formed in three elements in a line x_1, x_2, x_3 . These are located in a strip whose long dimension is perpendicular to the line of flight. Now assume that there is a mask strip as shown in Figure 2-48 (a). The aperture accepts three of these mask elements. Thus the mask looks successively as shown in Figure 2-48 (b). The equations for this diagram are:

$$x_1 + x_2 = V_1 \quad (63)$$

$$x_2 + x_3 = V_2 \quad (64)$$

$$x_3 + x_4 = V_3 \quad (65)$$

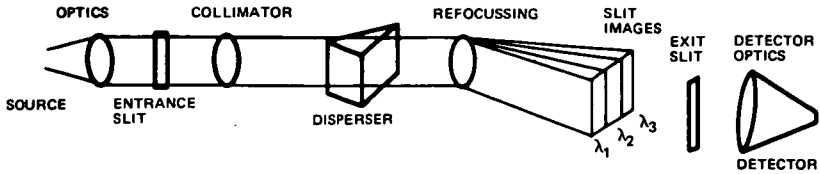


Figure 2-45. Conventional spectrometer

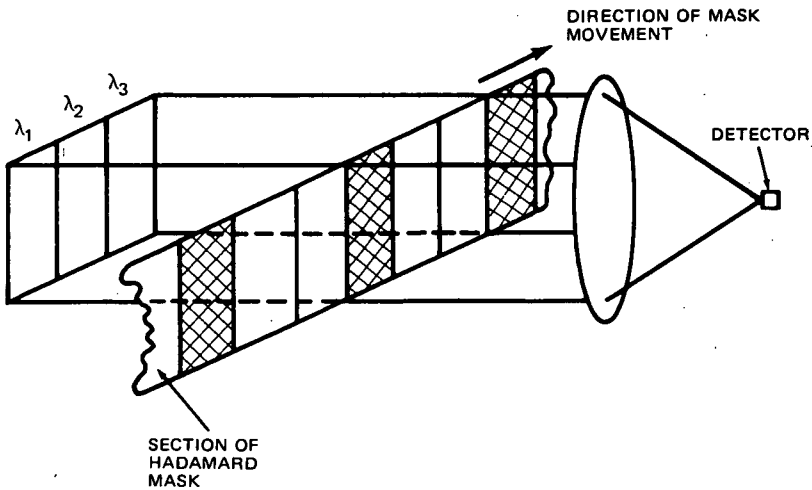


Figure 2-46. Schematic of the Hadamard system

Therefore there is a solution for spatial element. The x's stand for radiation levels in each of the resolution elements.

At each position the detector sees three elements, one of which is masked out. The conventional system sees one element. Thus the gain in irradiance is about $1/2 n$, where there are many elements.

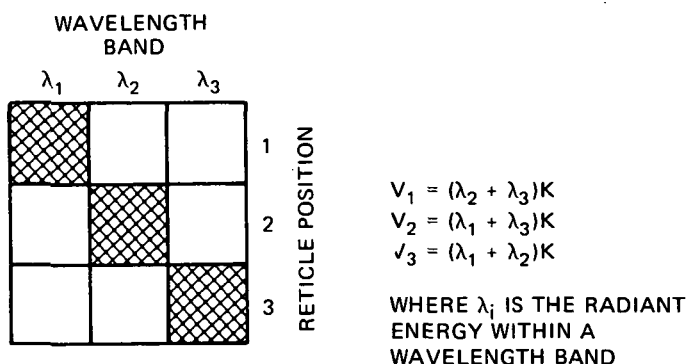


Figure 2-47. Example of a Hadamard Mask

Some Instrument Considerations

In this concept, what about noise and instrument effects? For a background (photon-noise) limited system, the noise will be proportional to the square root of the area. This gain is $1/2 \sqrt{n}$, where n is the number of elements. For a system like this, the entire scene must be imaged. It is an image space scanner. Any variations in the radiation from the opaque elements will cause variations in the apparent scene radiation. The non-uniformities will cause scene noise and uniform radiation can increase photon noise. Large aspect optics should be used, but this is not really different from the use of linear arrays. There must be n positions of the linear mask for each n resolution elements. If the line time is T , then the dwell time for each position of the Hadamard mask has time T/n . Radiation levels must be recorded for each of these so that the noise bandwidth corresponds to a sample time of T/n . This system is clearly of great advantage for sampling a scene with a few variations, compared to a single detector initially. Scanning noise will be a problem.

A comparison can be made with a system employing a linear array of detectors. For an array of n detectors to cover the n resolution elements of the scan line, the gain in signal-to-noise is $n^{1/2}$. The detectors probably cost more, have a varying responsivity from element to element and require a bias supply, cold shielding, preamplifiers, etc. The Hadamard scanner uses one detector which reduces the cost, the number of preamps and bias supplies, weight, cooling requirements but it requires a scanning mask, sampling system, and data processor for inverting the matrices.

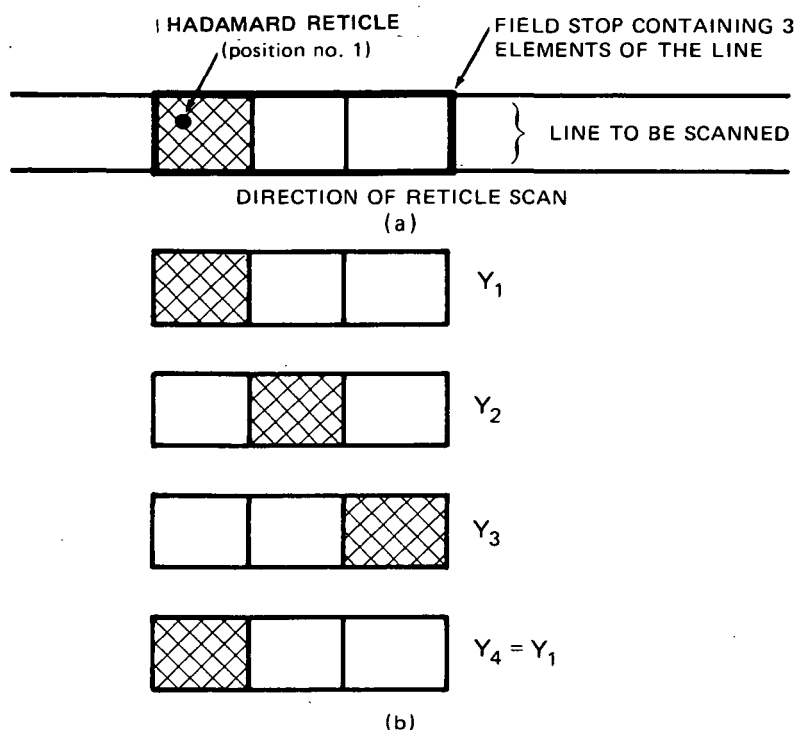


Figure 2-48. Three mask elements

Signal and Noise

The signal and noise relationships of the Hadamard are what really count. Suppose you have a three-element linear mask. Each time you will see two open apertures and an opaque mask. We assume the system is limited by the photon-noise of the background radiation.

Each measured voltage V_i represents the signals, and the noise is given by N_i .

$$V_1 = S_2 + S_3 + N_1 \quad (66)$$

$$V_2 = S_1 + S_3 + N_2 \quad (67)$$

$$V_3 = S_1 + S_2 + N_3 \quad (68)$$

The computer calculates the signal and noise as follows:

$$S_1 + \frac{N_2}{2} - \frac{N_1}{2} + \frac{N_3}{2} = \frac{V_2 - V_1 + V_3}{2} \quad (69)$$

This is to be compared to the signal and noise for a single detector and element.

$$S_1 + N_1 = V_1 \quad (70)$$

The signal is the mean value of $S + N$ and the noise N is the variance around this. The signal to noise ration is S/N . For the Hadamard system the signal to noise ratio is:

$$\frac{S_1}{[(N_2/2)^2 + (N_1/2)^2 + (N_3/2)^2]^{1/2}} \quad (71)$$

The noises are added in quadrature because they represent variances around the mean value. Thus, we compare S_1/N_1 to

$$\frac{2S_1}{[N_1^2 + N_2^2 + N_3^2]^{1/2}} \quad (72)$$

If the limit is photon noise, then the S/N comparison is between:

$$\sqrt{S_1} \text{ and } \sqrt{2S_1} \div (S_1 + S_2 + S_3)^{1/2} \quad (73)$$

If S_2 and S_3 are about the same as S_1 (a good approximation for earth resources scenes) then the result is:

$$\frac{\sqrt{2}}{\sqrt{3}} \sqrt{S_1} \quad (74)$$

The Hadamard disadvantage is $\sqrt{2/3}$. If S_2 and S_3 are small, the gain is $\sqrt{2}$. For bright sources on a dark background the system has a good advantage. Where does the 2 come from? How does one generalize to the N -element case?

The two came from the determinantal solution of the equation. Consideration of other cases shows that the codes only apply for odd numbers and that the 2 is one case of $1/2 (n + 1)$. Thus the gain for a photon-noise case is:

0110

0011

1001 .

This determinant is zero; the equations are linearly related.

If the following code is tried:

10101010 →

1010

0101

1010 ,

it is clear that this is a cycle 2 and the determinant is zero. Induction allows us to see that this is also true for all even codes. There are no Hadamard codes.

For the five-element code, the arrangement is:

111001110011100 →

11100

01110

00111

10011

11001 .

This determinant has a value of three.

The seven-element code is:

1111000111100 .

This consists of adding one zero and a one. The determinant has the value of five. The values of all the determinants, by mathematical induction, is $1/2 (n + 1)$. This is the signal gain kind of term corresponding to the 2 for the three-element case. For the n -element case, we compare S_1/N_1 to:

$$\frac{[1/2 (n + 1)]^{1/2} S_1}{[N_1^2 + N_2^2 + \dots]^{1/2}} = \frac{1/2 (n + 1) S_1}{[1/2 (n - 1) S_1]^{1/2}} = \sqrt{\frac{1/2 (n + 1) S_1}{1/2 (n - 1)}} \quad (76)$$

The gain is about 1 as claimed.

BIBLIOGRAPHY

- Annable, R.V., "Radiant Cooling," *Applied Optics*, 1970.
- Breckenridge, R.W. (Jr.), "A 3.6°K Reciprocating Refrigerator," Presented at the 1968 Cryogenic Engineering Conference, Cleveland, Ohio, 1968.
- Gabron, F., McCullough, J.E., Merriam, R.L., "Spaceborne Passive Radiator for Detector Cooling," Proceedings of 20th National Infrared Information Symposium (IRIS), 1972.
- Gessner, R.L., Colyer, D.B., "Miniature Claude and Reversed Brayton Cycle Turbomachinery Refrigerators," *Advances in Cryogenic Engineering*, Vol. 13, 1968.
- Goldberg, I.L. and McCulloch, A.W. "Annular Aperture Diffracted Energy Distribution for Extended Source," *Applied Optics*, Vol. 8, 1951-1958, July, 1969.
- Kollodge, J.C., et. al., "Nimbus Limb Radiometer, Apollo Fine Sun Sensor, and Skylab Multispectral Scanner," *Applied Optics*, 1972.
- Maddocks, F.E., "Application of Turbomachinery to Small-Capacity, Closed-Cycle, Cryogenic Systems," *Advances in Cryogenic Engineering*, Vol. 13, 1968.
- Prast, G., *The Vuilleumier (VM) Cycle. Cryogenics and Infrared Detection*, Boston Technical Publishers, Inc., Cambridge, Ma., 1970.
- Schulte, C.A., Fowle, A.A., Heuchling, T.P., Kronauer, R.E., "A cryogenic Refrigerator for Long-Life Application in Satellites," *Advances in Cryogenic Engineering*, Vol. 10, Plenum Press, New York, p. 477, 1965.
- Wolfe, W. L., (Editor), *Handbook of Military Infrared Technology*, U. S. Government Printing Office, Washington, D. C., 1965.

ATTACHMENT A
SYSTEMS THAT HAVE PROGRESSED
BEYOND THE PROTOTYPE STAGE

The spaceborne electromechanical imaging systems summarized in the attached tables represent most of the unclassified imaging systems developed by the United States that have performed in orbit or have progressed past the prototype stage of development.

Type	Spacecraft	First Launch Date	Orbit	Application	Type and Scan Angle	Instantaneous FOV, (μ) (Spectral Band Designation)
High-Resolution Infrared Radiometer (HRIR)	Nimbus I, II, III	8-28-64	1110 km (600 nmi) polar sun-synchronous (noon)	Day-night cloud maps and cloud temperature	Cross-course rotating mirror (45 r/min), 2.059 rad (118 deg)	7.5
Medium-Resolution IR Radiometer (MRIR)	Nimbus II, III	5-15-66 (II)	1110 km (600 nmi) polar sun-synchronous (noon)	Albedo, water vapor and CO ₂ distribution, day and night cloud maps, and cloud temperature.	Cross-course rotating mirror (8 r/min), 2.059 rad (118 deg)	43(A-E) ^a
Spin-Scan Cloud Camera (SSCC)	ATS I	12-6-66	Geostationary	Daytime cloud cover maps	Spacecraft spin (100 r/min) and latitude step of telescope, 0.314 rad (18 deg)	0.1
Multi-color Spin-Scan Cloud Camera (NSSCC)	ATS III	11-5-67	Geostationary	Three-color daytime cloud cover maps	Spacecraft spin (100 r/min) and latitude step of mirror 0.314 rad (18 deg)	0.1(A-C)
High-Resolution Scanning Radiometer (HRSR)	ITOS	1-23-70	1460 km (790 nmi) polar sun-synchronous (3 p.m.)	Day-night cloud maps and cloud temperature	Cross-course rotating mirror (48 r/min), 1.920 rad (110 deg)	2.7(A) 5.6(B)
Temperature-Humidity IR Radiometer (THIR)	Nimbus IV	4-8-70	1110 km (600 nmi) polar sun-synchronous (noon)	Water vapor distribution, day-night cloud maps, and cloud temperature	Cross-course rotating mirror (48 r/min), 2.059 rad (118 deg)	7(B) 21(A)
Multi-spectral Scanner (MSS)	ERTS I, B	7-23-72	930 km (500 nmi) polar sun-synchronous (10 a.m.)	Earth resources survey	Cross-course oscillating mirror (15 Hz), 0.202 rad (11.6 deg)	0.086(A-D) 0.2(E)
Imaging Photopolarimeter	Pioneer 10 C	3-2-72	Jupiter flyby at 203,830,000 km (110,000 nmi)	Photometry and polarization of zodiacal light, asteroids, and Jupiter. Two-color mapping of Jupiter	Spacecraft spin (4.8 r/min) and cone angle step of telescope, 0.506 rad (29 deg)	0.5(A,B)
Visible-IR Spin-Scan Radiometer (VISSR)	Synchronous Meteorological Satellite (SMS)	Fourth quarter, 1973	Geostationary	High-resolution day and night cloud maps and temperature	Spacecraft spin (100 r/min) and latitude step of mirror, 0.314 rad (18 deg)	0.025(A) 0.2(B)
Very-High Resolution Radiometer (VHRR)	ITOS-IV	10-15-72	1,460 km (790 nmi) polar sun-synchronous (3 p.m.)	High-resolution day and night cloud maps, and temperature	Cross-scan rotating mirror (400 r/min), 2.007 rad (115 deg)	0.6
Facsimile	Ranger			Lunar surface photo	Nodding mirror, camera rotation	1.5
	Explorer			Antenna position monitor	Rotating, nodding mirror 6.282 rad (360 deg)	2.3
Surface Composition Mapping Radiometer (SCMR)	NIMBUS V	12-12-72	1,110 km (600 nmi) polar sun-synchronous (noon)	High-resolution maps of terrestrial mineral characteristics	Cross-scan rotating mirror (600 r/min), 1.571 rad (90 deg)	0.6
Very-High Resolution Radiometer (VHRR)	ATS-F	1974	Geostationary	High-resolution day and night cloud maps	Raster scan of servo-stepped, gimballed flat mirror	0.3(A) 0.15(B)
S-192 Multispec-Scanner	Skylab (EREP)	Fourth Quarter 1973	435 km (235 nmi) circular	Earth Resources Survey	Image Space Conical Scan (6000 RPM) 2.09 rad (120 deg)	D.18rad (1-13)

^a Letters in parentheses refer to respective channels of multispectral scanners.

Type	Spacecraft	Optics Aperture and Focal Ratio (Including Relay and Imersion Optics)	Detector Type (Spectral Band)	Information Bandwidth	System Dynamic Range Radiance Temperature T_e Earth Albedo, ϵ ; Effective Bright Scene Radiance Range
High-Resolution Infrared Radiometer (HRIR)	Nimbus I, II, III	10.16 cm (4 in.): f/0.95 Cassegrain	PbSe Photoconductor	300 Hz	200-340 K (night) $33 \times 10^{-3} \text{ W cm}^{-2} \text{ sr}^{-1}$ (day)
Medium-Resolution IR Radiometer (MRIR)	Nimbus II, III	4.37 cm (1.72 in.): f/0.27 (B, D, E) 4.37 cm (1.72 in.): f/0.9 (A, C) Cassegrain	Thermistor bolometer	4 Hz (A-E)	0-80K (A) 0-270 K (B), 0-330 K (C) 0-270 K (D), 0-290 K (E)
Spin-Scan Cloud Camera (SSCC)	ATS I	12.70 cm (5 in.): f/2 folded paraboloid	S-11 PMT	160 kHz	1000:1
Multi-color Spin-Scan Cloud Camera (MSSCC)	ATS III	12.70 cm (5 in.): f/3 Wynne-Rosin	S-11 PMT (A, B) S-20 PMT (C)	160 kHz (A, B, C)	1000:1 (A, B, C)
High-Resolution Scanning Radiometer (HRSR)	ITOS	12.70 cm (5 in.): f/3.4 (A) 12.70 cm (5 in.): f/0.25 (B) Cassegrain	Silicon photodiode (A) Thermistor bolometer (B)	910 Hz (A) 435 Hz (B)	0-80K (A) 0-330 K (B)
Temperature-Humidity IR Radiometer (THIR)	Nimbus IV	12.70 cm (5 in.): f/0.26 (A), 12.70 cm (5 in.): f/0.26 (B) Cassegrain	Thermistor bolometer (A, B)	115 Hz (A) 345 Hz (B)	0-270 K (A) 0-330 K (B)
Multi-spectral Scanner (MSS)	ERTS I, B	22.86 cm (9 in.): f/3.6 (A-D) 22.86 cm (9 in.): f/2 (E) Ritchey-Chretien	S-20 PMT (A, B) S-25 PMT (C) Si PD (D) HgCdTe (E)	35.5 kHz (A-D) 13.7 kHz (E)	27×10^{-4} (A), 22×10^{-4} (B) 1.7×10^{-4} (C), 28×10^{-4} (D) $\text{W cm}^{-2} \text{ sr}^{-1}$ 0-310 K (E)
Imaging Photopolarimeter	Pioneer 10, G	2.54 cm (1 in.): f/3 Maksutov	S-20 Channel multiplier (A, B)	500 Hz (A, B)	8×10^{-5} (A), 4×10^{-5} (B) $\text{W cm}^{-2} \text{ sr}^{-1}$
Visible-IR Spin-Scan Radiometer (VISR)	Synchronous Meteorological Satellite (SMS)	40.64 cm (16 in.): f/6.3 (A) 40.64 cm (16 in.): f/1.3 (B) Ritchey-Chretien	S-23 PMT (A) HgCdTe photoconductor (B)	210 kHz (A) 26 kHz (B)	0-80K (A) 0-320 K (B)
Very-High Resolution Radiometer (VHR)	ITOS-IV	12.70 cm (5 in.): f/0.89 Dall-Kirkham	Silicon photodiode (A) HgCdTe photoconductor (B)	35 kHz	0.5-80K (A) 180-333 K (B)
Pacifile	Ranger	0.36 cm (0.14 in.): f/2.6	Silicon	100 Hz	$9.0-1500 \mu\text{W cm}^{-2} \text{ sr}^{-1}$
	Explorer	0.86 cm (0.34 in.): f/1	Photodiode	2.5 kHz	$6.5 \text{ to } 2800 \mu\text{W cm}^{-2} \text{ sr}^{-1}$
Surface Composition Mapping Radiometer (SCMR)	NIMBUS V	20.32 cm (8 in.): f/0.92	HgCdTe (A, B)	50 kHz	257-330 K (A, B)
Very-High Resolution Radiometer (VHR)	ATS-F	20.32 cm (8 in.): f/1.7	HgCdTe (A) Silicon Photodiode (B)	1200 Hz	185-335 K (A) 1-100K (B)
S-192 Multispectral Scanner	Skylab (MRP)	30.5 cm (12 in.) Instantaneous Clear Aperture: f/1.69 (1-12) f/1.17 (13)	HgCdTe All Channels [Cooled to 90° K]	167 kHz All channels	

Type	Spacecraft	NEAT at Scene Temperature K or Scene SNR at Irradiance, W cm ⁻²		Scanner Size		Total Weight		Maximum Power, W	Contractor
				cm	in.	kg	lb		
High-Resolution Infrared Radiometer (HRIR)	Nimbus I, II, III	0.22 K at 270 K (B)	25.40 x 40.64	10 x 16	x 9	8.62	19.0	4	ITT
		0.23 K at 330 K (C)	x 22.86						
		0.20 K at 270 K (D)							
		0.26 K at 290 K (E)							
Medium-Resolution IR Radiometer (MRIR)	Nimbus II, III		16.51 x 16.51	6.5 x 6.5	x 13	6.58	14.5	7.5	SBRC
Spin-Scan Cloud Camera (SSCC)	ATS I	30 at 10 ⁻¹¹ W cm ⁻²	25.40 x 27.94	10 x 11	x 17	9.07	20	21	SBRC
Multi-color Spin-Scan Cloud Camera (MSSCC)	ATS III	30 at 10 ⁻¹¹ W cm ⁻²	30.48 x 27.94	12 x 11	x 17	10.66	23.5	23	SBRC
High-Resolution Scanning Radiometer (HSR)	ITOS	19 at 0.5% (A)	16.26 x 40.39	6.4 x 15.9	x 8.4	8.30	18.3	6.5	SBRC
		3000 at 80% (A)	x 21.34						
		1.4 K at 185 K (B)							
Temperature Humidity IR Radiometer (THIR)	Nimbus IV	4 K at 185 K (A)	17.78 x 19.05	7 x 7.5	x 15.6	9.03	19.9	7.5	SBRC
		0.2 K at 300 K (A)	x 39.62						
		1.5 K at 185 K (B)							
Multi-Spectral Scanner (MSS)	ERTS I, B	100 at 1.6 x 10 ⁻¹¹ W cm ⁻² (A)	38.10 x 38.10	15 x 15	x 36	52.16	115	25	SBRC
		73 at 1.3 x 10 ⁻¹¹ W cm ⁻² (B)	x 91.44						
		44 at 1.0 x 10 ⁻¹¹ W cm ⁻² (C)							
		73 at 1.7 x 10 ⁻¹¹ W cm ⁻² (D)							
		1.2 K at 310 K (E)							
Imaging Photopolarimeter	Pioneer 10, G	25 at 2.2 x 10 ⁻¹¹ W cm ⁻² (A)	17.78 x 38.10	7 x 15 x 6		4.08	9	4	SBRC
		25 at 1.1 x 10 ⁻¹¹ W cm ⁻² (B)	x 15.24						
Visible-IR Spin-Scan Radiometer (VISSR)	Synchronous Meteorological Satellite (SMS)	3 at 0.5% (A)	50.80 x 50.80	20 x 20	x 58	60.10	132.5	23	SBRC
		1.7 K at 200 K (B)	x 147.32						
		0.4 K at 300 K (B)							
Very-High-Resolution Radiometer (VHR)	ITOS-IV	20 at 0.5% (A)	20.32 x 20.32	8 x 8 x 19		9.07	20	5.0	RCA
		1.5 K at 185 K (B)	x 48.26						
		0.5 K at 300 K (B)							
Facsimile	Ranger	3 at 5.6 x 10 ⁻¹¹ W cm ⁻² (at limiting bandwidth)	3.12 dia x 24.99	1.23 dia x 9.84		1.18	2.6	16	Philco-Ford
	Explorer	3 at 14.1 x 10 ⁻¹¹ W cm ⁻² (at limiting bandwidth)	3.81 dia x 16.51	1.5 dia x 6.5		00.50	1.1	3	
Surface Compulsion Mapping Radiometer (SCMR)	NIMBUS V	1.0 K at 280 K	22.86 x 42.16	9 x 16.6 x 21.6		19.05	42	15	ITT
Very-High-Resolution Radiometer (VHR)	ATS-F	1.0 K at 200 K (A)	67.31 x 53.34	26.5 x 21 x 15		27.22	60	35	ITT
S-192 Multispectral Scanner	SkyLab (EREP)	30 at 1% (B)							
			.55 cubic meters	19.3 cubic feet		159	350	266	Honeywell

CHAPTER 3
ELECTRON BEAM IMAGERS

PANEL MEMBERS

G. Barna — *Chairman*
O. Weinstein — *Associate Chairman*

K. J. Ando
F. Cook
O. Graham
M. Green
E. W. Koenig
F. Leccese
J. Lowrance
E. D. Savoye
M. St. John

Additional Technical Material Supplied By:

L. Freedman
J. Miller

ELECTRON BEAM IMAGERS

PANEL SUMMATION AND RECOMMENDED TECHNICAL APPROACHES

Electron-beam imagers are defined as those devices which, by means of a shutter or similar mechanism, put an image of an entire scene that is fixed in time on a photosensitive surface, and then read out the photosensitive surface by means of a beam of electrons after the shutter has closed. The common television camera and the ERTS Return-Beam Vidicon (RBV) are two examples of electron-beam imagers. Differences among electron-beam imagers generally are based upon either the method of reading the image on the photosensitive surface or on the material used as the surface.

In considering future space missions, the main argument for developing improved electron beam readout image sensors is based on the advantages of framing cameras over other imagers by providing performance essential to certain applications more easily than can be implemented with other sensor technologies.

Summary of Performance Characteristics

Table 3-1 compares performance characteristics for current (1972) electron beam sensor technology, and the estimates for performance levels that can be achieved in four and eight years. The actions that must be taken to achieve the performance levels shown are summarized here and discussed in detail in appropriate paragraphs of the text that follows.

In the table, the sensitivity, in joules/m², is defined at the surface of the sensor. The resolution is given at a relative response to a sine wave input, in cycles per mm. Total sensor resolution can be computed by multiplying this unit resolution by the format dimension. The format dimensions are given in millimeters. The "50 percent MTF" column corresponds to the EIFOV parameter, and the "20 percent MTF" column provides a measure of the MTF curve slope.

Recommendations

The Electron Beam Panel reached a number of technology options which they felt would offer the most promising performance for future applications. These were as follows.

SUMMARY TABLE
ELECTRON BEAM SENSOR PERFORMANCE CHARACTERISTICS

Device	Type	Format Size (mm)	1972			1976			1980		
			Sensitivity* J/m ² 10 : 1 S/N	Resolution**		Sensitivity* J/m ² 10 : 1 S/N	Resolution**		Sensitivity* J/m ² 10 : 1 S/N	Resolution**	
Return Beam Vidicons	2" ASOS	25 x 25	3 x 10 ⁻⁴	45	75	2 x 10 ⁻⁴	60	100			
	2" Silicon	25 x 25	3 x 10 ⁻⁵	40	60	3 x 10 ⁻⁵	50	70			
	4½" ASOS	50 x 50	3 x 10 ⁻⁴	45	75	2 x 10 ⁻⁴	60	100			
	4½" Silicon	50 x 50				3 x 10 ⁻⁵	50	70			
	Large Format	100 x 100				3 x 10 ⁻⁴	60	100			
FPS Vidicons	3" STD	45 x 45	2 x 10 ⁻⁴	32	44	2 x 10 ⁻⁴	50	70			
	Silicon	25 x 25	1 x 10 ⁻⁴	28	40	1 x 10 ⁻⁴	45	60			
	Large Format	90 x 90				2 x 10 ⁻⁴	50	70			
	Large Silicon	50 x 50				1 x 10 ⁻⁴	45	60			

Direct Beam Silicon Vidicons	Standard Photocon	25 x 25	1×10^{-4}	24	45							
	Silicon	18 x 18	3×10^{-5}	18	32							
	Large Silicon	50 x 50					3×10^{-5}	30	50	3×10^{-5}	40	80
Image Dissectors	Standard	25 x 25	20	35	55							
	Large Format	50 x 50	50	20	35		1	60	100			
Dielectric Tape Cameras	Large Format	50 x 50					4×10^{-6}	30	50	1×10^{-6}	60	100
	Large Format	50 x 50	3×10^{-7}	20	30		2×10^{-7}	40	60	2×10^{-7}	50	75
EBS Camera Tube and SIT	Standard	25 x 25	2×10^{-7}	10	15							
	Large Format	50 x 50					2×10^{-7}	30	45	2×10^{-7}	45	63

*For .55 micron monochromatic source and S/N in db

**In line pairs per millimeter

RBV Improvements

Striped filters for the large format tubes (i.e. 115 mm tube) should be developed to provide registered images from a single camera at the same resolution offered by the ERTS-1 RBV multispectral system. Improvements to the RBV in both shading and thermal and temporal signal stability can be achieved through field mesh and photoconductor improvement along with electro-optic modifications.

Higher Signal-to-Noise Sensors

The RBV is limited to signal-to-noise performance of the order of 40 dB, by the inherent nature of the return beam signal mechanisms. Three options are available to achieve higher signal-to-noise ratios.

1. The development of high resolution direct readout vidicons, and corresponding work to develop improved ultra low noise target pre-amplifiers. This approach would make the system signal-to-noise ratio bandwidth dependent, hence providing the means to achieve high sensitivity for low contrast applications by proper selection of system operating parameters and trading scan (or frame) time for signal-to-noise ratio.
2. Application of high velocity readout sensors currently under study to demonstrate feasibility. Performance data on these devices are expected early in 1973.
3. Application of isocon mode readout of high resolution vidicons, also currently under study. The isocon readout eliminates the beam noise dependence of return-beam readout, at the expense of a more complex electron optic.

Both options (2) and (3) would offer a free selection of frame times since they do not require bandwidth compromises. However, both of the options are early in their development, and any effort to pursue either of them should await further evidence of feasibility expected from on-going tests.

Larger Format Vidicons

Some of the problems experienced in current systems (e.g., ERTS) where "multiple-camera" cameras are used, are solvable using larger single sensors. It is expected that larger format electron beam sensors may have reduced resolution per mm, but that overall data packing density, which allows

simplified optics and reduced electronics, will prove most beneficial. Target formats as large as 100mm x 100mm should be studied.

Large Silicon Target Vidicons

The high quantum efficiency afforded by silicon in the visible and near IR gives it greater overall sensitivity than other vidicon photosensitive targets. A program to make large silicon diode array targets would be valuable and should be pursued

High-Sensitivity, High-Resolution, Fast-Erase Tube

Development of a camera tube, having high sensitivity and resolution with fast erase properties, is required for practical application of the Wide-range Image Spectro-Photometer (WISP) technique. A tube having a red-response photocathode, an image section with gain, and a high resolution electron gun similar to the return-beam vidicon is considered a feasible approach.

Optics

The current state-of-the-art in refractive optics needs to be improved to use the resolution available in the present electron-beam sensors. Large reflective and catadioptric optical systems should be studied as means of improving the optical performance. High resolution over relatively wide fields of view ($\sim 20^\circ$) together with large collecting apertures to promote sufficient signal in the narrow spectral bands of interests is important to this improvement.

Cold Cathode Development

Electron gun designs incorporating cold cathodes should be included in studies relating to development of new tubes. The cold cathode will provide solid state reliability, as well as significantly higher current density capabilities, increasing the spatial resolution. Recent developments in materials hold good promise for this technique and equipments utilizing cold cathodes are foreseen as off-the-shelf items within the near term.

CHAPTER 3

ELECTRON BEAM IMAGERS

INTRODUCTION

The designation "electron-beam imaging sensor" has been generally accepted to mean that class of imaging device that uses a focused electron beam to accomplish readout of a latent image on a photoconductor or photoemitter.

These imaging devices are evacuated to protect the internal elements and they generally use external components to focus and deflect the readout beam.

The panel's deliberations centered on technical material contributed by the panel's members. Material on the conventional silicon vidicon was contributed by K. Ando; F. Cook addressed dielectric tape cameras; M. Green addressed secondary electron conduction and electron bombarded silicon camera tubes; E. Koenig discussed image dissector tubes; F. Leccese discussed FPS camera tube and infrared vidicons; and E. Savoye addressed advanced technology (3-5 Photocathodes and solid state electron guns.) G. Barna prepared the introduction and survey material for the panel's report. A subgroup was formed to consider the technical options and recommendations. J. Lowrance headed this group which included O. Graham, M. St. John and O. Weinstein. Additional material was supplied by L. Freedman on return-beam-vidicons, by J. Miller on image motion and by H. Gurk on multispectral imaging systems using electron beam devices (H. Gurk worked with the user panel).

In this report, six devices along with their most significant permutations are discussed. The devices are: (1) Return-Beam Vidicon, (2) Focus Projection and Scanning (FPS) Vidicon, (3) Direct Beam Readout Vidicon, (4) Image Dissector Camera, (5) Dielectric Tape Camera, (6) Secondary Electron Conduction (SEC) and Electron Bombarded Silicon (EBS/SIT) Tube. The schematic arrangements for the operational concepts of these devices are shown in Figure 3-1. The discussion that follows centers on these basic operating principles of the different electron beam scanning devices.

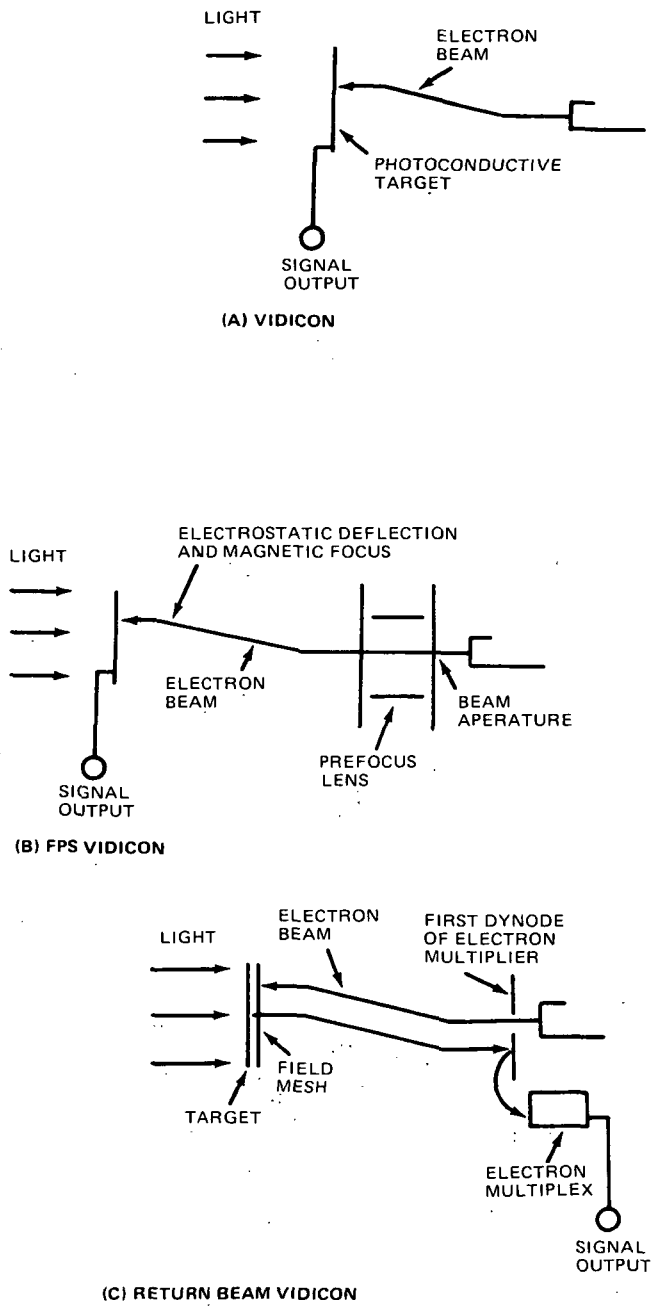


Figure 3-1. Schematic Representations of Electron Beam Sensors

Direct Beam Readout Vidicon

The vidicon, Figure 3-1(a), uses an electron gun to scan the photoconductive target. The target is coated on the front side with a transparent conductor which serves as the signal electrode. In operation, the scan beam is used to prepare the back-side of the target to a relatively negative potential. When the light pattern is focused on the photoconductor, the conductivity increases in the areas illuminated, with the back-side of the target being charged to a more positive value. The electron beam then reads the signal by depositing a negative charge on the positive areas resulting in a capacitively coupled signal to the front-side signal electrode.

Focus Projection and Scanning (FPS) Vidicon

The FPS vidicon refers to the tube's internal deflection plates (deflectron) which produce scanning (beam deflection) within the same volume where magnetic focusing occurs. The FPS produces signal current in a manner similar to the vidicon, as shown schematically in Figure 3-1(b).

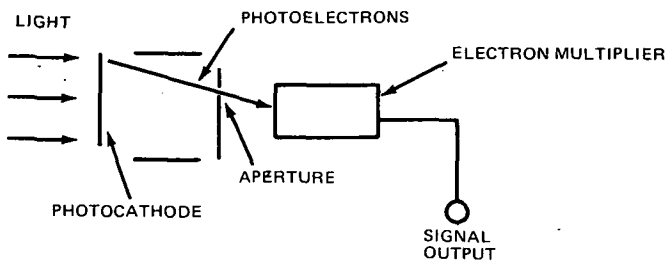
Return Beam Vidicon (RBV)

The RBV, shown in (c) of Figure 3-1, uses a photoconductor as the light detector. Photons are focused onto a thin target (normally antimony sulfide oxysulfide) which produces a charge pattern corresponding to the incident light image.

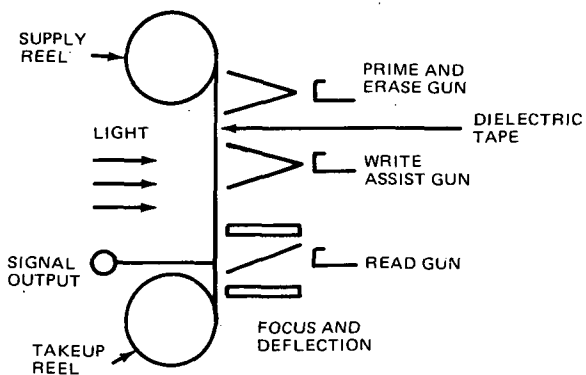
The electron beam from the gun scans the charge pattern, losing some of the electrons to the more positively charged areas, with the remainder of the beam returning to the electron multiplier surrounding the electron gun. The signal is the current output from the anode of the electron multiplier.

Image Dissectors

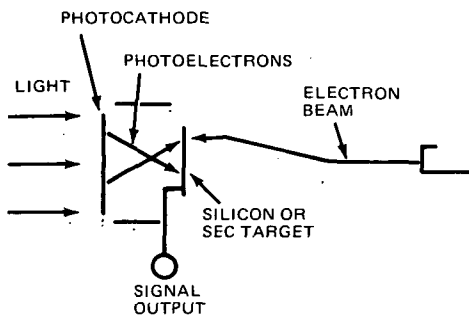
The image dissector shown in (a) of Figure 3-2, uses an image forming mechanism which is different from the previously described sensors. Electrons from the photocathode are accelerated and an image is translocated at a metallic plate in the plane identified in the illustration as "aperture." An aperture in the metallic plate samples the optical image. By moving the electron image across the aperture, using orthogonal magnetic deflection fields, the entire electron image can be sampled. Amplification in the electron multiplier increases levels of the electron samples to usable image signal levels. A principal feature of the image dissector is its operation without need for a separate electron beam source, leading to



(A) IMAGE DISSECTORS



(B) DIELECTRIC TAPE CAMERA (TYPICAL)



(C) SECONDARY ELECTRON CONDUCTION AND ELECTRON BOMBARDED SILICON TUBE

Figure 3-2. Schematic Representations of
Electron Beam Sensors

inherently higher reliability than those using tubes requiring a heater cathode to supply the electron beam.

Dielectric Tape Cameras

The dielectric tape camera, shown as (b) in the figure, has been configured in many variations, but in basic principle combines the ability to image and to store the image for indefinite periods through the use of dielectric tape. The imaging operation is similar to the operation of a vidicon, with the exception that recording of the image requires that the tape be flooded with electrons from a writing-assist gun. Thus, the system can be shuttered electronically, which is a distinct advantage over other forms of electron beam sensors. A separate set of electron-optics provides the readout function, which is similar to vidicon readout.

Secondary Electron Conduction (SEC) and Electron Bombarded Silicon (EBS/SIT) Tubes

The SEC tube, shown in (c) of the figure, uses a photocathode as the light detector. Photoelectrons are focused onto a thin target made of potassium chloride (KC1), which provides gain through secondary electron emission within the target. The SEC produces signal current via the electron scanning beam as defined for the vidicon.

The EBS/SIT tube operates in much the same way as the SEC tube; however, the target is a very thin silicon wafer of tightly spaced p-n junctions. Target gain is provided by photoelectrons focused onto the target, causing multiple dissociation of electron-hole pairs. The holes are collected at the p-side of the diode where the charge is neutralized by the scanning beam, producing signal current through the front side signal electrode, as defined for the vidicon.

APPLICATIONS OF ELECTRON BEAM SENSORS

Remote sensing of the earth and its environment is one of the principal current applications of satellites. Many of these applications require imagery either for direct photo interpretation, for further analysis and mensuration, as a base of reference for other data, or for computer processing. The user of the data — meteorologist, geographer, oceanographer, or other — is generally unconcerned about the device used to obtain the picture. His only concern is the quality, timeliness, and proper identification of the imagery.

Thus, requirements cannot be said to exist for electron beam readout imagers alone. Imaging requirements or desires exist for the various disciplines separately or in common. However, certain characteristics or easily implemented capabilities exist for electron-beam devices, which may make them likely candidates for some applications. Similarly, some limitations may make these devices not feasible or at least uneconomical for other applications.

Detailed discussions of the tube characteristics, their problems, status, and development requirements appear in later sections. However, some of the principal points about electron-beam imaging can be identified here to aid in the identification of likely applications. The most obviously advantageous characteristic of electron-beam imaging tubes is their use in frame cameras (with the exception of image dissectors). Neither mechanical scanners nor, for the present, solid-state detector arrays can be readily used in this mode.

A frame device with some latent storage capacity can be used to image a large area synoptically, to provide maximum exposure time with no smear, to provide a geometrically correctible reference base, and to take a snapshot and read it out either slowly to conserve bandwidth or quickly to permit another picture to be taken. The snapshot or shuttered operation avoids the need for severe long-term attitude control or for substantial ground processing to correct for variations during area coverage by a non-shuttered line-scan imager.

Electron beam tubes can also be used in line scan modes. Here the particular application and the system development time and cost requirements will determine whether a tube or one of the other imaging sensors will be used. The unique advantage that a tube system has over both the other imaging types is for either a very large number of spectral bands, or a programmable, variable number of bands using the MOCS (Multi-Channel Ocean Color Sensor), or the WISP (Wide Range Imaging Spectrophotometer). In both these devices, a grating or prism is used to spread a line of imagery (visible through a slit) over a full raster of a tube. The electron beam then scans the frame with the data handling system, combining data appropriately to generate the desired bands. Resolution for such a system is obviously limited since the bandwidth required to read out a frame is used for multiple copies of a single line.

For other line scan uses, tubes can be compared to the other imagers on more obvious bases. They require simpler data handling and are more advanced in development than arrays. They offer the possibility of enhancement through intensifier sections and multipliers. They are more efficient

than mechanical scanners and require no mechanical movement. On the other hand, tubes only operate in the visible and near IR, are more difficult to calibrate spectrally during flight, and may require longer focal lengths for high resolution than object plane mechanical scanners (image plane scanners have the same focal length).

CURRENT DEVICES

Return-Beam Vidicons

Less than 25 years have passed since the initial vidicon work (Weimer et al., 1951). A major accomplishment of the initial device was the operation of a practical TV camera tube without the use of a multiplier. The intervening development has traveled full circle with the practical application of a return beam vidicon (RBV) (Schade, 1970), where the multiplier is key to the useful realization of the vidicon resolution capabilities.

The RBV makes use of unique electron optics for a significant improvement in resolution. The inclusion of the electron multiplier permits a substantial improvement in signal-to-noise (S/N), essentially eliminating amplifier noise as a contributing factor to the overall system noise performance. This S/N increase is necessary for the practical utilization of the information packing density available in this device.

The following sections describe the operation of the RBV and the elements of that device that contribute to its high performance level. Considerations of the performance levels to be expected and a description of the RBV Multispectral Camera System presently orbiting on ERTS-1 are covered, as well as future improvements and enhanced levels of operation as projected.

Vidicon Operation

The Return Beam Vidicon (RBV), shown in Figure 3-3, contains the internal elements of the conventional vidicon with the addition of a multiplier structure and beam deflectors. The tube is surrounded by a specifically designed magnetic deflection yoke and focusing assembly that provide the potential for very high resolution operation. The RBV has been constructed in 115 mm (4½) and 50 mm (2-inch) versions. The following description, while applying in general, is numerically accurate for the 2-inch tube of the type employed in the ERTS multispectral camera system.

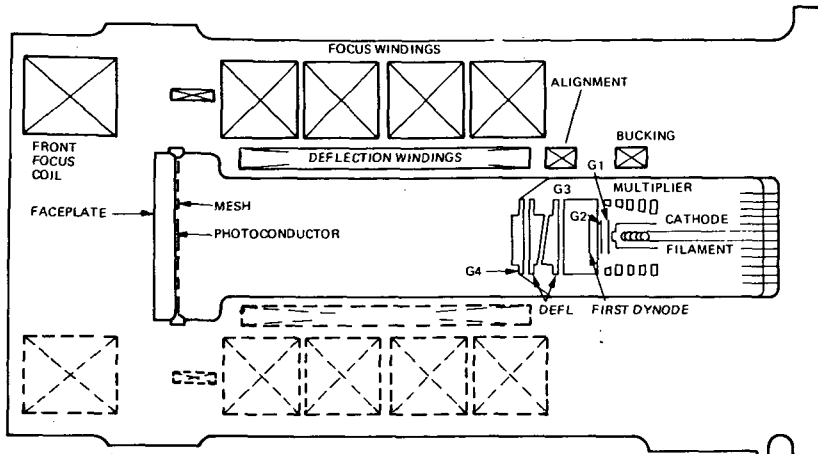


Figure 3-3. RBV

The electron beam cross section is defined by the G2 assembly which contains a 0.7 mm defining aperture. The beam is then demagnified by the electron optics providing the capability for limiting resolution of more than 90 lp/mm. As is conventional in vidicons, the beam lands on the photoconductor after passing through a closely spaced field mesh. The portion of the beam landing on the target during the readout scan is determined by the exposure discharge of the surface.

However, in contrast with the usual vidicon operation the portion of the beam not required to recharge the photoconductor contains the useful signal information. This reflected beam is returned along the same axial path toward the gun exit aperture. Prior to arriving at the gun the deflector electrodes act to deflect the returning beam so that the exit port in the first dynode of the multiplier is not scanned by the returning beam. The beam landing on the first dynode generates secondary electrons which in turn are amplified in the five-stage electron multiplier structure.

The gain provided by the multiplier is effectively doubled by employing both the last dynode and the anode as signal electrodes. The signals are out of phase for useful information and are processed in a differential amplifier to provide common mode rejection for any spurious pickup in the multiplier structure, or dynode supply.

The complete operational sequence is shown in the timing diagram of Figure 3-4. For repetitive shuttered-mode picture taking, the sequence begins with the erasure of old information. The photoconductor is first

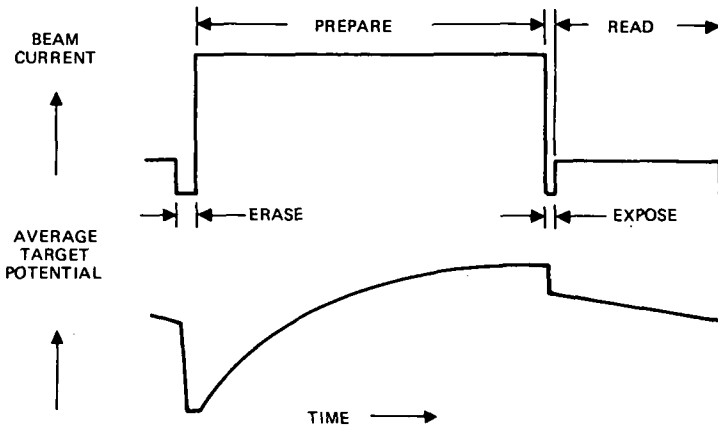


Figure 3-4. RBV Operational Sequence

discharged and then prepared for exposure by scanning the surface with a relatively high current beam.

Exposure is the next step in the operational sequence. The electro-optical process produces an electrical charge pattern by selective discharging of the elementary capacitance of the photoconductor surface, as for any vidicon. Reading is the final step in the process and is accomplished with a substantially lower value of beam current than that employed for surface preparation. The readout process is only partly destructive, depending on the type of photoconductor employed. Several readout scans may be employed at only small degradation in signal-to-noise ratio per scan. The whole operational sequence is repeated at time intervals and rates determined by the system application, as well as the operational requirements of the RBV.

The ASOS (antimony trisulfide oxysulfide) photoconductor is employed for aerospace applications. This type of target has good storage characteristics and is suited to the slow scan rates and long readout time required for the usual bandwidth limitation of its associated communication links. The characteristics of this photoconductor also largely determines the prepare-cycle requirements. Typically, a prepare time of the order of 5 to 15 seconds is required to establish equilibrium on the surface. Figure 3-5 shows the spectral response of the ASOS surface used for the ERTS-1 camera tubes.

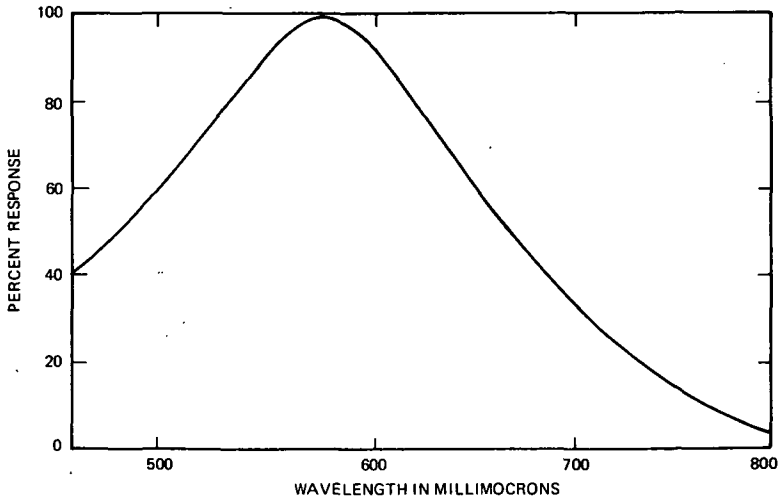


Figure 3-5. Spectral Sensitivity of RBV

Silicon Return Beam Vidicon

A Silicon diode array target can be substituted for the ASOS photoconductive target normally used in the 50 mm RBV high resolution camera tube, resulting in a high resolution sensor with improved sensitivity and spectral response.

Conventional silicon targets have a diode center-to-center spacing density of 72 per millimeter. In order to improve the resolution capability of the tube, special silicon targets having spacing density of 130 per millimeter have been used experimentally to demonstrate that such high-resolution silicon-target tubes are practical. Other than the target and minor variations in the faceplate construction, the experimental silicon RBV tube is identical in construction with the 50 mm RBV with the exception of format size and minor variations in face plate construction.

The performance of these targets retains the advantageous characteristics of conventional silicon-vidicon targets (See *Silicon Target Vidicons*, pages 217-225). Quantum efficiency approaches unity throughout the visible range. The spectral response extends from 0.35 to 1.1 μm (Refer to Figure 3-6). The ultraviolet response is limited practically by the faceplate transmission and the infrared by the bandgap of the silicon. Because the signal developed in the silicon target is proportional to the input radiation, the device has a unity gamma character in the operating range.

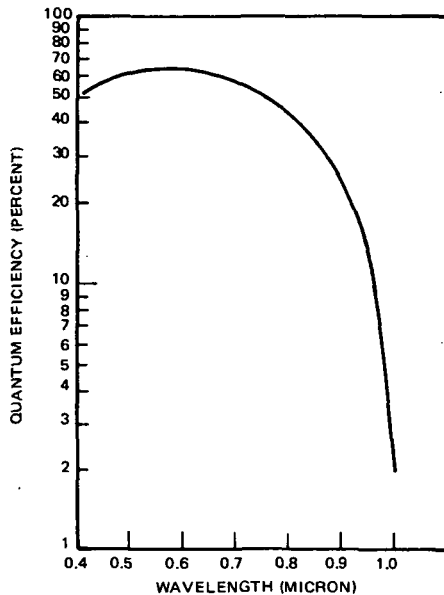


Figure 3-6. Spectral Sensitivity of Silicon

Performance Considerations

Tables 3-1 through 3-5 summarize the important performance characteristics for various RBV tube types. The tables reflect characteristics that range from the flight demonstrated performance of the ASOS-photoconductor 50 mm RBV (Table 3-1) to conceptual designs for a 175 mm RBV (Table 3-5). Figure 3-7 is a typical MTF characteristic that can be applied to any of the ASOS tubes, for describing present day performance. Figure 3-8 shows the light transfer characteristics of ASOS.

In each of the referenced performance tables, both the state of the art is described and the potential capability for each device is indicated. The following paragraphs summarize the steps that must be taken to achieve the indicated potential with the different RBV tube types.

50 mm RBV (ASOS Surface). Modest investments in tube development can be expected to improve both the resolution and sensitivity of the 2-inch RBV. Specifically, efforts to improve mesh fabrication techniques and thinner photoconductors will provide improved performance. Perhaps the largest possible avenue of resolution improvement will be achieved by reducing the beam cross section at the G2 gun aperture. This latter change

requires the development of higher current density electron gun designs to provide the same beam current within the smaller diameter beam.

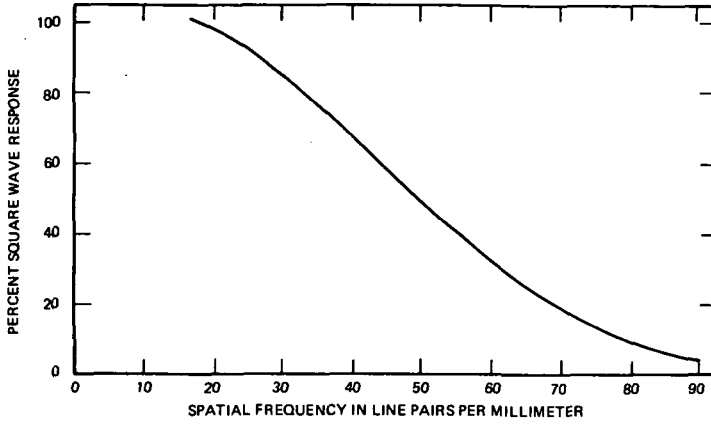


Figure 3-7. Square Wave Response of ERTS RBV Camera

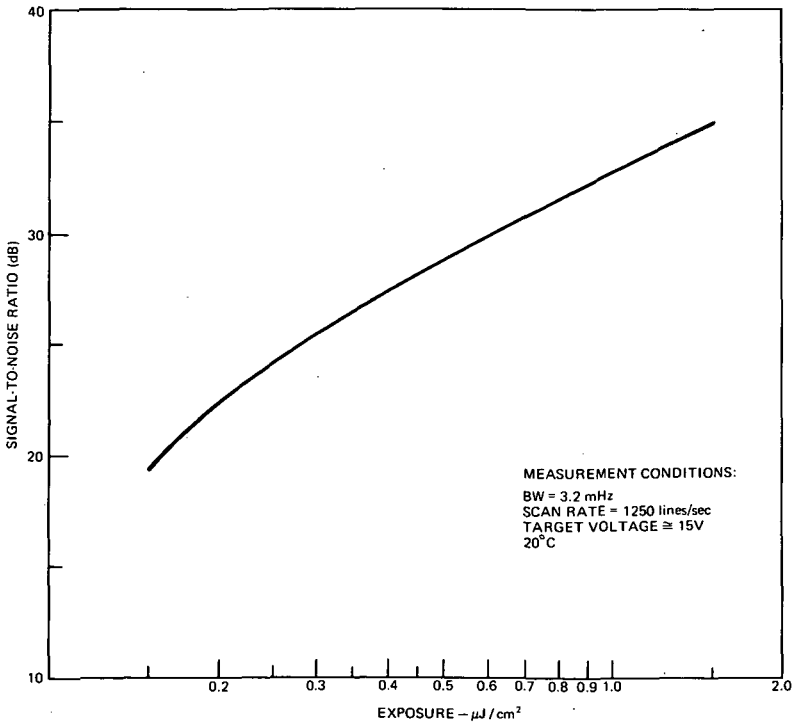


Figure 3-8. Light Transfer Characteristic RBV - ASOS Target

TABLE 3-1

50 mm RBV (ASOS Photoconductor)

	1972	Potential Capability
Status	flight status	
Resolution	50% @ 45 cy/mm 70% @ 75 cy/mm	50% @ 60 cy/mm
Sensitivity (10:1 SNR)	$3 \times 10^{-4} \text{ J/m}^2$	$2 \times 10^{-4} \text{ joules/m}^2$
Spectral Response	.48 to .67 μm (50%)	Same
Storage	90% after 15 sec	Same
Intra-scene dynamic range	80:1	>100:1
Format size	25mm x 25mm	Same
Radiometric Accuracy		Same
Operational BW	3.5 MHz (3.25 msec frame time)	Same
Geometric Distortion	1% (uncorrected) 2TVL (corrected)	Same
Weight (less optics)	18 kg	Same
Power	50 W	Same
Volume (less optics)	.013 m^3	Same
Deflection	Magnetic	Same
Special Requirement	Focus current supply to 0.5% stability moderate cooling required	Same

TABLE 3-2

50 mm RBV (Silicon Photoconductor)*

	1972	Potential Capability
Status	Developmental tube	
Resolution	70% @ 40 cy/mm 20% @ 50 cy/mm	<50% @ 50 cy/mm
Sensitivity (10:1 SNR)	3×10^{-5} joules/cm ²	
Spectral Response	<.4 to .9 μ m (50%)	
Storage	See special requirement	
Intra-scene dynamic range	100 to 1	
Format size	25mm x 25mm	
Special Requirement	Cooling required for storage. For 10-20 second storage, target temperature must be maintained at <-20°C. Only one frame required to prepare	

*All parameters except those noted are identical to ASOS RBV, Table 1.

TABLE 3-3

115 mm RBV (ASOS)

	1972	Potential Capability
Status	Brassboard camera	
Resolution (limiting)	50% @ 45 cy/mm 20% @ 75 cy/mm	50% @ 60 cy/mm
Sensitivity (10:1 SNR)	3×10^{-4} joules/m ²	2×10^{-4} joules/m ²
Spectral Response	.48 - .67 μ m (50%)	
Storage	90% in 15 sec	
Intra-scene dynamic range	100:1	
Format size	50mm x 50mm	
Radiometric Accuracy	poor	
Operational BW	3.5 MHz (10 sec frame time)	
Geometric Distortion	1% uncorrected	
Weight (less optics)	44 kg	
Power	200 W	
Volume (less optics)	.039 m ³	
Deflection	magnetic	
Special Requirement	same as 50 mm ASOS RBV	

TABLE 3-4

115 mm RBV (Silicon)

	1972	Potential Capability
Status	Conceptual	
Resolution		50% @ 50 cy/mm 20% @ 70 cy/mm
Sensitivity (10:1 SNR)		3×10^{-5} joules/m ²
Spectral Response		< .4 μ to 0.9 μ , 50% pts
Storage		Requires cooling for storage. For 10-20 second stor- age, target tem- perature must be maintained below -20°C. Only one prepare frame required.

TABLE 3-5

LARGE FORMAT RBV (ASOS)

	1972	Potential Capability
Status	Conceptual	
Resolution		50% @ 60 cy/mm
Sensitivity		3×10^{-4} joules/m ²
Format size		100 mm x 100 mm
Weight		90.7 - 136 kg
Power		300 - 400 W
Volume		.049 - 0.66 m ³

Initially, the M-type dispenser cathode can provide the increased cathode current density. However, the current density requirement is a natural application for the newer negative electron affinity (NEA) cathode, which could easily handle the increase in current density as well as providing solid state reliability, eliminating a potential life limiting item in the tube. (The NEA material status is described later in this chapter.)

Improvements in mesh and photoconductor technology may well offer improved shading characteristics. While present shading effects are contributed by the combination of electron optics and electron multiplier uniformity, the photoconductor and mesh are also important contributing factors. It is reasonable to expect improvements of the order of 2 to 1.

In summary, signal-to-noise improvements of the order of 3 to 6 dB can be anticipated. Combined with MTF improvements, the limiting resolution may well be extended to the range of 120 lp/mm. In addition substantial improvements in shading can be obtained.

50 mm RBV (Silicon Target). The developments noted previously for the ASOS tube are appropriate for the silicon RBV as well. The major development problem, however, resides in the target. Development tubes tested to date require additional work to approach expected sensitivity and resolution. Figures 3-9 and 3-10 show the present status of sensitivity and resolution measurements made with experimental tubes. Process work is required to achieve consistent quality targets of the required format size. Finally, the current diode density of 3300 diodes to the inch can be improved to better than 4000 diodes to the inch. Experimental targets of this density have been built.

Applications of the silicon tube requiring storage times of the order of 10 seconds requires operations at temperatures in the order of -20°C . This requirement is significantly different than that with ASOS targets, which require only moderate temperature control to prevent temperature from rising above $+30^{\circ}\text{C}$.

The major benefits expected with the silicon RBV will be availability of a big resolution tube with the broad spectral characteristic typical of silicon, as well as having improved sensitivity.

115 mm RBV (ASOS Target). The 115 mm RBV is currently being funded in a manufacturing methods program and is expected to be completed in mid 1973. The mesh, photoconductor and electron gun improvements described for the 50mm tube are applicable to the 115mm version as well.

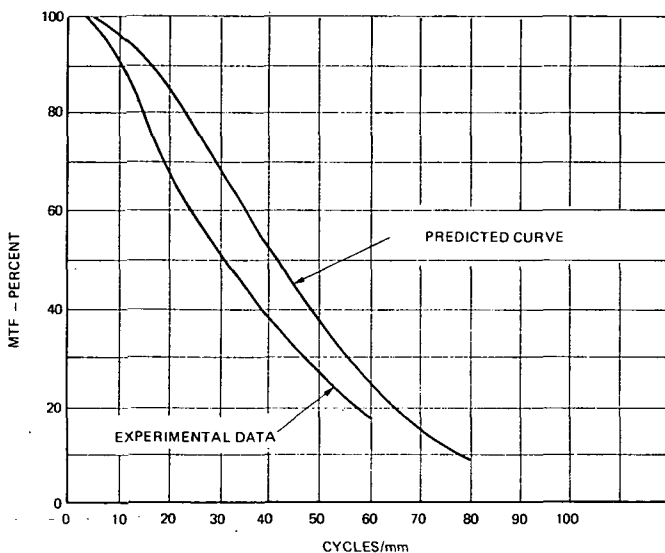


Figure 3-9. The predicted MTF curve for the Silicon RBV is shown. Experimental data are shown after corrections from square-wave to sine-wave response and for MTF losses in the optical system.

For space application, a determination is required of the potential problem of maintaining focus under both air and vacuum conditions. If the faceplate motion is shown to exceed the depth of focus, development of a tube with a thicker faceplate will be required. (6.4mm thickness is used in the 50mm tube compared to approximately 4mm in the current 115mm design.)

115 mm RBV (Silicon Target). The development requirements stated for the 50 mm tube apply. The degree of difficulty associated with achieving high quality 50 mm x 50 mm targets is significantly greater than that for a 25 mm target, but nevertheless is considered achievable, even in the 4000 diode/inch version.

Larger Format Vidicons. There is every reason to believe that RBVs up to 175 mm (100 mm x 100 mm active target) are achievable, at least in the ASOS version. This work has been studied conceptually, but no development work has been started. Device development would be followed by camera design work. Achievement of a breadboard design will require probably 4 - 6 years from the start of development efforts.

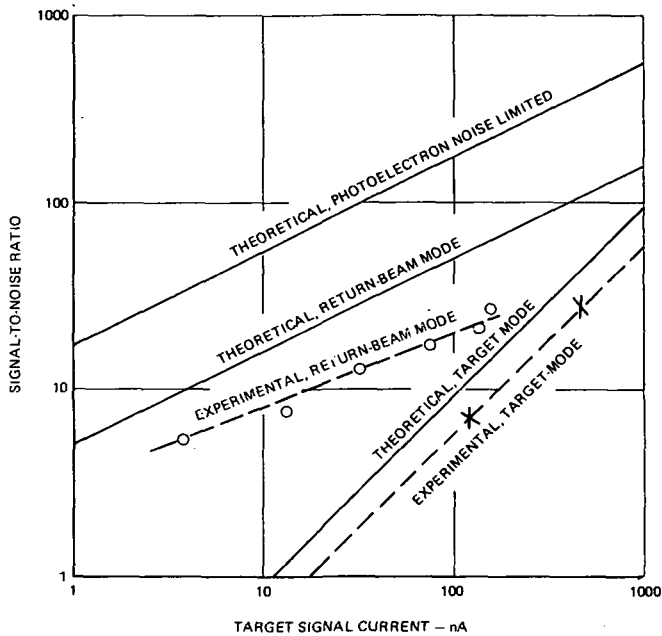


Figure 3-10. Calculated and measured signal-to-noise ratios for the Silicon RBV tube operated in the return-beam mode and in the target mode. Bandwidth is 10 MHz. Also shown is the calculated signal-to-noise ratio for the photocurrent only with no loss.

Multispectral Line Scan Sensor

A variation of the high resolution silicon-target RBV is the multispectral line scan sensor, which would use a specially configured silicon target to provide 8000 diodes (resolution elements) across a total line scanned format, in each of three spectral bands. With this sensor only the early stages of development have been completed, sufficient to demonstrate feasibility of line arrays and the fan-shaped electron beam required for readout of multiple lines.

This multispectral line scan sensor system is shown in concept in Figure 3-11. The ground scene is imaged onto the sensor through a dual modified-Schmidt optical imaging system. A dual system is required to split the image of the ground line across a 185 km (100 n.mi.) swath into two pieces for imaging on the silicon target of a 50mm vidicon. Each half of the optical system contains a 10.2 cm aperture, $f/3.25$ telescope.

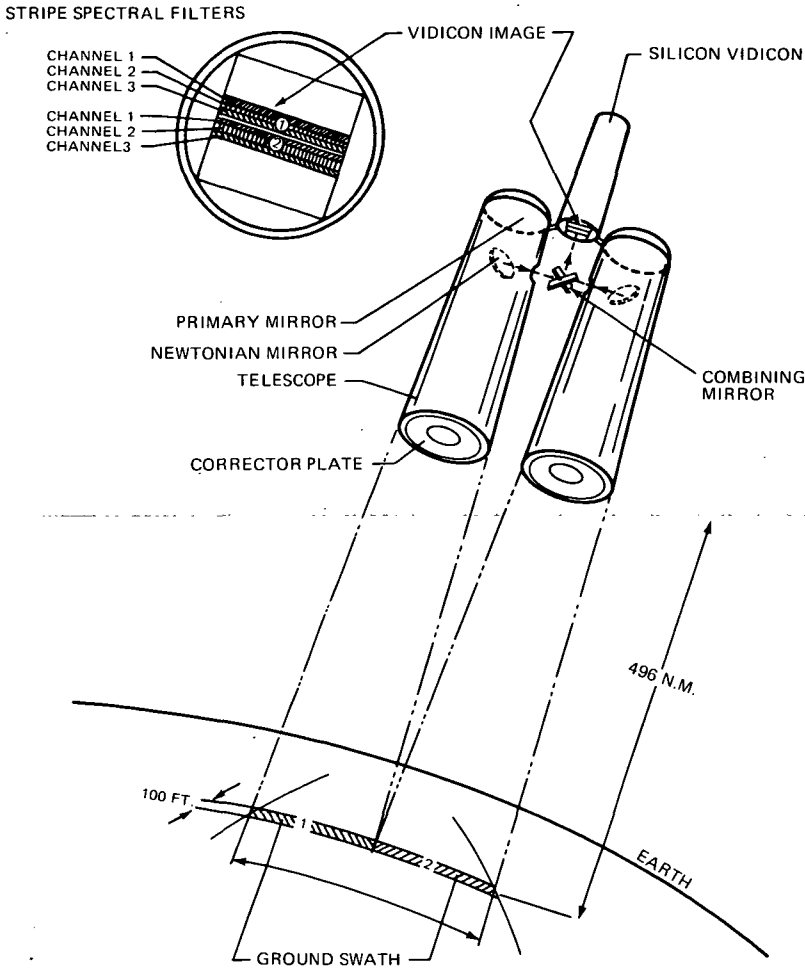


Figure 3-11. General System Concept

The line scan sensor contains a silicon target (conceptually shown in Figure 3-12) consisting of six electrically isolated lines of uniformly spaced p-n diodes formed on a strip of n-type silicon. The diode element density is 3000 diodes per 25mm along a 34mm line, resulting in 4000 diodes per line. The 185 km ground swath is imaged by the dual optical system onto two lines of diodes containing a total of 8000 diodes. Internal dichroic transmission filters of the sensor provide the three spectral bands.

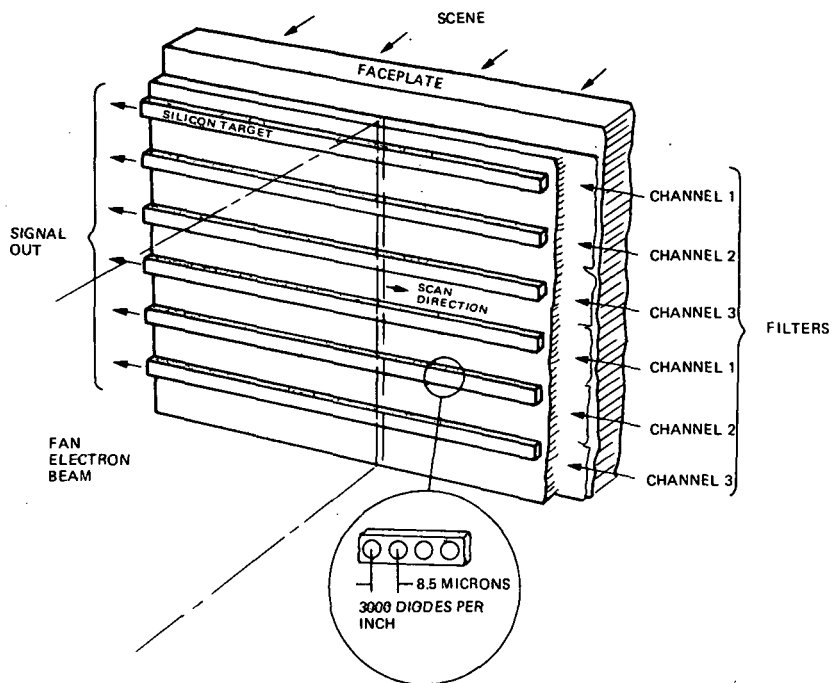


Figure 3-12. Multispectral Line Scan Sensor with Silicon Target

A fan beam, .01 x .89 mm, is used to obtain the simultaneous readout from the diode lines in a single 4 millisecond sweep of the scanning beam. The six simultaneous outputs from the sensor (two per ground swath for each of three spectral channels), suitably multiplexed, will feed a data link for transmission to earth ground station and reconstruction of the image. The line-scan sensor will provide 30 meter resolution per diode from the ERTS altitude of 910 km.

Table 3-6 summarizes the potential performance capability for the 50 mm multispectral line scan vidicon. Development efforts to date have concentrated on tube elements. The current status of development is:

- Silicon diode arrays have been epitaxially grown, using masks developed to produce the required 6 lines of 118 rectangular bales per mm (3000 per inch).
- Spectral filters have been evaporated on each line of the diodes

- Tests of an electron gun to develop the fan beam for readout have shown encouraging results, although more effort is required to achieve a beam with the proper electron density distribution.

To achieve breadboard status for this camera, the tube development needs to be continued to conclusion. Besides finalization of the cited items, the development of techniques for isolating the rows of diodes must be completed, as well as the final design of an integrated tube. This should be followed by the usual steps of process finalization, performance testing, and qualification. Because the tube operates as a line scan device, cooling is not required to enhance storage. The only other major development requiring attention will be the camera optics, to achieve the splitting of the ground line into two line segments on the tube target.

Focus Projection and Scanning Technology

Description of Technique

The Focus Projection and Scanning (FPS) technology combines electrostatic deflection and magnetic focusing into one electron-optic configuration. From the electron-optical standpoint, this device behaves like a scanning lens element that moves in a plane parallel to the target, while projecting on it an image of a spot-defining aperture. It is a simultaneous system, in that the deflection and focus are accomplished in a common volume. This simultaneous approach has many inherent advantages over the sequential technique. It is compact, achieves unity magnification, has no intercepting apertures, and contributes collimation as a byproduct of deflection. In addition, the FPS has the convenience of electrostatic deflection with its small size, power and weight, is magnetically self-shielding, and can be designed to perform a demagnification of the beam spot. This permits realization of high resolution in small envelopes and at low voltages.

A detailed description and analysis of FPS is given by Schlesinger and Wagner (1965 and 1967). As shown in Figure 3-13 a mixed-field cavity is formed by a cylindrical or conical deflectron (D), immersed in a solenoid (F), both being of equal length (ℓ). A factor contributing to the resolution of the FPS vidicon is that the scanning spot is a demagnified image rather than a 1:1 replica of the built-in object aperture (Ap). This is accomplished by the presence of a field-free drift tube which keeps the spot defining aperture (Ap) at a distance (a) from the input to the cavity. A demagnification of 0.7 can be achieved by this process.

TABLE 3-6

MULTISPECTRAL LINE SCAN VIDICON

	1972	Potential Capability
Status	Tube feasibility demonstrated	
Resolution		50% @ 40 cy/mm
Sensitivity		>40 db @ 1 $\mu\text{J}/\text{cm}^2$
Spectral Response		Can be configured to cover any three 100 nm channels in the range 0.4 - 1.0 μ
Intra-scene dynamic range		50:1
Format		linescan. . . 6 lines, 2 per spectral band; each line 33 mm long
Radiometric Accuracy		2% and repeatable
Operational BW		800 kHz (typical)
Geometric Distortion		1%
Weight (less optics)		13.6 kg
Power		35 W
Volume (less optics)		1.3 x 10 ⁴ cm ³
Deflection		magnetic
Special Requirements		focus current regulation to 0.05%

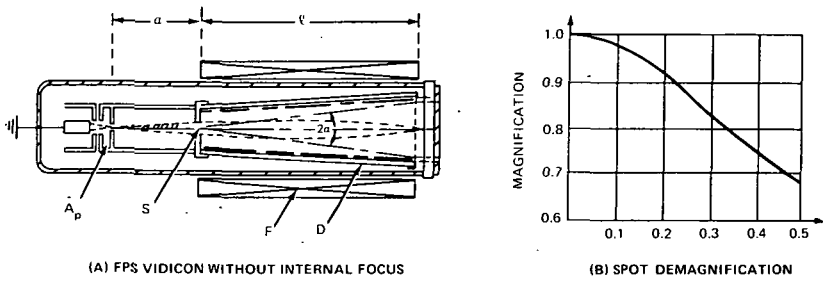
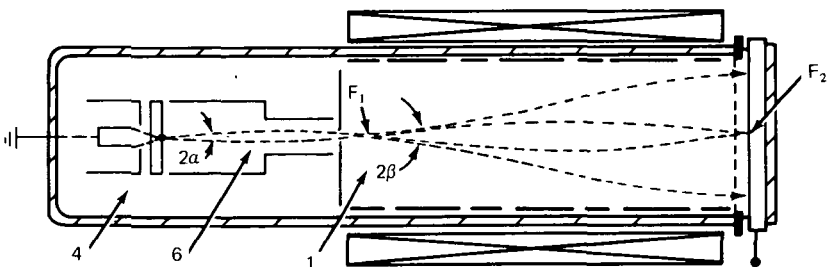


Figure 3-13. Relationship between Object-Distance and Shading

This technique of demagnifying the scanning spot by increasing the object distance cannot be pushed too far since it will affect the background uniformity. The relationship between object-distance and shading of the image due to beam landing errors indicates that shading will decrease with the square of the angle subtended by the target, i.e., the angle (2α) in Figure 3-13. However, for tubes used in applications requiring large target format sizes, the method of "internal-focus projection" was developed (Figure 3-14) as an effective means to reducing shading.

Theory has suggested that landing errors will disappear completely if the FPS cavity is magnetically focused from end to end of the electric field. However, since the target is located beyond the terminating mesh, and since the deceleration between the mesh and target makes the actual spacing appear twice as large to the beam, it becomes necessary to project an internal focus (F_1) to a point situated slightly inside the input plane to the FPS cavity. This is implemented by means of a strong pre-focus lens (6), in this case an electrostatic Einzel lens, projecting a real image of the aperture (4) into the FPS cavity (1). This first focus is virtually undeflected,



FPS VIDICON WITH INTERNAL FOCUS

Figure 3-14. FPS Vidicon with Internal Focus

but it can be shifted along the axis by varying the strength of the pre-focus lens. In addition, F_1 may be demagnified, by appropriate choice of distance ratios, such as to be smaller in size than the aperture itself. Since the scanning spot F_2 as relayed by the FPS cavity is a 1:1 image of F_1 , a demagnification of the aperture is obtained.

The electron ballistics of the FPS optics show that the electrostatic field component used for deflection adds just enough energy to the beam to conserve its axial velocity component during deflection. As a result, the flight time to the target is constant, whether or not the beam is deflected. This feature of the FPS optics provides an almost flat field of focus from center to edge.

High beam current density is important in image tubes in order to provide a wide dynamic range. As the spot size is made smaller, with constant scanning velocity, the beam current density must increase in order to satisfy this requirement for dynamic range. Also with the requirement for high resolution and large data bit storage capacity, vidicons need to have large-area targets which, for a constant frame rate, require a higher scanning velocity necessitating a higher beam current density. Another factor to consider is that for large data bandwidths the signal current must be large to overcome the amplifier noise. All these requirements point to the need of a high-intensity electron gun.

A special emission system with a potentially high radiance was developed for the 75 mm FPS vidicon. This gun is of the Pierce-type and uses a barium dispenser cathode running at an average of 1 A/cm^2 . Peak performance occurs at 3600 anode volts, where the gun has a radiance of $15,000 \text{ A/cm}^2\text{-steradian}$. This gun delivers up to $3 \mu\text{A}$ through a 0.5 mil aperture while at the same time maintaining a narrow beam half angle ($< 1.5^\circ$). Under these conditions an average spot size of 7 microns has been measured.

The FPS can be fabricated with either a Print on Wall (POW) or conical deflection. Although the POW configuration is longer it does offer some advantages:

1. It can be made more rugged since the deflectron is printed on the tube envelope wall
2. Better edge resolution
3. Improved edge shading.

Current Status

The FPS electron optics are used in a number of different vidicons of various sizes and with different target materials. The sizes vary from a 16 mm diameter x 75 mm long to a 75 mm diameter x 450 mm long. A summary of the tube characteristics are given in Table 3-7. Since the deflection assembly is inside the tube, the focusing coil can be made small. The 25 mm FPS vidicon with focusing coil has a maximum outside diameter of 32 mm. The target materials used with the FPS electron optics include antimony trisulfide, lead oxide, photon-in silicon diode targets, electron-in silicon diode targets and slow scan photoconductors.

TABLE 3-7

FPS VIDICON CHARACTERISTICS
(3 x 4 Scan Aspect Ratio)

Tube Diameter (mm)	16	25	38	75
Scan Diagonal (mm)	9	16	25	60
Scan Area (Square mm)	38.1	121	310	1780
Limiting Resolution (TVL/Pict. Hgt)				
Center	700	1200	1400	3600
Edge	600	1000	1200	3000
Corner	500	850	1000	2800
Lag (% @ 50 μ s)	10	18	35	40
Tube Length (cm)	8	16	24	47

The 75 mm FPS vidicon with a selenium-doped antimony trisulfide photoconductor and an FPS vidicon with a silicon photoconductor are the most practical tubes to use for earth observation missions.

Typical characteristics for the 75 mm FPS vidicon are shown in Figure 3-15 through Figure 3-18 and are summarized in Table 3-8 for the current tube and a projected future tube.

The characteristics of the FPS-silicon vidicon are similar to that of the all magnetic version with the exception of improved resolution. An important advantage the FPS electron optics have over magnetic readout when used with the silicon diode target is that high resolution can be obtained with a low field mesh potential (approximately 500 volts). This offers an excellent solution to the degradation of the silicon diode target caused by the soft X-rays generated by the reading beam striking the field mesh.

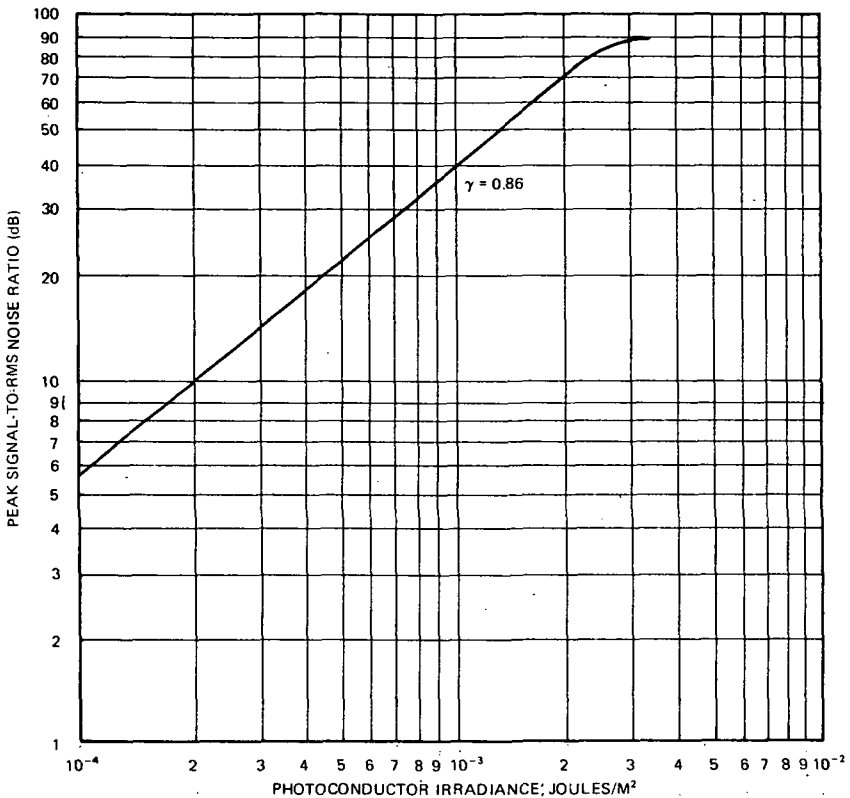


Figure 3-15. Photoconductor Irradiance, joules/m²

A summary of the characteristics of the 2-inch FPS silicon vidicon is given in Table 3-9 for a current developmental tube and a projected tube with improved electron optics and larger diameter photoconductor.

Growth Action Requirements

Advancements in the FPS-vidicon technology can be obtained in two areas: (1) increase in photoconductor size for larger format and (2) improvement in the electron gun and electron optic design for higher resolution.

An improved emission system with a Pierce-type gun, which delivers a beam current of 3 μ amp with a 0.3 mm gun anode aperture and a 1 degree beam defining aperture, was developed for an FPS-Isocon line scanner. In this tube the deflected beam leaves the FPS cavity parallel to the axis, before entering into the isocon-section which houses a 4-stage dynode multiplier. It is electron-coupled to a line scanning beam in such a manner than only

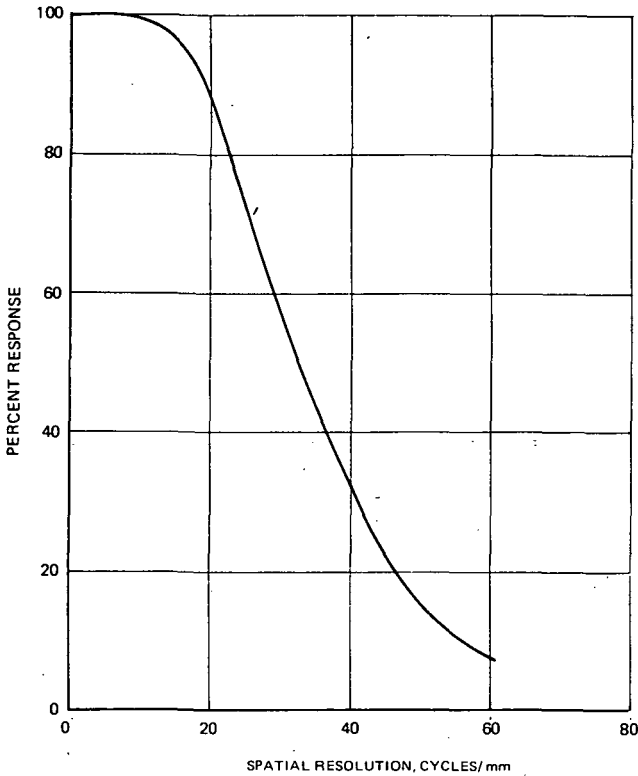


Figure 3-16. 75 mm FPS Vidicon Modulation Transfer Function

scattered electrons from the target can reach the multiplier, specular beam reflection from the target misses the multiplier and is absorbed in the FPS cavity. The measured spatial frequency response for this tube is shown in Figure 3-19.

A further improvement in resolution can be achieved with a reduction in aperture size to 0.2 mm. This would decrease the beam current capability to 1 μ amp which is still adequate for tube operation. The predicted MTF of this tube is 50 percent response at 50 lp/mm, 10 percent at 75 lp/mm, and a limiting response at 90 lp/mm. This electron gun design can also be applied to the FPS-vidicon for achieving a finer beam spot and subsequently higher resolution.

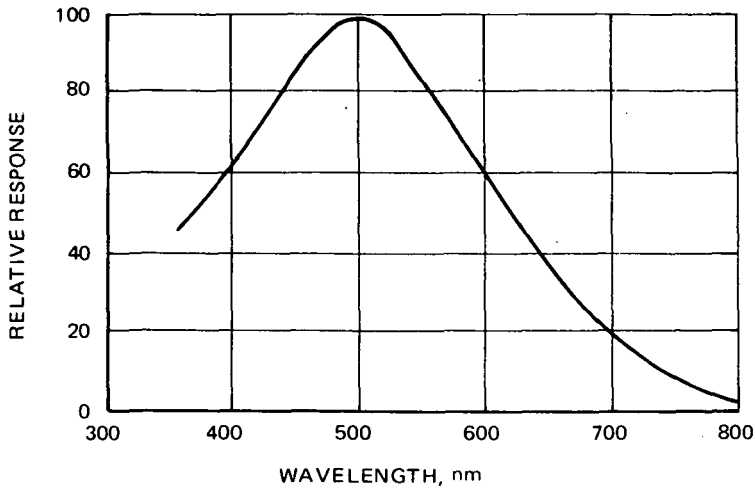


Figure 3-17. Spectral Response Selenium-Doped Antimony Trisulfide

Direct Beam Readout Vidicons with Silicon Diode Targets

A highly promising new material for use as photoconductors in imaging tubes is the silicon diode target. In this section, performance levels achieved with silicon targets are described, demonstrating its use as a photon-to-stored charged converter as required for conventional vidicon applications as well as an electron-to-stored charged converter as used in the silicon intensifier tube (SIT). The first application of the target has been to high resolution frame and line scan sensors. The second application is to provide high sensitivity sensor for low light level requirements (discussed in detail in a later section).

Silicon Target Vidicons

The application of semiconductor technology to camera devices is not new. As early as 1951, it was recognized that arrays of p-n junctions could be used effectively in vidicons (Reynolds, 1961). However, it is only recently that the technology, which resulted from the planar silicon concept and from large scale integration, has made possible a useful silicon camera tube. This was first demonstrated at Bell Laboratories, as recounted by Corwell, et al. (1967).

The silicon target vidicon is shown schematically in Figure 3-20. The target, Figure 3-21 consists of an array of individual p-n junctions produced in a single crystal of n-type silicon.

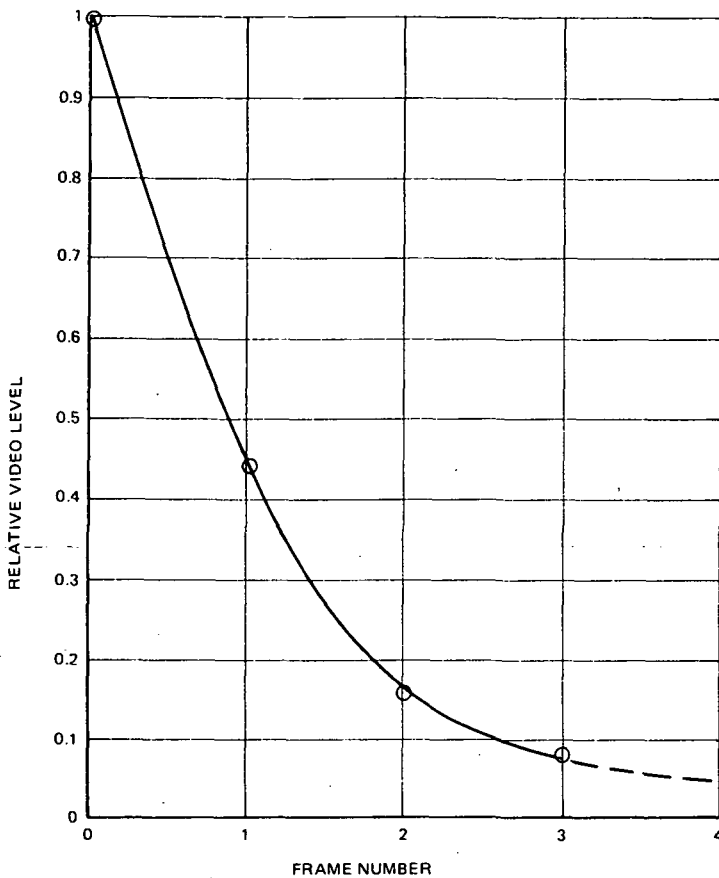


Figure 3-18. 75 mm FPS Vidicon Image Lag

The operation of this device is similar to that of a standard vidicon. A positive potential, relative to the thermionic cathode, is applied to the n-type region of the target. A low energy electron beam scans the surface of the silicon depositing charge such that the p-regions exposed to the beam are brought to cathode potential. Thus p-n junctions are reverse biased by the beam. During the time that the electron beam is not on an element, the reverse bias voltage across the p-n junction decreases as the result of transfer of charge across the junction. This charge arises from either internal generation of free carriers in the material or by photoexcited carriers in the material. These result in dark current and signal current respectively.

The output current is equal to the current which the electron beam must deliver to a p-region to restore it to cathode potential. This, in turn, is

TABLE 3-8
CHARACTERISTICS ON 3-INCH FPS VIDICON

Parameter	1972	Growth Potential
Photoconductor	Selenium-doped antimony Trisulfide	Same
Resolution		
50% response	32 lp/mm	50 lp/mm
20% response	44 lp/mm	70 lp/mm
Sensitivity		
Max. S/N	90	Same
joules/m ² @ 10:1 (dB)	2×10^{-4}	
gamma	.86	
Format size	45 mm x 45 mm	90 mm x 90 mm
Spectral Sensitivity (see curve)	Bandwidth -10% response 300 - 750 nm	Same
Operational Bandwidth	12 MHz \pm 1 db	as required for application
Dynamic Range	90	Same
Geometric Linearity	$\sim 1\%$	$\sim 0.5\%$
Power	50 watts	100 watts
Volume (less optics)	12.5 cm dia. x 56 cm long	23 cm dia. x 70 cm long
Weight (less optics)	5 kg	14 kg

TABLE 3-9

CHARACTERISTICS OF 2-INCH FPS SILICON VIDICON

Parameter	1972	Growth Potential
Photoconductor	Silicon	Same
Resolution		
50% response	28 lp/mm	45 lp/mm
20% response	40 lp/mm	60 lp/mm
Sensitivity		
Max. S/N	300:1	Same
joules/m ² @ 10:1 (db)	1×10^{-4}	
Format size	25 mm x 25 mm	55 mm x 55 mm
Spectral Sensitivity	Bandwidth -10% response 400 nm - 1000 nm	Same
Operational Bandwidth	25 MHz	as required by application
Dynamic range	300:1	Same
Geometric Linearity	~ 1%	~ 0.5%
Power	30 watts	50 watts
Volume (less optics)	7.5 cm dia. x 30 cm long	15 cm dia. x 50 cm long
Weight (less optics)	2 kg	7 kg

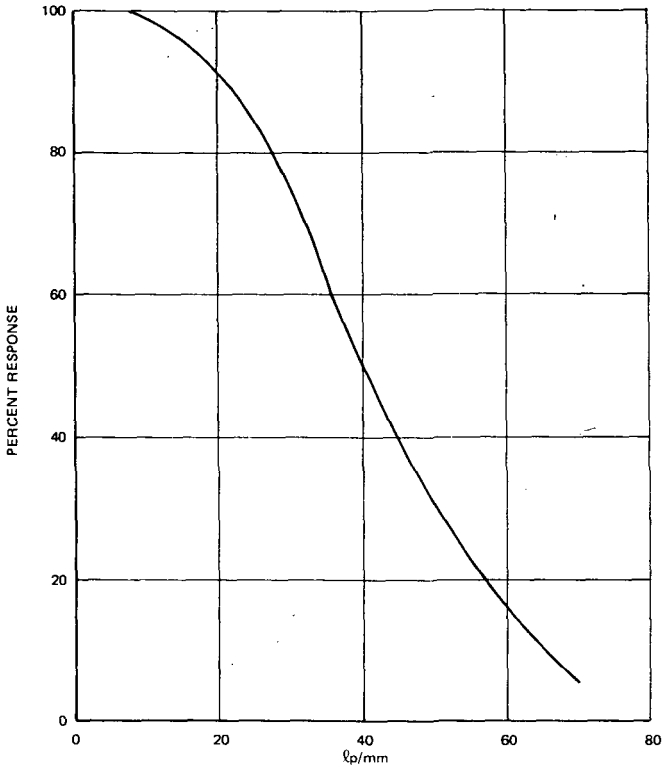


Figure 3-19. MTF of FPS Line Scan Isocon

equal to the dark current plus the signal current which flowed in the associated p-n junction during the time that the beam was not scanning this element.

The sensitivity of the silicon vidicon is shown in Figure 3-22 in terms of quantum efficiency or the number of electrons which flow in the external circuit for each incident photon. It can be seen that quantum efficiency as high as 70 percent can be achieved. Furthermore, the response extends in the infrared to $1.1 \mu\text{m}$. Thus the silicon target vidicon has considerably greater response in the near infrared region of the spectrum than any other vidicon now available. Figure 3-23 shows the response of a silicon-target especially treated for ultraviolet response and in an envelope with a quartz window. It can be seen that the high sensitivity extends to at least $.2 \mu\text{m}$.

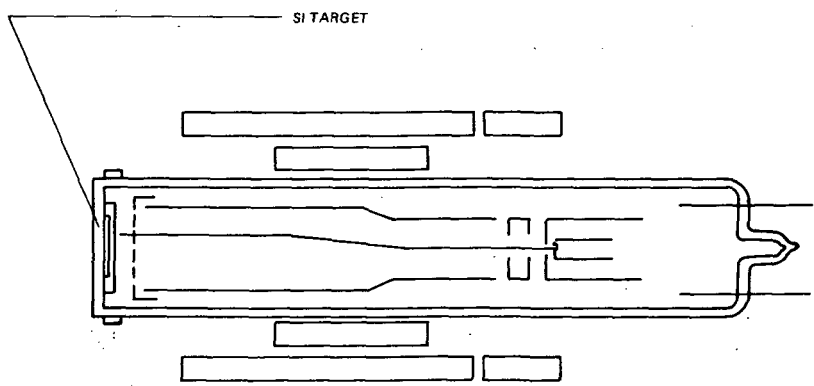


Figure 3-20. Schematic Diagram of a Silicon-Target Vidicon Pickup Tube

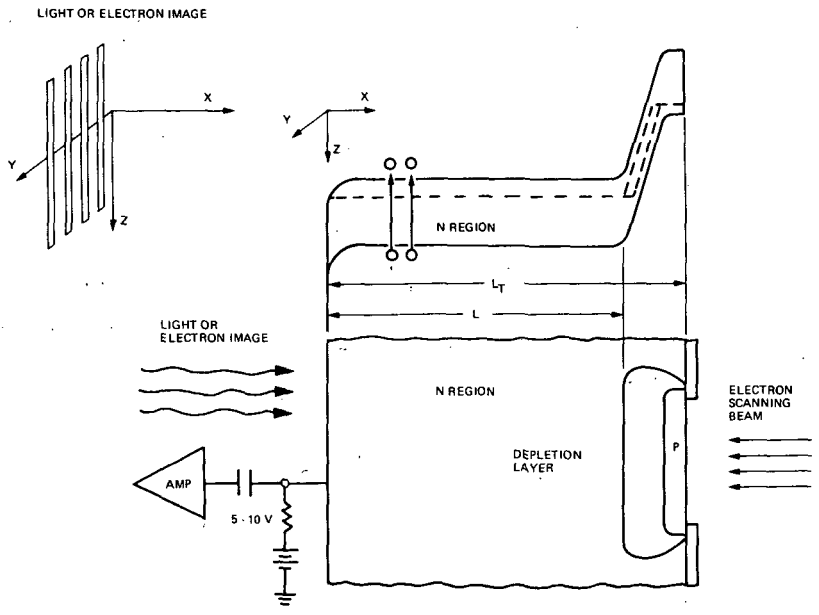


Figure 3-21. Diagram of Silicon Target

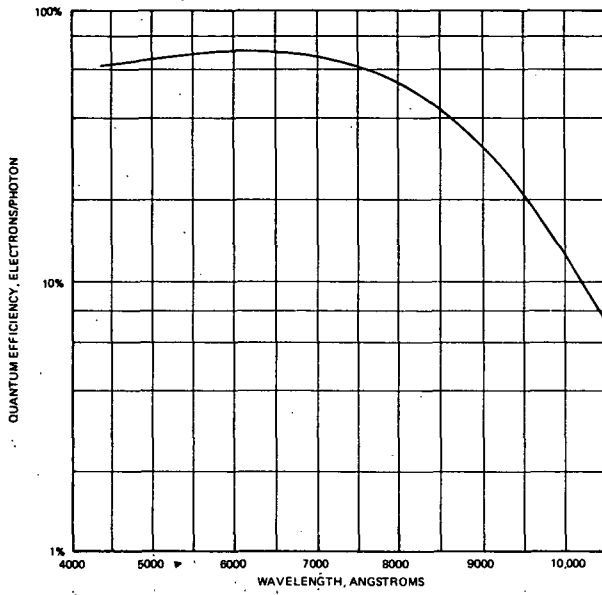


Figure 3-22. Spectral Response of a Silicon-Target Vidicon

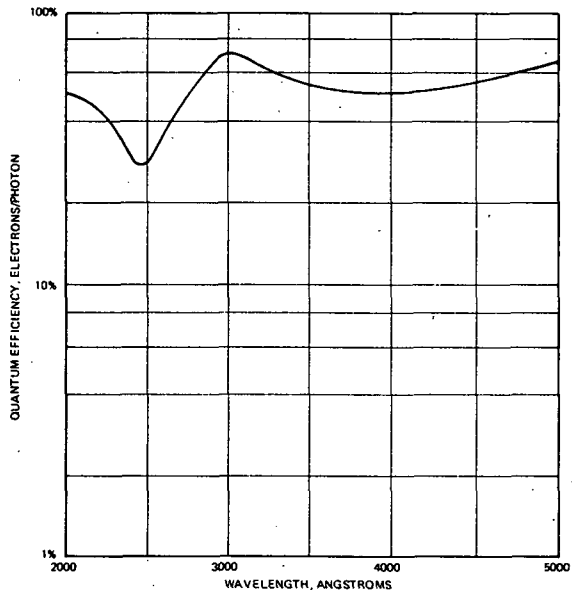


Figure 3-23. UV Response of a Silicon-Target Vidicon

Of particular interest are the slow-scan capabilities of the silicon-target vidicon. The silicon-target has the interesting property of not losing resolution as a function of storage time. The silicon-target vidicon is different in this respect than other vidicons where charge spreading and, therefore, loss of resolution, occurs with time. This performance is expected with silicon since once the photoexcited carriers are collected by a p-n junction, they can no longer spread sideways. A vidicon can be used in slow-scan applications only for times shorter than the time it takes the dark current to discharge the target. By use of a properly designed tube and cooling, it is possible to produce silicon-target vidicons with delayed readouts of minutes. For scan periods of the order of a few seconds, the target temperatures must be typically held at approximately -20°C .

State of the Art and Future Potentials of Silicon Vidicon Technology

Since the demonstration of the feasibility of the silicon vidicon by Bell Labs, the technology has advanced rapidly to the point where these devices are available in a variety of sizes from several manufacturers. Silicon vidicons with target sizes up to 25 mm have been fabricated. Targets with diode densities in the 60 to 70 diodes/mm are utilized in standard commercially available devices. As discussed in connection with the silicon RBV, special experimental targets with diode densities of 130 diodes/mm have also been fabricated. Furthermore, recent developments have shown that effective blooming control can be achieved, at least by one means, resulting in devices with effective intrascene dynamic ranges in excess of 10^5 .

The silicon vidicon represents an image tube with a good compromise between sensitivity, spectral response, and resolution and is rapidly finding widespread applications in both the commercial and military sector. Table 3-10 summarizes the current and anticipated performance levels for silicon vidicons.

For ERTS type missions improvements in several areas are desired. From a yield and fabrication standpoint, it is not likely that self supporting targets in excess of 40 mm will be fabricated without extensive development. Although wafers as large as 75 mm diameter are available, and some work has been done in photolithography with this size of wafer, 40 mm appears to be about the practical limit at the present time. Furthermore, the format size growth capability of silicon targets may be limited by the X-ray induced radiation damage effect phenomena. Large format silicon vidicons will require proportionately higher electrode voltages, compared to their small format counterparts, in order to maintain the same resolving power in the electron optics. These required higher voltages are not com-

patible with extended life operation. Either improvements in low voltage electron optics or the development of X-ray resistant targets will be required to realize the full resolving capability of large format silicon targets.

In other areas of performance, it is not anticipated that significant improvements will be made. Silicon vidicon technology advances in the next few years should be in the form of refinements of the basic existing characteristics, with improvements in yield being anticipated rather than dramatic new developments. Thus, the existing data on silicon vidicons should be a good basis for determining the applicability of the silicon vidicon to various types of ERTS missions.

However, besides the improvements in yields, several possible new approaches may be of significance later in the decade. One such development is the incorporation of an NEA cold cathode in a silicon vidicon. Preliminary data on such a tube was recently presented. Secondly is the continuous graded junction and the ion implanted silicon targets. Yield, cost, and cosmetic quality would be considerably improved by success with such approaches.

Finally it has been amply demonstrated that silicon vidicons have an extended slow scan and integration capability with cooling. Storage times in excess of 1 hour have been observed at temperatures of -40°C . The applicability of cooling as a means to achieve slow scan capability depends to a great extent upon the degree to which a simple implementation of cooling can be achieved in a camera system.

Direct Beam Readout Vidicons with Large Formats

In order to satisfy the need for a camera tube possessing a higher resolution than a conventional 25 mm vidicon at reasonable cost for video processing of printed documents, several vidicon types with large formats have been developed by various manufacturers. The approach taken was basically one of scaling up the 25 mm existing vidicon, incorporating all of the refinements that have been important to improved performance of that tube. The tube that has been developed is the 50 mm vidicon which provides a useful format of 25 x 25 mm.

This type of vidicon provides the advantage of a large format with simplicity of operation, a past history of reliability, and commercial availability. Table 3-11 gives the salient characteristics of this vidicon with the sectionalized coil especially designed for this vidicon. Figure 3-24 illustrates the square wave response of this vidicon in comparison with the 25 mm and 38 mm vidicon. Note that sensitivity and spectral response of the 50 mm

TABLE 3-10

CHARACTERISTICS OF LARGE FORMAT SILICON VIDICON CAMERAS

1. Silicon Vidicon Cameras -- Performance Summary			
Performance	Current Technology	1976	1980
Resolution 20% response 50% response	32 lp/mm 18 lp/mm	50 lp/mm 30 lp/mm	(80 lp/mm) (40 lp/mm)
Sensitivity J/m^2 5500 Å 10:1 S/N	3×10^{-5}	3×10^{-5}	3×10^{-5}
Gamma (γ)	1		
Maximum S/N (dB)	65	70	80
Format	25 mm	40 mm	50 mm
Spectral Response	(0.3 to 1.1 mm)	Same	Same
Bandwidth for Stated Performance	10 MHz	10 MHz	
Storage	< 1 sec at Room Temperature > 1 hour at -50°C		
Radiometric Accuracy	< 5% over long periods	2%	
Maximum bandwidth	30 MHz	60 MHz	
2. Silicon Vidicon Cameras -- Physical Summary			
Weight (less optics)	2 kg	2 kg	2 kg
Power (less optics)	15 watts	10 watts	5 watts
Volume (less optics)	1600 cm^3	1300 cm^3	
Special Requirement	Cooling required for slow scan operation		

TABLE 3-11

CHARACTERISTICS OF LARGE FORMAT VIDICONS

1. Large Format Standard Vidicon – Performance Summary			
Performance	Current Technology	1976	1980
Resolution (MTF)			
20% Response	45 lp/mm	67 lp/mm	--
50% Response	24 lp/mm	40 lp/mm	--
Sensitivity (J/m^2 at 5500 Å for S/N = 10:1)	10^{-4}	10^{-4}	
Gamma (γ)	≈ 0.8		
Maximum S/N (dB)	55	60	--
Format	25 mm x 25 mm	50 mm x 50 mm	
Spectral Response	Sb ₂ S ₃ or Se photocond	--	--
Bandwidth for stated performance	10 MHz	10 MHz	--
Radiometric Accuracy	--	5%	--
Maximum Bandwidth	30 MHz	60 MHz	
2. Large Format Standard Vidicon Camera – Physical Summary			
Physical	Current Technology	Future Potential	
Weight (less optics)	9 kg	7 kg	
Power (less optics)	50 watts	30 watts	
Volume (less optics)	$\approx 8200 \text{ cm}^3$	6600 cm ³	
Special Requirements	none	none	

vidicon are comparable to that of a 25 mm vidicon, if due consideration is taken of the increased format size and the photoconductor.

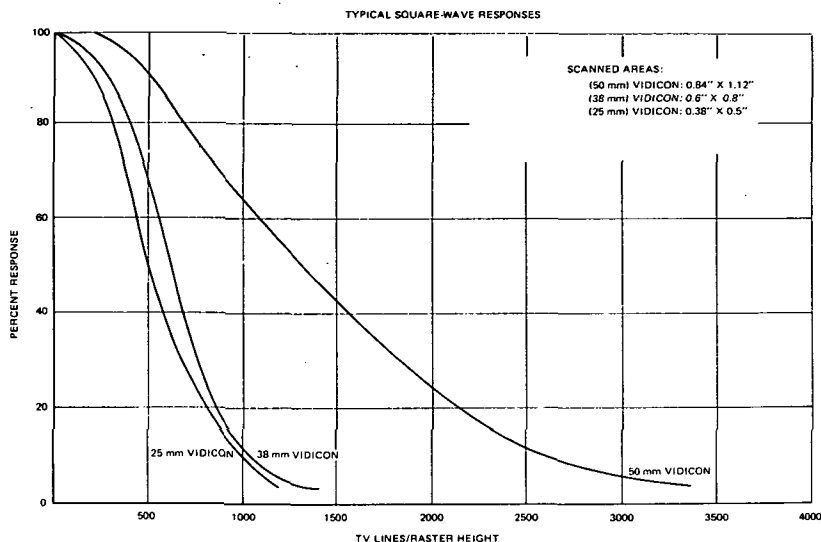


Figure 3-24. Square-Wave Responses of Three Vidicons

Figure 3-25 illustrates the spectral response of the four types of slow scan photoconductors available with the vidicon. As it now exists, the 50 mm vidicon does not possess the limiting resolution or the sensitivity of the 50 mm RBV. However some improvement can be anticipated in both areas. Consequently, the tradeoff between the cost and complexity of the RBV and its slightly better performance should be compared to the low cost and simplicity of the 50 mm vidicon.

Infrared Vidicons

A number of infrared vidicons have been developed for operation in the 1.5 to 15 μm spectral region. A variety of photoconductor materials (copper, nickel and zinc-doped-germanium, lead salts) have been used, with the higher performance tubes requiring cryogenic cooling to between 20 and 100 K. Format sizes have ranged from 10 mm to 35 mm scan diagonal with limiting resolution of 15 cycles/mm achievable. Tubes have been built with both magnetic and electrostatic focus and deflection systems which require camera electronics similar to visible vidicon sensors for operation. Sensitivity of approximately 3×10^{-5} joules/m² at the photoconductor

for a noise equivalent irradiance has been achieved under ambient background conditions with both a copper-doped-germanium vidicon ($1.7 - 3.5 \mu$) and a zinc-doped-germanium vidicon ($8 - 15 \mu$).

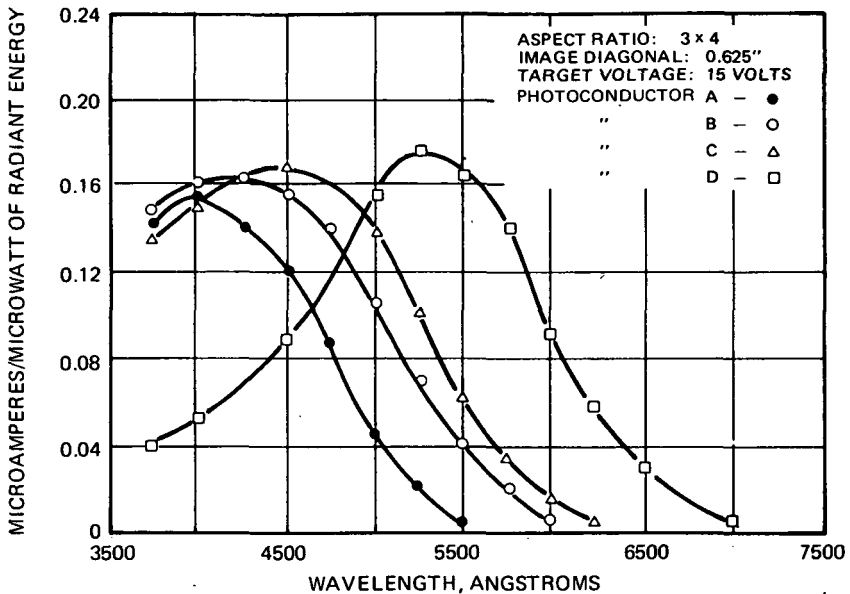


Figure 3-25. Spectral Response of Slow-Scan Vidicons

The infrared vidicon is a charge storage device which has the advantage of sensitivity improvement but the disadvantage of a strong dependence on background radiation levels. The photoconductor has a maximum charge storage capacity, and under high background radiation conditions, small signal levels are detected above a large background dc signal. This severely limits the effective tube responsivity and dynamic range. As a result the primary application for these devices has been directed towards the detection and imaging of targets against a low infrared radiating background (sky background). The earth observation mission is a high background application and consequently the vidicon performance is limited to high contrast scenes (large temperature difference $\approx 1 - 5 \text{ K}$).

Another disadvantage of the IR vidicon in the space application is the cryogenic requirements. These tubes in general require 10 - 15 watts for cooling the photoconductor as well as internal tube elements to 80 K (to minimize the background radiation). Closed cycle coolers with this

capability and adequate reliability and lifetime are not available at present and will have to be developed.

The development of solid state devices that do not suffer from the high background radiation limitation of the vidicon and that have a reduced cryogenic requirement appears to be more appropriate for earth observation in the thermal infrared band.

Image Dissector Cameras

Description

The image dissector camera has certain unique properties that are related to its detector method and image beam scanning, in contrast to cathode beam scanning of the more conventional image sensors. The independence of the scanning function and the ability to select tube components and components and combinations for a given application permit use of this sensor in selective and adaptive applications. These characteristics have been utilized in past programs for such functions as:

- Slow-scan image generation
- Spin satellite derotation
- Multiple outputs from a single sensor tube
- Electronic motion stabilization within the sensor tube
- Offset scanning of imagery
- Multiple functions of imaging, tracking, communication
- Fully electronic operation, eliminating shutters, iris, or motion devices
- Computer controlled scan positioning

These uses have led to the meteorological cameras for Nimbus and ATS-3, the generation of multiple color imagery from the Multispectral Ocean Color Scanner using a diffraction method of color separation, and the Multispectral Image Dissector Camera System using color separation filters and a three-aperture tube.

The future value of the image dissector may be in its ability to adapt to a specific set of mission requirements and its potential to tie into a real time information gathering and processing system. This has been found to be one of the most efficient of detectors and will doubtless continue to fulfill many requirements of the ecological, meteorological, and scientific community.

The Image Dissector Tube

Image dissector cameras are based on a particular type of electron beam sensor tube in which image forming is different from that of the electron gun. In the image dissector tube, as shown in Figure 3-26, the optical pattern from any type of lens or optical system excites a photo-emissive surface on the internal surface of the front plate of the tube. Electrons from the photocathode are accelerated toward a metallic screen by a potential of approximately 600 volts. Once having achieved a uniform potential, the total electron image is contained within a cylindrical magnetic focus field and is translocated to an aperture plane approximately 12 to 15 cm from the photocathode by refocusing each element of the original image to a corresponding point at the aperture plane.

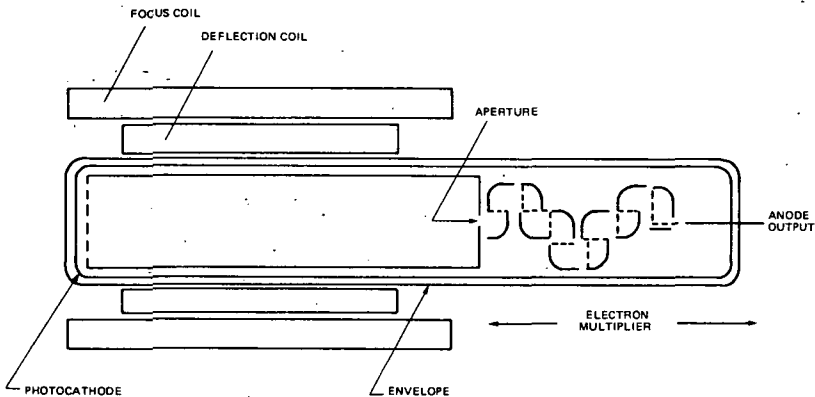


Figure 3-26. Image Dissector Tube, Schematic

The electron image at the aperture plane is a complete 2-dimensional representation of the optical input. If the aperture plane were to be a phosphor screen, it would be possible to view the optical image at that position; however, in the application of the image dissector tube as an imaging device, the aperture plane is a metallic plate with one small opening

(aperture) centrally located. In the case of a focused but undeflected image, the electrons arriving at this small aperture are those coming from the corresponding position on the photocathode. The size of the sampling aperture therefore determines the area of the photocathode from which the optical image is being sampled. By selecting the aperture size and shape, it is possible to adapt the image dissector tube to a wide variety of requirements and in many cases be able to trade off resolution for signal-to-noise ratio, image characteristic definition or other features.

A multiple stage electron multiplier follows the sampling apertures. In a typical tube there are ten multiplier stages, each with an electron gain of approximately 3.5. This generates 1 million electrons at the output of the electron multiplier for every electron that is passed through the sampling aperture. The box and grid type of electron multiplier is often used for its low noise characteristics and the ability to handle high currents at linear gain.

In the typical image dissector system, a single aperture placed at the center of the aperture plane is used to sample a given element of the optical image. When the focus field is augmented by orthogonal magnetic fields, the total electron image is moved across the aperture plane. The deflection rate and waveform are completely open to the designer permitting either raster scan, line scan or some form of combined scan such as offset, sub-raster, radial scan or tracking scan for a given application. The image dissector is capable of operating at all scan rates from zero motion to very rapid motion of the electron image across the sampling aperture. The trade-off and selection of scan mode is determined by the requirements of an end system, but in an adaptive application, the image dissector approach may provide specific capability not normally available with electron beam sensor devices.

The image dissector originated in the early days of television and was used in one of the first electronically scanned cameras. Because of sensitivity limitations, the dissector could not compete at high scan rates with sensors utilizing integrating type targets and its use became quite limited. In the past decade a multitude of new sensor requirements has developed which can be met best with a nonintegrating type of device. To meet these needs, the dissector has been redesigned and greatly improved.

Today it is a popular sensor for special applications and for experimental activities in many new fields of endeavor. The 25 mm image dissector, with an 18 mm format, is the design that was applied to the slow scanning camera system flown on the Nimbus III and Nimbus IV satellite in which

the slow scan capability and high resolution quality of the system provided excellent imagery of both ground and cloud cover. A more sophisticated application of the 25 mm image dissector in the ATS-3 satellite made use of the nonstoring property of the sensor tube to permit a derotation scan in one axis that offset the rotational characteristic of the satellite and an orthogonal scan which permitted a line scan across the face of the earth.

As a part of the earth resources technology satellite program, a high resolution image dissector system was developed. In this particular camera, a 57 mm diameter tube was utilized having a 45 mm diameter photocathode surface, a small aperture of 15 microns, and a combination of 3 apertures. Each aperture sensed a line from the image as it was translated from the photocathode to the aperture plane. By having three color strip filters in front of the photocathode, the 75 mm line apertures were capable of simultaneously recording the color content of the optical image as it passed across the photocathode. This program has been completed to the point of having airborne photography generated and reproduced and the usefulness of the color extraction and recombination features successfully demonstrated.

Signal Characteristics of the Image Dissector

The output signal from the image dissector results from an instantaneous sampling of the electron image. In a typical S25 photocathode, such as that shown in the spectral response curve of Figure 3-27, the quantum efficiency will reach 20 percent and will result in 60 milliamperes per square centimeter per watt of radiant flux. With the red response of the S25 photocathode extending out to beyond 900 nanometers, this type of sensor has the capability for extension of responsivity beyond that of many photoconductive surfaces but not yet equaling that of silicon diode array surfaces.

The output of the tube is set by the efficiency of the photocathode, the transmission factor of the accelerating screen, the size of the collecting aperture, and the gain of the electron multiplier. The typical dynamic range for an image dissector may extend over 4 orders of magnitude, since the lower limit of sensitivity is generally determined by a leakage current at the base structure of the tube where the electrical leakage from the base pins causes a small amount of current at the output. This leakage current is in the order of 10^{-11} amperes, compared to typical signal currents of 10^{-6} amperes. From this point, the output of the tube is linear with respect to input flux up to the point where the charge density at the final dynodes begins to limit the linearity of the output current. For applications where high tube currents may be anticipated, special dynode structures have been developed which permit output currents in the order of hundreds of milliamperes.

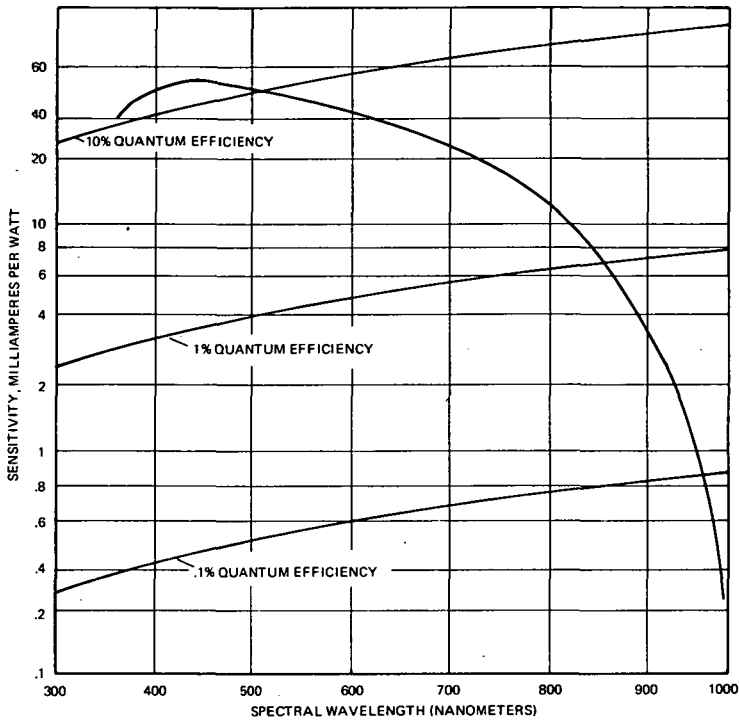


Figure 3-27. Photocathode Response

The fact that the sampling aperture receives electrons emitted from a very small part of the photocathode eliminates a source of noise which is often apparent in wide area photo tubes, that is, the thermal noise from the cathode itself. In this particular case, the only thermal noise detected is that coming from the part of the photocathode being sampled by the aperture and is in the order of 10^{-13} watts/m² on the photocathode. In the output signal, therefore, a linear variation of output current with input flux is found. A noise component is evident in the output signal as an increasing value as the input flux increases. This is shot noise, or the random variation of electron arrival at the dynodes and the random variation of energy levels within the electron beam. The noise current is therefore a direct function of the square root of the number of electrons flowing through the tube. An additional contribution of noise is provided in the dynode structure themselves, where there is a randomness of the multiplier gain that is a function of the dynode gain itself. The equation for signal-to-noise in an image dissector is given in Equation (1). This is the signal-to-noise ratio for a given condition of sampling time interval, since the effect of noise in the

system is a function of the sampling time, the size of the sampling aperture, the sensitivity of the photocathode, and the multiplier gain.

$$S/N = \left[\frac{J_K a K (\sigma-1)}{2 e f \sigma} \right]^{1/2} \quad (1)$$

where

- J_K = photocathode current density resulting from the integration of all radiant energy and the sensitivity of the photocathode
- a = area of sampling aperture
- K = transmission coefficient of the accelerating screen
- σ = dynode electron gain
- e = electronic charge 1.6×10^{-19}
- f = system noise bandwidth

Figure 3-28 shows the sensitivity of an image dissector under two conditions of aperture size (.25 mm or .010 inches, and .025 mm or .001 inches diameter), and two sample time intervals 2.5 and 25 microseconds. The values of selecting minimum resolution and signal bandwidths are recognizable as gains in sensitivity.

To compare input energy for total image generation with other sensors, a typical high resolution sensor is assumed (3200 elements per scan and 2.5 μ sec per element). There are 10^7 elements in a square segment of a reproduced scene. The time for scanning is therefore 250 seconds, and at 10:1 S/N, an input flux of 0.1 watts per square meter indicates a total energy requirement of 25 watt seconds/sq meter (joules/m²). A low resolution system (320 elements/scan, 25 microseconds per element) requires 2.5 seconds, and an energy input of 2.5×10^{-4} joules/meter².

The resolving power of the image dissector is determined by the magnetic field effects and the sampling aperture size. Figure 3-29 gives the modulation transfer function of a typical quality system having a 15 micron aperture diameter. This tube, in line scan mode, can generate imagery of 4800 TV lines in a 41 mm format.

Intensified Image Dissector

An image intensifier tube coupled to an image dissector provides both light gain and storage time to the detection process. Schematically, this is shown in Figure 3-30. The light gain is not valuable in itself since noise in signal is increased, and there are attendant problems of background noise, loss in

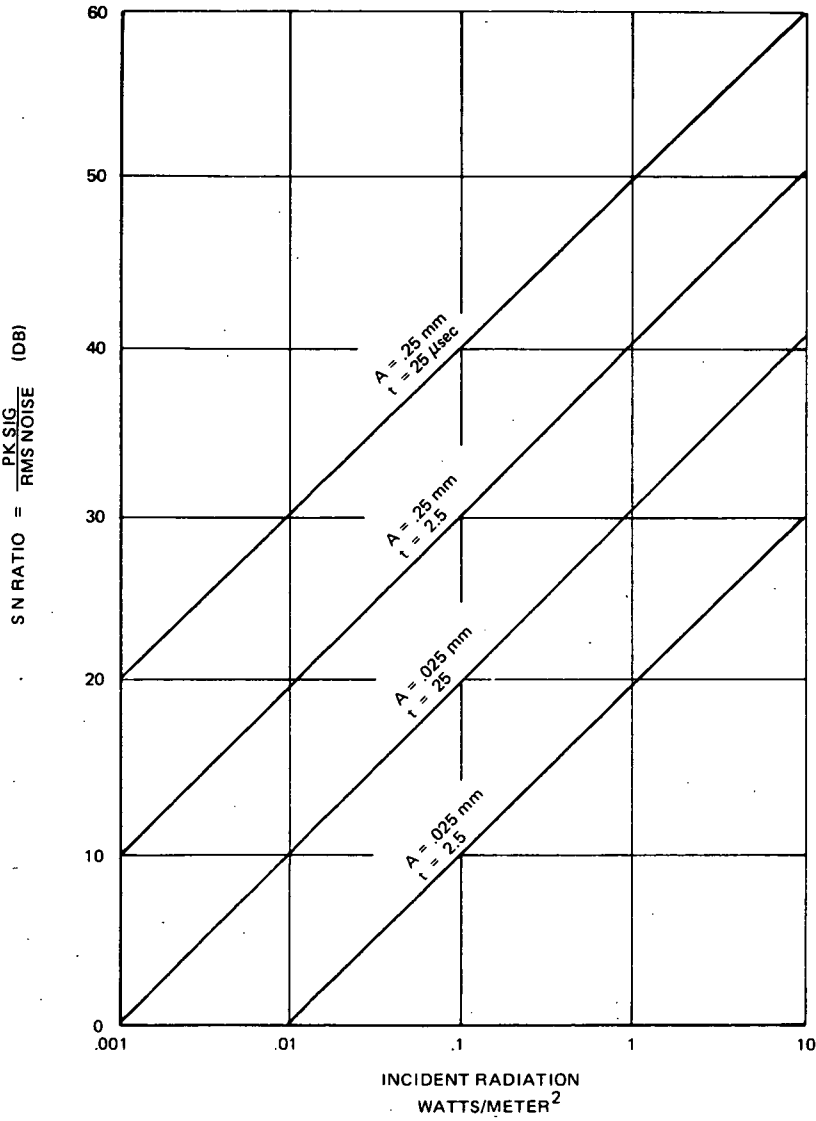


Figure 3-28. Image Dissector Sensitivity

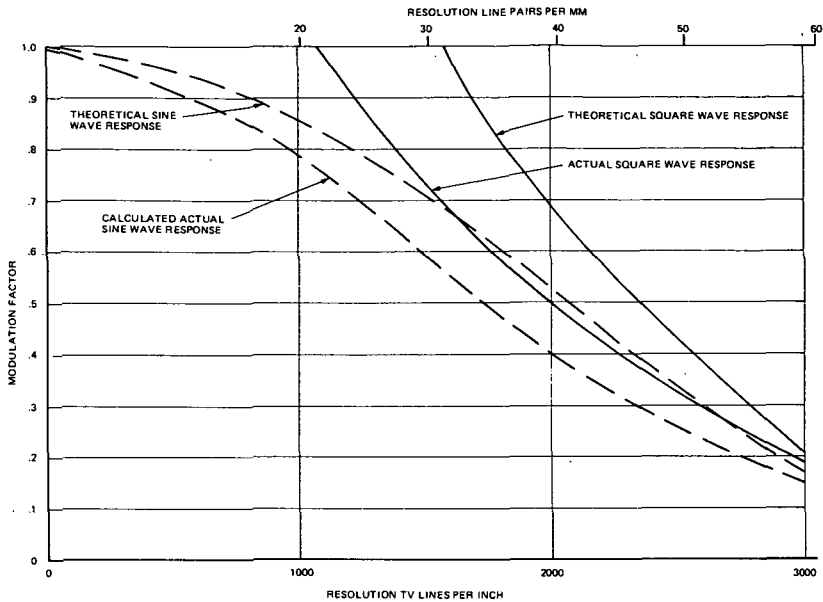


Figure 3-29. Image Dissector Resolution

definition, contrast, and geometry. An equivalent increase in signal strength could as easily be obtained by additional stages of electron multiplication within the image dissector tube. Of greater importance is the effect of the phosphor interface and its ability to continue phosphorescence after a light event has occurred. The phosphor decay, normally considered a hindrance in viewing devices, here adds the equivalent of a storage surface to the image dissector. The phosphor decay, being of a short time period (milliseconds), permits events to be detected that occurred at any time during that period. Two types of signal extraction are therefore to be considered.

Event Detection. Event detection may be performed by rapidly scanning the area of interest, with detection of photon events indicating an occurrence. Although of considerable interest in stellar imaging, the value of earth viewing is limited.

Line Scanning. Line scanning of an earth scene may be performed from a stabilized satellite, with detection of optical imagery as in the nonintensified system. The intensifier adds storage of all light inputs for an amplitude-time period determined by the decay characteristic. For a continuous scene image that is moving across the photocathode, the effect is one of summing the inputs over that time period, with the most recent input

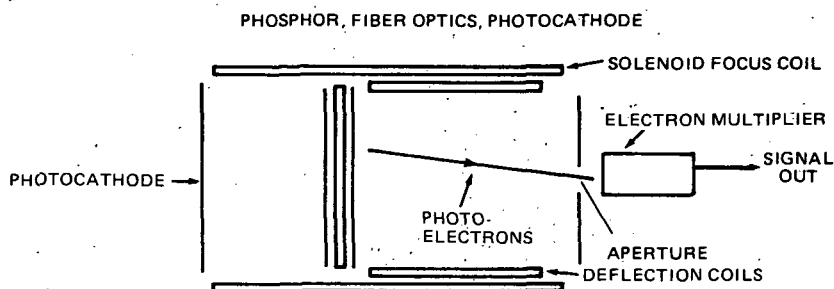


Figure 3-30. Intensifier Image Dissector

having the greatest effect. A typical sampling time for image dissector scanning is one to ten microseconds. A typical camera scans repetitively at ten millisecond intervals. A phosphor with a decay to $1/e$ in one-fifth of this time period would permit less than 1 percent residual image during a line scan period. Experimental gains in sensitivity from such systems indicate signal gains of 50 times or more.

The advantages of the intensified image dissector suggest a potential for a sensitive camera tube that requires no mechanical shutter and that does not depend on electron beam scanning for equalization of the scanning surface. Random scanning may be employed with this system.

Design factors to be considered in such an application include the optical coupling requirements, electrical and magnetic requirements of the tubes, geometric distortions and definition reduction of the intensifier, and the consequences of increasing the light loading on the image dissector photocathode.

Suggested applications of this technique include its use in multispectral scanners where narrow band filters or dispersive filters reduce the light loadings on the dissector photocathode, and in stabilized pointing cameras where long focal length optics reduce input light levels to a low value.

Correlation Techniques in Earth Sensing

The increasing volume of data from spaceborne systems is of concern to users and equipment suppliers alike. The potential for onboard image processing as a means of reducing data storage and transmission may be considered in future systems. When specific image characteristics are desired

and can be identified, a special modification of the image dissector may be considered.

The image correlation tube is a sensor capable of operating on a complete frame of imagery at one time. The tube, shown schematically in Figure 3-31, consists of a photoemissive surface, a transmissive storage surface, and one of several kinds of output detectors. An image is first stored on the storage screen as a variable electrostatic charge. The succeeding images are then imposed on the same screen, but, because of voltage changes, the image electrons are allowed to pass through the screen, being modulated spatially by the stored image. A diode detector plate then collects the difference electrons as a comparative function of the two images. Image electrons may be deflected in the space between photocathode and storage screen. Electronic magnification may also be impressed on the image.

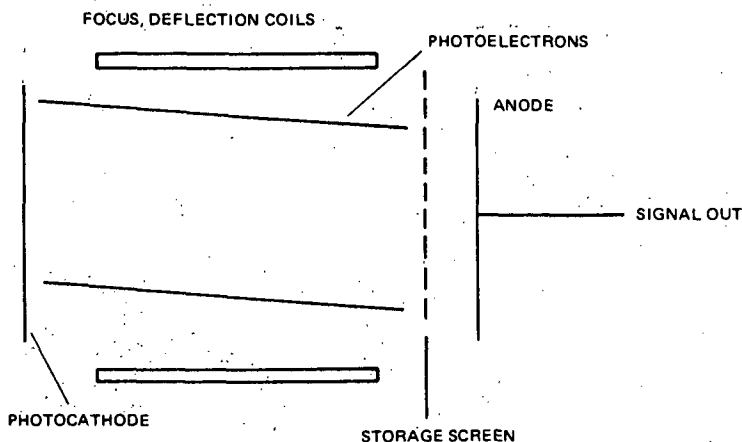


Figure 3-31. Image Correlation Tube

The process of operation includes image storage (write), mode change, read, and erase. Stored image may be held nondestructively for as long as useful. In repetitive situations, the reference image is removed by flooding the photocathode with a uniform light source and equalizing the charge on the storage screen. The output can occur as rapidly as the voltages can be changed. A write cycle may require only microseconds of exposure, and mode changes likewise. Reading of the correlation signal occurs continuously, and at high signal-to-noise because of the generally large signal currents involved. Areas of an image may be sampled in microseconds, permitting the interrogation of large areas (or colors, or sizes), rapidly.

Prime advantages of the image correlation tube are its speed, high sensitivity, variability of detection method (single or segmented anodes, etc.), and uniqueness of feature identification. The resolution of the stored and sensed image is limited by the transmissive screen to less than 30 line pairs per millimeter (although area position location may be much finer). The control of the storage screen voltage is critical for grey scale accuracy, and the system is not capable of image rotation electrically.

Application of the image correlation tube has been successful as area trackers for guidance, stabilization, v/h sensing, and automatic focus control. In the earth sensing role, the system may be useful in feature identification (shorelines, rivers, cities, etc., using programmed optical inputs). Color differences may be determined by contrast using successive optical filters or area separation on the faceplate. New techniques of data extraction and processing will be required to make full use of a device that can look at a whole scene and make an analysis of its size, form, position, contrast, spatial character, and time of occurrence.

Present and Future Characteristics of Image Dissector Systems

The most used image dissector tubes today come in three sizes, similar to vidicon and image orthicons and making use of the magnetic field technology of those commercial devices. A 25mm diameter tube with 18 mm photocathode was used on the Nimbus and ATS satellites for up to 1300 TV line system resolution. A 38 mm tube with 28 mm photocathode is used commercially, while the 57 mm diameter tube with a 43 mm photosurface is most often used for high quality imaging. A larger, 115 mm diameter tube has been used in special applications, but is generally found physically unwieldy.

Table 3-12 indicates the present capability of image dissector systems and an estimate of future characteristics obtainable with proper development support.

Table 3-13 describes a typical camera system at the present state-of-the-art in a space qualified configuration.

Each of the factors of Table 3-12 will be reviewed briefly here to indicate the limitation on growth in each area. The actions required to achieve growth are included.

TABLE 3-12
PRESENT AND FUTURE CAPABILITY
OF IMAGE DISSECTOR SENSORS

Characteristic	Present Capability	Potential Capability
Resolution	55 cy/mm on 45 mm surface (20% MTF) 35 cy/mm (50% MTF)	120 lp/mm on 100 mm surface
Sensitivity (surface)	Tri-Alkali 20% peak Q.E. .5% Q.E. at 900 nm Semiconductor 20% peak Q.E. 5% Q.E. at 900 nm .5% Q.E. at 1100 nm	40% peak Q.E. 2% Q.E. at 900 nm 40% peak Q.E. 10% Q.E. at 900 nm 1% Q.E. at 1200 nm
Sensitivity (system)	10:1 SNR high resolution 2.6 J/m^2 Low resolution $2.5 \times 10^{-4} \text{ J/m}^2$	10:1 SNR at 1 J/m^2 high resolution
Spectral Response	Tri-Alkali 250 to 900 nm Semiconductor 250 to 1100 nm	250 to 1000 nm 250 to 1200 nm
Geometry	.2% linearity over 45 mm surface Stability of 10^{-5} over 10^3 seconds Electronic Motion stabilization to 10^{-4}	.05% linearity over 100 mm 10^{-5} over 10^5 seconds Motion stabilization to 10^{-5}
Calibration	Preflight photometric calibration Continuous electronic calibration	Preflight and in-flight calibration Electronic grey scale and position calibration
Shading	Combined optic, cathode shading 5%	Automatic shading correction to .1%
Storage	No sensor surface storage	Augmented surface storage
Life Limitation	Photocathode life 3 years	Photocathode life 5 years
Dynamic Range, Intra-scene	100:1 Scene contrast 10^4 max range	1000:1 scene contrast
Radiometric Accuracy	0.5% calibration	0.1% calibration
Radiometric Stability	Non-uniform spectral decay	Spectral calibration to 0.1%
Operational Bandwidth	10^8 Hz max 5×10^5 Hz typical	10^7 Hz with multiple channel or intensifier

TABLE 3-13

SYSTEM DESCRIPTION MULTISPECTRAL CAMERA

Sensor	5.72 cm dia. x 30.5 cm long S25 photocathode, Strip Color Filters Three 15 mm apertures Magnetic Focus, Deflection Line scan
Data Output	Three video signals, 500 kHz each
Camera Size (less optics)	15 cm by 15 cm by 41 cm
Weight (less optics)	18 kg
Control Unit Size	15 cm by 15 cm by 31 cm (6600 cm ³)
Weight	9 kg
System Power	80 watts
Shutter or Iris	None
Heating Requirements	None

Resolution. Present limitations are set by aperture size and magnetic field optimization. The limit of resolution can be significantly expanded, since neither the photocathode nor sampling aperture should be the limiting factor. Improved magnetic field designs and optimization of the large tube configuration will permit consideration of sensors having 24,000 TV lines per diameter on a 100 mm format.

Sensitivity. The present tri-alkali photocathodes (S25, etc.) will be improved somewhat, but will gradually be replaced by semiconductor single crystal surfaces that are translucent and have high quantum efficiencies at the near infrared spectrum.

Spectral Response. The growth of semiconductor photoemitters will expand the spectral range to a useful 1.2 micrometers.

Geometry. Present field studies and systems are becoming more linear and geometrically accurate as design and experience are applied. Methods for producing ultra-linear systems are anticipated in the 1980 time frame.

Calibration. The image dissector can be easily and accurately calibrated before and during flight. This should permit photometric imagery having accuracies of 0.1 percent.

Shading. Vignetting of optics and electron multipliers are the present limiting factors. Modern video control methods permit compensation for these factors, allowing area calibration to approach 0.1 percent.

Storage. The photoemissive cathode is unique in having no image retention or storage. This is an aid in applications requiring motion compensation, etc. In order to improve sensitivity, storage may be added by the use of an image intensifier tube ahead of the image dissector. Gains of 20 times in signal to noise may be realized with such devices.

Life Limitations. Present life limitation is a gradual decay of photocathode sensitivity. Experience has shown this to not be a serious factor under normal life cycle conditions. No other failure mechanism exists, making this tube one of the most reliable of space sensors.

Dynamic Range. Contrast range within a scene is limited by scattered light from optics and interval tube parts. To increase this factor tubes must be designed for this requirement.

Radiometric Accuracy. With the aid of onboard calibration to determine time varying changes of system response, the radiometric accuracy may be excellent, aided by the negligible background noise and linear response of the photosurface. The life characteristics of the photocathode tend to indicate that the spectral response decays unevenly, with red response decaying before blue. A calibration system may compensate for this change.

Operational Bandwidth. High frequency operation of the image dissector is limited more by signal to noise factors than by physical factors. The photocathode, transit time spreads, and electron multiplier response have shown pulse response in the nanosecond range.

A present system operates at 500 kHz per spectral band and generates three simultaneous bands. Future systems using intensifiers can increase operating frequencies one order of magnitude. The use of added channels will likewise increase the data output by as much as ten times.

Actions Suggested

The general areas of system improvement that may be considered most fruitful are:

1. Photocathode development — increase quantum efficiency and extend spectral response.

2. Magnetic field developments — optimize field components for resolution, geometric accuracy, and speed of response.
3. Electron physics development — optimize electron multiplier structure design for uniformity, speed of response, noise reduction.
4. Tube size increase — develop large format systems having high resolution and multiple channel readout capacity.
5. Intensifier system — develop a compatible intensifier and dissector unit to realize potential gains of the approach.

Benefits and Applications

The image dissector can be applied in situations requiring instantaneous detection and multiple readout to great advantage. Systems for aircraft and poorly stabilized satellites may now have line scan imagers with electronic motion compensation.

Multiple readout may be used to advantage in high resolution multispectral imagers.

The high resolution line scanner is capable of partial scan at selected positions, permitting a large area coverage, with optimized scan format to relay only desired image information over low bandwidth lines to simple ground stations.

The high radiometric accuracy and multiple spectral output permit spectral identification of plant and ocean color.

Dielectric Tape Cameras

Several camera types have been developed to varying levels for recording, storing, reading out, transmitting and reconstructing images for applications requiring repetitive visual images and large capacity storage. Two of these cameras, the photoconductive dielectric tape camera and the grating-target tape camera were developed in the 1960's. A third type, the electrostatic storage camera, is currently under development. Each of these are discussed next in terms of operating principles and performance, both current and predicted. Table 3-14 presents a performance summary.

TABLE 3-14
DIELECTRIC TAPE CAMERAS — PERFORMANCE SUMMARY

Camera Characteristic Performance	Current Technology		1976 Electrostatic Camera	1980 Electrostatic Camera
	Photoconductive Tape	Grating Target		
Resolution @ 20% response	1500 TVL (30 lp/mm)	3000 TVL (60 lp/mm) (outer)	5000 TVL (50 lp/mm)	10,000 TVL (100 lp/mm)
@ 50% response	600 TVL (12 lp/mm)	1250 TVL (25 lp/mm) (outer)	3000 TVL (30 lp/mm)	4,000 TVL (40 lp/mm)
Sensitivity for 10:1 SNR	$1.5 \times 10^{-4} \text{ J/m}^2$	$5.5 \times 10^{-5} \text{ J/m}^2$	$4.5 \times 10^{-6} \text{ J/m}^2$	$1.1 \times 10^{-6} \text{ J/m}^2$
Format	25 mm strip	25 mm strip	50 mm strip	50 mm strip
Bandwidth for above	670 kHz	8 MHz	10 MHz	20 MHz
Spectral Response	Photoconductor	Photocathode	Photocathode	Photocathode
Storage	days @ < 10% signal loss	days @ < 10% signal loss	days @ < signal loss	days @ < 10% signal loss
Dynamic Range	25:1	100:1	> 100:1	> 150:1
Radiometric Stability	Requires in-flight calibration	Requires in-flight calibration	Requires in-flight calibration	Requires in-flight calibration
Geometric Linearity	1%	1%	< 1%	< 1%
Physical				
Weight (less optics)			25 kg	7 kg
Power (less optics)			60 watts	100 watts
Volume (less optics)			.057 m ³	.057 m ³
Special Requirement	None	None	None	None
Deflection	Magnetic	Magnetic	Electrostatic	Electrostatic

Photoconductive-Dielectric Tape Camera

Principle of Operation. The photoconductive-dielectric tape camera, developed by RCA, is shown in Figure 3-32. The camera system combines both the image sensor and storage medium in the camera head.

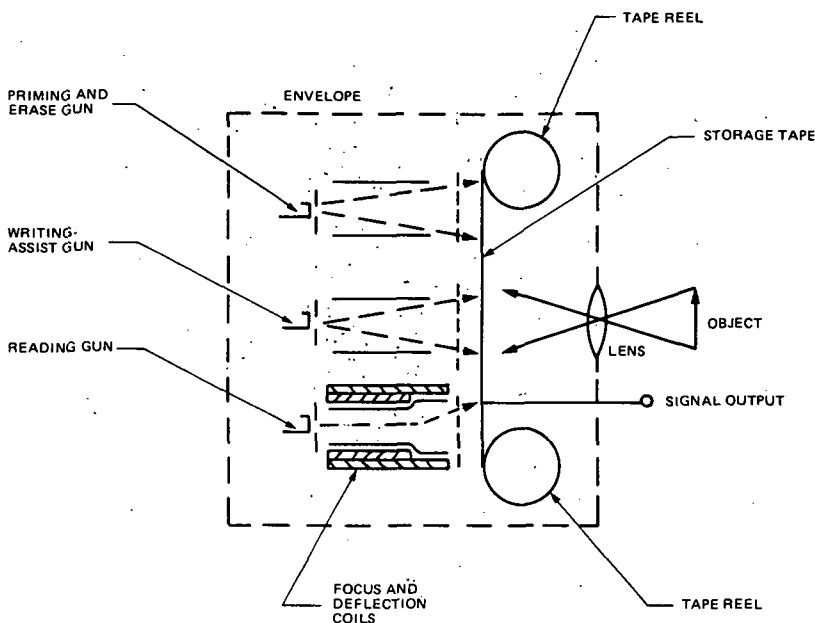


Figure 3-32. Photoconductive-Dielectric Tape Camera

The camera system is designed to record a large number of frames of high resolution picture information, during the orbit of a satellite for example. Then, when the satellite is near a particular ground receiving station, the camera is required to generate video signals corresponding to the sequence of stored images.

A target in the form of a tape is used to enable the storage of many images. The tape is moved between two reels into the writing and reading positions. For a typical meteorological system, the tape would be about 35 mm wide and 30 mm long. The tape consists of a flexible support layer, coated with a thin transparent photoconductive layer, on top of which is an insulating layer. The optical image is written onto the insulator surface and stored as charge patterns until readout or erased.

When the system is operating, the tape unwinds from a storage reel and is first exposed to a flood of electrons to erase past images and establish a uniform known potential. When primed, the optical image corresponding to the scene is imaged onto the photoconductor through the lens system. Recording, however, takes place only during the time interval that the tape is flooded with electrons from a writing-assist gun. The system is capable of being electronically shuttered by applying a writing gate pulse to the control grid of this gun.

Both framing and panoramic camera types have been developed. For reading the frame type camera, the target surface is moved to the reading position and raster scanned with a focused reading beam. In the panoramic camera, the tape is continuously moved at a constant rate as the reading beam scans across the tape width. By maintaining the proper potential of the read gun cathode, so that the secondary emission ratio is greater than unity, the readout process is achieved by collector potential stabilization of the target surface. The effect of the reading beam is to sequentially charge each bombarded area of the target to the collector mesh potential. In the process, a transient current flows through the series capacitance of the insulator and photoconductor, generating a time-varying output signal across a load resistor in series with the tape backplate.

Applications. Early work on the camera system was directed towards developing components for a high resolution, frame-type, dielectric tape camera. Around 1960, RCA began work on a meteorological panoramic camera. Subsequently, the company developed and space qualified the meteorological panoramic camera for the Nimbus satellite; however, it was never flown. The system has also been proposed for lunar mapping, Mars mapping and the entire class of missions requiring repetitive visual imaging and high-capacity data storage.

Resolution. A limiting resolution of 1500 TV lines per inch (30 lp/mm) has been obtained; at 50 percent response, a resolution of 600 TV lines per inch (12 lp/mm) has been obtained. The resolution is limited principally by the reading-beam diameter and secondary electron redistribution effects. The latter is a significant factor affecting growth potential. Alternative readout methods have been investigated.

Sensitivity. With a highlight exposure of about 0.1 meter candle seconds on the target surface, a peak signal-to-rms noise ratio of 5:1 can be obtained. Even though the quantum efficiency of the photoconductor can be quite high, approaching 50 percent, the overall sensitivity is limited by the absence of prestorage gain and noise sources originating in the readout

process. Some improvement may be possible with the use of an image intensifier, perhaps at the expense of spatial resolution.

Spectral Characteristics. The spectral characteristics are dependent on the type photoconductor used. For obtaining particular spectral responses, different photoconductors of appropriate dark resistivity and photosensitivity may be employed.

Unique Features/Limitations. The features of the dielectric tape camera (shared also with the grating and electrostatic cameras) are its multi-frame capacity for recording and storing pictures using both line scan and framing camera configurations, and its ability to store data for long periods before readout. The use of an organic material such as polystyrene as the storage tape base results in a severe limitation. The camera system cannot be outgassed by baking, and continuous pumping may be required. In cases where repetitive readout of the same information is required, limitations exist. Readout of the stored information is destructive and the greater part of it is gone in the first readout. A bandwidth limitation exists when using the tape as the signal electrode because of its large capacity. A return beam readout has been investigated to overcome this problem.

Grating-Target-Tape Camera

Principle of Operation. The grating-target tape camera (developed by Westinghouse Electric Corp.) is shown in Figure 3-33. This dielectric tape camera system, like the photoconductor-type system, combines both image sensor and storage in the camera head and is capable of storing a series of electrostatic images on a mechanically movable tape. The tape, with a sequence of stored images, can be rolled onto a takeup reel and unreeled for subsequent reading as desired. The camera includes, in addition to the storage tape and its associated transport mechanism, an erase and priming section, an input section, and a reading section.

The storage tape consists of a metallic base with fine grooves on the surface. The broader surface of each groove is coated with a thin insulating film (usually MgF_2) upon which the electrostatic charges are stored. The grooved storage tape is typically made of 35 mm wide nickel, with about 6,000 grooves per inch running perpendicular to the direction of the reading beam scan. Because of the grooved construction, charges on the surface of the insulating film written during exposure are not disturbed by contact with adjacent metallic surfaces when the tape is coiled.

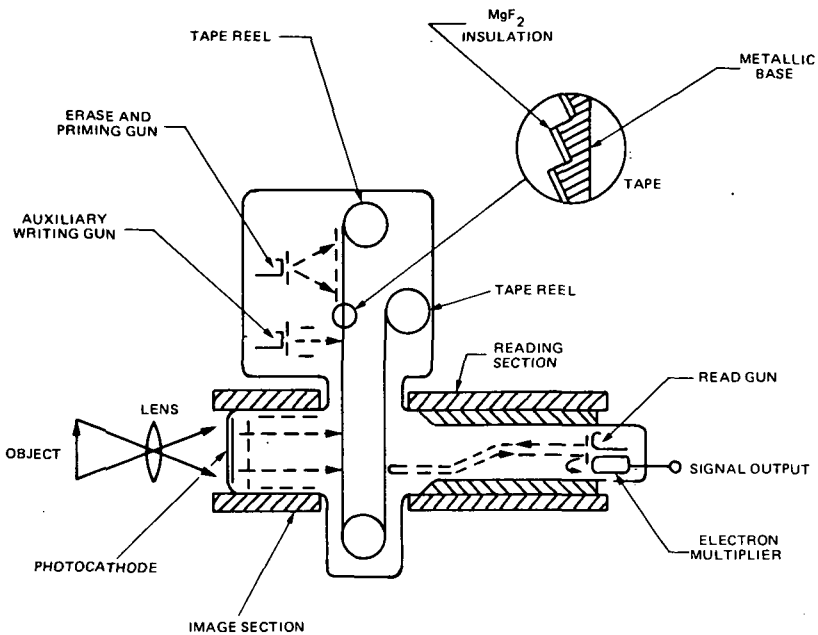


Figure 3-33. Grating-Target Tape Camera

Priming and erasing is first performed to insure that previous charge patterns stored on the insulator surface are removed and that the surface is shifted to a suitable potential for writing. During writing, exposure is controlled by pulsing the voltage on an electronic shutter grid located behind the photocathode. The pattern of photoelectrons, generated at the semitransparent photocathode by the scene, are accelerated during exposure and strike the target with 10 keV energy. These photoelectrons, magnetically focused at the target, produce bombardment induced conductivity in the insulator, causing its surface to partially discharge to the potential of the metallic backplate. A pattern of potential variations corresponding to the scene is thereby established on the insulating film of the target. Other methods of writing, such as secondary electron emission, are possible.

To readout the information, the portion of tape to be read out is first moved into the reading position, where it can be scanned by the focused reading beam. The cathode of the reading gun is held at a potential more positive than the target so that reading-beam electrons cannot land on the insulator. However by a coplanar-grid effect, the negatively charged insulator controls the amount of current that can land on the conductive base portions of the metal target. The fraction of the reading beam electrons that

will be reflected back to the multiplier will depend on how much the target was initially discharged during writing. After amplification in the multiplier, a modulated output signal is produced, corresponding to the stored charge pattern.

Applications. The grating target tape camera has been developed using several alternative configurations. The reel-to-reel tape version has been shown. An endless loop (about one foot long) experimental tube has been made by Westinghouse (tube type WX 30182). Another configuration (the Optechon) employs a rigid disc-shaped target with the same grating-structure as used in the tape-camera. Both frame imaging and line scan applications can be accommodated using grating-target tape camera designs. These can be effectively applied to a wide variety of satellite missions.

Resolution. With present cameras, the resolution at 50 percent response is 1250 TV lines per inch (25 lp/mm), while the limiting resolution at 5 percent response is 3750 TV lines per inch (75 lp/mm). Resolution is presently limited by reading the beam spot size, and improvement should be possible. Successful grating targets have been made up to 530 lp/mm.

Sensitivity. Both bialkali and trialkali photocathodes have been used. The photocathode can be selected on the basis of spectral response and photosensitivity desired. Exposures in excess of .02 meter candle seconds are required (equivalent to ASA 100).

Unique Features/Limitations. The grating-target tape camera features multi-frame capacity for recording and storing pictures. Pictures can be stored many hours. Repeated readout is possible. Signals do not spread to adjacent areas during writing because of the grating construction. The metal (uncoated) edge of the grooves acts as a Faraday shield so that the reading beam is unaffected by the charge pattern until it is within a groove spacing of the target. Geometric fidelity is thereby maintained. It is relatively easy to make the targets in large sizes. The sensitivity is limited by the low prestorage gain offered by the MgF_2 target and additional noise introduced at readout. Readout also limits the resolution performance.

Electrostatic Storage Camera

Principle of Operation. The electrostatic camera system (ECS), under development by CBS Laboratories, is shown in Figure 3-34. The camera utilizes a photoemissive detector, a high density large area electrostatic storage medium and electron beam readout.

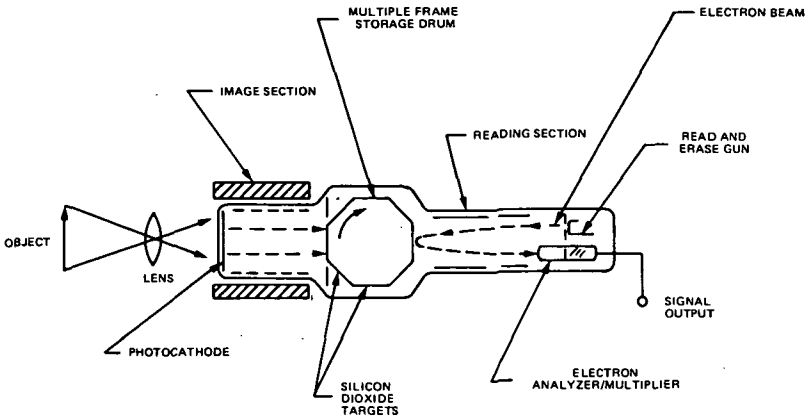


Figure 3-34. Electrostatic Storage Camera

The functions of exposure, storage, readout and erasure of electrostatic film are separate in the ECS operation. This results in the elimination of image retention without compromising the high performance of the readout process. The electrostatic storage material offers high gain and long term storage. This makes the ECS capable of low light level imaging and operation in a photon counting mode. The ECS offers higher image plane resolution than is available with vidicons or image orthicons.

The camera operation includes four steps: preparing the storage surface, exposure, storage, and readout.

Preparing Storage Surface. Priming the storage medium establishes a uniform surface potential. This is accomplished by flooding the surface with a low energy electron beam. This action erases any previous information that may have been retained and sets up an internal field gradient which is necessary for high electronic gain.

Exposure. During exposure the photocathode converts the optical image to an electron image. The photoelectrons are accelerated by the image section and focused onto the storage surface. These high energy photoelectrons discharge the storage surface by the process of electron bombardment induced conductivity (EBIC). This results in a charge pattern which corresponds to the intensity of the incoming optical image. Current gains of over 100X have been observed in this process.

Storage. Storage of the data written-in during exposure is achieved by maintaining the charge patterns (and resulting surface potentials) on the dielectric storage medium after exposure. Long term storage is achieved because of the very high surface and volume resistivity of the dielectric layer.

Readout. Readout is accomplished by positioning the desired exposure storage frame in front of the reading beam where it is scanned line by line. The energy of the electron beam is high enough to cause secondary electrons which are deflected and returned into a velocity selector. Electrons are accepted or rejected based on the target potential at the point where they originated. Since the potential is directly proportional to the charge stored, a video signal is generated which is related to the brightness variations in the input scene. The readout process does not erase and the images may be repeatedly scanned. Electrostatic focus and deflection are used and no field mesh is required.

Operating Characteristics. A typical set of operating characteristics for the electrostatic camera system is shown in Figure 3-35 at exposure levels similar to those for film cameras using 3404 film. Similar curves can be developed for low exposure operation. These characteristics were determined from laboratory measurements. Starting at the upper left hand diagram, the resultant charge density from the photocathode is given as a function of exposure. Although a $150 \mu\text{A}/1\text{m}$ (2854 K) S-20 photocathode is shown, the spectral response and sensitivity of the photoemitter can be selected to optimize performance depending on particular needs. The signal transfer for the storage medium is shown next with the surface potential plotted as a function of charge density. The slope of this characteristic (charge gain), target capacity, and resolution characteristics can be varied to suit a particular application. The output signal from the readout section is next related to the tape surface potential, and is finally shown as it effects the exposure density of the recording film. Considerable flexibility exists in tailoring the characteristic curves during the initial system design, as well as the selection of camera operating parameters of the ECS during use.

Unlike a film system, the exposure index of the electrostatic camera can be adjusted in flight for optimum operation under various scene conditions. It can also compensate for small shadow areas found within a larger scene and thus ensure the recovery of the necessary data regardless of variations in the scene illumination.

The electrostatic camera system can operate at a high overall quantum efficiency. The high gain associated with the storage process in effect

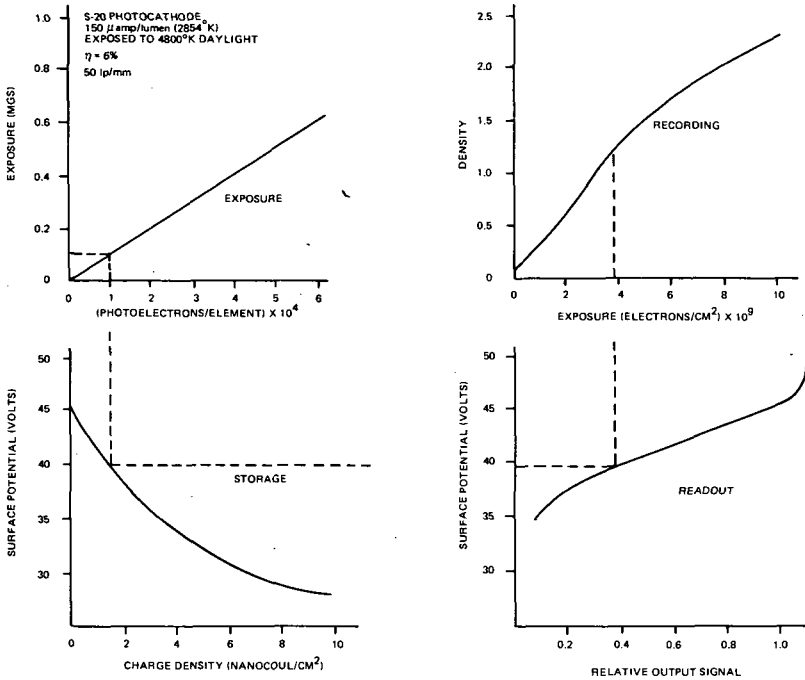


Figure 3-35. Electrostatic Camera Operation

preserves the high quantum efficiency obtained from the photoemitter. The high gain inherent in this process is required for high signal-to-noise ratio considerations and results in quantum-noise-limited camera operation over a wide dynamic range.

Applications. The electrostatic storage camera system design is extremely flexible. Both frame and slit camera configurations are possible. The size of the image and storage sections can readily be adjusted to accommodate varying format requirements. Although a multi-faceted drum configuration was shown in Figure 3-34, endless loop transports or a reel-to-reel transport are possible alternatives.

The technology is adaptable to any application where either large storage capacity, quick data delivery, long integration capability, reusability, and radiation immunity are of interest. These missions include a wide range of earth satellite applications.

The electrostatic camera system consists of two major subsystems, a sensor unit and a receiver station. The sensor unit acquires the imagery, stores a sequence of images, and finally scans and transmits the imagery to the receiver station. At the receiver station, the data are received, processed as desired, and recorded on film. A simplified block diagram of the ECS is shown in Figure 3-36.

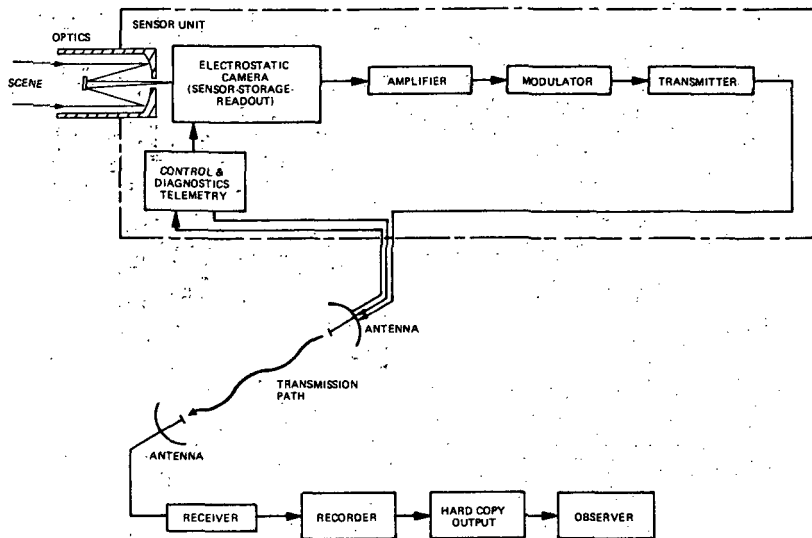


Figure 3-36. Electrostatic Camera System

Performance — Resolution and Sensitivity. Component performance levels have been studied in detail at CBS Laboratories. The camera performance characteristics presented in Figure 3-37 are based on these findings as are the produced values in the performance summary, Table 3-14 for 1976 availability. CBS Laboratories is presently conducting a program to verify these predictions by system tests. These results are expected early in 1974.

The electrostatic camera performance characteristics shown in Figure 3-37 are illustrative of operation in a system designed for the exposure of 3404 film. The spectral response of the system will depend primarily on the type of photoemitter selected. The threshold modulation function, and resolving power curves are shown. Comparisons with film, the return beam vidicon, and SEC camera tube are indicated for such a system with an $f/5.6$ lens.

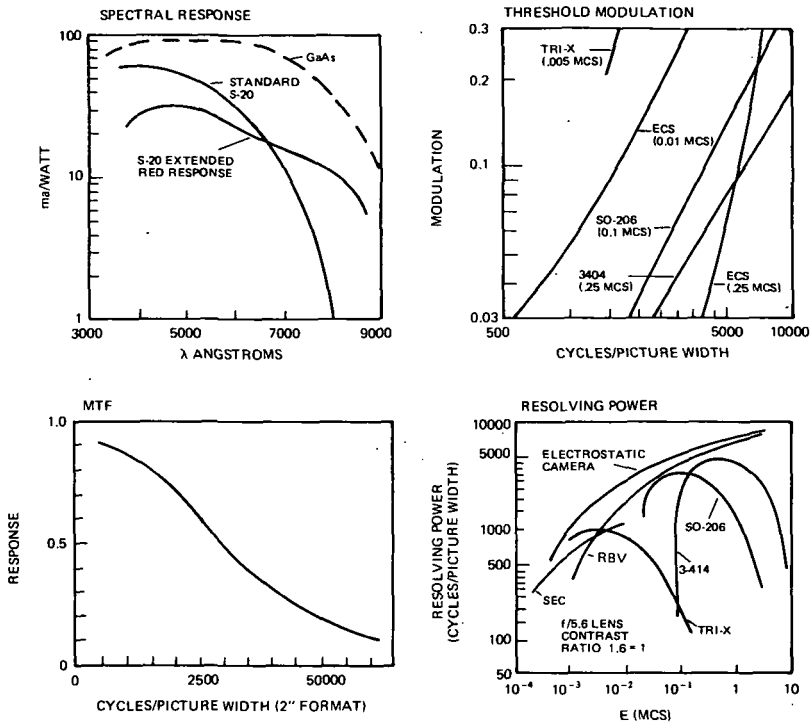


Figure 3-37. Performance Characteristics Electrostatic Storage Camera

Unique Features/Limitations. The electrostatic storage camera can be characterized by a number of special features. The camera is capable of high optical resolution over a large format and has a multiframe capacity for recording and storing pictures. The system provides for transmission of the stored information at arbitrary times (up to several weeks after exposure) and data rates.

A significant feature of a high resolution electrostatic camera is the ability to acquire an arbitrary number of frames at very high bandwidths, store, and transmit at data rates consistent with ground handling capabilities, without the use of ancillary storage equipment.

The readout process is nondestructive and repetitive scans are possible. The camera system essentially has a built-in data compression capability in that a cursory examination of pictures can be made at low resolution to identify areas of interest. These portions can be rescanned at high resolution.

The electrostatic camera system can operate at a high overall quantum efficiency. The high gain associated with the storage process in effect preserves the high quantum efficiency obtained from the photoemitter.

Development Requirements. The electrostatic camera system is still in the developmental stage. The basic operating principles have been demonstrated by laboratory tests at the component level. CBS Laboratories is presently funding a program to fabricate and evaluate a single frame camera tube for the purpose of evaluating the overall concept. Sensor performance verification is expected early in 1973 at levels consistent with the 1976 performance prediction of Table 3-14.

NASA funding would be required to design, fabricate and evaluate an application oriented breadboard.

The increased performance characteristics predicted for 1980 (Table 3-14) will require additional component development. These include improvement in photocathode response, storage material properties, and low noise electronics.

Secondary Electron Conduction and Electron Bombarded Silicon Camera Tubes

The majority of the television camera tubes used in the past for observation of the earth from satellites have been vidicons or image dissectors. These devices typically require integrated fluxes of 10^{-1} to 1 footcandle-second (10^{-4} to 10^{-3} joules per meter² at the wavelength of peak sensitivity) to produce fully exposed images of the best quality. In many remote sensing applications, this level of performance is adequate to generate high quality images because the spacecraft is viewing the daylight side of the earth. There are, however, certain situations where devices with higher sensitivity may be needed. Some of these are listed below:

1. *Very High Resolution Systems.* To achieve high resolution from satellite orbit, long focal length lenses are needed. In order to keep the aperture of the lens to a reasonable size, the focal ratio must be large and give low illumination levels in the focal plane. In addition, long focal length lenses accentuate image motion during exposure, and the short exposure times needed to control motion effects further limit the integrated flux available in the optical image.
2. *Imaging in Narrow Spectral Bands.* Filters used to restrict the illumination of the image to a narrow region of the spectrum reduce the

energy available to the sensor. In a system like WISP (Wide Range Imaging Spectrophotometer) where a grating or prism is used to spread a line of the image over the full camera tube raster, the integrated flux of the sensor may be 100 times lower than that found in normal imaging.

3. *Nondaylight Applications.* Imaging the dusk and dawn limb or the night side of the earth may be of interest for the detection of lightning strikes in thunderstorms, schools of fish by phosphorescence, auroral activity and night skyglow and various forms of human activity. In the later category, one can conceive of a satellite monitoring the position of ships and aircraft equipped with high intensity monochromatic identification lights.

The purpose of this discussion is to describe a class of television camera tubes that have sufficient sensitivity to produce fully exposed images with an integrated flux of 10^{-4} to 10^{-2} footcandle-seconds (10^{-7} to 10^{-5} joules per meter² at the wavelength of peak sensitivity) and are, therefore, suitable for the type of applications listed above. These devices are high sensitivity direct beam readout camera tubes of which SEC and EBS/SIT types are well known examples. The features they have in common are a photo-emissive image sensing surface, an electron bombarded storage target (EBT) and an electron beam readout mechanism, in which the video signal is taken directly to the preamplifier from the conducting backplate of the target.

Principles of Operation

Figure 3-38 illustrates an idealized version of a high sensitivity direct beam readout camera tube using an electron bombarded storage target. The device employs the magnetic focusing and deflection which is an appropriate choice for a high resolution application.

Photocathode and Image Section. An optical system forms an image of the scene to be recorded on a transmissive photocathode which is deposited on the inner surface of the faceplate of the tube. The faceplate may be any of a variety of materials. Magnesium fluoride transmits radiation from the far ultraviolet through the visible to the infrared, and this makes it a useful window for a tube requiring ultraviolet sensitivity. A conventional glass faceplate is suitable for a tube designed for near ultraviolet, visible and infrared response.

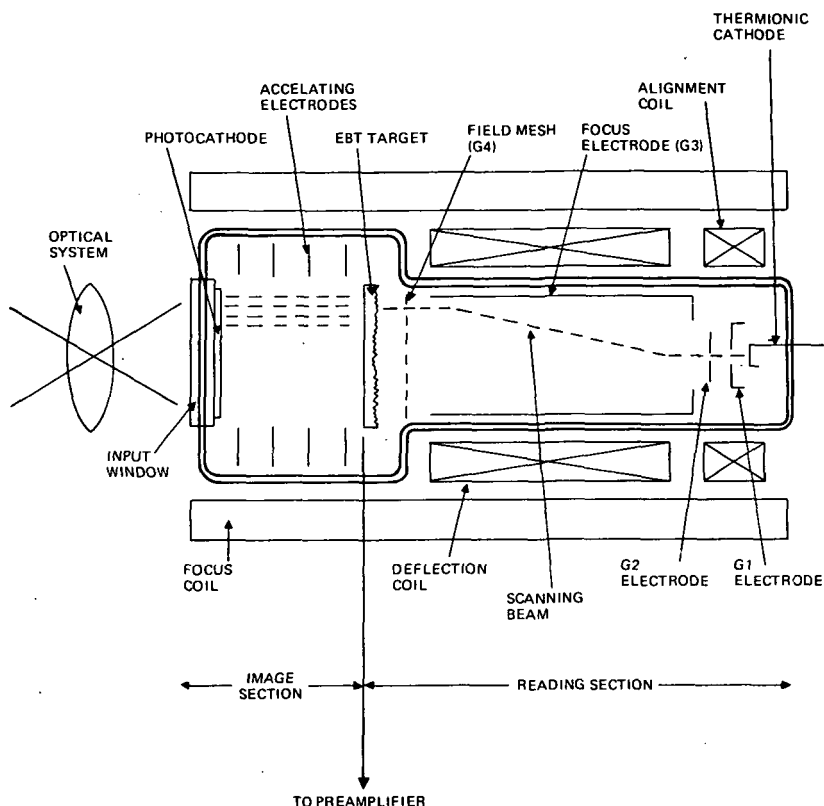


Figure 3-38. High Sensitivity Direct Beam Readout Camera Tube Using an Electron Bombarded Storage Target

The spectral range covered by presently available window-photocathode combinations used in SEC and EBS camera tubes is 0.1 to 0.9 μm . Fiber optic faceplates may be used to couple the camera tube to an image intensifier, image tube converter or a simple phosphor converter such as p-terphenyl. Intensifiers and converters can increase the sensitivity of the basic camera tube and extend its spectral coverage to include high energy particles, γ -rays, X-rays and 1 μm wavelength infrared radiation.

Whatever the faceplate-photocathode combination, the incoming photons interact with the photoemissive surface and release electrons which are accelerated across the image section of the tube by a voltage of -7 to -15 kV depending on the type of target employed. A series of ring electrodes is used to produce a uniform electric field through the image section. A

focusing solenoid generates an axial magnetic field, and a suitable combination of magnetic and electric field strengths causes the electron image to be transferred to the target. A correctly focused image on the target is achieved when the transit time of the electrons from photocathode to target is equal to the synchrotron period of the electron in the magnetic field.

Target and Reading Section. The accelerated photoelectrons enter the target and their kinetic energy is used to generate many charge carriers for each incident particle. This gain mechanism produces a large signal charge on the target that can more readily overcome the preamplifier noise during the subsequent readout of the signal, and thus increase the sensitivity of the tube.

A variety of electron bombarded targets have been used in high sensitivity direct beam readout camera tubes. At the present time, the secondary electron conduction (SEC) target and the electron bombarded silicon diode array (EBS) target are of greatest interest. However, consideration must be given to electron bombardment induced conductivity targets (EBIC), and future tubes may use electron bombarded versions of charge coupled devices (CCD). These are discussed later in this chapter. The specific gain mechanisms of these targets is also discussed.

The target not only provides gain, it also stores the charge image between the writing and reading processes. In a conventional broadcast camera tube where writing (deposition of a charge image on the target) and reading (removal of the charge image by the scanning beam) occur concurrently, the target need only store the image for a fraction of a second. However, in applications of the type under discussion, much longer storage times are usually needed. Because of limited electronic bandwidth, or the use of a large number of picture elements, it may take many seconds to read the image from the target. It may also be desirable to extend the writing period to permit the integration of very weak optical images. As will be seen later, exposures of several hours duration are not uncommon.

For these reasons, the storage characteristics of the target are important. To understand this aspect of image formation, the description of the tube should be completed by examining the reading section. The conductive backplate of the target is maintained at 5 to 15 volts positive with respect to the cathode of the electron gun which generates the reading beam. The reading beam is made to scan the surface of the target in a raster by deflection coils located around the tube between the target and the electron gun. As the well-focused reading beam passes over the surface of the target it

returns the surface to ground and establishes an electric field between the free surface of the target and the conductive backplate.

Then, during the writing period, charge carriers are generated in the target by the photoelectrons. The charge carriers move through the target under the influence of the electric field causing a positive charge to accumulate on the surface in those areas of the target which correspond to highlights of the optical image. During the next scan cycle these charged areas are neutralized by electrons from the reading beam which land on the positively charged areas of the target surface. A corresponding video current is generated in the target backplate by capacitive coupling through the target, and thus, current flows through a load resistor which is connected to the input of the video preamplifier.

It is clear that, in the absence of photoelectrons, it is desirable that no charges should accumulate on the target surface. If such charges do appear in the absence of an optical input, the target is said to have a measurable "dark current" which, by filling up the available storage capacity of the target, limits the storage time of the target. In addition to a low dark current, the target should have a high lateral resistivity to prevent spreading and blurring of the charge image during the storage period.

Performance Characteristics

Direct beam readout EBT camera tubes offer the following desirable characteristics:

- Ability to produce pictures at light levels as much as 1000 times lower than those needed to operate vidicons and image dissectors.
- Sufficient resolution to generate 4×10^6 picture elements at an MTF of 45 percent.
- Using the SEC target, the ability to integrate and store images for periods of many hours duration.
- A direct beam readout process, the same as that used in the vidicon. This is simple to set up and operate compared to the return beam technique used in other high sensitivity tubes, and the noise content of the signal is unaffected by the beam current setting.
- A variety of window-photocathode combinations offering sensitivity over a wide spectral range.

- An image section which can be modified to permit image motion compensation and electronic shuttering.
- Tube structures capable of surviving rocket launch and operating in the space environment.

In the present context, the sensitivity of the direct beam readout EBT tube is perhaps its most significant feature.

SEC Camera Tubes. The SEC camera tube derives its name from the gain mechanism in its target, Secondary Electron Conduction. The SEC target consists of three layers: an aluminum oxide support layer approximately $0.07\text{ }\mu\text{m}$ thick, and a low-density layer of potassium chloride approximately $20\text{ }\mu\text{m}$ thick. The potassium chloride layer has a density of only 2 percent of the normal density of KCl and is formed by evaporating the material in an inert gas atmosphere at a pressure of approximately 2 torr. Where added strength and protection against damage from intense light sources is needed, the aluminum oxide support layer may be replaced by a copper mesh.

The operation of the SEC target follows the general scheme described in the previous section. The charge carriers released by the high energy photoelectrons are free secondary electrons that move to the signal plate through the vacuum interstices of the target structure under the influence of the electric field within the target. This process is called secondary electron conduction. In order to understand the electrical behavior of the low density layer it must be emphasized that 98 percent of its volume is a vacuum. The SEC target has the following characteristics.

- *Gain.* A peak gain of about 80 to 100 is obtained when the photocathode voltage is 8 kV.
- *Signal Storage.* Potassium chloride is a wideband/gap material. In the low density state used in the SEC target, it has extremely high resistivity, and both dark current and lateral leakage are essentially nonexistent. Charge images can be stored on the target without degradation for periods of at least hundreds of hours.
- *Storage Capacity of Target.* Standard SEC targets can store 7×10^4 electrons in a $36\text{ }\mu\text{m} \times 48\text{ }\mu\text{m}$ picture element or 4×10^9 electrons per cm^2 . Higher capacity SEC targets are now available that increase these values by a factor of two to 8×10^9 electrons per cm^2 .

A variety of SEC camera tubes have been developed for military, space and commercial applications, and many of these are available as standard production types. Of particular interest in connection with remote sensing of the

earth are two high resolution tubes developed by Westinghouse for Princeton University under contract to NASA. These tubes are candidates for the imaging sensor in the Large Space Telescope. The WX-31958 is a magnetic focus and deflection SEC camera tube with a 25 mm x 25 mm photocathode and target format. It has a diameter of 8 cm and a length of 45 cm. The WX-32193 also employs magnetic focus and deflection but is a larger device with a 50 mm x 50 mm photocathode and target format, a maximum diameter of 13 cm and a length of 49 cm. At the present time, the WX-32193 has characteristics shown in Table 3-15.

Further improvements in the performance of SEC camera tubes may be anticipated in three areas: photoresponse, resolution and target gain. New developments in photocathodes and cold cathodes described elsewhere in this report, may be expected to be incorporated in SEC tubes and improve spectral coverage and restoration. Improvements in resolution should also arise from a reduction in effective target thickness. Lowrance and Zuchino (1971) have shown that, in present SEC tubes, resolution performance is probably dominated by mirror image charge effects in the target. They have calculated an effective target thickness of about $7\text{ }\mu\text{m}$, for the WX-31958. Use of an EBIC zinc sulfide layer of the type described by Dawes (1971) may be one way of improving resolution and gain. The ZnS target is reported to have a thickness of $0.8\text{ }\mu\text{m}$, a gain of 300 to 500 and a low enough dark current to permit integration for several minutes.

TABLE 3-15

SEC 1972 SUMMARY CHART

Resolution for 20% MTF:	30 cycles/mm
Resolution for 50% MTF:	20 cycles/mm (Figure 3-39)
Sensitivity at 550 nm:	3×10^{-7} joules/m ² (Figure 3-40)
Format size:	50 mm x 50 mm
Geometry:	less than 1% distortion
Bandwidth for stated performance:	50 kHz
Bandwidth maximum:	20 MHz
Spectral sensitivity:	$0.1\text{ }\mu\text{m}$ to $0.9\text{ }\mu\text{m}$
Storage time:	greater than 100 hours at 25°C
Dynamic range:	(See Figure 3-40)
Weight (less optics)	40 kg
Power (less optics)	75 W
Volume (less optics)	$1.6 \times 10^4\text{ cm}^3$

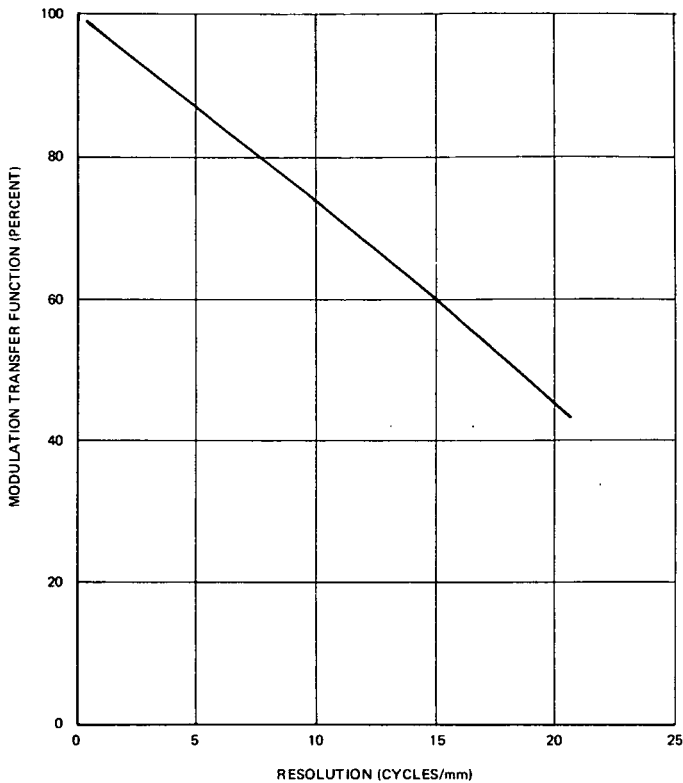


Figure 3-39. Modulation Transfer Functions of the WX-31958 and WX 32193-SEC Camera Tubes in 1972 Time Frame

A further development effort is required to incorporate improved photocathode and cold cathode technology in SEC tubes when this becomes available. Incorporation of EBIC layers will also need a solution to the compatibility of these targets with 50 mm x 50 mm target support layers. The characteristics shown in Table 3-16 for four years and Table 3-17 for eight may be anticipated for future versions of SEC tubes incorporating EBIC targets using the same tube envelope as the current WX-32193.

EBS/SIT Camera Tubes. High sensitivity, direct beam readout camera tubes using silicon diode array targets are designated Electron Bombarded Silicon (EBS) or Silicon Intensified Target (SIT) tubes. The targets used in the EBS devices are very similar to targets used in the silicon vidicons. In an EBS tube, the p-type islands face the reading section. The silicon target is excited by photoelectrons with an energy of typically 10 keV.

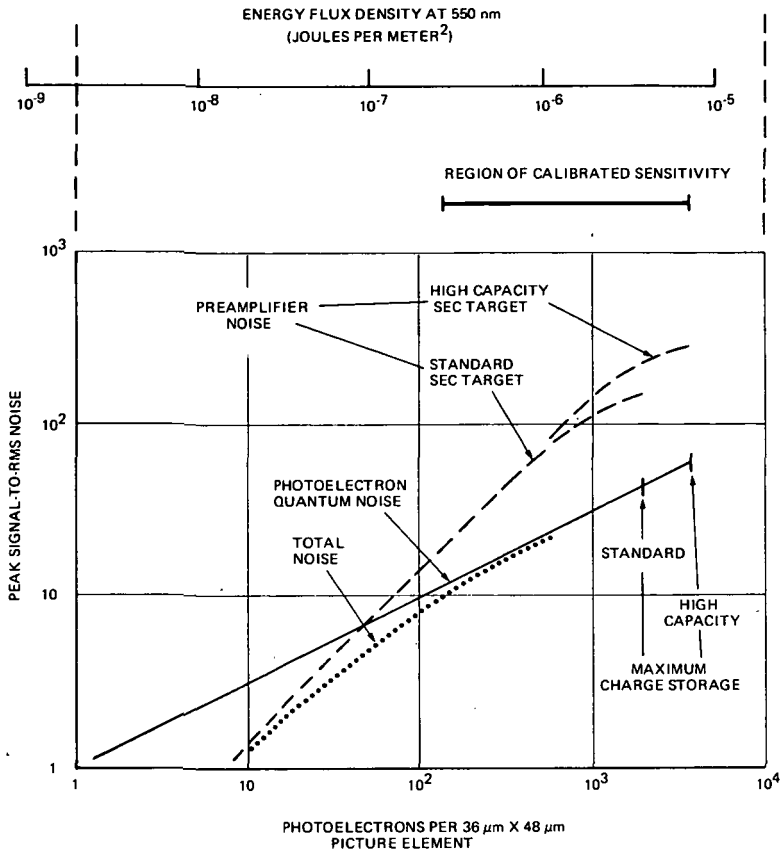


Figure 3-40. Sensitivity of the WX-31958 and WX-32193 SEC Camera Tubes in 1972 Time Frame

A dark coating is placed on the surface of the target facing the photocathode to prevent direct excitation by light. Since the photoelectrons penetrate only $1\ \mu\text{m}$ into the silicon, it is necessary to thin the silicon wafer more than is normally required for vidicon operation with direct light excitation. If the target is too thick, the holes generated by photoelectrons will diffuse laterally before being collected by the p-type islands, thereby degrading the resolution of the target.

The electron bombarded silicon diode array target has the following characteristics:

- **Gain.** Due to background effects in the image section, the photocathode is usually operated with a voltage $\leq 10\ \text{kV}$, giving a gain of about 1600 to 2000.

TABLE 3-16

SEC 1976 SUMMARY CHART

Resolution for 20% MTF:	60 cycles/mm
Resolution for 50% MTF:	40 cycles/mm
Sensitivity at 550 nm:	2×10^{-7} joules/m ²
Format size:	50 mm x 50 mm
Geometry:	same as 1972 value
Bandwidth for stated performance:	50 kHz
Bandwidth maximum:	20 MHz
Spectral Sensitivity:	0.1 μ m to 0.9 μ m
Storage time:	several minutes to several hours
Dynamic range:	twice 1972 value
Weight:	same as 1972 value
Power:	same as 1972 value
Volume:	same as 1972 value

TABLE 3-17

SEC 1980 SUMMARY CHART

Resolution for 20% MTF:	75 cycles/mm
Resolution for 50% MTF:	50 cycles/mm
Sensitivity at 550 nm:	2×10^{-7} joules/m ²
Format size:	50 mm x 50 mm
Geometry:	same as 1972 value
Bandwidth for stated performance:	200 KHz
Bandwidth maximum:	20 MHz
Spectral sensitivity:	0.1 μ m to 1.1 μ m
Storage time:	several minutes to several hours
Dynamic range:	twice 1972 value
Weight:	same as 1972 value
Power:	same as 1972 value
Volume:	same as 1972 value

- *Signal Storage.* Thermally generated charge carriers cause silicon diode array targets to have a significant dark current at room temperature, and this dark current limits the integration time to a few seconds. Since dark current decreases by a factor of two for every 10°C drop in temperature, the integration time can be increased by cooling. This, however, can involve practical difficulties and the use of a large amount of power. Lateral leakage does not appear to be a limitation to target resolution if resistive sea targets are avoided, but further measurements are needed to investigate this aspect of performance.
- *Storage Capacity.* The storage characteristics of silicon targets vary depending on the structure and the resistivity of the silicon wafer. A value of 80×10^9 electrons per cm^2 is typical.

The EBS camera tube is a relatively new device compared to the SEC tube. So far, a variety of EBS tubes have been developed for military applications employing electrostatically focused image sections and offering 600 to 900 TV line resolution. The characteristics of such a tube with a 25 mm x 25 mm image format are described in Table 3-18. This information is typical of the Westinghouse WX-31841 camera tube which uses a 1½-inch diameter scan section.

TABLE 3-18

EBS/SIT 1972 SUMMARY CHART

Resolution for 20% MTF:	15 cycles/mm
Resolution for 50% MTF:	10 cycles/mm
Sensitivity at 550 nm:	2×10^{-7} joules/ m^2
Format size:	25 mm x 25 mm
Geometry:	approximately 3% distortion
Bandwidth for stated performance:	10 MHz
Bandwidth maximum:	20 MHz
Spectral sensitivity:	0.4 μm to 0.9 μm
Storage time:	30 seconds at -20° C
Dynamic range:	greater than SEC at reduced gain
Weight:	15 kg
Power:	25 W
Volume:	$5 \times 10^2 \text{ cm}^3$

High resolution, large image format, slow scan EBS/SIT types comparable to the WX-31958 and WX-32193 SEC tubes are not yet in existence. However, to make a valid comparison with other sensors suitable for remote sensing of the earth, the following performance analysis is based on a hypothetical tube of the WX-31958 or WX-32193 type using a silicon diode array target. The construction of such a tube will be feasible as soon as targets using current technology, but of a sufficient size, are available.

Extrapolation from EBS tubes with 16 mm and 25 mm diameter targets suggests that resolution comparable to that shown in Figure 3-39 for the SEC tubes can be achieved soon in large EBS devices. However, larger tubes require high field mesh (G4) voltages of the order of 1000V to maintain good MTF. Many silicon diode array targets are damaged by the X-rays produced when field mesh voltages higher than 350 to 400 V are used. A silicon target currently being developed by Westinghouse that can operate without damage with G4 at 1000V may be the answer to this problem.

EBS tubes have 20 to 25 times the target gain of an SEC tube. Their charge storage capability is perhaps 10 to 20 times greater. However, operated at full gain, the ratio of charge storage capability to gain is no greater for an EBS tube than for an SEC tube. As a result, the maximum signal to noise ratio set by charge storage considerations is about the same for both tubes. The higher gain of the EBS tube is only useful at very low light levels where it can more easily override the preamplifier noise. However, at these light levels signal-to-noise ratios are so poor that they are of little interest for remote earth sensing applications. EBS tubes will probably be of greatest use in remote earth sensing applications when operated with photocathode voltages that give less than the maximum gain.

The development of an EBS tube with a 50 mm x 50 mm image format using a target with 80 to 120 diodes per mm is possible within the next four to eight years. Such a tube operated at reduced gain could offer comparable resolution and improved signal-to-noise ratio over present SEC tubes, provided problems related to dark current and X-ray damage at high G4 voltage are solved. Its characteristics are indicated in the Tables 3-19 and 3-20. Such a tube would use the same tube envelope as the WX-32193 SEC type discussed earlier.

TABLE 3-19

EBS/SIT 1976 SUMMARY CHART

Resolution for 20% MTF:	45 cycles/mm
Resolution for 50% MTF:	30 cycles/mm
Sensitivity at 550 nm:	same as 1972 value
Format size:	50 mm x 50 mm
Geometry:	less than 1% distortion
Bandwidth for stated performance:	50 kHz
Bandwidth maximum:	20 MHz
Spectral sensitivity:	0.1 μm to 0.9 μm
Storage time:	same as 1972 value
Dynamic range:	same as 1972 value
Weight (less optics):	40 kg
Power (less optics):	75 W
Volume (less optics):	$1.6 \times 10^4 \text{ cm}^3$

TABLE 3-20

EBS/SIT 1980 SUMMARY CHART

Resolution for 20% MTF:	63 cycles/mm
Resolution for 50% MTF:	45 cycles/mm
Sensitivity at 550 nm:	same as 1972 value
Format size:	50 mm x 50 mm
Geometry:	less than 1% distortion
Bandwidth for stated performance:	200 kHz
Bandwidth maximum:	20 MHz
Spectral sensitivity:	0.1 μm to 1.1 μm
Storage time:	same as 1972 value
Dynamic range:	same as 1972 value
Weight:	same as 1976 value
Power:	same as 1976 value
Volume:	same as 1976 value

Further improvements in the resolution of SEC camera tubes may be anticipated. When large, low dark current silicon diode array targets are developed, EBS tubes operated at reduced gain may become the preferred sensor because of their potential for higher signal-to-noise ratios. On a longer time scale, electron bombarded tubes with charge coupled device targets could become important sensors for low flux level applications.

ADVANCED TECHNOLOGY

The previous section of this chapter has presented existing technology, as well as potential extension of that technology to achieve higher performance levels. Various other technology efforts related to improving imaging devices are also under development and promise to extend performance even beyond the limits which have been indicated. These areas of advanced technology are discussed next.

Negative Electron Affinity

The basic principles of Negative-Electron-Affinity (NEA) emitters were first enunciated almost 10 years ago, and during the ensuing decade, increasingly rapid progress has been made in exploiting the practical advantages of this new electron emission concept. Recent developments have now made it possible to realize these advantages in high resolution, high sensitivity imaging types of devices operating in the near-IR, as well as the visible portion of the spectrum. In addition, it is now possible to develop a cold cathode electron source with a very high emission current density capability, together with a very narrow velocity distribution of the emitted electrons.

NEA emitters represent a radically different technology from that of conventional electron emitting surfaces. This is indicated in Figure 3-41 which shows the energy-band diagrams appropriate for (a) a conventional photocathode (e.g., S-20 multialkali) and (b) a NEA photocathode (e.g., GaAs:Cs-O) of approximately the same long-wavelength photo-threshold. The vacuum interface of a conventional emitter, as indicated in (a) of the figure, presents an energy barrier, the "electron affinity," to the emission of electrons. Thus, only "hot" electrons, with energy sufficient to surmount this barrier, can be emitted into vacuum. In contrast to this, the NEA emitter, as indicated in (b) of this figure, effectively removes this electron-affinity barrier to electron emission. This can be accomplished, as indicated schematically, through treatment of the semiconductor surface (e.g., with Cs and O) to reduce the work function to a value less than the band-gap

of the p-type bulk material. Thus, under the proper conditions the bottom of the conduction band, which is nearly the full band-gap in energy above the Fermi energy for strongly p-type material, lies above the vacuum energy level.

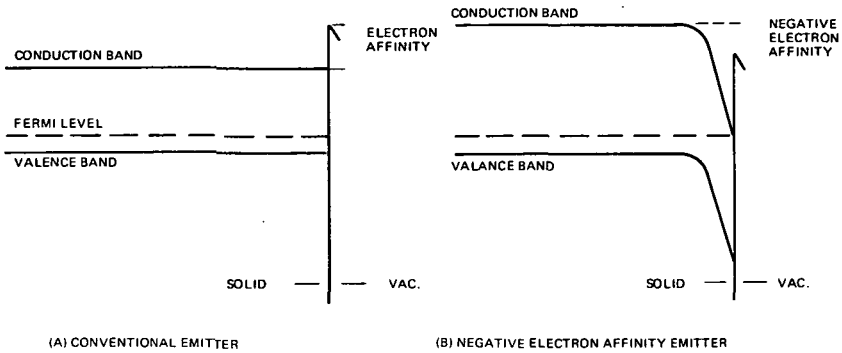


Figure 3-41. Simplified Energy Band Diagrams

The outstanding advantage of NEA emitters, therefore, lies in the fact that electrons with only thermal energies at the bottom of the conduction band can be emitted into vacuum.

Photoemitters

The revolutionary effect of the NEA technology on electron emission can be seen from Figure 3-42, which shows photoemission sensitivity (to 2854 K tungsten lamp) and secondary electron yield as functions of time over the last 30 years. The rapid advances made in the last five years are a result of this concept.

The major effort in the development of NEA emitters has been directed toward use of III-V materials (e.g., GaAs) as photoemitters with enhanced sensitivity in the infrared region of the spectrum. The first significant result was reported by Scheer and VanLaar (1965), who observed high sensitivity photoemission from surfaces of GaAs produced by cleavage in high vacuum and treated with cesium.

Subsequent efforts have included the extension of the NEA concept to compounds such as GaAsP, which have shorter wavelength thresholds than GaAs, and InGaAs which has response further in the infrared than GaAs. Figure 3-43 compares the response of GaAs and InGaAs cathodes with

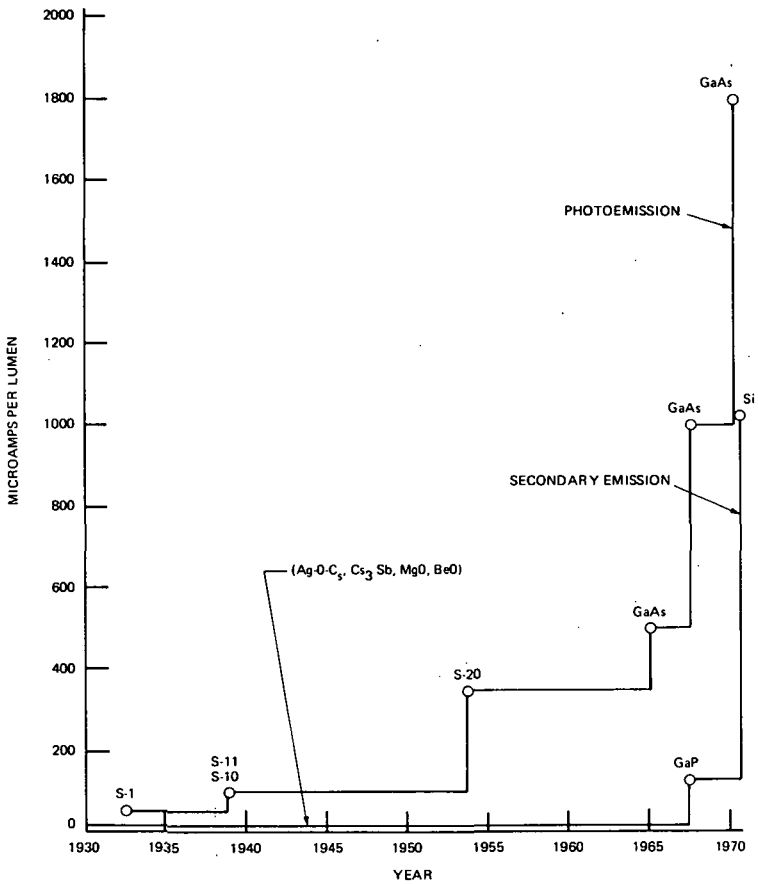


Figure 3-42. History of Photo and Secondary Emission

conventional S-25 (extended red multialkali) and S-1 cathodes covering the same spectral regions showing the substantial improvement which has been achieved using the negative electron affinity concept in practical tubes. Considerable effort has been aimed at producing NEA cathodes in a form which is compatible with conventional tube geometries, and which have the stability required in practical tubes. This effort has resulted in the development of over 50 photomultiplier tube types, including tubes with GaAs cathodes with sensitivities in excess of 1000 $\mu\text{A}/\text{lumen}$ (compared to 100-300 $\mu\text{A}/\text{lumen}$ in conventional tubes). Tubes containing GaAsP cathodes are also available. In addition to the high sensitivity of these tubes, the III-V NEA photocathodes have low dark currents ($\sim 10^{-16}$ A/cm²) which make them advantageous for detection of extremely small light signals.

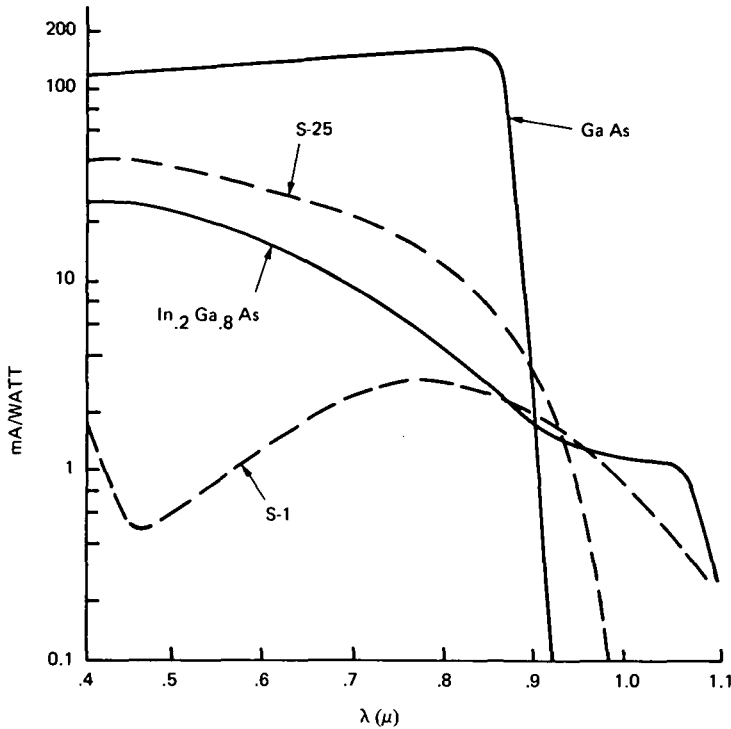


Figure 3-43. Photocathode Spectral Response in Practical Devices

For imaging devices it is necessary to produce photocathodes which operate in the transmission mode in which electrons are emitted from the side opposite that on which the radiation is incident. This mode differs from that used in photomultiplier tubes where opaque or reflection mode cathodes can be used without upsetting the electron optical focusing. The major effort in this work at present is the development of large area thin single crystal films of III-V semiconductors.

There are three basic approaches to this problem: (a) thinned self-supporting films, (b) films bonded to a supporting substrate, thinned either before or after bonding, and (c) thin films grown epitaxially on a suitable transmitting substrate. The first two approaches require bulk III-V material of sufficient size, uniformity and quality be available and that methods be developed to form thin films uniformly to the order of 2-5 μ m in thickness. A major advantage of these approaches is that of broad-band spectral response, extending throughout the visible and into the near IR (to about

9300 Å for GaAs). At present GaAs can be obtained approximately 38 mm in diameter. Ternary III-V material (e.g., InGaAs for longer wavelength response) is not available in bulk form larger than about one cm diameter, and extensive development would be required to make large sizes available.

In addition there is a problem with mechanical stability of the thinned films since the materials cleave readily. In spite of these difficulties, a considerable effort is being devoted to these approaches at present. If successful, extension to sizes larger than about 40 mm diameter would require a substantial additional effort, even for GaAs.

A major effort at present is directed to approach (c) — thin films grown epitaxially on a suitable substrate. This work utilizes GaP as substrate material, which is available to about 45 mm diameter, and employs an intermediate layer grown epitaxially between the GaP substrate and the photo-emitter to minimize lattice mismatch, and hence, obtain the required high quality photocathode material.

This technique potentially can be extended to produce very large area cathodes (51 to 76 mm diameter) through the use of single crystal sapphire as substrate material on which would be grown in sequence: GaP, the intermediate layer to match lattice parameters, and finally the photocathode material.

The spectral response in all such cases of GaP — intermediate layer substrates for the photocathode itself is limited at the short-wavelength end of the spectrum by optical absorption in the substrate. In a typical case, using GaInP as an intermediate layer to match GaAs lattice parameter, the short wavelength cut-off occurs at about 650 nanometers. This provides a serious limitation for ERTS-types of applications, in which response in the visible is normally required. It is possible to consider approaches combining the cited (b) and (c) approaches to avoid this problem. For example, available III-V material could be used as substrate to grow epitaxial layers of the desired photocathode composition. The photocathode material could then be bonded to a transparent faceplate, and the original substrate removed by a selective etching technique. Regardless of the exact approach adopted, it is clear that the special requirements of large area and broad spectral responses including the visible will require extensive specialized developmental programs.

The photosensitivity potentially achievable with NEA emitters is extremely high. Commercial tubes using reflection mode GaAs cathodes have already

demonstrated $QE > 25$ percent, and in laboratory experiments $QE > 50$ percent has been observed. In transmission mode cathodes suitable for imaging, antireflection coatings can be utilized which would increase the above values by about 25 percent for equivalent quality material.

The resolution capability of the NEA cathodes is expected to be excellent for imaging applications utilizing conventional high-performance electron optics, in view of the narrow emission velocity distribution. The major resolution degradation mechanism may be that resulting from diffusion of carriers within the photocathode material. Figure 3-44 presents an estimate of the resolution loss due to diffusion in a cathode $2\text{ }\mu\text{m}$ thick. Notice that 50 percent MTF occurs at about 130 cycles/mm, and 20 percent at about 220 cycles/mm. This effect is thickness-dependent, for example, a $4\text{ }\mu\text{m}$ thick cathode would be expected to have 50 percent and 20 percent MTF at 65 and 100 cycles/mm respectively.

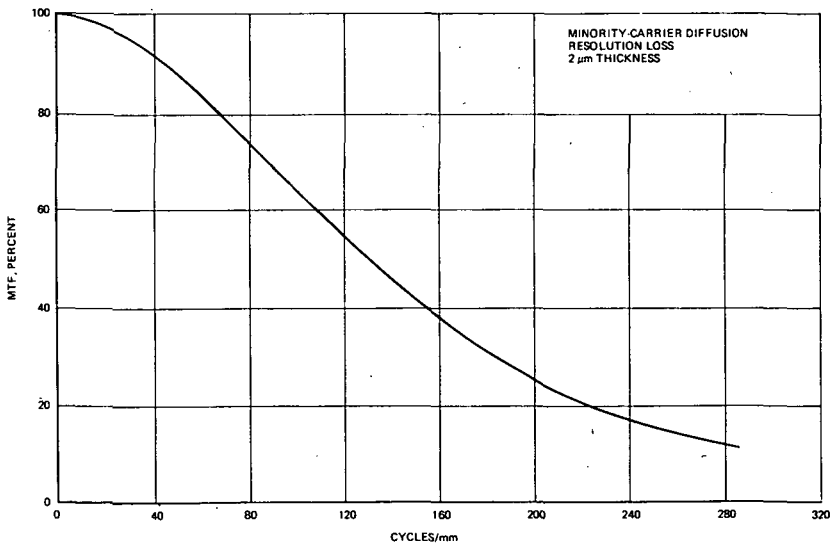


Figure 3-44. Estimate of Resolution Loss

Electron Bombarded CCD

As discussed in Chapter 4, linear arrays of silicon diodes, read out with integrated circuit shift registers and amplifiers, are available and under intensive development. While these devices are being designed to respond to light, those made of silicon are also sensitive to high energy electrons, with a conversion efficiency of about one carrier per 3.5 electron volts. The silicon diode targets used in the SIT or EBS tubes provide typical gains of more than 2000.

The readout noise of the CCD arrays is currently a few hundred electrons per diode and can be expected to decrease in future devices. Therefore, it appears quite feasible to detect single photoelectrons from a photocathode using accelerating voltages of 10 to 15 kV. A sensor of this type could be used in conjunction with a digital memory to achieve quantum noise limited signal-to-noise ratios at the lowest possible illumination levels. In Figure 3-45, the signal-to-noise ratio is plotted versus exposure for a light illuminated silicon diode array with a readout noise of 100 electrons rms and a CCD plus III-V photocathode.

For applications where the exposure will be very low, such as narrowband spectra, the CCD plus Photocathode is approximately 2 orders of magnitude more sensitive when judged on the basis of S/N. At high illumination levels, the S/N is dominated by the statistical or quantum noise in both devices.

The image intensifier arrangement also affords the system advantages associated with image intensifiers in standard television tubes. These advantages are:

- a. Ability to vary gain as a function of scene illumination
- b. Image motion can be compensated electronically and altered in flight if necessary
- c. Magnification varied between photocathode and CCD to provide electronic "zoom," to adjust the system's focal length in flight depending on the scene of interest
- d. Use in the "WISP" mode to look at different narrow spectral bands by deflecting the electron image between photocathode and array.

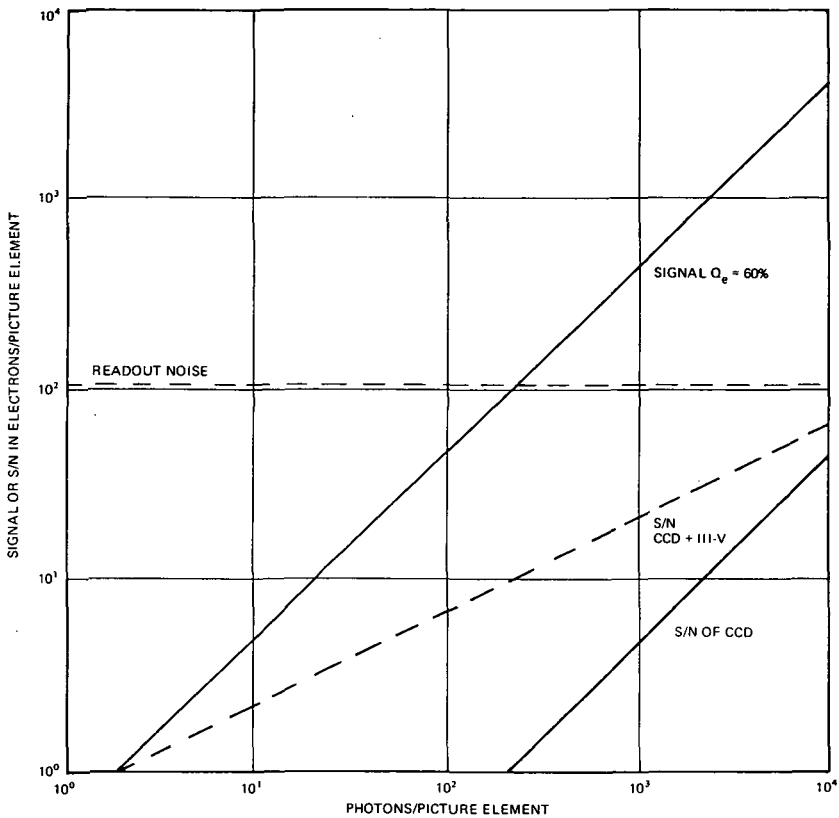


Figure 3-45. CCD + Photocathode Sensor

The technology is at hand to make these sensors, capitalizing on the major effort to develop the solid state arrays. Some work would be required to adapt the CCD devices to the photocathode processing temperatures and constituents used to make photocathodes. This would be relatively inexpensive, in comparison with the substantial investment now being made in optically-sensitive CCD technology.

Cold Cathode Emitter

The negative electron affinity concept offers the possibility of a direct replacement for the thermionic cathode. As described, the negative electron affinity emitter is one in which electrons in the conduction band can be emitted into vacuum. A way of introducing electrons into the conduction band is through the injection of carriers by means of a forward biased p-n junction. The resulting structure is a cold cathode emitter.

The band diagram of a p-n junction cold cathode emitter is shown in Figure 3-46. By forward biasing the injecting contact, a high density of carriers is injected into the p-type region. These carriers diffuse across the p-region to the surface which has been treated to have negative electron affinity and are emitted into vacuum. The structure is similar to an n-p-n transistor in which the collector is a vacuum electrode. The treatment of the injecting structure follows that of the junction transistor.

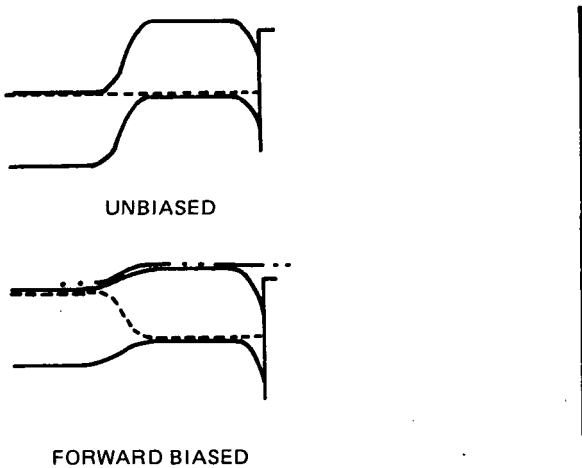


Figure 3-46. Junction Cold Cathode Emitter

The first observation of cold cathode emission, made using a structure in which the p-n junction was perpendicular to the emitting surface showed feasibility of the concept. More recent work has resulted in the development of a silicon cathode with geometry shown in Figure 3-47. Using this cathode with an emitting area of $2.5 \times 10^{-5} \text{ cm}^2$, an emission density of 20 amps/cm² was observed on a continuous basis. More than 200 amps/cm² were obtained on a pulsed basis. This emission density is nearly an order of magnitude greater than that observed from thermionic cathodes. The emission efficiency defined as the ratio of emitted current to injected current observed was as high as 10 percent. Promising results have also been obtained with a III-V version of this type of emitter.

A major advantage of this type of cathode for ERTS applications is the potential for extremely high resolution capability. The cathode injecting area itself defines the limiting aperture, and the narrow velocity distribution of the emitted electrons provides excellent imaging characteristics. For example, Figure 3-48 presents an estimate of the MTF limitation to electron-gun

performance provided by a cold-cathode with $5\text{ }\mu\text{m}$ emitting diameter. This estimate is based on O. Shade (1970) expressions for cos-squared distribution in angle. The cold-cathode is expected to provide a high degree of forward-focus, hence actual performance may exceed this estimate. A beam current of $5\text{ }\mu\text{A}$ would be provided by such a cathode at 20 A/cm^2 .

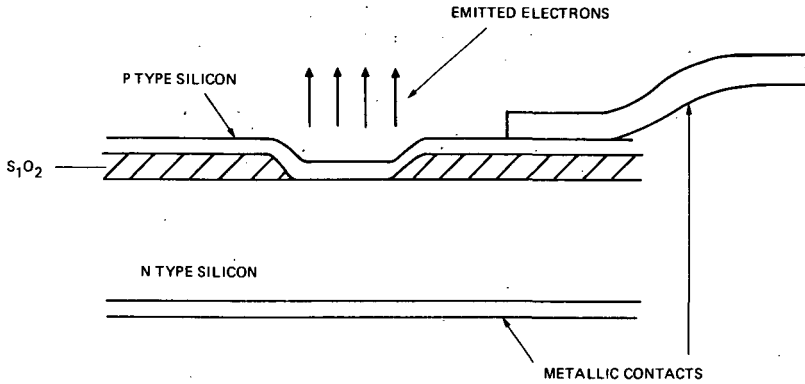


Figure 3-47. Silicon Cathode

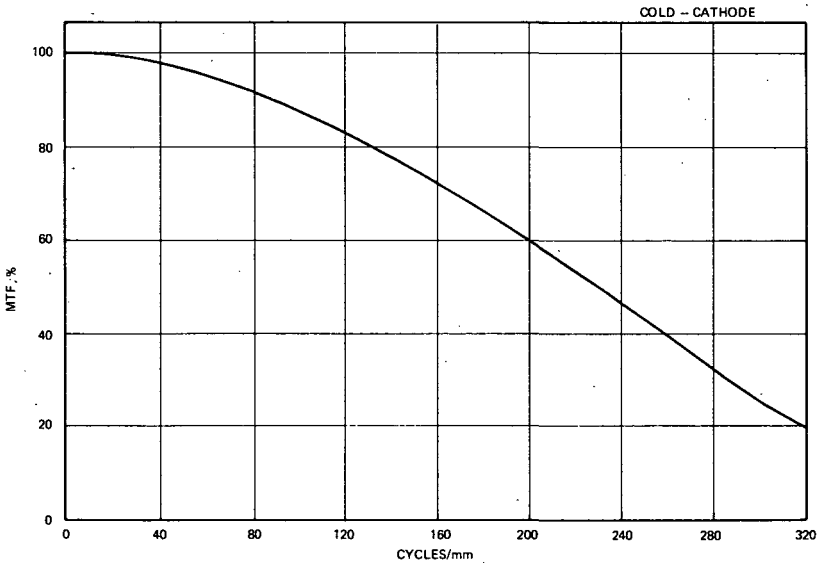


Figure 3-48. MTF Limitation to Electro-Gun Performance

Notice that 50 percent MTF occurs at 230 cycles/mm, with 20 percent response at about 320 cycles/mm. Although there are other resolution degradation mechanisms in the operation of beam-scanned tubes, such as the field mesh, target, etc., these results indicate that the cold-cathode should effectively remove the electron optics as a major limiting factor.

SYSTEMS AND ACCESSORIES

Growth of electron beam imaging devices both in quality of data and application to user requirements has brought a maturity of sophistication. With ever-increasing numbers of users now recognizing the features of specific instruments and the degree of utility afforded by each, it is possible to look at new approaches with confidence, and be able to better specify the requirements of present state-of-the-art devices to meet newly uncovered applications.

The world of electron beam devices has its own set of constraints, capabilities, and potential. Typical of this is the discussion on optics for these devices in the next section, and the projection of performance indicated in previous sections by expanding sensor configurations. New ideas are being formed. The use of image motion compensation may eliminate the short operating time required for shuttered sensors. The use of striped filters gives multispectral capability to normally monochrome sensors, and new techniques of color separation and detection will add capability to present devices.

In the present consideration of future systems, related accessories of data storage systems, mechanical mounts, off-axis pointing systems, data encoding and processing devices and others are not reviewed here, since the study effort was limited in time and scope. Some mention is made in a previous section of image correlation methods and a sensor capable of extracting feature information on a total scene basis. Perhaps this and other data optimizing schemes will call for a new class of accessory devices and a new system approach for preprocessed imagery. In the near future, the general growth of imaging devices is expected to provide an increased variety of image data that are useful to a significant number of uses.

Wide Area Image Detection

The wide area image detection process requires that the related optical field of view be large enough to cover the area or swath of interest. To do this effectively, the lens must be designed for minimum degradation at the edges

of the field. The effect of stray light, vignetting, and light flux density varying at the fourth power of the cosine of the angle are all significant. The spectral irradiance at the image plane is proportional to the product of the spectral transmittance of the lens and the spectral radiant flux incident at the lens. Some of the flux that is not transmitted is absorbed by the lens elements, and some is reflected out of the camera.

Of great importance is the spectral transmittance due to scattering by surface imperfections, dust, scratches, and microinhomogeneities within the lens elements. In addition there are reflections and multiple reflections from lens surfaces, tube surfaces, mounting fixtures, diaphragm, and shutter edges and surfaces. These sources of stray light give rise to additional spectral irradiance over the image surface, which reduces the contrast in the image and is commonly referred to as veiling glare. This veiling glare may become the limiting factor in a system designed for wide intra-scene dynamic range.

The modulation transfer function of a lens is a measure of its spatial frequency response. With a low frequency measurement as a baseline (100 percent) the effect of increasing frequencies may be determined and applied to system analysis, where the combined effects of lens, sensor, amplifier, recorder, transmitter, multiply receiver and display may all be considered.

A lens designed to provide quality imagery with a designated resolving power, should have an MTF characteristic that drops very slowly before the limiting resolution of the sensor takes effect. Figure 3-49 is the modulation response of the ERTS-I return beam vidicon camera lens. The lens was designed for a 0.1 micrometer wide spectral band, and a 35 mm wide image plane. The lens is an f2.5, with a focal length of 126 mm, manufactured by Fairchild. Few lenses in existence can approach this quality.

For sensor systems requiring long focal length and chromatic correction over an extended wavelength range, a reflective optical system may be used. All-reflective systems have a limited field of view. In catadioptric systems the field of view can be widened by corrector plates or field widening elements near the focal plane. For electron beam devices, such systems would probably not be used for fields of view above 10 degrees. The reflective optic system is also effective in reducing telescope length and space component weight while providing a low-f number at long effective focal lengths.

Detailed optical design and system definitions are described in the literature. The importance of extreme care in optical requirement definition, design, and testing cannot be overemphasized in a high performance system.

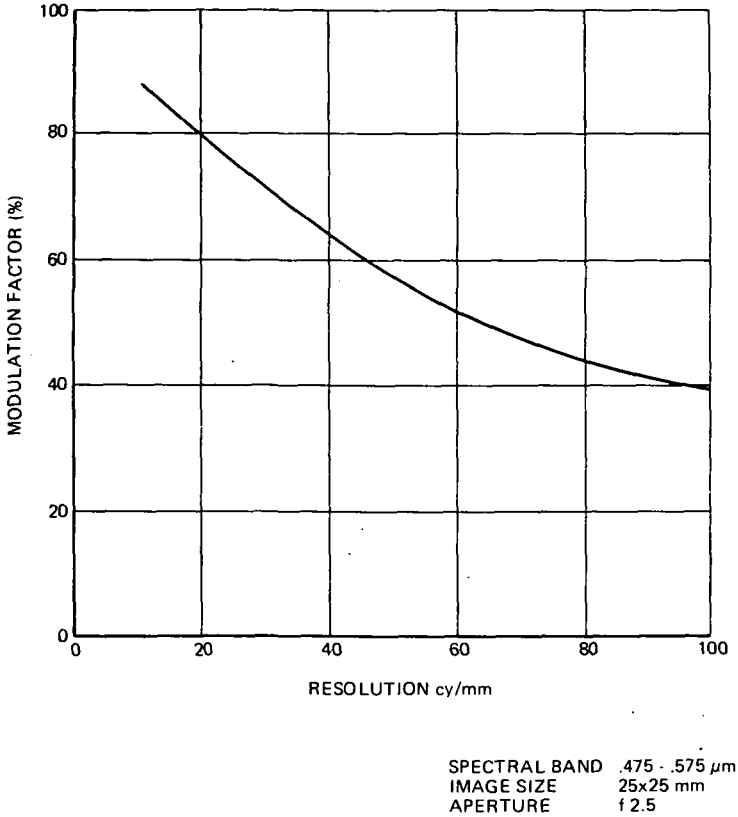


Figure 3-49. Modulation Response of High Performance ERTS-1 RBV Camera Lens

Techniques for Multispectral Separated Signals

Alternative Possibilities

The usefulness of multispectral data both for presentation as color imagery to facilitate photo interpretation and for use in quantitative spectral signature analysis has been clearly demonstrated by ERTS. When considering electron-beam tubes as the sensors, the most obvious way to obtain several separate spectral bands is to use multiple sensors, i.e., one tube for each band, as done with the ERTS RBV cameras and with most commercial color TV.

Such a scheme has several obvious advantages. The spatial resolution per band is the highest possible with the tube selected. Spectral resolution also should approach the maximum since the filter and optics both can be optimized for the band. The basic design of the sensor system is simple since the only difference for each band is the optics/filter system.

The principal disadvantage for such a system is the difficulty of registration of the data from all bands. Problems include differences in electron optics in each tube, differences in focal lengths and fields of view, and misalignment. In addition, multisensor systems have obvious disadvantages in size and weight.

The alternative ways to obtain multispectral separated signals all involve the use of a single tube. Two of these alternatives have already been discussed in detail: the line-scan multispectral silicon vidicon, and the multiaperture image dissector. Two other single tube techniques also show considerable promise and are described here. The first is the use of criss-crossing patterns of striped filters for several spectral bands. These striped filters are used across a full frame tube to provide multiple bands over a two-dimensional area image. The second is the WISP, Widerange Image Spectrophotometer, in which one dimension of a tube's format is used for spatial information, and the other for spectral information. This type of device which itself has several different forms is spatially a line-scan device, which provides a second dimension spatially by the movement of the sensor carrying vehicle.

Striped Filters

General Description and Features. A system using a single frame sensor with striped filters is capable of providing high resolution multispectral images by employing a technique to encode the spectral information into different frequency channels. In simplest form, the system uses for each spectral band alternate stripes of a filter corresponding to that band and a completely transparent material. Each set of stripes for a different band is placed on (or in front of) the tube face at a different angle to the scan lines of the tube. The angle differences make each pattern's stripes appear of different width and frequency to the scan lines and permit a separation of spectral data. Each band is then encoded into a different frequency channel of the total bandwidth of the tube. By appropriately choosing the widths and angles of the stripes, high resolution, registered, multispectral images can be achieved.

This multispectral framing camera system offers the following features:

1. A single camera can supply high-resolution imagery in three or more spectral channels, thereby reducing the weight, volume, and power requirements when compared to a multisensor system using, for example, three RBV cameras.
2. All channels are in perfect registration and are available simultaneously at the ground station.
3. A single electrical signal containing encoded information about all the channels is available for recording or transmission, reducing the on-board storage requirements.
4. The problem of sensor calibration is greatly simplified since only a single camera tube is used.
5. Additional channels, reduced in resolution but in perfect registration, can be added in a simple manner.
6. The encoding configuration facilitates the use of the "mixed highs" principle where the high-resolution information is common to a number of spectral channels, thus taking advantage of the redundancy present in the spectral channels.
7. The attitude requirements placed on the spacecraft are identical to those of any shuttered framing camera system, and image motion compensation can be employed for increased light sensitivity, if required.

This multispectral single sensor suffers from the following disadvantages in comparison with a multispectral-multisensor system:

1. Lower output signal-to-noise ratio due to light loss caused by the color encoding technique.
2. Lower resolution within a given spectral channel separation, but not necessarily for a spectral composite. In the case of a "mixed highs" mode of operation, the resolution of a spectral channel separation is only slightly reduced, due to the optical system. In the equal bandwidth mode the resolution is reduced by an additional factor.

Typical System Operation. A description of the operation of a single camera, three spectral channel system should help to clarify the principles of operation. Figure 3-50 is a schematic diagram of the optical system. Lens 1 is used to image the scene to be televised onto the filter plane. Lens 2 is a relay lens that images the filter plane onto the sensitive surface of the television camera tube, e.g., a vidicon. The image on the vidicon photoconductor will then be the scene to be televised, modified by the transmission characteristic of the filter. Figure 3-51 shows the details of the filter. The vertical lines represent alternate strips of transparent and cyan filter material. The diagonal lines represent alternate strips of transparent and yellow filter material. The line density (spatial frequency) is the same for the yellow and cyan gratings. A cyan filter has the property that it is transparent to blue light and to green light, but opaque to red light. This, therefore appears as a vertical grating structure only to red light, since it does not perturb either green or blue light. A yellow filter has the property that it transmits red and green light and is opaque to blue light. The structure then appears to be a grating with a 45 degree orientation to blue light only, since the red and green components are not perturbed. If the entire filter structure is illuminated by white light, the red component of the light will be modulated by a vertical grating, the blue component of the light will sense no grating structure at all.

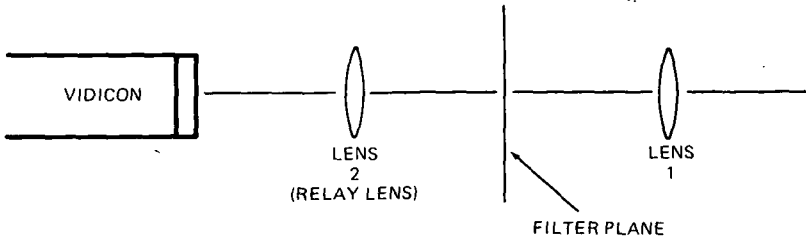


Figure 3-50. Television Camera Optical System

Assume for a moment that the filter plane is illuminated with red light and the structure is imaged onto the vidicon faceplate. A grid pattern will appear on the vidicon faceplate with a vertical orientation. As the electron beam scans the photoconductor, a carrier signal will be generated due to the grating structure image. The frequency of this carrier will be determined by the velocity of the scanning beam, the number of lines per inch of the grating at the vidicon faceplate, and the angle between the scan direction and grating axis. If the structure is illuminated with blue light instead of red light, a different grating structure will appear on the vidicon faceplate,

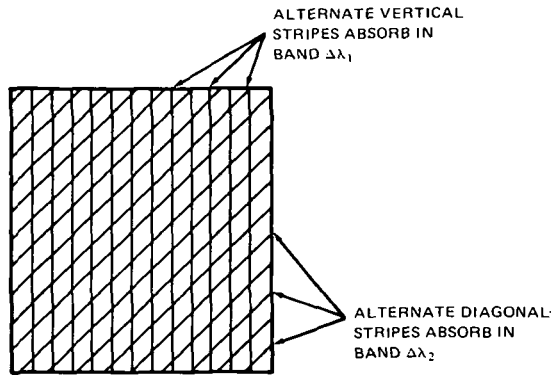


Figure 3-51. Filter Detail

this time with a 45 degree orientation. As the beam is now scanned, a carrier signal will be generated that is lower by a factor of $\sqrt{2}$ than the first case. In a commercial television system, these two carriers become the color subcarriers for red and blue. A system that has been designed and tested uses 5.0 MHz and 3.5 MHz as the two color-carrier frequencies.

Figure 3-52 shows the resulting signal spectrum from the vidicon when the camera is looking at a live scene. The red information appears as sidebands around the 5 megacycle carrier; the blue information appears as sidebands around the 3.5 megacycle carrier; and the luminance is representative of the total information in the signal. The three components can be matrixed to extract the standard blue, red, and green components of the signal.

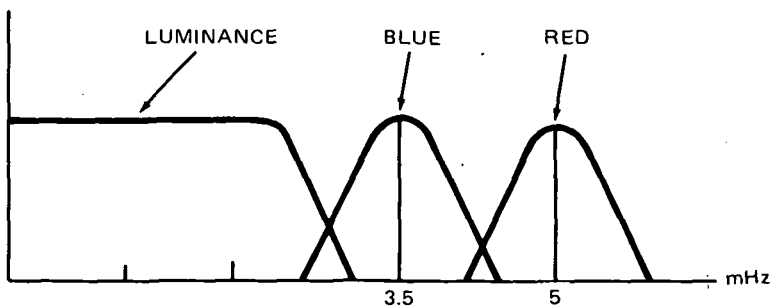


Figure 3-52. Vidicon Signal Spectrum

The system described is designed for accurate reproduction of color. The color spectrum of the image is divided into components defined by the colorimetry of the filter material used. These are carefully selected to match the colors of the reconstruction process; in the commercial case, this is the color television receiver. However, if the filter material in the grating is selective in the infrared (e.g., for an ERTS application) that component of the image can be encoded. It could then be reconstructed in any desired color on a color display or displayed separately as individual spectral separations.

The basic configuration of a satellite camera system is illustrated in Figure 3-53. The surface of the earth is imaged by an objective lens onto a filter plane where a spectral encoding filter is placed. A relay lens images this filter plane onto the sensitive surface of a single camera tube. The electrical output of the camera tube is then available for recording on-board the spacecraft or for direct transmission to a ground station. As described previously, the spectral encoding filter for a three-channel system is made of two sets of color grating stripes on a single transparent substrate. These gratings are displaced at different angles relative to each other. Their presence causes the scene information to be modulated onto electrical carriers in the output spectrum.

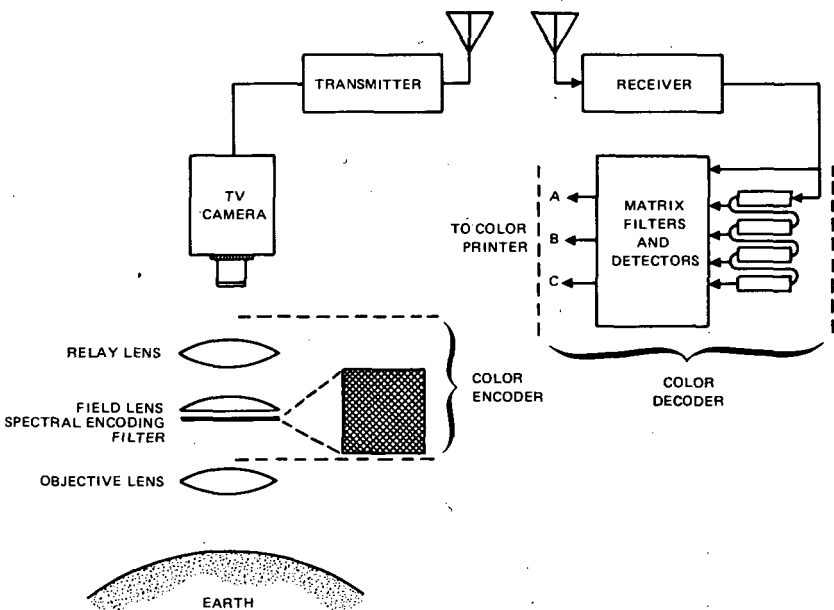


Figure 3-53. Spectral Encoding and Decoding System

At the ground station a filtering operation is incorporated to separate the various channels. To separate the channels efficiently and with a minimum of crosstalk, two-dimensional spatial frequency filtering is required (Macovski and Schaefer, 1972). This filtering is accomplished by obtaining a weighted sum of a two-dimensional scanned array. The array is realized in the ground station by use of a number of delay elements, each of which stores a complete scanned line. Note that for the simple illustrative case described earlier, only simple bandpass filters were required to recover the individual spectral channels. However, to make the most effective use of the information handling capabilities of the sensor, two-dimensional filters are required.

Status and Potential of Striped Filter Cameras. Striped filter systems are now available for commercial and closed-circuit color television applications. Stanford Research Institute has developed a laboratory simulation of a high resolution 3-color striped filter system for NASA and used the simulator as the basis for a comprehensive analysis. Determination of the effects of crosstalk and development of coding schemes to reduce these effects have been the principal foci of this investigation. Single band resolutions of 50-60 percent of the basic camera resolutions have been achieved for the simulated system, and it is anticipated that such results can be achieved for up to four bands in an "equal band" system. Such a system could have many applications on future satellites where high resolution multispectral, frame cameras are desired.

The full potential of these systems depends on several key parameters.

1. The number of encoded channels in this type of multispectral sensor is limited by signal-to-noise ratio considerations. As more spectral channels are added, the finite dynamic range of the sensor is divided into smaller allocations for each spectral band. The noise output of the sensor is not divided in a corresponding way but is present equally in all channels. This electrical noise can be reduced only by electrical filtering (i.e., bandlimiting). A practical upper limit for the number of encoded channels is probably in the order of six.
2. The registration of the system from the vidicon faceplate to the output printing device is essentially perfect. The only possible limitation to spectral channel registration might result from the optical system imaging the different spectral images onto slightly different

regions of the vidicon faceplate. However, this type of chromatic aberration should be very small.

3. This system, using a single sensor, is inherently more stable than a multisensor system. A multisensor system can exhibit much larger differential drifts between spectral channels than a single sensor system. If even small differential drift between two channels were very important (e.g., between the green and infrared levels from some vegetation), a color difference encoding technique could be used. In this technique, instead of encoding each color with a separate set of stripes, the difference between two colors is encoded by one set of stripes, and one of these colors is encoded by another set of stripes. Although both arrangements encode the same information in two sets of stripes, the color difference set of stripes is more immune to decoding errors in determining the relative strength of the two colors. Thus, by considering some spectral information more important than others, the system can be designed to favor the more important.
4. The output signal-to-noise ratio of the single sensor multispectral system described is less than that of a multisensor system employing separate lenses and filters. The principal reasons for this are: (a) the dynamic range of the sensor for any one color is appreciably less than the total dynamic range, and (b) the MTF of the sensor at the carrier frequency of the striped filters is less than one. The signal-to-noise ratio can be improved by reducing the frequency of the stripes (improving the MTF factor) and filtering the electrical signals accordingly (reducing the electrical noise). This produces a situation where S/N can be traded off for resolution (or bandwidth) of the spectral channel. The one tube color television cameras designed for commercial television have achieved a good balance between S/N and resolution.
5. The resolution of the system depends upon the mode in which the system is used. In the "equal band" mode, all the information for each spectral channel is derived from its encoded signal. In this mode, the resolution or bandwidth of the system corresponds to approximately 60 percent of the frequency of the encoding stripes. The frequency of the encoding stripes is usually set somewhere between the 25 and 50 percent points of the MTF of the sensor plus relay lens.

The resolution of the system in the "mixed highs" mode (Bedford, 1950) is nearly equal to the resolution of a multisensor system, being essentially that of the sensor plus relay lens. In the mixed highs mode, the spectral information encoded in the stripes provides the low frequency information for a particular spectral band. The high frequency information is supplied to all spectral channels (in common) by the nonencoded, high frequency information.

Both the equal band system and mixed highs system will have their resolution increased somewhat if the relay lens is removed. This may be done by depositing the stripes on the vidicon faceplate, or using fiber optics to couple the light from the stripes to the vidicon photoconductive surface.

Widerange Image Spectrophotometer (WISP)

Basic Concept. The WISP concept uses a two-dimensional, full frame image tube to record spatial information parallel to one axis and spectral information parallel to the other. It does this by taking a one-dimensional (line) image and spreading it spectrally in the perpendicular direction. Figure 3-54 illustrates the basic operation. An objective lens focuses the incident radiation on a narrow slit which determines the field of view. Radiation passing through the slit is converted into a beam of parallel rays by a collimating lens. A diffraction grating breaks up the beam into its individual wavelength components which leave the grating at different angles. Another lens assembly focuses these spectral components on the photosensitive surface of an imaging tube. Each component is focused on a unique location of the tube surface. The tube electronically scans the image and divides the spectrum into a preselected number of wavelength bands. Thus, the tube's operation is comparable to viewing the image first with a camera which is sensitive only to radiation in one wavelength range, say 4000 - 4150 Å. Next, it views the image like a camera which senses only a second band, say 4150 - 4300 Å, and so on until the entire multispectral range of interest is covered.

In most cases, the spectral bandwidths for each band of interest are equal, and the specific bands for a particular implementation of WISP are fixed. But neither of these conditions are requirements of the concept. Within the limits of the electrical bandwidth, sensitivity, and operating features of the tube and its control circuitry, many variations of the WISP concept are possible. Some of the more interesting will be discussed in the next section.

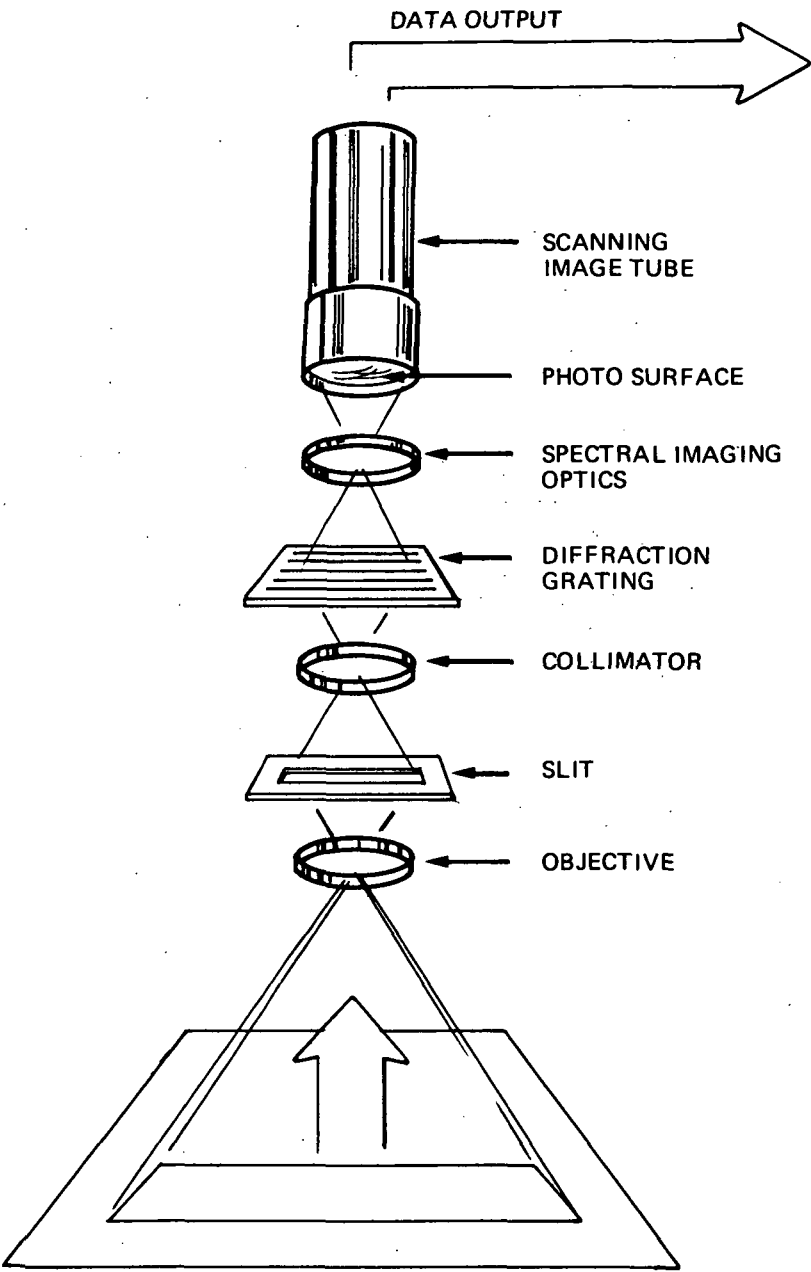


Figure 3-54. WISP Concept Schematic

In order to obtain two-dimensional spatial imagery, the WISP must be mounted on a platform which moves in a direction perpendicular to the slit. Consequently, the entire spectrum of interest must be scanned in the image tube, while the camera moves the equivalent of one slit's width in the object plane. Thus, for a given ground speed and sensitivity of the tube/optics combination, there is a tradeoff between spectral and spatial resolution.

The readout operation of the WISP will depend both on the kind of image tube being used and on the number and size of the spectral bands. In all cases, however, in order to assure registration of the data in all spectral bands, from the same ground point, the scan is made across the whole spectrum of interest for each ground point before stepping to the next point. The output of the WISP is a video signal that can be processed in many ways both on the spacecraft and on the ground to select or combine the data from different bands according to the needs of the user.

Alternate Implementations. The original version of WISP, built and tested by TRW Systems as a laboratory version, featured an interesting variation which has not been incorporated since then into any flight model, but which could prove very useful in the future. In this device it was possible to vary the location, and number of spectral bands by command. The number of the bands had an upper bound, and, of course, the bands could not overlap. Nevertheless, the flexibility offered by this concept could be very useful for an experimental mission in which the usefulness of particular bands may not be known in advance or in which different scenes may require different spectral bands. This flexibility requires additional complexity in the camera: in the control circuits and scanning mechanism, the data handling logic, and perhaps even in beam shaping. The difficulty of implementation and limits of capability of such systems should be investigated.

Two other WISP implementations have been investigated and implemented under NASA contracts by TRW. The MOCS, Multichannel Ocean Color Sensor, was an AAFE experiment flown on a NASA aircraft in 1972 over both ocean and lake waters. It uses an image dissector tube to record the image in twenty 150\AA bands from 4000 to 7000\AA . The spectra are scanned in sequence over a 150-point line on the tube. MOCS's principal application is the measurement of water color which is an indicator of subsurface phenomena such as plankton growth and pollution diffusion. The need for 20 bands has been questioned, and it is still to be determined whether a much smaller number, say 6 to 10 bands, would be sufficient if they were centered at the most important wavelengths. However, chlorophyll, planktons containing different pigments, sewage composed of many components,

different types of sediments, and oils which fluoresce at many wavelengths will be targets. Figure 3-55 illustrates a sampling of reflectance curves showing a diversity of signatures. Hence, the number of bands has not yet been reduced.

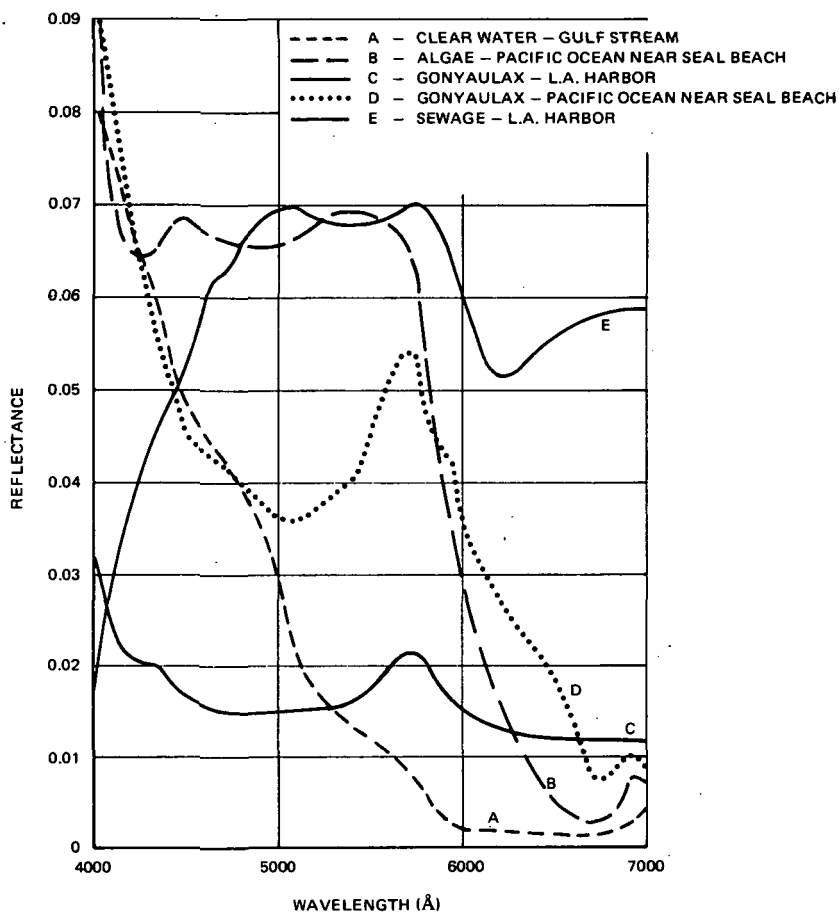


Figure 3-55. Spectral Reflectance of Five Water Bodies

The Scanning Imaging Spectroradiometer (SIS) is a dual mode WISP. In the land mode it has a spatial resolution of 1380 elements and uses twelve 375Å bands between 4000 and 8500Å. In the ocean mode, the spatial resolution is down to 138 elements, but the spectral resolution is improved to permit sixty 75Å bands. SIS is to fly on an RB57 aircraft. Signal-to-noise ratios for large targets have been measured at 30 dB for the ocean

mode and 28 dB for land. The scan pattern differs for the land mode, where it is linear, and the ocean mode, where it is "dithered" as shown in Figure 3-56. An FPS vidicon is used to permit this scan pattern variation and the performance range required of SIS. The SIS can be changed from one operating mode to the other by command.

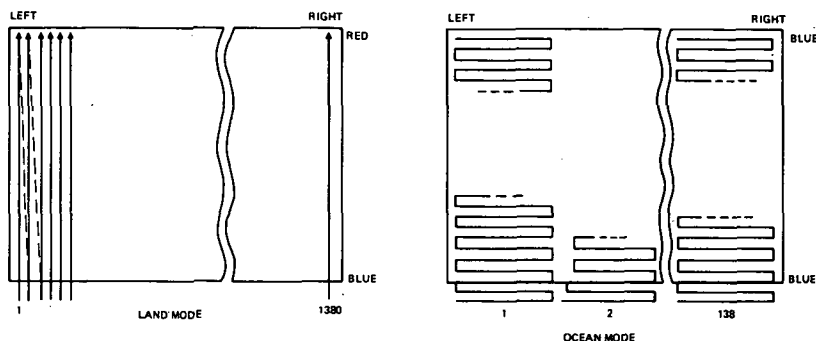


Figure 3-56. Scanning Imaging Spectroradiometer Vidicon Scanning Patterns

As noted, two types of tubes — image dissectors and vidicons — have been principally used for the WISP. The former is limited in beam shape by its fixed aperture and in the kind of scanning patterns it can use since it has no storage and thus cannot integrate the radiant energy at a particular point over any period longer than the instant that point is being scanned. However, it is more linear than the FPS vidicon, requires simpler data handling, and because it does not integrate, it has no lag effect, which the vidicon does and which causes some problems in adjacent element interference. The vidicon, on the other hand, is more flexible in its control capabilities, provides energy storage, and is more sensitive than the dissector. A flexible WISP would, therefore, likely use a vidicon although with either device, the location of the bands could be shifted by a voltage change. Likewise, in either case not all of the bands provided by the sensor need be sent to the ground if communications bandwidth is a problem.

Some improvements in dissector sensitivity are now being investigated which might improve its flexibility. Recent tests have been conducted by TRW and ITT on "smoothing dissectors" using both one and two stages of intensification. These devices show promise of retaining the linearity and no-lag characteristics of the dissector while giving S/N gains of from 5 to 20 times.

The WISP thus offers considerable promise for multispectral applications. In general, it is useful where extra high resolution is not required but many spectral bands are.

Forward Motion Compensation

Nongeostationary spacecraft and any point on the earth's surface are always in motion relative to one another. This motion is caused primarily by the spacecraft's orbital velocity, but the rotation of the earth and random spacecraft motions also contribute. Because of this motion, any image taken over a finite exposure time will contain a certain amount of smear which may reduce the effective spatial resolution of the image. However, the exposure times of the ERTS-1 RBV and similar cameras are on the order of 10 milliseconds, which is short enough so that the resulting smear of about $1\frac{1}{2}$ TV lines does not unacceptably degrade the images produced. Hence there are no motion compensation techniques on ERTS-1 or ERTS-B.

Future cameras may be required to observe specialized scenes, such as those with low contrast ratios. Low contrast scenes require a longer exposure time to maintain the same spatial resolution as achievable with short exposures of high contrast scenes. The maximum exposure time that can be accommodated without significant degradation in image quality is a function of spacecraft orbital altitude and sensor resolution.

With respect to electron-beam imagers, motion smear is usually expressed in terms of TV lines. Table 3-21 relates the number of TV lines of smear to the present degradation in image spatial resolution.

TABLE 3-21

EFFECT OF SMEAR ON RESOLUTION

Amount of Smear (TV Lines)	Response (%)
$\frac{1}{2}$	90
1	63
$1\frac{1}{2}$	29
2	0

It is possible to compensate for a large portion of relative image motion, and thus operate with long exposure times without degradation in image

quality. Many techniques have been proposed and implemented for use with electron-beam imagers to accomplish this compensation. They have included sensor platform, reflective and refractive optical, and electronic techniques. Typical nonelectronic motion compensation systems weigh about 10 pounds and require about 50 watts peak and 1 watt average power.

Electronic motion compensation may be applied in a sensor where the optical image is focused on a photoemitter, and the resulting electron image is magnetically refocused at a second plane (target, phosphor sandwich, or aperture plane). In these cases a magnetic field may be applied to the image during translocation, and this field provides an angular motion equivalent to the optical scene motion. This type of compensation has been used in image intensifier tubes and image dissectors with considerable success.

Forward motion of a spacecraft may be estimated from altitude and velocity, with variations controlled by ground command. The limit of exposure time is determined by the allowable limit of obscuration, since the photoemitted image is being moved across and off the sensing surface. The stabilized image could increase exposure times by more than one order of magnitude.

Other spacecraft motions, such as roll, pitch, and yaw require either predicted motion correction signals or on-board sensors for detection. High accuracy two-axis gyros can detect motions of one arc-second, which may be used for pitch and roll correction. Normal two dimensional images cannot be corrected electronically for yaw (rotation). The image dissector in a line-scan mode has successfully demonstrated roll correction in aircraft imaging experiments, and has the capacity for all axis compensation with the appropriate sensors.

One of the most promising optical motion compensation techniques, based on studies by RCA and Dynatronics, is based on the use of a pair of counter-rotating wedges with identical apex angles forming a variable geometry prism (Figure 3-57). In its initial position, the prism does not deviate the optical path of the incoming light. During exposure, the wedges are counter-rotated by an angle θ from this original position. The deflection of the optical path caused by the wedge rotation is in the direction of the bisector of the apex axis and the deflection angle is $2(n-1)\phi \sin \theta$, where n is the index of refraction of the wedge material and ϕ is the wedge angle.

Provided the counter rotation angle θ is small, the optical deflection can be regarded as a linear function of the rotating angle. Consequently, when the

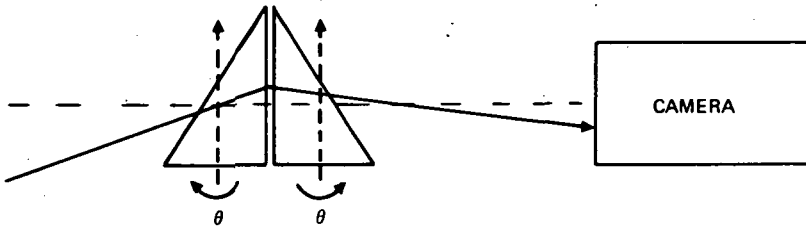


Figure 3-57. Counter-Rotating Wedges for FMC

wedges are counter-rotated at a constant rate and the bisect line is aligned with the orbital path, this optical element can provide motion compensation at and near its complementary (initial) position (Figure 3-58).

The rotation wedges can provide compensation for 97 percent of the motion over an exposure time of up to 200 milliseconds. Light transmission efficiency is 95 percent and its limiting resolution is $16 \mu\text{rad}$ which will not be noticeable at spatial resolutions currently achievable from space.

TECHNOLOGY OPTIONS REACHED BY PANEL

The conclusions arrived at by the panel as to the technology options that offer the most effective performance-cost benefits for future user applications are summarized in this section.

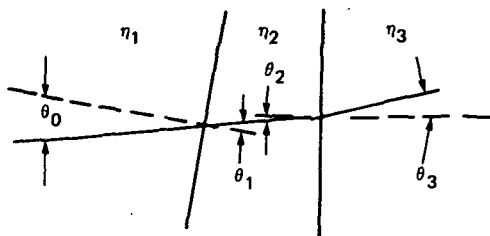
RBV Improvements

It is believed that a large number of user applications can be satisfied by improvements to the existing RBV Camera. Improvement in shading and thermal and temporal signal stability can be accomplished by mesh and photoconductor improvement, and electro-optical modifications to achieve more desirable tube characteristics. Both the 50 mm and 115 mm versions should be pursued.

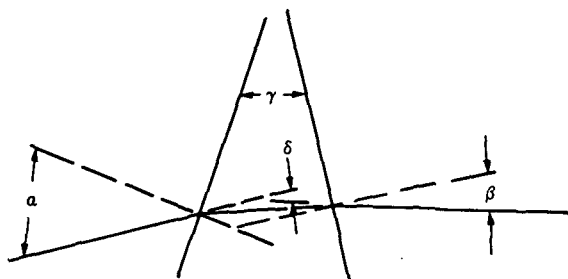
Higher Signal-to-Noise Sensors

The RBV is limited to signal-to-noise performance of the order of 40 dB, by the inherent nature of the return beam signal mechanisms. Three options are available to achieve higher signal-to-noise ratios.

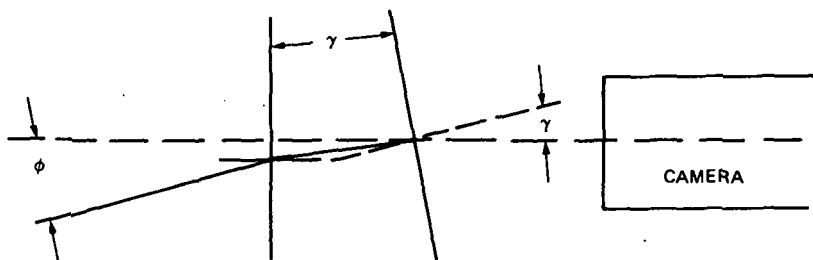
1. The development of high resolution direct readout vidicons, and corresponding work to develop improved ultra low noise target



(a) Deflection of light beam at boundaries



(b) Deflection of light beam by a prism



(c) Motion compensation

Figure 3-58. Optical Motion Compensation Techniques

preamplifiers. This approach would make the system signal-to-noise ratio bandwidth dependent, hence providing the means to achieve high signal-to-noise for low contrast applications by proper selection of system operating parameters and trading scan (or frame) time for signal-to-noise ratio.

2. Application of high velocity readout sensors currently under study to demonstrate feasibility. Performance data on these devices is expected early in 1973.
3. Application of isocon mode readout of high resolution vidicons, also currently under study. The isocon readout eliminates the beam noise dependence of return-beam readout, at the expense of a more complex electron optic.

Both options (2) and (3) would offer a free selection of frame times since they do not require bandwidth compromises. However, both of the options are early in their development, and any effort to pursue either of them should await further evidence of feasibility expected from on-going tests.

Large Format Vidicons

Some of the problems experienced in current systems, like ERTS where multiple cameras are used, are solvable by using larger single sensors. It is expected that larger format sensors may have reduced resolution per mm, but that overall data packing density which allows simplified optics and reduced electronics will prove more beneficial. The larger tubes with striped filters could offer acceptable resolution performance in multiple spectral bands, with registered images, and relatively simple electronics. Target formats as large as 100 x 100 mm should be studied.

Large Silicon Target Vidicons

The high quantum efficiency in the visible and near IR afforded by silicon makes it a decided improvement over other vidicon photosensitive targets. Since its resolution is limited by the target structure, it should be incorporated in large format tubes that can provide the necessary overall resolution at relatively low spatial frequency. It is recommended that a program be funded to make large silicon diode array targets. This would be followed by a program to use these targets in the large vidicons also recommended in this study.

As a part of this option, a supporting effort to develop the techniques for cooling the target to below 0°C (to provide slow scan operation) is considered essential. The cooling problem should be considered in the tube design.

High Sensitivity, High Resolution, Fast-Erase Camera Tube

Development of a camera tube having high sensitivity, high resolution and fast erase is recommended for applications such as WISP. A tube having an extended red response photocathode, an image section with gain and a high resolution electron gun similar to that used in the return beam vidicon is considered a feasible approach for the development of a tube having the desired characteristics. The extended red photocathode would provide spectral response over the 400 - 900 nanometer wavelength region. The gain mechanism would provide the sensitivity required of a camera tube operating in the manner described for WISP. The tetrode version of the RBV electron gun is recommended because this gun can be operated in two modes; a high resolution mode for readout and a high current mode for preparation.

As a part of this option, support should be provided to develop negative electron affinity (NEA) materials for the lower part of the visible spectrum, for the image section photoemitter.

The recent invention and intensive development of negative electron affinity (NEA) photocathodes has extended the long wavelength sensitivity of photocathode devices. It has also increased the quantum efficiency in the visible spectrum. Negative affinity photoemitters also have the potential of increasing the resolution of image tubes because of these low velocity spread characteristics of NEA photoemission. The ongoing programs are directed toward military applications and will in general not provide sensors suitable for earth observation missions.

Funds should be allocated for developing III-V photocathodes that are large (70 mm diameter) and with high quantum efficiency over the spectral band from .3 to 1 micron. This development would be followed by the application of these photocathodes to the high resolution television tubes discussed previously.

Optics

Current state-of-the-art in refractive optics allows about 50 percent MTF at 100 line pairs/mm. Clearly the optical chains need to be improved to use

the available resolution in the present electron beam sensors. With the increased payload capability provided by the shuttle, large reflective and catadioptric optical systems should be studied and designed. These would provide high resolution over relatively wide fields of view and large collecting apertures that will develop sufficient signal in the narrow spectral bands of interest for many of the user applications.

Cold Cathodes (Negative Electron Affinity Materials)

There have been recent developments of negative electron affinity materials which seem promising for cold electron beam cathodes. Indications are that adequate effort is being expended on this device to make it an off the shelf reality within the next few years.

If the technical options for new tube developments are pursued, it is recommended that gun designs incorporating the cold cathode be included in the new devices. The use of the cold cathode will provide state reliability, as well as significantly higher current density capabilities.

Dielectric Tape Camera

The dielectric tape camera offers significant data storage advantages for specific utilities over current magnetic tape. The working group panel felt that it could not recommend additional effort into the dielectric tape camera design, without a specific planned application. However, for completeness, the user group should be aware of the significant increase by a factor of 100 that this tape camera offers in data storage density. Its potential, therefore, is important for long-term considerations.

BIBLIOGRAPHY

- Bedford, A. V.; "Mixed Highs in Color Television," *Prdc. IRE*, 38, 9; 1003, September 1950.
- Crowell, M. H.; Buck, T. M.; Labunda, E. E.; Dalton, J. V.; and Walsh, E. J.; "A Camera Tube with a Silicon Diode Array Target," in *Bell System Tech. J.*, 46 (2), 491-495, 1967.
- Dawes, *Electron Bombarded Induced Conductivity* (1971).
- Lowrance and Zuchino *Secondary Electron Conduction* (1971).
- Reynolds, F. W., "Solid State Light Sensitive Storage Device," U.S. Patent No. 3,011,089, applied for April 15, 1958, issued November 21, 1961.
- Schade, O. H., Sr., "Electron Optics and Signal Readout of High-Definition Return-Beam Vidicon Cameras," in *RCA Review*, 31, No. 1, March 1970.
- Macovski, A. and Schaefer, L. F., *IEEE Transactions on Computers*, Vol. C-21, No. 7, 642, 1972.
- Scheer, J. J. and VanLaar, J., *Solid State Commun.*, 3, 189, 1965.
- Schlesinger, K. and Wagner, R. A.; "A Mixed-Field Type of Vidicon," *IEEE Trans. on Electron Devices*, ED-14, No. 3, March 1967.
- Weimer, P. K., Forque, J. V., and Goodrich, R. R., "The Vidicon Photoconductive Camera Tube," *RCA Review*, 12 (1), 306-313, 1951.

CHAPTER 4

SOLID-STATE SENSOR ARRAYS FOR MULTISPECTRAL IMAGING FROM EARTH ORBIT

PANEL MEMBERS

J. M. Early – *Chairman*

L. L. Thompson – *Associate Chairman*

D. E. Bode

R. Ennulat

F. Huck

A. Koso

N. Lavery

J. Mudar

B. Rubin

P. N. Slater

G. Strull

P. K. Weimer

SOLID-STATE SENSOR ARRAYS FOR MULTISPECTRAL IMAGING FROM EARTH ORBIT

PANEL SUMMATION OF SOLID-STATE SENSOR TECHNOLOGY

The discussions of the panel members centered on the current and projected state-of-the-art in monolithic self-scanned solid-state sensors, together with complex arrays of such devices, for sensing the resources of the earth from earth-orbiting satellites. The types of sensors considered were those sensitive to electromagnetic radiation in the visible and near-infrared range of the spectrum from 0.4 to 1.1 microns, and to a minor degree those sensitive to radiation in the infrared range of the spectrum from 1 to 13 microns. The prime emphasis was on the former—the visible and near-infrared range, or in the photosensitivity range of silicon. These sensors consist of monolithic arrays of photodiodes, phototransistors, and charge-coupled devices formed on silicon using microelectronic fabrication techniques. The infrared devices consist of high-density arrays of infrared detectors (photoconductive and photovoltaic) made from semiconductor materials which are not integrated (i.e., fabricated on the same semiconductor wafer) with associated electronics.

Self-scanned solid state sensors, in general, comprise discrete photosensitive elements which are scanned by means of integrated registers driven by clock voltages. Currently, long linear arrays are formed by assembling a number of individual silicon chips. Two-dimensional area arrays (500 x 500) will become available in a few years, with even larger arrays possible.

Silicon Detector Arrays

Silicon, self-scanned, solid-state image sensor arrays are intrinsically small and require little power. They have solid-state reliability and are not damaged by high radiant overloads (e.g., direct solar input). These characteristics and superior photosensitive performance make cost reductions possible both in the sensing elements and the associated optics.

The high quantum efficiency of silicon, in conjunction with high scanning efficiency and low-noise, on-chip amplification, leads to high signal-to-noise (S/N) ratios and wide intrascene dynamic range. Electronics on the chip ordinarily include detector element scanning and signal current amplification.

Theoretically, these may be expanded readily to create other important performance features.

Using discrete photo-sensing elements fabricated with high geometric accuracy, a built-in metric and coordinate system is provided. Once aligned to the optics, geometric calibration is maintained. Individual detector characteristics are similar, but each discrete detector must be calibrated to eliminate the effect of dark current variations noise and pattern noise due to nonuniformity in responsivity of the individual photosensitive elements.

In silicon detector arrays there are three candidate types of sensors: photodiodes, phototransistors and charge-coupled devices (CCD). Two self-scanning modes are used: digital multiplexing and analog charge-transfer. The photodiodes and phototransistors have ordinarily used digital multiplexers driven by on-chip shift registers; the CCD sensors use the newer analog charge-transfer readout mode. Being silicon, the spectral response is restricted to the visible and near infrared (to 1.1 micrometers). The readout circuitry is generally on the same silicon chip as the multiple sensors (usually more than 100 sensors per chip).

The different solid-state sensors can be matched in their overall mechanical characteristics and in their gross electrical input and output requirements. All of the modes have approximately the same weight, volume and power consumption. They all operate at low voltage (less than 20 volts) and can easily be formatted to provide the same output to the additional onboard processing.

Status and Outlook

Solid-state imaging sensor systems are currently feasible, and they can be developed for advanced earth resource missions anticipated for the late 1970's and early 1980's. Photodiode and phototransistor arrays are in an advanced stage of development. A sensor using these arrays can be developed for space flight in a period of about four years. Charge-coupled devices are in the early developmental stage. A sensor using them can probably be developed for space flight in about six years.

At present, silicon photodetector elements can be assembled into line arrays of several thousands of elements with a center-to-center element spacing of 15 micrometers (0.6 mil) for high resolution pushbroom mode of scanning.

The fixed geometry and spatially quantized nature of the arrays make possible accurate geometric relationships in the imaged scene in the cross-track direction.

Registered multispectral data can be obtained by using precise alignment between the arrays in each spectral band of a pushbroom scan mode system. Currently calibration information must be stored for *each* detector element. This has significant software impact in that there are thousands of elements in the typical multispectral solid-state imaging system.

Infrared Detector Arrays

The motivations for the development of IR solid-state, self-scanned imaging systems are:

- To increase performance potential by integrating photoelectrons over a line or frame scan time
- To reduce electronic complexity and cost
- To increase reliability by elimination of mechanical scanning
- To simplify registration of thermal imagery through compatibility with solid-state imaging in the visible spectrum.

Current Status of IR Solid State Imaging

It is possible at present to make high-density arrays of infrared detectors (photoconductive and photovoltaic) out of semi-conductors having energy gaps between 0.1 and 0.5 eV. However, it is not yet possible to integrate these detectors with associated electronics on one chip, because the technology for fabricating transistors in materials such as InAs, InSb, HgCdTe, PbSnTe, etc., has not been established. It is possible to consider hybrid devices consisting of infrared detector arrays cemented to a silicon chip containing the necessary readout circuitry; these would require interconnections made by stitch bonds or by leads evaporated over glue lines.

Near-Term Prospects of IR Solid-State Imaging Devices (Four Years)

Another form of hybrid device, consisting of conventional infrared detector arrays connected to silicon charge-coupled devices via appropriate interfacing electronics integrated on the same silicon chip, could possibly be developed within six years.

Long-Term Prospects of IR Solid-State Imaging Devices (Eight Years)

Infrared detector arrays utilizing temperature sensitivity effects (such as thermistor bolometers, pyroelectric detectors, and thermopiles) may be

advantageous for special and auxiliary imaging applications. However, their technology growth potential is so limited in terms of sensitivity, response time, and element size that their development appears to be of low priority in terms of present and anticipated NASA applications. It is recommended that NASA limit funding of device research in this area. However, research efforts are recommended to investigate the feasibility of preparing charge-coupled devices in indium antimonide.

CHAPTER 4

SOLID-STATE SENSOR ARRAYS FOR MULTISPECTRAL IMAGING FROM EARTH ORBIT

INTRODUCTION

Solid-state self-scanned arrays offer important advantages for future earth-orbit satellite missions. Advantages include: no mechanical scanning, built-in geometric accuracy, the high quantum efficiency of silicon for the visible, high resolution, good stability, low-voltage operation, and improved signal-to-noise performance. The principal disadvantage of these arrays is their relatively early state of development at the present time, but their potential for the late 1970's and 1980's appears very high.

Self-scanned arrays also appear worth exploring for infrared applications, although the advantages in the infrared range appear not to be as significant as in the visible spectrum. The limitations result from the fact that the devices are still in the early developmental stage and low noise performance has not yet been achieved.

Scope

This chapter discusses silicon detector arrays and their potential for the visible and near IR spectrum. Infrared detectors are discussed as possible hybrid devices connected to silicon charge-coupled devices. This discussion is followed by an evaluation of various system considerations (e.g., optical design, environmental considerations, and multispectral imaging).

A short paper on spectroradiometric accuracy is included as Attachment 1 at the end of this chapter, along with a reference bibliography.

The panel members addressed the general areas of self-addressed silicon array technology, self-addressed infrared arrays, optics design considerations, and systems concepts. Addressing silicon devices were J. Early, F. Huck, B. Rubin, G. Strull and P. K. Weimer. The area of infrared arrays was addressed by D. E. Bode, R. Ennulat, and J. Mudar. Optics and radiometry were handled by P. N. Slater, and systems were handled by A. Koso, N. Laverty, and L. Thompson.

Overview

Potentials and limitations of monolithic, solid-state, self-scanned sensors and arrays of such devices for multispectral earth imaging from orbit are discussed

in this chapter. Specifically, monolithic arrays of active devices are considered with the capability of accumulating photogenerated charge carriers across reversed biased depletion layers operated in a storage mode, with integrated scanning of the stored charge depletion layers. Not included are such items as the nonmonolithic photoconductive or photovoltaic arrays for the infrared, except those in which monolithically integrated multi-element scanning is utilized.

The wavelength range of interest is from ultraviolet to the infrared. Prime emphasis is placed, however, on the photosensitive range of silicon. Not only linear arrays but also area arrays and moving-target-area arrays used in the linear array mode are considered. Devices discussed include the photodiode, the phototransistor, the charge-coupled types, and potential infrared self-scanned sensors.

General Performance Criteria

The fundamental performance criteria for integrated self-scanned solid-state arrays closely parallel those for alternative sensors. Among the important criteria area:

- Geometric resolution which is determined by element size, spacing, and number
- Quantum efficiency and its variation with wavelength, as determined by reflection and absorption losses in layers overlying the silicon, with the characteristic absorption depth and electrode structure of the devices that interact with the geometric resolution particularly at wavelengths approaching the silicon band edge
- Scan rates using integration and, together with element size, quantum efficiency, and available light, determine available signal.

These factors set limits on dynamic range and boundary conditions on signal-to-noise potential of the sensor itself.

Of importance in practical systems is device stability, particularly short term and, although of lesser consequence, power supply requirements. Scan rate, taken with the number of elements, imposes bandwidth requirements per monolithic chip and for the total system. Dynamic range requirements and signal compression and encoding requirements are dictated by system constraints on the one hand; on the other, they are limited by available transmission bandwidth and by precompression and precoding noise associated with the signal.

Calibration Requirements

As with other sensors, solid-state self-scanned arrays require geometric, radiometric, and electrical calibration. Intrinsically, geometric calibration is straightforward and, once established, is subject only to mechanical distortions of the sensor structure. Element-to-element variations in photosensitivity or dark current must, as with other sensors, be calibrated out. Depending on the particular sensor design, additional calibration must be provided when additional per-element variations exist; for example, phototransistors require gain or linearity calibration, usually at two or more points, plus additional calibration for temperature variation. To some degree responsivity may be power-supply dependent so that calibration for such effects is desirable. Intrinsically, however, determination of photosensor geometry by the photomasking process during fabrication, and the chemical stability of the silicon/silicon dioxide system make geometric, radiometric, and electrical characteristics of solid-state self-scanned arrays very stable.

SILICON DETECTOR ARRAYS

Silicon detector arrays represent an imaging technique that makes use of linear arrays of solid-state detectors operating in what is termed a "pushbroom scan" mode. In such a system, a detector array is used to image the scene in the cross-track direction, and spacecraft motion is used to provide the orthogonal scan component. Figure 4-1 illustrates the principle of this technique. The figure shows that one array can provide data in a single spectral channel; however, additional spectral channels can be covered by using multiple arrays and appropriate spectral band selection techniques.

The recent development of high-density linear silicon arrays offers unique advantages in sensor design for earth observation applications. The primary advantages resulting from the use of these arrays are:

1. With the array oriented in a cross-track configuration, continuous coverage of a wide swath width of terrain can be obtained. Mechanical scanning is eliminated, since the satellite subpoint motion along the ground track provides the single-axis scanning motion that is required, and the detector elements are interrogated electronically.
2. Large arrays can be formed containing several thousand detector elements. The use of high-density arrays offers high resolution capability.
3. The precise geometric alignment of the detector elements resulting from the use of microcircuit fabrication techniques, in addition to the precision of alignment within the optical system, offers an advantage in accuracy of ground reconstruction of images.

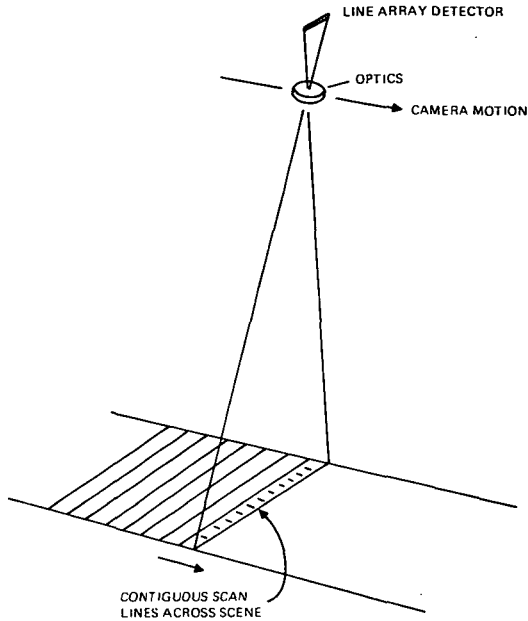


Figure 4-1. Illustration of the Pushbroom Scan Technique

4. The detectors are operated in an integration mode, thus providing high scan efficiency. The exposure time of each detector element is limited only by the permissible image motion at the optical focal plane. The high scanning efficiency results in a long exposure time, increasing the signal-to-noise ratio and resolution.

The various silicon self-scanned array devices are similar in the mechanisms, limitations, and potential of the sensing portions, but differ most significantly in the arrangements for signal amplification and scanning. Light sensing is accomplished by photoemission into a reversed biased depletion layer operated in the storage mode. Scanning may be accomplished by switching (as with photodiode and phototransistor arrays) or by the movement of potential wells (as in charge-coupled devices). Amplification may be based on one amplifier per sensor (as in phototransistor arrays) or on one amplifier for many photosensors, or on a single amplifier for an entire array.

The common means of sensing across a reverse biased silicon depletion layer leads to similar sensing performance. The size of the photosensitive area largely determines sensitivity and geometric resolution. The basic characteristics of silicon determine quantum efficiency, although overlying electrode layers can modify this property significantly. Each type of photosensor has a common source of noise in the dark current.

The sections that follow discuss the three candidate sensors: photodiodes, phototransistors and charge-coupled devices (CCD). In general, there are two self-scanning modes: digital multiplexing and analog charge-transfer. The photodiodes and phototransistors have ordinarily used digital multiplexing, although photodiodes have also been operated in connection with analog charge transfer in bucket-brigade sensors. The CCD sensors have analog charge-transfer readout. It is possible that other combinations may prove useful.

Since all of these sensors are silicon, their operation is restricted to the visible and near infrared (to $1.1 \mu\text{m}$). The readout circuitry is generally on the same silicon chip as the array of detector elements (usually more than 100 sensors per chip).

Photodiode Technology

The advent of silicon integrated circuit technology has made possible the construction of linear photodiode arrays which meet the requirements for earth resources missions. The elements of a system using silicon integrated circuit photodiode technology are illustrated in Figure 4-2.

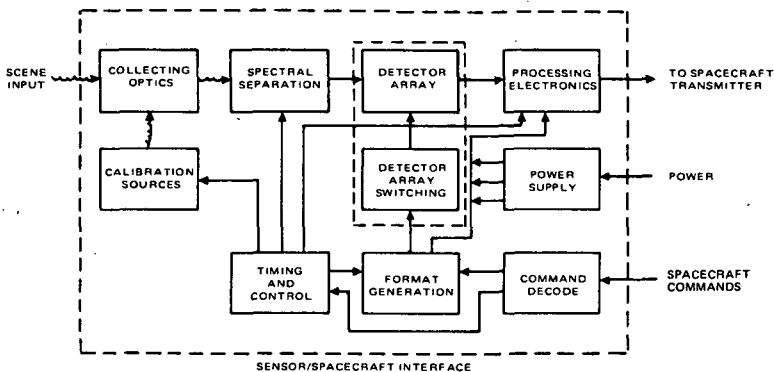


Figure 4-2. Solid-state Multispectral Imager Block Diagram

Large-scale integration technology can provide area phototransistor mosaics consisting of 400×500 elements in a 1-inch format; such configurations are currently being delivered to Marshall Space Flight Center. Mosaics of this size are difficult to fabricate because of the infinitesimal probability for achieving perfect arrays in view of material and photographic limitations. Linear arrays of phototransistors have also been constructed. All of these

are subject to: (a) limitations imposed by the finite charge required to turn the transistor on to the point where gain is realized, (b) variation in gain between large numbers of elements, and (c) large number of leads required for array connection.

The use of CMOS (complementary metal oxide Semiconductor) technology has permitted the combination of the detector sampling and commutation circuitry on the same chip as the silicon diode detectors. This is shown in the functional diagram of Figure 4-2, where the detector array and associated logic and switching (bounded by dashed lines) are fabricated on the same monolithic chip. Several chips may of course be required, depending on the total array length needed.

In the photodiode arrays, an amplifier is coupled to each photodiode on the chip to increase the output signal level. The addition of a shift register on the chip makes possible a self-scanning photodiode array sensor. This approach, using CMOS electronics to furnish detection, multiplexing, and first-level amplification, is practical and will provide a suitable configuration for use in a pushbroom scan-system. The design details of the detector array configuration are discussed next.

Photodiode Array Design Considerations

The candidate chip for this application consists of 96 or more photodiodes on 0.6 mil centers with the associated electronics necessary to form an array of sensors for image scanning. (See Figure 4-3.) The video signal is formed by periodically sampling each photodiode in the array. The electronics, which along with the photodiodes complete the sensor, furnish the first level of preamplification and multiplexing necessary to periodically sample each sensor and commutate the sensor inputs onto one of several output buses.

To perform the necessary functions of the array, a sensor, an amplifier, and address and control circuitry are associated with each diode position. A schematic diagram of the sensor and the amplifier is shown in Figure 4-4. The photodiode, operating in the integration mode, and a reset switch form the sensor whose output is taken from the node between the two devices. The output of the sensor is connected to the gate of a single Metal-Oxide-Silicon Transistor (MOST) whose drain current is the measured variable commutated to the output line. The address circuitry consists of a shift register stage and an AND gate to control the reset switch.

Q_1 is the reset switch, Q_2 is the amplifier, Q_3 is the amplifier commutating switch, and the external amplifier is the output current detector.

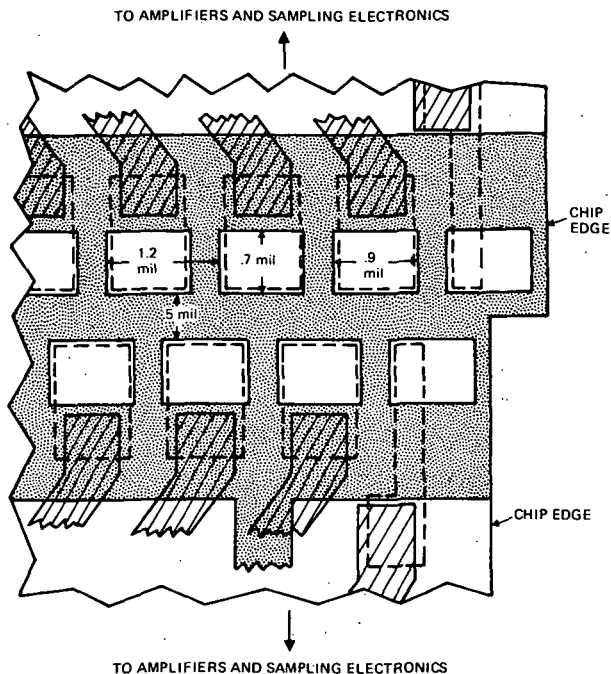


Figure 4-3. Diode Array and Chip Edge Geometry

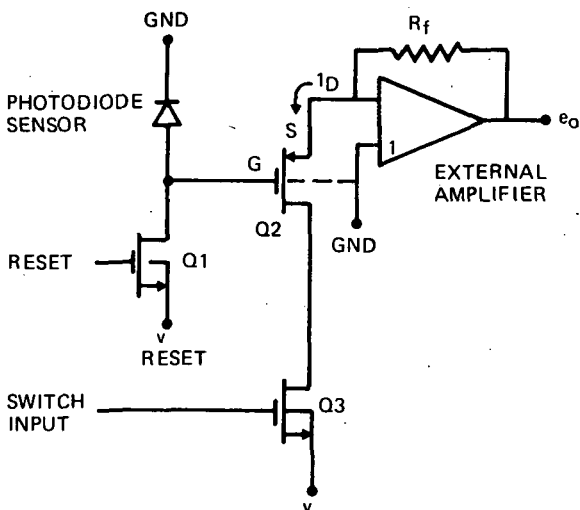


Figure 4-4. Sensor and Amplifier Element Equivalent Circuit

The integration mode of the photodiode has been discussed extensively in the literature and will only be reviewed briefly below. Initial conditions for the integration mode are established when the photodiode is reverse biased by switching on Q_1 . When Q_1 is switched off, the photodiode remains reverse biased because of the charge stored on the input capacitance of the amplifier, the parasitic capacitance of the interconnects and the reset switch, and the capacitance of the diode itself. The rate with which this voltage will decay toward zero is proportional to the leakage of the diode, the parasitic leakage of the node, and the light proportional reverse current of the photodiode. After a period t , Q_1 is again turned on and the capacitance is recharged.

This mode of operation ensures that the diode is detecting during the entire period between reset pulses and offers an efficiency proportional to the ratio of the integration period to the total period from reset pulse to reset pulse. The measure of illumination may be the peak recharge current, the total replaced charge, or the voltage across the diode prior to reset. This photodetector uses the voltage across the diode at the reset switch drain (prior to reset) as its detected variable.

The amplifier is the single p-channel MOST, Q_2 as shown in Figure 4-4. The voltage between its gate and the output bus is the integrated signal which in turn determines the source current flowing through R_f (the measured variable). The series n-channel MOST, Q_3 , between the supply and the amplifier, enables this current to flow through the amplifier when addressed by a "one" during the sample period and inhibits the current when addressed with a zero between samples.

Figure 4-4 shows that the output bus is connected to the summing node of an operational amplifier which is referenced to ground. The output bus is thus a virtual ground with an impedance of R_f/A_v . This being the case, many amplifiers may be multiplexed onto this line without channel interaction. Consequently, a substantial reduction in the number of output leads is made possible.

Sensitivity. The sensor/amplifier element sensitivity is limited by the $1/f$ noise (a noise characteristic proportional to the inverse of the frequency) present in the sensor signal voltage, inherent amplifier noise, and amplifier transient turn-off signal. However, if one is attempting to form the electrical image of a scene from a large number of such elements, variations of dc leakage, sensitivity, gain, threshold, and charge coupled by the reset switch will add spatial noise to the image. Little can be done in operation of the chip to reduce spatial noise due to difference in gains and leakage or sensitivity. Threshold

voltages and coupled voltages may most easily be removed by measuring only the signal change over the integration period. How this is done is illustrated by the timing and external amplifier output waveforms shown in Figure 4-5 and explained next.

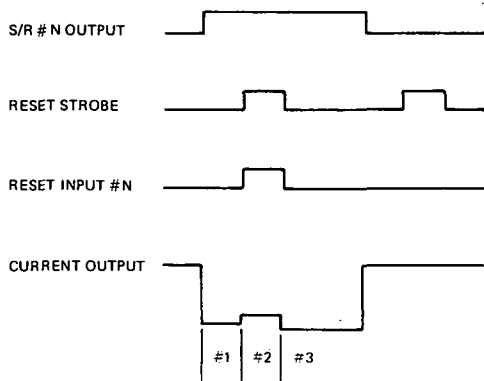


Figure 4-5. Sensor Timing and Output

The output waveform of the amplifier during its address period may be divided into three periods: prereset, reset, and initial conditions. (These correspond to periods numbered 1, 2, 3 on Figure 4-5.) The prereset sensor amplifier gate voltage is a function of the initial starting voltage, leakage and signal current, and amplifier gain, as well as the amplifier threshold voltages and parasitic coupled charges. During reset, the amplifier output is a measure of the reset voltage. After reset, the output of the amplifier is a measure of the starting level for the next integration period and is a function of the reset reference voltage and the charge coupled through the reset switch.

If one assumes that the initial conditions are exactly the same at the beginning of each integration period in the channel, then the signal may be taken as the difference between the first and third periods. An additional advantage obtained by this method of signal measurements is reduction of ac noise associated with the p-channel MOST amplifier. If the readout time is chosen properly, the effect of the poor $1/f$ noise characteristics of the MOST at low frequencies may be minimized.

Address Circuitry. To avoid the necessity of generating the sequential amplifier address pulses externally and inputting them to each sensor channel, a shift register (SR) is incorporated on the chip to control the amplifier switch. A "one" is input to the first cell of the register and stepped through successive

cells by the two-phase register clock. The "one" appears at interstage points as gate pulses input to the amplifier commutating switch. Each SR stage may address more than one amplifier, but the number of output buses required on the chip must equal the number addressed simultaneously.

The shift register is identified in the composite circuit diagram of Figure 4-6. The SR is the dynamic type and is clocked by two phases, 180 degrees from each other. It will be noted that the interstage transmission switch is a single p-channel MOST. To reliably transmit both a one and a zero, the phase voltage must swing between the voltage level associated with the one, and the p-channel threshold voltage below the zero level.

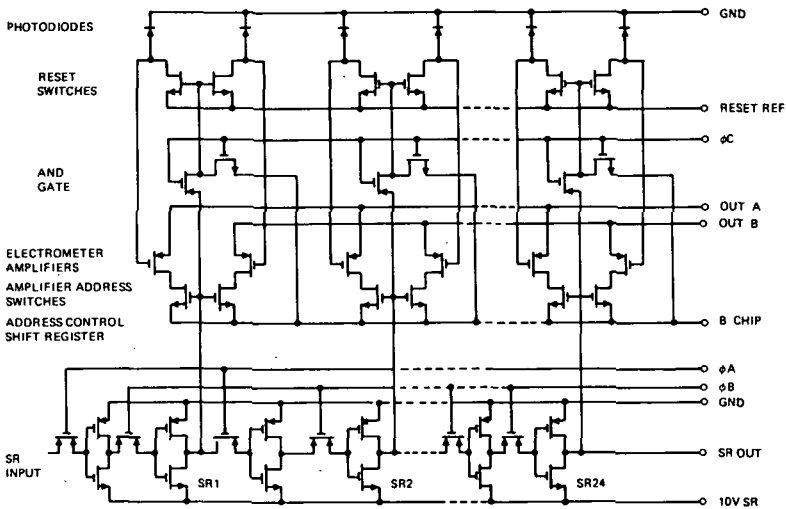


Figure 4-6. Shift Register Composite Circuit

The nested reset pulse required by the reset switch is also a logical one and occurs simultaneously but not coincident with either the beginning or end SR output. It can be generated at the SR stage by an AND gate whose inputs are an external clock (called phase C in Figure 4-6) common to all AND gates of the array, and the SR output as shown.

Array Performance

The following section presents measured performance data for the photodiode arrays.

Spectral Response. The typical diode spectral response is shown in Figure 4-7. The basic spectral response is that of silicon with sensitivity extending from the blue to the near IR. Figure 4-8 shows a typical aperture profile made using a 1.0 micron diameter (at its 20% points) spot of white light.

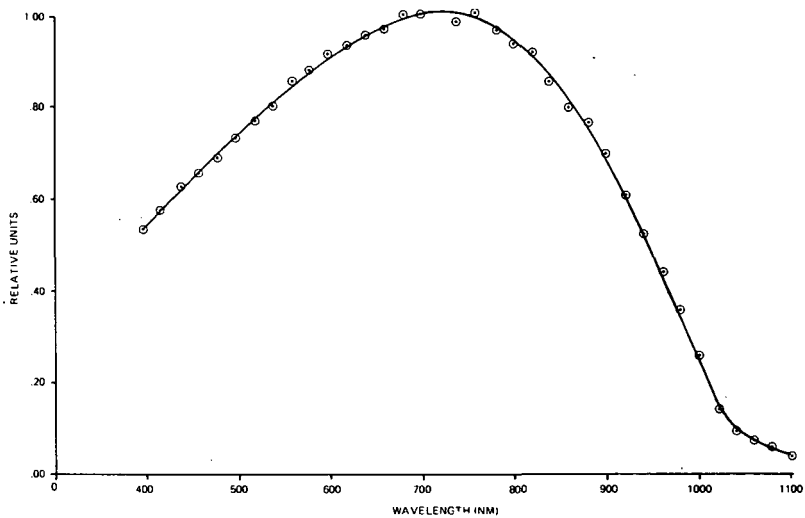
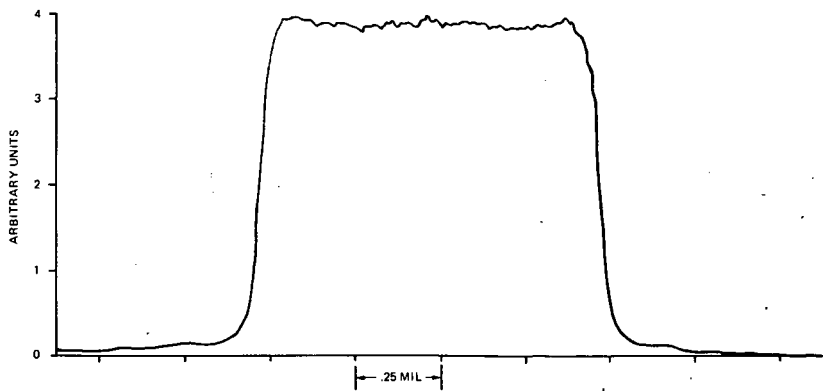


Figure 4-7. Spectral Response



Detector Sensitivity. Detector sensitivity plotted for a sample of 25 chips is shown in Figure 4-9. The curves shown represent the mean response for each array; however, the lower levels are variable because of measurement error at those levels, but at high levels the curves shown are linear in response, with very closely matched responsivities over nearly a 1000:1 dynamic range.

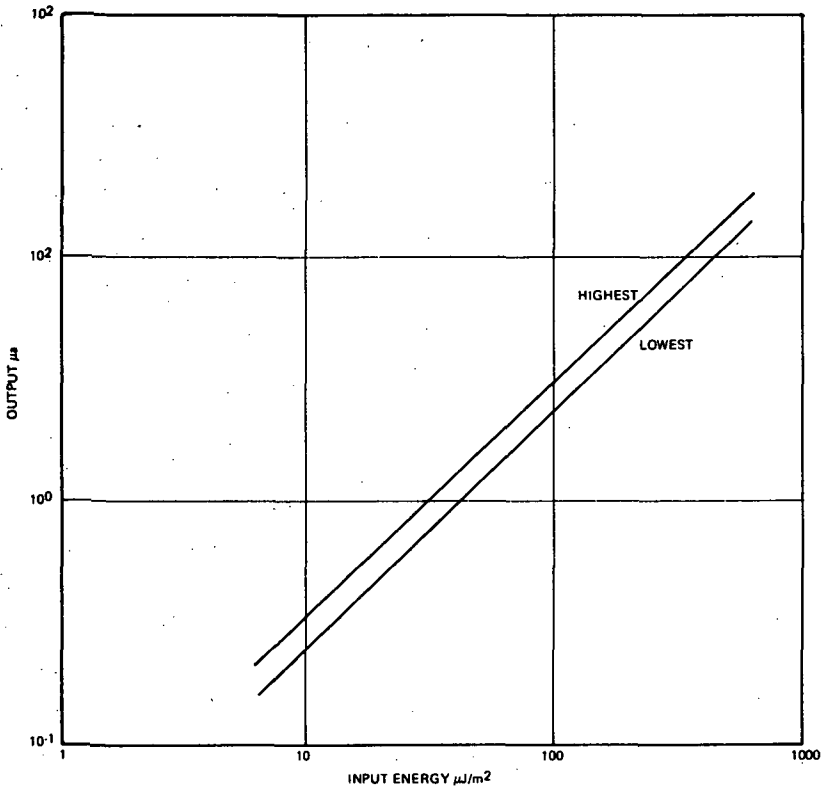


Figure 4-9. Transfer Characteristic, Self-scanned Photodiode Array

Figure 4-10 shows the noise equivalent signal (NES) for a sample of 25 chips. Since the diodes are operated in an integration mode, the equivalent signal is in terms of irradiance on the detector ($\text{milliwatt}/\text{meter}^2$) times the integration time (millisecond) which gives $\text{microjoules}/\text{meter}^2$. The NES corresponds to that integrated irradiance which gives a signal-to-noise (S/N) ratio of 1.

Figure 4-11 shows the variation of detector-to-detector response for a typical chip. The increase in variation at low irradiance levels can be attributed to poor S/N in the measurement.

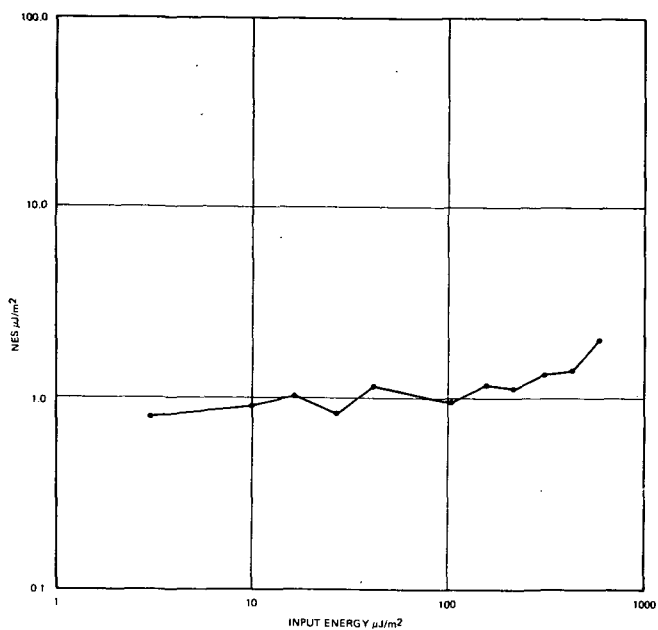


Figure 4-10

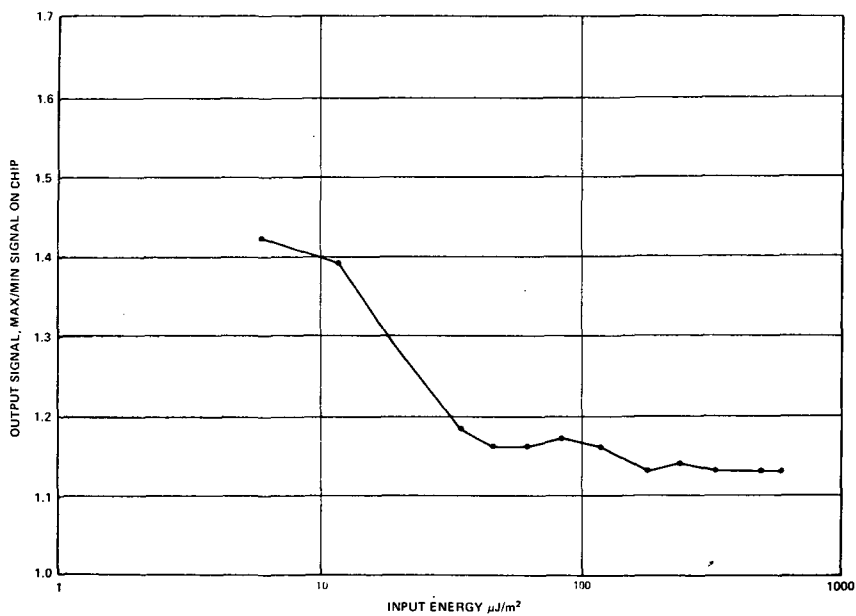


Figure 4-11

The conditions under which all the response measurements were taken were 6000 K illumination filtered to 400 to 800 nanometers. The integration time of the detector was one millisecond.

Formation of Long Arrays. Because of the difficulty in making very long-line arrays monolithically, smaller arrays are used; however, smaller arrays pose problems in maintaining image contiguity. To achieve image contiguity, the edge of the chip must be placed to within 0.3 mil of the end diodes. Figure 4-12 shows how a number of chips may be butted together to form a long array.

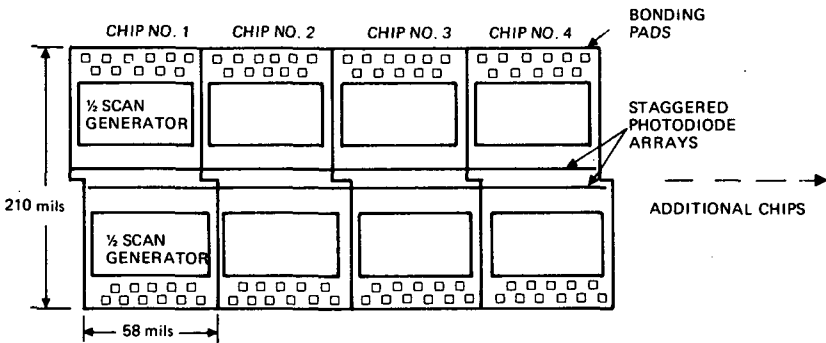


Figure 4-12. Butted Assembly of Chips with Staggered Photodiode Arrays

An analysis of systems performance for photodiode arrays is given later in this chapter (see pp. 381-387).

Phototransistors

A study has been completed to determine the configuration and performance of a multispectral imaging sensor using linear arrays of silicon phototransistors to observe the resources of the earth from earth-orbiting satellites. The bipolar transistor arrays were fabricated by microelectronic techniques using triple-diffusion in silicon.

One unique requirement associated with the use of phototransistor arrays is that the effect of pattern noise, due to variations in both the responsivity and dark current of the individual phototransistors and preamplifiers, must be eliminated either through the use of onboard electronic signal processing or through the use of calibration data in image reconstruction.

The primary conclusions resulting from the study are as follows:

1. It is feasible to obtain high-resolution imagery in individual spectral bands of a multispectral imaging sensor using linear arrays of silicon phototransistors.
2. The production of multispectral imagery can be accomplished.
3. Computer processing of video data to eliminate the effect of variations in phototransistor responsivity and dark current is feasible.
4. In order to meet the future requirements of the NASA for both ground coverage and spatial resolution, increased data rate capability or the use of data compression techniques, or a combination of both, will be required.

More detailed phototransistor information is presented in the following categories:

- Physical and performance characteristics of the silicon phototransistor arrays
- Definition of the performance requirements of future earth-orbiting multispectral imaging systems for the observation of earth resources
- Analysis, specifications, and preliminary design configurations of three satellite-borne sensors which fulfill the performance requirements (discussed pp. 387-404).
- Results obtained with an engineering model of an imaging system using the silicon phototransistor arrays, in which the capability of obtaining high-resolution imagery was demonstrated.

Characteristics of Phototransistor Arrays

The basic element of the photodetector array consists of an LSA (large scale array) chip consisting of 195 phototransistors and preamplifiers and a second SCE (signal conditioning electronics) chip containing five amplifier channels mounted on a common LSA substructure assembly (Figure 4-13). The five signals from the SCE require additional signal conditioning, multiplexing, and digital data processing.

LSA Configuration. The LSA consists of the 195 phototransistors, fabricated by triple-diffusion in silicon on a single chip (Figure 4-14). The array consists

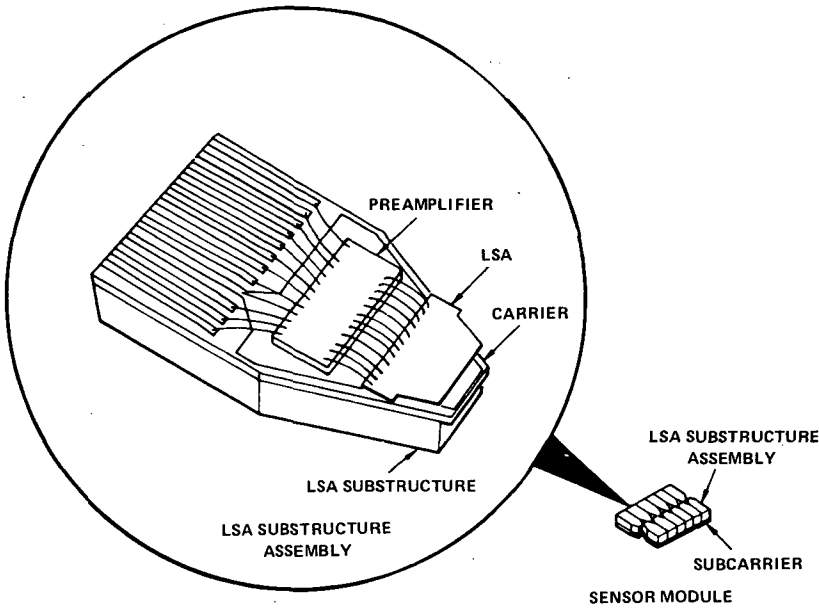


Figure 4-13. Detector Array Structural Configuration

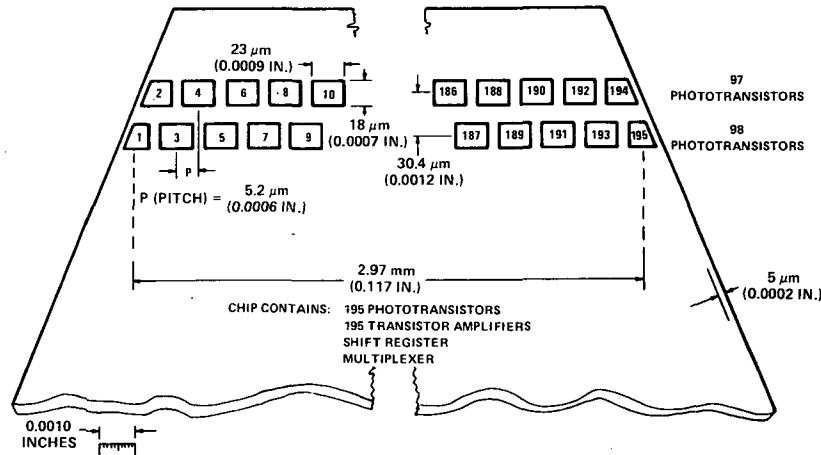


Figure 4-14. LSA Chip Geometry

of two rows of phototransistors, one row of 97 elements and the other of 98 elements. This configuration is used to provide sufficient spacing between adjacent elements due to penetration of the incident radiation into the base material. If a single row of closely spaced elements were used, excessive crosstalk would result. The use of the staggered configuration reduces the amount of crosstalk between adjacent detector elements to a value less than two percent.

The size of the photosensitive area of each phototransistor is 18×23 microns ($0.7 \times 10^{-3} \times 0.9 \times 10^{-3}$ inches), and the pitch spacing along the array is 15.2 microns (0.6×10^{-3} inches). The two rows of phototransistors are separated by a distance of 30.4 microns (1.2×10^{-3} inches). The overall length of the total array of 195 phototransistors is 2.97 millimeters (0.117 inch). To form an extended array, adjacent chips can be aligned within a tolerance of 2.5 microns (0.1×10^{-3} inch) along or normal to the array, and the vertical (z-axis) positioning of the chips can be held to the same tolerance. Extended arrays can be made to conform to either a flat or curved surface.

The LSA chip consists not only of the phototransistor elements, but also of 195 stages of amplification (one for each element), as well as a shift register and multiplexer. The multiplexer is used to commutate the outputs of the 195 preamplifiers onto five signal leads, each containing the serial output of 39 preamplifiers. These five signal leads are hard-wired to the second chip, containing the five SCE amplifiers that further amplify the five serial signals prior to digital processing of the signals. The digital processing electronics, external to the LSA and SCE chip, are fabricated of integrated circuits and discrete components.

Equivalent Circuit. The equivalent circuit of the LSA consists of a phototransistor and amplifier transistor arranged in a Darlington configuration (Figure 4-15). Initially, the charge on the base-collector capacitance of the phototransistor is neutralized by a pumping transistor (denoted by "erase" switch). Bias is then applied to the base-collector capacitance by the S3 switch. During the light exposure interval, radiation incident on this junction generates electron-hole pairs that result in discharge of the bias applied to the junction. The amount of discharge is proportional to the amount of energy absorbed during the exposure interval. This change in the current output of the phototransistor during the sampling interval is increased by the gain of the amplifier transistor (preamplifier).

Multiplexing of the 195 signals from the phototransistors is accomplished as follows: The collectors of the 195 amplifier transistors (preamplifiers) are connected together in five groups of 39 (195 total). Readout is accomplished

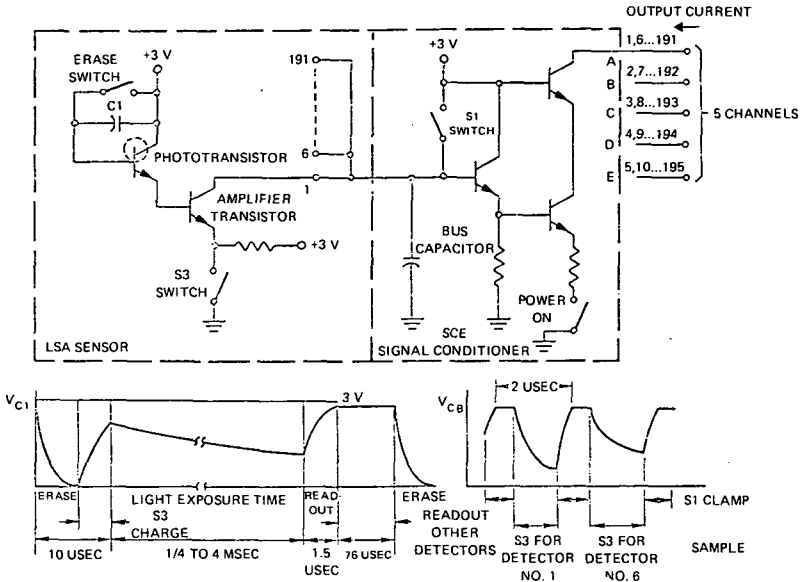


Figure 4-15. LSA/SCE Circuit Diagram

by closing of the readout switches (S3), in sequence, controlled by a shift register. Switching of 39 switch transistors in sequence results in a serial output from 39 preamplifiers. With five groups of 39 being interrogated in parallel, readout of the signal from the 195 phototransistors is accomplished. The readout, or sampling, of the output of each preamplifier is accomplished in $2 \mu\text{sec}$, with $78 \mu\text{sec}$ being required for serial sampling of a group of 39. After this sampling, the photojunctions of the phototransistors are again biased, and the cycle is repeated.

On the SCE chip, five amplifiers are used to increase the level of the five signals from the LSA chip prior to analog to digital (A/D) conversion of the video signal. Each of the amplifiers has two stages of gain. The clamp switch, S1, is used to reset the signal to a reference level between each of the 39 serial samples from the LSA sensor. The "power on" switch is used to apply power to the SCE amplifier to initiate operation.

Performance Characteristics

The quantum efficiency of the phototransistors is illustrated in Figure 4-16 for two values of base-collector diffusion depth. A diffusion depth of 5.2 microns is currently used. If increased sensitivity in the near infrared range

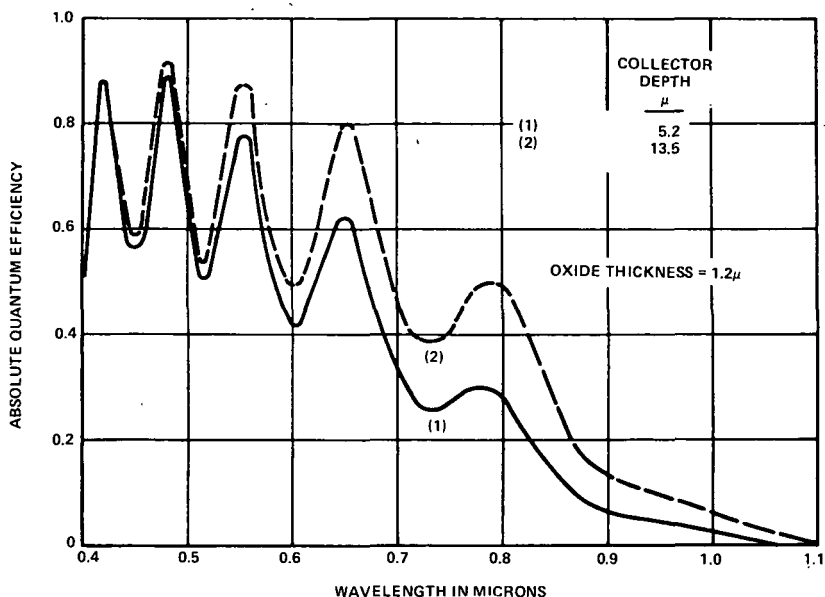


Figure 4-16. Absolute Quantum Efficiency of Detector Array (Theoretical)

is desired, this can be obtained by using the deeper diffusion depth of 13.5 microns. The inflections in the curves are caused by the interference of light in the silicon dioxide passivation layer on the photodetectors.

The variation in responsivity of the current from the LSA/SCE combination is illustrated in Figure 4-17. The gamma is near unity, with a dynamic range of $10^3/1$. Three-sigma variation in output at maximum integrated exposure level is 2/1, and the dark noise level, expressed as noise equivalent signal (NES) is 1.2×10^{-3} watts/meter² using an integration time of 10^{-3} seconds, corresponding to an integrated energy density of 1.2 microjoules/meter².

The spatial frequency response of the arrays, defined by the modulation transfer functions both parallel and normal to the array, is approximately 30 percent at the limiting resolution of 32.8 line-pair/mm (Figure 4-18). The shapes of the modulation transfer functions are determined not only by the geometrical size of the photosensitive area of the phototransistors, but also by the sensitivity contour of the photosensitive areas. These contours are measured by the use of a laser beam probe, with an effective beam diameter of approximately one micron. An analysis of system performance and the results of an in-house development program are presented in the systems section of this chapter.

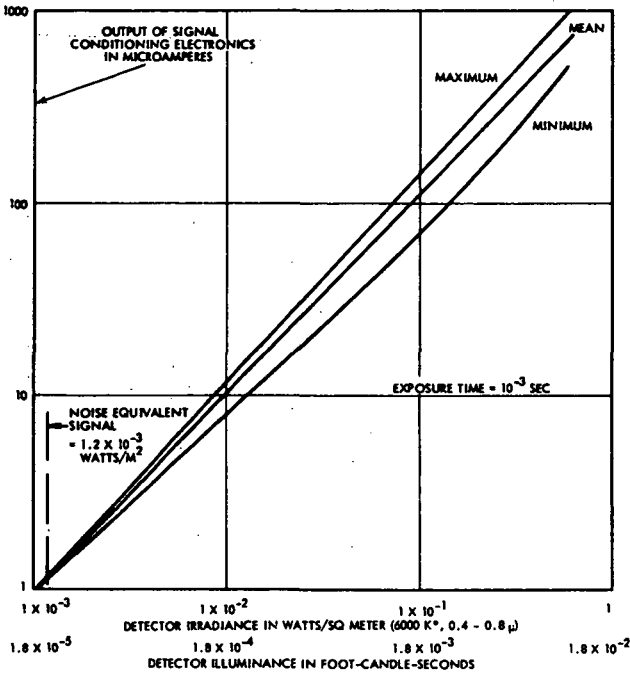


Figure 4-17. Variation in Responsivity of 195 Detector Elements on a Single Large Scale Array

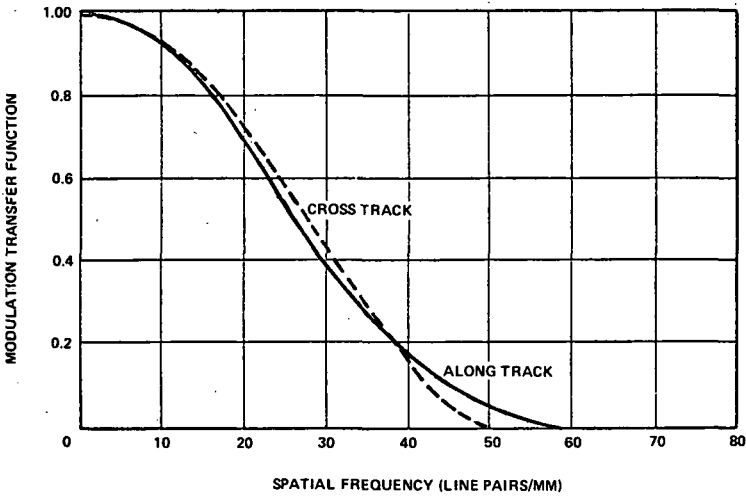


Figure 4-18. Phototransistor Modulation Transfer Function

Charge-Coupled Devices

This section discusses the principles of charged-coupled imaging devices and their potential performance capabilities for multispectral earth imaging from orbit.

Technical Considerations

Using the basic CCD principle, it is possible to transport a photon-generated signal charge over long distances within a chip and to sense the charge with a preamplifier having potentially an extremely small input capacitance. This in turn leads to amplification with very low input noise levels. Using the buried channel CCD concept, it is possible to achieve very high transfer efficiencies over wide dynamic ranges, which minimizes image distortion. Using transparent gates over the photosensing regions, it is possible to achieve high net quantum efficiencies commensurate with those of the best silicon sensors; polycrystalline silicon films make good transparent gates for wavelengths greater than about 0.45 microns. Because of the inherent simplicity of the CCD unit cell (one photosensing element plus one "bit" of register), it is possible to make imaging devices with more detector elements than was previously possible.

CCD Basic Technology. CCD is a new class of semiconductor structures normally operating in (thermal) nonequilibrium and utilizing, as the signal carriers, minority charge transported by moving potential wells. In essence, therefore, a CCD is a nearly ideal semiconductor analog shift register. The CCD concept permits the design of highly complex functional devices at potentially low cost.

A functional CCD device implies a viewpoint distinct from that of conventional integrated circuit technology. An integrated circuit is composed of a large number of discrete devices fabricated on a common silicon wafer and interconnected by conductors. Such a structure can be unambiguously represented by conventional equivalent circuits. In a CCD this is not possible and the device as a whole performs a unique function. The concept emphasizes the organized manipulation of information in the form of charge packets, as opposed to integrated circuit elements which depend on current and gain. Thus many functions can be performed in a much simpler way with a much simpler structure.

Despite the fact that CCD is a new device concept, it is based on well developed semiconductor technology which is one of its chief advantages. In addition, CCD has the attributes of: (1) silicon fabrication simplicity, (2) high packing

density, (3) high reliability, (4) low power requirements, and (5) potentially low-noise analog signal processing. Such features imply major device advantages in the area of imaging devices.

Concept and Basic Operation. In its original form the CCD was envisioned as merely an array of closely spaced metal insulator semiconductor (MIS) capacitors. Although from an operational point of view, this perspective is now realized to be somewhat naive, a physical understanding of the basic MIS capacitor is vital in comprehending CCD operation.

For the sake of analysis, consider a p-type conductivity semiconductor on which there is an insulating layer and a metal electrode. If, at time $t=0$, a positive voltage V_G with respect to the substrate is instantaneously applied to the electrode, a depletion region will be formed in the semiconductor as shown by the familiar energy band diagram in the upper portion of Figure 4-19. The surface potential ϕ_s will increase to the value

$$\phi_s = \frac{qN_D w^2}{2\epsilon_s}, \quad (1)$$

where w is the depletion depth, N_D is the acceptor doping density and ϵ_s is the semiconductor dielectric constant. The depletion depth w is dependent on the gate voltage and the device parameters. If w is eliminated from Equation (1) a relation between the gate voltage V_G and the surface potential is obtained

$$V_G = \phi_s + \frac{\sqrt{2\epsilon_s qN_D}}{C_o} \cdot \phi_s^{1/2}, \quad (2)$$

where C_o is the oxide capacitance, and the constant offset due to work function differences and fixed ionic charge has been ignored for clarity.

With the presence of a large depletion region, the device is not in thermal equilibrium; therefore, minority carriers (electrons in this case) will begin to accumulate at the interface between the semiconductor and the insulator. The surface potential decreases and a larger voltage appears across the insulator until equilibrium is reached (lower portion of Figure 4-19). The density of electrons stored in this inversion layer is given by the equation:

$$Q = C_o (V_G - \phi_s) - \sqrt{2\epsilon_s qN_D \phi_s}. \quad (3)$$

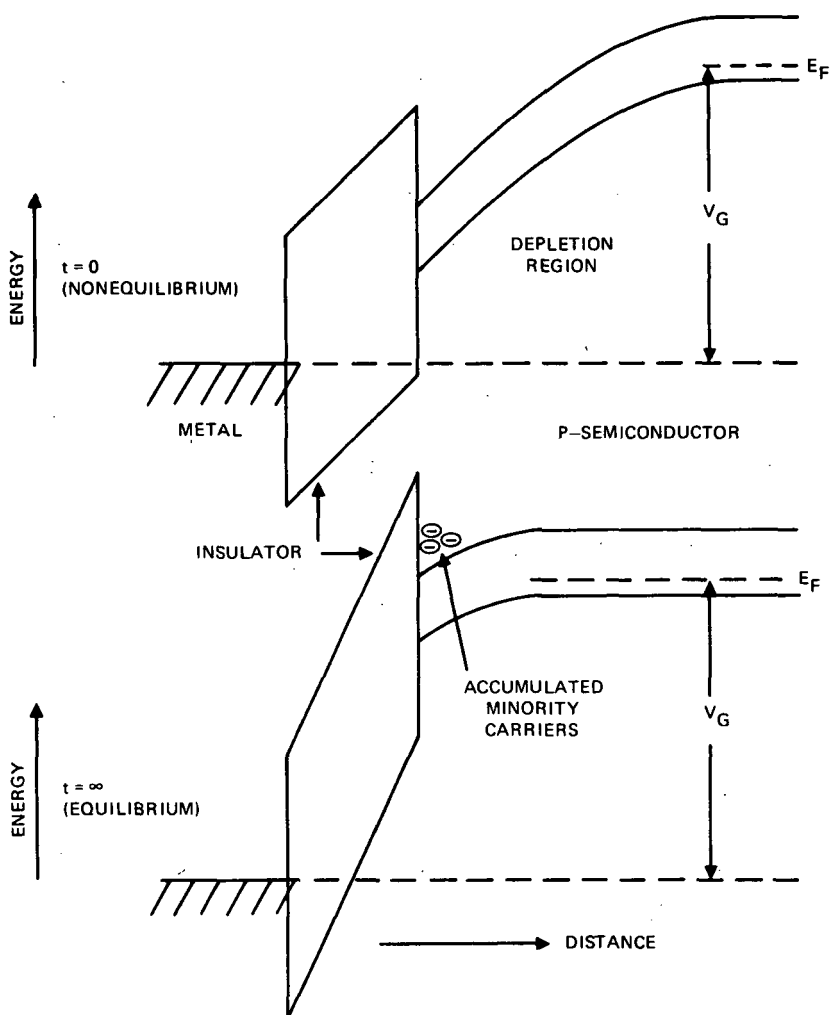


Figure 4-19. MIS Capacitor

The inherent source of minority carriers is thermal generation. In high quality devices, however, the thermal generation current may be so low that equilibrium is achieved only after many seconds. In such cases, the minority carriers may be introduced artificially by incident photons, surface avalanching or a forward biased junction, and they are then used to represent information. If this "information" can be transferred to a detection circuit and read, the basis for a usable device is established.

An important concern in CCD design is the efficiency of charge transfer from one electrode region to the next. A detailed discussion of transfer efficiency

is given in the next section. Qualitatively, it can be stated that the electrode pattern must be so configured that signal carriers can move freely from one electrode region to the next when appropriate voltages are applied. An early problem in CCD performance was the ineffective coupling of charge across the interelectrode gaps. This problem existed because the electrode pattern in the original structures was formed by etching away the metalization, thereby exposing the active oxide region. Thus the potential in these regions was not effectively controlled by the clocking voltages, and unreliable performance was characteristic of these early devices.

One way to eliminate this problem is to employ silicon gate technology. With this approach, the electrode pattern is formed by selective diffusion on an undoped polysilicon sheet. Thus the gaps are now replaced by an undoped polysilicon film between the doped polysilicon electrodes. This undoped region is a highly resistive dielectric and serves to define the potential in the interelectrode space and to protect the active oxide from the ambient environment. The potential is determined by the electrode voltages and the real and displacement currents within the film. Experimental results showed that this approach was highly successful in eliminating electrostatic uncertainties associated with the interelectrode gaps. Other ways to eliminate the gap problem make use of overlapping gates or planar gates with an additional electrode covering the gaps.

Overall device transfer efficiency, however, was still limited by surface state trapping effects. Since the intimate juxtaposition of minority carriers with the silicon/silicon dioxide interface was an intrinsic property of the original CCD design, either surface states had to be eliminated or the basic design of the CCDs had to be altered. Pursuit of the latter alternative has led to the "buried channel" concept. In the conventional CCD, the basic storage element is the MIS capacitor normally operated in nonequilibrium (Figure 4-19). The potential minimum for minority carriers exists at the silicon/insulator interface. If now an appropriate impurity distribution of polarity opposite to the substrate is introduced over a small region (approximately $0.5\ \mu\text{m}$) adjacent to the surface, the potential minimum for the case of nonequilibrium will move away from the surface to a location within the impurity layer (Figure 4-20).

Use of this type of storage element in a CCD structure prevents contact of the signal carriers with the interface during normal operation and essentially eliminates long time constant trapping. With this design, transfer efficiency becomes first order independent of charge level. The speed of charge transfer is enhanced, because the carriers are now further away from the electrodes, and, therefore, subject to more fringing field effects, and because bulk mobility rather than the lower surface mobility applies.

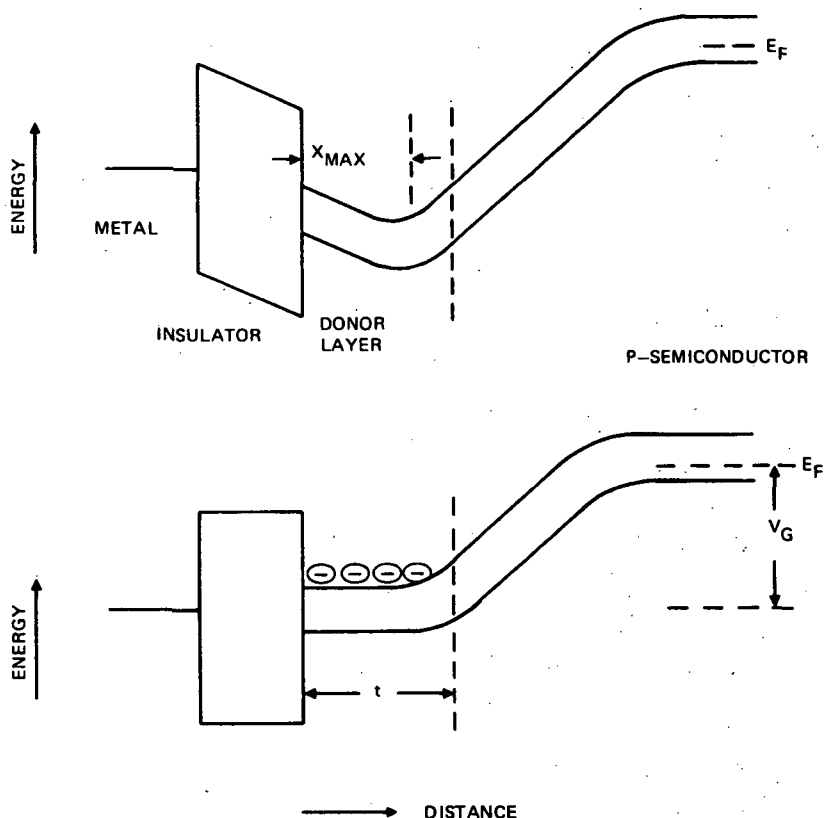


Figure 4-20. MIS Capacitor with Donor Layer

There are several ways in which to configure a CCD so that unidirectional charge transfer is assured. Perhaps the most obvious way is a three-phase arrangement as shown in cross-section in Figure 4-21. Electrode sets $\phi 2$ and $\phi 3$ are held at a resting voltage V_r ($V_r \geq \text{threshold voltage}$) and electrode set $\phi 1$ is held at an applied voltage V_a ($V_a > V_r$). Any carriers present in the surface region will localize in the potential wells under the first phase electrodes. If it is desired to transfer the charge to the right, electrode set $\phi 2$ is pulsed to a voltage V_p ($V_p > V_a$) and the potential minimum for electrons is displaced to the right. At a later time, electrode set $\phi 1$ is reduced to the resting potential and the transfer process is completed. The electrodes of phase two are then lowered to V_a in preparation for the next transfer. In this way a device of many electrodes can be made with only three independent driving connections.

Another configuration frequently discussed in the literature is the so-called two-phase/four-phase design. This was introduced historically because of the

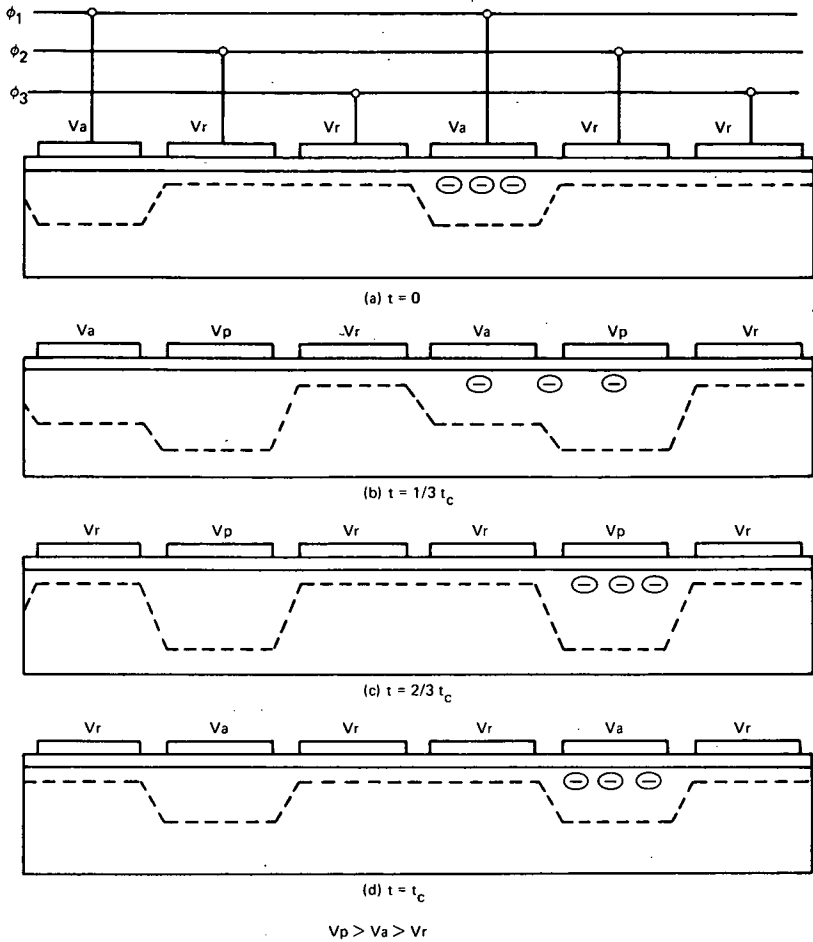


Figure 4-21. Three-phase Unidirectional Charge Coupling

traditional problem with etching the interelectrode gaps in the three-phase structures. It was thought, therefore, that use of the two-level gate technology would eliminate the exposed gaps and produce more reliable devices. A cross-section of this configuration is shown in Figure 4-22. In this figure each gate is shown equal in size; hence charge may be stored under each gate during the transfer process. Alternatively the upper electrodes may be made smaller and used as control gates to allow transfer between buried electrodes.

The difference in oxide thickness between the even and odd phases can be used to permit a true two-phase operation. Here the upper and lower electrodes are connected in pairs and, with a common voltage applied to each pair, a step

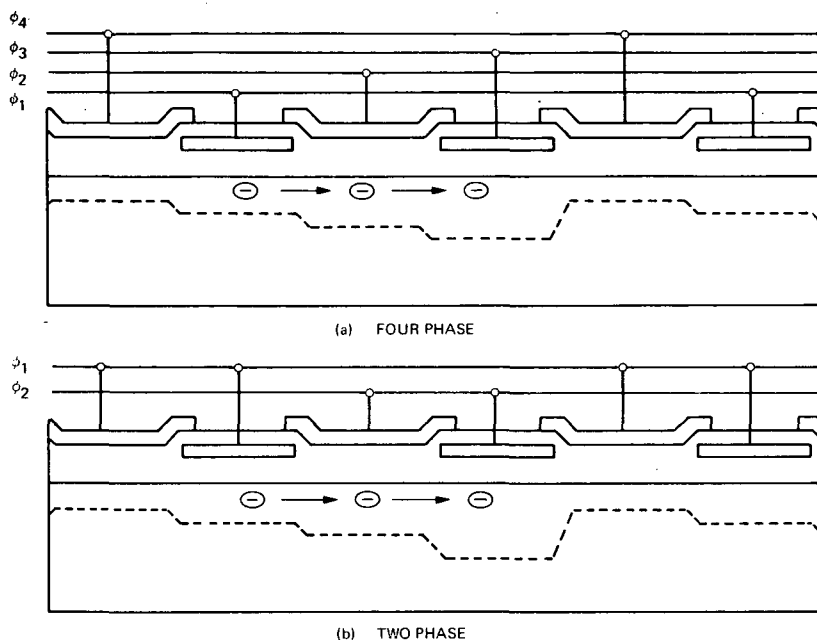


Figure 4-22. Sealed Channel CCD's

in the surface potential exists due to the difference in oxide thickness, resulting in an asymmetric potential well. Alternate pulsing of the two phases results in a preferred direction of charge transfer. The principal disadvantages of this structure are (a) the dependence of the charge handling capability on the clock voltage offset, and (b) the design does not extrapolate favorably to a buried channel configuration. A superior two-phase arrangement which does not have these disadvantages is the implanted asymmetry CCD.

A unique characteristic of an ideal CCD is that the only free carriers in the channel are signal carriers. This feature makes the CCD potentially a very low noise semiconductor device. (A more detailed discussion of noise characteristics as well as charge detection and dynamic range are given later in this chapter.) Another result of having to transfer a limited number of free carriers is the minimization of on-chip power dissipation. The theory indicates that the energy requirements for CCD are among the lowest for semiconductor structures. Energy requirements for element transfers as low as 1 pJ per element transfer appear easily realizable.

Thus, the CCD is a nonequilibrium minority carrier structure characterized by low power, low noise and simplicity of design.

Considerations of Transfer Efficiency. A thorough understanding of charge transport mechanisms is vital to the proper design of charge-coupled imaging devices. An imaging device should exhibit an analog (preferably linear) behavior; that is, the output charge attributable to a given photo sensor element should be directly related to the integrated light intensity incident on that element. This is fundamental to charge-coupled imaging devices unless charge is left behind, added, or lost during transfer. In these cases signal will be attenuated and spatial resolution will be degraded.

The quality of charge transport, or transfer efficiency, is an important parameter in the characterization of a CCD. Qualitatively, the mechanism of charge transport is easy to understand. At time $t=0$, the beginning of the transfer, the packet is very dense and localized and the gradient of the carrier density at the edges of the packet is large. When the channel potential of the adjacent electrode becomes more positive than the local potential, namely, when the adjacent MIS structures couple, a considerable fraction of the packet transfers very quickly due to the strong drift forces felt by these electrons. As time passes, this force decreases and becomes asymptotic to a value given by considerations of thermal diffusion and surface electric field intensity. The final charge decay is therefore exponential and may be characterized by a time constant.

Transfer Inefficiency Effects. The influence of transfer inefficiency on the propagation of information along a CCD shift register can be studied analytically if it is assumed that the loss per transfer is a constant fraction of the charge present. Such an analysis has been done by Joyce and Bertram (1971) who reported that the effect of inefficiency in charge transfer is to deteriorate image quality by reducing the MTF or sine wave response and by producing a phase shift for different spatial frequencies. The interpretation of the transfer efficiency in terms of a sine wave input enables the quantitative degradation to be calculated as shown in the following discussion.

Theory of Charge Transport. The rate at which charge transfer takes place is governed by drift, diffusion, and field-aided forces. The magnitude of these forces depends on the charge density in the packet and on the geometrical and electrical parameters of the device. At large charge densities, charge transfer is dominated by drift forces. At lower charge densities, charge moves under the action of diffusion and fringe-field drift. The magnitude and extent of the fringe fields at the ends of each gate can make a great difference in the transfer efficiency at high transfer frequencies. The diffusion decay time constant is given by the equation:

$$\tau_{\text{diff}} = \left(\frac{2w}{\pi} \right)^2 \cdot \frac{1}{D} \quad (4)$$

where $D = \mu \frac{kt}{q}$ is the diffusion coefficient and w is the electrode center-to-center spacing.

For representative dimensions τ_{diff} is typically on the order of 10^2 nanoseconds. Since transfer time must be many time constants long to obtain a transfer inefficiency ϵ of less than 10^{-3} , a many-shift operation at frequencies significantly beyond 1 MHz is not practical for devices that operate in the diffusion transfer mode. In the field-aided case, the asymptotic decay time constant is given by:

$$\tau_{\text{field-aided}} = \frac{w}{\mu E_s} \quad (5)$$

where E_s is the average tangential electric field. Since $\tau_{\text{field-aided}}$ is typically on the order of 1 nanosecond for representative values, devices should be designed to operate in this mode for low transfer inefficiency and high frequency operation.

Noise in CCD Signal Processing. In a CCD the signal charge is composed of minority carriers that are stored and transferred in potential wells. These wells are formed in a depletion region inside a semiconductor. Therefore, the signal charge is isolated from external electronics until it is detected at the output circuit. Moreover, in an ideal CCD, the signal carriers are not mixed with other carriers (except thermally generated dark charge). Therefore, an ideal charge-coupled device is intrinsically a low-noise semiconductor device.

In this section, the noise associated with CCD sensing and scanning will be considered. As a standard measure of noise behavior, noise equivalent signal (NES) has been selected. The noise level in charge-coupled devices is so low that NES may be calculated and measured in terms of signal electrons per picture element (pixel). Although NES will vary with scanning rate and other parameters, it is nonetheless a simple and convenient measure of noise. The noise sources to be considered are the signal itself, the photosensor, the transfer registers, and the output amplifiers which are dealt with at length in the next paragraphs.

Noise in Signal. The photoelectrons collected by the sensor constitute a Gaussian population having an intrinsic steady state statistical fluctuation equal to the square root of the number of events. The so-called photon noise in the signal is, therefore, given by:

$$\text{NES}_s \cong \sqrt{S} \quad (6)$$

where S is the number of electrons detected. If a precision of 0.2 percent is needed, S must be at least 250,000, which has a square root of 500, and an intrinsic S/N ratio of the same value.

Sensor and Transfer Noise. The principal sources of noise in the sensing and transfer process are the thermally generated charge carriers arising from recombination centers in the silicon, and the statistical variations associated with the charge transfer process. The latter process includes both charge carriers failing to transfer, although available for transfer, and charge carriers trapped temporarily in the oxide. Transfer noise is directly proportional to total charge transfer inefficiency; that is, to Ne . For example, if transfer inefficiency is 10^{-3} and 1000 transfers are made, $Ne = 10^{-3} \times 10^3 = 1$. If then, a population of 10^6 electrons is being transferred, a randomness in transfer occurs to the extent of 10^6 with a resulting NES of 10^3 electrons. In calculations of transfer noise, both signal charge and any required bias charge necessary to promote transfer efficiency must be considered. The NES for transfer may be calculated as:

$$NES_T = \sqrt{Ne (S + B)} \quad (7)$$

where B is the number of bias charges per pixel and the other symbols are as defined above. It should be noted that, if a bias is employed, the bias-charge is uncertain to the extent of the square root of the number of thermal electrons on the bias-charge determining capacitance (C_{BD}), giving a component $NES_B \cong 400 \times \sqrt{C_{BD}}$.

The final source of noise in sensing and transfer is the thermally generated or dark charge. Assuming geometric, but not temporal, uniformity of dark charge generation and equal area for each sensor, dark charge will again be simply a statistically fluctuating fixed number giving rise to a noise equivalent signal of $NES_D = \sqrt{D}$ where D is the dark charge per pixel. The total noise arriving at the amplifier input might then be written as:

$$NES_I^2 = NES_S^2 + NES_B^2 + NES_T^2 + NES_D^2 = (1 + Ne) S + B + D + 400^2 C_{BD}. \quad (8)$$

This NES value may be compared with that for the amplifier to determine the degradation in S/N ratio introduced by the amplifier. It should be pointed out that the noise introduced by the transfer process is highly correlated since the carriers left behind at any transfer appear also in the following potential well. If the Ne product is small, the noise is so highly correlated that virtually all of it appears in the upper half of the bandwidth, as can be seen from the fact that appropriately formed combinations of successive pairs of output signals would almost entirely eliminate it.

Dark Current. There are three dark current sources: depletion region, neutral bulk silicon, and the oxide-silicon interface. These can be expressed as:

$$I_{gd} = \frac{1}{2} \frac{qn_i w}{\tau_o} \text{ (depletion region)} \quad (9)$$

$$I_{gb} = \frac{qn_i n_i L_n}{\tau_o N} \text{ (neutral region)} \quad (10)$$

$$I_{gs} = \frac{1}{2} qn_i s_o \text{ (surface)} \quad (11)$$

where in these equations:

- n_i = intrinsic conductivity of silicon
- L_n = electron diffusion length
- N = doping density
- s_o = surface recombination velocity
- w = depletion width
- τ_o = bulk lifetime.

At or below room temperature, Equation 10 contributes very little current, thus the dominant terms of Equations 9 and 11 can be combined and the total dark current can be expressed as:

$$I = \frac{1}{2} qn_i \left(\frac{w}{\tau_o} + s_o \right) \quad (12)$$

Experimental values for τ_o and s_o obtained from a self-scanned photoarray are:

- τ_o = 0.5 millisecond
- s_o = 1 centimeter/second.

For 10μ depletion width, this gives:

$$I = 3.6 \text{ nA/cm}^2 \quad (13)$$

which is about 1/3 of the typical dark current for a silicon vidicon (10 nA/cm^2). For a sensor plus scanning area of 1.2 mil x 5 mil per pixel and integration time

of 40 microsecond, the charge due to dark current is:

$$Q \cong 5 \times 10^{-18} \text{ coulomb}$$

or

(14)

$$D \cong 30 \text{ (number of dark electrons per pixel).}$$

A more serious problem will be the variation of dark current across the array. This variation will depend on any change in the generation centers which may arise from the starting material or from the fabrication process. Therefore, a good starting material and careful processing are absolute requirements for low dark current (with small variations). Experimentally, a maximum dark current variation as low as ± 1.5 percent of saturation has been obtained for a 500 element linear CCD array.

In summary this analysis indicates that the dominant noise contributions in the charge reaching the amplifier input arise from the transfer process and the dark charge. Therefore, in order to fully exploit the capability of CCD sensors, close attention to detail is important in the design of the systems electronics and hardware.

Charge Detection. In this subsection various charge detecting alternatives with some limits on their performance are considered. The signal from any charge-coupled device consists of a packet of minority carriers. The detector circuit is required to sense this charge and output an amplified version to other components that are connected to it. The requirements for the output amplifier are numerous: (a) the amplifier must possess sufficient gain to adequately drive the next stage; (b) the equivalent input noise must be small enough to allow detection of the desired minimum charge at the desired signal-to-noise ratio; (c) the dynamic range must be capable of handling the largest expected input signal; (d) the frequency response must be broad enough for the intended application; and (e) linearity of gain over the full dynamic range must be adequate to meet system requirements. In addition to these factors, the influence of ambient conditions on amplifier performance may be important.

Gated Charge Integrator (Single Ended). The simplest approach to designing an output circuit utilizes the CCD output diode itself as a gated charge integrator as shown in Figure 4-23. In this mode, the diode is charged to some fixed value of reverse voltage, V_{bias} , by a reset MOST during a time when no signal is being transferred out of the register. The reset switch is then opened, allowing the output diode to function as a charge-storage detector for minority

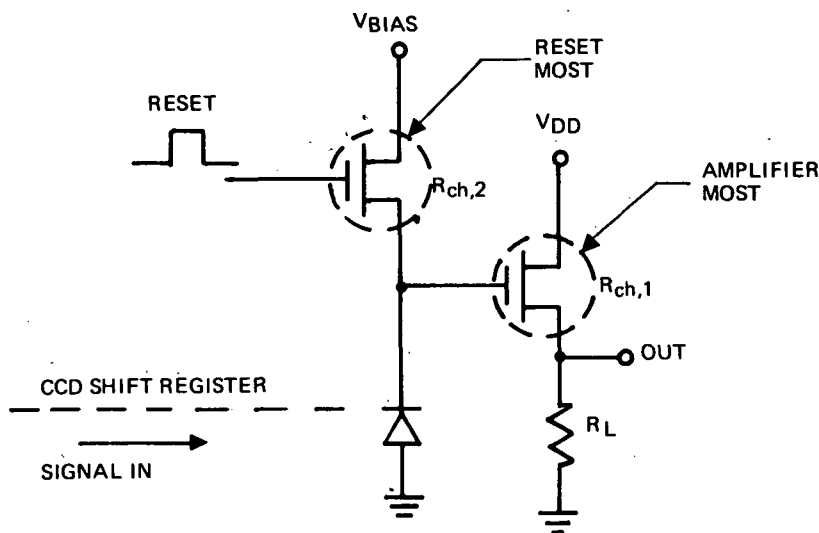


Figure 4-23. Most Gated Charge Detector

carriers. At the next transfer, the signal charge is thus stored on the equivalent diode capacitance, resulting in a corresponding change in the voltage across the diode.

The voltage swing can then be monitored by a high input-impedance source-follower stage, which in turn could drive a second common source stage to achieve additional voltage gain.

a. Basic transfer function and linearity. Most of the properties of this configuration are determined primarily by the charge-detecting diode itself. Because it functions as an integrating capacitor, the overriding consideration in the design of the diode is to minimize its capacitance. By so doing, the charge-to-voltage transfer function (Q/C in the idealized case) is maximized. The total capacitance consists of two components: C_J , the depletion-layer capacitance of the reverse-biased diode, and C_{MOS} , the oxide capacitance of the source-follower gate and the interconnection thereto. The largest output voltage will therefore result from minimizing the dimension of both structures.

Assuming an output junction geometry of $35\mu\text{m} \times 35\mu\text{m}$ on the surface with $500\mu\text{m}^2$ of source-follower gate area, and also assuming a 10V reverse bias on the junction and 1500 Å oxide thickness, the capacitance would be:

$$C_{\text{out}} = C_J + C_{MOS} = 0.01 \text{ pF} + 0.1 \text{ pF} = 0.11 \text{ pF}. \quad (15)$$

In other words, at least 90 percent of the total output capacitance is simple MOS capacitance. (Note also that these values give rise to a voltage responsivity of almost 10V/pC.)

Because only C_J varies with respect to applied voltage, the basic charge-to-voltage transfer function is highly linear. This linearity is further enhanced by the fact that the C_J , itself, is under moderately strong reverse bias and in percentage is nearly constant for small voltage swings. This behavior is illustrated in Figure 4-24, where the voltage response of a depletion-layer capacitance

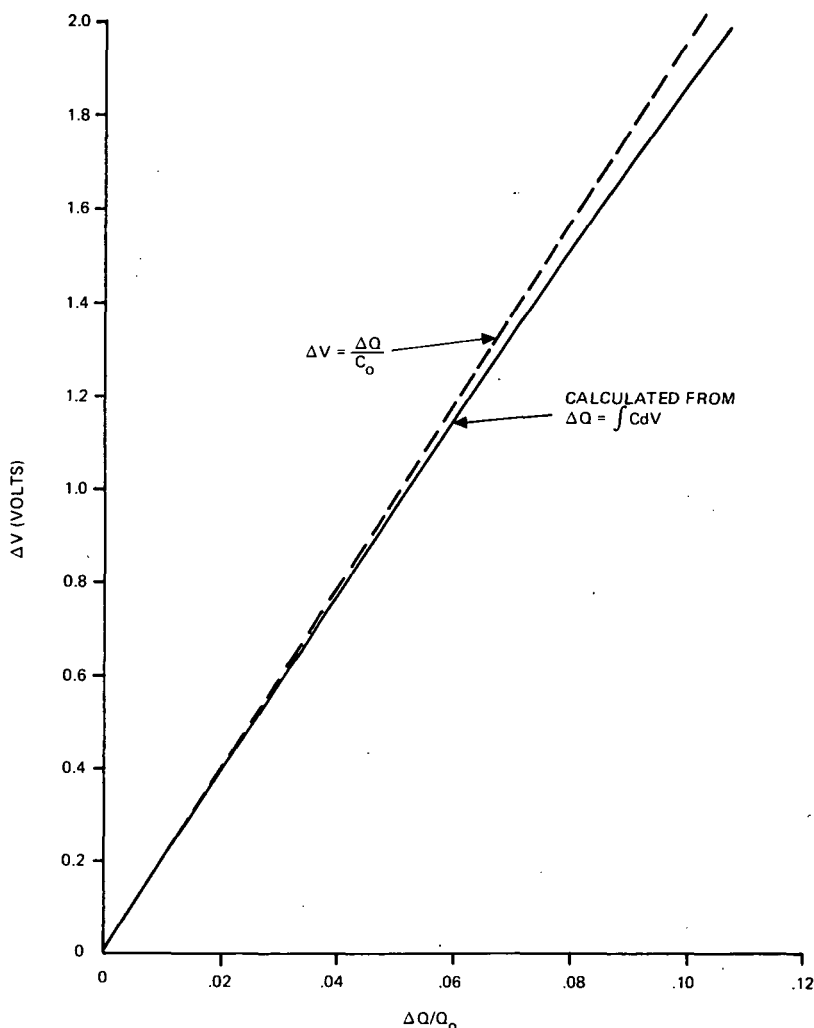


Figure 4-24. Nonlinearity of Depletion Layer, Capacitance $V_R = 10V$

(biased initially at $V_R = 10V$) is compared with its linearized equivalent. These calculations are based on the fact that for moderate reverse bias V_R , the depletion layer capacitance of a diffused pn junction is proportional to $V_R^{-1/2}$, written here as:

$$C_J \approx K_c V_R^{-1/2} \quad (16)$$

where K_c depends on substrate doping, dielectric constant, etc.

The increment of charge, ΔQ , necessary to discharge the junction from V_2 to V_1 is thus given by the equation:

$$\Delta Q = \int_{V_1}^{V_2} C_J dV = 2K_c (\sqrt{V_2} - \sqrt{V_1}) \quad (17)$$

Normalizing to Q_o , the total stored charge at $V_R = V_2$, the equation becomes:

$$\frac{\Delta Q}{Q_o} = 1 - \sqrt{V_1/V_2} \quad (18)$$

which is used to calculate $\Delta V (V_2 - V_1)$ vs $\Delta Q/Q_o$ (solid line). This result is compared to the linearized case (dotted line) where C_J is assumed to remain constant at the original bias level $V_R = V_2$, giving the equation:

$$\frac{\Delta Q}{Q_o} = \frac{V_2 - V_1}{2V_2} \quad (19)$$

As shown, constancy of C_J is satisfactory for small ΔV ; the error for a 1V swing is about 1.5 percent, rising to a 5 percent error at $\Delta V = 2V$. The total variation in output capacitance, for the case of $C_J = 0.1 C_{out}$ and $\Delta V = 2V$, is thus ~ 0.5 percent.

b. Signal saturation level. The output diode will not "saturate" until it loses all the charge initially stored on it during the reset time. For $V_{bias} = 10V$ and $C_{out} = 0.1$ pF, the saturation level corresponds to 1 pC. However, one would probably not wish to utilize the full extent of this signal handling capability because of the sacrifice in linearity at the upper end (error in linearity approaches 50 percent during the final few volts).

Fortunately, the maximum signal charge in a high-density CCD structure will be limited to ~ 0.2 pC strictly because of geometrical limitations. Hence, the output swing will be restricted to ~ 2 volt maximum, where the nearly ideal behavior predominates.

c. Additional effects of source-follower. The primary purpose of the source-follower is to buffer the output diode and provide a low impedance output capable of driving the desired load to the maximum frequency of interest. The optimum design of this stage therefore represents a tradeoff between voltage gain A_V ($A_V = 1$, ideally) and output resistance, R_O . For a MOST with transconductance g_m and source resistance R_s :

$$A_V = \frac{g_m R_s}{1 + g_m R_s} \quad (20)$$

and

$$R_O = \frac{R_s}{1 + g_m R_s} \quad (21)$$

Clearly, maximizing g_m is desirable from the standpoints both of maximizing A_V and minimizing R_O . From a device point of view, this requires maximizing mobility, oxide capacitance, gate width (Z/L), and gate drive (V_G). Many of these quantities, however, must be chosen on the basis of other factors. Oxide capacitance is dictated by process considerations, gate size must be minimized to limit input capacitance, and quiescent gate drive is determined by V_{bias} .

d. Principal limitation of the gated charge integrator. The limitations of the simple gated charge integrator are twofold. First, from a practical standpoint, the output is subject to a strong component of "coherent noise" originating from the reset gate. This noise consists of a feedthrough of the reset pulse to the output through the gate-to-source capacitance C_{Gs} of the reset switch. The magnitude of this feedthrough is proportional to the amplitude of the reset pulse and the ratio of C_{Gs} to the output capacitance.

Since C_{out} is intentionally made as small as possible, the coherent reset noise may be comparable to the maximum output signal. Although this noise does not limit S/N in the strictest theoretical sense, it does add to the complexity of the signal processing task and hence is undesirable.

The second, and more fundamental, limitation of this technique arises from the mixing that occurs between the signal of interest and the majority carrier population of the sensing diffusion. This mixing leads to transfer noise in connection with the discharging (or resetting) of the sensing diffusion. Stated briefly, the consequences of these contaminating effects are: (a) a limit on the precision to which the voltage of the sensing region can be set, and (b) a randomness in the resetting process.

Transimpedance Amplifier. The transimpedance amplifier of Figure 4-26 is a possible alternate for the gated charge integrator. In this scheme, a high-gain operational amplifier maintains the input diode at a virtual dc potential of V_{bias} . As charge enters the output diffusion, it is forced through the feedback resistor R_f , producing a corresponding voltage swing at the amplifier output.

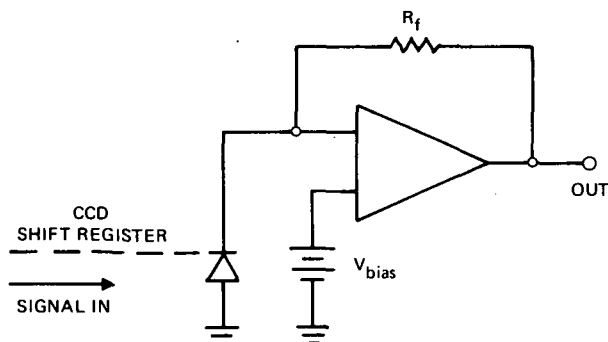


Figure 4-26. Transimpedance Amplifier

The method of detection does not require a reset pulse and is therefore quieter than the gated charge integrator. However, the output voltage produced is now proportional to signal current rather than charge, requiring the use of either a peak voltage detector or a separate integrator as the next stage. The most serious disadvantage lies in the requirements for the amplifier itself. Satisfactory operation depends on a large open-loop gain at frequencies well above the maximum signal frequency. Based on state-of-the-art for operational amplifier performance, this automatically excludes CCD operation above a few MHz. Moreover, fabrication of this type of amplifier is not compatible with MOS technology, ruling out the possibility of an on-chip amplifier. This amplifier is, therefore, not considered acceptable for CCD applications.

Sample-and-Hold Differential Gated Charge Amplifier. In a paper presented at the 1972 IEDM (December 6, 1972, Washington, D.C.), a gated charge amplifier was discussed that avoids capacitance noise (White, et al., 1972). Specifically, after reset, the amplifier output is integrated for an interval and stored on a capacitance. The capacitance is then isolated, the charge to be sensed is brought to the sensing diffusion, and a second capacitor is similarly charged by the same amplifier. This capacitor is then isolated and the charges on the two capacitors are compared by a differential amplifier. In principal, the charges accumulated on the two capacitors differ only by the charge sensed,

multiplied by the amplification factor of the amplifier. Obviously, there is capacitance noise associated with the pair of output capacitors, but this noise occurs under high-level signal conditions and when referred to the input is far smaller than the usual capacitance noise of the sensing diffusion.

The principal noise source in this type of amplifier is the shot noise of the output current of the amplifier. For a charge sensing electrode of 2×10^{-13} farads driving an output MOS transistor of 7.5μ gate width, the NES is estimated as 35 to 50 electrons. This may be compared to an NES of about 100 for the comparable ordinary gated charge amplifier. At reduced sampling rates the advantage of the sample-and-hold amplifier is even greater as the capacitance noise dominates the performance of the ordinary gated charge amplifier.

In summary, the extremely low noise properties of the basic charge-coupled device impose demanding requirements for on-chip amplifiers in order to realize the full benefits of using CCD technology.

Power Dissipation (On-Chip). One of the attractive features of CCD technology is the very low power dissipated by the device. On-chip power dissipation can be divided into two distinct categories: the first associated with the clocking of charge through a CCD register, and the second associated with the output amplifier. An upper limit can readily be placed on the power consumed by the first category, and the result represents one of the principal advantages of CCDs. Amplifier power, on the other hand, is more difficult to quantify because of its dependence on circuit design and operating point. However, it is expected that the on-chip amplifier can be optimized in such a way that its power dissipation will be compatible with the rest of the device.

Charge Transfer Power. The peak current drawn from the CCD clock drivers consists of two main components. The first item results from the capacitance loading from clock line to substrate, and will include the displacement current to the substrate through this capacitance. The second item will stem from the current that flows between clock lines as a result of the charge transfer itself. Other dissipative components include the finite resistance along the clock lines and the leakage resistance between them. These are negligible, however, and are not included in this discussion.

Assuming the series resistance of the substrate is also negligible, the major source of on-chip dissipation is associated with the second component of current. The power dissipation per bit, P_{diss} , is then given by the energy loss per cycle multiplied by the number of transfers per clock period and by the clock frequency, f_c .

In the two-phase CCD, it can be shown that the power dissipation is given by:

$$P_{\text{diss}} = 2Q_s f_c \left[V_b + V_{\text{av}} - \frac{Q_s}{2C_p} \right] \quad (22)$$

where, Q_s = signal charge

V_b = barrier height

V_{av} = average driving voltage above V_b

C_p = the capacitance of [(half-bit area) - (barrier area)] .

Representative values for a 1 mil²/bit, two-phase structure are:

$$Q_s = 0.1 \text{ pC}$$

$$V_b + V_{\text{av}} = 10\text{V}$$

$$C_p = 1.2 \text{ pF}$$

leading to an energy per transfer of approximately 1 pJ/bit. The resulting power dissipation per bit vs. f_c for this example is plotted in Figure 4-27 (upper curve).

For completeness, this dissipation is compared with that of a polyphase CCD carrying the same charge of $Q_s = 0.1 \text{ pC}$. This bottom curve is based on the results of Strain (1972). This trace indicates that a lower limit on power dissipation in a polyphase CCD is given by the equation:

$$P_{\text{diss}} = Q_s \frac{16 L_p^2 f_c^2}{\mu} \quad (23)$$

This is true where μ is the mobility and L_p is the electrode spacing. As shown, on-chip dissipation can be less for a polyphase clocking system, a direct result of the fact that directionality in such a CCD is achieved by proper phasing of clock lines rather than by building in a potential step. Because of the dependence on f_c^2 , this advantage loses importance for frequencies above ~50 MHz. However, even the two-phase value of 1 pJ/bit results in conservative operation for all designs presently being considered. For example, a 500 x 500 two-phase image sensing array operating at a bit rate of 10 MHz would dissipate a maximum of 10 milliwatts, with 5 milliwatts consumed by the high-speed output register and 5 milliwatts consumed by the slower registers. (This calculation assumes the unlikely worst-case situation of a uniformly saturated array.)

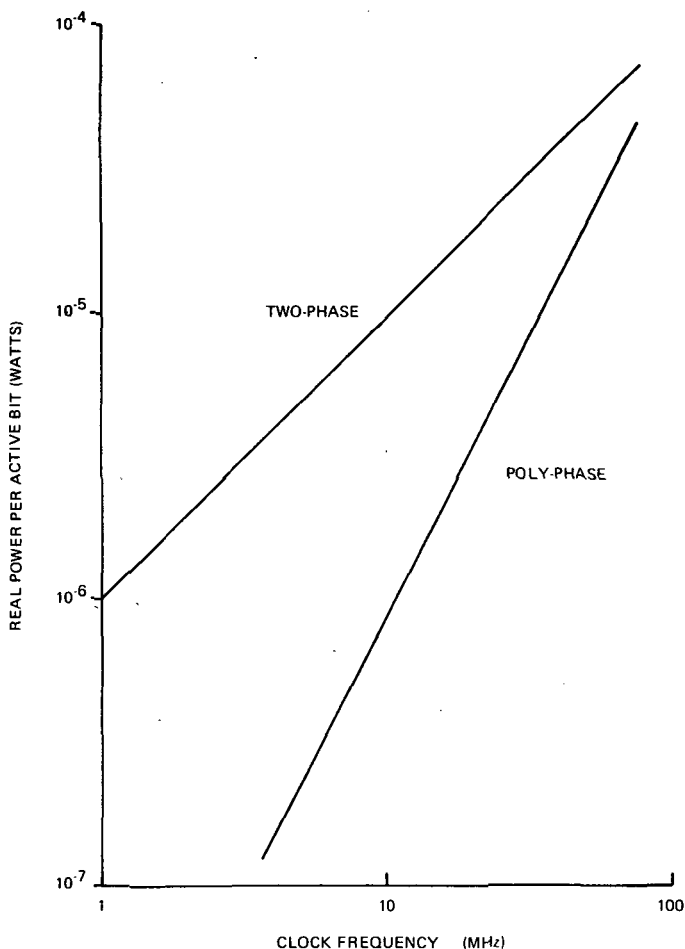


Figure 4-27. Power Dissipation per Bit Versus Frequency

In general, the power dissipation of a two-phase CCD is not likely to limit the performance of the devices considered here. In addition, the numerous other advantages of two-phase over three-phase configurations far outweigh the minor sacrifice in power.

Output Amplifier Power. As mentioned earlier, dissipation in the output amplifier depends strongly on the type of circuit employed and the choice of operating point. For example, initial investigation of the gated charge detector has been conducted with the source-follower biased in a region of strong conduction where it consumes ~ 50 milliwatts of power. In this situation the amplifier becomes the largest power sink, even on a large x-y array.

The same device, however, could be operated in a manner entirely different from a source-follower. If channel conductance were measured instead of source voltage, an operating point possessing extremely low quiescent drain current and source-to-drain voltage could be chosen. Amplifier dissipation could thus be reduced by more than an order of magnitude. Because of the complex relation between operating point, linearity, and signal-to-noise, optimization of the output amplifier, as previously discussed, represents a significant task in the development of this type of amplifier.

CCD Image Sensors Basic Technology

The sections that follow discuss the technology relating to the silicon detector arrays with particular reference to CCD devices.

General Design of CCD Image Sensors. The CCD concept offers a major breakthrough in the field of solid-state image sensor development. This new concept, coupled with state-of-the-art MOS integrated circuit technology, provides a means of producing image sensors which have a great many more sensor elements per monolithic array and provide improved performance.

This section treats both linear and area imaging devices. Specific design variables discussed in this section include those influencing: (a) unit cell packing density, (b) the relationship between element spacing and resolution, and (c) net quantum efficiency.

Linear Imaging Requirements. The linear imaging array requirement of major interest includes the general problem of air-to-ground and space-to-ground daylight imaging and other similar tasks. Resolution requirements range approximately from 500 Hz to 25 KHz. A dynamic range capability of approximately 1000:1 or more is desirable. Thus, it is desired to maximize the number of sensor elements per monolithic array, maximize the scanning speed and still achieve a dynamic range capability of the order of 1000:1 or better. Quantum efficiency is not as important in most of the applications of this type as it would be in low-light-level applications, but it is still important in connection with the dynamic range requirement.

Other aspects of the image sensor design problem have already been discussed, such as the need for particular levels of transfer efficiency, freedom from trapping effects, and the importance of a low-noise, on-chip preamplifier.

The Organization of a Complete Linear Imaging Device. Whereas a primitive linear imaging device could be nothing more than a CCD shift register and

output circuit, a practical design requires a more complex organization. Only in applications with very long integration times, that is, ≥ 100 times the line scan time, could a simple CCD shift register suffice. The reason for this limitation is the image smearing that results when the shift register is driven while it is being illuminated.

Specifically, a linear CCD imaging device should consist of a sensor array plus a transport array. One such organization is shown in Figure 4-28. In this illustration the signal charge from the two transport arrays is shifted into a two-bit register for delivery to the amplifier.

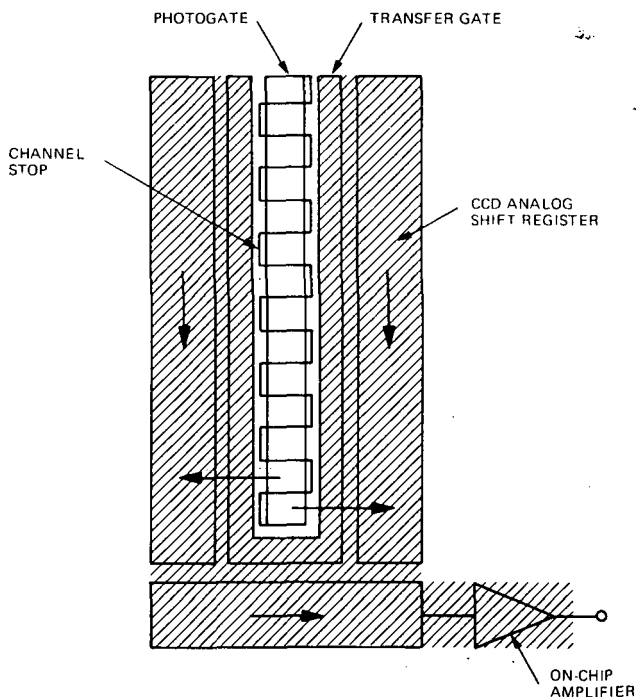


Figure 4-28. CCD Linear Imaging

Photoelement Pitch. The use of two transport registers in the design of charge-coupled linear imaging devices permits smaller photoelement-to-photoelement spacings than have been possible previously. As an example, for the case of a two-phase design in which the minimum dimension in any mask plane is 0.2 mil, it is readily seen that a sensor pitch of 2000 per inch is feasible.

For imaging in the visible spectral range for which the absorption coefficient in the silicon is greater than $2 \times 10^{-3} \text{ cm}^{-1}$ or 5 mil^{-1} , the optical cross-talk (due to light incident in one sensor area producing a signal in a neighboring sensor) is small even at 2000 sensors per inch. For longer wavelengths the absorption coefficient decreases rapidly, and it becomes more important to consider the width of the depletion layer and the numerical aperture of the imaging optics in order to predict optical cross-talk accurately.

In principle, the image can be incident either on the front or on the back of the device, provided it is thinned sufficiently to avoid sacrificing a significant portion of the resolution. Since thinning greatly complicates fabrication, it should be done only for some clear advantage. For example, if polycrystalline silicon (poly-Si) is used as the gate material, and if increased quantum efficiency is required for wavelengths less than 0.45 microns, it might be necessary to resort to thinning in order to use back side illumination.

MTF Considerations. In order to maximize a signal for a given sensor pitch, the elemental sensor areas should be approximately square and without any "dead" space between them. The modulation transfer functions (MTFs) along the device axis and in the image motion direction are functions of the sensor area and aspect ratio. Depending on the MTF desired in each direction, modifications of the "maximum square" sensor element would have to be made. For equal areas under the two MTF curves, it is necessary to compensate for image motion smearing by making the sensor dimension in the image motion direction less than the other dimension; the quantitative treatment depends on image velocity. A more detailed discussion of MTF considerations is given later in this chapter.

Linearity of Photoresponse. Although an extensive investigation of CCD photo-response characteristics is yet to be conducted, preliminary results from a small statistical sample indicate only a small departure from linearity. This is illustrated in Figure 4-29, which shows a curve relating illumination level to signal output for a charge-coupled linear imaging device. This device incorporates on-chip a single-ended MOS gated charge amplifier such as previously described.

The observed nonlinearity is attributable in part to at least two factors; the first is related to the linearity of the charge detector amplifier as discussed earlier, and the second to depletion region modulation due to different levels of stored charge. Assuming a surface channel configuration for simplicity of analysis, the depletion width is given in the following equation:

$$w = \left\{ \frac{q\epsilon_s}{qN} \left[V_0 + V - \left(V_0^2 + 2V V_0 \right)^{1/2} \right] \right\}^{1/2} \quad (24)$$

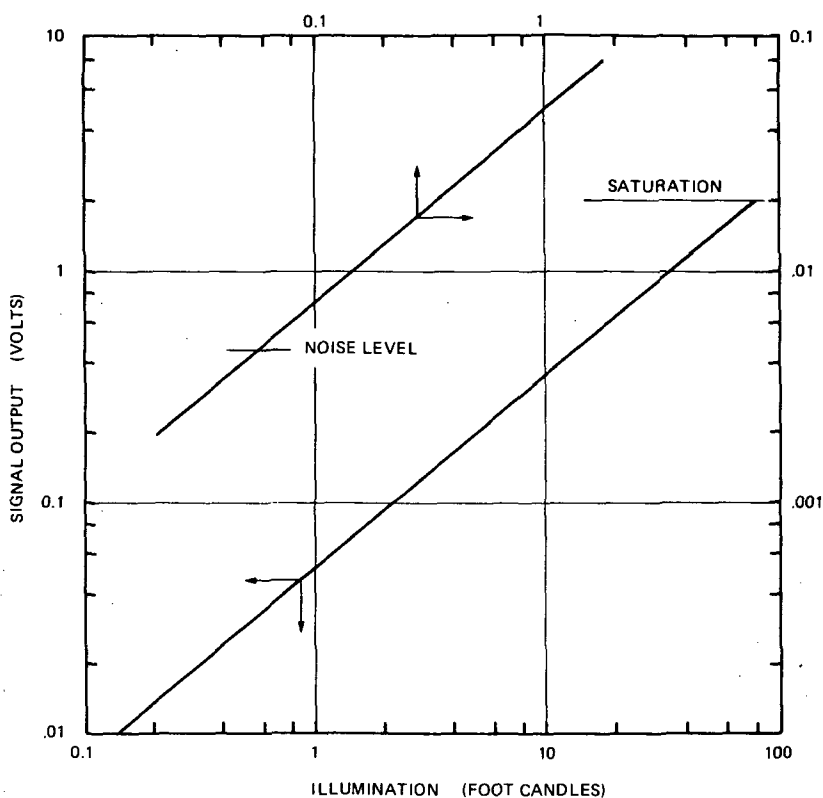


Figure 4-29. Linearity of Photo Response

where,

$$V_o = \frac{\epsilon_s q N}{C_o^2} \quad (25)$$

$$V = V_G - V_{FB} - \frac{q_{sig}}{C_o} \quad (26)$$

- w = depletion width
- ϵ_s = semiconductor dielectric constant
- q = electronic charge
- N = doping density
- q_{sig} = input signal charge

V_{FB} = flat band voltage

V_G = applied gate voltage

C_o = oxide capacitance per unit area.

For representative parameters, the depletion region will vary on the order of 3 microns. This will result in a change of probability of capture for electrons created by photon absorption in the neutral bulk. In the blue part of the spectrum, most carriers are absorbed well within the depletion region and are unaffected by the width variation. In the red, where most carriers are absorbed in the neutral bulk, the change in capture probability (for the case $L \gg w$) is proportional to the equation:

$$[1 - \exp(-\Delta w/L)] \quad (27)$$

where L is the minority carrier diffusion length.

In the high quality material that is used in CCD fabrication, the diffusion length L is on the order of 10^2 micron. Thus the anticipated nonlinearity for the red part of the spectrum is less than 3 percent. Therefore, the photoresponse of CCD image sensors is highly linear and should not present difficulties in establishing correlation with incident photon flux.

MTF Requirements on Transfer Efficiency. Periodically, the photogenerated charge accumulated at each photosensing element in the array must be interrogated. In an ideal sensor the readout mechanism should provide an accurate rendering of the information stored. In an imaging device employing charge-coupled shift registers, the quality of image reproduction will be degraded if the transfer efficiency is not sufficiently high and will result in significant and clearly undesirable variations in the spatial resolution across the sensor. This subject can be quantified by introducing the modulation transfer function.

The standard description of the resolution of an imaging system is generally given in terms of the MTF for a sinewave input and is represented by a plot of normalized amplitude versus spatial frequency out to the Nyquist limit. Qualitatively, the greater the area under this MTF curve the better is the fidelity of the reproduced image. This measure of imaging fidelity is conveniently expressed as the equivalent number of TV lines per picture, N_{eq} , which is the maximum number of resolvable lines per picture in a hypothetical system having the same area under the MTF curve but with a flat response. To be sure, there are other criteria for defining an optimum imaging system. The most common being "limiting resolution," but none is so widely accepted for precision characterization as the MTF curve itself.

The Effect of Transfer Inefficiency on MTF. The effect of inefficiency in charge transfer is to deteriorate image quality by reducing MTF or sinewave response and by producing a phase shift for different spatial frequencies. The interpretation of the transfer efficiency in terms of a sinewave input enables the quantitative degradation to be calculated.

Consider a charge-coupled imaging device in which N transfers are required to bring the accumulated photocharge to the output circuit. If the transfer inefficiency per transfer is ϵ , then the normalized modulation transfer function is given by the equation:

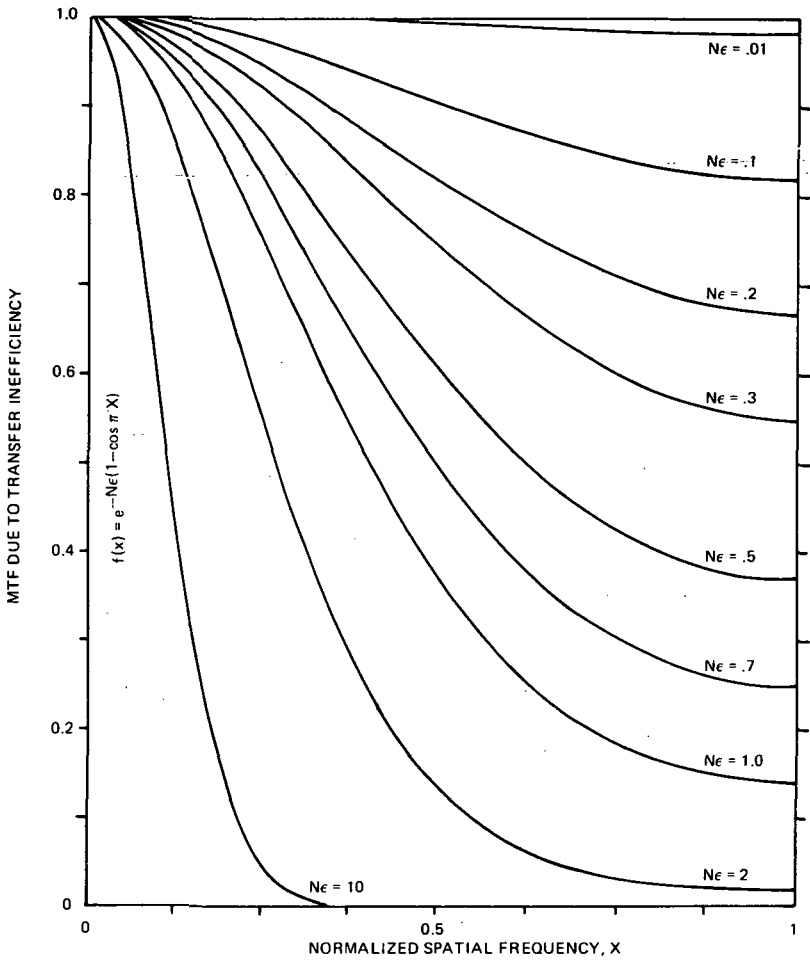
$$\text{MTF}(x) = e^{-N\epsilon (1 - \cos \pi x)} \quad (28)$$

where x is the normalized spatial frequency and the maximum useful spatial frequency is $x=1$ (Nyquist limit), in which case there is just one TV line per sensor imaged onto the array. This equation is the same as that given by Amelio, et al., (1971) except for notation. The derivation is attributed to Joyce and Bertram (1971).

A family of MTF curves are shown in Figure 4-30 for different values of N . Since the number of shifts, N , depends on the photoelement location, the MTF response will vary across the sensor from a near perfect response for elements near the output to some smaller value depending on $N\epsilon$ and the spatial frequency x . Assuming a variation at the Nyquist limit of less than a factor of two is acceptable, values of the $N\epsilon$ product should be less than about 0.3. On the other hand, extremely small values of $N\epsilon$ (<0.05) are probably not necessary because of other limiting elements in the camera system. As an example, if it is desired to have $N\epsilon = 0.1$ for an imaging device requiring a maximum of 10^3 transfers, then an inefficiency of less than 10^{-4} must be achieved.

Effect of Transfer Inefficiency on Image Phase Shift. Phase shift is an effect that distorts the image. Amelio (1971) and Joyce and Bertram (1971) consider that phase shift is proportional to N , and that the worst-case phase shift is one-element spacing when $N\epsilon = 1 - N\epsilon\pi$ in their angular notation. Thus, in view of the previous observation that the $N\epsilon$ product should be <1 , phase shift will generally not be a significant effect.

Blooming Control/Exposure Control. Use of the CCD concept in the design of solid-state photosensors requires the implementation of electronic anti-blooming and exposure control features. In a CCD photosensor, the photocharge is stored in potential wells near the surface in the form of minority carriers. These wells are localized underneath an optically transparent electrode

Figure 4-30. MTF Curves for Various Values of Ne

and are bounded on two of the sides parallel to the surface by the presence of a so-called channel-stop diffusion. On the other two sides, parallel to the surface, they are bounded by a gated CCD analog shift register, and usually, by a third channel-stop diffusion. In the axis perpendicular to the surface, the well is formed by the usual parabolic potential profiles formed by the field lines terminating on the donors and acceptors in the implanted layer and bulk, respectively. When this three-dimensional well becomes saturated with charge, carriers will flow away from the desired point of integration and "blooming" will occur. This can be prevented by incorporating an overflow protection that will drain off excess carriers just before the well saturates.

One possible planar configuration is shown in Figure 4-31. In this design the usual channel-stop boundary has been replaced by an exposure gate and a sink diode. The sink diode is always reverse biased to drain any minority carriers coming into the vicinity. In the exposure control mode, the exposure gate is turned on hard during the first part of the device scanning cycle and all photon-generated carriers are drained through the sink diode (STANDBY in Figure 4-31). During the latter part of the device scanning cycle, the exposure gate is turned off and photon-generated carriers are integrated under the photogate (EXPOSE in Figure 4-31). Without this exposure control, the integration time is equal to the total device scanning period. With the exposure control, however, the true integration time is the exposure time which can be varied for different light intensities. Therefore, a wide range of light intensity can be handled without saturating the device. This is desirable if the nominal background lighting is high as in a daylight scene.

In the blooming control mode of operation, the exposure gate is turned on slightly so that excessive carriers are drained through the sink diode instead of filling the adjacent photoelement. Thus, the potential wells under the photogate are never permitted to fully saturate, and blooming cannot occur. In this way, an image with a contrast range far exceeding the dynamic range of the device can be handled without destroying the resolution. This function is illustrated in Figure 4-32.

This scheme can be thought of as an active approach in that the control is actively achieved with external voltages. A passive approach with a simpler structure is also conceivable, but with limited versatility. One possible scheme is to have a region of implanted asymmetry at the photogate with no exposure gate. In this way, a built-in barrier can be obtained on one side of the photogate which determines the saturation signal. Any excessive carriers will then spill over the built-in barrier and antiblooming can be obtained. Although blooming control would be easier with this scheme, exposure control cannot be accomplished.

Note that these remarks are equally applicable to linear or area devices. However, in an area array one suffers the expense of increased chip size and reduced resolution.

An alternative approach to the planar structure is to bury the sink diode under the photogate. With this structure, there is no sacrifice in terms of chip size and resolution. However, careful design and good process control will be required for successful fabrication and operation of this structure.

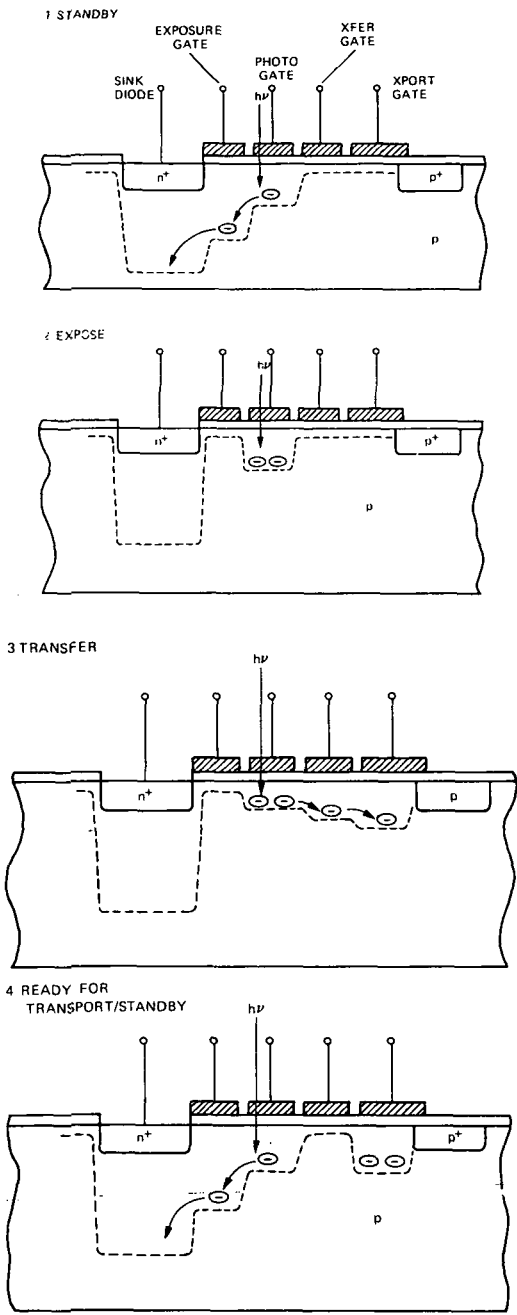
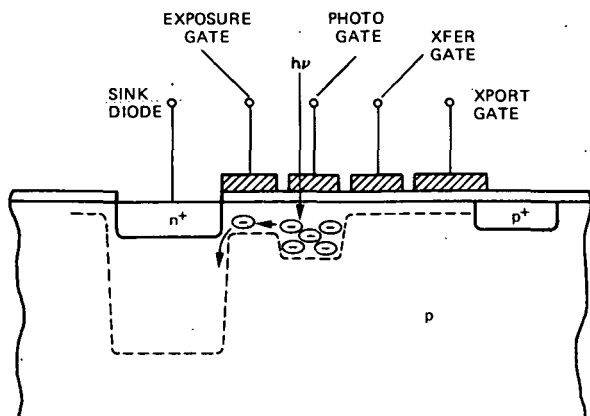


Figure 4-31. CCLID with Exposure Control

1 IN SATURATION - TRANSVERSE VIEW



2 IN SATURATION - LONGITUDINAL VIEW THROUGH PHOTOGATE

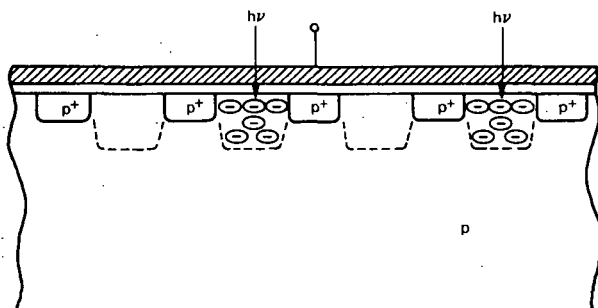


Figure 4-32. Exposure Control Device Operating in
Anti-blooming Mode

Variable Exchange of Resolution and S/N Ratio in CCD Sensors

Scanning by charge transfer in CCD sensors offers a unique opportunity for signal processing within the sensor itself, which does not exist with other modes of scanning of solid state sensors. For example the output S/N ratio delivered by the sensor can be increased at the expense of resolution by remote control to optimize performance under varying conditions of scene illumination and signal transmission.

The controllable exchange of resolution and sensitivity in charge-coupled sensors is accomplished by combining the signal charges from a variable number of adjoining elements to obtain larger individual charge packets with a corresponding decrease in the total number of packets. Since the internal summary process of the charges is into the sensor output amplifier, the ratio of signal

to amplifier noise is increased in direct proportion to the increase in size of the individual charge packets. Similarly the effect of other noise sources within the sensor can be reduced in a variable degree depending upon the character of the noise source.

The modifications required in a CCD sensor to permit controllable exchange of resolution and sensitivity are minor, and affect in no way its performance capabilities under normal operating conditions. The summing of adjacent charges is carried out under one or more clock electrodes which have been connected to a special clock voltage source. Adjustment of this voltage source controls the number and location of the elements to be summed into groups. No changes are required in external scan rates for summing to be effective.

The summing method of exchange of sensitivity and resolution has been demonstrated in both single-line and two-dimensional CCD sensor arrays (Weimer, et al., 1973).

Performance of Charge-Coupled Imaging Devices (Through December 1972)

Because of the newness of the CCD technology, only a few device types have been built and very little performance data are available. Performance data on one device type—the 500-element buried channel linear imaging device—is presented here. (This device was discussed broadly in the section on Basic Technology.)

Transfer Efficiency. At a 1-MHz element rate (three transfers per element) inefficiencies between 10^{-4} and 10^{-5} are nominally measured. Moreover, these values have been found to be independent of the charge level.

Spectral Response. Figure 4-33 shows a typical relative spectral response curve. In this device the polysilicon gate, which covers the photosensors, is approximately 0.5 micron thick. The sharp drop in response at $\lambda < 0.5$ micron is due primarily to optical absorption in the polysilicon gate. By proper design, it may be possible to reduce the polysilicon gate thickness substantially and thereby extend the response spectrum to shorter wavelengths.

Imaging Performance and Dynamic Range. Figure 4-34 shows a block diagram of the imaging circuit used to characterize the imaging performance of this device over a wide dynamic range. The results presented here were obtained using a 1 MHz element sampling frequency and an integration time of 500 microseconds. Figure 4-35 shows four pictures taken at different light levels. The source

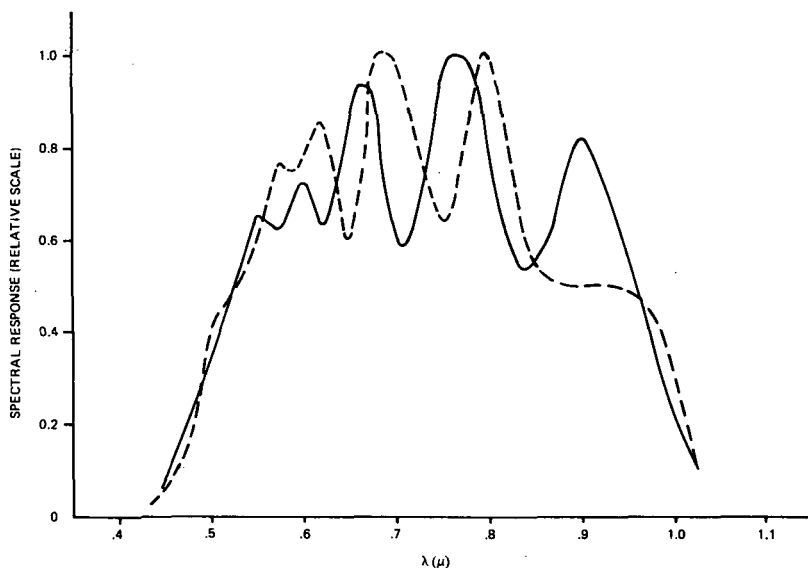


Figure 4-33. Spectral Responses of Two Samples of the 500-element Imaging Device

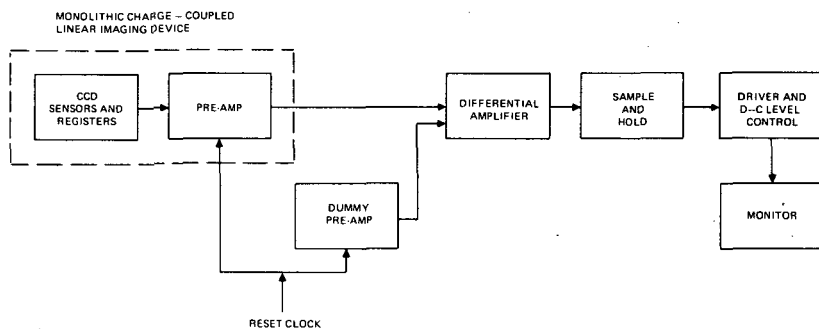


Figure 4-34. Block Diagram of the Imaging System

illumination in each case was a tungsten source at a color temperature of approximately 2800 K and filtered to remove wavelengths greater than approximately 0.9 microns. The highlight signal level in picture (a) (upper left hand corner) is near saturation. In pictures (b), (c) and (d), light levels are reduced by 10X, 100X and 1000X, respectively. Picture (d) is degraded by random noise originating in the preamplifier, but the subject is still clearly recognizable. In lieu of an accurate dynamic range determination it appears that the dynamic range exceeds 1000:1.

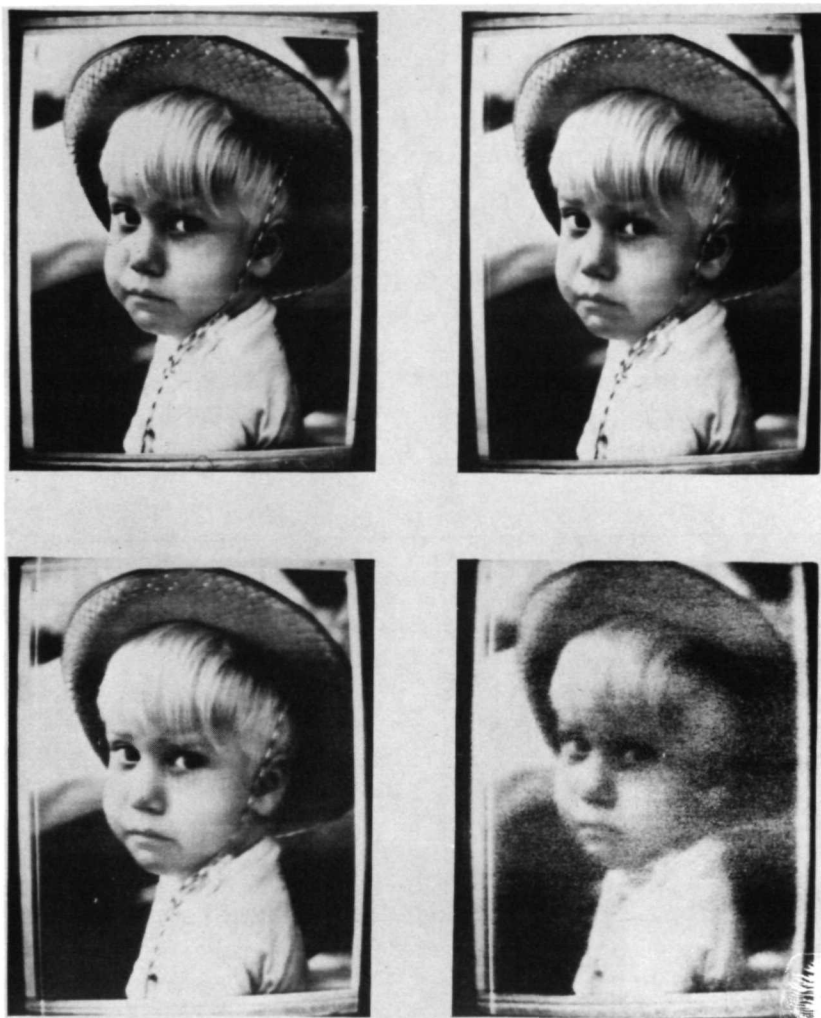


Figure 4-35. Images Produced with the 500-element Linear Imaging Device. The Relative Illumination Levels Are: (a) 1, (b) 10^{-1} , (c) 10^{-2} and (d) 10^{-3}

It can also be seen that the uniformity of response is excellent. The primary causes of nonuniformities are expected to be variations in element size and number of transfers required to reach the output.

Chip Butting Requirements. One of the requirements of the monolithic imaging chip to be used for earth-orbital imaging is that it be capable of butting to similar chips so as to give a mosaic imaging system that can reproduce a high-quality picture. This requirement is essentially the same for all solid-state

images made on silicon. A few minor points of differences that are specific to charge-coupled imaging devices are noted next.

There will be a need for new device designs to cope with the lack of space on the chip either at the ends or along one edge of the linear photosensing region. More gate and bus crossovers will be needed, very likely requiring an additional conductive layer relative to simpler linear imaging devices. Some ingenuity will also be needed to design a very sharp 90-degree turn in the CCD register(s) so that the preamplifier can be situated away from the immediate end of the sensor region.

It appears, however, that it will be possible to fabricate charge-coupled imaging device chips with considerably more sensing elements per chip than is possible with photodiode and phototransistor arrays. This means that there can be fewer interfaces for a given total number of sensors, and therefore a smaller fraction of the image data which would require special processing to give a smoothed video signal, regardless of the specific requirements on smoothing at the interface. It is too early to say whether or not CCD imaging sensor that would have an essentially uniform sensor pitch across a chip-to-chip interface would be feasible.

One chip-butting concept of interest for a pushbroom-mode CCD orbital imager is depicted in Figure 4-36. In this concept each chip has a parallelogram shape and consists of a main sensor array and a secondary sensor array. The displacement of the secondary array frame, the axis of the main array, and the length of the secondary array are minimized. The direction of image motion is such that, to read one line of the image, the signal from the smaller array is stored (off-chip) until the larger array scans that same line. This minimizes the amount of memory storage required. An advantage of this concept is that the ends of the sensor array are more accessible for charge detection and amplification.

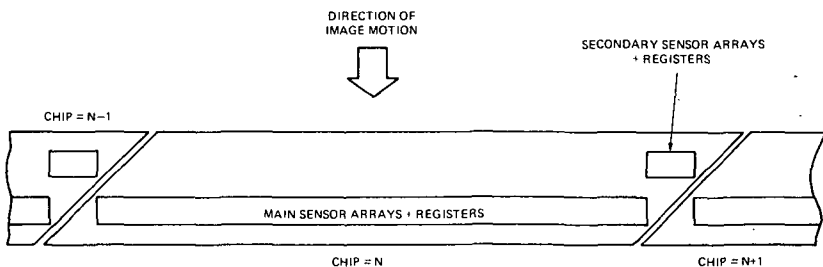


Figure 4-36. A Pushbroom-mode Orbital Image Sensor Concept

INFRARED DETECTOR ARRAYS

IR System Considerations

Infrared array development has not at this time reached the technological maturity of silicon detectors and arrays. Major differences are contained in the following: (a) present HgCdTe detectors operate generally in the photoconductive mode; (b) small scale (approximately 100-element) IR arrays have been manufactured only through the physical assembling of individual detectors; and (c) $1/f$ noise in the infrared detectors is considerably higher than in silicon detectors. The implications of these differences for the IR systems are as follows: (a) present systems require a drop in the incoming radiation; (b) detector bias (≈ 1 mW per detector) is required; and (c) the low impedance of the detectors (25-250 Ω) requires high-power preamplifier stages.

However, the infrared detector manufacturing community is at present capable of manufacturing high density arrays of IR detectors for use in mechanical scanners. The problems of uniformity have now been solved to an extent that high performance can be expected from these arrays. Multispectral capability has also been incorporated in these array systems. In view of this proven performance in mechanical scanners, it is legitimate to ask, "Why should efforts be expended on the development of self-scanned imaging systems?"

The motivation for developing IR solid-state, self-scanned imaging systems are found in the following objectives:

1. Increase performance potential by integrating over a frame time.
2. Reduce electronic complexity and cost by using a single amplifier in a multiplexed mode.
3. Increase reliability by eliminating mechanical scanning.
4. Provide compatibility with solid state imaging in the visible to simplify registration of thermal imagery.

Current Status of IR Solid-State Imaging and Readout

It is currently possible to make high density arrays of IR detectors (photoconductive, photovoltaic) out of narrow band-gap (0.1 to 0.5 eV) semiconductors. However, it is not possible, as yet, to integrate these detectors with their associated electronics onto one chip, because the technology for fabricating transistors in materials such as InAs, InSb, HgCdTe, PbSnTe, etc., has not been established. It is possible to consider hybrid devices consisting of IR detector arrays cemented to a silicon chip that contains the necessary

read-out circuitry. This would require interconnections made by stitch bonds or by leads evaporated over glue lines.

In brief, although feasibility studies for the design of self-scanned, solid-state IR imaging systems have been conducted over a number of years, at this date, no imager has been constructed that can compare in performance with the current generation of mechanical scanned IR systems.

Near Future Prospects of IR-CCD Devices (4 years hence)

Currently there are no IR-CCD devices which are operable. Furthermore, it has not been established, at this date, whether the common candidate semi-conducting materials for near-IR (1 to 5-micron) imaging, PbS, PbSe, PbTe, InAs, InSb, and short wavelength HgCdTe, can be processed to yield surface characteristics that would be amenable to IR-CCD device fabrication. Considering the vast research program that has gone into the development of silicon devices, it is a reasonably safe prediction that there will be no IR-CCD devices available for incorporation in an operational satellite sensing system four years from now. This prediction is based on an estimate of the funding required to bring a material such as InSb to the current state of silicon versus the funding now allocated for such a development program. Hybrid devices, using IR detectors as the sensors and using the CCD concept only as signal processors, could possibly be available during this time period; however, the CCD mode of charge transfer and readout would be in competition with other means of processing, and the advantage of charge storage or single integration would not be utilized.

An approach that could alter the situation somewhat would be the development of extrinsic silicon detectors in the 1 to 5-micron interval that would also be amenable to CCD processing. However, this would also involve a development program. The fruition of such a program in time for launch dates four years hence is unlikely.

Long Term Prospects (8 years hence)

At substantial developmental funding levels, the probability of achieving an IR-CCD by 1980 is estimated to be approximately 50 percent, if the process of understanding the surface properties of the candidate materials does not unearth some fundamental barriers. However, again based on the current rate of funding, the probability that an IR-CCD system will be operational eight years hence is also quite small (~10%).

Technical Considerations

While CCD operation in the visible region using silicon technology may be a relatively appealing approach, this mode of operation in the near-IR (1 to 5 microns) is beset with a number of fundamental difficulties.

Cooling Requirements

The potential well or bucket that is available for charge storage in a frame time is finite. Present capability is of the order of 10^{12} electrons/centimeter². Room temperatures would result in carrier generation rates that would fill the wells at an unacceptable rate. Thus, cooling of the detector arrays would be necessary. While cooling is inconvenient, it is not an insurmountable barrier.

For 5-micron operation the usual operating temperatures are in the range of 77 to 100 K. It has been estimated that the power dissipation per element could be as low as 15 microwatts for a 1 megaHertz bandwidth. Thus for a $10^3 \times 10^3$ array, the power dissipation would be a minimum of 15 milliwatts. These calculations were based on silicon technology; the use of higher conductivity materials would undoubtedly lead to higher heat loads.

Present 10-micron HgCdTe detectors operate in the photoconductive mode, requiring approximately 1 milliwatt of bias power. In addition, since these devices have very low impedance, the preamplifier stages require several milliwatts. The high responsivity of the photoconductor may allow switching at the detector; thus a single preamplifier could possibly be used. Moreover, even under these conditions, 2000-6000 element arrays will require several watts of cooling power. Feasibility of radiative coolers at these power levels is questionable. Vuilleumier (VM) coolers with this capacity are under development by NASA. It can be expected that, within four to eight years, coolers with the required capacity will be available.

In addition, development of photovoltaic detectors in the 1 to 3-micron and 10 to 14-micron region is in progress. Development of these detectors should allow the use of the technology described in the section of this report discussing near and far infrared systems (Chapter 2).

Background Generation of Charge

The generation of charge carriers by the background photon flux is a more formidable barrier. Some calculations and examples will demonstrate this point.

Assume the following system:

$$\text{Well storage capability} = 10^{11} \text{ e/centimeter}^2$$

$$\text{Frame time} = 1/30\text{sec}$$

$$\text{Long wavelength limit} = \sim 5.5 \text{ micron}$$

$$\text{Background temperature} = 300\text{K}$$

$$\text{Optical/f number} = f/2$$

$$\text{Quantum efficiency } (\eta) = 0.5$$

Then,

$$Q \text{ at background} = 4 \times 10^{18} \text{ photon/second-centimeter}^2 \quad (29)$$

$$Q_{0-5.5 \mu\text{m}} = 2 \times 10^{16} \text{ photon/second-centimeter}^2 \quad (30)$$

$$Q_{0-5.5 \mu\text{m}} \text{ at image plane} = \frac{2 \times 10^{16}}{4(f/2)^2} = 0.12 \times 10^{16} \cong 10^{15} \text{ photon/} \\ \text{second-centimeter}^2 \quad (31)$$

Therefore, the charge generated at wells is:

$$q = 5 \times 10^{14} \text{ e/centimeter}^2\text{-second}$$

and the charge generated during a frame time is approximately 0.6×10^{13} e/centimeter².

However, this is almost 2 orders of magnitude larger than the charge required for saturation.

Since optical surfaces and structures radiate at the wavelength of interest (10 to 12 microns), it is necessary to design optical systems that have very low f numbers at the detector—a condition that will be difficult to achieve in the pushbroom mode where off-axis performance is required. This fact will further aggravate the dynamic range requirements of the amplifiers associated with IR detectors.

To alleviate the problems associated with the measurement of small variations in a very large background, it will be necessary either to modulate the incoming radiation and to develop techniques for ac coupling in large arrays, or to develop techniques for dc restoration in the first amplifier stages. At this time feasibility of these approaches has not been demonstrated.

Power Considerations

As mentioned previously, the power dissipation in an $10^3 \times 10^3$ array alone would be a minimum of 15 milliwatts that would require cooling. The electrical-thermal cooling conversion efficiencies are quite low in current cryogenic systems. Therefore, 1–10 watts of electrical power would be necessary to provide cooling for such an array. Other requirements such as signal processing and telemetry would be additional loads.

Element and Array Fabrication

The technology and methodology of fabricating CCD imaging arrays from silicon materials is discussed elsewhere in this report. The areas that are discussed here are the problems peculiar to the extension of CCD imaging to the infrared.

The extension of self-scanned solid state imaging to the infrared spectral region will be accomplished by the development of the surface technology of semiconductors other than silicon or the use of extrinsically doped silicon materials. A third possible approach is the use of lowband-gap semiconductor detectors electrically connected to silicon charge transfer elements in a hybrid arrangement. However, this latter approach ignores many of the advantages of CCD operation; namely, signal generation, processing, amplification, and readout of single elements using integrated circuitry techniques.

High density detector arrays have been constructed on lowband-gap semiconductor wafers. However, the surface physics of such well known materials as InSb and InAs are not known to a sufficient degree to permit charge transfer and shift register functions to be constructed on the same element. The problems of forming high density arrays by geometrically selective doping, insulator formation and metallized contact deposition are indeed formidable.

The approach of using extrinsic silicon arrays is an interesting one. Although high density arrays have been fabricated from extrinsic silicon, these have been stacked element arrays and, to date, the fabrication of 5-micron silicon detector arrays on a monolithic wafer has not been reported. The problems to be solved here, are whether the doping of the silicon to provide 5-micron operation in the infrared can be made compatible with charge localization and storage and transfer. Since the signal generation would be essentially a bulk effect, the problems to overcome would be to minimize crosstalk between adjacent elements.

IR System Summary

Infrared detection array utilizing temperature sensitive effects (such as thermistor bolometers, pyroelectric detectors, and thermopiles) may be advantageous for special and auxiliary imaging applications. However, their technological growth potential is so limited in terms of sensitivity, response time, and element size that their development appears to be of low priority in terms of present and anticipated NASA applications. NASA should limit funding of device research in this area.

In addition, the feasibility of preparing charge-coupled devices in InSb should be investigated.

SYSTEM CONSIDERATIONS

Optical Design

Although long linear IR arrays for the 8 to 14-micron range are not currently available, work presently in hand indicates that hybrid self-scanned IR detectors requiring cooling to ~ 100 K could be available in four years; and that it

is conceivable for hybrid CCD-IR detectors requiring cooling to only $\sim 240\text{K}$ to be available in eight years (see IR Detector Section pp. 364).

There are basically three approaches involving use of self-scanned arrays in multispectral system design:

- A hybrid system in which a whiskbroom scanner (electro-mechanical scanner) includes self-scanned rectangular area silicon arrays as well as conventional IR detectors.
- A multiple optical channel system in which silicon linear arrays are operated in a pushbroom mode and the IR channels are obtained from a conventional whiskbroom scanner.
- A multispectral system in which all imagery is obtained by pushbroom scanning.

The hybrid system has an inherent advantage in that with only the one optical system involved, the imagery in the various bands is in perfect register. Three disadvantages, however, are: (1) although in perfect register, the imagery suffers from the distortion inherent in the whiskbroom (panoramic) mode of operation; (2) area silicon arrays have to be used to increase the dwell time on these detectors (therefore involving greater array complexity); and (3) the rate of charge translation across the area array has to be accurately synchronized with image motion.

The multiple-channel approach, which includes both whiskbroom and pushbroom scanners, has the advantage of choice of f-number and focal length to optimize sensitivity and resolution match between channels. The imagery produced is not in perfect register because of the different scanning actions involved.

An all-pushbroom system has none of the disadvantages listed above. Careful optical and mechanical design and fabrication can yield imagery of excellent registration and freedom from optical distortion, for example, as provided by the S190 multiband frame cameras on Skylab (6 precision 70 mm film cameras). A disadvantage to the approach is that for cartographic applications the imagery has to be corrected for spacecraft attitude changes.

A comparison of the all-pushbroom system using linear self-scanned arrays and *present* photodiode technology with the multispectral scanner on ERTS 1 shows a dramatic reduction in system size that should be reflected in system cost. The lack of mechanical moving parts and possibilities for future array developments make this a highly regarded choice for advanced multi-band sensor systems.

For purposes of discussing imaging systems, it is necessary to identify a set of system requirements. The following table lists a reasonable set of requirements for a high-resolution multispectral imager to operate on an earth observation satellite.

Table 4-1

System Specifications

ORBIT REQUIREMENTS

- Spacecraft Altitude: 920 kilometer (496 nautical miles)
- Near polar, sun synchronous orbit
- Sun angle: 60 degree solar zenith at 50 degree north latitude at vernal equinox

SENSOR REQUIREMENTS

- 185 kilometer (100 nautical miles) swathwidth
- Contiguous coverage at equator
- 30 meters IFOV to 7.6 meters IFOV
- Spectral region: visible to 1.2 microns
- 0.1-micron spectral channel bandwidth (3 channels minimum)
- Scene reflectance: less than 20 percent
- Background reflectance: 2 to 20 percent
- Geometric linearity: better than 0.1 percent
- Inherent spatial registration between all channels
- Relative radiometric accuracy between channels: better than 5 percent

Primary Optics Design

The primary optics, as part of the array sensor/optics subsystem, should fulfill the following system requirements:

Field of View: Less than 12 degrees

Optics Speed: $f/4$ or faster, as determined by sensor array configuration and ground scene characteristics

Focal Length: Determined by sensor array configuration

Resolution: Basically sensor limited; therefore optics MTF = 0.5 to 0.7, or better, at the limiting spatial frequency determined by the array geometry (ground resolution cells to be selected, but within the range 25–100 feet)

Spectral Band: The optics will be polychromatic for parallel operation in the following spectral bands: 0.5–0.6, 0.6–0.7, 0.7–0.8 and 0.8–1.1 microns

Image Plane Flatness: Due to the line character of the image, no special requirements on image flatness are needed. That is, the arrays consist of many small array chips which may be mounted on a curved surface to follow any reasonable image curvature ($R = 20$ inches or thereabouts) with satisfactory accuracy.

There are four classes of optical designs, which are in use or have been used, that approach the above specifications:

1. *Derivations of Double-Gauss lens design.* These are characterized by near uniform sharpness over the whole field of view, at speeds $f/6$ to $f/3.5$. The optical system length is slightly larger than the focal length (FL) (1.1 – $1.2 \times FL$). The Fecker Division of Owens-Illinois, Pacific Optical, Itek, and Perkin-Elmer are among the suppliers of such lenses.
2. *Petzval-type lenses.* These are lightweight and show excellent image sharpness on-axis with, in general, appreciable fall-off in the field. System speed is $f/3.5$ to $f/5$, and the system is long, typical $1.3 \times FL$. The major producer is Itek Corporation.
3. *Catadioptric systems such as the Schmidt, the Concentric Bouwers-Maksutov, and combinations of these (by Baker, and other).* Their length is typically 1 – $2 \times FL$. Schmidt and Baker camera lenses are made by Perkin-Elmer Corporation, among others. Concentric systems applicable to high-altitude aerial work are made by Old Delft Optical Company of Holland. They excel in uniformity of imagery for FOV up to 20 degrees and more.

4. *High-resolution mirror systems with image correction by small-diameter lens groups near the image plane.* Examples are the Ritchey-Chretien systems by American Optical Company and Fecker. These systems differ from the Schmidt and Bouwers systems in which image correction is accomplished by full-size corrector elements. Although they show excellent performance on-axis, the usable field of view is too small (1 to 3 degrees) to be of further consideration here.

When considering optics weight for the same optical parameters as focal length, etc., the Petzval lenses are the lightest, the double-Gauss types are heavier, and the concentric mirror types somewhat heavier still. When comparing the optics barrel lengths, the Petzvals are the longest, and the double-Gauss the shortest.

Figure 4-37 shows a typical diagram of each of the three optical systems to be considered, scaled to the same focal length and effective optical speed, and all capable of imagery over 12 degrees FOV.

Performance Considerations

A major advantage of the solid-state array is that the one-dimension optical image (line image) and the sensor array, which consists of a series of small chips, can be made to follow any image curvature within reason. Thus the optical designer does not have to trade off optical performance against image flatness or uniform image curvature.

The major problem is the high resolution imagery that is required over a very wide spectral range, spanning more than an octave (0.5 to 1.1 microns). This poses a formidable color correction task.

For the refractive systems, Fecker and Itek made a short study of the performance of their systems when optimized for this spectral range. In each case the minimum 100 percent blur circle was approximately 38 micrometers, whereas for the 2-mirror concentric, the minimum 100 percent blur circle ranged from 9 μm to 23 μm over this broad spectral region. Here the optics are assumed to be focused for minimum blur circle diameter (geometric, without diffraction effects) which still contains 100 percent of the transmitted energy. These values are typical for low-contrast resolution.

With respect to MTF, the idea is to have the entire optics blur circle fall within one detector elemental area. For the photodiode array, this would limit the spot size to 15.2 microns (0.6 mils). To sense edges in the scene, the edge transition in the optical image should be no wider than one-diode spacing,

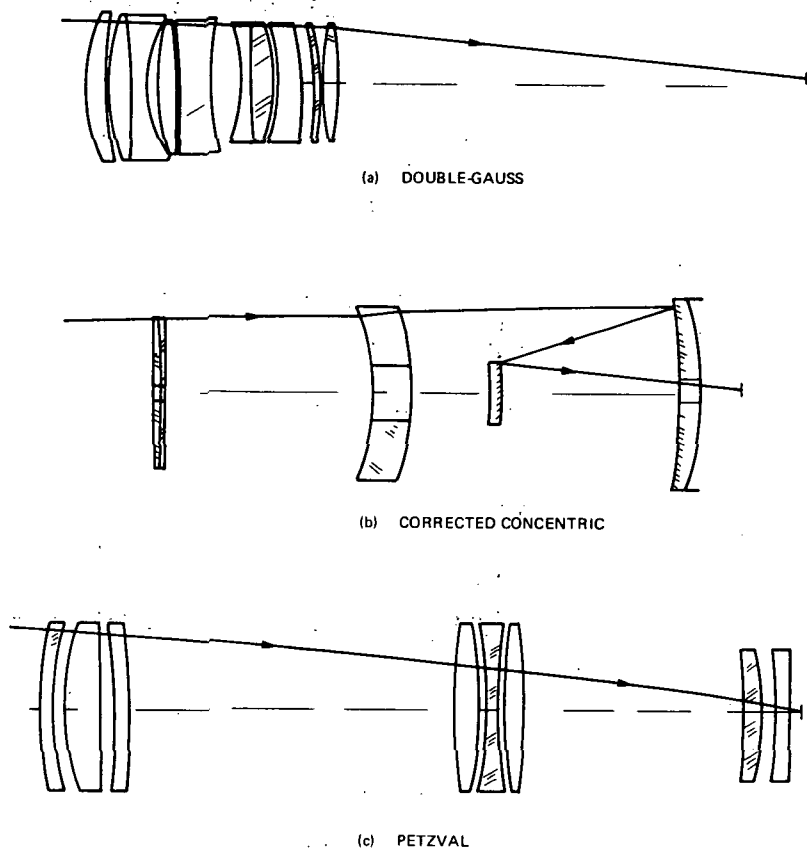


Figure 4-37. Three Candidate Optical Systems

which in the present case is 7.6 microns (0.3 mils), leading again to an optics point-spread function diameter of 15.2 microns. At this diameter, diffraction effects will be relatively small (2.5 microns at 0.5μ and 5.1 microns at 1.1μ). Therefore the optics spread function can be assumed to have the characteristics of the minimum geometrical 100 percent blur circle, and thus shows an essentially uniform energy density. Figure 4-38 shows the relative MTF performance of comparable refractive and reflector optics.

The optics focal length and f/number are determined by (a) the effective detector pitch and (b) the sensor sensitivity, scene characteristics, and optics spectral transmission, respectively.

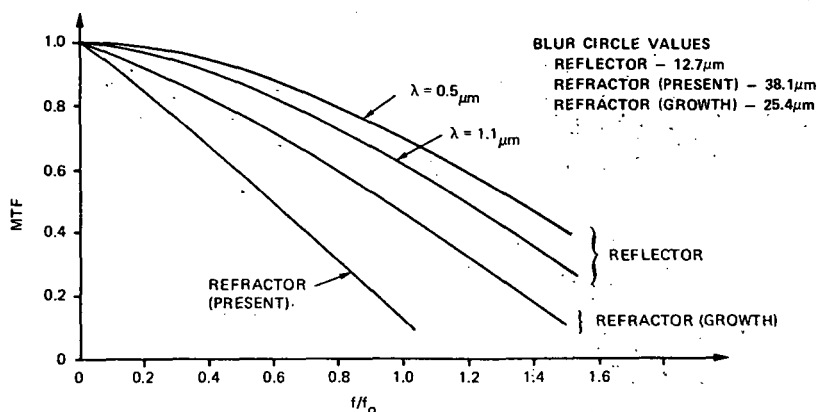


Figure 4-38. Optics Modulation Transfer Function Comparable Optics—
 $f/2.5$, FL-61 cm (24 in.)

Spectral Separation and Registration

The problem of spectral separation involves tradeoffs of purity of separation versus spectral channel transmission, using as large a part of the optics entrance area as possible, while introducing only a minimum of image degradation. The image registration, on a diode-by-diode basis, requires uniformity of arrays, a high-precision array mounting, and control of optical imagery being sent into the various spectral channels.

A survey of image separation techniques and image registration aspects are discussed next.

Spectral Image Separation

There are four spectral bands to be separated that have been chosen to facilitate comparison with existing ERTS systems. Their bandwidth are not to be exceeded, and the radiant energy transported through them is to be maximized.

The spectral bands each have an optical image in the form of a straight line. The four line images correspond to a common line object on the ground.

Candidate techniques for spectral image evaluation are:

1. Project four identical images onto individual image sensors, each sensor supplied with its own spectral bandpass filter.

2. Making use of the fact that the optical image of interest has one dimension only (line images), one may spread this line image out into a spectrum, by means of a prism or grating, and sense four narrow strips from this spectrum.
3. An imaging beam may be separated into four components by a successive application of beam splitters that have long-pass characteristics. Long-pass beam splitters are of the multilayer interference type to minimize energy losses. They are sensitive to changes in incidence angle, such as caused by FOV angles or an optics aperture angle.

The last technique is the preferred because it uses 100% of the radiant energy in each spectral channel from the entire entrance aperture, giving the highest efficiency. Figure 4-39 shows one conception of this technique that uses dichroic beam splitters at normal incidence.

Spectral Image Registration

The registration of the spectral images will have been fully carried out if the four mounted arrays, when viewed from the object space looking into the optics, are completely coincident (on a diode by diode basis). This ideal situation can be further specified as follows:

1. The orientation angles for all four arrays, taken in a plane perpendicular to the optical axis, will be identical.
2. The apparent distance between the four arrays displayed as in Figure 4-39 will be zero.
3. Relative shifts between the arrays parallel to the array axis will be zero.
4. The arrays will all be within the corresponding spectral optical image planes.

The technique needed to carry out these requirements to a satisfactory accuracy, with a resulting registration error $1/3$ to $1/2$ array diode spacing for any two corresponding diodes, can be selected from a variety of approaches, bounded by two limiting cases:

1. All array chips are individually adjustable in linear and angular position.
2. All array diodes are permanently arranged and mounted as one complete array assembly, and each completed array is then "dropped in place" in an array mounting fixture, without any further adjustments.

A decision on the optimum approach really depends on the engineering experience developed with the current research effort involving the photodiode arrays.

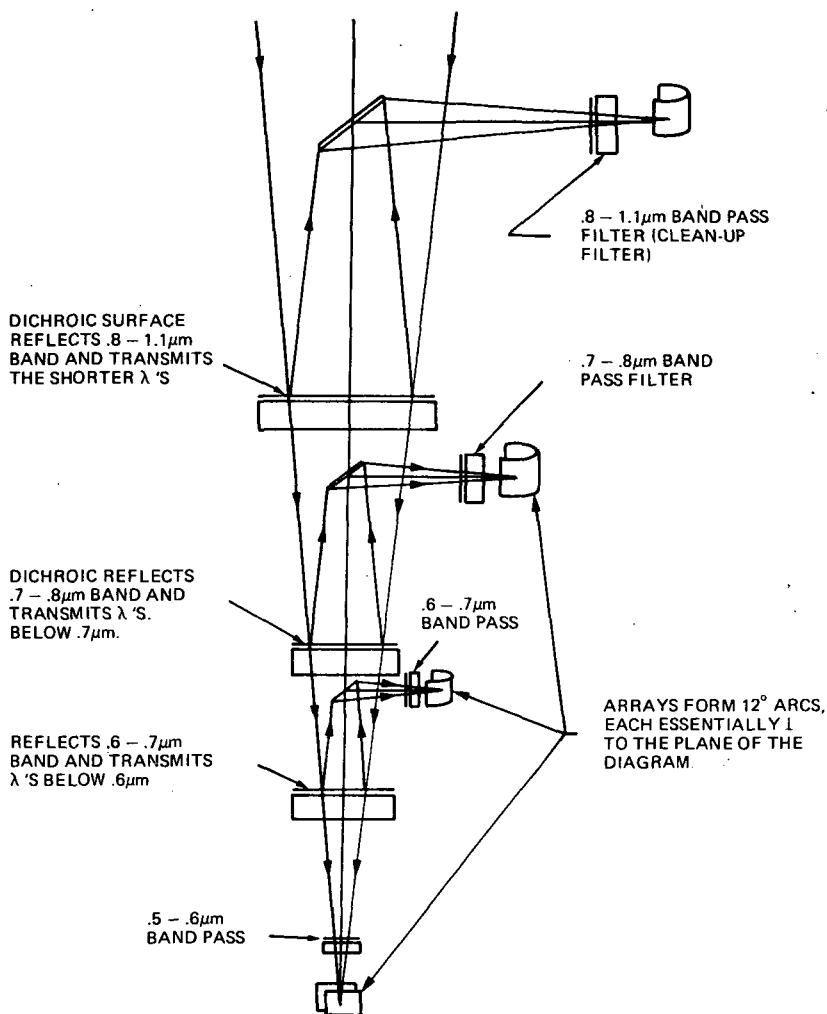


Figure 4-39. Schematic of Multispectral Optics

Environmental Considerations

The thermal/radiation environment can affect the operation of the sensor in various ways. The changes produced in the optical system can be broadly categorized as changes in dimensional stability and changes in the lattice structure of the optical materials. An attempt at a listing of the major environmental factors, the changes they produce, and the countermeasures that can be taken to complete or partly restore these changes, is given in Table 4-2. These environmental factors are discussed in general in the following sections.

Table 4-2
Environmental Factors Affecting Sensor Operation

Environmental Factor	Parameters Involved	Effects	Countermeasure	Remaining Limits
Average temperature	Linear dimensions	Shifts in focus, cross-track mapping error	Material selection of mirrors, barrels, sensor assembly	$\Delta T = 100^{\circ}\text{C}$ (focus shifts) $\Delta T = 100^{\circ}\text{C}$ (array expansion)
Temperature cycles and gradients	Refractive index (As above)	Focus shift, image degradation Dynamic focal shifts, alignment errors, image degradation	Restriction in glass selection Conducting barrel, insulating jacket (As above)	$\Delta T = 50^{\circ}\text{C}$ (reflector) 5°C (refractor) $\Delta T = 20^{\circ}\text{C}$
Shock and vibrations pre-launch & launch	Linear dimensions	Alignment errors	Construction & mounting, favors concentric system	Mechanical design
Attitude control	Imagery, mapping acc'y	Image smear, mapping errors	Attitude stabilization	0.06 degree/sec.
Vacuum	Outgassing phenomena	Degrading by optical surface films	Avoid outgassing sources inside optics/sensor structure	Restricted selection of sensor bonding materials & cabling
Micrometeorites	Scattering coefficient of outermost optical surface	Surface erosion	Continuous pointing at nearby earth	Effect largely suppressed (life > 10 years)
Atomic particles	(As above) Boron glass lattice spectral transmission	Surface sputtering, lattice damage formation of color centers, changes in spectral transmission in bands 1 and 2	(As above) (As above) (Cerium-stabilized glasses)	(As above) (As above) Restrictions in optical design
Hard radiation	(As above)	(As above)	Shielding (aided by down-looking char.)	None

Temperature

Changes in temperature can set up temperature distribution fields, for instance a homogeneous field, a linear field, a radial field—all being functions of time as well. The affected parameters are primarily linear dimensions and indices of refraction. Dimensional changes affect a component's shape and its location, while refractive index changes produce image shifts and image degradation.

The thermal time constant of the optical glass elements is of the order of hours. The orbital period is about 1.5 hours; therefore, a uniform temperature value will not be attained, and temperature gradients will be present in the lenses. A more detailed thermal analysis is therefore essential prior to the design of the flight model.

Shock and Vibration

Shock and vibrations tend to do structural and optical damage, and at smaller intensities can cause permanent changes in alignment. A concentric optical system is especially effective in counteracting misalignment since the optical elements may be allowed to rotate around their common center of curvature. They do not have to "return" to their original position after shock, and the limiting stops can therefore be of a softer, absorbent nature, rather than stiff springs that press the lens back against hard stops. This reduces considerably the chances of damage to the optical elements.

Other Environmental Factors

Aside from the factors listed in Table 4-2, high-resolution imagery requires attitude stabilization on the order of 0.005 degree/second per axis. The effects of micrometeorites, of ions, and of fast neutral atomic particles are largely suppressed because the sensor system is always looking at the earth, which occupies a large effective fraction of the half sphere from which such particles can enter the optics. The addition of a short extension to the optics barrel will shade the front optical element from the sun. Standard shielding techniques may be used to protect the optics and sensors from hard radiation.

MULTISPECTRAL IMAGING SYSTEMS FOR EARTH RESOURCE SURVEY

A multispectral imaging system is frequently used for the identification of surface features based on differences in their spectral characteristics.

For purposes of preliminary discussions, it is assumed that four wavelengths (in Angstroms) are significant for the analysis of vegetation: 5500, 6500, 7500, and 9000. The actual bands utilized may not be centered at these wavelengths because of the asymmetry of the spectral features. The system must be capable of providing spatially registered images in these (or other selected bands) to permit meaningful decisions based on the differential spectral reflectances. The output S/N ratio must be sufficient for these purposes.

The spatial resolution of the multispectral imager is ultimately limited by the projected size of the individual detectors. The size of the optical aperture for a given set of parameters depends inversely upon the ground resolution, and the video data rate depends upon the inverse square of the ground resolution. As illustrated in Figure 4-40, the video bandwidth of a line-array imaging system with a 100-foot IFOV and coverage in N spectral channels is given by the equation:

$$BW = \frac{NWV}{\Delta^2} \quad (32)$$

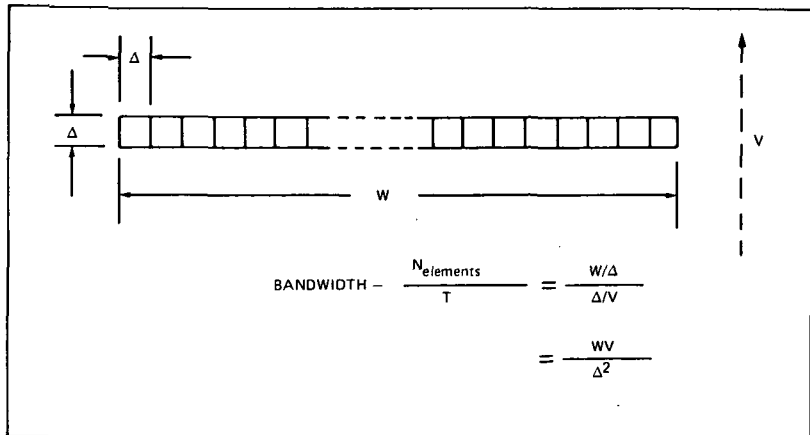


Figure 4-40. Video Bandwidth Calculation

where,

- W = swathwidth in feet
= 0.608×10^6 feet (100 nautical miles)
- V = velocity of subsatellite point in feet/second
= 2.5×10^4 feet/second
- Δ = length of resolution element in feet
= 100 feet

therefore, $\text{BW} = 1.52 N \times 10^6$ Hz.

This is the total analog video bandwidth that must be handled by the spacecraft system. Using a separate detector and amplifier for each resolution element and each spectral band (N line arrays), the individual detector amplifier bandwidth is seen to be:

$$\text{bandwidth}_{\text{det}} = \frac{V}{2\Delta} = 125 \text{ Hz} . \quad (33)$$

The angular resolution corresponding to a 100-foot IFOV system is 33 microradians or 7 arc-seconds. The modulation transfer function (MTF) of the optical system must be as high as possible at 33 microradians/half cycle to avoid loss of modulation at the focal surface. Optical considerations are covered in another section.

Characteristics of High Resolution Photodiode Self-Scanned Solid-State Systems

Table 4-3 identifies the characteristics of three possible photodiode arrays with IFOVs (ground sample distance) of 30.5 m (10 ft), 15.25 m (50 ft) and with 7.6 m (25 ft). The S/N ratios were calculated using the following equation:

$$S/N = (\pi H_{\lambda} M) \frac{(1-\phi) T_{\lambda}}{4 (f/No.)^2} \frac{\eta_o t}{NES} (MTF) \quad (34)$$

Table 4-3

Characteristics of High Resolution Self-Scanned Photodiode Solid-State Systems

IFOV	30.5m	15.25m	7.6m
Detectors/Band	6,000	12,000	24,000
Integration Time	4.7 msec	2.36 msec	1.2 msec
Video Encoding (bits)	8	8	8
Data Rate (Megabit/sec)	41	167	640
Optics Focal Length	46 cm	92 cm	185 cm
f-Number	5	4	4
High Contrast S/N Ratio at 32.8 lp/m			
Band 1	5.3	4.7	2.4
Band 4	3.4	2.9	1.5
High Contrast S/N Ratio at Low Spatial Frequency			
Band 1	26.5	23.5	12
Band 4	17.14	14.5	7.5
Approximate System Volume	0.037 m ³	0.074 m ³	0.335 m ³
Approximate System Weight	80 lbs	150 lbs	500 lbs
Approximate System Power	40 W	30 W	200 W

where,

H_λ = Radiance at the optics aperture within a given spectral band

M = Scene modulation = $\frac{C-1}{C+1}$; C = Contrast ratio

ϕ = Optics obscuration

T_λ = Optics transmission

η_o = Relative response

t = Integration time

NES = Noise equivalent signal = (mw) (msec)/m² = $\mu\text{J}/\text{m}^2$

MTF = System (MTF includes optics, detector, and image motion effects).

In each of the systems the use of catadioptric optics is anticipated, thus a typical obscuration factor of 50 percent has been chosen. The weight, power, and size numbers represent an average of results obtained from a number of independent studies, and therefore may be considered to be reasonably representative.

The following parameters have been held constant in order to present the data in parametric form.

Orbit Altitude: 926 km (500 nautical miles)

Field of View: 11.5° (185/km/100 nautical miles)

Detector Spacing: 15.2 μm (0.6 mil)

Detector NES: 1.2 $\mu\text{J}/\text{m}^2$

System MTF (including image motion): 0.2 (at 32.8 lp/mm)

Spectral Band	Radiance (W/cm ² -sr)	Optics Transmission	Relative Response
1) 0.5 – 0.6 μm	1.1×10^{-4}	0.68	0.65
2) 0.6 – 0.7 μm	0.9×10^{-4}	0.63	0.76
3) 0.7 – 0.8 μm	0.7×10^{-4}	0.58	0.80
4) 0.8 – 1.1 μm	1.1×10^{-4}	0.65	0.42

Comparison with Mechanical Scanning. At this time it is perhaps of interest to consider comparing a self-scanned solid-state imager with an advanced mechanical scanning system. Table 4-4 lists the major parameters and predicted

Table 4-4

An Advanced Mechanical Scanner Versus a Solid-State Imager

	Solid State	Mechanical
Altitude	1000 kilometer	1000 kilometer
IFOV	12°	12°
IFOV	15 microradians	43 microradians
Detectors/Band	12,000	9
Optics	f/4 Catadioptric	Catoptric (41 cm Aperture)
S/N* – High-Contrast Target, Low Spatial Frequency		
Band 1	23.5	12
Band 2	20.8	9
Band 3	15.7	5
Band 4	14.5	3
IR Bands	No Capability	3 Additional Bands 1.55–1.75 μ , 2–2.4 μ , 10.4–12.6 μ
Estimates		
Data Rate	170 megabit/second	30 megabit/second
Size	0.9 x 0.3 x 0.3 meters	2 x 1 x 0.6 meters
Weight	150 pounds	270 pounds
Power	80 watts	75 watts

*Based on parameters at the beginning of this section.

performance values for each two such systems. This comparison is for comparison's sake, and not with the idea of one system replacing the other. The mechanical scanner has the clear advantage with respect to multiband sensing, where self-scanned silicon technology offers no IR sensing capability. Also, for the three times smaller IFOV, the solid state imager requires use of 48,000 detectors. Calibration of this large number of detectors will be a formidable task compared to the relatively few point detectors of the mechanical scanning system.

There are other systems that can be conceived; however, further tradeoff analysis will be dependent on the interaction of user needs with the capabilities of technology.

Image Detection Electronic Subsystem

Figure 4-41 shows a simplified block diagram of the image detection electronic subsystem. The system consists of five functional major subsystems: photodiode array, analog processor, digital processor, timing and control, and power conditioning. The linear array photodiode chip is an LSI CMOS integrated circuit and contains a staggered linear array of photodiodes and the first levels of preamplification and multiplexing. The analog processor reduces the dynamic

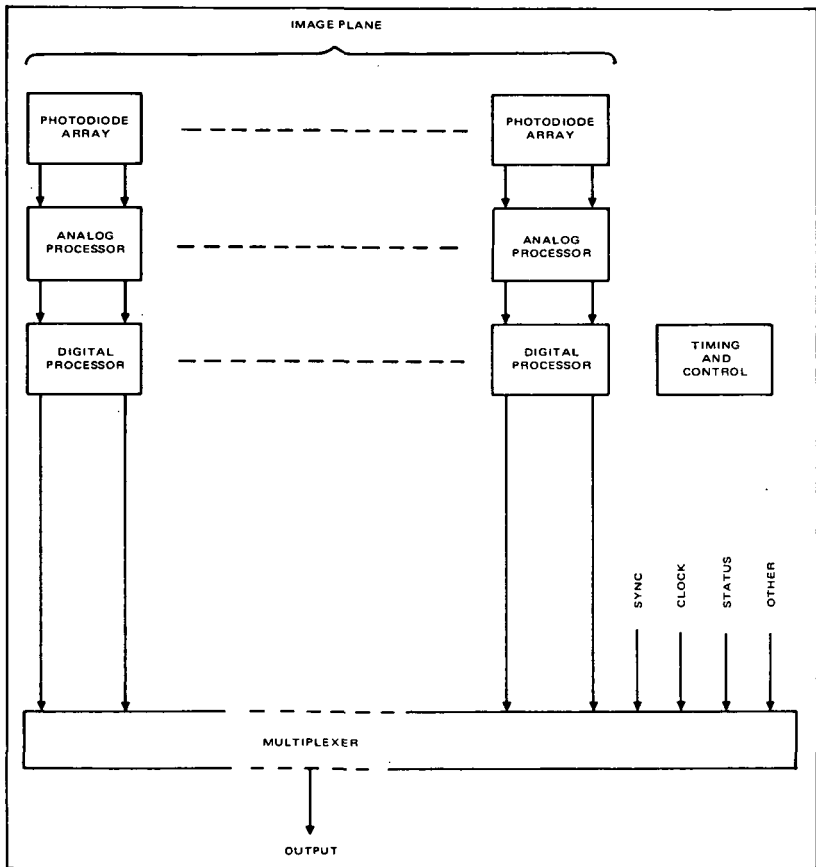


Figure 4-41. Simplified Block Diagram of Image Detection Electronic Subsystem

range requirements placed on the subsequent circuitry and increases immunity to noise generated by the detectors and its preamplifier. The digital processor converts the analog signal to digital form in order to preserve signal accuracy. After encoding, the signals are multiplexed out of a single output line. The timing and control circuits include the master clock and the necessary control circuits to properly synchronize the photodiode array, analog processors, and digital processor. The power conditioning circuitry processes the main supply power to provide regulated voltages required by all portions of the system.

Readout Approaches

There are various approaches to the readout of a diode line array. These include a pure sequential readout, a combination sequential/parallel, and an all-parallel approach. For present purposes, it is assumed that the line scan video information will be transmitted via the spacecraft over a single-channel transmitter; therefore, the readout logic of the line array can be implemented in any form as long as it is eventually reconstructed into sequential video format.

The simultaneous parallel readout of all diodes is difficult to achieve due to excessive bandwidth requirements and to the fact that the diode dual role of integration and intermediate storage would be lost.

A fully serial sequential readout of all diodes appears to be an outstanding candidate approach. The advantages are that it truly represents a line-scan system and that the output video requires no reconstruction, interleaving, or reformatting. A disadvantage is that the monolithic circuitry associated with the sequential access and readout of 6,000 or more diodes requires that the basic sampling interval system be 1 MHz whereas, inherent solid-state properties of silicon diode CMOS switching and sensing arrays limit the sequential sampling rate to lower values.

Digital Processor

The purpose of the digital processor is to convert the sampled output of the analog processor to a digital signal. To accomplish this, two primary operations on the analog data are required: (1) conversion from analog to digital, and (2) multiplexing or the division of the data stream for the integration time into frames of digital information. In addition to the basic data frame, there are frames for synchronization, error correction, and ancillary information. In addition, data restoration requirements dictate the addition of synchronization and housekeeping information into the output bit stream.

Noise and Compensation

In arrays used for imaging, there are two major sources of image degradation frequently referred to as noise. One is the random variation in output level from the individual array elements attributable to shot noise in the detectors and other conducting devices, Johnson noise in resistors, $1/f$ noise in semiconductors, and perhaps other less important sources of random fluctuations. This will be considered true noise. The other major source is variation in output level from different elements in the array due to differences in element characteristics, such as sensitivity and leakage of the detectors and offset and other variations in associated amplifiers and samplers. This type of image degradation called pattern noise is not random, and in principle, it can be measured and eliminated from the image.

Pattern Noise. Experience shows that pattern noise is primarily due to an interelement variation in dark current and, secondarily, to a variation in sensitivity. The effects of the interelement variation in a linear array sweeping over an area shows up in an image as dark and light lines parallel to the track. In a system where the ratio of two outputs is assumed to be the ratio of the input light intensities for special analysis, the results of low-light levels would be grossly inaccurate without dark-level compensation. To a large extent, the dark-level variation is due to leakage that can be reduced substantially by cooling the array. Therefore, array cooling is a major factor in reducing the uncompensated pattern noise.

Compensation. In addition to reducing the cause of pattern noise by cooling, it is possible to compensate for it to a large extent. Dark-current compensation will certainly be a function of temperature and, to a less extent, of time.

It is possible to obtain patterns of dark output at various temperatures before launch and use the data on the ground after selecting the appropriate pattern from telemetered temperature data. It is also possible to obtain dark patterns in orbit at night to check the original data with either the temperature variations naturally occurring or artificially induced. A commandable shutter could be used to provide dark current data at any time in orbit. If mounted near the focal plane, the shutter motion could be only a few thousandths of an inch so that flexing of spring material could be used, avoiding sliding or rotating surface friction with its chance of failure. This approach may require the use of a mechanically actuated shutter to obtain the black background pattern. However, the storage of this information is infrequently required and could be commanded via the spacecraft. Because this shuttering is aperiodic and commandable, it is not subject to the normal long-term wearout considerations in a space environment.

Even without any previous information, it should be possible with recorded data to adjust the bias and gain characteristics of a ground compensator for each element in the array so as to eliminate (or minimize) along-track streaking in a display. Again, this adjustment would change with array temperature and perhaps with time.

Adjustment of a bias amounts to a two-point compensation instead of the one-point compensation achieved by bias (correction for dark current) alone. However, in practice it is possible that five-point compensation will be required.

Characteristics of Phototransistor Solid-State Systems

The anticipated performance of the multispectral sensors using silicon photo-detector arrays has been analyzed, based upon the characteristics of the arrays. The method of analysis is based upon the theory developed by Shade (1967) in determining the resolving power of television camera systems, and it includes the attenuating effects of image motion, the optical system, detector size, and the frequency response of the electronic amplifier upon signal-to-noise (S/N) ratio at high spatial frequencies.

Referring to Figure 4-42, with the radiance and contrast of the scene defined, the optical parameters determine the irradiance incident upon the detector array during the exposure interval. With knowledge of detector element size and quantum efficiency, the number of photoelectrons, n , generated by each detector element during the exposure interval is determined. Assuming random distribution of the photoelectrons, the noise in this signal can be considered to be the square root of the number of photoelectrons, or $n^{1/2}$. The S/N

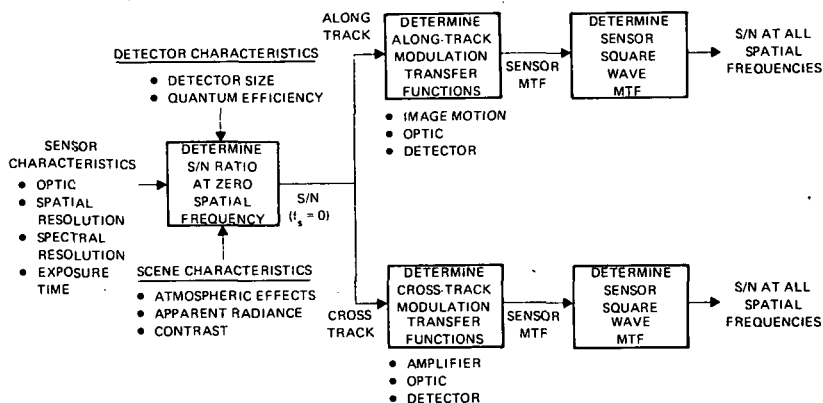


Figure 4-42. Method of Analysis of Sensor Performance

ratio at low spatial frequencies will then be $n^{1/2}$, and the S/N ratio at higher spatial frequencies can be determined by the quantity $n^{1/2} \times T(k)$, where $T(k)$ is the sensor modulation transfer function. Assuming the target and background model to be in the form of a square wave bar pattern of increasing spatial frequency, the square-wave modulation transfer function (MTF) is used. This can be obtained from the sinusoidal MTF of the sensor, which is the product of the individual MTFs defining the attenuating effects of image motion, optical resolution, detector size, and electronic/amplifier frequency response.

The spectral reflectance of typical natural objects on the terrain are illustrated in Figure 4-43 from the *Handbook of Geophysics for Air Force Designers* (1957). The apparent spectral radiance of objects of specified reflectance, as seen from orbital altitude has been computed, including the effect of atmospheric scattering of solar radiation, and is defined in Figure 4-44, from Fraser and Ramsey (1968). From these two figures, the apparent spectral radiance of objects of known reflectance from orbital altitude can be determined.

The phototransistor array is fabricated in the form of a large scale array (LSA) using triple-diffusion bipolar technology and operates in the four-step charge discharge cycle illustrated in Figure 4-45. With the photojunction initially

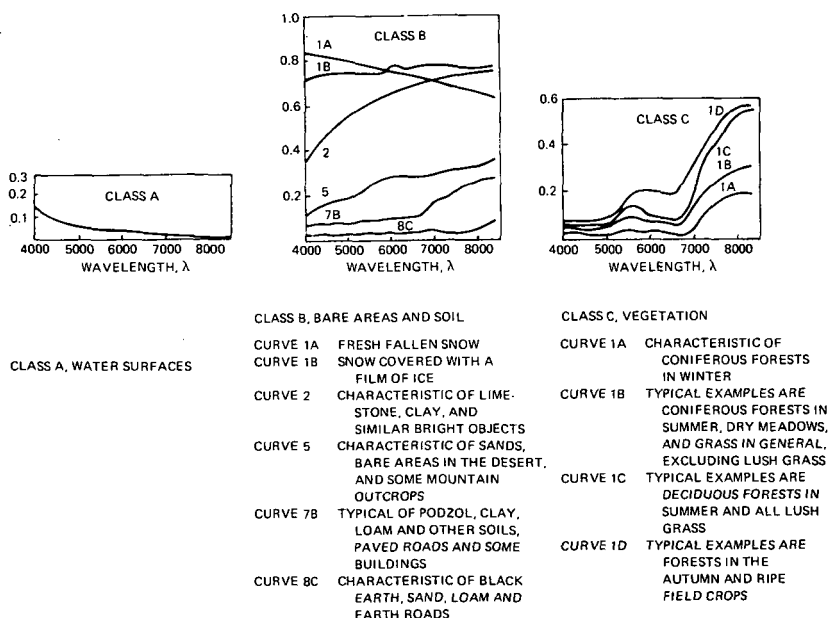


Figure 4-43. Spectral Reflectance for Eleven Types of Natural Objects as Measured by Krinov

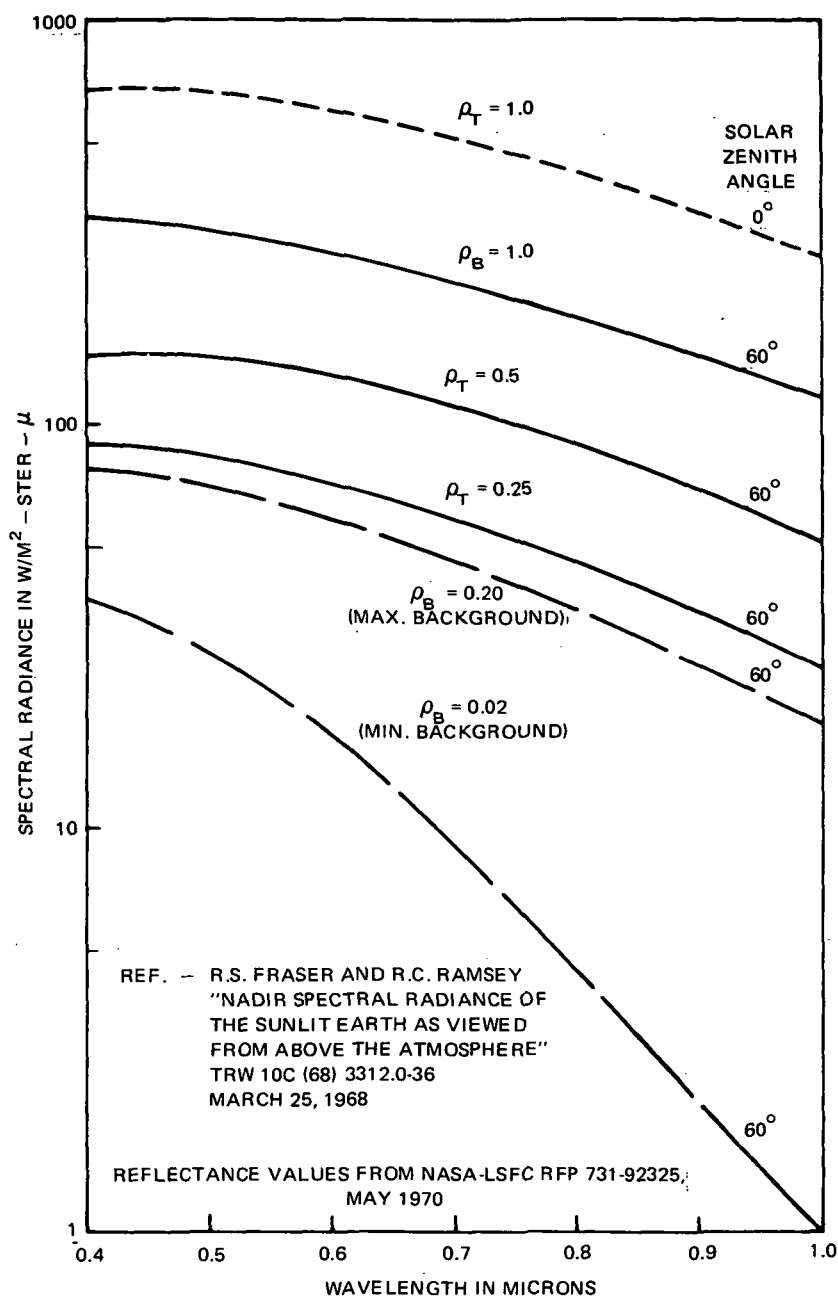


Figure 4-44. Apparent Spectral Radiance of Targets and Background from Orbit

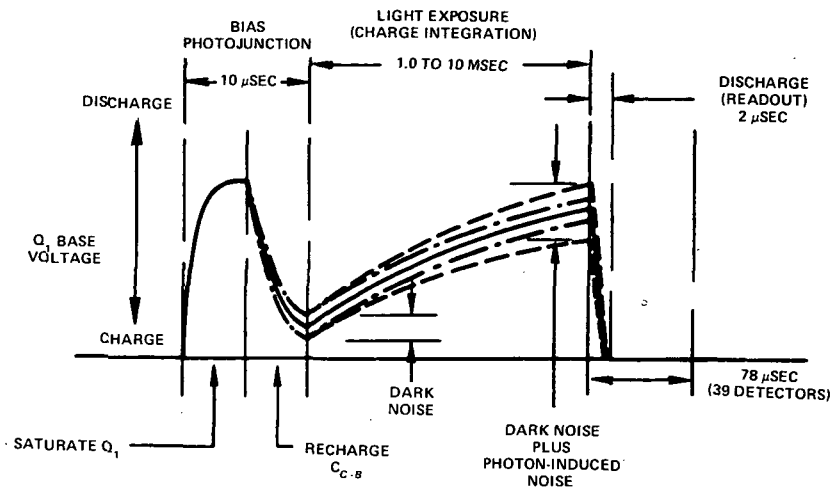


Figure 4-45. LSA Phototransistor Charge and Discharge Cycle

saturated after readout during the previous cycle, the photojunction is discharged. It is then recharged to a predetermined value prior to the light exposure interval. At this time, noise is induced in the photojunction due to the electron charge which is present, which may be considered to be dark noise. Exposure to light then causes discharge of the junction, with additional noise being induced by conversion of photons to photoelectrons, and the resultant current flow causes discharge of the photojunction. The last event in the cycle is that of restoring the charge on the photojunction to the initial value, with the amount of current required to accomplish restoration of charge comprising the signal.

The absolute quantum efficiency of the detector array for two values of junction diffusion depth, 5.2 and 13.5 microns, is shown in Figure 4-46. (This illustration was previously given as Figure 4-16 and is repeated here for convenience.) The latter diffusion depth is assumed in order to obtain increased response in the near-infrared range.

The equations used to compute performance are defined in Table 4-5, and the variables and constants in Table 4-6. With the exception of the consideration of the dark noise level of the phototransistors, the use of the equations corresponds to the method of analysis defined by O. H. Shade. Using the first equation, with the dark-noise level or NES being 1.2×10^{-6} Joules/meter², the corresponding value in terms of photoelectrons is computed to be 792 photoelectrons rms.

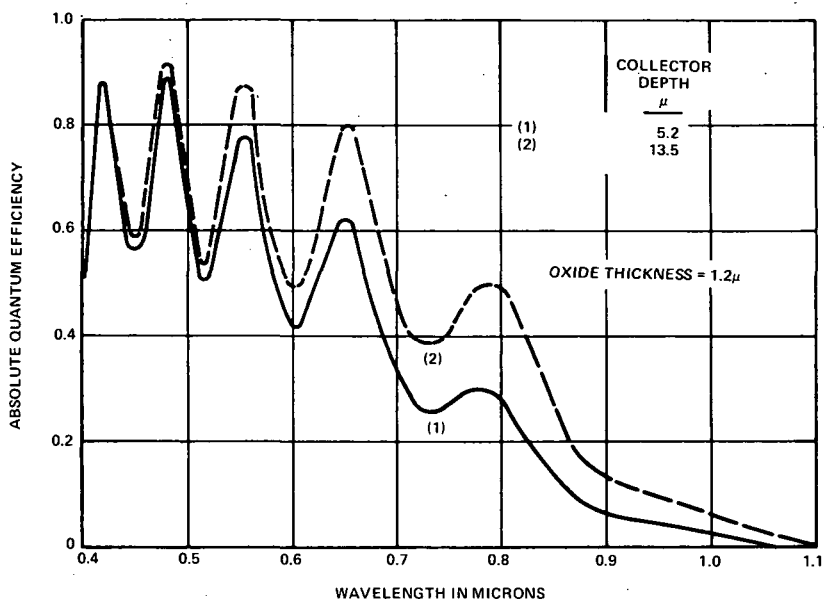


Figure 4-46. Absolute Quantum Efficiency of Detector Array (Theoretical)

Table 4-5

Parametric Equations for Calculation of Performance

RMS ELECTRON NOISE ON COLLECTOR-BASE JUNCTION AT END OF CHARGE CYCLE

$$n_1 = \frac{a}{h c} \int_{0.4\mu}^{0.8\mu} U(\lambda) \epsilon(\lambda) \lambda d\lambda \quad \text{WHERE} \quad \int_{0.4\mu}^{0.8\mu} U_{\lambda} d\lambda = N E S$$

PHOTOELECTRONS GENERATED DURING EXPOSURE INTERVAL

$$n_2 = \frac{\pi a t_o t_1}{4 F^2 h c} \int_{\lambda_1}^{\lambda_2} N(\lambda) \epsilon(\lambda) f(\lambda) \lambda d\lambda$$

S/N RATIO DURING READOUT INTERVAL (AT ANY SPATIAL FREQUENCY)

$$S/N = \frac{n_2 \Delta p T(k)}{\left[n_1^2 + n_2 \bar{p} \right]^{1/2}} \quad \text{P-P/RMS}$$

Table 4-6

Definition of Variables and Constants

n_1	= ELECTRON NOISE ON COLLECTOR-BASE JUNCTION AT END OF CHARGE CYCLE, ELECTRONS RMS
a	= AREA OF DETECTOR ELEMENT, M^2
h	= PLANCK'S CONSTANT, JOULE - SECONDS
c	= VELOCITY OF LIGHT, MICRONS/SEC.
$U(\lambda)$	= ENERGY PER UNIT AREA PER UNIT WAVELENGTH / INTERVAL ($6000K^\circ$ RADIATION), JOULES/ M^2
$\epsilon(\lambda)$	= SPECTRAL QUANTUM EFFICIENCY, PHOTOELEC- TRONS/PHOTON
λ	= WAVELENGTH, MICRONS
NES	= DARK NOISE LEVEL, ($6000K^\circ$ RADIATION $0.4-0.8 \mu$) (NOISE EQUIVALENT ENERGY DENSITY), 1.20μ JOULES/ M^2
n_2	= PHOTOELECTRONS GENERATED DURING EXPOSURE INTERVAL
t_o	= OPTICAL TRANSMISSION
t_1	= EXPOSURE TIME, SEC.
$N(\lambda)$	= SPECTRAL RADIANCE OF SCENE WITH UNITY REFLECTANCE, $W/M^2\text{-st-}\mu$
$f(\lambda)$	= SPECTRAL TRANSMISSION OF OPTICAL FILTER
F	= f-NUMBER OF OPTICAL SYSTEM
$\Delta\rho$	= DIFFERENCE IN REFLECTANCE BETWEEN SCENE HIGHLIGHT AND LOWLIGHT
$\bar{\rho}$	= AVERAGE REFLECTANCE OF SCENE
$T(k)$	= RESPONSE OF SENSOR TO SQUARE WAVE OF IN- CREASING SPATIAL FREQUENCY

The second equation is used to compute the number of photoelectrons generated during the exposure interval induced by the scene highlight radiance, with reflectance assumed to be unity. The wavelength intervals of integration are assumed to be 0.1, 0.1, 0.1, and 0.3 microns for the four spectral bands of the system, centered at 0.55, 0.65, 0.75, and 0.95 microns.

In the third equation, the S/N ratio is computed. The numerator includes the quantity $\Delta\rho$ to account for scene modulation, and $T(k)$ represents the MTF response of the sensor to a square-wave input signal. The denominator includes two items, with n_1 being the dark noise term and n_2 representing the photoelectrons induced by the average scene radiance.

The MTF in the cross-track direction is illustrated in Figure 4-47. The amplifier MTF has negligible attenuation upon the signal, having a bandwidth of 5 MHz. The optical system MTF is assumed to have a value of zero at

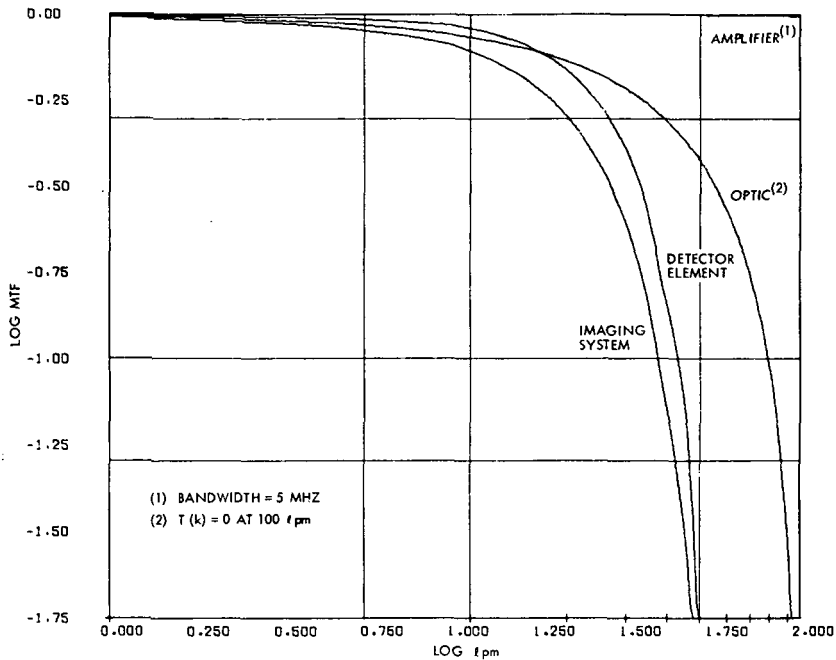


Figure 4-47. Modulation Transfer Functions (Cross-track)

100 lp/mm (limiting resolution). The MTF of the detector element is empirically determined. The product of the three MTFs is the sinusoidal MTF of the imaging system in the cross-track direction. Similarly, the sinusoidal MTF of the imaging system in the along-track direction is determined in Figure 4-48. Using a computer program developed for this purpose, the corresponding square wave MTFs of the sensor in Figure 4-49 are determined.

Results of Performance Analysis. A computer program has been developed for solution of the equations defined in Table 4-2 to permit the computation

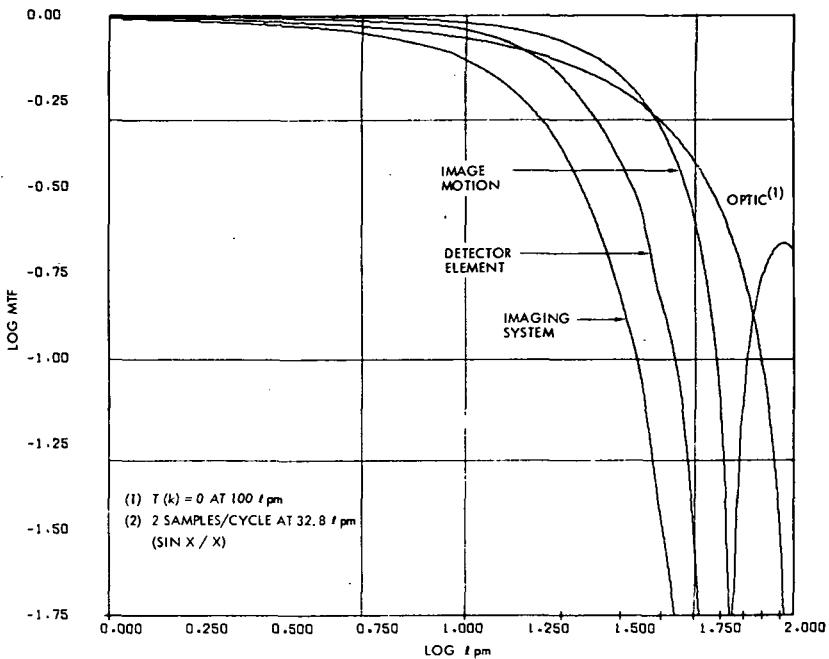


Figure 4-48. Modulation Transfer Functions (Along-track)

of S/N ratio for various levels of scene reflectance and modulation. The performance of three configurations of the sensor system, with 30-, 15-, and 7.5-meter (100-, 50-, and 25-foot) ground resolution, has been determined using this program. The results are illustrated in Figures 4-50, 4-51, and 4-52.

For the near future applications, the sensor with a 30-meter ground resolution is recommended. Referring to Figure 4-50, it is seen that at an image plane frequency of 32.8 ℓ pm, corresponding to 30 meters per object line on the terrain, an S/N ratio between 8.2 and 15 is obtained for the four spectral bands of the system, with an average scene reflectance of 0.10 and with a difference between highlight and lowlight reflectance of 0.05. Thus, it may be concluded that a very satisfactory S/N ratio will be obtained with the desired resolution of 30 meters, when observing objects on the terrain with very low reflectance and with a very small reflectance difference between the highlights and lowlights of the scene.

Imaging System Configurations and Performance

The anticipated performance of three phototransistor imaging system configurations has been determined, each having a ground coverage (swath width) of

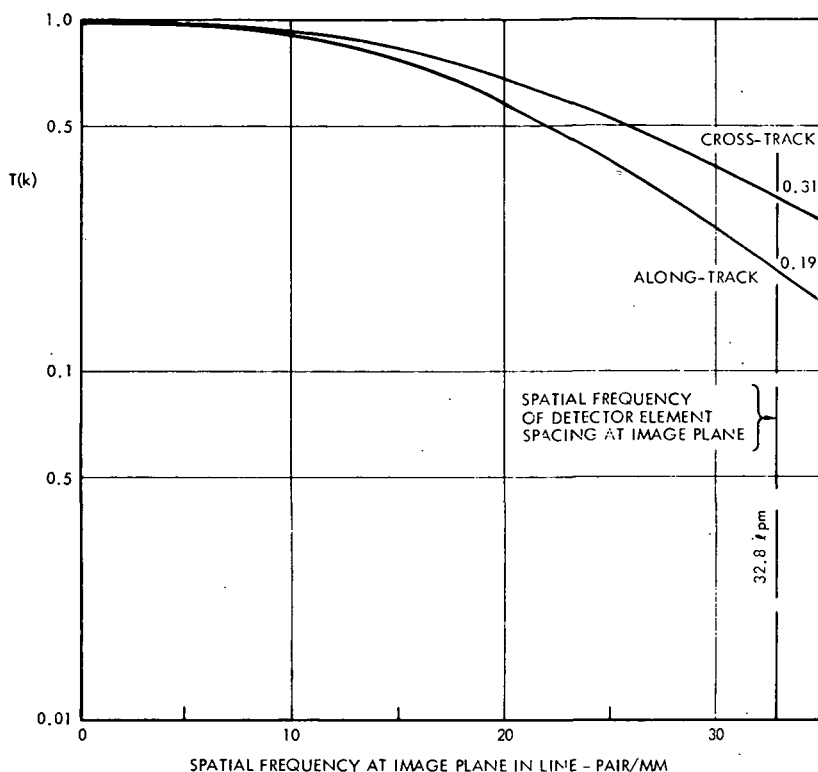


Figure 4-49. Response of Sensor to Continuous Square Wave Pattern of Increasing Line Density

185 kilometers (100 nautical miles) normal to the orbital plane, and with three values of ground resolution—7.5, 15, and 30 meters (25, 50, and 100 feet).

Imaging Sensor Specifications. Detailed specifications for the several multi-spectral sensor configurations are contained in Table 4-7. The most significant characteristic is that of data rate. For the configuration with a ground resolution of 100 feet, the uncompressed data rate will be 51.3 megabits/second. However, a number of data compression techniques may be used to make this rate compatible with current data-link capabilities. By compressing the data by a factor of 2.5/1, a data rate of 21.7 megabits/second may be obtained, which is compatible with current data bandwidth capability.

Preliminary Design Configuration

The physical configurations of the three sensors are illustrated in Figure 4-53. These estimates are based upon a detailed examination of the component count

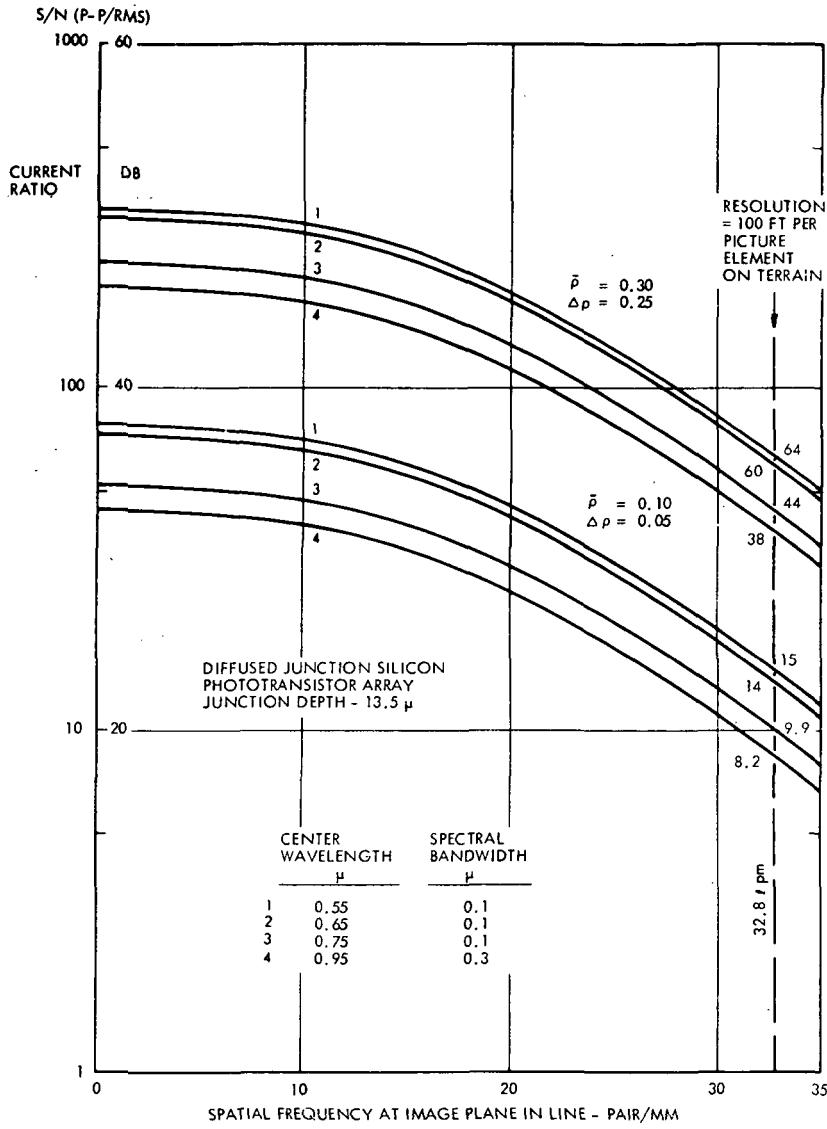


Figure 4-50. Solid State Multispectral Sensor S/N Ratio and Resolution for Two Values of Scene Contrast (30M Resolution, 46 cm FL f/5.4 Optic)

for each of the three sensors. For the sensor with 30 meter resolution, a refractive optic with an f-number of 5.4 and a focal length of 46 centimeters will be used. A pointing mirror will be used for off-nadir pointing capability (Figure 4-54). Separation of the energy from the scene into the four spectral bands will be accomplished by the use of dichroic filters and prismatic beam

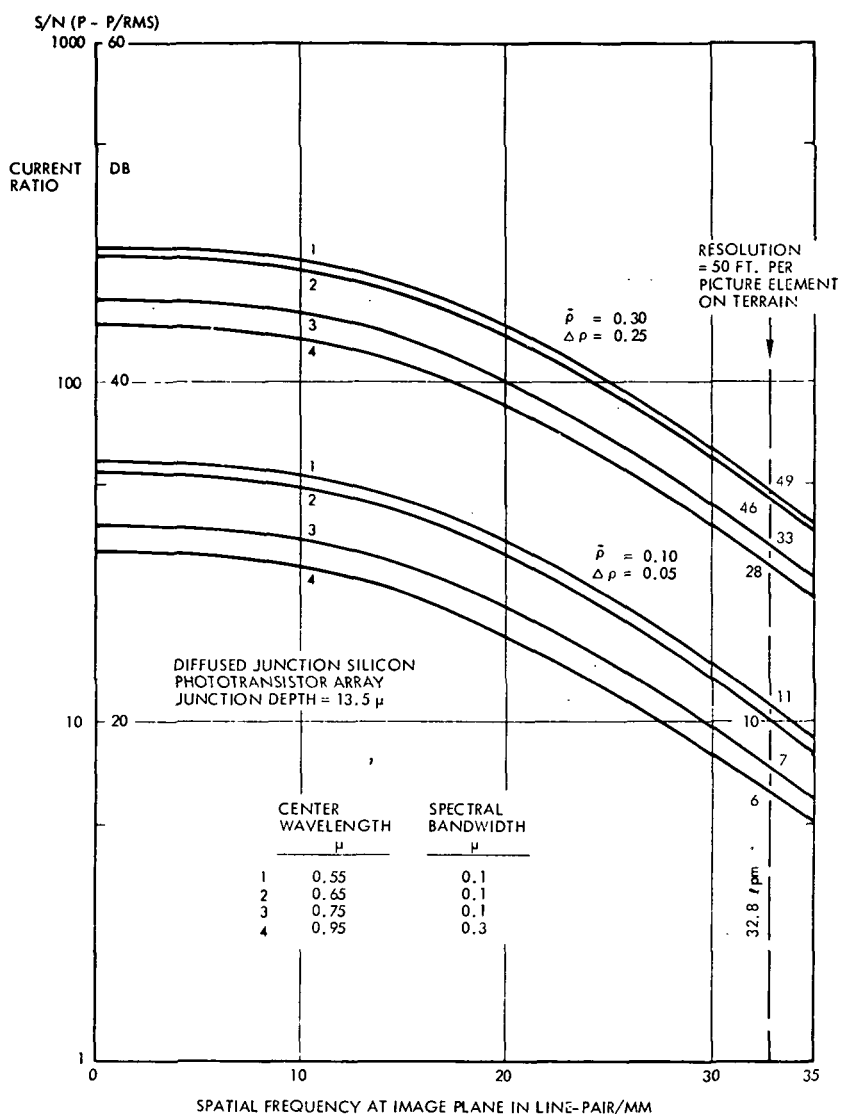


Figure 4-51. Solid State Multispectral Sensor S/N Ratio and Resolution for Two Values of Scene Contrast (15M Resolution, 90 cm FL $f/4.5$ Optic)

splitters. A feasibility model of this optical system has been developed. Four arrays of detectors are used, one for each spectral band, with each array consisting of 6045 detector elements. Data processing (conversion of analog data to digital form in five parallel data channels) is accomplished in a data processing electronics unit external to the detector array and preamplifier assemblies.

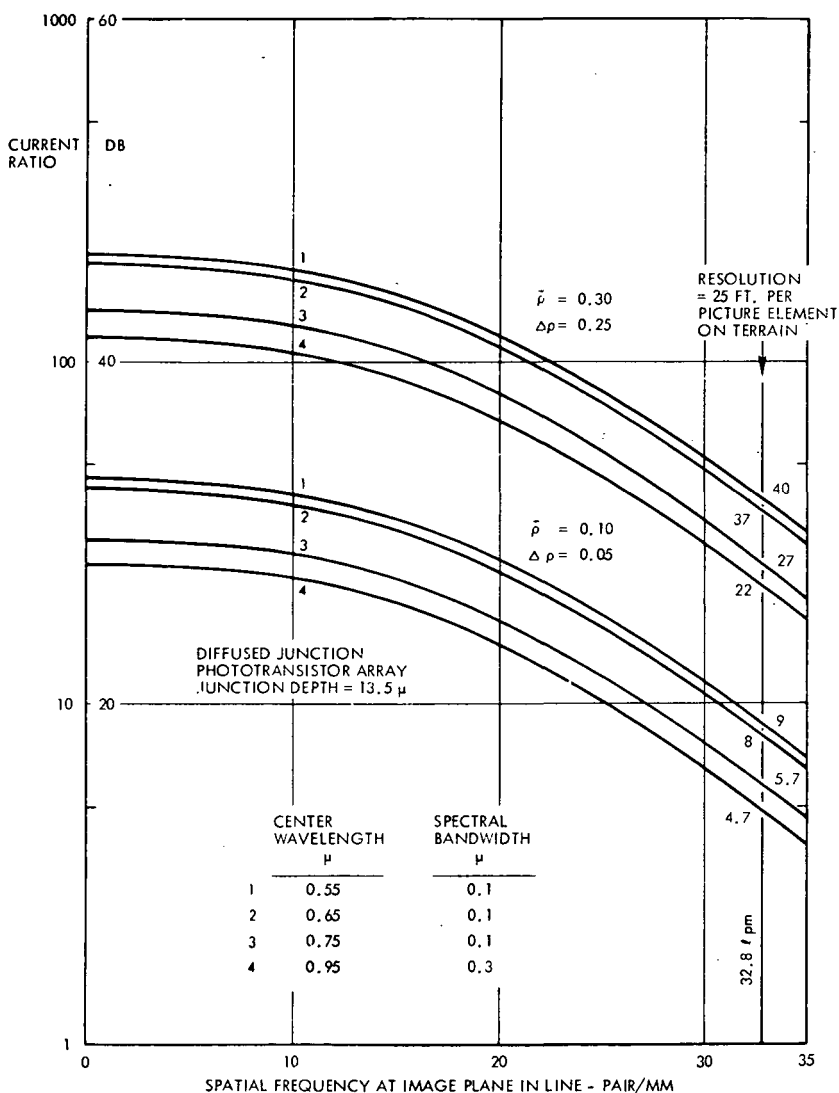
$S/N (P = P/RMS)$ 

Figure 4-52. Solid State Multispectral Sensor S/N Ratio and Resolution for Two Values of Scene Contrast (7.5M Resolution, 185 cm FL f/3.8 Optic)

Total weight, volume, and power estimates for the instrument are: 32 kilograms (70 pounds), 0.04 meters^3 (1.3 feet³), and 134 watts.

Data Collection Facility. The data collection facility consists of a data collection processor, a disc memory and magnetic tape transport with formatter.

Table 4-7
Characteristics of Multispectral Sensors for 30, 15, and 7.5 M
Ground Resolution

Item	30 M Resolution	15 M Resolution	7.5 M Resolution
• Mission Parameters Altitude Swath width Ground resolution Pointing capability	920 km (496 n. mi.) 185 km (100 n. mi.) 30 M/picture element ± 185 km Cross-track	920 km (496 n. mi.) 185 km (100 n. mi.) 15 M/picture element ± 185 km Cross-track	920 km (496 n. mi.) 185 km (100 n. mi.) 7.5 M/picture element ± 185 km Cross-track
• Spectral Parameters Number of bands Center wavelengths Spectral bandwidths	4 0.55, 0.65, 0.75, 0.95 μ 0.1, 0.1, 0.1, 0.3 μ	4 0.55, 0.65, 0.75, 0.95 μ 0.1, 0.1, 0.1, 0.3 μ	4 0.55, 0.65, 0.75, 0.95 μ 0.1, 0.1, 0.1, 0.3 μ
• Detector Parameters Number of arrays Elements/array ¹ Detector spacing on terrain	4 6045 (31 chips) 30 M	4 12090 (62 chips) 15 M	4 24180 (124 chips) 7.5 M
• Intensity Parameters (at 0.55 μ) Required S/N at $\Delta\rho = 0.05$ (at max. scene frequency) MTF at max. scene freq. S/N at zero scene freq. ($\Delta\rho = 0.05$) Max. scene reflectance range Max. scene radiance range Required dynamic range	4/1 0.19 21/1 0.02 to 0.76 12.5/1 ² 263/1	4/1 0.19 21/1 0.02 to 0.76 12.5/1 ² 263/1	4/1 0.19 21/1 0.02 to 0.76 12.5/1 ² 263/1
• Data Parameters Video encoding level LSA gain variation (3 σ) Analog electronics variation (3 σ) Total encoding level Exposure time ¹ Data rate (w/o compression) Data rate (2.5/1 compression) Data rate (3.33/1 compression)	8 bit (256 levels) 2/1 2/1 10 bit 4.7 msec 51.3 mb/s 21.7 mb/s 16.8 mb/s	8 bit (256 levels) 2/1 2/1 10 bit 2.36 msec 205.2 mb/s 86.8 mb/s 67.3 mb/s	8 bit (256 levels) 2/1 2/1 10 bit 1.18 msec 820.8 mb/sec 347.2 mb/sec 269.2 mb/sec
• Optical System Type Focal length f-number	Refractive 46 cm 5.4	Catadioptric 36 cm 4.5	Bouwers - Maksutov 185 cm 3.8

¹Kell factor of 1.0 both cross-track and along-track

²Includes atmospheric backscatter

Input data are received from analog to digital converters working in parallel and controlled by a five 10-bit programmer. A block diagram of the system is shown in Figure 4-55.

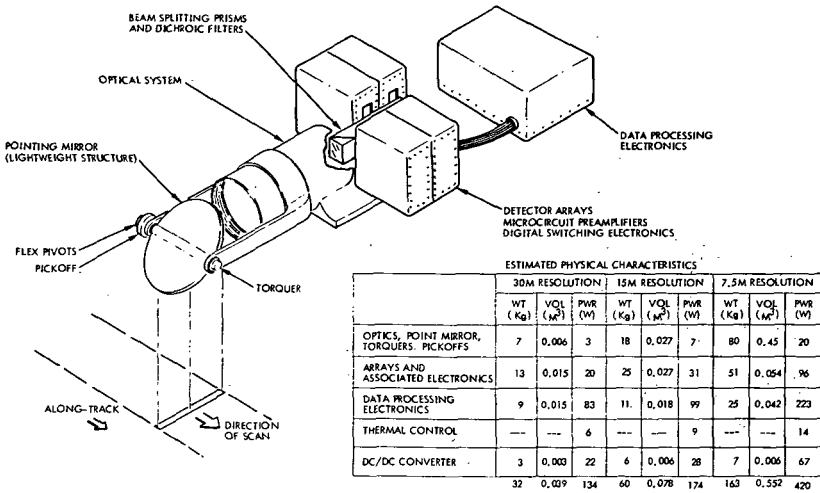


Figure 4-53. Flight Hardware Configurations

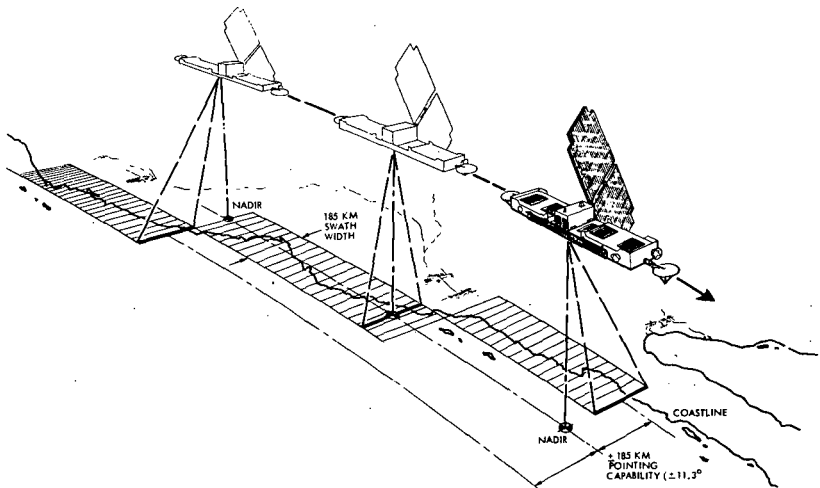


Figure 4-54. Off-Nadir Pointing Capability

The data collection facility performs the function of recording input data on magnetic tape in a format suitable for computer processing. Data buffering in the form of an LSI random-access memory in the processor and the disc memory is required to attain data rate compatibility with the tape recorder.

The solid-state multispectral imaging sensor and data collection facility are illustrated in Figure 4-56.

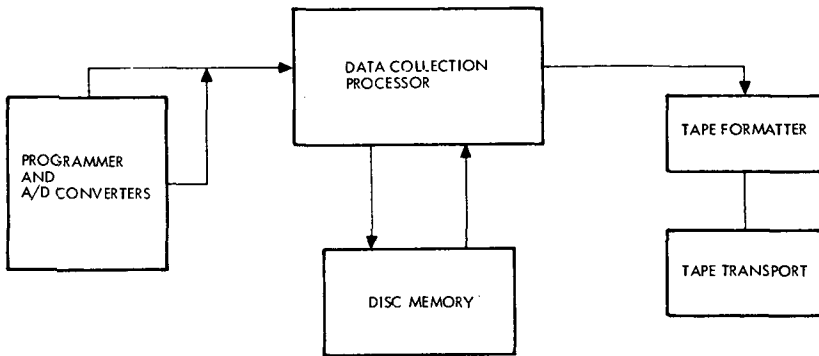


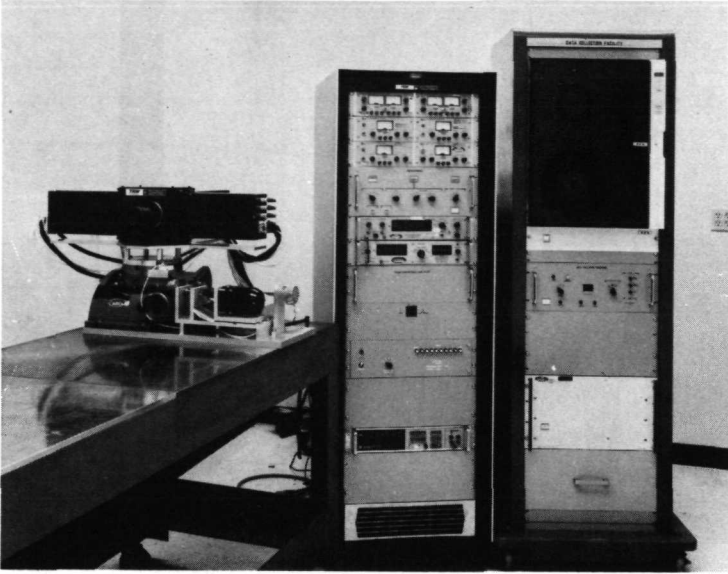
Figure 4-55. Data Collection Facility

Image Generation Software. A software program was developed for reformatting of the data collected on digital tape to obtain compatibility with the laser beam film writer used for image reconstruction at a vendor's facility. This program also provided for calibration of the detector arrays, using 160 samples of the output of each detector element at each level of a grey scale containing seven shades of grey, in order to eliminate the effect of nonuniform responsivity of the detector elements of the phototransistor array. Linear interpolation of the detector current levels between grey scale calibrations was employed. A 16-step grey scale was also printed on film by the laser beam film writer, in conjunction with the record of the imagery obtained in the laboratory.

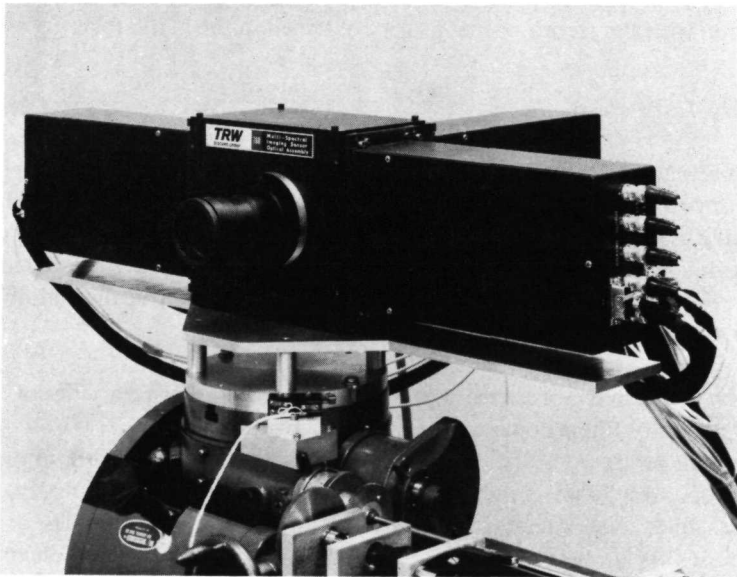
Laboratory Test Results

Two high-resolution images were obtained in the laboratory tests using illuminated negatives of typical aerial scenes as test patterns. These images were obtained using one array of the sensor, sensitive in the 0.5 to 0.6 micron range of the spectrum. The array consisted of five active chips, each having 195 detector elements, for a total of 975 elements. (One additional chip at the end of the array was inactive, being damaged in assembly.)

Calibration of the detector elements was first performed by using a series of six neutral-density filters in place of the negative of the aerial scene. The irradiance levels produced at the image plane of the sensor during calibration ranged from 0 to 0.54 watts/meter² within the 0.1 micron spectral bandpass. This corresponds to an integrated energy level from 0 to 600 microjoules/meter² during the array integration interval of 1.14 millisecond. The nominal operating range of the detector array is from 0 to 540 microjoules/meter². The calibration data recorded on magnetic tape was used in subsequent reconstruction of the video data.



Solid State Multispectral Sensor



Sensor and Data Collection Facility

Figure 4-56. Feasibility Model of Imaging Sensor and Data Collection Facility

In order to record the video data on magnetic tape, a disc memory was used to permit high-speed recording of data from the array and slow-speed playback onto magnetic tape. The capacity of the disc corresponded to 160 sequential exposures of data at an encoding level of 10 bits, for a total load of $160 \times 975 \times 10 = 1.56 \times 10^6$ bits. The time required to load the disc was 192 msec; the disc was then played back over a time period of 12 seconds into the magnetic tape recorder. With the capacity of the disc being limited to 160 exposures of the array, six sequential loads of the disc were required to collect the full frame of data, consisting of 960 sequential exposures. This required scanning of the test pattern in six sequential operations, with the rotary head being reindexed between each operation. Indexing was accomplished by use of a Norden digital encoder on the rotary head, geared up with a gear ratio of 120/1, and with 1024 counts per revolution of the encoder. Each count corresponded to one-third of one picture element. The sensor was rotated at a rate of 0.25 radians/second.

Referring to the photographic print of the first image obtained (Figure 4-57), the information content of the photograph is as follows. On the left hand side



Figure 4-57. Initial Image Obtained in Laboratory Tests

of the photograph a computer-generated grey scale is reproduced to determine the linearity and dynamic range of the laser beam film writer. This grey scale consists of 16 steps, over a total density range from 0.08 to 1.18 in the film negative reproduction. This density range corresponds to 83 percent to 6.6 percent in terms of transmission. Each individual step of the grey scale represents a change in density of 0.069, corresponding to an increase in scene brightness by a factor of 1.18 per step. In the original film negative produced by the laser film recorder, 13 shades of grey are apparent, representing the limit in dynamic range of the recording system.

The fine dotted line on the right edge of the grey scale indicated the density of the detector elements, with a white dot and a black dash each corresponding to one detector element. The image was scanned from left to right with a total of 960 sequential exposures of the array, each cycle interval being of 1.20 milliseconds average duration. The total time to scan the image was 1.15 seconds.

With respect to resolution, an examination of the image of the barge in the lower left corner of the photograph reveals that objects approximately twice the size of a picture element are clearly discernible. The size of a picture element is indicated by either a dot or dash on the right side of the grey scale. The density of the detectors on the array of the sensor corresponds to 32.8 line-pair/millimeter.

Some noise and several streaks are apparent in the upper portion of the image. It was subsequently determined that this was due to cross-talk in the random-access memory used for buffering of the video data prior to recording on the data disc. In subsequent recording of data this effect was eliminated by sequentially loading and unloading of the memory. In the second image these defects were eliminated (Figure 4-58).

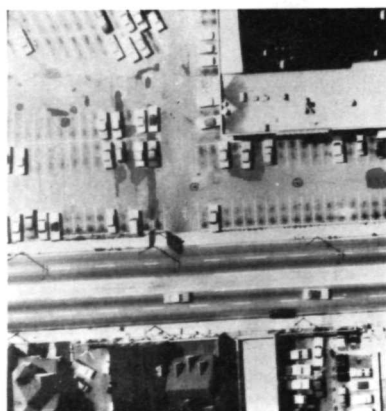


Figure 4-58. Second Image Obtained in Laboratory Tests

BIBLIOGRAPHY

- G. F. Amelio, W. J. Bertram, Jr., and M. F. Tomsett, "Charge-Coupled Imaging Devices: Design Considerations," IEEE Trans. on Electron Devices, ED-18, No. 11, pp. 986-992, 1971.
- R. S. Fraser and R. C. Ramsey, "Nadir Spectral Radiance of the Sunlit Earth as Viewed from Above the Atmosphere," TRW IOC (68) 3312-36, March 25, 1968.
- W. B. Joyce and W. J. Bertram, "Linearized Dispersion Relation and Green's Function for Discreet-Charge-Transfer Devices with Incomplete Transfer," Bell System Technical Journal, Vol. 50, pp. 1741-1759, 1971.
- O. Shade, Sr., "The Resolving-Power Functions and Quantum Processes of Television Cameras," RCA Review, Vol. XXVIII, No. 3, pp. 460-534, Sept. 1967.
- R. J. Strain, "Properties of an Idealized Traveling-Wave Charge-Coupled Device," IEEE Trans. on Electron Devices, ED-19, No. 10, 1972.
- U.S. Air Force *Handbook of Geophysics for Air Force Design*, U.S.A.F. Cambridge Research Center, pp. 14-1 to 14-2, 1957.
- P. K. Weimer, W. S. Pike, M. G. Kovac, and F. V. Shallcross, "The Design and Operation of Charge-Coupled Image Sensors," Paper Presented to the IEEE Solid State Circuits Conference, Philadelphia, Feb. 15, 1973.
- M. H. White, D. R. Lampe, F. C. Blaha, and I. A. Mack, "Characteristics of Surface Channel CCD Image Arrays at Low Light Levels," Solid State Circuits Conference Journal, 1973.

ATTACHMENT A

SPECTRORADIOMETRIC ACCURACY—ATMOSPHERE AND INTERNAL AND EXTERNAL CALIBRATION

(Notes by P. N. Slater)

Visual and Near-IR Range

Even at its clearest, the atmosphere does not approximate a Rayleigh atmosphere where scattering increases in inverse proportion to λ^4 . A clear atmosphere scatters according to a $\lambda^{-0.7}$ to $\lambda^{-2.0}$ law. A clear atmosphere with a large component of nonselective scattering, typically shows 50 percent more scattering in the blue than the red. The effect of atmospheric scattering on spectral signatures is a function of many variables:

- Sensor altitude
- Atmospheric haze condition
- Solar altitude
- Wavelength band
- Angle of view from nadir
- Azimuth of angle of view
- Polarization.

A brief indication of the variability in spectral signatures is seen if all the above factors are constant except atmospheric haze condition and solar altitude. Weather observers categorize atmospheric haze as follows:

<u>Visibility</u>	<u>Atmospheric luminance in candles/meters²</u>
Very clear	2500
Light haze	3500
Medium haze	5000
Heavy haze	7000

To a first approximation the illuminance level at the aperture of the sensor E_s is given by

$$E_s = E\rho\tau + \pi L \quad (1-1)$$

where E is the solar and sky illuminance at the ground scene of reflectance ρ , τ is the atmospheric transmittance assumed 0.8, and L is the atmospheric luminance. E varies from 5×10^4 meter candles at 30 degrees solar altitude to 15×10^4 meter candles at 90 degrees. Now, the extreme values of the range of illuminance levels at the sensor is given by

$$E_s = 5 \times 10^4 \times 0.05 \times 0.8 + 7000 \pi \cong (0.2 + 2.0) \times 10^4 \quad (1-2)$$

and

$$E_s = 15 \times 10^4 \times 0.05 \times 0.8 + 2500 \pi \cong (0.6 + 0.8) \times 10^4 \quad (1-3)$$

The total illuminance varies from 2.2×10^4 meter candles to 1.4 meter candles. It is of vital significance to those interested in extracting reflectance values from image plane illuminance values that in one case the light reflected from the scene is 43 percent of the total light incident at the sensor and in the other case it is 9 percent.

Some in the user community have planned on measuring ground reflectance differences from day to day, with sun altitude, etc.; the same, to accuracies of 1 percent or better. If we look at the most favorable solar altitude angle of 90 degrees, the variation in the signal at the sensor can be 100 percent due to changes in atmospheric haze from day to day, for a ground reflectance of 5 percent.

There are also higher frequency variations in haze effects. These have been measured at the Optical Sciences Center, University of Arizona, to vary from 0 to 5 percent in the frequency range 0–1 KHz. The measurements are preliminary and by themselves indicate that a reasonable limit on sensor calibration accuracy is 0.5 to 1 percent as a relative value. These measurements were made in the visible spectrum. Corresponding measurements in the IR are not known to exist.

IR Range

In the 10-12 micron range it is no longer necessary to consider the atmospheric path radiance and its effect on the signal. However, due to variations

in atmospheric constituents—mostly water vapor—the atmospheric transmission does vary. This variation causes an apparent error in the measurement of earth surface temperature.

The transmission of the atmosphere varies from approximately 0.45 for a tropical atmosphere to 0.9 for a dry arctic atmosphere. This effect alone produces an error of approximately 50 K in the absolute temperature reading.

Conclusions and Recommendations

The band to sum-of-all-bands ratioing technique is a frequently used way of reducing variability due to atmospheric conditions in spectral signatures. However, substantial ($\sim 10\%$) variations can still occur in spectral signature determinations particularly in the visible spectrum. Measurements of ground reflectance values from high altitudes can vary by 100 percent due to atmospheric conditions, again in the visible. Reference to atmospheric models can reduce these variations.

A more direct solution is the utilization of simple, automatic, ground-based equipment designed to make atmospheric measurements in the visible and IR at the time of spacecraft overflight. Corrections to spectral reflectance data could be relayed to the spacecraft. Corrected reflectance data would be relayed to ground and uncorrectable reflectance data would be relayed to ground and uncorrectable reflectance data, owing to poor atmospheric conditions, would be erased. A global network of such automatic atmosphere sensing ground stations is conceivable, the density varying according to interest in the surrounding earth surface, rapidity of average change-with-distance of prevailing atmospheric conditions, and so forth.

With regard to internal calibration of the sensor, it would seem that ± 1 percent relative spectroradiometric accuracy is meaningful during monthly periods. In terms of absolute values the calibration should probably be as good as ± 10 percent.

CHAPTER 5
SENSOR RELATED TECHNOLOGY

PANEL MEMBERS

M. Maxwell – *Chairman*

**F. C. Billingsley
J. Edmond
R. Fenn
A. Guha
D. Landgrebe
B. Steiner**

Additional Technical Material Supplied By:

**J. Moyer
J. Hayes**

SENSOR RELATED TECHNOLOGY

PANEL CONCLUSIONS AND RECOMMENDATIONS

This panel investigated various sensor-related systems, programs, techniques and equipment concepts as they relate to the advanced sensor requirements being developed by the other panels. Various factors—calibration, atmospheric effects, platform attitude, and ground data processing—all affect the ability of imagers and scanners to produce the information desired by users. In some cases, these factors constrain the sensor performance, while in others they afford opportunities for information enhancement by image manipulation and data management. The panel members placed major emphasis on identifying those specific factors that might constrain or otherwise limit the development and utility of data to be acquired through advanced imaging and scanning sensors.

The discussion categories established by this panel in the course of investigating sensor related technology were:

- Atmospheric Effects
- Radiometric Calibration
- Platform Effects
- Sensor Data Systems
- Data Correction and Image Generation
- Image Processing
- Sensor Related Aspects of User Data Analysis.

Atmospheric Effects

Conclusions

The current understanding of the atmosphere makes it very difficult to estimate the absolute surface reflectance of elements in a scene. However, atmospheric effects can be estimated with sufficient accuracy to allow meaningful information on reflectance ratios between near elements (both spatially and spectrally) to be extracted from the data. Future NASA programs should include auxiliary

sensors, flown with imagers, to locate and allow the automatic identification of regions where the data are significantly disturbed by haze or thin cirrus clouds.

Recommendations for Future Efforts in Atmospheric Transmission Studies

Atmospheric optical effects may reduce the imaging capabilities of satellite-borne optical systems to about 50-90 percent of their performance in the absence of an atmosphere for a clear atmospheric condition, and to less than 10 percent of their performance in a hazy atmosphere, or for low sun angles and very short wavelength. A variability with space and time must be expected of approximately a factor of 10. It is, therefore, quite obvious that any quantitative remote sensing experiment of surface properties will require a rather accurate knowledge of the atmospheric effects on the image quality of the optical/IR imaging system. In this way a correction for these effects can be made and the inherent features and characteristics of the object scene can be restored.

Efforts in two directions will be required to achieve this:

- Develop improved atmospheric models and theoretical concepts which can be used to compute the specific atmospheric attenuation or noise parameters.
- Conduct concurrent measurements of atmospheric optical quantities with the remote sensing observations.

Since it can be shown that the contrast transmittance of the atmosphere varies by about 50 to 60 percent of its value per one mile change in surface visibility, assuming similar vertical distributions of haze particles, the prediction accuracy for atmospheric contrast transmittance can be improved by about 50 percent if one applies atmospheric models with different surface visibilities as an input. With sufficiently detailed and representative atmospheric models, it should be possible to predict optical parameters from model calculations to an accuracy of 30 to 50 percent of the actual value for most conditions. Any further improvement will require direct concurrent measurements.

Measurement programs for improvements in atmospheric models, as well as for concurrent monitoring, will have to include total atmospheric beam transmittance, contrast transmittance, modulation transfer function (MTF), atmospheric IR emission depending on the conditions of the sensing system (wavelength band, receiver aperture, etc.). Such measurements are basically within the present state of the art; however, they will require new developments in technology.

Atmospheric transmittance is independent of direction of path and can, therefore, be obtained from ground measurements. A program of solar transmission measurements at a selected number of weather stations should be initiated as soon as possible. Theoretical relationships between upward and downward directed (sky radiance) path radiances should be examined to establish possible methods for deriving upward directed path radiances and contrast transmittances from surface measurements. One area of promising potential would be the development of the airborne (or satellite-borne) LIDAR backscatter system.

Radiometric Calibration

Present Situation

NASA has done a commendable job of defining its broadest radiometric goals for present sensors. These goals are remarkably close to those still being specified four to eight years hence by many users. The 5 percent absolute accuracy goal of ERTS-1 remains a suitable general target for future platforms. However, NASA is not yet able to assure its users of the detailed radiometric fidelity that they would like. Problem areas are as follows:

- Detailed Radiometric specifications for present systems were either not provided by NASA, as was the case for VISSR, or were furnished initially only in general fashion, such as the "5 percent absolute accuracy" figure for ERTS-1.
- Detailed assurance of compliance with these few specifications has generally not been provided either by the vendors or by NASA. This deficiency arises partly because the best laboratory standards of spectral irradiance until recently have been only 5 percent standards, which is the total ERTS-1 tolerance.
- NASA/JSC does not yet possess the facilities required to verify compliance with radiometric specifications. NASA/GSFC has not been supplied by NBS with the standards and techniques to assure compliance with the ERTS-1 specification for "5 percent absolute accuracy."

Recommendations

The following recommendations are stated for radiometric calibration. Activity in the cited areas would be small compared with the total effort involved in future systems. But such activity would provide the only reasonable assurance that quantitative user needs would be fulfilled.

- Radiometric calibration performance should be considered at the start and throughout the design of future remote sensing systems. This performance should become a conscious part of all trade-offs involved.
- The two different fundamental approaches to on-board calibration, large diffuse sources and focal-point sources, should be evaluated quantitatively.
- Radiometric specifications for future platforms should be made sufficiently complete to assure fulfillment of user expectations or realistic trade-offs of these should be made. For example, distinctions among the various types of calibration, absolute, relative spectral, temporal stability, should be drawn explicitly.
- Firm demonstration of fulfillment of these specifications should be required of suppliers.
- Independent radiometric test facilities of 1 to 5 percent accuracy with simulated space environment would facilitate fulfillment of the NASA mission.
- The long term performance of potential radiometer components, optics, detectors, and calibration sources, must be examined, both in the laboratory and under simulated space environment, so that intelligent trade-offs can be made in the components and systems selected.
- SkyLab might usefully be employed to verify the stability of the most promising components under real space environment and to compare the scanner data with local data at five-day intervals in order to explore atmospheric changes.

Platform Effects

State-of-the-Art Survey

Orbit estimation accuracies of 10-30 meters, one sigma, for an ERTS-type orbit should be possible in 4 to 8 years with presently planned developments. This seems adequate to position earth sensor imagery in a cartographic reference system. In absence of significant internal distortions in the sensor picture display, excellent positioning may be achieved by using ground control points.

Pointing errors in pitch and roll affect local verticality and distort the frame. Rotation about the local vertical (yaw error) affects cartographic positioning and, in a digital data processing system, increases complexity of data processing.

Stabilization errors (short term attitude variations, or jitter) affect line-to-line registration of the image produced by a scanning sensor. Present state-of-the-art for ERTS-1 is ± 0.4 degrees and ± 0.015 degrees per second. Significant improvements are practicable within 4 to 8 years and the main question is to establish the definite needs of the user. One order of magnitude improvement is a routine developmental task and does not require a technological breakthrough.

Attitude determination is one area that needs immediate attention. Present state-of-the-art for ERTS is about one-tenth of a degree. This may need to be improved by approximately two orders of magnitude so that geometric corrections may be applied to minimize loss of resolution as well as to remove internal distortions in the image produced by a scanning sensor. At present there is no operational system which can meet this need. Design and development work in this area is under way and should be pursued.

Recommendations

The following recommendations are made as a result of the platform effects investigation:

- In the future spacecraft designs, spacecraft rotation about local vertical (yaw motion) should be controlled as closely as practicable. This would reduce storage requirements for applying geometric corrections and simplify digital data processing.
- Spacecraft verticality (pitch and roll motions) should be stabilized to maintain the integrity of one frame of picture produced by scanning sensors. This stabilization of short term attitude behavior should be controlled to at least one-sixth of the IFOV per line to maintain reasonable MTF. No great effort need be made in precision pointing control of the spacecraft unless it can be controlled to these accuracies. This assumes that the spacecraft does not carry an accurately pointable gimbaled sensor, and that local readout ground stations do not require cartographic accuracy in their pictures.
- A precision attitude determination system should generate attitude annotation data to accuracies of at least one-fourth of an IFOV which can be fed into digital data processing systems for automatic image rectification on a line-to-line basis. This system should provide geometric corrections for attitude (and residual orbit ephemeris) errors and be based on a gyro-star sensor and possibly ground control point measurements.

- It is recommended that a meeting be organized between several experts from various disciplines to examine the methodology of geometric corrections of scanned images in a digital data processing system. The results of this meeting will allow minimization of total program cost; both spacecraft and ground data processing systems.

Sensor Data Systems Concepts

State-of-the-Art

Data rates under 280 million bits per second (megabits/sec) and 7 bit accuracy can be multiplexed at the present time. Onboard storage systems could be developed to store from 30 to 200 megabits/sec. Ground data recorders currently can accept data at 30 megabits/sec, with 60 megabits/sec a reasonable improvement. Rates of 100 to 200 megabits/sec are within reach, but will require considerable development.

Conclusions

As stated, multiplexers for high resolution sensors with output rates to 280 megabits/sec have been demonstrated in a breadboard system. At a maximum analog-to-digital conversion of 20 megasamples/sec, 7-bit accuracy is marginal, while 8 to 9-bit accuracy is unattainable using currently designed circuitry. At lower sampling rates (10 megasamples/sec), higher accuracy (8 or 9 bits) is feasible. Thus the development of a time division Pulse Code Modulation multiplexer for these data rates is within the state-of-the-art; but, if higher accuracy ($< 1/4$ of 1%) is required, more development will be required.

Data Correction and Image Generation

Conclusions and Recommendations

A number of standard ground processing operations will be required to convert as-received data from advanced sensors into images and data forms which facilitate analysis and interpretation. These operations include:

- Radiometric calibration and compensation of detector variations
- Geometric registration, as required of sensor data
- Conversion of sensor data to computer-compatible tapes

- Generation of standard-scale annotated imagery, corrected for sensor geometry, platform altitude, attitude rates, earth rotation, and perhaps atmospheric effects.
- Upon request, generation of imagery with the grey scale expanded in selected portions of the signal range for critical interpretation.
- Upon request, provision of sensor data transformed into a standard coordinate system for temporal analysis (change detection).
- Upon request, provision of sensor data calibrated for locally known atmospheric parameters.

Limitations of the present Earth Resources Technology Satellite (ERTS) ground data processing system with respect to the above requirements are as follows:

The present Electron Beam Recorder (EBR) is format-size limited for handling any conical-scan sensor geometry, and becomes resolution-limited for line-scan formats beyond 6000 elements per line. A new EBR with a larger format may be capable of handling both kinds of sensors within the present system. An improved enlarger is necessary to obtain higher output image quality. The increased resolution of the advanced sensors may require a 2X increase in the output image scale and format size to permit easy interpretation without using magnifying lenses.

Increased digital processing capability is required to satisfy calibration requirements for solid-state array sensors, conversion of conical scan data to orthogonal form and precision data rectification. Major hardware improvements will be required to provide the extreme speeds and large memories required.

Present digital tape techniques are inadequate for large scale storage and dissemination of digital pictures, and therefore development is needed in this area.

Techniques for producing many band color and/or color separation outputs are also required to allow easy registration and use by analysts.

Image Processing

Conclusions

Digital image processing has proven its worth over the past 10 years and is now an accepted method of image analysis. At this point, it is a fairly expensive process due primarily to the fact that the image processing systems presently

available (e.g., VICAR at the Jet Propulsion Laboratory, LARSYS at Purdue University, and their various offspring) are all first generation processes. That is, they have been primarily designed for batch operations and, although they allow interactive processing, they are not optimal.

Different types of sensors have a varying impact on ground system design. The line array scanners or pushbroom sensors will require the development of a specialized high speed digital system to radiometrically calibrate the data from many thousands of detectors at very high rates. The built-in geometric accuracy of these arrays will, however, simplify the geometric correction problems.

Recommendations

The following seven specific topics are suggested as core items for further research. The first four listed are considered short-term or 4-year items and the second three, long-term or 8-year items.

- Archival image storage and distribution. Although images stored on film as images will always be part of the system, large-scale storage of images in digital form will be required. Present computer compatible magnetic tapes are very inefficient in this respect. Digital image storage on film is becoming available; what is needed now is the implementation of such devices in configurations useful for image processing.

Modern magnetic tape digital recording techniques allow packing densities to about 16 kilobits/inch per track. At this density it may be practical to continue to use magnetic tape as the archival or interchange medium, in spite of the disadvantages of tape. Examples of disadvantages are the need to make individual recordings for duplicates (as contrasted to making contact prints for film media) and the possibility of deterioration over time. Techniques need to be developed, perhaps using commercial-type video cassettes as the medium, to distribute digital images for user processing.

- Hardware. A number of the algorithms currently used for image processing could be greatly speeded up if they were implemented in hardware. This hardware may be utilized in two manners: (1) as a direct part of the computer CPU to replace software functions and (2) as peripheral or perhaps even noncomputer associated devices. The candidates for conversion to hardware most clearly seen at this point are for correlation and Fourier transform, geometric rubber sheet stretching and

various parts of the multispectral analysis. The multimegabit memory development must be continued to provide multipicture storage for immediate access to the computing system, and also to provide video rate readout to volatile displays.

- High quality data entry. High quality image scanning is relatively slow. Devices are required that can be easily operated to allow the analyst or computer operator to rapidly and correctly enter film images into a digital system.
- Algorithm development. Although a large number of individual processes are currently available (over 100 programs are available for execution under VICAR at JPL), new algorithms are continually required, either to perform new functions or to upgrade the present functions. The support of continued algorithm development must be preplanned activity, rather than ad hoc, to allow mission operations to take maximum advantage of the latest techniques.
- System software design. Similarly, system software development must continue to provide ability to handle higher resolution pictures and to provide multipartition processing and better interactive capabilities. Although these capabilities are becoming available in the larger operating systems, the price paid in system overhead is extremely high. The image processing efficiency may actually be lower than in the simpler batch systems. This comes about generally because of the extreme flexibility provided by these major systems. The research and development of systems particularly geared to the image processing job is indicated.
- Parallel numerical processing. This will include such areas as electronic large-scale-integrated circuits, magnetic bubble research, holographic logic, and the like.
- Optical processing and optical to optical converters. Digitally controlled optical processors may be required with input and output either directly as images or through digital to optical converters interconnected with digital systems.

Sensor Related Aspects of User Data Analysis

The key parameters of the typical sensor which bear most directly on its ability to acquire data are spatial and spectral resolution and signal-to-noise ratio. The interrelation between these parameters relative to sensor performance and the relation between all of these and ancillary information was considered by the panel and confirmed as significant. It is concluded that 4-6 spectral bands,

picked appropriately from the visible, reflective and thermal IR data with a signal-to-noise ratio suggesting 7 to 8 bit data (128 to 256 shades of gray), are usually adequate for typical analysis problems.

One important aspect of the data system not having adequately been emphasized elsewhere, is the time delay in delivering data to the user. There are two separate and distinct costs which arise as this delay increases. (1) There may be a time critical need on the part of a particular user for information derived from the data. Thus a delay in availability of the information derived may reduce its value. There are many examples of this throughout user agencies, especially federal agencies.

(2) It must be recognized that the analysis step (i.e. changing data to information) involves the utilization of data from the sensor and from other sources. These other sources usually involve data of a non-quantitative nature. The quality of data of this type can deteriorate significantly in a period of several weeks; it does not archive well. Further, even after operational status is achieved, it may be necessary to gather data selectively on a basis which is interactive with the remotely sensed data. The ability to do this rapidly deteriorates with time. The essence of this second point is both the quality of the information derived and the cost of deriving it deteriorates with time delay in data delivery, by reason of the added difficulties in analysis which it causes.

CHAPTER 5

SENSOR RELATED TECHNOLOGY

INTRODUCTION

In order to develop the organization of this chapter and to focus the discussion accurately, Figure 5-1 is provided as an overview of an entire system in block diagram form, with candidate operations and key parameters listed with each block. This diagram is intended to highlight that portion of the system between the sensors themselves and the user. Note that the total system is considered to include not only the hardware elements but also the sun, the atmosphere, the scene, and the user as integral parts. Since both the sensors and the user portions of the system are extensively treated in other chapters of this report, they are not specifically discussed in this chapter.

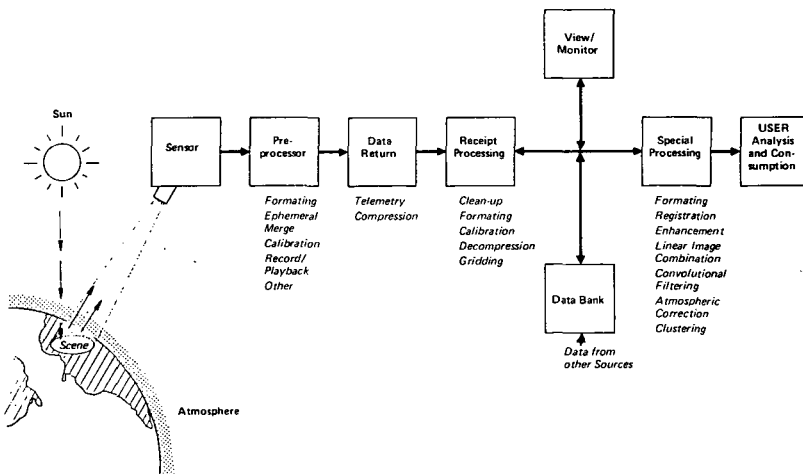


Figure 5-1. An Example of a System Functional Block Diagram

In Figure 5-1, it is proposed that data from the sensors proceed immediately to a preprocessing section, where potential operations are merging of the ephemeral and the calibration information with the data stream (or at least establishing the proper data labeling so that this step can become a part of ground processing during data receipt), forming the data, possibly recording and playback of the data, and all other tasks that are necessary before actual ground processing. It is assumed that all data will then be in digital form and will remain so through subsequent conversion to imagery or delivery to the user.

The next step is transmission of the data to the earth through the use of a telemetry system. Since photographic sensors are not a subject of extensive consideration here, the use of direct photo-package return is not recommended for any application having a short repeat cycle requirement. This approach would unnecessarily add complexity to the physical system and delay to the delivery of data to the users. Data compression is a definite possibility, both at this point in the system and in connection with the accumulated data bank, provided that the measurable effects of such compression can be made acceptable to the user.

Receipt processing on the ground includes all those data processing tasks which must be carried out regardless of the user or the format in which the data is to be delivered. This includes accomplishing the radiometric and basic geometric calibration, formatting and minor clean-up, gridding, rough annotation and decompression as required.

Completion of receipt processing results in data ready for archiving, for delivery to the user in standard product form, or for subsection to further standardized processing steps. The standard product at this point would be available in either "computer" compatible tape or a limited number of image formats and would have the following attributes: The data would have been cleaned up and calibrated, it would be in a vertical projection and a standard scale, and it would be longitude-latitude oriented.

A menu of optional special processing functions are envisioned to be available. Example possibilities are precision registration, image enhancement, convolutional filtering, gamma curve adjustment and nonsupervised machine classification (clustering). The size of this list is dependent not only upon available processing resources but also upon the ability of the user to specify and use them knowledgeably. Output at this stage would again be in the form of "computer" compatible tape and film.

Again it should be emphasized that the diagram of Figure 5-1 is provided to serve more as a vehicle to organize and focus this report rather than as a specific proposal as to how a future system should be designed. The remaining portions of this chapter develop in detail the various aspects of this diagram from a sensor-related point of view.

Regarding individual contributions to sensor related technology: R. Fenn discusses atmospheric effects on sensor performance; B. Steiner discusses radiometry; A. Guha discusses platform stability for satellite control systems; Data Correction and Image Generation are discussed by J. Edmond;

Image Processing Considerations are discussed by F. Billingsley; and D. Landgrebe discusses Sensor Related Aspects of User Data Analysis and also helped prepare the summary of recommendations with M. Maxwell. M. Maxwell contributed Sensor Data Systems, J. Moyer supplied the Representative System Descriptions, and J. Hayes supplied Wide-Band Tape Recorder information.

Scope of Chapter

The section which precedes this chapter, provides some conclusions and some general recommendations. Note that the more specific conclusions and recommendations are contained near the end of each subsection as well as in the summary.

The second section of this chapter entitled "Atmospheric Effects" discusses scene irradiance levels and the effects from the atmosphere that attenuate, scatter, distort or otherwise disturb the radiance reflected or emitted from the ground before it reaches the sensor. Any system requiring absolute estimates of the reflectivity of a scene will have very significant limitations in the accuracy that may be achieved when all measurements are from orbital altitude. However, data acquired from aircraft will suffer significantly less distortion from the same limiting effects. This section presents a discussion of the sources of these limitations and how accurately they can be countered or removed.

The next section, entitled "Radiometric Calibration," presents information on the problems and limitations of radiometric calibration of sensors. The state-of-the-art in primary and secondary standards of radiance and irradiance at various wavelengths is presented. Information is also given concerning difficulties in meeting the various requirements delineated from both a long- and short-term basis.

"Platform Effects" is the title of the next section and presents a discussion of the limitations that spacecraft platforms impose on the performance of sensors. The principal problem considered is the effect of errors in spacecraft position and attitude on the geometric accuracy of pictures produced by scanners. Information is presented as to the current state-of-the-art in attitude sensing and control and performance possibilities projected for the near future are discussed.

The next section, entitled "Sensor Data Systems," is a collection of short papers discussing various related data systems. This section presents

information on the projected characteristics and availability of high speed multiplexers to take the data from the sensors, a discussion of the present and projected state-of-the-art in high capacity tape recorders for data storage on a spacecraft, and information as to the current state-of-the-art and the projected performance capabilities of ground data recorders to accept the data.

The next section, entitled "Data Correction and Image Generation" presents a discussion of data correction and image generation. Radiometric and geometric requirements are treated, as well as basic processing operations and systems.

This is followed by a section entitled "Image Processing Considerations" which discusses a number of techniques for image processing, including hardware and software considerations and real-time and on-board processing.

Some sensor-related aspects of the data analysis step are presented next. Since the analysis step is necessarily individualized to the particular user problem, a detailed treatment of this process is not given. Rather, the relationship of spatial and spectral resolution, signal-to-noise ratio and ancillary information as to the identifiability of scene areas are explored here.

A total system description relative to some representative sensors is next presented to illustrate how the sensor fits into a complete system. The Earth Resources Technology Satellite-1 (ERTS-1) Multispectral Scanner and the Synchronous Meteorological Satellite (SMS) VISSR systems are used as examples here.

At the end of this chapter, attachments are provided along with a reference bibliography. Attachments 1 and 2 are discussions of calibration procedures for the MSS and VISSR, respectively. Attachments 3 and 4 are published papers discussing spacecraft recorder technology in direct support of pertinent data in the chapter.

ATMOSPHERIC EFFECTS

The performance of any optical/IR imaging device is dependent first of all on the radiation energy available for image formation from the object scene, and secondly, on the effects of the intervening atmosphere on this radiation. Attachment 1 provides a mathematical evaluation of inherent atmospheric limitations as a background for the discussions that follow.

In the visible and near IR portion of the electromagnetic spectrum, the image forming radiation for passive systems originates from natural sources (sun, moon, airglow, starlight); for active systems, from artificial sources (flares, LASER illuminators). The object signature is then determined by its reflectance properties. In the middle and far IR, the image forming radiation for the most part is emitted as thermal radiation from the object scene itself; this radiation is a function of object temperature and emittance.

The atmospheric parameters that most affect the image quality of a particular optical system are determined by the system itself. For instance, atmospheric backscattering, which is an important factor in active laser illuminating systems, can be greatly reduced in range-gated systems. For visual systems at high light levels, the major effect of the intervening atmosphere is the reduction in contrast. However, for low radiation level systems which are photon noise limited, such as image intensifiers or infrared passive imaging systems, the important atmospheric effect is the reduction in signal-to-noise ratio (Baily and Mundie, 1969).

Therefore, the proper application of atmospheric optical properties to a particular system is imperative.

Object Scene Irradiance Levels

The irradiance level at the earth's surface due to direct sunlight, sky radiation, moonlight, starlight, and airglow varies over approximately nine orders of magnitude (Figure 5-2).

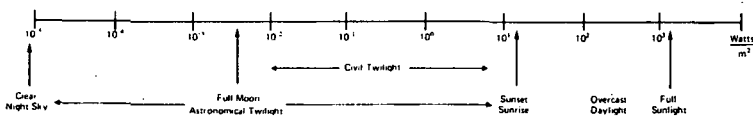


Figure 5-2. Range of Natural Irradiance Levels

Variations of the irradiance levels are due to astronomical factors (sun elevation, moon phase) and atmospheric conditions (scattering and absorption by air molecules, haze particles and clouds). The atmospheric attenuation not only reduces the irradiance levels on the ground but also changes the spectral distribution of radiance, since scattering and absorption are wavelength dependent processes.

Directional Solar and Lunar Radiation

At a mean distance of the sun from the earth, the irradiance on top of the earth's atmosphere is 1.36 kW/m^2 with an uncertainty of ± 2 percent (Johnson, 1954; Drummond, 1968). The variation due to changing sun-to-earth distance amounts to -3.27 percent at aphelion and +3.42 percent at perihelion. MacDonald (1963) has calculated the extraterrestrial radiation for each $1/2$ degree of latitude and for each day of the year. Tables of nocturnal illumination for four lunar months by day and hour have been computed by Biberman et al. (1966). Still of considerable value, and a standard reference for day and nighttime illumination levels are the "Natural Illumination Charts" by D. R. E. Brown (1952).

Figure 5-3 gives solar spectral irradiance curves at sea level for various optical air masses. Ninety-nine percent of the total irradiance is included in the interval 0.22 to $11 \text{ } \mu\text{m}$. Detailed data in tabular form for extraterrestrial and terrestrial spectral irradiance are given in the AF Handbook of Geophysics and Space Environment (1965).

Diffuse Sky Radiation and Global Radiation

Part of the scattered solar radiation reaches the earth's surface as diffuse skylight. The ratio of skylight to direct solar radiation varies on a clear day with solar elevation angle: from about 0.6 at a sun elevation of 10 degrees, to 0.08 with the sun near zenith. For the hazy conditions of a large city, the corresponding values would be 1 and 0.13. For a pure molecular Rayleigh-scattering atmosphere, the spectral and spatial distribution of sky radiation has been calculated by Deirmendjian and Sekera (1954, 1956) and Coulson, Dave, and Sekera (1960). The spectral distribution of skylight varies considerably with the amount of atmospheric turbidity. (See also the discussion of atmospheric attenuation that follows.)

The total incident radiation illuminating the earth's surface is equal to the sum of direct solar and sky radiation, which in meteorology is called "global

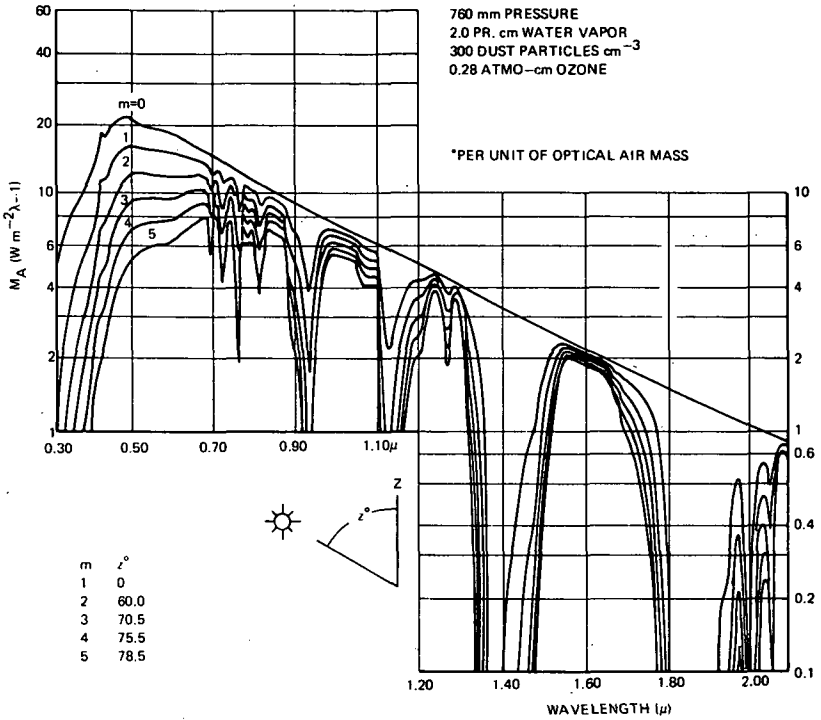


Figure 5-3. Solar Spectral Irradiance Curves at Sea Level for Various Optical Air Masses (The Value of the Solar Constant Used in This Calculation was 1322 W m^{-2} ; after P. Moon, J. Franklin Institute, v. 230, No. 5, p. 583, 1940)

radiation.” It varies on a clear day between about 0.1 kW/m^2 near sunrise or sunset, to 1.15 kW/m^2 at noon.

The total global irradiance is less dependent on atmospheric turbidity than the direct solar radiation. It may vary by 10 to 15 percent. Also high ground albedo (snow cover) may increase total irradiance by several percent. A considerable amount of data on the total global radiation over the total solar spectrum, the dependence on time of day, season and geographic distribution, has been accumulated in the meteorological literature (e.g., Robinson 1966, Geiger 1961). These data usually give total radiation over a wide spectral band and have, therefore, to be weighed with a spectral distribution curve to make them applicable to narrow spectral band irradiance estimates. However, such data do provide a highly representative climatological basis for different amounts of cloud cover.

Effect of Haze and Clouds on Irradiance

Since a portion of the scattered direct solar radiation is redirected as diffuse skylight to the ground, the effect of haze on the total global radiation is less than on direct solar and sky radiation separately. Similarly, the change in spectral distribution of global radiation is only a few percent, with a slight reduction in the short wavelength end and a slight increase in the near infrared. Table 5-1 shows a comparison of irradiance levels due to direct sunlight and diffuse skylight for clear and hazy atmospheric conditions for low and high sun.

Table 5-1
Irradiance on a Horizontal Receiver at the Earth's Surface
(According to R. Schulze, 1970)

	Solar Elevation	Direct Sun kW/m ²	Skylight kW/m ²	Sun + Sky = Global kW/m ²	Relat. Irradiance = Global/Extra- terr. (%)
Clear Atmosphere (rural areas)	90°	1.10	0.09	1.20	0.83
	10°	0.09	0.05	0.14	0.55
Hazy Atmosphere (urban-industrial)	90°	0.90	0.17	1.07	0.74
	10°	0.04	0.06	0.10	0.39

Clouds may reduce the global radiation by as much as 90 percent or more. Irradiance values for broken cloud conditions are highly variable and depend on the altitude, distribution, and type of clouds.

Atmospheric Attenuation Effects

Description of Atmospheric Effects

The radiation originating from an object scene element is affected along its path through the atmosphere by three different physical processes:

- Absorption of radiation energy by atmospheric molecules and haze (aerosol particles)

- Scattering of radiation out of the direction of the image forming ray, occurring on air molecules and aerosol particles
- Redirection of radiation energy by inhomogeneities in atmospheric air density and refractive index due to atmospheric turbulence.

All three processes are linear; i.e., the energy transmitted through an air volume is proportional to the incident energy. They also do not change the frequency of the incident radiation. (Raman scattering is not being considered here.) However, these processes are more or less wavelength dependent, and therefore the spectral distribution of radiation will be changed.

The absorption of radiation by aerosol particles depends on the refractive index of the particle, its size and shape, and the wavelength of the incident radiation. Aerosol absorption is mostly limited to infrared radiation and is a relative smoothly varying function of wavelength (Volz, 1972).

The variation of molecular absorption is much more complex and a highly oscillatory function of wavelength due to the existence of a large number of molecular absorption bands, each consisting of a large number of narrow absorption lines. Molecular absorption is primarily due to (in order of importance) water vapor H_2O , carbon dioxide CO_2 , ozone O_3 , nitrous oxide N_2O , carbon monoxide CO , methane CH_4 , oxygen O_2 , and nitrogen N_2 . Molecular absorption is not only a function of the amount of absorbing gas, but also of the temperature and pressure of the gas.

Molecular scattering depends on the number and type of molecules in the atmospheric path only and is very nearly inversely proportional to the fourth power of the wavelength. Aerosol scattering is more complex and depends, in a way similar to aerosol absorption, on the aerosol particle size distribution, shape and refractive index.

If an optical medium (such as the atmosphere) is not homogeneous but contains density variations, a transmitted wavefront will be distorted. This means that, for each object point, the wavefront arriving at the receiver will have random variations in amplitude, phase, direction and polarization.

Atmospheric density inhomogeneities are caused by dynamic disturbances (wind pressure) as well as by temperature variations causing vertical motions in the atmosphere.

Images formed through a turbulent medium show three properties:

- Scintillation or fluctuations in total image intensity

- Image motion
- Blur or spreading of the image beyond the diffraction pattern.

The information content of an image depends not only on the radiation intensity arriving from a particular object point, but it is also a function of the degree of capability to differentiate between two image elements; i.e., the contrast between them. Contrast is defined in several different ways. One definition for contrast, which is frequently used, is the modulation contrast:

$$C_{\text{modul.}} = \frac{\text{max. radiance} - \text{min. radiance}}{\text{max. radiance} + \text{min. radiance}} \quad (1)$$

The apparent contrast, C_a , in the image plane is proportional to the inherent object contrast:

$$C_a = C_o \cdot \tau_c \quad (2)$$

where τ_c is the contrast transmittance. The inherent object plane contrast is reduced by atmospheric scattering, absorption, and turbulence in the visible spectrum and by atmospheric absorption and thermal emission in the infrared. In a transitional spectral region all these processes may be equally significant.

If the object scene spatial resolution is defined as the minimum separation between two scene elements, which the receiver optical system can resolve, it becomes apparent that spatial resolution is a function of atmospheric contrast reduction.

The modulation transfer function (MTF) is the contrast transmittance for a target with sinusoidally varying brightness. In a turbulent atmosphere the MTF decreases with increasing spatial frequency of the object scene. For near zero spatial frequencies, turbulence phenomena vanish and contrast loss is only due to atmospheric scattering processes. In this case the apparent radiance of a distant object is the sum of two radiation flux components:

- Residual image forming radiation from the object after propagating through the atmosphere, and
- Radiance caused by scattering of ambient light, incident on the optical path, in the direction of the receiver.

This second quantity is called path radiance; it obviously does not contain any information about the object scene. It can be shown (Duntley et al.,

1957) that if the contrast is defined as:

$$C_{\text{universal}} = \frac{\text{object radiance} - \text{background radiance}}{\text{background radiance}}, \quad (3)$$

a universal contrast transmittance can be derived as:

$$\tau'_{c, \text{universal}} = \frac{1}{1 + P/N_{Bo}(T)}, \quad (4)$$

where P is the path radiance, N_{Bo} the inherent background radiance, and T the beam transmittance. The universal contrast transmittance is only a function of atmospheric and background properties.

Although the path radiance in the visible spectrum is due to scattered radiation, the physical process for path radiance in the infrared is thermal emitted radiation by each path element. This path emission is a function of the atmospheric composition and its emittance, and also of the temperature of the path element. The path emission is related to the absorption by Kirchhoff's law, and it is those gases (and aerosols) which absorb infrared radiation that also emit radiation.

Magnitude of Atmospheric Effects

The relative contribution of molecular scattering and absorption, and of aerosol scattering and absorption is illustrated in Figure 5-4. Table 5-2 lists the symbols in the equations and with the illustrations supporting the discussion. This figure gives transmission values for a vertical path through the whole atmosphere. The atmospheric properties correspond to a mid-latitude winter condition. The spectral resolution is approximately 20 wavenumbers or:

$$\nu = 1/\lambda \text{ (cm}^{-1}\text{)}. \quad (5)$$

which would mean, for example, if the wavenumber for $\lambda = 1 \mu\text{m}$ is $1/\lambda = 10,000 \text{ cm}^{-1}$, then a resolution of $\Delta\nu = 20 \text{ cm}^{-1}$ corresponds to a resolution in wavelength of 20 Angstroms.

Figure 5-4(a) shows the transmission due to water vapor and ozone; Figure 5-4(b), due to uniformly mixed gases (CO_2 , N_2O , CO , CH_4 , and O_2), due to molecular scattering, and also due to scattering and absorption from aerosol components corresponding to 23 km and 5 km surface visibility. This figure demonstrates the relative contribution of various atmospheric constituents to the total attenuation; it can, therefore, assess the effect in changes of concentration of various components on the total transmittance. The total

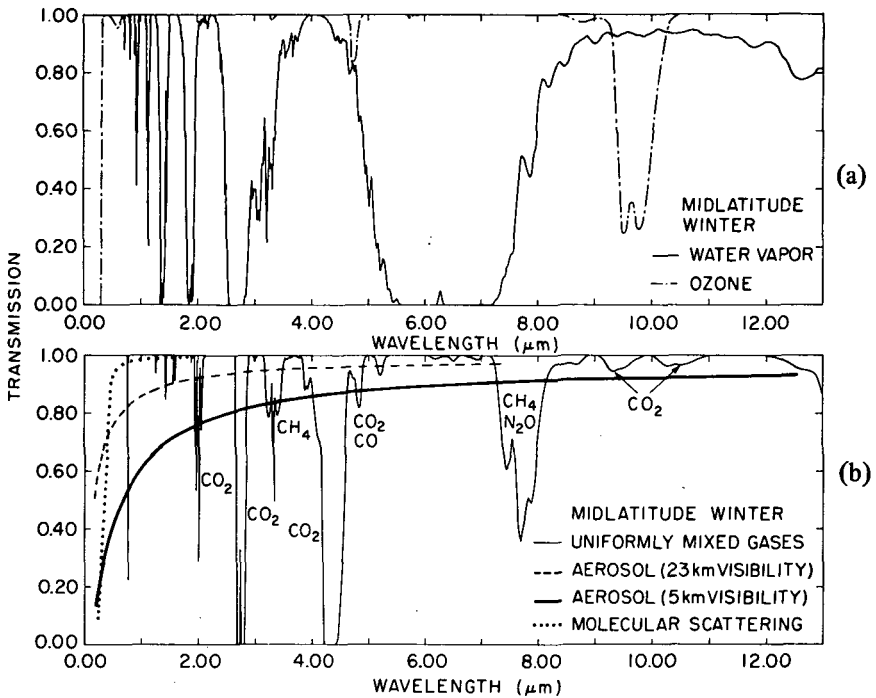


Figure 5-4. Effects of Water Vapor and Ozone & Molecular Scattering from Aerosol Particles

atmospheric transmission can be obtained by multiplying together the transmission values for the individual components.

Figure 5-5(a) and (b) shows the total transmission for the two extreme models of a tropical and subarctic winter atmosphere. Both atmospheric models contain the 23 km visibility aerosol component. The difference in transmission between the two models is almost completely due to the differences in water vapor and ozone content and distribution. In the illustration, the well-known atmospheric transmission windows can be seen in the visible, near IR, at 3.5-4 μm with the 9.6 μm ozone band. The transmission of the 8-12 μm window shows the largest difference between the two models, almost a factor of 2. The transmission in the visible, of course, is primarily determined by aerosol scattering. Molecular scattering is very nearly proportional to λ^{-4} . Aerosol scattering is approximately proportional to λ^{-1} . One notices that the absorption bands not only become deeper (smaller transmission) but also wider as the absorber optical path increases.

Table 5-2
Symbols Used in Discussion of
Atmospheric Effects

A	= ground albedo
C_a	= apparent contrast (modulation)
C_o	= inherent contrast (modulation)
τ_c	= contrast transmittance (modulation)
τ_c	= contrast transmittance (universal)
C_a	= apparent contrast (universal)
C_o	= inherent contrast (universal)
P	= path radiance
T	= beam transmittance
N_{Bo}	= radiance from background at 0 distance
I	= beam intensity
R	= receiver range
D	= receiver aperture
λ	= wavelength [μm]
ν	= wave number [cm^{-1}]

It should be remembered that these are model atmospheres, and that day-to-day variations can be significant. Integrated transmittance values pertaining to the total solar radiation over the whole solar spectrum show that 75-80 percent of molecular absorption is due to water vapor absorption, primarily in the infrared absorption bands. It is important to note that variations in atmospheric water vapor change the total direct solar radiation only by a few percent, because amounts of water vapor that are already small absorb almost completely in the narrow spectral absorption bands and additional water vapor only has the effect of widening the absorption bands, as mentioned earlier. Ozone accounts for about 20 percent of the total absorbed energy and oxygen for about 1-3 percent. Ozone absorbs mainly in the ultraviolet and visible spectrum and in the 9.6 μm band.

For an optical system with very small aperture, turbulence-induced intensity fluctuations in a wave front element from the object scene may also be a factor in the signal-to-noise characteristics (Weiner, 1967).

Experimental data (Höhn, 1966; Paulson et al, 1962) show that the intensity fluctuations have frequencies ranging from 0-1000 Hz. For a vertical path from ground to 1 km altitude Weiner derives intensity fluctuations ($\Delta I/I$)

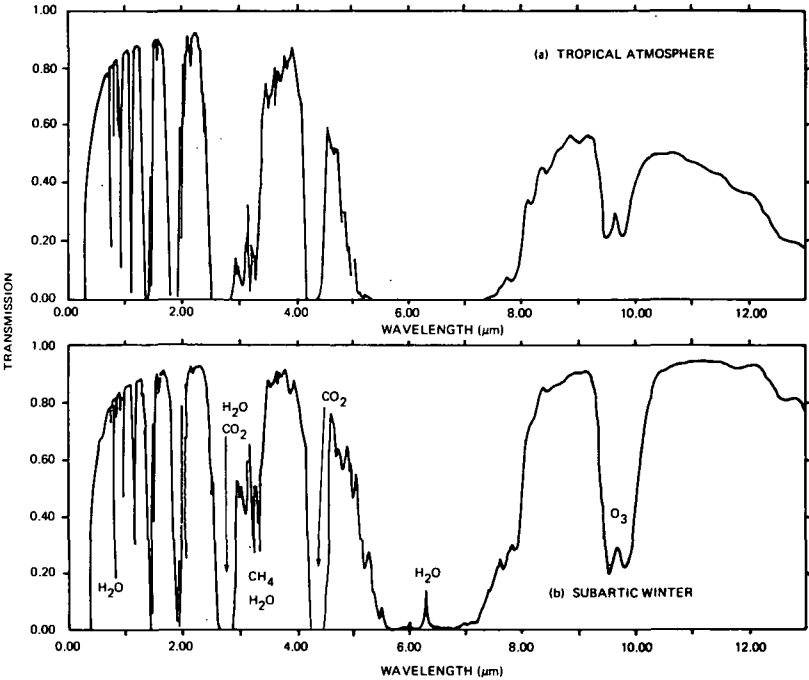


Figure 5-5. Total Transmission for Two Extreme Models

for a receiver with a 4-cm diameter aperture of approximately 0.40; for a receiver with a 40-cm aperture, approximately 0.06.

Reduction of scene contrast due to atmospheric scattering varies over several orders of magnitude depending on wavelength, atmospheric turbidity, source-slant path geometry and ground albedo.

Figure 5-6 gives the universal contrast transmission:

$$\tau'_c = \frac{C'_{\text{apparent}}}{C'_{\text{inherent}}} \tag{6}$$

for a receiver located on top of the atmosphere looking straight down. The ground albedo, A, is 10, 30, and 60 percent (ground albedo is the ratio of total incident to total reflected radiance from the ground). The contrast transmittance is shown for two different atmospheric models, one corresponding to clear conditions with 23 km surface visibility, and also for a hazy

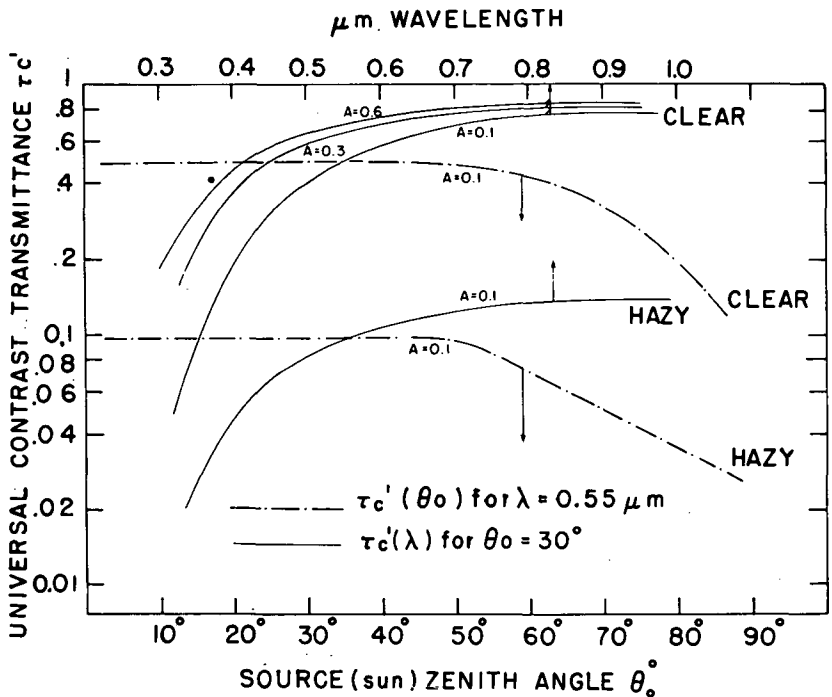


Figure 5-6. Transmission Values for Vertical Path through Whole Atmosphere

atmosphere with 3 km visibility on the ground. The figure shows the dependence of τ_c' on wavelength, sun zenith angle and albedo. The results of these model calculations illustrate the range of contrast transmittance values which has to be considered in the interpretation of imagery from a satellite platform.

The variation in contrast transmittance values also gives an indication of the extreme requirements for atmospheric turbidity and scattering data if a prediction accuracy of for example 10 percent or better is desired in background or object inherent radiance. Even if the contrast reduction due to light scattering were extremely small, atmospheric turbulence will put an upper limit on the quality of an image transmitted through the atmosphere. Theoretical considerations (Fried, 1966) show that the limiting ground resolution is in the order of 5-10 cm. This resolution is approached as an asymptotic limit at an altitude around 10 kilometers and cannot be exceeded no matter how large the receiving lens aperture.

The performance of optical systems at high light levels (e.g., photopic vision, photographic systems) is primarily limited by image contrast. On the other hand the performance of systems for low radiation energy levels (image intensifiers, passive infrared systems) is mainly limited by photon noise and it can be shown (Bailey and Mundie, 1969) that the signal to noise at range R is equal to the product of the signal to noise at range zero times the infrared beam transmittance, with little effect of the path radiance.

Atmospheric infrared emission, which constitutes the path radiance for infrared wavelengths can be computed from radiation transfer models and radiation diagrams. Considerable interest has recently been directed at the effect of aerosol particles on the infrared thermal emitted and absorbed atmospheric radiance, especially in the water vapor absorption window from 8-12 μm . The objective of these studies has been to determine errors in surface temperature derived from airborne radiometric measurements. Results of these studies (Jacobowitz, 1972) show that atmospheric aerosols will absorb more energy than they emit. This will reduce the outgoing radiation flux so that the radiometrically determined temperature appears less than the actual surface temperature. This temperature error is generally about 0.2 to 0.5 K, and may become as large as 2 K in a very hazy atmosphere. Only for arctic winter conditions, haziness will cause a radiation temperature higher than the true surface temperature.

Present Prediction Capabilities for Atmospheric Effects

Mathematical and Computer Models. Existing theories allow for most practical applications exact or nearly exact computations of most atmospheric optical parameters related to atmospheric absorption, scattering and emission. Uncertainties in predictions are not so much in the algorithm used, but in the representativeness of the input data on atmospheric properties. Beam transmittance calculations for monochromatic radiation (LASERs) or broad-band radiation, degraded to any given spectral bandwidth, can be performed to include the effects of atmospheric molecular absorption, aerosol absorption and scattering (Altshuler, 1961; McClatchey et al, 1971). The error in the computational method is for most spectral regions a few percent or less. Additional uncertainties are in the input parameters: molecular and aerosol absorption and scattering characteristics.

Considerable progress has been made during the last decade in developing computational procedures to calculate multiple scattering radiation transfer in atmospheres containing nonuniformly distributed aerosol particles. Approximation methods and numerical techniques have been developed to

calculate any optical parameter (sky radiance, path radiance, atmospheric reflected radiance) including all orders of higher scattering (Churchill et al, 1961; Coulson et al, 1960; Hermann 1965; Wells et al, 1968; Thompson and Wells, 1971; Plass, 1968, 1972). These computational techniques, however, are in general rather complex and require computers with large memories and high speed capability. Even then, the computer time requirements do not permit very extensive calculations for a large variety of input parameters.

However, sufficient model calculations exist to provide an understanding of the effect and relative significance of various parameters for contrast transmission. The error in these computational techniques is estimated to be a few percent or less, except for extremely low sun elevation angles or look angles near the horizon where the accuracy decreases rapidly. A number of these computational methods do account for the polarization of scattered radiation. An evaluation of the accuracy of multiple scattering radiation transfer programs is very difficult, since no rigorous solutions exist and a comparison with experimental data lacks the necessary detail in measurement of the basic atmospheric parameters on aerosols, albedo, etc., required as inputs into the computational schemes.

Present computational capabilities are less satisfactory for predicting atmospheric turbulence effects. Several researchers have developed analytical techniques to obtain estimates of the atmospheric modulation transfer function (Hufnagel and Stanley, 1964; Fried, 1966; Tatarski, 1961; Lutomirski and Yura, 1971). However, the agreement between these different methods is often only limited to some very special condition. Present predictions for atmospheric turbulence effects are mostly based on experimental data.

Atmospheric Models. In order to perform computations of atmospheric transmittance, contrast reduction or other parameters for the purpose of establishing design criteria for systems development, atmospheric models are required which provide the input data for the optical calculations. Such models have to include the spatial and temporal variation of all atmospheric parameters and environmental factors which affect the propagation of optical/IR radiation. These atmospheric models obviously have to be based on extended series of measurements from which a climatology of the various parameters can be derived.

Atmospheric models for the basic atmospheric parameters pressure, density, temperature, and as supplements humidity have been established in the "U.S. Standard Atmosphere," 1962, and "U.S. Standard Atmosphere Supplement," 1966, (Handbook of Geophysics and Space Environment, AFCRL, 1965). There are also well founded models for ozone distribution and of course for the uniformly mixed atmospheric gases.

Several attempts have been made to formulate analogous models for atmospheric aerosols (Elterman, 1968, 1970; Deirmendjian, 1969; McClatchey et al, 1971). These aerosol models, however, at the present definitely lack the experimental data basis to give them the statistical significance of a standard atmosphere. They should only be regarded as guidelines to indicate trends in atmospheric optical parameters. There exists no generally accepted concept of the variability of aerosol distributions (concentrations, size, composition, refractive index) with geographical location, altitude, season, meteorological conditions, etc., except for some very gross features such as an inverse power law aerosol size distribution and the 18-20 km aerosol layer.

Only a very generalized concept exists at this time for the atmospheric structure constants which describe the turbulent conditions of the atmosphere (Fried, 1965). The user has to refer to the limited number of original measurement results (Lawrence, 1970; Wyngaard, 1971). A considerable amount of field measurements will be required before reliable models can be established.

For the effectiveness of any airborne surveillance and remote sensing system, the spatial and temporal distribution of cloudcover is perhaps the most important quantity to be considered, since clouds with the exception of cirrus clouds are completely opaque to optical wavelengths. It has been shown that cloud data from surface observations are not very applicable to airborne optical systems. Very useful data on the probability of a cloudfree clear line of sight have been obtained during recent years from an aircraft in-flight observation program (Bertoni, 1967), from which a climatology of cloud distribution for the continental U.S. and some other portions of the world have been derived.

Present Capabilities for Real Time Atmospheric Data Collection

The only atmospheric optical parameter which has been measured on a routine basis is surface visibility as part of the meteorological observations. In many instances reported surface visibilities are not even based on measurements but on observer visual estimates. The values get increasingly unreliable if the visibilities become in the order of 5-10 miles or better. As shown earlier, surface visibility or extinction coefficients are only one of several parameters determining the total atmospheric transmittance or contrast reduction. There is hardly any correlation with turbulence parameters. Total atmospheric transmission measurements are limited to a few specific programs connected with solar radiation measurements (e.g., the Astrophysical Observatory of the Smithsonian Institute) or other research programs.

No instrumentational capability exists at present for implementing any ground-based or airborne measurement program of atmospheric optical parameters with sufficient vertical, horizontal and temporal coverage to derive corrections for atmospheric transmission effects with an accuracy substantially superior to that of predictions or analysis based on atmospheric models.

Global meteorological satellite coverage has provided a completely new capability for cloud distribution analysis and prediction. However, no satellite experiment exists at present, or has been implemented for global coverage of atmospheric transmission properties.

Air pollution monitoring programs, such as the Environmental Protection Agency's air quality surveillance network, can provide useful data which will indicate trends in optical atmospheric properties.

Recommendations for Future Efforts in Atmospheric Transmission Studies for Remote Sensing

Atmospheric optical effects may reduce the imaging capabilities of satellite born optical systems to about 50-90 percent in a clear atmosphere, and to less than 10 percent in a hazy atmosphere, or for low sun angles or very short wavelength. A variability of about a factor 10 with space and time must be expected. It is, therefore, quite obvious that any quantitative remote sensing experiment of surface properties will require a rather accurate knowledge of the atmospheric effects on the image quality of the optical/IR imaging system, so that a correction for these effects can be made and the inherent object scene features and characteristics be restored.

Efforts in two directions will be required to achieve this:

- Develop improved atmospheric models and theoretical concepts which can be used to compute the specific atmospheric attenuation or noise parameters
- Conduct concurrent measurements of atmospheric optical quantities with the remote sensing observations.

It can be shown for instance that the contrast transmittance of the atmosphere varies by about 50 to 60 percent of its value per one mile change in surface visibility, assuming similar vertical distributions of haze particles. This indicates that one can improve the prediction accuracy for atmospheric contrast transmittance by about 50 percent if one applies atmospheric

models with different surface visibilities. With sufficiently detailed and representative atmospheric models, it should be possible to predict optical parameters from model calculations to an accuracy of 30-50 percent of the actual value for most conditions. Any further improvement will require direct concurrent measurements.

Measurement programs for improvements in atmospheric models, as well as for concurrent monitoring, will have to include total atmospheric beam transmittance, contrast transmittance, modulation transfer function (MTF), atmospheric IR emission depending on the conditions of the sensing system (wavelength band, receiver aperture, etc.). Such measurements are basically within the present state of the art, however, they will require new development in technology.

Atmospheric transmittance is independent of direction of path and can, therefore, be obtained from ground measurements. A program of solar transmission measurements at a selected number of weather stations should be initiated as soon as possible. Theoretical relationships between upward and downward directed (sky radiance) path radiances should be examined to establish possible methods for deriving upward directed path radiances and contrast transmittances from surface measurements (Gordon, 1969). One area of promising potential would be development of airborne (or satellite borne) LIDAR backscatter system (Elterman, 1972). [See also the NASA report on "Remote Measurement of Pollution," NASA SP-285, pp 33-35 (1971).]

Representative atmospheric optical models must be developed which describe the environmental conditions with regard to their geographical, seasonal, and meteorological variability. Since contrast transmittance varies by about 50 to 60 percent of its value per 1 mile change in surface visibility, one can conclude that by applying atmospheric models for different visibility conditions, one will be able to predict atmospheric optical parameters with an accuracy of 30 to 50 percent of the actual value for most conditions.

Theoretical relationships between upward and downward directed path radiance (sky radiance) should be examined to establish possible methods for denoting upward directed path radiance and contrast transmittance for ground measurements (Gordon, 1969).

The Earth Resources Experiment Package (EREP) on SkyLab has a multi-spectral scanner (S192) and a spectrometer (S191). S192 has 13 channels in the frequency range 0.4 to 13 μm and S191 has the same range. The cone of the instantaneous field of view of S191 on the surface is 0.4 km and the IFOV of S192 is 80 m.

It should be possible to find large enough targets, e.g., wheat fields, sand or water areas that have a response in all of the bands of the scanner and that can be viewed sequentially under a variety of atmospheric conditions. The orbit of SkyLab has now been fixed and observations of the same area may be possible every 5 days. The stability of the scanner varies with each band but it is possibly in the range from 1 to 3 percent. The spectrometer requires a 2-second dwell which is provided by the astronaut tracking using the telescope which is a part of the spectrometer. Field measurements can be made at the time of overflights so that measurements can be compared. If this experiment is to be performed, a reference standard should be selected and measurements made through preflight of all of the instruments used for both surface and space.

The field data collected by Purdue University and the Soil and Water Conservation Division, USDA, using the Esotech Field Spectrometer should be digitized and analyzed to determine the degree of correlation in both shape and amplitude between spectral values measured in the frequency domains where the atmosphere has a severe effect, and where its effect is less. In addition it may be possible to describe transmissivity as a function of the bandwidth.

It is recommended that a program of solar transmission and sky radiance measurements at a selected number of sites be implemented as soon as possible. Such measurements are very simple and relatively inexpensive.

For a near term capability for indication and discrimination of haze and thin cirrus clouds, onboard near IR and thermal IR radiometer channels, in addition to the visual spectral bands, can provide qualitative information. Long range atmospheric measurement programs should include ground, aircraft and balloon measurements of radiance, atmospheric transmittance, contrast reduction, MTF and IR emission, depending on the sensor involved. Such measurements are basically within the present state of the art; however, some will require new instrumentational development.

RADIOMETRIC CALIBRATION

As stated in the summary of this chapter, NASA has done a commendable job of defining its broadest radiometric goals for present platforms. These goals are remarkably close to those being specified by many users for periods four to eight years hence. The 5 percent absolute accuracy goal of ERTS-1 remains a suitable general target for future platforms. However, NASA is not at the present time able to guarantee all the detailed radiometric fidelity that

users would like. Such limitations and problem areas result from the following:

1. Detailed radiometric specifications for present systems were either not provided by NASA, as was the case for VISSR, or were furnished initially only in general fashion, such as the "5 percent absolute accuracy" figure of the ERTS-1.
2. Detailed assurance of compliance with these few specifications has generally not been provided either by the vendors or by NASA. This deficiency arises partly because the best laboratory standards of spectral irradiance until recently have been only 5 percent, which is the total ERTS-1 tolerance.
3. NASA/JSC does not yet possess the facilities required to verify compliance with radiometric specifications. NASA/GSFC has not been supplied by NBS with the standards and techniques to assure compliance with the ERTS-1 "5 percent absolute accuracy" specification.

A definite set of radiometric requirements can be anticipated in connection with each operational stage of remote radiation sensing. First, decisions concerning the operating levels must be made. Second, the satisfactory performance of the sensor system must be established. And third, the interpretation of the images formed will depend on certain auxiliary data. All of these requirements dictate periodic reference in a sufficiently careful manner to a source whose performance is known.

Furthermore, not only these various stages of sensor operation monitoring but also the technical system constraints must be jointly considered at the earliest planning stage if a generally satisfactory operating system is to result. Anticipating certain conclusions of this chapter, the satisfactory production and utilization of remotely generated data will involve more information than is now available. Some of this information must be in hand before the design of a sensor is started. Then, with the assistance of other background data, remote observations can be decoded, understood, and interpreted to fulfill much of the promise of useful results.

Types of Radiometric Requirements

Amplifier Gain Setting Adjustment

An initial decision to be made for a radiation sensor performing remotely is the choice of amplifier gain setting. On the one hand, the amplifier cannot be permitted to be overloaded by its input signal. On the other hand, the

amplifier operating level cannot be permitted to drop to the point that the output is unnecessarily degraded by noise introduced by the telemetry system. Therefore, if expensive excess dynamic range is not to be required, decisions on amplifier gain settings must be available during flight. For this purpose alone, 10 percent calibration stability over the lifetime of the platform with respect to an arbitrary standard is considered desirable.

Verification of Radiometer Operation

Once the choice of an amplifier gain has been made, the satisfactory performance of the radiation measuring system must be verified periodically. The greater the fraction of the entire operating system that is involved in this verification, the less the likelihood of intolerable system performance. However, a partial system check is sometimes much simpler and less costly in terms of cost, weight, and power. The consequences of a performance change in any unchecked optical system components must be weighed against the higher costs of a full periodic optical system check. For the general testing of system operation, 25 percent stability for the life of the system is minimally satisfactory.

Channel Gain-Match

The utilization of large images derived from any scanning system will be severely hampered if artificial, systematic differences exist in information channels. For example, a striped picture is more difficult to interpret than a uniform one, no matter how sophisticated the interpreter. The relative electro-optical gain in adjacent channels must thus either be matched or the degree of mismatch be determined. That is, if reference data on mismatch is provided, the image can be processed later to remove artificial differences in adjacent channels. For destriping, 1 percent relative accuracy is highly desirable.

Inter- and Intra-Orbit Comparison of Data

Not only a uniform picture is desirable, even for qualitative purposes; but increasingly, users desire to compare images that differ in time and position. An example is the comparison of data from adjacent geographical areas, but necessarily taken from successive orbits. Another widely useful comparison is that of the same area on successive passes over it. In order for such comparisons to be meaningful, they must be referred to a stable reference.

The accuracy required will depend on specific use. In general, however, the intercomparability of data from different radiometers is also highly desirable. Accuracy at least with respect to a given stable standard to a few percent will also be necessary. If changes of 5 percent are not detectable with certainty, many potential users may be unsatisfied.

Spectral Bandpass Shape

The interpretation of spectral information can depend on knowledge of the spectral resolution under which the data was taken. This resolution will generally have to be determined before launch of a platform. If a bandpass stability under flight conditions is a problem, then in-flight determination capability will also be desirable. In general, however, variation in spectral resolution will be much less of a problem than radiometric level stability.

Because of other constraints, such as observation time and spacial resolution, the spectral resolution desirable now and in the foreseeable future for remote sensing of the earth is sufficiently within the state of the art, if addressed seriously. The spectral resolution required for atmospheric observations of meteorological significance is much more difficult to provide and maintain. Such work is not the main focus of this study; nevertheless, for both atmospheric and earth surface sensing, reliable data must be obtained in advance of flight if interpretation of the spectral data are to be reliable.

Spectral Signatures

The relative fidelity of the spectral data obtained, that is the system's relative spectral response, can be approached in one of two ways. In one case, all data in a given frame can be treated as unique and essentially nonintercomparable with other data. This approach has been necessary up until now, partly because of system stability and partly because of the differing spectral regions observed from each platform. For such operation, stability of the system must be assessed at 2 to 5 percent depending on the use. Accuracy here is unimportant, but the utilization of such data is severely restricted. A complete library of signatures must be generated either for each frame, or for each new system, or when an existing system undergoes changes.

If consistent systems can be designed, then intercomparable absolute spectral calibration becomes feasible and useful. In order to insure intercomparability, assurance of relative spectral accuracy should be made to 2 to 5 percent. Such accuracy would avoid the necessity for the generation of new spectral signature libraries with each new platform. Spectral data taken at different times

could then be compared directly after suitable data handling. Relative spectral accuracy would provide intercomparability of spectral data without the necessity for absolute accuracy.

Benchmark Data

Finally, in the hierarchy of desirable information, certain tasks will require not only stability but absolute radiometric accuracy. The promise that remote sensing offers of a synoptic approach to global problems will be realized with long-term knowledge of absolute radiometric levels. In principle, satellites could be intercompared in chain fashion, once the stability of a single satellite were assured; but in practice, such chain measurements become progressively more uncertain. For example, if the heat balance of the earth is indeed changing due to natural or man-made causes, quantitative knowledge of changes and their spectral character would indeed be essential to the design of corrective measures. Both stability and accuracy within 1 to 2 percent over several years will be of long range global significance.

Table 5-3 summarizes the radiometric requirements in the various areas just discussed. Because the *stability* of the optical radiation monitor system must be assured, regardless of the degree of measurement sophistication, determination of absolute accuracy is not such an additional burden as might initially be assumed. If the time-dependent and environmental aspects of radiation measurement have been seriously addressed to assure stability, the requirement for absolute accuracy primarily implies special additional attention only to preflight calibration. This is a relatively straightforward fraction of the entire calibration problem. However, all aspects of optical radiation calibration require serious attention if the desired results are to be obtained.

Quality of Radiometric Measurement Required

Visible and Near Infrared

The utilization of remote sensing data is still in its infancy. Because of the very short history of these measurements, a precise quantitative estimate of the desirable data quality is difficult to predict. Nevertheless, estimates can be made based on laboratory data in hand. For example, useful discrimination of geologic utility must approach 5 percent relative spectral accuracy in order for the observer to distinguish differing geologic formations (Vincent). Observations of agricultural interest, on the other hand, must distinguish between types and status of foliage. This information is sometimes less widely

Table 5-3
Radiometric Requirements

Purpose	Stability/2 Years (percent)	Accuracy	
		Relative (percent)	Absolute (percent)
Amplifier Gain	10		
Operation Verification	25		
Channel Gain Match		1	
Long-term Data Comparison		2-5	
Band Pass Identification			2-5
Spectral Signatures		2-5	
Benchmark Data			1-2

varying in spectral distribution than is that for geologic structures. Preliminary airborne platform data indicate that measurements good for at least 2 to 3 percent relative spectral accuracy must be made in order to identify soil utilization or crop statistics with useful accuracy. Since the study of spectral signatures is still so new, later work may well indicate that data good to 1 percent relative spectral accuracy are useful for work on a global scale under less severely restricted conditions.

Thermal Infrared

As an example of the quality requirements for thermal I/R data, in geology applications, Vincent has shown that a useful survey can be made of silica content with two channels in the 8-14 μm band up to a 5 percent absolute accuracy. Data of similar quality is expected to yield useful information in stress analysis for agricultural surveys.

Oceanographers can chart ocean behavior with thermal information better than 1°C absolute accuracy. Moreover, ocean and stress pollution can be identified with data of similar quality. Ocean productivity is also associated with similar quality measurements.

Present State of Radiometry

The most accurate radiometric measurement that can now be made is that of irradiance at a level of one solar constant. This measurement is performed with an electrically calibrated radiometer (Geist 1972, NBS). With substantial effort, this measurement can be made in a few laboratories to ± 0.5 percent. Unless there is fortuitous cancellation of errors, the spread of such measurements can thus be expected to be about 1 percent. This most accurate measurement requires a full hour of measurement data, with an elaborate laboratory apparatus and data handlers. The lamp to which the first transfer is made operates at atmospheric pressure, room temperature, in a vertical position, under earth gravity, and without vibration.

On the basis of the experience of experts (Geist 1972, OSA, Zalewski 1972) variation in these conditions is expected to affect the performance of lamps, but in presently unquantified ways. The most accurate lamps used to transfer scales of *spectral* irradiance at the level of one solar constant have an uncertainty between 1-1/2 percent in the visible and near IR and 3 percent in the ultraviolet (Saunders 1972). Their long term stability is variable.

Spectral radiance measurements can be made at best in the laboratory to about 1 percent (Kostkowski 1970). This measurement is painstakingly performed at atmospheric pressure and room temperature, vertically under earth gravity, and without vibration. Between 225 nm and 2.4 μm , the area of the lamp filament whose radiance is determined is at most a few square millimeters. Measurements at the 1 percent level require the radiance mapping of the parts of the filament under direct observation. Between 1.5 μm and 15 μm , blackbodies are commonly used directly. These have been designed for operation under laboratory conditions.

In summary, a number of small but important factors essential to reliable radiometric measurements from space are to be studied. For example, the various limiting factors for determining the radiance of relatively large sources remain to be studied quantitatively. The independent capability to perform accurate radiometry at the state-of-the-art 1 to 2 percent level must be acquired. The long-term performance of promising detectors remains to be studied at this level. The stability of visible sources under space environment remains to be determined. The stability of surfaces and optical components under space environment remains to be examined. But, substantial promise is contained in the recent development of blackbody theory sufficiently comprehensive for unquestionable application to large-area sources being used or contemplated.

New Technical Constraints

Space radiometry thus introduces several new factors and challenges to traditional optical radiation measurement systems. These constraints suggest the generation of a new body of background information and of special remote hardware.

Time Behavior

One essential characteristic of space calibration is the relatively long period of time and/or large distances between initial system performance checks and the critical measurements that need to be characterized. This constraint is in marked contrast to conventional radiometry. The time behavior of calibrated sources and detectors even under normal atmospheric pressure and normal ambient radiation levels has not yet been widely studied. From presently available data, calibrated detector performance a few months or years hence cannot be predicted with certainty. Space radiometry thus requires extension of previous radiometric experience.

Environment

In many cases an unusual environment is even more influential on space radiation measurement than the mere passage of time. On the one hand vacuum or unconventional vapor constituents can play a major role in radiation measurements. On the other hand relatively high photon and ionizing particle fluxes can also play a role. In addition, the combination of the two—unconventional pressures and particle fluxes—can apparently generate effects that neither does alone.

Aperture

Because of the importance of maximizing the amount of data obtained, space systems produce relatively large image fields of view. The desire for increasingly high spacial and spectral resolution as well has led to increasingly large angular apertures to obtain sufficiently detectable signals. If the data obtained with these increasingly large systems is to be quantified reliably, the entire system aperture must be calibrated. The challenges arising in the calibration of such large apertures are also relatively new to radiometry. Therefore, reference to past experience again proves an insufficient guide to future decision making.

Spectral Regions of Greatest Importance

Two different spectral regions of primary interest need to be distinguished. They differ both in the types of user requirements and in the technical solutions to such requirements. In the visible and near infrared spectral regions, the dominant radiation in remote sensing is that reflected from the sun. The physical quantity of primary interest is a reflectivity—the ratio of the earth's surface radiance to solar irradiance. Solar irradiation corresponds very roughly in spectral distribution to that of a blackbody near 5500 K. This radiation occurs primarily in the visible and near infrared regions short of $2.5\ \mu\text{m}$. The integrated irradiance from the sun is about $140\ \text{mw}/\text{cm}^2$. (In order to develop a similar irradiance from a 100-watt lamp, a surface must be placed within a few centimeters of it, but the spectral distribution of the lamp will be much more heavily weighted in the infrared.)

The primary radiation from the earth itself, on the other hand, is similar in spectral distribution to that of blackbodies ranging from 250 K to 300 K, which emit primarily in the middle infrared ($\sim 10\ \mu\text{m}$). The absolute radiance of specific regions of the earth's surface is the quantity of primary significance here. Because of atmospheric absorption by water vapor, two specific spectral regions are of much greater earth sensing interest than the others: 3.5 to $5\ \mu\text{m}$ and 8 to $14\ \mu\text{m}$. In all of these spectral regions observed, however, the reflective and the emissive, the surface of interest occurs below a physically interfering atmosphere, while the sensor is above most of this atmosphere. In order to achieve measurements of the desired accuracy, the effect of this atmosphere in these spectral regions must be understood. Thus meteorology, although not the primary focus of this report, plays a role that will have to be examined quantitatively if measurements of the desired reliability are to be achieved.

Systems Currently Operating or Being Planned

Current system uses of radiometry are discussed next. Representative systems are discussed in fuller detail at the end of this chapter.

Multispectral Data System (MSDS)

This system employs a 24-channel spectrometer that is designed for manual operation and is much closer in time (and position) to data taken than space-borne systems. Both visible, quartz-halogen, and infrared, thermal quasi-blackbody, calibration sources are utilized by this object-plane scanning system. The entire scanner optics systems is calibrated. The surface of a partial

sphere, illuminated by the quartz-halogen lamp, provides a relatively uniform secondary source for visible calibration in the reflective region scanning system. The operating lifetime is designed for about 100 hours, during which manual attention is available.

This system is not directly suitable to space, both because of the required continual calibration with a 100-hour-lifetime source and because of the manual attention required. Reflective region calibration is designed for 1 percent relative spectral performance and 10 percent absolute fidelity. The thermal channels are designed for 0.2 K relative accuracy with regard to each other, and 0.5 K absolute accuracy. Substantially more care and a substantially larger fraction of the system as a whole has gone into the calibration of this system than into spaceborne systems. Nevertheless, the actual performance of this system has not been independently checked experimentally.

Earth Resources Technology Satellite (ERTS)

The multispectral scanner in the ERTS system is limited to four channels in the visible and near infrared. Fiber optics are used to convey sections of the object-scanned image to filtered detectors. A filtered grain-of-wheat lamp is imaged onto the fibers during the nonobserving part of each second sweep. The electro-optic gain of adjacent channels is in principle adjusted for uniformity within 2 percent on the basis of this signal. In practice, striping in pictures is obvious, however. In addition, once in each orbit, a small area of the sun is scanned across the fibers. The accuracy of this system was initially unspecified. Calibration has been performed with a unit developed at GSFC and interchanged with the contractor. Later independent experiments were performed as well as possible. (See Attachment 2.)

SkyLab

The 13-channel multispectral scanner in SkyLab is designed for intermittent operation, 100 hours total operating time. The image plane is scanned; internal calibration involves only part of the optical system. A "grain-of-wheat" lamp is supplied for reflective channel calibration, and two quasi-blackbodies at temperatures above and below scenes to be observed are used in the calibration of thermal infrared. Relative calibration accuracy is specified for 1 percent; absolute accuracy, 5 percent and 0.5 K respectively. Linearity is specified for 0.5 percent. At this writing (December 1972) the radiometric accuracy has not been verified.

Visible-Infrared Spin-Scan Radiometer (VISSR)

This multispectral instrument in (high) synchronous orbit is being planned primarily as a cloud monitor. No on-board calibration capability was initially designated. More recently, both pre-flight and on-board calibration capability of the order of 1 percent has been incorporated in the VISSR. (See Attachment 3.)

Recommendations

If the radiometric fidelity identified in the previous sections of this report and specified by NASA itself for some of its platforms is to be actually achieved, considerable work will have to be undertaken.

Timing of Design

Radiometric calibration performance should be considered at the start and throughout the design of future remote sensing systems. This performance should become a conscious part of all trade-offs involved.

Evaluation of Basic Approaches to Calibration

The various factors involved in the two different fundamental calibration system approaches remain to be evaluated. Large area, diffuse sources are inefficient but relatively uniform. Focused fiber-optics systems are relatively efficient and stable with respect to surface contamination. But they are substantially less uniform and are sensitive to vibration. Quantitative evaluation of these two different approaches will be necessary before optimum systems can be designed. Radiometric problems in systems operating and being integrated underline the importance of this analysis.

Specification Detail

Radiometric specifications for future platforms should be made sufficiently complete to assure fulfillment of user expectations or realistic trade-offs. For example, distinctions among the various types of calibration—absolute, relative spectral, temporal stability—should be drawn explicitly.

Fulfillment of Specifications

Firm demonstration of fulfillment of the new and complete specifications should be required of suppliers.

Establishment of Calibration Capability on the Ground

The present inability of NASA to evaluate independently and quantitatively the radiometric performance of its remote sensing systems can have very serious consequences in the performance of the systems now operating and being designed. Compliance even with the few specifications that have been designated cannot be verified. Indeed there are reasons to suspect that some of the systems as supplied will not meet their designated specifications, minimal as these are in terms of performance required by users. The performance of future systems will have to be specified more carefully and then evaluated reliably after delivery.

Detectors

The achievement of measurements of the required reliability may well hinge on the development of detectors of greater stability and verification of that stability. New solid state detectors in both the visible and infrared probably permit greater stability with sufficient sensitivity. Nevertheless, this stability must be verified under simulated space environment for a sufficient length of time. Because of the questionability of forced aging in such work, preparations for such testing should be inaugurated immediately.

Visible Sources of Radiation

Even with the promise of more stable detectors, the useful life of calibration sources, operational limitations, and necessary constraints must be studied and research performed to permit greater reliability and substantiation of predicted life. Here, too, the questionability of forced aging and the large amount of work required to achieve the desired improvement dictate the immediate inauguration of suitable programs to provide standards of extended and proven reliability.

Blackbody Theory

Reliable measurements in the infrared require use of blackbodies of known characteristics. Blackbody theory sufficiently comprehensive to encompass

realistic space observation conditions must be developed. It must then be proven in the laboratory.

Stability of Surfaces

The stability both of primary infrared blackbodies and of diffuse surfaces used in periodic measurements of the sun in visible spectral region is unknown. Knowledge of the stability of diffusing and specular surfaces under aging space conditions must be developed. The preparation of reliable measurements of such stability should be inaugurated immediately.

Cryogenic Factors in Infrared Measurements

Infrared measurements in the 8-14 μm region require cooled detectors. Cryodeposited contaminants can affect the performance of such cooled radiometers in ways not yet determined. A quantitative study of the effects of such contaminants must be undertaken if the long-term performance of such radiometers is to be reliable.

On-Going Program—SkyLab

SkyLab might be employed usefully (a) to verify the stability of the most promising components under real space environment and (b) to compare the scanner data with local data at five-day intervals in order to explore atmospheric changes.

Activity in these areas would be small compared with the total effort involved in future systems. But such activity would provide the only reasonable assurance that quantitative user needs would be fulfilled.

PLATFORM EFFECTS

Most aerospace vehicles can be used as remote platforms for earth observation with varying degrees of effectiveness. Aircraft and spacecraft have been used commonly for this purpose; balloons and sounding rockets can also serve as suitable platforms for certain applications. The operating characteristics of these vehicles are sufficiently different so that for the most part they compliment, rather than compete with, one another (Table 5-4). A referenced document prepared by NASA Langley Research Center, entitled "Remote Measurement of Pollution," contains a discussion of these platforms, much

Table 5-4
Platform Characteristics

Platform	Capability	Applicability
Aircraft	Low altitudes (<20 km) Short duration (few hrs)	Intensive local coverage in selected areas, very high resolution possible, flexible scheduling
Balloons	Low altitudes (<50 km) Medium duration (few wks)	Hovering over selected areas, somewhat difficult to control coverage, attractive for testing spacecraft payload sensors through atmosphere
Sounding Rockets	Variable altitude Short duration (few hrs)	Good mainly for vertical profiling
Spacecraft	Selected altitude (500-36,000 km) Long life (many months) Payload weight limited by launch vehicle capability	Automatic routine global coverage for long periods of time, high resolution coverage of large areas feasible

of it is applicable to the general problem of earth observation. The more important properties that determine the suitability of a platform for a particular earth observation program are:

- Physical support features such as allowable payload weight, power, volume and data handling capacity
- Cost and availability
- Nature, duration, and quality of viewing coverage as determined by altitude, range, trajectory, life expectancy, and the accuracy and stability with which the sensor can be pointed to the desired target on earth.

The present discussion concentrates on the last item, with emphasis on platform stability, as it affects or limits high resolution earth observation from remote platforms.

Aircraft have been used extensively for oil and mineral exploration, forestry and agricultural surveys, and cartography. A recent survey paper by Syvertson and Mulholland provides information on the present and projected future role of aircraft in earth observation. Aircraft are very well suited for intensive coverage of small selected areas, and also for study of shortlived phenomena with rapid and unpredictable changes where flexible scheduling is desirable. Although an aircraft cannot be as free from vibration as a spacecraft, the lower operating altitude implies a higher allowable level of attitude perturbation for the same ground resolution (see Figure 5-7). The main limitation is the impracticality of global coverage using only aircraft. Spacecraft and aircraft should play complementary roles in a unified and well coordinated earth observation program.

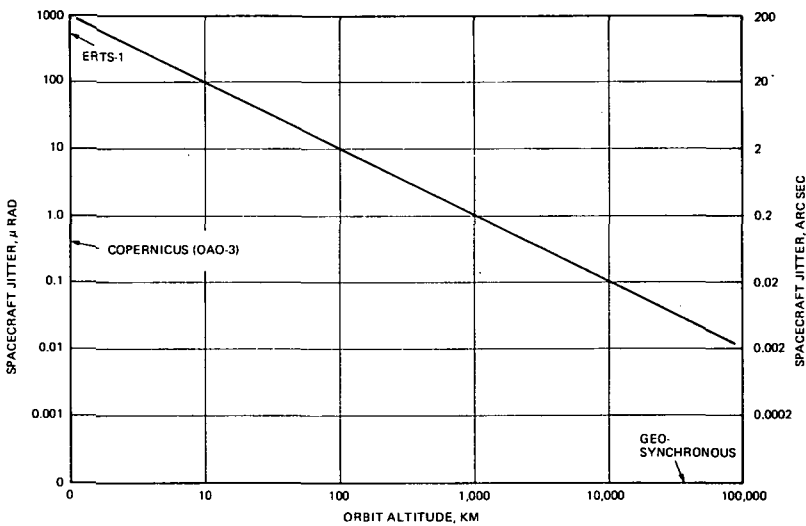


Figure 5-7. Allowable Attitude Error per Meter of Error on Ground

A global overview at predetermined intervals may be provided by earth observation satellites while frequent and on-demand local coverage may be obtained by use of aircraft. Sounding rockets and balloons may also fit in such a unified program to perform specific support functions. Sounding rockets are useful for vertical profiling and have otherwise limited applicability. Balloons have been extensively used by several agencies of the government. A reference document from the bibliography to this chapter, entitled "Proceedings of the Symposium on Earth Observation from Balloons," deals specifically with the problems of earth observation from balloons.

The present trend is to make more extensive use of spacecraft as platforms. They have the obvious advantage of providing unattended service on a global scale for a fairly long time and can provide respectable resolution on ground. Table 5-5 presents a brief survey of recent, on-going and planned spacecraft programs with potentialities of earth observation.

Table 5-5
Survey of Recent or Planned NASA Programs with
Potential for Earth Observation

Program Name	Approximate Weight, (kg) Gross/Payload	Orbit	Attitude
ERTS-1	816/204	Circular Polar Sunsynchronous 912 km	3-axis stabilization $\pm 0.4^\circ$, $\pm 0.015^\circ/\text{sec}$
ITOS-D	308/99	Circular 78° Retro 1460 km	Momentum bias (dual spin) stabilization $\pm 0.4^\circ$, $\pm 0.005^\circ/\text{sec}$
ATS-F	930/272	Geosynchronous Equatorial 90°W	3-axis control normal $\pm 0.1^\circ$, low jitter mode $\pm 0.01^\circ$, $\pm 0.001^\circ/\text{sec}$ for up to 24 minutes
SMS	243/84	Geosynchronous	Spin stabilized 2.4 microradians nutation half-cone angle
Copernicus (OAO-3)	2204/--	Circular, 35° inclination, 740 km	3-axis control ± 0.24 microradians under PEP control
EREP/ SKYLAB	975/420	Circular, 50° in- clination, 435 km	
SHUTTLE	-----	185 km-500 km, various inclinations	$\pm 0.03^\circ/\text{sec}$

The next two subsections describe the orbit and attitude requirements, and the current and projected state-of-the-art.

Orbit Requirements and State-of-the-Art

The satellite orbit is chosen to satisfy, as far as practicable, the required viewing area coverage and the subsatellite ground track pattern. Some compromises between conflicting requirements are almost always necessary. Fuchs and Stratella (1970) provide a sample orbit analysis for a specific earth observation mission. A NASA report in 1970, "The Definition Phase Report for the Earth Observatory Satellite (EOS)" (from the reference bibliography) includes other aspects of spacecraft design. A circular orbit is usually preferred so as to maintain a nearly uniform distance from the ground. Variations in the solar illumination angle at the subsatellite point for a given latitude is also considered undesirable and usually minimized by using a sunsynchronous orbit. The launch window is chosen to satisfy the solar illumination angle requirement. The angle between the spacecraft orbit plane and the equatorial plane determines the latitude limits of the ground track. (A 50-degree inclination angle or greater is needed to cover the continental United States excluding Alaska.)

However, the requirement of sunsynchronism forces a constraint between the altitude and the inclination angle. It turns out that for altitudes up to a few thousand kilometers, sunsynchronous orbits are near polar so that global coverage is possible. In the absence of any other overriding factor, an orbit is usually chosen to be low enough for large weight and good resolution but high enough to reduce atmospheric drag and disturbance (for longer life and easier stabilization), to provide a fairly large swathwidth on the ground, and to result in reasonably long contact time with ground station. The last consideration may disappear if geostationary data relay satellites are utilized.

A major alternative to a sunsynchronous orbit is a geosynchronous orbit in which the spacecraft remains approximately stationary relative to ground at an altitude of about 35,900 km. The obvious advantage is that a number of such spacecraft with pointable gimballed sensors can continuously monitor the earth with near global coverage, while maintaining a continuous communication and command link with appropriate ground stations. Disadvantages include the large launch vehicle requirements for the spacecraft, the extreme stabilization and control requirements, and the more difficult sensor design for the necessary resolution. Added to these possibly is the station keeping requirement since only a few equilibrium positions are appropriate for such satellites.

The altitude and the required ground resolution determine the accuracy with which the orbit elements and attitude variables must be known. The error sources do not have comparable effects on image quality. An error in altitude

affects scaling whereas along-track and cross-track errors in orbit elements affect positioning. An angle error about the local vertical does not have the same kind of effect as angular errors about the other two axes. Moreover, some of these error sources may not be clearly distinguishable. For example, an angular error about the velocity vector has effects somewhat similar to a cross-track orbit error. Therefore, the overall picture quality depends heavily on how these errors are estimated and eliminated. (This is discussed in a later section.)

To simplify discussions, the required ground resolution is normalized to one meter. The needed accuracy of along-track and cross-track orbit elements is then given by $1 + h/R$ where h is the orbit altitude and R is the radius of the earth. Figure 5-8 is a plot of this relationship. The regularity of spacecraft motions, use of an extensive tracking network and accurate modeling of geopotential field permits fairly precise estimates of spacecraft positions. An accuracy in the range of 30-100 m is quite reasonable (discussed in the NASA EOS report referenced previously). A recent study entitled "EOS Mapping-Accuracy Study" by Bendix Research Laboratories considers 5 m achievable and 20 m practicable. These are all one sigma values in an ERTS type orbit. (See Table 5-5.) Space navigation techniques now available are capable of determining the position of a site on the earth's surface with an accuracy of the order of ten meters or better (Siry, 1972). The orbit estimation errors are not equally distributed in all directions; the error in the direction of motion is usually significantly larger than the error in other two axes. At synchronous altitude, the error is of the order of 100 meters one sigma; the longitudinal error usually being much larger than the errors in other directions.

Identifiable landmark features within the earth observation payload sensor imagery, also called ground truth data and ground control points, can be used to improve orbit (and attitude) estimation. Photogrammetrists have utilized such techniques for quite some time. In conjunction with modern statistical filtering methods, which have proved so efficient in orbit estimation schemes, this use of ground truth data holds great promise for providing an efficient and practical data processing tool.

Attitude Requirements and State-of-the-Art

The earth observing sensor carried as a payload on a platform naturally imposes certain requirements on the nature and quality of platform motions, and the knowledge of such motions. To accurately locate a desired target on the ground within the sensor field of view, it must be possible to orient a platform-to-ground line-of-sight vector to adequate accuracies. The variables

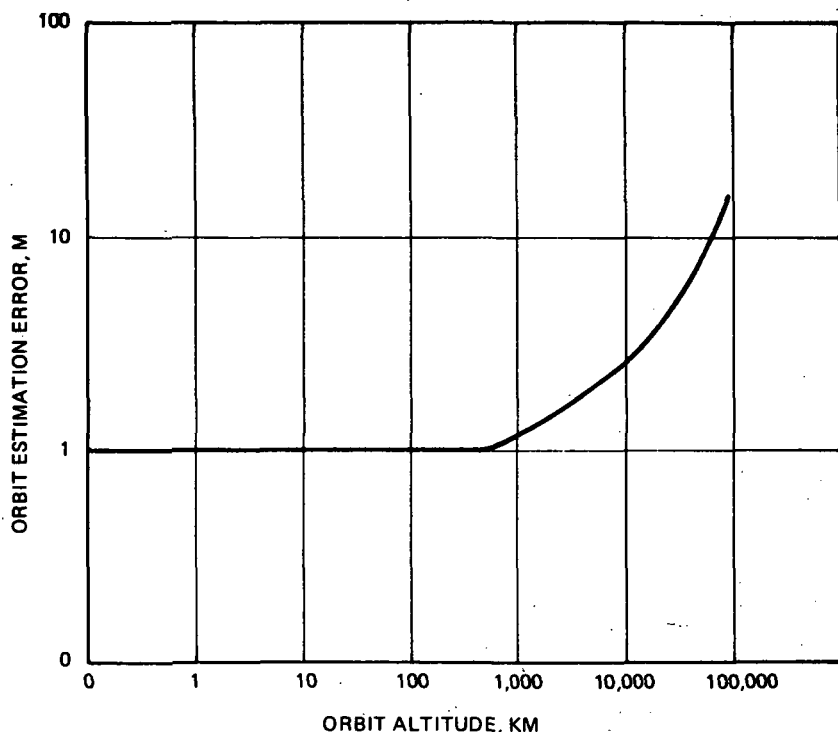


Figure 5-8. Allowable Orbit Estimation Error per Meter of Error on Ground

defining the platform trajectory (or orbit) and orientation (or attitude) must be known accurately to allow precise identification of the intersection point of the line-of-sight vector with earth's surface. Several different levels of accuracy can be specified for these variables.

Quite modest accuracies in real time knowledge of ephemeris and attitude are usually adequate to acquire the target within the sensor field-of-view and provide desired coverage. The temporal registration, or the exactness with which two pictures of the same ground scene taken at two different times may be made to overlap, is determined by the total error in orbit and orientation. In the absence of significant internal distortions within the frames, it may be easier to match the frames during data analysis rather than design the platform attitude control and orbit determination systems to meet severe accuracy requirements.

Very close control of short term variations (or jitter) is required for picture qualities consistent with high resolution payload sensor capabilities. Jitter

affects the spatial registration, or the ability to reproduce the shapes of large objects faithfully and determine the relative locations of small ground features within the same frame exactly. For the usual case of an earth observation sensor rigidly fixed to the platform, it is obvious that rapid and random jitter motions are much more significant in image degradation than large bias type errors that are fixed or vary slowly.

Finally, the accuracies with which the platform motions can be easily controlled are far exceeded by the accuracies with which these can be measured or estimated, particularly if post-flight smoothing is carried out. It is therefore possible to apply attitude and orbit corrections during data processing to improve image quality. A viable strategy for achieving good performance is to use ground based precision orbit and attitude determination systems with a loosely controlled low jitter platform.

The nature of the payload sensor determines the type of jitter requirements that must be imposed on the platform. For shuttered framing sensors taking "snapshot" pictures, the stability during the very short duration of exposure is critical; the orbit and attitude motions are utilized only to change the field-of-view coverage. An example is the Return Beam Vidicon (RBV) camera on the ERTS spacecraft. Much more severe stability requirements are imposed by multispectral electromechanical scanners which utilize platform motions as essential features of sensor operation. Examples are the Multispectral Scanner (MSS) on ERTS, and the VISSR on SMS. In such cases, the perturbations must be below acceptable levels for many tens of seconds or several minutes.

For a given ground resolution, allowable error in attitude (jitter) has an inverse relationship with altitude. The log-log plot is therefore a straight line and is shown in Figure 5-7. The yaw error (rotation about local vertical) is usually not very critical for picture quality but is more difficult to compensate in digital data processing. Figure 5-7 refers to attitude jitters in the other two axes. These are either the short term stability errors, or attitude estimation errors if a precision attitude determination system is used, which affect the spatial registration within one frame. The overall pointing accuracy may be much inferior. The approximate jitter performance of two spacecraft are also shown to provide benchmarks. The quoted performance of Copernicus can be considered the limit for all practical purposes for any spacecraft within the next ten years. (See Table 5-5 for an indication of the present state-of-the-art.)

The example of Copernicus—an astronomical observatory—is not directly applicable for earth observation missions. In this case, a large astronomical

telescope meant for stellar observation also produces a fine guidance error signal for satellite control. Tracking a cooperative target is always a desirable feature of a control system. Earth observation payload sensors are not likely to be able to generate attitude error signals in real time (although they may effectively do so for post flight data processing) and auxiliary independent attitude sensors must be used for attitude determination and control.

Requirements on attitude stabilization and attitude determination may be established by referring to Figure 5-9 which was generated by F.C. Billingsley of the Jet Propulsion Laboratories. The loss of resolution because of uncertainty of geometric locations of pixels starts to become significant when the location error is about one tenth of an IFOV.

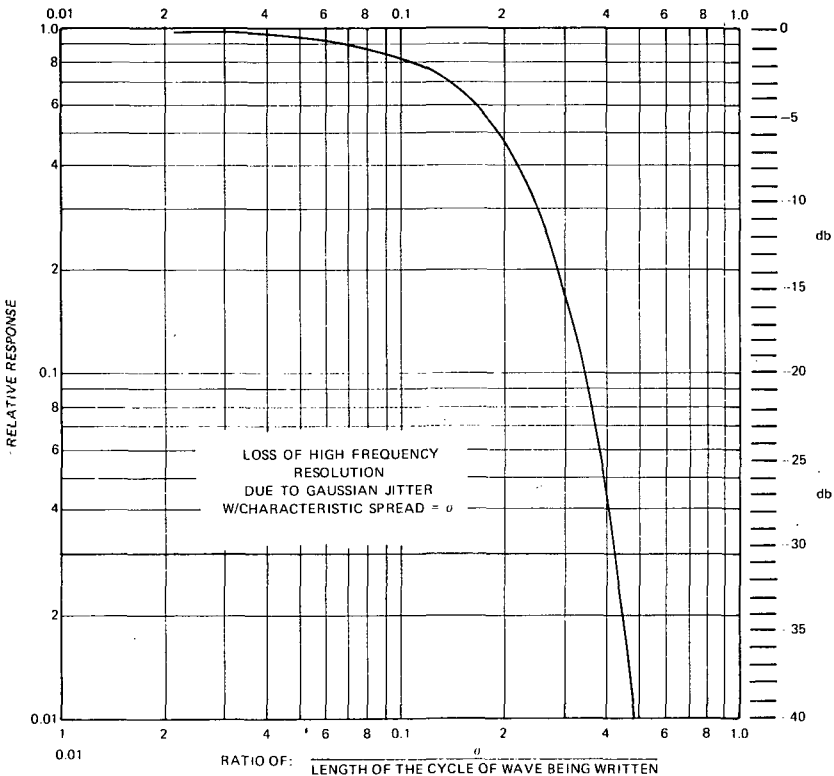


Figure 5-9. Loss of High Frequency Resolution Because of Jitter

The problem of precision attitude determination and control has not received the same attention in the past as precision orbit determination and precision

image data processing. These are of course different facets of the same problem. Studies and design efforts by Draper Laboratories (1972), TRW and Honeywell, indicate that attitude accuracy of 18 microradians (0.001 degree) one sigma, or better, without using payload sensor data, may be achievable within the next several years if adequate efforts are made. The nearest thing to an operational system is the one being built by Honeywell under an Air Force project, but the accuracy is likely to be significantly less than the above number. However, there is no insurmountable technological barrier in achieving post flight attitude determination accuracies below 10 microradians for the several minutes of time an ERTS-type satellite takes to pass over the continental United States.

Spacecraft Error Sources and Attitude Motions

Attitude motions can be put into proper perspective by considering the major geometric error sources. At the low end of the frequency spectrum are bias-type slowly varying errors such as thermally induced flexures, axis misalignments, orbit irregularities, and errors produced by atmospheric, solar, gravitational, and magnetic torques. These range up to a few thousandths of a hertz and have predominant components at daily and orbit frequencies, and their multiples. These are largely deterministic and, therefore, can be calibrated out if a high accuracy attitude sensor is available.

For earth observation missions, the payload sensor can serve as the precision attitude sensor in conjunction with ground control points. Attitude motions of spin stabilized spacecrafts are usually concentrated at certain discrete frequencies depending on design and operating conditions. For the more usual case of three axis stabilized spacecrafts, the attitude variations usually range from orbit frequency up to a few hertz. They fall off rapidly with frequency, as discussed below, and the frequency at which they cease to be significant clearly depends on the desired attitude accuracy. A horizon sensor is the usual attitude sensor used for closed loop attitude control and it can provide, at best, ± 0.05 degree accuracy up to very small fractions of a hertz. (This is discussed in NASA SP-8033, entitled *Spacecraft-Earth Horizon Sensors*, 1969.)

A horizon sensor is a two-axis device, and therefore, for the third (yaw or local vertical) axis, a rate gyro in the gyrocompass mode is commonly used. Also, if the bandwidth of the horizon sensor is not adequate, gyros in the other two axes may be used for rate damping. Three axis precision gyro systems may also be used, independently of the attitude control system, for attitude determination. Precision gyros are capable of measuring rates up to many hertz with short term (few minutes to an hour) stabilities of the order

of 0.001 - 0.01 degrees per hour provided great care is taken to calibrate a slowly varying bias drift rate of 1.0 - 10.0 degrees per hour. A precision attitude sensor may be used to estimate the bias at frequent (but not necessarily regular) intervals. The length of the interval depends on the quality of the gyro system and the desired accuracy. It may vary from a few minutes to few tens of minutes.

In the proposed Stellar-Inertial Measurement System (SIMS) a star sensor is considered for this purpose (Draper Laboratory 1972). Within reasonable weight and size limitations, star sensors can deliver several microradians accuracy up to several tenths of a hertz. Significantly better performance is possible with large optics—Copernicus is an example—but it may not be cost effective to do so. Ground control points in the payload sensor imagery can also be used in place of, or in addition to, the star sensor and preliminary investigations have established the feasibility of this concept. (See the Draper Laboratory study mentioned previously.) One nice feature of this method is that the attitude measurement accuracy is automatically normalized to the payload sensor requirements.

Mechanical jitter at frequencies above one hertz may be within the electro-mechanical scanner itself, induced by the spacecraft attitude motions. They may also be due to flexibility and excitation of natural modes of the spacecraft, coupled with a fluttering solar array. In the case of spinning spacecraft, nutational motions may cause jitter. These are as much structural as attitude control problems. Effort is usually made to reduce these to acceptable levels. If desired, some of these motions may be measured by using accelerometers, gyros, and encoders for eventual compensation. Earth observation sensors are usually made passive to separate out the problems of sensor design and spacecraft design. However, it is the overall performance of the system that is of interest and as the scanners get more complex, some simplification may be achieved by coordinating spacecraft and sensor designs.

Mathematical Model

A very simple linear mathematical model of spacecraft altitude motions is developed next to provide a feel for the platform behavior.

For a three axis stabilized spacecraft, the simplest model for the spacecraft on a single axis basis is the double integral plant:

$$\ddot{\theta} = T \quad (7)$$

where θ is an inertial angular variable defining the spacecraft rotation and T is the total normalized torque (or acceleration) given by:

$$T = T_c + T_d, \quad (8)$$

where T_c is the control torque and T_d is the disturbance torque. The control system intends to maintain θ indentially zero so that θ is the perturbation about a nominal altitude. Normally, it is desired that the behavior be described by:

$$\theta + 2\zeta \omega_o \dot{\theta} + \omega_o^2 \theta = 0, \quad (9)$$

when control actions are included. This second order damped system has desirable stability and response characteristics when appropriate values of the two parameters—damping ratio ζ and natural frequency ω_o —are used. To get (9) from (7) and (8), it is required that:

$$T_c = -T_d - 2\zeta \omega_o \dot{\theta} - \omega_o^2 \theta. \quad (10)$$

The torque is generated by some electromechanical torquing device and assuming it to be linear:

$$T_c = bu, \quad (11)$$

where u is the control voltage and b is the scale factor. Therefore, it is the aim of the control system designer to generate a signal u given by:

$$u = -\frac{1}{b} (T_d + 2\zeta \omega_o \dot{\theta} + \omega_o^2 \theta). \quad (12)$$

In practice, the signal actually generated uses the estimated values of scale factor and variables:

$$u = -\frac{1}{\hat{b}} (\hat{T}_d + 2\zeta \omega_o \dot{\hat{\theta}} + \omega_o^2 \hat{\theta}). \quad (13)$$

because these are not known exactly and are defined as the following:

$$\hat{b} (1 - \epsilon_b) = b$$

$$\hat{T}_d + \epsilon_d = T_d$$

$$\hat{\dot{\theta}} + \epsilon_{\dot{\theta}} = \dot{\theta}$$

$$\hat{\theta} + \epsilon_{\theta} = \theta$$

where the epsilons with appropriate subscripts are estimation or measurement errors. The resulting actively controlled system is then given by:

$$\begin{aligned} \ddot{\theta} + 2\zeta \omega_o \dot{\theta} + \omega_o^2 \theta = & (\epsilon_d + 2\zeta \omega_o \epsilon_{\dot{\theta}} + \omega_o^2 \epsilon_{\theta}) \\ & + \epsilon_b (\hat{T}_d + 2\zeta \omega_o \hat{\dot{\theta}} + \omega_o^2 \theta). \end{aligned} \quad (14)$$

Equation (14) is then used in place of (9). This is a second order system driven by noise: the first term on the right-hand side represents measurement noise and the second the effects of scale factor error. In most cases, these can be described only in a probabilistic sense. The noise on the right-hand side of (14) is assumed to be white with equal power at all frequencies. The power spectral density of the altitude angle response is shown in Figure 5-10. Increasing ω_o increases accuracy and control bandwidth but consumes more control power and requires better quality sensors. Usually ω_o is chosen so that the control system counteracts the most significant disturbance inputs, because it is impractical to control the spacecraft at very high frequencies. This does not imply necessarily poor performance because normally the disturbance level drops off with increasing frequency. The assumption of white noise in the right-hand side of (14) can be justified by invoking the principle of superposition: all deterministic effects can be taken into account separately to modify the total response.

One important thing to note is that the attitude-sensor-measurement errors and torque-scale-factor uncertainties would produce attitude motions even in the hypothetical case of no external disturbances.

It must be emphasized that the above discussion is not complete in any sense and excludes potentially important effects of such factors as cross-coupling between axes, nonlinear elements such as deadbands quantization, saturation and hysteresis, and limit cycle operation. This model should, however, provide better communication between attitude control engineers and sensor engineers. As a description of attitude motions, it can be used in a statistical error analysis of the overall system. Also, sensor designers may be able to specify attitude control system performance in terms of frequency response characteristics such as the one presented above.

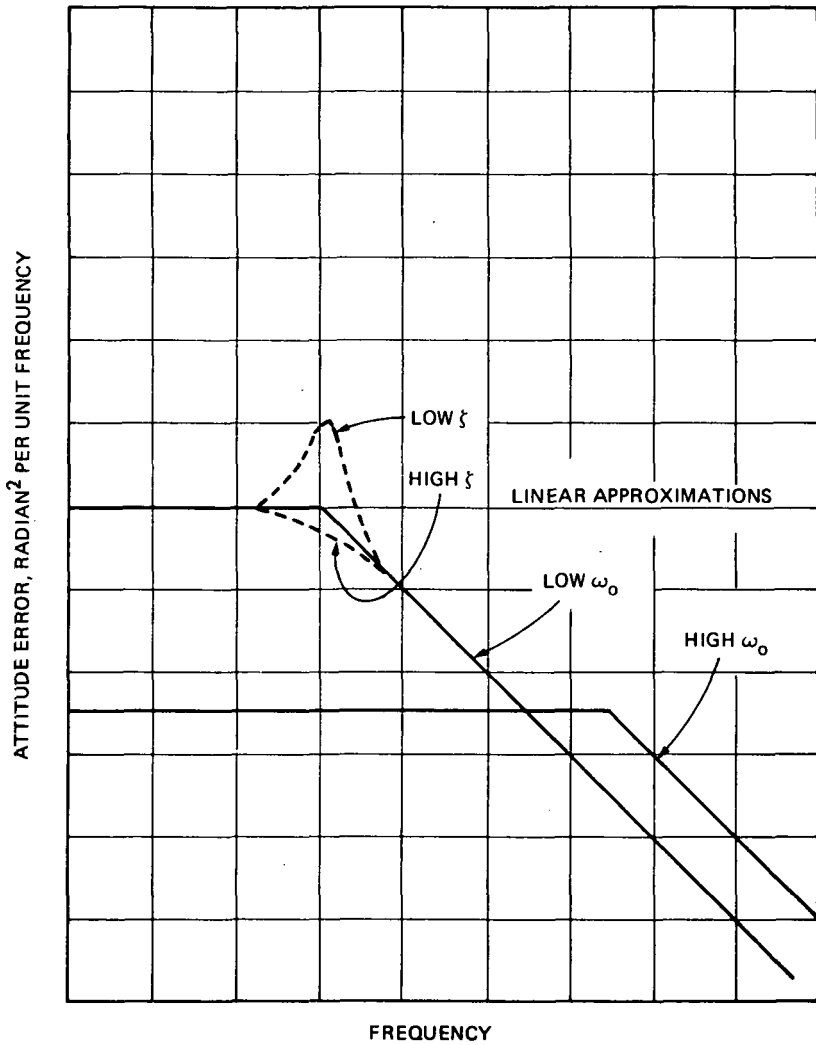


Figure 5-10. Power Spectral Density of Random Attitude Motions

Future Developments and Recommendations

Three major areas that need attention to increase the capability of high resolution earth observation are:

- Sensors (attitude, rate, alignment)

- On-board logic
- Ground processing of attitude data.

High-quality gyros should be considered for more extensive use in future earth observation missions. In many missions, smooth attitude motions and absence of random jitter is more important than absolute pointing accuracy. Good rate gyros, or inertial grade rate integrating gyros used in the rate mode, may provide better rate damping in such cases. This would also permit better yaw control which is a very desirable feature if digital image processing is used. Precision rate integrating gyros may also be used as attitude reference. When properly calibrated and used, these may be depended on to maintain attitude memory within one-to-ten microradians for several tens of minutes.

Sophisticated computational schemes must be used for operation at this performance level. If the gyros are used in a precision attitude determination system on a loosely controlled spacecraft, these computations can be done on ground computers as part of post flight data processing. On the other hand, if these are used in a closed loop attitude control system, a programmable flight computer may be required. In any case, a precise attitude sensor would be needed for periodic removal of low frequency gyro errors.

For automated global coverage, a star sensor may be used for this purpose and the Draper Laboratory study previously referred to discusses stellar-inertial measurement systems (SIMS) for post flight determination of attitude history. The accuracy limiting item in such a system would probably be the star sensor because its physical size increases rapidly with increased resolution and accuracy. A cost versus benefit analysis would limit the star sensor accuracy to a certain value beyond which the attendant increase in volume, weight and power may have adverse effects on other aspects of system performance. These trade-off considerations, of course, may be drastically different for conventionally launched and shuttle launched spacecraft.

The limitations on star sensor accuracy may be circumvented by using ground control points within the payload sensor imagery for attitude updates. A star in the star sensor field-of-view defines a line-of-sight vector from the platform to the outside world and so does an identifiable ground feature in the earth observation imagery. The important difference is that, because of the relative distances involved, orbit ephemeris errors do not corrupt the stellar attitude measurement nearly as much as the ground control point attitude indication. In other words, although the dynamic and kinematic equations of motion of the spacecraft may be usually separated as two disjointed parts (translational

motion of the center of mass or orbit motion, and rotational motion about the center of mass or attitude motion), external effects can become coupled through the measurement equation using ground control points. The solution to such a problem may be obtained efficiently and accurately by augmenting traditional photogrammetric methods with modern filtering theory which has been used very successfully in orbit estimation programs.

The usual photogrammetric method is very well suited for analysis of instantaneous "snapshot" type pictures such as the image produced by the Return Beam Vidicon camera. Ground control points within the frame are used to solve the purely geometric problem of determining the location and orientation of the platform at the instant of picture taking. Usually, the accuracy is improved by computing the least squares solution in an overdetermined system of equations (i.e., one with more than the minimum necessary number of ground control points).

For the image formed by an electromechanical scanner, platform motions during the imaging interval cannot be ignored. In such a case, a straightforward extension of the usual photogrammetric method is to find the nominal trajectory and attitude history during the interval, and obtain least squares solutions for certain orbit elements and/or attitude variables which are perturbations around the nominal. Quite often, the orbit is assumed to be known as determined by orbit estimation programs and low order polynomial models are least square fitted to describe attitude variations. (See Bendix Report on EOS Mapping Accuracy Study.) These estimates of attitude motions must also include significant amounts of orbit repeatability errors. This is essentially an adaptation of a geometric approach to solve a dynamic problem.

Better accuracy should be obtainable at increased computational efficiency by explicitly using the equations of motion in a recursive stochastic filtering algorithm as is done in most orbit estimation programs. This may be used as a refinement over the baseline accuracy values of orbit errors and inertial attitude errors, and simultaneous improvements in orbit and attitude estimates may be accomplished, for example, by employing a 12 element state vector to define orbit and attitude uncertainties.

There is extensive interest in the aerospace industry today in the development of autonomous navigation technology for orbit estimation using landmarks and without ground tracking. The basic ingredients necessary for such estimation by post flight data analysis are already present in earth observation missions. The refinement of orbit estimation of course is a simpler problem than autonomous navigation. On the other hand, it is well established that attitudes can be precisely estimated using gyros and star sensors. Recent

preliminary investigations have established the feasibility of replacing star sensor data with ground truth data. These are examples of independent solutions of orbit and attitude determinations problems using landmarks. Although not usable in the present context, some orbit estimation routines do exist which simultaneously estimate many variables necessary to define orbit and attitude motions. (See Martin Marietta Corporation report entitled *Formulation of Statistical Trajectory Estimation Programs.*)

There is little doubt about the feasibility of this approach from a theoretical point of view. Enough measurement equations may be mechanized to make the system completely observable in the sense of Kalman so that some of the many variants of recursive filtering routines may be implemented. The development needed is essentially of a practical nature: to develop a well-conditioned computational scheme for this specific problem. The advantages that this method can offer over the present approach (as used for ERTS) is better accuracy obtainable through better modeling of the dynamical system, considerable savings in computational requirements because of the use of recursive algorithm and also because the inherently better accuracy permits use of fewer ground control points, and a more streamlined and more nearly automatic operation.

To summarize, a digital image processing system should use geometric correction and annotation data generated by a measurement system using gyros and star sensors for high and low frequency spacecraft attitude data and, in addition, ground control points for calibration and positioning.

Ground control points, without precise attitude data, have been used in ERTS "precision" image processing. Gyro and star sensor based systems are well developed and one such system is going to be flown in near future. A systems approach should now be taken to combine these two methods and synthesize a data processing scheme for geometric image correction which minimizes the total system cost, both spacecraft and ground systems.

SENSOR DATA SYSTEMS

High Speed Multiplexers

A new generation of high resolution sensors are being developed for earth observation missions, and new high-data-rate multiplexers are required which will become forerunners of a new class needed in the near future. Some characteristics of the high rate multiplexers in current use are as follows:

- Data rates: 15 to 60 megabits/sec

- A/D accuracy: 6 to 8 bits
Sampling bandwidths to 219 kHz
- Input capacity: 10-25 channels.

Other programs have been initiated to provide multiplexers for much higher rate requirements of the near future. One of these programs, the Multi-megabit Operation Multiplexer System (MOMS) development, is the result of a GSFC SRT program for a high data rate PCM processor that is capable of accepting a wide variety of analog inputs and producing an output stream at rates of 280 megabits/sec. Although primarily intended to process wideband video data, such as generated by a vidicon or scanning radiometer, the system can be used for any application requiring up to 40 megasamples/sec. Of particular significance is the projected low power consumption of 27 watts while operating at the full 280 megabits/sec rate thereby representing a significant speed/power performance improvement over systems heretofore obtainable.

The MOMS will multiplex and digitize to 7-bit accuracy 60 channels of linear and nonlinear radiometer data at 250 kilosample/second/channel and 4 channels of vidicon data at 5 megasamples/seond/channel. The MOMS will be about 625 cu. in. in size and 25 lbs. in weight.

Each analog input is sampled in accordance with a format controlled by a read-only memory (ROM), and the resulting analog level is converted to a 7-bit binary code in the analog-to-digital (A/D) converter. Considerable flexibility has been provided in the choice of channel sampling rates and format to accommodate changing data requirements. In addition to the analog inputs, provision has been made to accept an external parallel digital input from a housekeeping or equivalent source, and to multiplex that data into the composite digital bit stream.

The overall system consists of two 140 megabits/sec blocks. Each block contains an analog multiplexer, and A/D converter, and optional sample-and-hold and/or compression amplifiers.

All programmer logic has been implemented with a new Current Feedback Logic design (CFL) which is a major factor in realizing these data rates at low power levels. Using this technology, it is possible to achieve a 2 nanoseconds/2 milliwatts logic gate which represents a significant improvement over the closest commercially available logic element. The data format and channel sample rates are controlled by read only memories which provide flexibility to accommodate a wide range of data requirements. The overall format is constrained by the upper limit of 280 megabits/sec, but within that constraint,

any combination of sample rates from 20 megasamples/sec to 160 kilosamples/sec is possible. Although not included in the basic design, further submultiplexing is possible to achieve a large number of channels at lower rates such as encountered in "pushbroom" scanners.

The system provides two out-of-phase output ports, each of NRZ-L format and 140 megabits/sec suitable for use with quadrature modulators. System block redundancy has been employed to achieve a predicted 0.9 probability of success for a one year mission.

A basic accuracy problem has been uncovered during the MOMS development that may be related to high speed multiplexers in general. The present MOMS A/D converter operates at a 20 megasamples/sec (50 ns) rate, of which 20 ns is used to multiplex the analog data and 30 ns is used for the A/D conversion. To implement such a system, requires use of state-of-the-art small geometry transistor with f_t in excess of 1.0 GHz at 1.0 mA. Because of the extremely shallow base widths of these devices, production yields are relatively low, thereby making the selection of high gain matched pairs economically feasible for only a laboratory demonstration prototype. Consequently, the circuits implemented with these devices exhibit a considerably larger worst-case error than would be expected from lower speed circuits where use of matched devices is feasible. It must be noted, also, that the quoted worst-case errors include high speed analog multiplexer error which does not exist in single channel systems.

Table 5-6 demonstrates the worst-case performance that can be expected for combinations of A/D converter bits and transistor size/speed/match. The present approach with a 7-bit design utilizing the small geometry device is shown to have a 2.28 percent error excluding quantizing whereas the same design operating at half the speed and implemented with larger geometry matched devices has a corresponding error of 0.85 percent.

When combined with the vidicon sensor characteristics, the present processor far exceeds the requirement of the vidicon from a dynamic range and noise standpoint, but due to the marginal sampling rate, rather excessive (20%) interpolation errors result. A possible change to this system would be to reduce the number of bits from 7 to 5 and increase the sampling rate from 5 megasamples/sec to 8.7 megasamples/sec. At five bits, it is feasible to employ an all parallel design that permits the use of a nonlinear compression transfer function as well as improving the overall accuracy. The resulting system exhibits a much more consistent and overall improved accuracy.

Table 5-6

Hardware Limitations

		# Bits	Quan Error	Accuracy Excluding Quantizing Error			Sampling Rate Megasamples/sec.
				A/D	Mux	Total	
Unmatched Devices	Present	7	±0.4%	1.32%	0.96%	2.28%	20.00
		6	±0.8%	1.32%	0.96%	2.28%	20.00
		5	±1.6%	0.90%	1.29%	2.19%	34.80
Matched Pairs		8	±0.2%	0.60%	0.25%	0.85%	10.24
		7	±0.4%	0.60%	0.25%	0.85%	10.24

Because of the greatly improved radiometer characteristics, the overall accuracy of the system is constrained by the processing rather than the sensor itself. Consequently, the changes upgrade the processing performance by increasing from 7 bits to 8 bits and by implementing the slower large geometry devices.

Inasmuch as the study design of the present MOMS functional blocks is completely applicable to the aforementioned system changes, a more optimum system could be considered in the future.

Definition of these optimum system parameters has been a direct outgrowth of the significant amount of information derived from the effort on this study program to date, particularly as it relates to actual system implementation with components available now and in the immediate foreseeable future.

To summarize, multiplexers for high resolution sensors with output rates to 280 megabits/sec have been demonstrated. At a maximum A/D converter of 20 megabits/sec, 7 bit accuracy is marginal while 8 to 9 bit accuracy would be unattainable using currently designed circuitry. At lower sampling rates, higher accuracy (8 or 9 bits) is feasible. Thus the development of a time division Pulse Code Modulation multiplexer for these data rates is within the state-of-the-art. However, if high accuracy (<1/4 of 1%) is required, more development will be required.

On-Board Storage

Spacecraft Tape Recorders—Present

The past and near future capabilities of spacecraft magnetic tape recorders are described in Attachment D, "High Data Rate Spacecraft Tape Recorders."

Below are some specifics included in the paper, some additional notes on spacecraft recorders, and comments on what is available in associated ground tape recorders.

The highest data rate recorders now in use are the ERTS Wideband Video Tape Recorder (WBVTR) and the SkyLab Earth Resources Experiment Package (EREP) recorder.

ERTS-WBVTR. This device operates either in an analog mode with an information bandwidth of 4 MHz or in a digital mode at 15 megabits/sec. Additional details are included in Attachment 4 (previously cited) and Attachment 5, "Wideband Image Recorder for ERTS." This device will also record and reproduce television on SkyLab. Its characteristics are as follows:

Data Rates:

Analog: 4 MHz at 42 dB SNR (6 MHz proven)

Digital: 15 Mbs (30 Mbs possible)

Capacity: 30 minutes = 3×10^{10} bits

Size: 2 cu. ft.

Weight: 76 lbs.

Power: 95 watts (250 watts peak).

SkyLab EREP. The EREP recorder stores digital data from a scanner on 28 tracks at 1 megabit/sec per track. It is a record only device and the 7000-ft reels are removed from the machine by the astronauts and returned to Earth for reproduction. Significant additional development would be required to provide in-space playback.

Other. Many other recorders of lesser data rate are available; from ERTS telemetry at 1 kilobit/sec to Viking Orbiter at up to 2.2 megabits/sec for short periods.

Spacecraft Tape Recorders—Future.

See Table 5-7.

"EOS" — (1 megabit/sec record/30 megabits/sec playback.) A task referred to as EOS, although not exclusively applicable to that program, is the storage of data at 1.2 megabits/sec and playback at 30 megabits/sec. Two programs are addressing this. The most likely to achieve early success is an adaptation

Table 5-7
Spacecraft Recorders

	Data Rate	Capacity-Bits	Date (Technology Achieved)	Cost K\$	
				Develop	Per Copy
ERTS	15×10^6 BPS	30×10^9	1970	2200.	400.
EOS Study	30×10^6 BPS	60×10^9	1973	500.	450.
Transverse (2 channel)	60×10^6 BPS	60×10^9	1973	500.	500.
Multitrack	$60\text{-}200 \times 10^6$ BPS	250×10^9	1974	2000.	500.

of the ERTS—WBVTR. Here the rotating headwheel of this transverse scan device is slowed to provide a record head/tape speed of 80 ips. Playback is performed at the normal ERTS speed of about 2000 ips at 30 megabits/sec. The increase in rate from the 15 megabits per second of ERTS to 30 megabits/sec will be achieved by using a double density code in direct recording rather than the FM/FSK technique of ERTS. The other question, predicted life due to head or tape wear, is still being evaluated. So far, a modified ERTS breadboard has exceeded 5000 hours without head/tape degradation.

Five-Year Tape Recorder. A program primarily devoted to long life has been configured to be ultimately capable of storing 1.2 megabits/sec in record and playing back at 30 megabits/sec. This will demonstrate longitudinal multi-channel capability on a one-inch-wide machine.

ERTS—"EOS" Plus. Several rotary head ground recorders have been multi-channel devices (i.e., instead of the four heads used on ERTS, they employ eight or more). Moving the tape longitudinally at twice the speed then allows the operation of the headwheel at the same original speed, while storing two channels of data. This is one conceivable, albeit complex, way of achieving a 60 megabit/sec capability.

Multitrack Tape Recorders. It appears that pressing the rotary head beyond 30 megabits/sec may be very difficult. For greater data rates, the use of many longitudinal tracks may be more fruitful. Some work is being done. See Final Report Contract No. NAS5-21511, Design Study for Multichannel Tape Recorder System. This approach to 60 megabit/sec and greater is not unreasonable but will require considerable development.

Ground Recorders (See Table 5-8)

Table 5-8
Ground Station Recorders

	Digital Data			
	Rate	Capacity-Bits	BER	Year (Technology Achieved)
ERTS/TR70	15×10^6 BPS	100×10^9	10^{-7}	1971
Transverse (2 channel)	30×10^6 BPS	200×10^9	10^{-6}	1973
Multitrack	$60\text{-}200 \times 10^6$ BPS	400×10^9	10^{-6}	1974 & Up

There is now significant interest and effort in the development of higher data rate and larger capacity ground recorders, both analog and digital. Some of the more pertinent programs are described in the following paragraphs.

ERTS Rotary Head Recorders. These devices are adaptations of commercial television recorders. In ERTS they are configured to an analog bandwidth of 4 MHz at a signal to noise ratio of about 45 dB. This recorder also stores digital data at 15 megabits/sec with a bit error rate of about 10^{-6} .

Extension of Rotary Head Recorders. Several programs indicate that the analog and digital capacities can be extended. It is reported that 15 MHz at 34-40 dB is in the hardware development phase; 6 MHz has been done several times. The modification of a flight recorder to achieve 30 megabits/sec that appears feasible, would certainly be more easily achieved on the ground. This approach employs direct recording of a double density code instead of the FM used on ERTS. Another method that has been used to extend data rates is the use of multiple channels (i.e., the rotating headwheel has 8 or 16 heads on the wheel in place of the 4 necessary for a single channel). This latter method is achievable but, of course, somewhat expensive in that duplicate electronics are required.

ERTS Longitudinal Recorder. The primary digital ground recorder for ERTS is a 28-track, 1-inch-wide tape, longitudinal recorder. It stores demultiplexed 15 megabits/sec ERTS data at a rate of 0.6×10^6 bits per second per track.

It employs a double density code with a packing density of 10,000 bits per inch. Capacity is about 20 minutes.

Extension of Longitudinal Recording. The above ERTS recorder could probably be extended to a data rate of 30 megabits/sec by employing a higher packing density. Also, another group reports 30 megabits/sec on 1/2 inch tape for 20 minutes. Further extensions are underway. Higher longitudinal packing densities of up to 40,000 bits per inch and lateral track densities of up to 160 tracks per inch have been achieved in the lab. One proposal for a ground recorder promised 100 megabits/sec for 20 minutes. Such rates are achievable but the costs are significant. A rough estimate of the cost of such a program might be two million dollars development and 150 thousand dollars per copy. Also, a current baseline design for EOS A requires a ground recorder with data rates up to 200 Mbs.

Laser Recording. Analog devices are conceivable at up to 100 MHz. A feasibility model of a 40 MHz unit exists. Only isolated developments have pursued digital recording. Not too much is available now, but future digital use should not be discounted.

DATA CORRECTION AND IMAGE GENERATION

This section considers the ground processing operations that convert the sensor data from the form received into the output form that facilitate its display, interpretation and use. The ground processing requirements are defined by differences between the characteristics of as-received data, and the image and data characteristics desired as output.

In addition to the physical format in which it is acquired, the as-received sensor information will have various geometric and radiometric characteristics inherent from the acquisition process. These will restrict the usefulness of the output images and data if they are not "corrected." The term "corrected" is therefore used in a collective sense to include operations that redistribute the data into a more desirable form, as well as operations that remove known "errors."

The standard ground processing operations that will be required to convert as-received data from advanced sensors into the required images and data will include:

- Radiometric calibration and compensation of detector variations
- Geometric registration, as required, of sensor data

- Conversion of sensor data to computer-compatible tapes
- Generation of standard-scale annotated imagery, corrected for sensor geometry, platform altitude, attitude, and earth rotation

Other ground-processing operations that would be applied to specific data upon user request might include:

- Generation of imagery expanded in specified portions of the signal range for critical interpretation
- Provision of sensor data transformed into a standard coordinate system and registered with previous data for temporal analysis
- Provision of sensor data calibrated for locally known atmospheric parameters.

In this section, the general processing requirements and associated sensor-related, platform-related and earth-related effects are briefly reviewed. This is followed by discussion of processing operations and instrumentation applicable to the correction and generation of user-compatible images and data.

Radiometric Requirements

The received data must possess at least two radiometric characteristics fundamental to the purposes of remote sensing:

- Spectral Calibration—defining the relationship between data quantization level and received radiance per spectral band in order to determine scene radiance and permit comparison with other sensors.
- Radiometric Stability—maintaining calibration throughout the operational life of the sensor—to permit accurate detection and analysis of temporally varying scene phenomena.

It is also desirable for the obtained scene radiance data to be compensated, or corrected, for the variable and spectrally dependent absorption and scattering effects of the atmosphere.

Since the sensors may have arbitrary radiance transfer characteristics, which will tend to drift or change with time, the corresponding radiometric data processing functions are: first, to normalize the data to an apriori transfer relationship; second, to compensate the data for changes in detector response by utilizing calibration signals obtained from reference radiant sources within the sensor; and third, to compensate the data for atmospheric effects according to some atmospheric model.

For the image outputs, two corresponding radiometric processing requirements are: first, to convert the corrected data to image form with a relationship between signal level and film density which optimizes the human perception of scene contrast over the signal range (or over user-selected portions of the signal range); and second, to apply to each image a gray scale, identifying the signal-to-density relationship.

Geometric Requirements

Three geometric characteristics of the output images and image data are fundamental to the purposes of multispectral remote sensing:

- **Spatial Registration**—elemental registration of the scene information in different spectral bands—for image interpretation and spectral data analysis.
- **Positioning**—determining the geographic coordinates of the scene information—for locating and delineating observed phenomena on the earth's surface.
- **Temporal Registration**—elemental registration of scene information from different coverages—for interpretation and analysis of time-dependent phenomena.

These three characteristics constitute the *geometric* functional requirements for ground processing. They are listed in order of increasing difficulty. The difficulty of each also varies with the type of sensor, stability of the platform, the processing techniques employed, and volume of images and data to be produced.

Some basic considerations with regard to these three functional requirements are given in the following paragraphs.

Spatial Registration

The data from different spectral bands in many advanced sensors will be "inherently" registered. For such sensors the correction required to "achieve" spatial registration of the data in different spectral bands may be absent (or minimal, such as compensating for small fixed offsets between bands). On the other hand, spectral data from noninherently-registered sensors must be geometrically transformed to achieve registration.

Positioning

This geometric functional requirement can be considered two ways. It can involve: (1) identification of earth coordinates in images and/or data remaining in or recorded in the sensor-coordinate system or (2) transformation of the sensor data into images and/or data in an earth-based coordinate system. The first approach requires determination of the sensor-to-earth coordinate relationship in a way unique to that image and/or data set. Since it does not transform the data itself, the processing implementation is simpler than the second approach, the conversion of the data into an earth-based coordinate system, which increases the amount of processing required. In general, the second approach involves a transformation of the data according to the known projective geometry and orientation of the sensor into a standard projection, and then identifying the position and orientation of the transformed data set on the earth's surface.

A consequence of the first approach (from a user standpoint), is that the user must apply the earth-sensor relationship that is unique to that data set in order to find the points of interest in his data. With images, where only certain earth locations (e.g., grid intersections) are identified, determining the position of points other than those identified requires a nonuniform spatial interpolation unique to that image. With the latter approach the relationship between image points or data points to earth coordinates is uniform. Depending on the type of image recorder used (discussed later), it may be easier to apply a uniform geometric transformation to all images than to all digital data and in view of this, the volume of images relative to the volume of digital output data desired becomes an important consideration.

Temporal Registration

Transformation of scene information from different coverages into element-by-element registration is the most difficult processing task, particularly for digital data outputs. For images which have been corrected to a common output geometry (as discussed in the previous paragraph) some degree of registration automatically applies between images of different coverages. Here registration errors are dependent on spatial repeatability (rather than absolute accuracy) of the geometric conversion and positioning. If alignment is based on matching "image content," registration error will be the difference between the two transformations. If alignment is based on matching geographic "tick marks," the registration error may increase since it will include differences in the accuracy of locating the two images.

Note: In this discussion, reference has been to the transformation of the remotely sensed data into cartographic coordinates. It should perhaps be emphasized that this is not done for purposes of cartographic mapping per se: it is done *to facilitate comparison of data records with one another and with the surface of the earth.*

Image Geometry

In geometry of remotely sensed image data is determined by three factors:

- Imaging characteristics of the sensor
- Sensor orientation
- Geometry of the earth scene.

Sensor Geometry

Sensors are commonly characterized according to the way the image is formed, such as, frame-imaging sensors, line-imaging sensors or arrays, object-plane scanners and image-plane scanners. These distinctions do not always define a unique imaging geometry, although they have some common characteristics. Many imaging geometries are possible for the latter two types.

Frame-imaging sensors obtain a two-dimensional image of the scene formed at one brief interval of time. In camera tubes such as vidicons and orthicons, an optical image formed by a lens is briefly exposed on the sensing surface by a mechanical shutter. The sensing surface converts the optical image to a charge distribution, which is then read out by an electron beam in a prescribed scanning raster. In an ideal framing sensor, depicted in Figure 5-11, image coordinates x, y relate to object coordinates X, Y by a constant scale factor (f/h) , where f is the focal length of the imaging lens and h is the sensor altitude. Practical constraints however limit the geometric accuracy of the scan readout in spaceborne camera-tube sensors. Therefore, the faceplate of the sensing surface is often equipped with a calibrated reseau which superimposes the video information to enable subsequent recovery of the image-plane geometry.

Line-imaging sensors obtain a succession of one-dimensional images of the earth scene along a line normal to the spacecraft motion. Sensors of this type include solid-state linear-array sensors and image dissectors. The ideal geometry is depicted in Figure 5-12; a lens without a shutter forms a moving

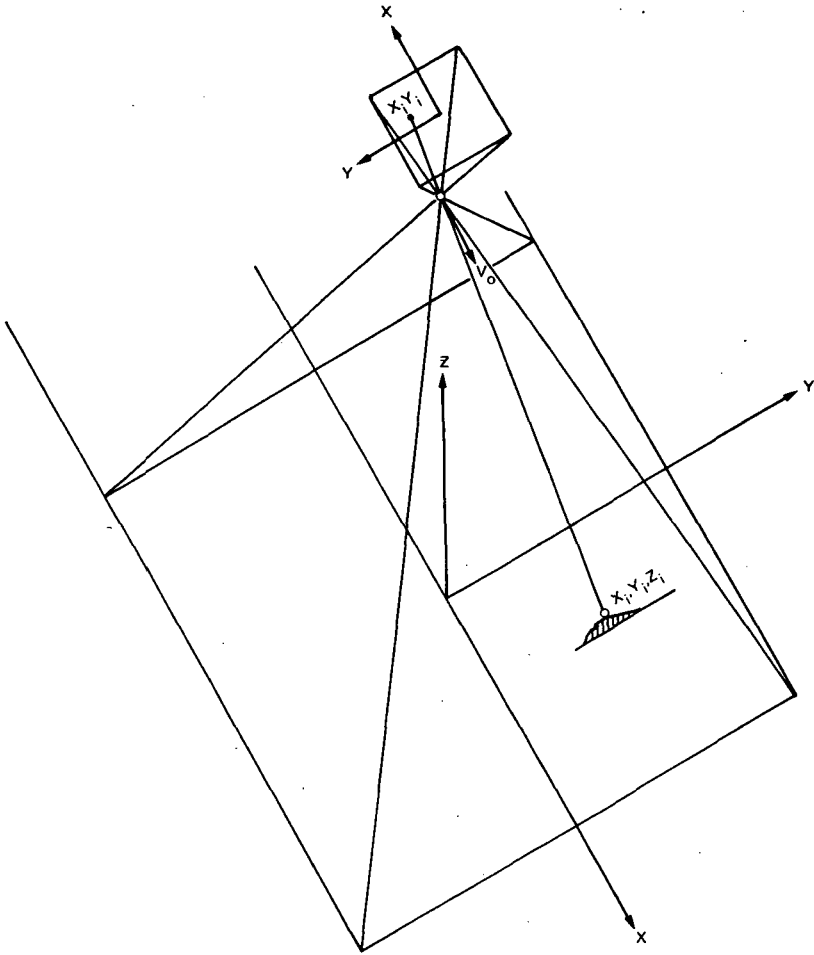


Figure 5-11. Imaging Geometry of a Frame Imaging Sensor

image upon the plane containing the linear detector. The geometry of the line-imager differs in a practical sense from that of a framing imager; it is more like a scanner in which the two-dimensional projection of the scene information varies with changing attitude of the platform.

The basic distinction between *scanners* and imaging sensors is in the way they obtain across-track image information. Scanners utilize relative motion between the optical image and a single detector to obtain each line of spectral

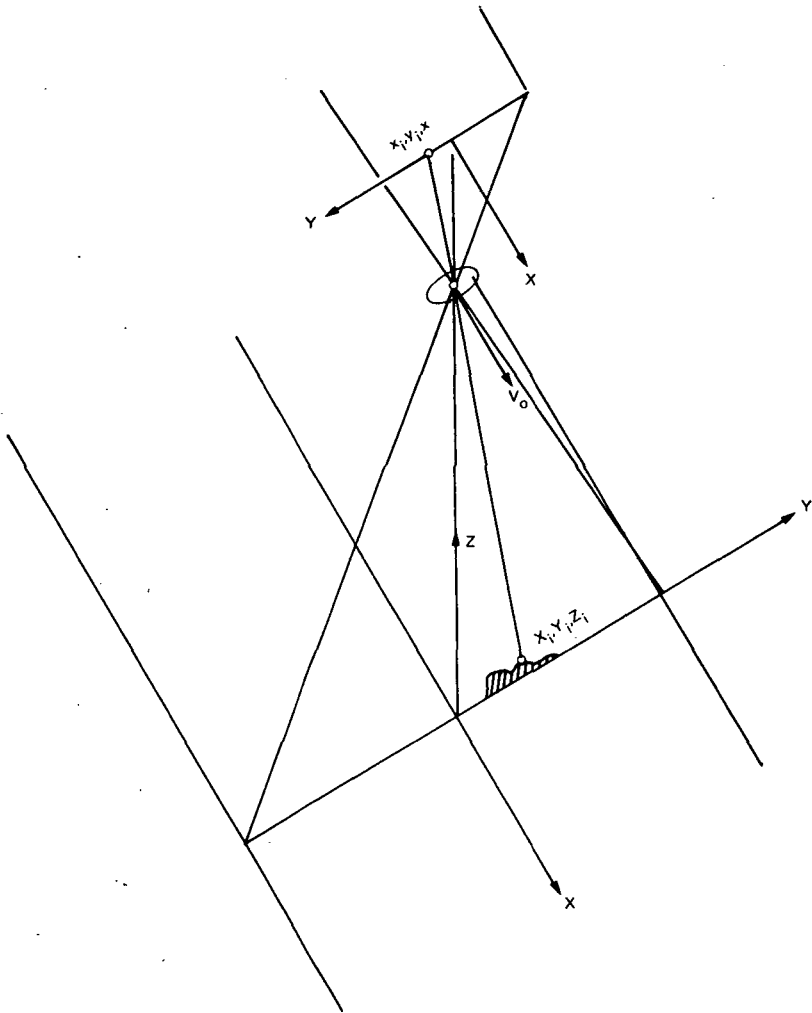


Figure 5-12.. Imaging Geometry of a Line Imaging Sensor

data; imagers use an extended one- or two-dimensional sensing surface or a linear detector array which remains stationary relative to the cross-track dimension of the optical image.

Object-plane scanners (e.g., ERTS MSS) use a telescope with a small working field focused on the detector and a scanning mirror to sweep the field across the ground track. *Image-plane* scanners (e.g., one proposed EOS Thematic

Mapper) use a telescope which images the width of the ground track upon a stationary intermediate plane, of which a small zone is scanned and relayed to or reimaged upon the detectors.

The imaging geometry of advanced scanners, therefore, depends on the particular way the object space or image plane is formed and scanned. A representative linear-scan geometry using an oscillating object space mirror, is shown in Figure 5-13. Each scan traces a linear path orthogonal to the ground track, each trace obtains a number of scan lines. This is a geometry similar to the ERTS MSS sensor, obtained by a vibrating mirror. Other advanced scanners may use a rotating wheel to scan a curved image plane and thus providing a nonlinear imaging geometry.

A conical scan geometry, Figure 5-14, is representative of one present approach toward an advanced high-duty cycle scanner. The cone axis is tilted forward about one-half the included angle so that the active scan is nearly vertical beneath the satellite, and each scan sweeps an elliptical segment across the ground track. Vertical orientation of the axis would produce a circular scan segment with a constant nadir angle, but this is undesirable from standpoints of decreased ground resolution, increased position error for given attitude uncertainty, and increased displacement error due to terrain relief. (The latter effect would be valuable for stereomapping, utilizing both fore-and aft segments of the cone, but such cartographic-related missions are not considered to be within the primary data-acquisition role of the sensor.)

Figures 5-15 through 5-17 depict the image-geometry effects of various types of sensors. The first column depicts the inherent geometry of the image resulting from sensing a flat plane. The second column depicts the resulting geometry when sensing a flat plane containing a pattern of terrain relief (diagrammed in perspective at the top of the illustration). The relief pattern shown consists of an array of pyramids whose peaks are above the datum plane in their bases. The third column shows the image geometry after rectification, that is, after conversion of the as-received geometry to that of a standard projection. The residual distortion due to terrain relief is shown by the shaded portions, in which the darker portions correspond to slopes which slope "downward" relative to the horizontal direction from local vertical. The last column is a vector diagram of the local displacement of those image points above the datum. Figure 5-15 depicts these effects for frame- and line-imaging sensors having vertical and tilted orientations. Figure 5-16 depicts the geometric effects for line-scan and conical-scan sensors having vertical and tilted orientations. For reference, Figure 5-17 depicts the imaging geometry for a panoramic two-dimensional imager such as a panoramic film camera.

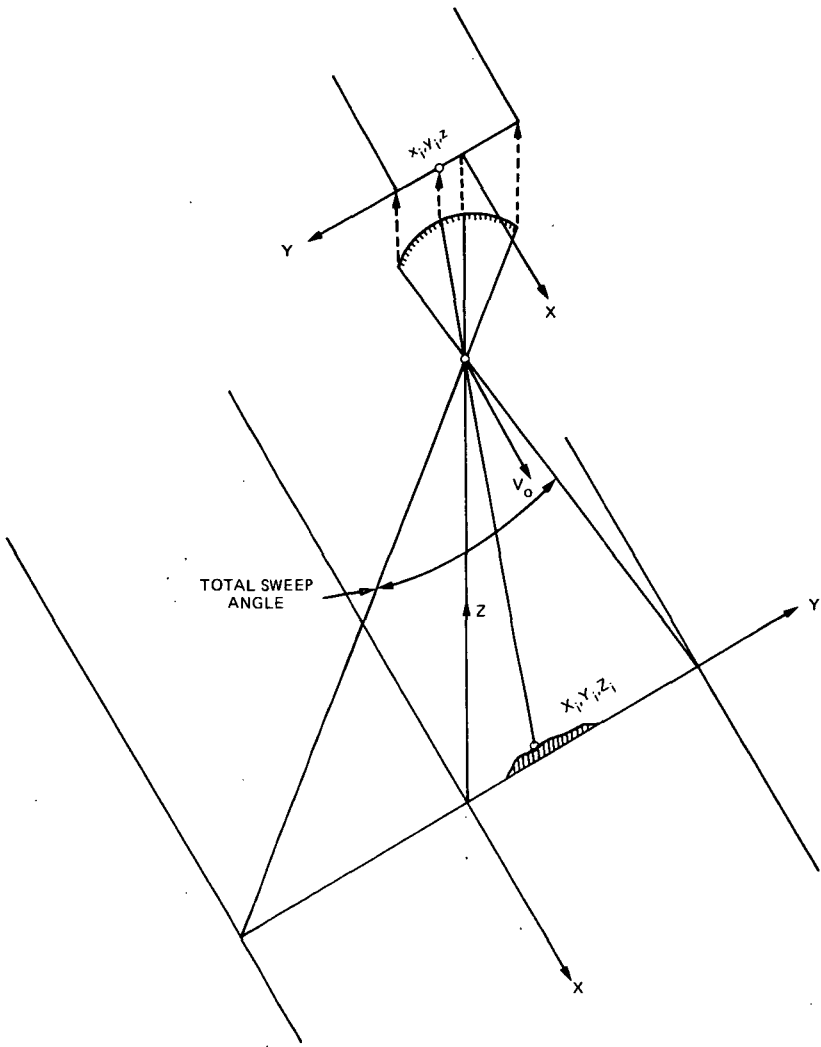


Figure 5-13. Imaging Geometry of an Object Plane Line Scan Sensor

It should perhaps be mentioned that at satellite altitudes, the magnitude of terrain relief effects as depicted in Figure 5-15 and 5-16 is exaggerated; relief effects are considerably reduced (though not absent) in narrow-angle vertically oriented satellite image data.

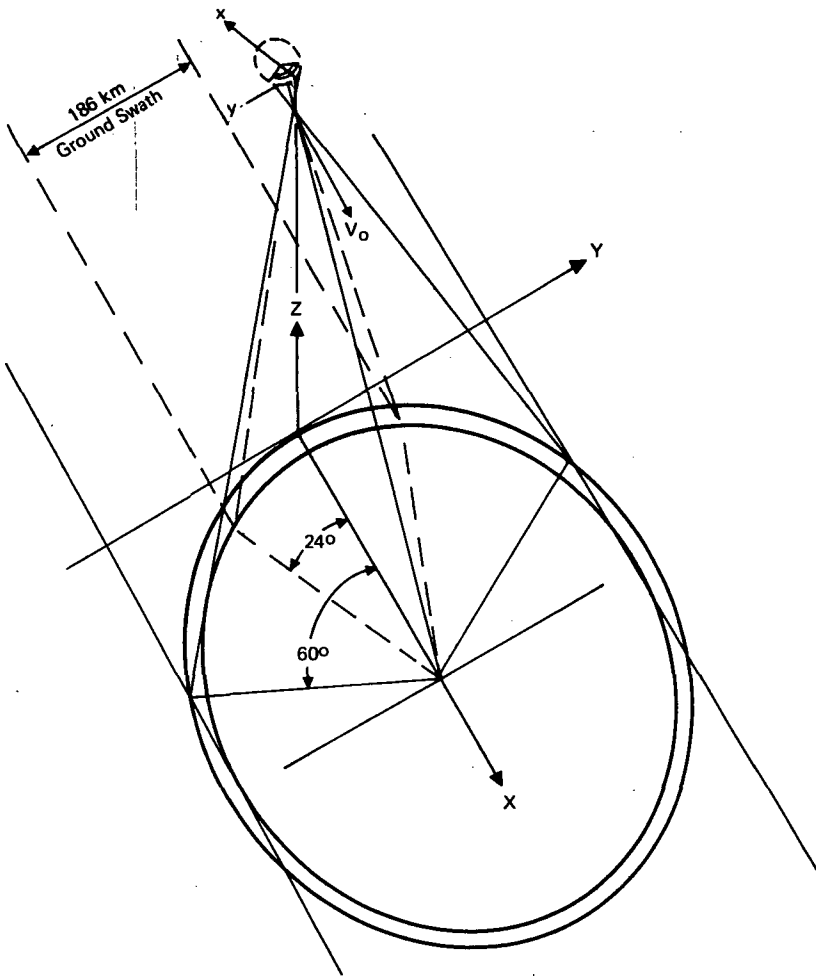


Figure 5-14. Imaging Geometry of an Image Plane Line Scanning Sensor
 (Conical, Forward Tilted Polar Axis)
 $\pm 24^\circ$ scan angle: thematic mapper
 $\pm 60^\circ$ scan angle: skylab

Sensor Geometry Calibration

Any image data correction process requires an accurate calibration of the internal imaging geometry of the sensor. As noted, the projective geometry of some sensors may be complex, but in this regard accurate knowledge of the geometry is more important than its complexity. The complexity of the geometry however may significantly impact the processing required.

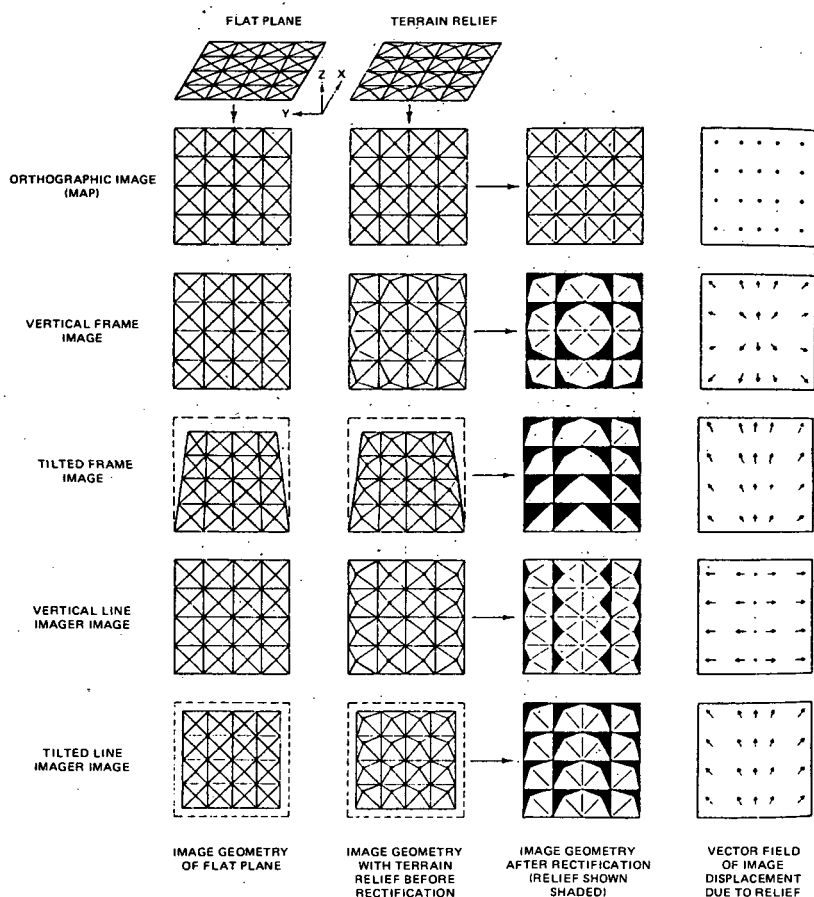


Figure 5-15. Image Geometry and Terrain Relief Distortions for
Frame and Line Imagers

Care must be taken to ensure that the calibration determined on the ground or in thermal vacuum will be the same in zero gravity. Stability of the sensor geometry is also important. When required stability cannot be ensured in the sensor design, an on-board geometric reference (analogous to a *reseau*) is necessary to compensate or reconstruct the geometry on the ground. The reference should be easily detectable in the signal, preferably at the beginning and end of the sweep, and might be incorporated with the radiometric reference.

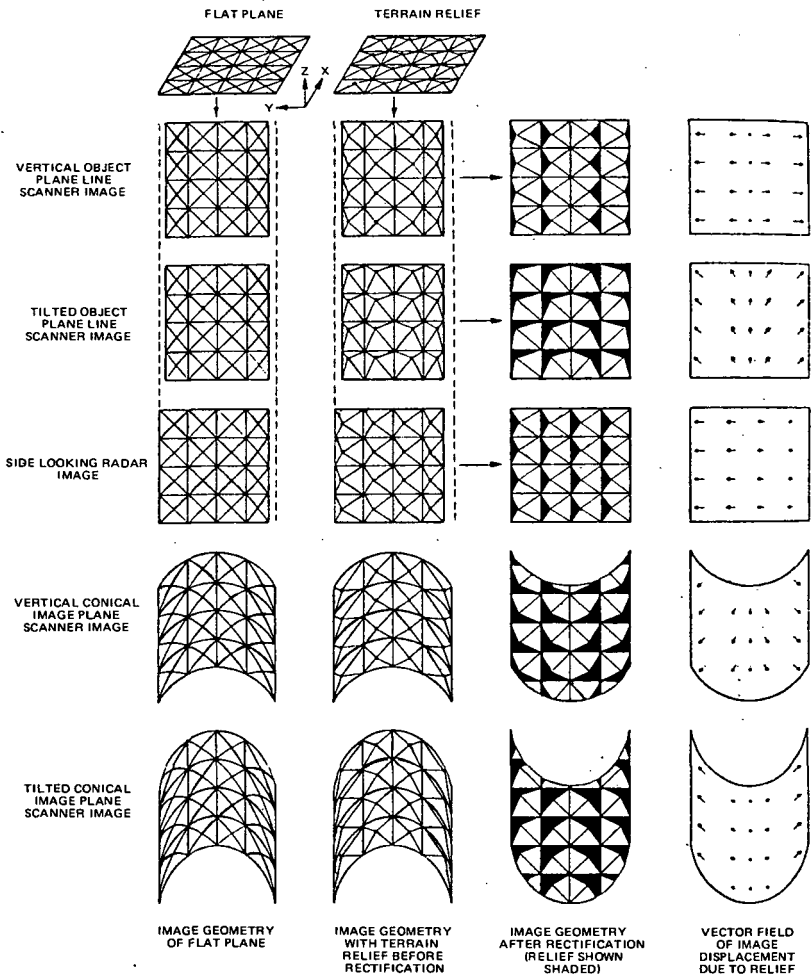


Figure 5-16. Image Geometry and Terrain Relief Distortions for Object Plane Line Scanner, Side Looking Radar, and Conical Image Plane Scanners

External Geometric Effects

Platform Attitude and Position. One basic set of image-geometry considerations external to the sensor are those introduced by variation in the angular attitude and altitude of the platform. With a frame-imaging sensor, the instantaneous attitude is fixed for that frame. A small attitude error from vertical will affect primarily the position of the image (on the earth); such

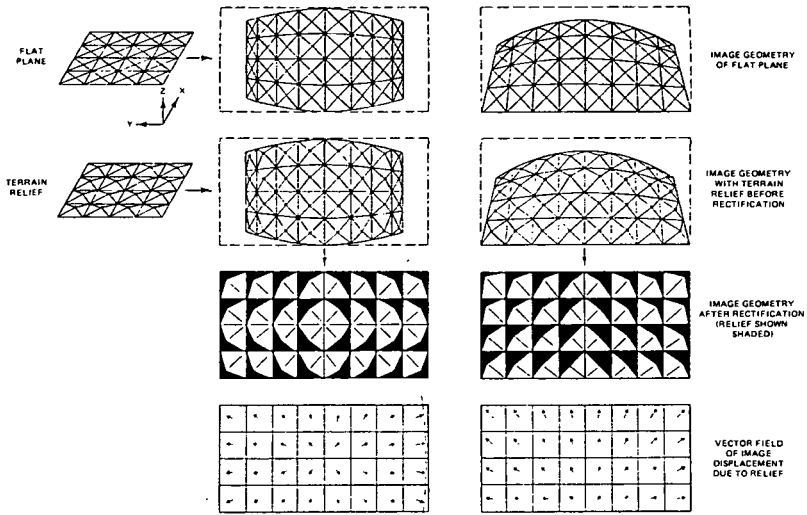


Figure 5-17. Terrain Relief Distortions for a Panoramic Film Sensor

errors will have relatively minor effect on the image geometry. In all other (nonframing) sensors, the orientation errors can have an effect on both the position and geometry. The severity depends on the particular attitude axis and the magnitudes of error, error rate, and rate of change. For instance, a small constant pitch or roll error affects image position but not geometry. A constant yaw error affects image geometry but not position. A constant pitch rate affects image scale in the direction of motion. A constant roll rate introduces first-order image skew. A constant yaw rate introduces higher-order skew. Higher-order effects are introduced by nonconstant rates, when the change of attitude rate is appreciable within the ground interval of interest. These effects however do not necessarily imply that the satellite need be ultrastabilized to minimize such consequences in processing the image data; other (more severe) processing consequences may already exist due to the inherent geometry of the sensor. More important criteria are to ensure that the platform attitude varies smoothly and that its attitude is accurately determined or determinable.

Sensor Pointing. Advanced sensors will include off-axis pointing capabilities to increase coverage effectiveness. For "primary" sensors (i.e., those which cover the maximum ground track width) pointing may occur as a one-track-width offset (to either side of center), thus obtaining the same coverage along the offset track as would be obtained by an adjacent normal track. For

high-resolution (HRPI-type) sensors which cover a smaller field of view, the pointing might be in finer increments (or continuously variable) within three normal track widths. The off-axis pointing modes add to both the geometric positioning requirements (analogous to spacecraft roll attitude) and involve additional geometric transformation requirements.

Earth Rotation skews continuously-acquired scene information eastward relative to the direction of satellite motion and introduces higher-order effects in scanner data. The skew affect is appreciable for the 100 km near-polar orbit; amounting to over 5 degrees at the equator, decreasing with increasing latitude.

Earth Curvature causes a radially-inward displacement of image points with increasing radius from the subsatellite point. This introduces a variable scale effect (common to all representations or projections of the spherical earth on a flat plane) which is compensated to a small standardized error by appropriate choice of the projection plane.

Terrain Relief, as diagrammed earlier, causes image points whose elevation is above (below) some reference datum to be displaced radially outward (inward) from the subsatellite point. The magnitude of displacement increases with the radial distance to and the elevation of the point. (In precision-processed ERTS images, relief effects are minimized by scaling the images to the elevation datum of the image center rather than to sea level, but areas of relief within the scene are not locally compensated. For a 185 km scene, this leads to horizontal errors on the order of 10% of the vertical relief at the edge relative to the center.)

Atmospheric Refraction effects, causing outward displacement of image points with increasing radius from the subsatellite point. They are negligible in narrow-angle vertical images, and even the larger errors introduced in images pointed off-axis can probably be ignored.

Basic Processing Operations

From the foregoing review of the basic processing requirements and potential error sources, the following describes the general operations that are performed to process the received data into the output form:

- Radiometric data correction relative to the sensor and atmospheric effects prescribed earlier
- Relevant image recording techniques, formats, and annotation

- Derivation and use of satellite attitude and position information
- Geometric data processing, including some considerations relating to sensor geometry
- Basic tradeoffs between platform-derived and ground-control data for precise image positioning
- Alternative processing system approaches.

Sensor Radiometric Correction

For sensors which employ on-board calibration references, the ground-processing radiometric correction operation involves (a) extracting the radiometric reference signal from the sensor data, (b) comparing it with the calibrated reference, (c) deriving, from differences between the two, the functional correction required, and (d) applying the correction to the sensor data. The simplest correction involves a level (ΔL) and gain coefficient (G).

$$S_{out} = (S_{in} + \Delta L) G. \quad (15)$$

When the sensor response is nonlinear, or if different detectors have different nonlinearities, exponential or higher-order corrections are involved, such as:

$$S_{out} = (S_{in} + \Delta L)^\gamma \quad (16)$$

or more generally,

$$S_{out} = S_{in} \pm G_1 (S_{in})^2 \pm G_2 (S_{in})^3 \pm \dots \pm \Delta L. \quad (17)$$

Rather than perform multiplicative operations, a table-lookup may be involved to "linearize" the nonlinear effects, or normalize nonlinear differences. One consideration in this regard is that any linear or nonlinear correction of discrete data values implies an output quantization level higher than that of the input data being corrected. Since this may not be desirable from a data volume standpoint, performing a nonlinear correction operation with the same output quantization involves some information loss, as well as some compromise in the data certainty. A philosophical point here is that it might be desirable to *not* "linearize" sensor data that is inherently nonlinear (i.e., relative to the radiance domain, other than correcting for nonlinear differences between detectors. Instead, appropriate radiance calibration tables that define the nonlinear characteristic of the detectors should be issued to the users. When it is desirable to write such data on film with a linearized (or any other) transfer characteristics, the desired characteristic could be provided by a table look-up, or a function generator following D/A conversion.

For sensors employing more than one detector per spectral band, the on-board calibration reference also permits continuous correction of relative response differences between detectors. An extremely stable reference is necessary to maintain "absolute" calibration.

For relative correction between detectors an alternative, or back-up, approach to an on-board reference is to derive the correction coefficients per detector by statistical comparison of the image data from the different detectors. This approach is made possible by the fact that, on the average, local image levels do not change very fast (i.e., the probability that the average level of one line of image information will be like the next is much higher than the probability that it would be different). From this there are many methods for determining the gain and level correction coefficients relative to a "reference" detector. Three such methods that have been proposed for ERTS including (a) statistical averaging, (b) linear regression and (c) measured residue minimization. The latter may be easiest to implement in the present system; in any case, the instantaneous coefficients per line would be filtered before application to minimize the relative normalization error.

Atmospheric Radiometric Correction

Correction for atmospheric effects could range from simple operations to those that are relatively complex. One relatively simple type of correction might be to expand the green-band signal modulation to compensate for the correspondingly severe contrast attenuation of the atmosphere in this band. The "stretch" function applied to the instantaneous signal varies with the average level; thus, the average level of the signal would need to be continuously sensed to determine the magnitude of correction to be applied to instantaneous data values above or below the average level. Contrast expansion to appropriately lesser degrees could also be applied to the other (red, IR) bands.

Such an approach implies a "standard" atmospheric model, or a standardized model with varying seasonal or regional characteristics. The definition of an agreeable model might be a difficult task. Another level of sophistication (and also perhaps the most valuable) would be to determine by "ground truth" platforms or other dedicated means, the important atmospheric parameters of a particular area of interest, then relay these parameters to the processing facility before the sensor data arrives. Such inputs could then be handled in a way similar to other standard ancillary information (such as platform attitude and tracking data), and they would be fed into the processing system to apply the specifically determined atmospheric correction to that data of interest. The special correction would be suitably annotated on the

output images and data; all other images would receive the standard (or zero) correction.

Image Recording

The important performance characteristics of the film recorder are:

- Spatial Frequency Response (MTF)
- Geometric Stability
- Writing Flexibility
- Radiometric Stability
- Data Rate (Video Bandwidth).

The spatial frequency response or modulation transfer function of the film recorder is the dominant requirement to minimize degradation of the spatial resolution of the sensor. Three types of film recorders capable of the resolution required are crater-lamp recorders (CLR), electron beam recorders (EBR), and laser beam recorders (LBR).

For ERTS, the limiting sensor resolution corresponds to 4000 elements per scan line, with the additional requirement of operation at a 4 MHz (RBV video) analog bandwidth, and at lower bandwidth for recording MSS images. The state-of-the-art (1970) for the above three recorders relative to the ERTS requirement is shown in Figure 5-18. All three types have 80 to 90 percent modulation response at the RBV and MSS resolution limits (solid arrows).

The EBR was selected for the ERTS application primarily for its flexibility: the electron beam can be easily and rapidly steered in an arbitrary writing path. The CLR and LBR scans cannot be easily steered at present. In the ERTS system, the EBR enables the on-line correction of essentially all major image errors while the video tapes from the receiving sites are converted directly to film.

For MSS images, these corrections include compensation of mirror velocity error, variation of spacecraft altitude attitude and earth-rotation effects over the frame interval, and framing the continuous MSS data into individual rectified images with 10 percent overlap between frames. MSS spectral images are recorded at an 8.8 megabit/sec data rate, with four tape passes to produce the four spectral bands.

For RBV images, the corrections include compensation of altitude and attitude errors, shading errors, boresight errors, and the different high-order internal

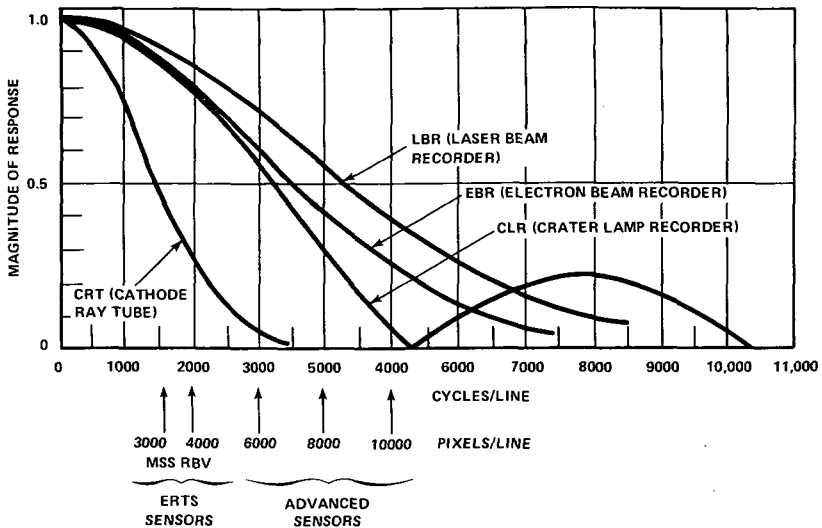


Figure 5-18. Representative Film Recorder Spatial Frequency Response (1970)

distortions of each camera, producing registered triplets at the 4 MHz RBV data rate. The RBV and MSS images are generated with a common scale, format center and geographic annotation.

The use of a Laser Beam Recorder (LBR) as the primary film recorder would require that corrections, other than the most simple, be performed on the data in the digital domain. This is a basic tradeoff between the two image recording approaches, which will be summarized later.

Operationally, the EBR accuracy and stability is better than one part in 5,000. Relative to the residual errors of the sensor, this does not seriously degrade the geometric accuracy of the recorded image. The CLR and LBR being optical-mechanical devices, have a considerably higher stability.

Radiometric stability is important during the interval it takes to record an image and its associated gray scale. The stability variation is less than the random density variations of the film, typically between 0.005 and 0.01 density units, or about 1 to 2 percent.

Image Resolution, Scale and Format Size

It is desirable to present image information at an output scale in which essentially all of the information present can be perceived with the unaided

eye. The unaided limit at high contrast is about 10 cycles/mm; in an image, a lower frequency limit is more reasonable for perception of low contrast detail.

The ERTS output images have an 80 meter projected ground IFOV and a scale of 1:1,000,000. Assuming two elements (IFOV's) per spatial cycle, the sensor spatial frequency limit is about 6 cycles/mm on the 9-1/2 inch image format. Thus, assuming a similar 6 cycle/mm limiting frequency in the image being viewed, the following table summarizes the effect of changing ground element size and number of elements per image width, on the image scale and output format size.

Table 5-9
Relation of Ground Element and Number to Image Scale
and Output Size in Six Sensors
(6 cycles/mm)

Sensor Type	Ground Element (meters)	Number of Elements	Image Scale ¹	Format Size (inches)
ERTS	80	3-4,000	1:1,000,000	9.5
	40	4,000	1:500,000	9.5
(EOS TM)	40	8,000	1:500,000	19.0
(Adv TM)	40	16,000	1:500,000	39.0 ¹
(HRPI)	20	2,000	1:250,000	5.0
(Adv HRPI)	20	4,000	1:250,000	9.5
(Adv HRPI)	20	8,000	1:250,000	19.0

Increasing the output format size to 19 inches is not a technological problem, but it may pose some problems in film handling, particularly for photographic processing equipment and facilities which can handle only up to 10-inch film at present.

The increasing number of picture elements is seen to be a more difficult problem for the film recorder. The modulation response at 8000 elements (4000 spatial cycles) per line, Figure 5-18, is considerably lower than at 4000 elements per line. The recorder-film system MTF and film-grain signal-to-noise ratio both tend to improve with increasing format size. In view of the

increase in output image format accompanying increased sensor performance, it may also be desirable to enlarge the recorder writing format.

Data Interpolation

Fundamental to the geometric transformation of discrete data points from a given line or array into a different line or array is the manner by which values are determined for output points which fall between points in the input data.

The simplest decision, taking the value of the closest neighboring point, introduces plus or minus one-element discontinuities in the output data, but this approach is the easiest to implement. Another approach, forming the output data points as the appropriately weighted average of neighboring points, avoids such discontinuities by increasing the amount of local processing.

Either of the above introduces data modulation loss at spatial frequencies approaching the limiting resolution of the sensor. This effect can be compensated by examining an array of surrounding points with an algorithm to determine the local spatial frequency characteristics of the data, and applying a local deconvolution appropriate to the sensor aperture to determine the intermediate data values. This sharpens local data transitions, but increases the processing required and accentuates data noise. Thus, the choice of interpolation method involves a tradeoff between the processing cost and speed versus the advantages to be gained.

Sensor-Geometry Correction

Geometric distortions of the sensor are corrected by applying a transformation to the data derived from the calibrated projective geometry of a particular sensor.

For frame-imaging sensors employing electron-beam readout, the projective errors will tend to include first-order scale and skew errors, plus a variety of higher-order errors due to nonlinearities in the beam deflection. Most of the distortion components may tend to be stationary, such that a fixed transformation derived from measurements of reseau positions might be capable of removing most of the geometric error. The transformation, however, may tend to be geometrically complex. For precision correction, it may remain necessary to measure all reseau positions to derive the specific transformation required per image.

For scanning sensors which have a linear sweep across the ground track, a one-dimensional correction is required to normalize the variation in cross-track scale, proportional to the tangent of the instantaneous sweep angle from vertical.

Pushbroom type detector arrays will tend to have a fixed one-dimensional correction, corresponding to the variations in spacing of the particular detector array and the radial distortion of the lens.

The transformation required for compensation of the internal geometry in scanners employing a conical scan pattern is two-dimensional, as discussed in the paragraph that follows.

Conical-Scan Conversion

The curved image geometry of the conical scanner, Figure 5-19, results in a number of consequences. First, the curved geometry must obviously be compensated in the generation of film images, either by writing the image with a curved scan format or by converting the sensor data to a linear-scan format for recording with a straight-line film recorder. Second, the curved scan format is seen to be a considerable nuisance to data users, particularly when the data is to be displayed or printed out in graphical form or when it is desired to delineate the boundaries of a data set to be analyzed, or when spatially-oriented operations (such as geological lineament location, etc.) are to be performed.

To avoid these and other unforeseen user problems, it appears desirable to transform the data from the curved format into an orthogonal format. In Figure 5-19, one output line AB correspond to appropriate data points from input scan lines 1 through N. The input lines are obtained serially, so the data in the shaded portion from lines 1 through N have to be contained in rapid-access storage as the output lines are formed. Assuming a 48 degree polar scan angle, the minimum storage in bytes is on the order of $0.04 E^2 S$, where E is the number of elements per line and S is the number of spectral bands.

For an advanced 7-band conical scanner with a resolution of 8000 elements (bytes) per line, the amount of data contained in the shaded area is on the order of 18 megabytes. The data storage requirements can be reduced by multiple tape passes, i.e., by transforming only a portion of the data on one pass. With this approach, the reduction in storage tends to decrease as only a linear function of the number of passes. Alternative approaches, based on

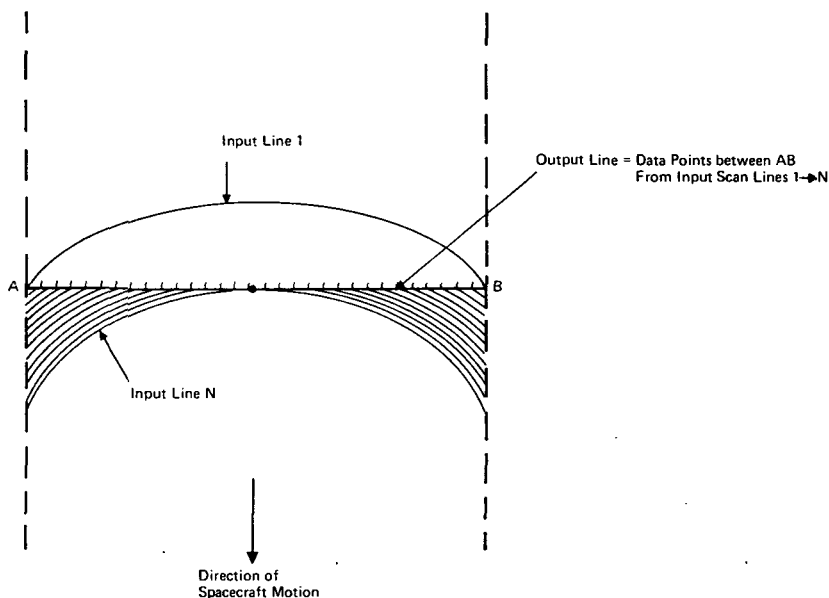


Figure 5-19. Conical Scan to Linear Scan Conversion

cascading multiple delay-storage devices with a smaller amount of rapid-access storage, can be considered for transforming the data in one tape pass. This may be a feasible initial approach to conical data reformatting; however, it might be cost-effective to reformat only that data requested by users rather than reformatting all the data as a matter of course.

Assuming a uniform quantization rate, outer portions of the conically scanned image are over-sampled relative to a spatially uniform sampling interval in the across-track direction. A simple nearest-neighbor conversion of data points would not utilize all of the input data.

In addition to the above trigonometric considerations, the conical scan geometry has other subtle effects. Assuming a uniform detector signal quantization rate is chosen to obtain data points at adjacent on-axis IFOVs, earth rotation causes the adjacent IFOVs between scans to become overlapped at one edge of the scan and underlapped at the other (Figure 5-20). Another effect dependent on the design of the scanner is potential rotation of the detector field (Figure 5-21). Off-axis pointing capability may involve rotation of the scan swath, as well as, the detector field.

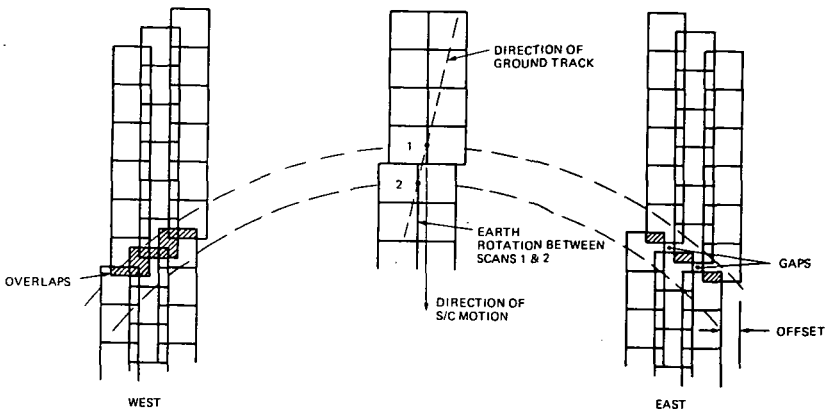


Figure 5-20. Variation of Data Coverage Between Scans Due to Earth Rotation

All of these effects must be taken into account in the conical scan data processing requirements, with respect to the performance advantages obtained by the conical scan concept.

The corresponding problems of image recording of conically scanned data are considerably less severe, though not without consequence. For example, data which is digitally reformatted per user request can be recorded with a conventional straight-line image recorder, of which there are many types. But since it is probably desirable to convert all received data to image form, for this task a film recorder with a curved-scan-format capability would appear highly desirable. The conical scan format can be generated with the present ERTS 70 mm EBR recorder, with some compromise of format size, resolution, and the elimination of frame overlap. These effects are a result of the present 16 mm height of the EBR beam deflection window in the along-track dimension. Doubling the window size would enable conical-scan recording in the same format as the present ERTS images.

The various effects of the conical scan geometry for a nominal 6000 element per line conical scanner are currently being analyzed under a NASA contract with respect to the present ERTS image processing system. The results of this study should establish the advantages and limitations of present facilities, near-term implementation requirements, and identify longer-term limitations and requirements for conical scan processing.

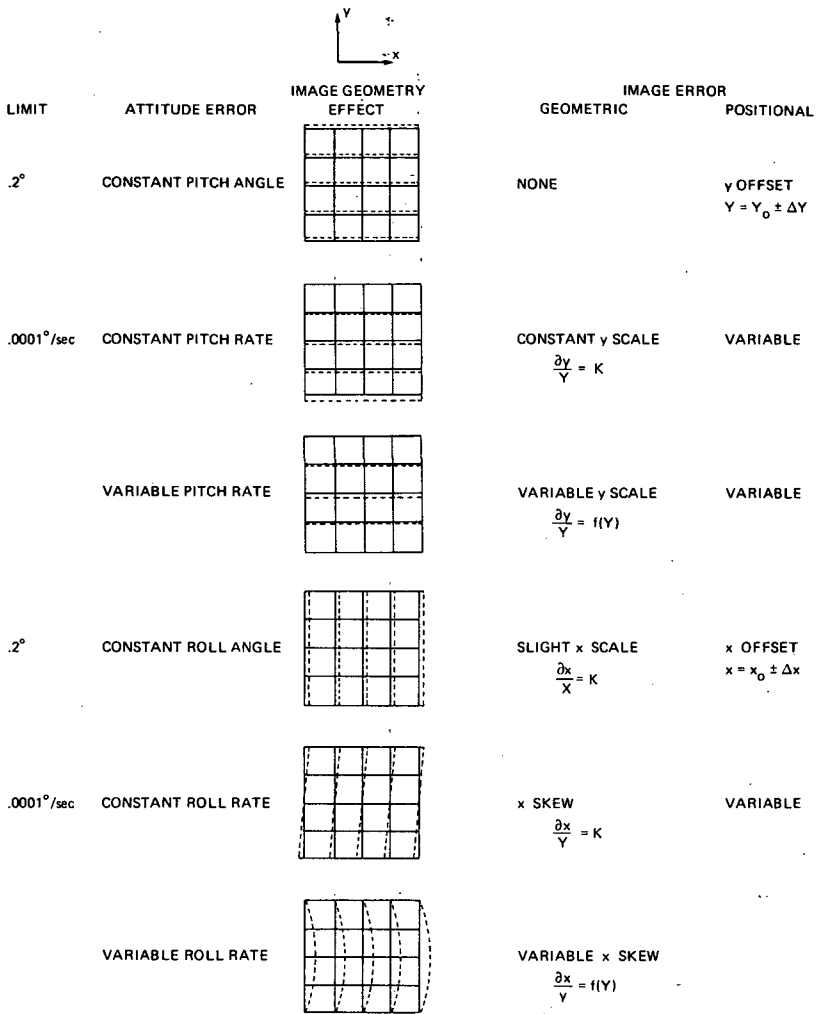


Figure 5-21. Attitude Effects on Image Geometry

Correction of Platform Effects

The transformation for compensating platform variation can be resolved for discussion purposes by considering the effects of the various attitude and attitude rate components. The basic considerations involved are the processing complexity and data-storage requirements, summarized in the two right-hand columns of Figure 5-21. These diagrams relate to a data set from an

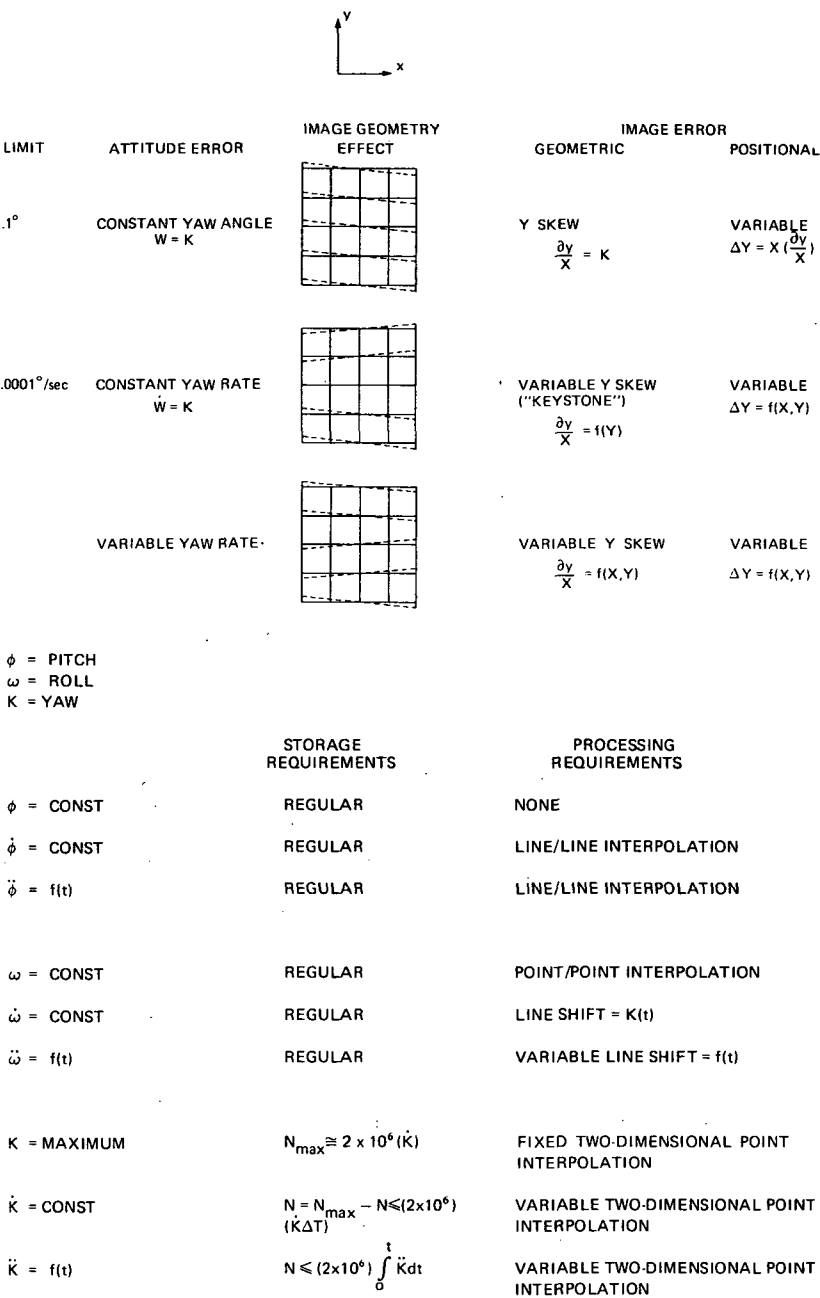


Figure 5-21 (cont). Attitude Effects on Image Geometry

ideal sensor, or to the data after internal-geometry correction, although the attitude corrections would probably be applied simultaneously with the internal correction. A constant pitch angle has the least impact. Pitch-rate effects require interpolation of new lines of data values between the lines in the data set, according to the known temporal variation in the pitch angle. A constant roll angle involves a point-by-point interpolation of new values along each line in the data set. A varying roll angle requires interpolation of points between adjacent lines, to shift the data proportional to the local skew. The compensation of purely pitch and roll effects is inherently one-dimensional, or at best two-dimensional between adjacent lines; therefore, minimal data storage is required.

Roll effects introduce two-dimensional data skew (for scanners) or data rotation (for frame imagers) relative to the satellite heading. Therefore, two-dimensional data storage and two-dimensional data point interpolation are required to obtain the corrected output data. The amount of data to be stored is directly proportional to the maximum yaw angle. For an 8000 element 7-band sensor, the storage necessary is on the order of 2 megabytes per degree of yaw. Therefore from this standpoint it may be desirable to restrict the maximum yaw angle of the spacecraft. Variations in the yaw angle correspondingly vary the orientation of the output line through the stored data, and also vary the amount of data stored up to the peak-yaw angle case.

Present ERTS Ground Data Processing System Operations

A diagram of the functional operations performed by the ERTS ground data processing system is shown in Figure 5-22.

The *preprocessing* operations involve (1) determining from the telemetry tapes the spacecraft attitude and attitude rates at selected intervals of time along the orbit, and (2) determining from tracking data the position of the spacecraft vs. time. These two sets of data are processed to determine the attitudes, attitude rates, and earth position (latitude/longitude) of each image format center, which is given an ID number derived from the nearest tenth-second of the time of acquisition. These data, plus a number of other information, are recorded on what are called *annotation tapes*.

Three annotation tapes are generated, one for Bulk (BIAT), one for Precision (PIAT), and for Special (SIAT). The BIAT contains position, attitude, and annotation for all the images contained on the RBV/MSS video tape. The PIAT and SIAT contain specific processing instructions for the particular images and data sets requested by users.

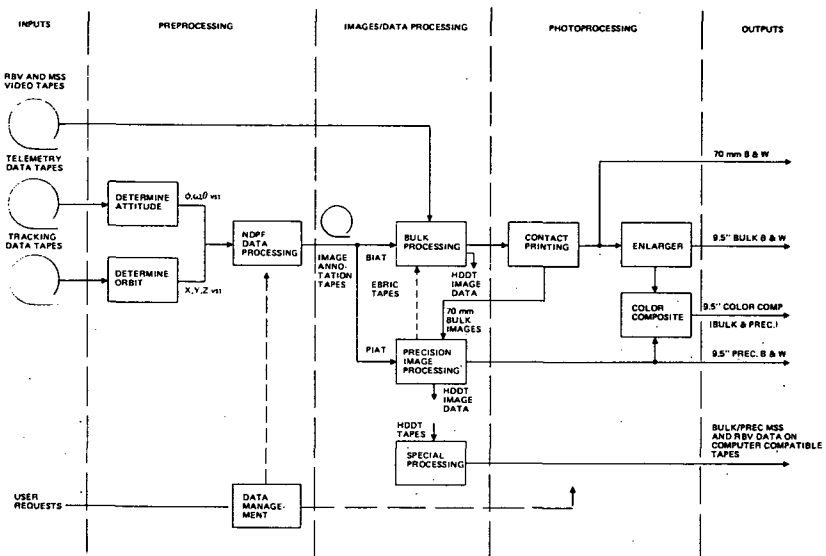


Figure 5-22. ERTS Ground Data Processing System Operations

In the bulk processing subsystem, the RBV or MSS video tape received from the test site is mounted with the appropriate BIAT, and that video tape is bulk processed. The outputs from this operation are 70 mm film and high-density digital tapes (HDDT), with the following processing operations applied:

- Registered RBV images, corrected for shading registration (camera distortion and boresight offsets), spacecraft attitude and attitude errors positioned with respect to latitude and longitude coordinates and annotated with acquisition information and a gray scale.
- Framed MSS images, radiometrically corrected for detector variations, geometrically corrected for mirror sweep errors, spacecraft attitude and altitude variations, framed (corresponding to the RBV image centers) with 10 percent image overlaps, positioned in latitude/longitude coordinates, and annotated with acquisition information and a gray scale.
- HDDT tapes of 25-mile image strips, in a common intermediate HDDT format, converted from the MSS 28-track digital data format and the RBV FM analog video tape format.
- Precision Image Processing received 70 mm contract-print copies of the images to be processed, determines and automatically measures position of ground control points in each MSS/RBV set, measures all RBV

reseau, measures and compensates for input density variations, and transforms each image by incremental scanning and reprinting in an 8 x 8 array on 9-1/2 inch film. The outputs of this precision processing operations are:

- RBV or MSS images at 1:1,000,000 scale, precisely positioned and annotated in UTM or Polar Stereographic coordinates.
- High density digital tapes of the scanned image data.
- Special Processing performs the following operations:
 - From Bulk HDDTs, it applies radiometric correction of MSS detector variations and scanned line-length variations, and produces MSS output data on 800 bpi computer-compatible tapes.
 - From precision HDDTs, it converts the RBV and MSS data into 512 x 512-element data blocks on 800 bpi computer-compatible tapes.
- Photo Processing includes the following operations:
 - Provision of 70 mm B&W outputs.
 - Enlargement of the 70 mm bulk images and provision of 1:1,000,000 9-1/2 inch B&W image outputs.
 - Generation of bulk and precision 9-1/2 inch color-composite outputs.

Discussion of the Summary of the Conclusions

The limitations of the present (ERTS) ground data processing system with respect to the above requirements are as follows:

- The present EBR is format-size limited for handling any conical-scan sensor geometry, and it becomes resolution-limited for line-scan formats beyond 6000 elements per line. An additional EBR with a larger format may be capable of handling both kinds of sensors within the present system.

An improved enlarger is necessary to obtain higher output image quality. The increased resolution of the advanced sensors may require a 2X increase in the output image scale and format size to permit unaided visual interpretation.

- Increased digital processing capability is required to satisfy calibration requirements for solid-state array sensors, conversion of conical scan data to orthogonal form and precision data rectification. Major hardware improvements will be required to provide the extreme speeds and large memories required.

- Certain types of mission functions strongly indicate the usefulness of an on-board image processing computer.
- Present digital tape techniques will be inadequate for large scale storage and dissemination of digital pictures, and therefore improvements are needed in this area.
- Techniques for producing many band color and/or color separation outputs for each band with easy registration and use by analysts are required.

IMAGE PROCESSING CONSIDERATIONS

Image processing of various sorts will be required both on board the spacecraft and on the ground. It is not clear at this time exactly what the division of the specific tasks should be. Processing on board the spacecraft will be particularly useful when it is required for making an on board decision to avoid the necessity of transmitting image data to the ground for data compression and editing and for information storage and cataloging, including the correlation of new imagery with previously stored images. It is anticipated that the same image processing applications will be useful on the ground where the possibilities of larger computers will allow these processes to be carried out more thoroughly or at greater depth. In addition, other processes not feasible on board may be attempted on the ground, and very large libraries of past images may be accumulated and retrieved as appropriate.

Some of the many processes required may be accomplished by optical processing such as with coherent light or various photographic techniques. Huang (1967) discusses the two prime contenders, digital processing and coherent optics. In general, it can be stated that the main advantages of a coherent optical system are its efficient storage of the large amount of data in a picture and high processing speed due to the implicit parallel processing of all elements simultaneously. Coherent processing has the disadvantages of being rather touchy to operate properly and being subject to errors; it is also unable to easily handle nonlinear problems and has a relatively high cost for large aperture systems. Digital processing has the advantages of being extremely flexible, rather trouble-free and easy to use, once the programming system has been worked out. It also has the ability to handle problems which are nonlinear in both intensity and geometry and can solve these with an accuracy limited only by the user's knowledge of the incoming data.

To gain the advantages of digital processing requires high quality signals with low noise, and associated accurate analog-to-digital conversion equipment.

To maintain data quality, the data from most advanced sensors will be obtained by digitizing the sensor signal on board the spacecraft. Although the possible large cost of a digital computer system is a potential disadvantage, this cost can be traded for processing speed by using a smaller computer which will require longer to do the processing. Alternatively, special purpose peripherals may be utilized to gain processing speed. This discussion is only concerned with the digital image processing techniques since these allow the possibilities of complex analyses and can produce numerical output results when required.

A breakdown of the broad area of image processing into six application areas, with some examples of the kinds of processing which may be applied in each, is given in Table 5-10. Illustrations of the results of some of these processing techniques have been published. It is not the intent of this discussion to further illustrate these possibilities, but rather to consider what is involved in image processing.

Image Processing Software Considerations

A large amount of picture processing can be done with normal general-purpose computers and standard Fortran language. Although Fortran or similar languages are convenient for programming, they generally do not result in high efficiency of operation compared to properly coded assembly language routines. For this reason, with a large number of pictures to be processed, or where fast turnaround time is required, special attention must be given to reducing or bypassing the inefficient parts of the Fortran and/or doing programming in machine language. In addition, the image processing laboratory should make available to the analyst an efficient data handling system for the development of algorithms and for the recording, processing, retrieval and display of pictures.

To facilitate the use of the system by the analyst and to enable him to rapidly call for new processes, it is desirable that the image processing software system be based upon English language commands and require a minimum of programming knowledge and data inputs from the analyst. In addition, it should perform automatically the input/output processing and routine book-keeping which will be required. Such a language has been in use at the Jet Propulsion Laboratory since 1966 where it has been running on an IBM 360/44 computer. (A version for 360/OS is also available.)

The fundamental philosophy of this system, called VICAR, is that the image analyst in accomplishing his picture processing will call for execution of one

Table 5-10
Image Processing Applications

Area	Technique	Used for:
Generation	Computer-Originated Computer substitutions	Test targets and graphical displays Insert windows in pictures Insert good data for bad
Intensity Manipulation	Intensity calibration of systems Non-linear lookups	Photometry Film curve corrections Grey scale alterations
Geometric Manipulation	Chromaticity calculations Geometric calibration of systems Reprojection	Color shift, balance, alteration Good geometry needed for stereo Convert slant picture to ground projection
Spatial Frequency Operations	Overlay match of two pictures Independent X and Y adjustments Spatial high frequency boost Spatial low frequency reduction	Rubber sheet stretching Aspect ratio corrections Correct for detail losses in system Minimize broad-brush shading Remove effects of glare
Analysis	Single frequency filtering Fourier transform Image light distribution Pattern extraction	Remove coherent noise Analysis in spatial frequency plane Star cluster analysis Counting blood cells, autos, stars, etc. and analyzing shapes of objects
Multi- picture	Convolution Subtraction Addition Multiplication Division	Filtering, correlation Change detection Stereo information extraction Averaging, noise removal Spatial domain filtering Normalizing

or more of the programs from the system library. He may enter parameters at the time of execution to suit his particular needs, as the library programs are written to be flexible in application. These programs have been previously debugged and documented and are available for any analyst to call on. A continually growing system is thus provided as various analysts require new

processes and write the required executable programs. The language has proven to be easy to use after an initial learning period and makes possible much simpler and more error-free job set-ups than would be possible without it. An interactive mode is available in which the analyst may iterate with the processing by using an interactive console containing the required communication gear and several volatile and hard-copy displays.

The primary advantages of this system over separate programs are:

- Easier to use due to standardization of procedures and formats and the reduction in the number of control cards or statements.
- Saves time and money in programming by providing buffering, house-keeping, label processing and many other capabilities to the programmer.
- Allows the analyst to set up many and varied programming strings by calling the various executable programs in the desired order.
- Can be improved and expanded in the future without necessarily modifying the executable programs.
- Faster execution due to the elimination of returns to the operating system between tasks.

Although this system at JPL has proven extremely satisfactory, it has a number of distinct limitations which must be considered as newer systems are designed and implemented. VICAR has been designed as a batch processing system and as such it performs quite efficiently in the actual processing of images. However, it requires that the images be available in digital form, usually on magnetic tape. Presently available film scanners are not easy to set up and adjust on line during operations. Therefore, VICAR-controlled film scanning is not normally recommended as a way of entering data into the system except in some special cases where the analyst is working interactively with the processing. Therefore, a system designed for use in an environment in which the processing is to be done as part of the mission operations must have careful thought given to the input source of image data and its conversion into a system standard format.

System Hardware Considerations

In designing an image processing system, a number of things must be considered more or less simultaneously. Some of these will be found to have practical hardware limitations due to the current state-of-the-art, while others

may be open ended in this respect, but limited by cost of implementation. Briefly, the considerations to be covered in detail are:

- Quantizing accuracy: The finer the digital steps used to characterize the points, the better. This will ultimately be limited by noise.
- Recording and display considerations: Practical image recording equipment faces several limitations. Conversion to digital form must be done properly to avoid degradations. Interactive volatile image quality displays must be properly designed and implemented.
- Data processing: Minimization of computer time suggests that a small picture is desirable, but this limits either resolution or area coverage. Design of a data handling system geared to picture processing will greatly facilitate this procedure.

Data Recording and Dissemination

For this discussion, it is assumed that the bulk of the images to be handled will be obtained by transmission from the spacecraft. At the present state of the art, there is no device for recording large quantities of digital samples in computer accessible format at the high sample rates anticipated. If, for some reason, extremely high digitizing rates must be employed, nonstandard techniques such as digital recording on analog tape using Miller or similar modulation (which allows extreme packing density and hence, high digital rates) must be used. If the required data rate is above that which the computer can handle, a longitudinal tape recorder may be used which may be subsequently replayed at slow speeds, or a video recorder may be used which may be played back without tape advance to give repeated presentations of the same image to allow piece-wise readout. Since neither of these approaches is a standard ADP technique, development is required to produce working systems.

Digital image dissemination to users must be made more economical, and properly formatted to allow easy use in low cost devices (e.g., film recorders) by the user.

A near-time solution may be to further develop the techniques for digital recording on video tape, with the expectation of using low cost commercial video playback machines at the user site. If the playback is primarily for film recording, the slowdown capabilities outlined for computer interfacing will not be required.

A complete system will require some sort of output recording device to produce hard copy. For pictures of 2000 x 2000 or perhaps 4000 x 4000 pixels,

a cathode ray tube device may be satisfactory. Above this picture size, direct electron beam recording or facsimile type devices on film may be used. This technique allows picture sizes up to the range of 10,000 pixels, and, since there is no phosphor noise, the pictures are very "clean."

In conversion of images to film, the film grain contributes to the apparent picture noise. The maximum allowable RMS film noise in units are normally published, for a 6-bit system with noise = $1/3$ step, may be derived to be:

$$\sigma_D = 0.00025 \times SA \quad (18)$$

where

σ_D = maximum allowable RMS density fluctuations at $D = 1$
and aperture = 48 micrometers

SA = scanning aperture diameter in micrometers.

Perusal of film specifications will show that normal film has noise considerably higher than this value for small apertures, and hence the system will be film-limited at small pixel size. For this reason it is desirable to keep film image formats large wherever possible.

Black-and-White Films

Because of the wide range of reflectivities of various materials which will be imaged, the corresponding signal levels will also vary widely. As a result, the capabilities of black-and-white film will be taxed, since desired scene detail will fall not only in the linear parts of the film curves, but also in the low-gamma toe and shoulder regions. To avoid loss of information in these regions, several processes may be used, and should be considered as tradeoffs:

- Approach 1: Black and White (B/W) film at normal gamma could be used, with the exposure optimized for maximum contrast for desired parts of the image. This could be produced either by special playback of digital tapes on request with parameters to satisfy the requestor, or by a group of films made on-line for the archives and suitable exposure made to produce the requestor copy. A possible disadvantage of this latter general type of product is the probability of complete saturation and hence loss of data outside of the requested range.
- Approach 2: B/W film at low gamma, which will "hold" the entire brightness range encountered, could be used. A standard product

could be defined and distributed, but the lower contrast may reduce the visibility of some targets. However, this may be fine grain film, which can stand subsequent enlargement and reprinting at high contrast without serious degradation.

- Approach 3: Use of multilayer extended range color film is possible. Such material is available, but produces a product which is unusual in appearance and which might therefore not gain user acceptance.
- Approach 4: A nonlinear contrast stretch by computer to precompensate for film toe and shoulder saturation could be produced. A much wider range on the film may then be used without the loss of visible detail in the very dark and light areas. This works excellently, and may also be used to avoid color shifts with brightness which may otherwise occur if these films are used to produce color composites.
- Approach 5: Digital filtering or optical techniques could be used (e.g., the Log-e-tronics printer) to reduce low spatial frequency information (broad-brush shading). This destroys photometry, but it is very useful in visibly presenting detail in all areas of the image independent of local gross scene brightness. This type of output has been a standard product for the Mariner '71 Mars Orbiter mission.
- Approach 6: Upon user request, the desired range could be extracted by computer, stretched, and printed optimally on film. The deleted areas may be brought deliberately to black or white saturation or otherwise specially treated. This will unambiguously tag areas of poor photometry and help avoid user analysis anomalies. This approach may result in a high processing load, but should result in better control of selection of the desired image brightness range than Approach 1. It also provides contrast stretch and hence increased visibility in the desired brightness range.

Note that Approaches 1, 3, 5 and 6 destroy photometry in the attempt to make details visible. Approaches 2 and 4 attempt to retain photometry as well as present details, but at a sacrifice of contrast in the middle-brightness range.

Black and white output negatives to be used for paper prints should not have a density range greater than approximately 1, if all the picture detail in the negative is to be reproduced in a print, but could have a density range up to perhaps 2, if it is to be viewed as a transparency.

Color Film Outputs

It has become evident that optimum color combination will vary with the users and with what they are trying to see. This will be further aggravated as more spectral bands are incorporated in the sensors.

Because of the familiarity of users with false color infrared photography, this combination is expected to be one standard output, available on color film. It is not yet clear from ERTS-1 experience whether band 6 or band 7 is better for the IR contribution; it is likely that this will vary depending on the circumstance.

Other combinations favored vary widely. For this reason, it is suggested the B/W separations (properly compensated for film density-log E curvature) be supplied to the user to allow him to make his own composites. This in turn makes it desirable that these films be easily registered by the user, either for color printing or for color additive viewing.

For printing, a relatively foolproof method could be to pin-punch-register the outgoing films at the data processing facility, using standard color photography techniques. It is not clear at this point whether prepunched film could be used with fixed image placement relative to it, or whether manual registration must be used as is presently done in the NDPF. As an alternate or supplement to the punched holes, accurate fiducials recorded on the film during image recording will provide other landmarks for registration.

For color combination for viewing, isolated pieces of film (e.g., the ones mentioned above for color printing) which are pin registered may be supplied. Alternatively, a single piece of film may be supplied which has all the images, accurately displaced from one another. A special matching viewer may then be used for recombination without requiring extensive alignment by the user. Note that the use of isolated pieces of film will allow the use of different gammas or even negatives for the different colors, a capability not readily available with the single multiple-image film. A viewer which could take either input would be desirable.

As a number of picture elements per line increases, the severity of image registration problems also goes up. This will be further aggravated if the multiple image film is used. A study of film dimensional stability vs. image size for various resolutions and formats should be carried out. Larger images will ease the registration but will increase the cost of the recombining optics.

Volatile Display

The development of processing techniques and the determination of the parameters to be applied during the processing are quite subjective and require the continued attention of the analyst to the results of his processing. This is a time-consuming iterative procedure in which the analyst examines his latest results and submits new processing accordingly. The time required to obtain a picture from the computer system will be minimized if a data display is available. This display must be of high enough quality to present the details required by the analyst and may take the form of either hard-copy printout or cathode-ray tube display.

Volatile displays are usually based on cathode-ray tube presentation, and may take several forms depending on the type of memory used for the refreshing process:

- Refreshing directly from computer: This is very satisfactory but ties up the computer. It allows the analyst to provide flicker mode A-B comparisons for presentation of new data immediately upon computation.
- External self-clocked picture-size memories: These memories are now becoming available and allow refreshing the display without further attention from the computer once the memory has been loaded. This frees the computer for other tasks while the analyst is inspecting his picture. Availability of such a memory may have some advantages in that it may also be used during computation (when no interactive display is occurring) to avoid multiple disk head seek.
- Multiple head rotating drum or disk memories: If properly designed, these may also provide the video rate digital data required for display. However, many tracks with simultaneous head accesses are required to achieve the required data rate.
- Storage tube memories: Modern silicon diode vidicon storage tubes are approaching a quality adequate for monochrome presentation of pictures up to 1024 x 1024 in size. These are quite moderate in price and should be seriously considered. However, if multiple channels are used with the intent of overlaying the displayed images, as in 3-channel use for color display, there could be a possibility of severe maintenance problems in maintaining overlay matching.

In addition to the normal high quality film recording required for archival image output, a CRT recorder using Polaroid film has been found to be extremely valuable. With this recorder, which may be treated as a computer

peripheral and serviced by the computer operator, the analyst can obtain either in real time at the console or with his listings as a result of batch processing, a high quality image on Polaroid paper. Use of this device greatly minimizes turnaround time in that the images are immediately available and obviates the film processing/enlarger route. Such a device, in operation at JPL since about 1968, is currently being modified to provide direct color output.

In the demarcation of areas for processing such as the definition of training sample for multispectral scanning, location data may be obtained by the use of light pens, Rand tablets, Grafpen or similar devices. These will operate directly with the volatile displays in the interactive mode.

Advanced Hardware Development

It must be considered that conventional "computer compatible" magnetic tape will become an obsolete method of storing large quantities of archival images. At the present popular 800 bpi tape density, with images formatted one record per picture line, one standard reel of tape will hold only one picture of 4096 x 4096 size. Higher tape packing densities and/or other recording formats or data compression may be used to increase storage efficiency; however, it is not felt that even one order of magnitude improvement is available in the near future by this route. However, modification of video recorders to store digital data may achieve an improvement in the packing factor (number of bits/cm²) by 50 over conventional 800 bpi tapes. Alternatively, it is felt that digital data storage on film may provide much higher volume data packing efficiency for archival purposes. The multi-megabyte memories currently being developed can provide the capability for on-line use where many pictures must be available for instant recall.

As indicated, it is anticipated that most of the pictures will be received in computer compatible form. However, where pictures are received in the form of film images, a major bottleneck may develop in preparing these input pictures for computer operations. Film scanning to the spatial resolution and required signal-to-noise ratio is not a trivial task. Based on the experience at JPL, it is recommended that entry of film data be accomplished in two steps:

- Generate from the archival film an intermediate film which has been brought as closely as possible to the desired scale and photogrammetrically rectified. This will minimize much of the digital processing required for rectification and will minimize handling of the archival films.

- Scan this intermediate film to produce the required system compatible formatted picture.

Special purpose peripherals may be used with a general purpose computer system to reduce the processing time for certain of the processes. Consider, for example, geometric rubber sheet stretching of the pictures. This will be required for rectification, for the correction of camera geometric distortion, and for the overlay matching of pictures for interpicture comparisons. If the input picture is reproduced with variable spacing at the output to accomplish the geometrical corrections, this variable spacing will cause an intensity modulation to occur. This, of course, is undesirable, and suggests that the output picture elements (pixels) should be equally spaced. This in turn requires that, in building up the output picture matrix, the data must be selected from the proper location in the input picture. If the system has been designed to provide operating picture storage on disk (the normal practical approach), many head seeks will be required when the requisite input data are transferred to core for processing.

To minimize the bookkeeping and the number of head accesses, as many lines as possible should therefore be read into core simultaneously, and this number determines the amount of output picture matrix which can be built up in one pass. The availability of multiple head drums or full picture size memories can *greatly* reduce the amount of computer processing time required for the geometric manipulations. In addition, because of the nature of the interpolations required, further significant reductions in processing time can be obtained by special purpose interpolation peripheral devices. It is estimated that a factor of 100 or more in processing time could be saved by these techniques.

Spatial frequency filtering may be accomplished either by convolution or through operations in the Fourier domain. In both of these processes, the mutual effects of a whole neighborhood of pixels is calculated at each pixel location. In convolution, for example, a 15×15 filter will require 225×10^6 multiply-summations for filtering of a 1000×1000 pixel picture.

The usefulness of a special purpose device for performing these operations is evident. Peripheral boxes for this operation and a related one, the Fourier transform, are now available. These devices obtain their high speed primarily through the use of parallel processing and microprogramming.

Modern techniques in large scale integrated circuits, magnetic bubbles and various optical techniques lead naturally to the possibilities of parallel processing. One parallel machine, the Illiac IV, has been designed. Although this

machine is capable of extremely fast operation, it is not clear at this point how it could be used for image processing by remotely located users. It is therefore anticipated that parallel image processing techniques will be used in more modest sized configurations, probably associated with general purpose computers. It is not clear at this point how specialized such devices would be (i.e., whether they themselves will be programmable or whether each device will have a specific processing function).

Techniques presently being developed may use various optical processes in conjunction with digital processing. This will require the development of adequate interfaces to convert from digital to optical and vice-versa. Such techniques are presently being developed at the Jet Propulsion Laboratory and other places under the sponsorship of GSFC. It is to be expected that such optical processing in the midst of a digital operation will not be used to solve all problems in spite of the inherently high speed, inasmuch as normal optical processing is analog and will introduce errors into the output pictures which would not have been produced in an all-digital system. Used in the proper place, however (that is, where the extreme precision or where numerical output is not required), these techniques could appreciably improve throughout.

GSFC Program to Develop "Real Time" Image Processing Systems

The Goddard Space Flight Center has a program to develop computing systems that can accept "real" images (such as those sensed from an orbiting spacecraft) and extract useful information from such images on a real time basis. The major part of this effort is directed toward developing data processors known as "Tse Computers." The word "tse" (American pronunciation: "see") is Chinese for "pictograph character." The most basic computational entity of a digital computer is a binary "bit." Similarly, the most basic computational entity of a tse computer is a binary image (or tse).

A tse computer consists of a collection of two-dimensional logic components, storage component, and components for precisely positioning images. Because operations are being performed on entire images, tse computers have the ability to perform many thousands of logical operations simultaneously. Therefore, one is able to conceive of computers four or five orders of magnitude faster than digital computers.

Laboratory breadboards of simple tse systems utilizing liquid crystal logic elements have been built and operated. The logic elements used were able to perform sixteen thousand (NOR) operations simultaneously.

It is anticipated that, by the end of 1975, components that will allow for computing speeds of 10^8 bits per second will be available. At these speeds, an image processing task that now takes a half hour would take two seconds. By the late 1980s, developments allowing effective computation rates of 10^{12} bits per second with images of 1024×1024 resolution are expected. At these speeds and resolutions, the present half hour task would take around 200 microseconds.

In addition to the work on tse computers, the Goddard program includes the development of real time coherent optical data processing systems. Prototype real time noncoherent-to-coherent image converters have been delivered. In addition, electrically alterable Fourier plane filters have been developed. The use of coherent optical systems for tracking moving objects (such as clouds) and for recognizing stellar constellations is also being investigated.

Data Processing

The development of the processing algorithms and the accomplishment of some moderate amount of actual processing can be done on almost any general-purpose computer. It will be found, however, that the smaller computers will be quite inefficient for picture processing. The smaller machines do not have adequate capability for the large amount of pixel manipulation which must be done to handle the large arrays present in pictures. Therefore, if the analyst is concerned with either fast turnaround from the computer, or with processing either large pictures or a large number of small pictures, he must eventually consider going to a medium or large size computer.

Since even large computer installations do not normally have adequate core memory for storing an entire picture, some form of picture roll-through is required. In this mode a few lines of picture at a time are read into core, processed, and then read out to allow room for more lines for further processing. In addition to the core space required for the program storage, capacity must be provided for pixel storage. Some of the processing algorithms operate on one pixel at a time, and could conceivably work with a picture memory as small as a few pixels. Other programs, such as the two-dimensional convolution program for filtering, require simultaneously a number of picture lines at least as high as the convolution matrix size, and for efficient operation such program should have room for several times this amount. But for a picture of 4000 pixels per line, the total memory size for one picture storage (1.6×10^7 bytes) rapidly gets out of hand. The state-of-the-art in computer memories is now such that memories of 130,000 to 1×10^6 bytes are now quite practical (but expensive).

Whether or not magnetic tape and disks are useful will depend upon the type and mix of the processing to be done. It is convenient to group the pixels in an integral number of lines per record, with a complete picture occupying one file or data set. The lines are normally recorded sequentially along the recording medium. For those processes in which sequential line access is adequate, obtaining a picture from tape is entirely satisfactory. However, for those processes in which a number of lines simultaneously must be accessed, or for which nonsequential pixels from several lines must be used, magnetic tape is very inconvenient. In this case, it will be better to serially read a complete picture from tape onto disk and then to randomly access the required pixels or lines from the disk. If the disks are organized in a cylindrical mode, access time will be further reduced. At least two disk drives are recommended.

Modern techniques in random access mass memories should be investigated since these will provide immediate access to various parts of the picture required for the filtering and geometrical rectification operations. As indicated earlier, it is expected that when such devices become generally available they will reduce the time for certain processes by extreme factors. This not only reduces the computing time for a given operation but, perhaps more importantly, will make the computation system available to many more processes in a given block of time, thus greatly reducing queuing delays.

Rationale for On-Board Image Processing Computer

There are three major potential uses of a computer of sufficient size (e.g., 360/44) to do on-board image processing for advanced earth resources type missions:

- Processing for decision making
- Analysis as a form of data compression and editing
- Information storage, retrieval, and cataloging.

Decision making implies near-real time analysis aboard the spacecraft. For instance, if the position of fish schools is desired and the detection of such schools requires manipulation of the imagery, the usefulness of the information is lost if no computer is available to make an on-the-spot analysis.

Detecting forest fires from orbit will probably require some type of enhancement of the thermal imagery for proper detection. In addition the coordinates of the fire must be known accurately. A computer is, therefore, essential to make proper and timely use of the information. Change detection will

play a role in any type of analysis of transient phenomena. Since transient phenomena by their nature require quick response, the capability for that type of analysis must be available. Simple photographic overlays are not feasible because of the variations in viewing geometry between different orbits or times in one orbit. Cross-correlation and rubber sheet stretching techniques can conveniently be done with a digital computer.

In line with cost reduction attempts, some form of massive data compression and editing is required. It is expected that man assisted by a computer will make an efficient data editor. Editing will take place in the process of target selection as well as in the on-board analysis and rejection of substandard data.

An additional form of data compression will consist of combining data before return to earth for further analysis. For instance, a particular Karhunen-Loeve transformation could be carried out to reduce the 12-band scanner data to 4-band, according to the target objectives, for later analysis. On-board, real time analysis could also assure that the proper mix of bands was being made.

Information storage and retrieval requires a computer and, while it might not be justified on its own, it is a valuable adjunct to the decision making and analysis functions. For instance, for change detection it will be necessary to retrieve images taken at an earlier date. For analysis, stored ground truth information will be necessary. In addition the computer will provide a valuable bookkeeping service to apply picture coordinates, sun altitude, etc., to the images and save appreciable time and confusion in the returned data.

General Philosophical Considerations

In addition to all previous considerations, there are number of more or less isolated items affecting the ground system and the possibilities for image processing and analysis which should be considered in the overall design of the mission. To some extent these are of an operational and philosophical nature, and as such are more properly considered in terms of mission design philosophy. These areas are broken down here into two groups—spacecraft data techniques and ground data processing.

Spacecraft Data Techniques

- **Onboard Storage:** Onboard storage of vast quantities of data and on-board processing of that data will be required. It is anticipated that

magnetic tape may be inadequate and that development of new storage methods will be a major cost item.

- Onboard Processors: Preprocessing of data onboard the spacecraft can avoid the transmission of trivial, redundant or otherwise uninteresting data; if done before onboard storage, preprocessing can reduce the storage problem. It is unclear whether these processors should be programmable, completely special purpose or somewhere between.
- Data Compression: The effects of data compression upon subsequent ground processing must be considered. Adequate consensus of all experimenters must be obtained in the determination of whether the data compression is to be data destroying or data retaining.
- Multi-Experiment Organization: In order to make optimum use of spacecraft and astronaut time, careful consideration must be given to the symbiotic combination of multiple experiments.
- Onboard Computer Control: Maximum advantage should be taken of the ability of a computer to untiringly perform such tasks as target selection, selection of data to be taken, selection of data to be transmitted, etc. This will have the side advantage of forcing the experimenters to more carefully plan the entire mission.
- Sensor Selection: Adequate design attention must be given to the matching of the sensor type and/or the type of data to the processing technique to be employed. It is entirely possible otherwise to design experiments from which data is hard if not impossible to extricate.
- Clean Detectors: Although calibration can be applied to compensate for detector artifacts, its use should be to further improve the accuracy of presentable data. Calibration or ground processing should not be relied upon as a prerequisite to rapid and accurate data presentation as the required turnaround time may well be longer than permitted by mission operations.
- Automated Maintenance and Graceful Failure: The experiment design should utilize error detection and correction with possibly some form of coded redundancy to provide at least the flagging of dubious data and preferably, automatic failure detection and by-passing.
- Diagnostic Instrumentation of On-Board Computer: On-board computers must be adequately instrumented to detect incipient failures.

Ground Data Processing

- More Efficient Programming: With the current price of \$3 to \$10 per instruction and the tendency toward larger and more complex

programs, more efficient methods of programming and debugging must be developed. Adequate consideration must be given to analyst interaction with his processing.

- Mass Storage: The entire data processing system must contain storage of quantities of pictures for recall and comparison by the experimenters. For this to be done in a reasonable time, new techniques of mass storage capable of recalling pictures in a very few seconds from a memory of 10^{12} bits may be required.
- Pattern Recognition: The entire area of pattern recognition and information extraction from pictures must be given further emphasis with the development of hardware and/or software techniques as required.

Image Processing Recommendations

Digital image processing has proven its worth over the past 10 years and is now an accepted method of image analysis. At this point, it is a fairly expensive process due primarily to the fact that the image processing systems presently available (e.g., VICAR at the Jet Propulsion Laboratory, LARSYS at Purdue University, and their various offspring) are all first generation processes. That is, they have been primarily designed for batch operations and, although they allow interactive processing, they are not optimal.

As a summarizing recommendation, the panel suggested the following seven specific topics as core items for further research.

Short Term Payoff

- Archival Image Storage and Distribution. Although images stored on film as images will always be part of the system, large-scale storage of images in digital form will be required. Present computer compatible magnetic tapes are very inefficient in this respect. Digital image storage on film is becoming available; what is needed now is the implementation of such devices in configurations useful for image processing.

Modern magnetic tape digital recording techniques allow packing densities to about 16 kilobits/inch per track. At this density it may be practical to continue to use magnetic tape as the archival or interchange medium. This is possible in spite of the disadvantages of tape, such as the need to make individual recordings for duplicates (as contrasted to making contact prints for film media) and the possibility of

deterioration over time. The digital techniques need to be developed, perhaps using commercial-type video cassettes as the medium.

- Hardware. A number of the algorithms currently used for image processing could be greatly speeded up if they were implemented in hardware. This hardware may be utilized in two manners: as a direct part of the computer CPU to replace software functions and as peripheral or perhaps even noncomputer associated devices. The candidates for conversion to hardware most clearly seen at this point are for correlation and Fourier transform, geometric rubber sheet stretching and various parts of the multispectral analysis. The multimegabit memory development must be continued to provide multi-picture storage for immediate access to the computing system, and also to provide video rate readout to volatile displays.
- High Quality Data Entry. High quality image scanning is relatively slow. Easily operated devices are required to allow the analyst or computer operator to rapidly and correctly enter film images into the system.
- Algorithm Development. Although a large number of individual processes are currently available (over 100 programs are available for execution under VICAR at JPL), new algorithms are continually required, either to perform new functions or to upgrade the present functions. The support of continued algorithm development must be a preplanned activity rather than ad hoc, to allow mission operations to take maximum advantage of the latest techniques.

Long Term Payoff

- System Software Design. Similarly, system software development must continue to provide ability to handle larger pictures and to provide multipartition processing and better interactive capabilities. Although these capabilities are becoming available in the larger operating systems, the price paid in system overhead is extremely high. The image processing efficiency may actually be lower than in the simpler batch systems. This comes about generally because of the extreme flexibility provided by these major systems. The research and development of systems particularly geared to the image processing job is indicated. This system research must be a specifically defined task to be successful, and not left as an ad hoc exercise forced upon an image processing laboratory by circumstances.
- Parallel Numerical Processing. This will include such areas as electronic LSI, magnetic bubble research, holographic logic, and the like.

- Optical Processing and Optical Converters. Digitally controlled optical processors will be required, either to process the images directly or through optical converters interconnected with the digital systems.

SENSOR-RELATED ASPECTS OF USER DATA ANALYSIS

Sample Identification

Given a sample material that is distinguishable by some means from all other materials in a particular scene, it is the purpose of this discussion to describe in a qualitative way, the interrelationships between the key parameters of that distinguishability. Although the studies leading to the understanding of these relationships were carried out with regard to numerically-oriented systems, the same basic principles probably to apply to systems utilizing human interpreters.

Since the ability to identify the material of a given sample area on the ground (i.e., to distinguish between it and all other materials in the scene) rests on measurements of the energy emanating from the scene elements, the key identification parameters are those relating the various aspects of energy measurements. Such a parametric set involves:

- Spatial Resolution
- Spectral Resolution
- Signal-to-Noise Ratio, S/N

Spatial, Spectral Resolution and S/N Interdependencies

It is apparent that these three parameters are very much interrelated. A given amount of energy emanates from a given scene area, and the choice must be made as to how many scene elements (pixels) that particular area should be subdivided into in order to achieve the desired amount of spatial detail. Also to be chosen is the number of spectral bands into which the energy from each scene element is to be resolved and measured. However, having selected values for the above two, the value for the third, in this particular case S/N, can readily be determined for a specific sensor.

All three parameters have a direct and also an interrelated bearing on distinguishability. In general it is not possible to identify a material which does not occupy a significant portion of the instantaneous field of view; thus the relation to spatial resolution is obvious. The relation of spectral resolution and S/N to identifiability may be a little less obvious, however. Although

this specific problem has not been treated in the literature, some insight can be gained from the results of related studies.

For example, G. F. Hughes, in correspondence with the IEEE Transactions on Information Theory in January 1968, studied the relationship between classifier performance (probability of correct classification) and a quantity defined as measurement complexity. In the present case, this measurement complexity can be thought of as the product of the number of spectral bands times the signal quantization precision expressed in terms of the number of discrete bins used. In a well designed data system, the number of such bins is usually closely related to the S/N ratio of the signals. In the case of ERTS, for example, if one assumed that the entire dynamic range of the sensor and data system were actively being utilized, the measurement complexity would be 4 bands times 64 bins or 256.

Hughes found theoretically that for the case of two equally likely classes, with unlimited amounts of training data available, the plot of classifier performance (probability of correct classification) versus measurement complexity increases monotonically to the right. This suggests that the more spectral bands and the more S/N, the better. There is a definite knee and saturation in the curve, however, with the result that beyond a certain point the performance improvement for increased measurement complexity is very marginal.

Note that this result, however, applies to the infinite training data case. That is, one assumes exact and complete knowledge of the classes of data to be identified. A more practical situation is the finite training data case. Hughes presents a similar (theoretical) result for the latter case, and the significant difference is that this curve does not monotonically increase but has a maximum occurring at a certain measurement complexity. The practical importance of this result is considerably enhanced by the fact that this phenomenon has been observed to occur experimentally using multiband earth observational data.

The values of both the performance and the measurement complexity at which the peak occurs depends on the amount of training data available. Again, assuming that these same principles apply across the spectrum of data analysis procedures, and a study of the basis for them would tend to suggest that they may, this suggests a fourth significant and interrelated parameter should be added to the above three, namely the specific knowledge of the ground scene and the classes to be used. Ordinarily this knowledge comes from the ground or lower altitude observations.

Further results are available by which to separate to some extent the contributions made by the S/N and by the spectral resolution. During the course of data compression studies, it was found that, for multiband earth observational data concerning the visible and near IR, the intrinsic dimensionality of this data seems to be about four. This means that, although the range from 0.4 to 1.5 μm could be divided into many subbands, it should be possible in the data system to linearly recombine (i.e., additively mix) them in such a way that only four channels must be transmitted. If the middle and far IR regions are added in, this number may not rise above six.

A study regarding the effects on analysis performance of decreasing S/N suggests that, when data has significantly less than 6-bit precision (64 shades of gray), performance begins to deteriorate rather rapidly for a classification task of intermediate difficulty (crop species identification) and that increasing precision above 7 bits (128 shades of gray) will still result in improved performance. In general more difficult (sophisticated) classifications require higher S/N, and further there is some indication that, as the S/N is increased, it is possible to effectively utilize data in increased numbers of spectral bands.

Conclusions

Summarizing, although the evidence is not at all complete and the needs in individual situations may differ, the following provides useful working conclusions to use at this time. These are subject to change based upon later evidence.

- Spectral and spatial resolution, S/N and ground observational knowledge are parameters directly related to identifiability and interrelated to one another.
- Generally, spatial resolution must be chosen, for identifiability purposes, so that the instantaneous field of view is commensurate with the material to be identified. Note that too fine a resolution may be just as damaging as too coarse (e.g., seeing the spaces between rows of a row crop), and that the choice of resolution for mensuration purposes may conflict with that for identification.
- For typical classification situations, 4-6 spectral bands are adequate, although improved performance is possible. If adequate energy is available to be able to generate data in a larger number of spectral bands, the specific 4-6 spectral bands should be selected based upon the planned use of the data. A typical band set selected in this way will include 2-3 in the visible spectrum, 1-2 in the reflective IR, and 1 in the emissive IR region.

- For typical classification, S/N ratios high enough to justify 7-bit data systems (128 shades of gray) are very desirable, while even higher ones may be classed as useful in some cases.
- Whatever the value of data obtained from remote platforms in terms of the quality of information that can be produced, increased information about the scene (i.e., increased training information) will only serve to improve it.

REPRESENTATIVE SYSTEM DESCRIPTIONS

General

This section presents representative systems concepts to form the basis of a total system description through reference to existing programs. Discussion centers on the Earth Resources Technology Satellite (ERTS) Multispectral Scanner System (MSS) and a system which is to be in operation in 1974, the Synchronous Meteorological Spacecraft (SMS) Visible Infrared Spin Scan Radiometer (VISSR).

The ERTS-MSS description includes the sensor, multiplexer, transmission and receiving equipment, ground data recorder and checkout display system. An overview of the MSS display/system for ERTS-1 experimenters is also presented.

The SMS-VISSR description covers the sensor and its operations modes: multiplex, communication, demultiplex, and synchronizer/data buffer or line stretcher which organizes the data for retransmission from the spacecraft to a direct-readout ground station generating a high quality picture.

ERTS-1-MSS

The Earth Resources Technology Satellite (ERTS) Multispectral Scanner System (MSS) is one of two major sensor experiments in earth orbit aboard the ERTS-1 spacecraft. The scanner system mission on ERTS is to provide imaging of earth scenes simultaneously in four spectral bands. Each one of 24 detectors views a 78 m x 78 m area of the earth's surface. The dimensions of the area imaged by each scan of the MSS comprise a swath 185 km (100 nautical miles) by 468 meters. The scan rate is 13.62 scans per second.

Sensor Subsystems

The Multispectral Scanner System is composed of several subsystems. These subsystems are the scan mirror, the telescope, the imaging electro-optics and the multiplexer.

The scan mirror of the MSS (Figure 5-23) is an oscillating mirror, which provides a cross-track scan, 100 nautical miles wide, of the earth's surface, while the progress of the spacecraft provides the scan along the orbital track.

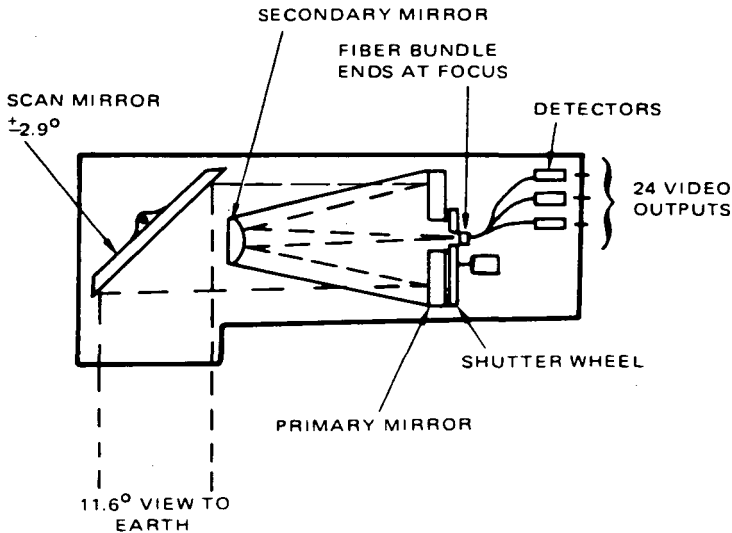


Figure 5-23. Four-Band Scanner Configuration

The telescope incorporating reflective optics to ensure the widest spectral bandwidth possible, receives the reflected earth image from the scan mirror and projects it as a point image into the imaging electro-optics. The imaging electro-optics receives the point image at one end of a fiber optic element, which routes the image through a spectral bandpass filter to a photodetector. The sweeping of this point by the scanner mirror generates an earth image line. The output of the photodetector represents the video history of this line and has a frequency range from DC to 50 kHz. Six lines of image information are generated by this method simultaneously in each of four spectral bands by locating a 4 x 6 fiber optic matrix in the image plane. Each fiber optic element (0.002791 x 0.002791 inch) is connected through an optical (spectral) bandpass filter to a separate photodetector. The generation of six images (A to F) in each band (Figure 5-24) during one scan sweep permits a suitable dwell time for each picture element that is needed to obtain a signal to noise voltage ratio of 25 to 50 on low reflectance scenes.

The multiplexer samples the four spectral band signals in a 10-microsecond time frame. The sensor data are formatted in the multiplexer with various synchronizing and calibration information into a serial digital signal as the

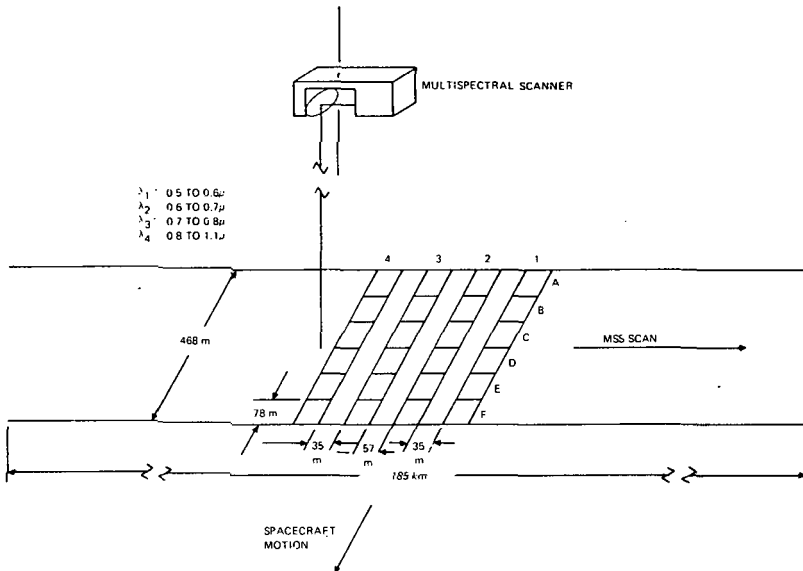


Figure 5-24. MSS Sensor Identification as Projected on Earth Surface

output of the multiplexer to be recorded on the satellite video tape recorder and/or transmitted in real time to a ground receiving station. The multiplexer also provides the MSS timing.

The MSS multiplexer is comprised of five functional sections (Figure 5-25): an analog multiplexer, analog-to-digital converter, timing logic, output buffer and power supply. Because of the high sampling rate required (2.5 MHz), two track-and-hold circuits are used in an alternating mode, one tracking the analog output of sensor 2A, while the stored value of sensor 1A is being digitized by the analog-to-digital converter from the other track-and-hold circuit. The track-and-hold circuit, in effect, requires a response time of only one-half the word rate of 2.5 MHz or 1.25 MHz. The word rate or sensor sampling rate of 2.5 MHz results in slightly over-sampling the data. One sample of a sensor represents an earth image 78 meters wide in the direction of scan. At this sampling rate, the image of the scanner has moved approximately 165 feet in the 10 microseconds it takes to sample all 24 sensors.

The sequence of sampling of the four spectral bands (1 through 4) by six rows (A through F) in the sensor matrix is such that less than 5 microseconds, or 1/4 a resolution element, exist between the first and last of the six sensor images in one spectral band. This produces a skew affect of 1/4 resolution

of a particular sensor in one scan to the instant of sample of the same sensor in preceding and succeeding scans.

The output of the track-and-hold circuits are switched to the analog-to-digital converter through a linear amplifier or a logarithmic amplifier (Figure 5-26). The 0.0 to 4.0-volt signal of the sensors in three spectral bands are processed in accordance with the logarithmic function:

$$V_{out} = 2.515 L_n (0.98 V_{in}) \text{ volts.} \tag{19}$$

This logarithmic scaling along with its inverse, minimizes the degradation of signal-to-noise ratio due to quantization in the small signal regions of primary importance.

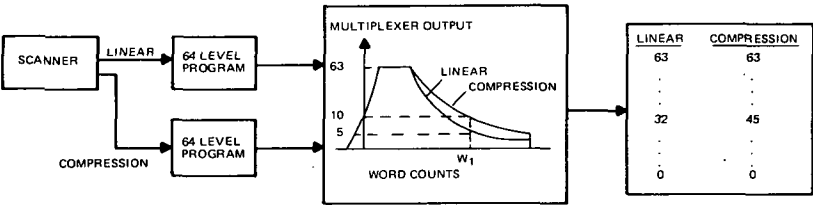


Figure 5-26. Calculation of Multiplexer Compression Curve

The analog-to-digital converter used in the MSS multiplexer makes 2.5 mega conversion per second. This conversion is performed in two steps. In the first step, the input analog voltage is compared by seven comparitor circuits set at equally spaced levels from 0 to 4 volts. The output of these comparitors is converted to the 3 most significant bits of a 6-bit digital word and stored in the output format register. This value is fed back through a 3-bit digital-to-analog converter to the input of a “times 8” amplifier and the remainder amplified eight times and applied to the seven comparitors. The output of the comparitors is converted to a 3-bit digital word and stored as the 3-least-significant bits in the output format register. From each word, 2 bits are complemented before they are entered into the output format register to ensure that each word will contain level transitions for ground equipment synchronization for most codes and specifically for the zero and full scale values. The format register content is then shifted out as one word into the output data format. This process is repeated for each sensor sample.

The timing logic of the MSS multiplexer organizes the output data format, generates all code and synchronizing words inserted into the format, generates the timing signals for the analog multiplexer and the analog-to-digital converter, generates the scan mirror and shutter drive signals, generates time-code |

gating and performs the logic detection of the scan start and end of scan pulses. The timing reference for the multiplexer is a 29.9 MHz crystal oscillator, with a stability of 1 part in 10^5 over a temperature of -20°C to $+80^{\circ}\text{C}$. The 30.12 MHz signal is divided down to provide the multiplexer bit rate of 15.06 MHz and word rate of 2.49 MHz. The analog-to-digital converter and analog multiplexer timing are derived from the bit and word rate signals with conventional ring counters, dividers and gating logic techniques.

The digital formatter accepts digitized sensor data from the converter and digital codes from the preamble and synchronizer codes generator and the jitter measure code generators and combines them into a serial digital bit stream. It provides the timing signals to the spacecraft to clock time code into the data format in the 24 words following SPS-1 and minor frame sync code of each major frame.

The preamble and sync codes generator of the timing logic provides the various digital codes which enable the ground equipment to synchronize with each mirror scan and each minor frame (150 words) of data transmitted. The 6-bit preamble (000111) and its complement, the start of line scan code (111000) are generated continuously to be inserted into the previously described format.

A pseudo start-of-line scan pulse is generated 6 milliseconds after the latest time at which the start of line scan pulse is expected to occur, assuring MSS operation in the event of loss of this scan pulse from the scanner.

The timing logic provides a power inverter synchronizing signal of 249 kHz, and a scan mirror and a shutter drive synchronizing signal to the scanner electronics.

The internal power requirements of the multiplexer are supplied by its own conventional dc to dc converter operating off the spacecraft power bus.

The command interface in the multiplexer utilizes latching relays with steering and protection diodes. The output interfaces of 15 MHz signals incorporate a complementary current source output driver.

Table 5-11 describes the interface characteristics of the MSS. Table 5-12 summarizes the system parameters of the spacecraft MSS equipment.

Transmission and Receiving Equipment

The Multispectral Scanner System data that is transmitted as Pulse Code Modulated PCM-FM over the rf link to the ERTS ground station is

Table 5-11.

MSS Interface Parameters

Item	Specification
Scanner Weight	105 lbs
Multiplexer Weight	6 lbs
Scanner Size	Approx 14 x 15 x 35 inches
Multiplexer Size	4 x 6 x 6.5 inches
Regulated Power, -24.5 volts	20 watts scanner plus 19.6 watts multiplexer
Unregulated Power, -39 volts	22 watts
Command Capability	72 (55 assigned)
Telemetry Channels	97

demodulated, processed by a bit synchronizer and sent to the Receiving Site Equipment (RSE). The RSE processes the PCM data, presents the processed information on a status monitor ("A scope") for on-line content and quality inspection, and records the processed data on magnetic tape for further processing. The RSE (Figure 5-27) consists of a demultiplexer, a digital tape recorder, a status monitor oscilloscope, and an RSE test set. The RSE accepts serial digital data and clock signals from a bit synchronizer to perform word and frame synchronization. It decommutates the input data into 25 parallel data channels, 24 of which contain the data separated by channel from each of the 24 sensors. The 25 data channels are recorded on parallel tracks on magnetic tape, along with a tape speed control reference frequency and the serial time code provided by the station. Each channel can be displayed in analog form on the status monitor oscilloscope. Table 5-13 illustrates some of the characteristics of the demultiplexer portion of the RSE.

The RSE test set provides simulated serial digital data for the demultiplexer and permits the display of either the selected demultiplexer output digital data or selected tape recorder output data on the status monitor oscilloscope, together with a display of line measurement data. The RSE test set also tests the demultiplexer acquisition and error detection logic by introducing selected errors into the simulated data stream. Table 5-14 illustrates some of the characteristics of the RSE test set.

The RSE uses a wideband multitrack tape recorder, an Ampex FR 1900-28. The tape recorder records at 60 ips the 25 channels of decommutated Non

Table 5-12

Summary of MSS Parameters

SPACECRAFT EQUIPMENT

Scanner

Telescope optics	9 inch Ritchey-Chretien type with 3.5 inch secondary mirror, f/3.6
Scanning method	Flat mirror oscillating ± 2.9 degrees at 13.62 Hz
Scan duty cycle (forward trace)	31.5 ms of 73.42 ms cycle minimum
Instantaneous field of view	0.086 mr (includes fiber cladding)
Optical fiber core	2.8 milli-inches
Spectral band and detectors	0.5 to 0.6 microns, PMT 0.6 to 0.7 microns, PMT 0.7 to 0.8 microns, PMT 0.8 to 1.1 microns, SiPd
Focal length	32.5 inches
Number of lines scanned per scan per band	6
Limiting resolution from 496 n.mi.	100 feet
Operational resolution	225 feet
Sampling distance	184 feet
Video bandwidth (-3 dB)	42.3 kHz per channel

Multiplexer

Number of channels	24
Quantization	6 bits
Quantization accuracy	With ± 30 mv at any quantum level
Processing modes	Linear and signal compression
Clock stability	$\pm 1 \times 10^{-4}$ /year
Output bit rate	15.06×10^6 bps
Sampling rate (each channel)	100,418 samples/second
Crosstalk	>40 db rejection

Return to Zero (NRZ) digital data, one channel of modulated carrier serial time code, one channel of capstan servo reference frequency and a voice log. The tape recorder incorporates Miller Code encoding and decoding logic in record and playback modes.

Ground Data Recorder

The tape recorder is capable of reproducing the MSS data along with an individual bit clock for each of the 25 digital channels at 60 ips and at 15 ips

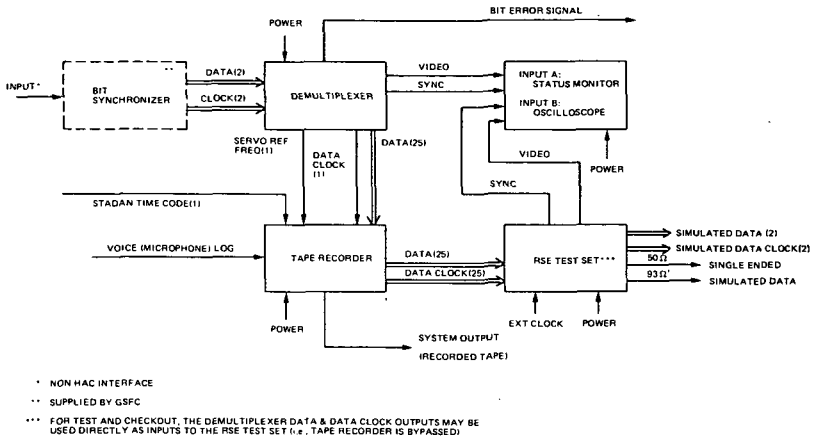


Figure 5-27. RSE Functional Block Diagram

Table 5-13

Demultiplexer Characteristics

<u>Functional</u>	
Input bit rate	15 Mb/s
Output bit rate (each channel)	600 kb/s
Output channels	25
<u>Acquisition and Maintenance</u>	
Probability of acquisition of major frame sync	>0.99 in first frame for a bit error rate of 1×10^{-5}
Major frame miss rate	$<1 \times 10^{-8}$ per major frame, once acquired
End of scan detection	RMS error ≤ 1 DEMUX input word for bit error rate of 1×10^{-5} .
Minor frame sync	Output bit stream phase jump $\leq 1/4$ of output bit period for downlink, bit slippages of 6 bits or less.
Power requirement	<140 W of 115 V 60 Hz.
<u>Physical</u>	
Weight	75 lb (max)
Depth	25.97 inch (max)
Width	19.03 inch (max)
Height	12.22 inch (max)

Table 5-14
RSE Test Set Characteristics

Function	Characteristic
Output bit rate	15 Mb/s NRZ data
Output data stream	(1) single ended at impedance levels of 50 and 93 ohms (2) simulated data and clock of bit synchronizer
Error(s) simulation	Single or multiple error capability
Input bit rate	600 kb/s
Input channels	25
Maximum external clock frequency	15.5 MHz
Power requirement	<100 w of 115 v, 60 Hz
<u>Physical</u>	
Weight	<65 lb
Depth	<22 inch
Width	<19 inch
Height	<14 inch

(4:1 speed reduction). It will also operate in conjunction with a second machine to permit duplication of tapes at 60 ips. Playback speed control is obtained either by phase referencing the capstan tachometer to a control frequency or by phase referencing the recorded capstan servo reference frequency to a control frequency. The control frequency may be either an internal standard or an external standard between 380 kHz and 420 kHz.

The tape recorder records in parallel tracks on 1-inch magnetic tape wound on 14-1/2-inch reels having standard National Association of Broadcasters (NAB) hubs. The recorder is capable of simultaneous record and playback to permit the recorded quality of the received signal to be examined by the RSE test set during a pass. Meters are provided in the recorder for all tracks, to permit monitoring of the level of the recorded signal to determine whether the recording being produced (or reproduced) is within the limits set for recording level.

A fast-forward and reverse-wind provision enables a reel containing 9200 feet of tape to be wound in approximately 6 minutes.

The tape recorder is expandable to 32 tracks by replacement of the present 28-track head stack assembly with a 32-track head stack assembly and the addition of the electronics for the additional tracks. Card slots and rack wiring necessary to accommodate the expansion capability are included in the recorder. Table 5-15 presents the major functional and physical characteristics of the RSE tape recorder.

Checkout Display System

The Ground Processing Equipment (GPE) of the Multispectral Scanner System is a piece of support equipment that reads and processes magnetic tape recorded multispectral scanner data and converts the processed data using a crater lamp photo recorder into photographic images of the earth's surface.

The GPE is not used in the operational ground station, but was used to verify the proper operation of the MSS during its development and qualification. The photographic imaging at the operational ground station is produced on an electron beam recorder. The GPE consists of a magnetic tape recorder (Ampex FR 1900-28), a digital processor, and a crater lamp photo recorder. The tape recorder reads into the digital processor 25 channels (tracks) of prerecorded multispectral digital data and a ground station time code track. The tape recorder receives a tape speed sync signal (servo reference) from the digital processor.

The digital processor processes the multispectral data and converts it into analog video to drive the photo recorder(s). This equipment also provides digital video to the ERTS computer. The digital processor functions are controlled manually, by data read in from punched paper tapes and by the ERTS computer. The digital processor may be operated manually or automatically by the ERTS computer.

The photo recorder converts the analog video output of the digital processor into positive or negative photo transparencies. This equipment receives drive and sync control from the digital processor and sends status signals back to the digital processor.

Paper tapes prepared by the ERTS computer are used to input video correction data into the digital processor. The ERTS computer also prepares annotation paper tapes that are used to input latitude-longitude tick marks and other annotation data into the digital processor for read-out by the photo recorder.

Table 5-15
RSE Tape Recorder Characteristics

Function	Characteristic
Number of channels	28
DEMUX digital outputs	25 NRZ PCM
Servo reference frequency	1
Station timing	1
Blank track	1
Voice log	Auxiliary edge track
Head assembly	28 tracks in two 14-track head stacks
Data rate	600 kb/s
Packing density	10,000 bits per inch
Data skew	
Max. data displacement errors	<6.25 bits across any one band, <36 bits between tracks on separate heads
Data transfer reliability	
Bit error rate	$<1 \times 10^{-6}$
Record speed	60 ips
Playback speeds	
Digital data	60 ips, 15 ips
STADAN time code	120 ips, 60 ips, 30 ips, 15 ips
Start/stop time	<8 sec/4 sec
Power requirement	<2.5 kw of 115 v, 60 Hz

Table 5-16 gives some of the characteristics of the GPE.

The picture format for the ground processing equipment is shown in Figure 5-28, which represents the information for one band. All four bands are processed in the same operation and appear side by side on a common photographic transparency.

Table 5-16
Ground Processing Equipment

Item	Characteristics
<u>Digital Processor</u>	
Inputs	25 video tape channels, STADAN time code from tape channel, annotation and indexing paper tape, and video correction paper tape
Output	Video signals polarized for either negative or positive transparency
<u>Photo Recorder</u>	
Type	Mechanical facsimile
Format	Four spectral bands at 10^6 to 1 scale
Rate of reproduction	One-fourth record rate
Gray scale fidelity	$16 \sqrt{2}$ gray shades
Optical system	Two optic heads on a common carriage
Light source	Zirconium arc crater lamp
Drum speed	1225.8 rpm

Referring to Figure 5-28, everything outside the picture itself (i.e., tick marks, gray scales, and title block) will be positioned relative to drum rotation, not memory location. There will be approximately 360 lines per inch down the drum and 360 counts per inch around the drum. Since the lines and counts are the same width, they will both be called "lines" when speaking of the dimensions of the picture annotation.

There will be one elongated tick on each side of each photograph. The cross-mark reference lines are the same size as the normal ticks and are lined up with them as in Figure 5-28. All tick marks are two lines long. The basic constraints on picture layout are the limits of 9 inches wide by 8 inches high. The title block consists of paper tape controlled annotation plus a 12-digit number selected by the operator using thumbwheel switches.

(Note: Much of the preceding information has been extracted from the monthly progress reports published by Hughes Aircraft Company on contract NAS 5-11255 and the "Final Report, Volume 1" titled "Multispectral Scanner Systems for ERTS Four Band Scanner System" also published by Hughes Aircraft Company.)

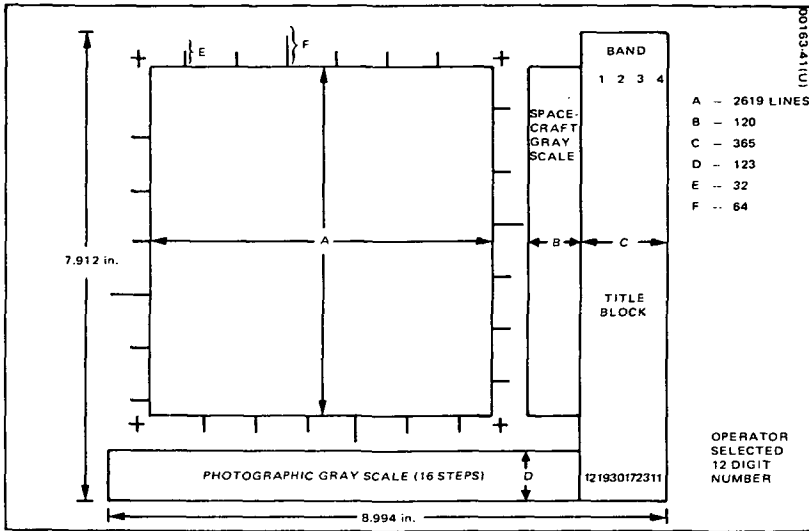


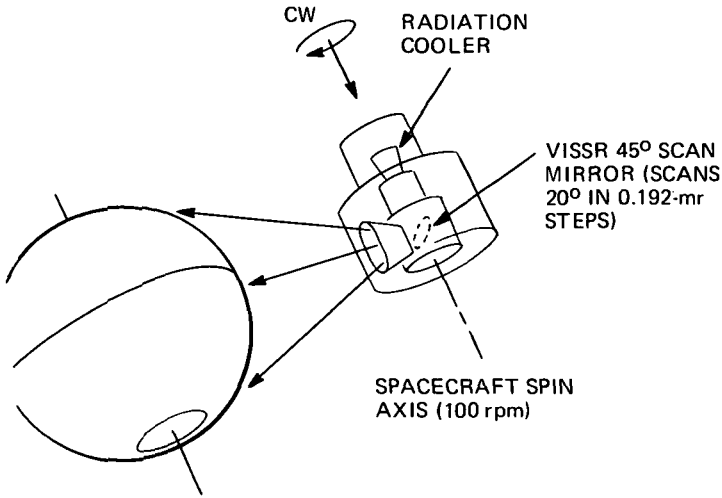
Figure 5-28. GPE Picture Format

SMS-VISSR

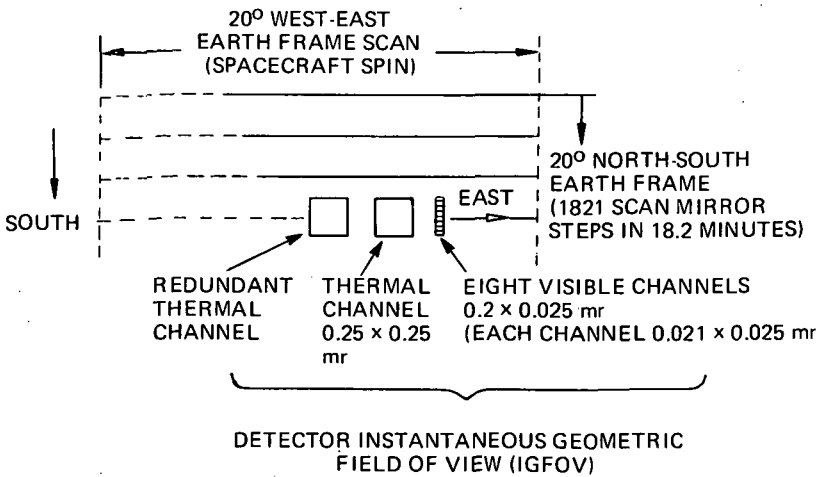
The Visible Infrared Spin Scan Radiometer (VISSR) is the earth imaging sensor on the Synchronous Meteorological Satellite (SMS). The VISSR operates as an integral part of the SMS, a synchronous spin-stabilized geostationary satellite with a planned operational life of three years. VISSR provides both day and night mapping capability with a satellite subpoint resolution of one-half mile in daylight and five miles at night. Cloud altitude is determined by infrared radiometric measurement of cloud top temperature. VISSR instrumentation provides a substantial improvement in resolution in the visible region and extends measurement capabilities to the infrared region when compared to the previous smaller ATS Spin-Scan Cameras. The capability is provided for future growth in the infrared region of vertical temperature profile measurements through the use of additional infrared channels with different spectral and field-of-view characteristics.

Sensor

The VISSR arrangement as used in the synchronous spin-stabilized geostationary satellite is shown in Figure 5-29. As indicated in this figure, the mapping raster is formed by a combination of the satellite spin motion and a step action of the scanner optics. One raster line, corresponding to the earth's west-east



(a) SPIN-SCAN GEOMETRY



(b) PICTURE DATA FORMAT

Figure 5-29. VISSR/Spacecraft Spin-Scan Geometry and Picture Data Format Arrangement

axis, is formed for each revolution of the spinning satellite (100 rpm), and the scanner positions each successive line in the north-south axis. Each north-south axis scan step corresponds to the instrument's instantaneous geometric field of view (IGFOV). This 0.192-milliradian step corresponds to the thermal channel 5-mile resolution, when related to the satellite's 22,000 statute mile distance from the earth and considering there is a 1-mile overlap between successive scan lines.

The one-half mile resolution in the visible region is obtained by using a linear array of eight detectors aligned so that they sweep out the same scan line path. The IGFOV of each visible channel is 0.025×0.021 mr, allowing 20 percent underlap between detectors for fabrication considerations. The earth is covered in the north-south plane with successive latitude steps until 20 degrees coverage is attained (± 10 degrees about the nominal radiometer optical axis). Following the normal frame, the scanner retraces to the original start position at a rate approximately ten times faster than the normal step scan period.

The VISSR instrumentation permits the following four modes of scanning.

- Normal Frame: This covers the entire earth with a ± 10 degree frame, and consists of 1821 latitude steps in 18.2 minutes. It automatically retraces to the original start position in 1.71 minutes to make a complete scan cycle in 19.93 minutes. Each normal frame is initiated by ground command.
- Variable Frame: Selected frame sector and position within the normal earth view are acquired by ground command.
- Single-Line: Interruption of the scan step sequence at any selected north-south position makes a single-line scan. Scan position is determined by command timing.
- Rapid Forward Scan: A rapid forward scan (ten times normal scan rate) is initiated by command to permit rapid positioning of the scan to any selected position within the normal frame.

The scanner assembly consists of a telescope and a separate electronics module. The telescope is a 16-inch diameter aperture optical system which includes an object-space scan mirror for accomplishing the step north-south scan. The assembly includes a radiation cooler and detectors with supporting electronics. It is approximately 60 inches long and 25.5 inches in diameter, and weighs 143.4 pounds. The electronics module occupies approximately 450 cubic inches and weighs 13 pounds. It contains the circuitry for interfacing the scanner electronics with the spacecraft electronics, the circuitry necessary for conditioning the scanner signal channels, and the logic circuitry concerned

with the scan drive and calibration sequence. The nominal electrical power required by the radiometer is 22 watts.

The mechanical-optical layout of the telescope is shown in Figure 5-30. Referring to this figure, radiation is received by the primary optics via the 45-degree object-space scan mirror. This is an elliptically shaped plane mirror, which is tilted about its minor axis to obtain the north-south scan steps. This mirror is servo-positioned using a torque motor drive, together with a digital encoder for completing the servo loop. A redundant identical assembly is on the opposite side of the mirror. The servo electronics include the logic necessary to step position the mirror at 0.096-mr steps (0.192-mr optical steps) in the required sequence to make the selected scan mode.

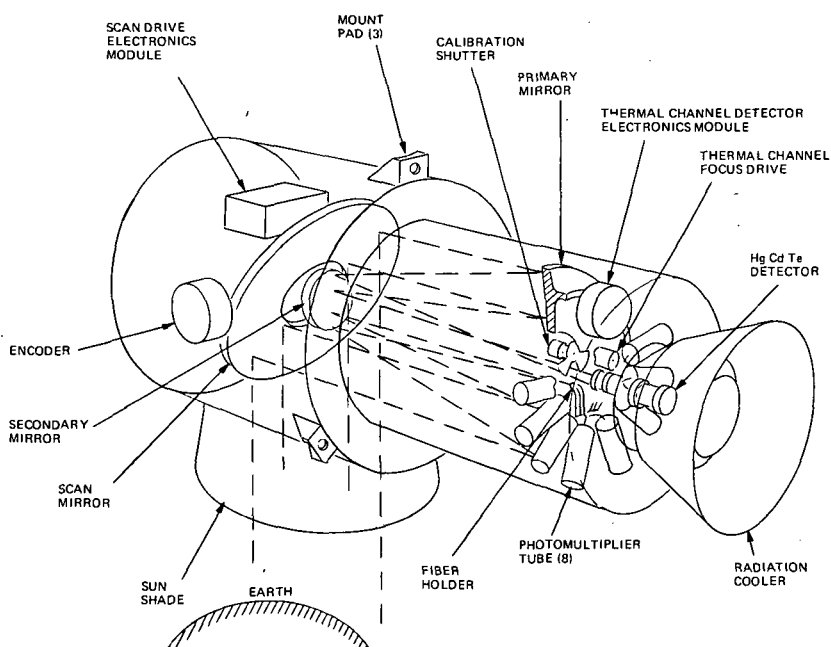


Figure 5-30. VISSR/SMS Schematic

Energy from the scan mirror is collected by a Ritchey-Chretien optical system. The 16-inch diameter optical system has a 114.7-inch focal length. The system includes a baffle that extends from the primary mirror center section to minimize the effects of scattered radiation. Energy in the visible region is detected at the prime focus, using eight fiber optics arranged at the focal plane to form the defining 0.2×0.025 -mr (field stop) linear array (with each fiber 0.025×0.021 -mr). The other ends of the individual fibers are optically

integrated with the eight photomultiplier tubes having the desired 0.55- to 0.75-micron response. In addition, the prime focal plane is relayed to the radiation cooler cold plate using two germanium relay lenses. The relay configuration also is used to increase the overall optical speed to $f/1.28$ relative to the thermal detectors. The 0.005×0.005 inch HgCdTe long-wavelength detector is mounted on the radiation cooler cold plate, together with the identical redundant detector. An optical filter between the final relay lens and the detectors restricts the energy to the 10.5- to 12.6-micron wavelength bandpass.

A radiation cooler is used to cool the intrinsic long-wavelength detectors (HgCdTe) in the thermal channel to a nominal temperature of 90 K, the controlled temperature value selected for optimum performance of the particular detector in the scanner. The cooler has actually demonstrated low-temperature performance of 81 K. It uses two cold stages plus an ambient shield. The outside shield is 18 inches in diameter.

Table 5-17 provides a summary of the design, performance, and physical characteristics of VISSR.

Multiplexer

The video outputs of the VISSR visible and infrared sensors are prepared for transmission over the rf link to the ground receiving site by the VISSR digital multiplexer (mux). The VISSR mux sequentially samples the 10 VISSR video channels, performs analog-to-digital conversions, and generates a quadri-phase compatible serial waveform.

The VISSR subsystem provides eight visual and two infrared channels. The information bandwidth of the former is 225 kHz and that of the latter is 26 kHz. Prealiasing filters are provided in the mux to ensure the aliasing error in the reconstructed video is sufficiently reduced that the system signal-to-noise ratio degradation does not exceed 1 dB. The VISSR subsystem also provides 12 encoder signals to the VISSR mux. The encoder signals contain the line scan identification number which is transmitted once-per-scan to the CDA ground station. The VISSR mux accepts the eight visual and two infrared analog signals from the VISSR electronics assembly, performs the analog-to-digital conversion, and provides quadriphase compatible serial outputs. The VISSR mux operates in one of two modes, as directed by the telemetry and command subsystem, and contains redundant elements to increase the overall Mean Time To Failure (MTTF). Table 5-18 delineates the mux operating modes.

Table 5-17
Design Summary

Design Parameters	Visible Channel	Thermal Channel
Number of Channels	8	1 plus 1 redundant channel
Wavelength Band of Operation, Half-Power Points	0.55-0.7 microns	10.5-12.6 microns
Instantaneous Geometric Field of View (IGFOV)	0.025 x 0.021 mr	0.2 x 0.2 mr
Collecting Aperture	1090 cm ²	1090 cm ²
Detector	EMR541E-01 PMT	HgCdTe
Size	—	0.105 x 0.105 m
Response	S-20 (enhanced)	—
Scan Period	0.6 sec	0.6 sec
Dwell Time	2.4 x 10 ⁻⁶ sec	1.9 x 10 ⁻⁵ sec
Information Bandwidth ⁽²⁾	210 kHz	26 kHz
Dynamic Range, Albedo (%); Target Temperature (°K)	0 to 80	0 to 330
Performance Characteristics	Visible Channel	Thermal Channel
Noise Equivalent Radiance NEN for an Extended Source (watt-cm ⁻² -sterad ⁻¹)	—	1 x 10 ⁻⁵
Noise Equivalent Differential Temperature for an Extended Source	—	1.5 K at 200 K 0.4 K at 300 K
S/N at 0.5% Albedo, for an Extended Source	3:1	
Modulation Transfer Function	0.34 at 2 x 10 ⁴ cycles/rad	0.42 at 2.5 x 10 ³ cycles/rad
V _p /V _{ss} , Target Size Equal to IGTOV's Includes Optical Response Factors (Approximate)	0.45	0.55
Physical Characteristics	Scanner	Electronics Module
Weight	143.4 lb	13 lb
Size ^(b)	60 x 25.5 x 25.5	450 in. ³
Power Requirements	22 watts	
Inflight Calibration Provisions		
Visible Channel	1. Sun and Space	
Thermal Channel	1. Sun and Space 2. Calibration Blackbody and Space 3. Electronics Gain and Linearity	

(a) Physical location of information bandwidth filters (i.e., VISSR or SMS data link) to be determined by NASA.

(b) Excluding entrance aperture sun shade.

Table 5-18

VISSR Multiplexer Data Transmission Modes

Mode	Input* Channels	Samples** Rate (kHz)	Visible Channel Resolution		Data Mb/sec	Symbol Rate Mb/sec
			N-S (n.m.)	E-W (n.m.)		
1	8 visible +2 IR	500	0.5	0.5	28.0	14.0
2	4 visible +2 IR	437	1.0	0.5	14.0	7.0

*Reduction in number of visible channels is accomplished by paralleling individual visible sensor outputs (i.e., 4 visible = 4 groups consisting of 2 adjacent sensors per group; 2 visible = 2 groups consisting of 4 adjacent sensors per group; 1 visible = 1 group consisting of all eight sensors in parallel).

**Predicated on 100 rpm spin rate.

The general block diagram of the VISSR mux is illustrated in Figure 5-31. The unit features input signal multiplexing, redundant analog-to-digital converters

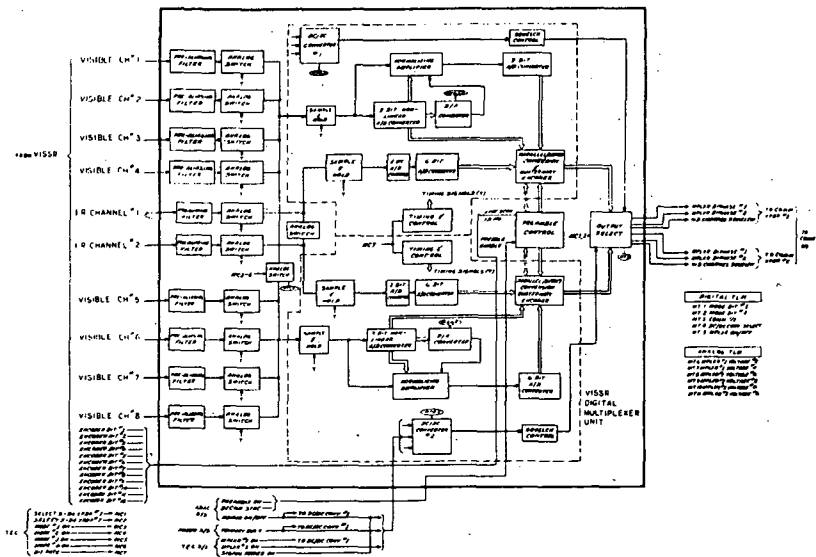


Figure 5-31. SMS VISSR Multiplexer Block Diagram

with their associated dc/dc converters for reliability enhancement, and output differential encoding for quadriphase modulation. Each VISSR analog output signal to the mux is bandlimited by presampling filters, which reduce the alias error in the output analog data at the ground station. Analog switches follow each filter and sequentially multiplex each of the input signals to the analog-to-digital converters. Track-and-hold elements are inserted between the switches and the converters to provide a constant-amplitude signal during the conversion process. Finally, two types of converters are used: an 8-bit linear analog-to-digital converter for the IR channels and a 6-bit nonlinear analog-to-digital converter for the visual channels.

The eight visible and two infrared analog video signals from the scanner enter the multiplexer through input prealiasing filters and buffer amplifiers. The analog video multiplexer sequentially combines the eight visual video signals into a sampled video stream for conversion by one of the two redundant nonlinear, 6-bit analog-to-digital converters. Similarly, the multiplexer sequentially combines the two IR signals for one of the two redundant 8-bit linear converters. Figures 5-32 and 5-33 provide block diagrams of the visible and infrared analog switching and track-and-hold portions of the VISSR multiplexer.

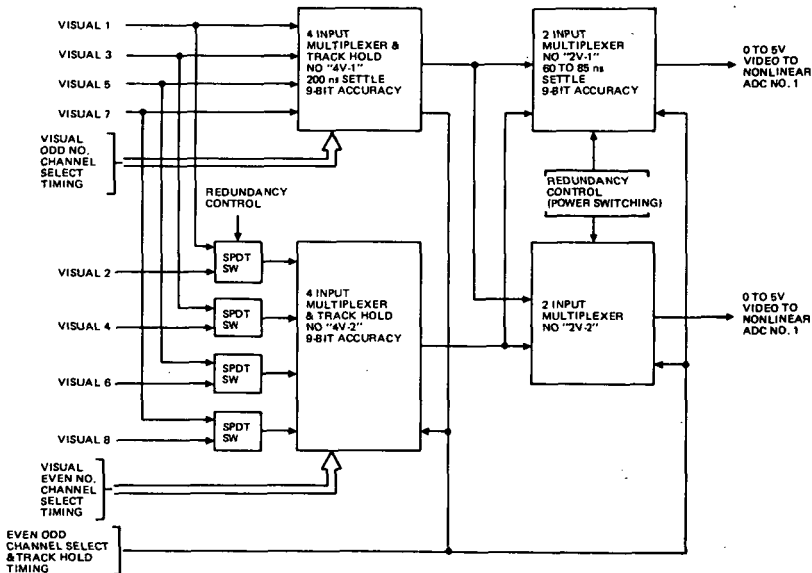


Figure 5-32. SMS VISSR MUX, Analog Multiplexer

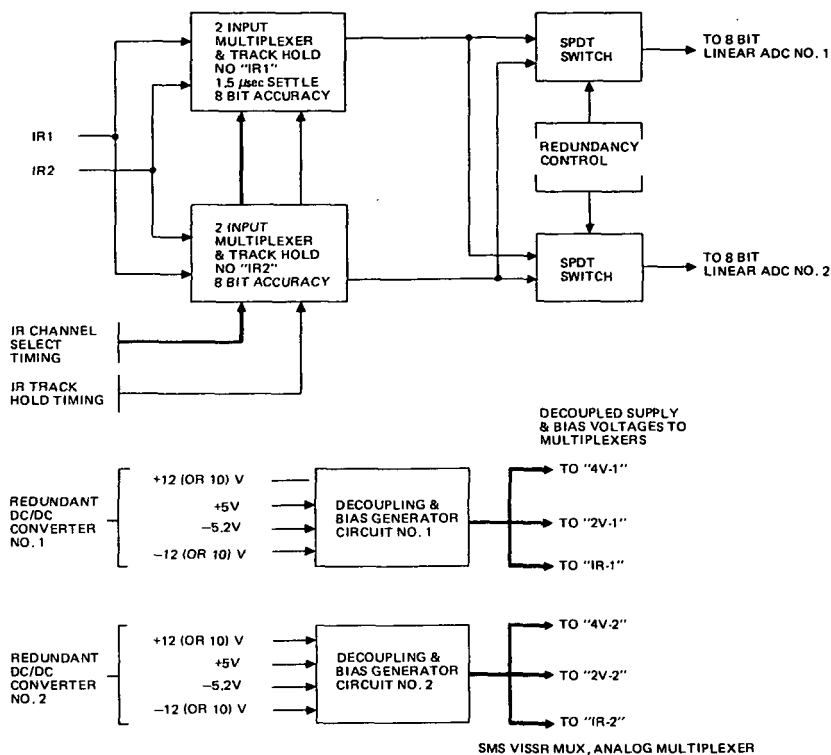


Figure 5-33. SMS VISSR MUX, Analog Multiplexer

The visual channels are divided into odd and even groups. A four-input multiplexer is normally assigned to each group, that is, the unit numbered 4V-1 multiplexes visual inputs 1, 3, 5, and 7, and 4V-2 the even inputs. The outputs of 4V-1 and 4V-2 are connected to two input multiplexers 2V-1 and 2V-2. The redundancy control signal energizes only one of these two input multiplexers corresponding to the nonlinear analog-to-digital converter currently in use.

The four-input multiplexers also combine a track-and-hold function. In mode 1 (28 megabits/sec and all eight visual signals utilized) one multiplexer is tracking and stabilizing while the other is holding and outputting through the two-input multiplexer to the analog-to-digital converter. On the next video conversion, the roles are reversed. Thus, the four-input multiplexer has one word time (approximately 214 nanoseconds) to stabilize to the required accuracy of 0.1 percent. As will be seen, this timing remains the same in mode 2.

In mode 2, the data rate drops to 14 megabits/sec, and the even channels are no longer normally multiplexed. The even-channel signals are previously combined linearly with their odd twins, as described in the section on the prealiasing filters. Therefore, the two-input multiplexer in use does not commutate in mode 2.

The linear averaging function is accomplished in the prealiasing filter section, resulting in no change for the multiplexer.

The four Single Pole Double Throw (SPDT) video switches normally connect the inputs of 4V-2 to the even-numbered channels. In the event of any malfunction affecting multiplexer 4V-1, the switches are optionally thrown to substitute 4V-2, thus maintaining 50 percent channel capability for mode 1 and full capability for modes 2, 3, and 4. The redundancy control to the multiplexers 2V-1 and 2V-2 allows the system to maintain full capability in the event of malfunction in either of these multiplexers or the related analog-to-digital converter.

All multiplexers employ voltage limiting in their analog inputs at approximately +5.8V and -0.8V so that erroneous out-of-range input signals do not cause failure on the remaining good channels. To prevent failure in subsequent units, in the event of malfunction, the multiplexer outputs are dc current limited.

The IR channels are handled by two parallel, completely redundant two-input multiplexers and track-hold circuits, IR-1 and IR-2. Either is connected to either of the redundant 8-bit linear converters by redundancy control signals applied to the SPDT switches. The IR conversion rate is 250 kHz, and up to 1.5 μ s is allocated for multiplexers IR-1 and IR-2 to stabilize.

Table 5-19 delineates the digital multiplexer specifications.

The VISSR data demultiplexer is designed to decommutate serial PCM data from the receiving site quadriphase demodulator. The VISSR data demultiplexer accepts the outputs from the demodulator which consists of two serial bit streams (x and y), at 14 MHz clock rate and a 28-MHz clock. It demultiplexes the bit streams and generates eight visual and two IR analog outputs. It also provides a digital display of any selected visual or IR data words. A self-check panel provides for checking the demultiplexer in the absence of an input signal.

Table 5-19
Digital Multiplexer Specifications

Parameter	Specification
A. VISSR outputs (multiplexer input)	
1. Visual channels	
Quantity	8 each (full capability)
Video bandwidth (3 db)	0.05 Hz to 225 kHz
Peak signal to RMS noise	9 db at black level (noise level 10 mv) 32 db at white level (noise level 120 mv)
Dynamic range	54 db (10 mv to 5000 mv) precompanding 32 db (10 mv to 400 mv) postcompanding
Minimum noise level	10 mv
Maximum noise level	120 mv (increases as a square root of signal voltage)
2. IR channels	
Quantity	2 each (full capability)
Bandwidth	0.02 Hz to 2 kHz
Peak signal to RMS noise	10 db (target temp. 180 K) 48 db (target temp. 300 K)
Dynamic range	48 db (20 mv to 5000 mv)
Noise level	20 mv
B. Multiplexer	
1. Visual channels	
Encoding	6-bit
Linearity	Companded (= square root)
S/N degradation	1 db due to quantization (i.e., $S/N_Q = 38$ db)
Gain stability (per channel)	± 0.5 db over any 12-hour interval
2. IR channels	
Encoding	8-bits linear
Linearity	1 percent of full scale from straight line
S/N degradation	< 1 db due to quantization and inter-modulation (i.e., $S/N_Q = 54$ db)
Gain stability (per channel)	± 0.5 db over any 12-hour interval
Size	651 in.
Weight	14.4 lbs
Power	Maximum average power 6.5 w Peak pulse power (51 ms) 42.8 w

Spacecraft to Ground Communication

The 24 megabit/sec PCM data is transmitted as quadrature phase modulation on the S-band downlink to the data acquisition or processing site. A quadrature phase demodulation and bit synchronizer convert the data to a serial bit stream which is sent to the demultiplexer.

Demultiplexer

The demultiplexer outputs the VISSR channel information, in parallel digital form to the Synchronizer/Data Buffer (S/DB). It also provides clock, identification, status and strobe signals for the S/DB.

Figure 5-34 is the functional block diagram of the demultiplexer. It shows the functional configuration and general signal flow.

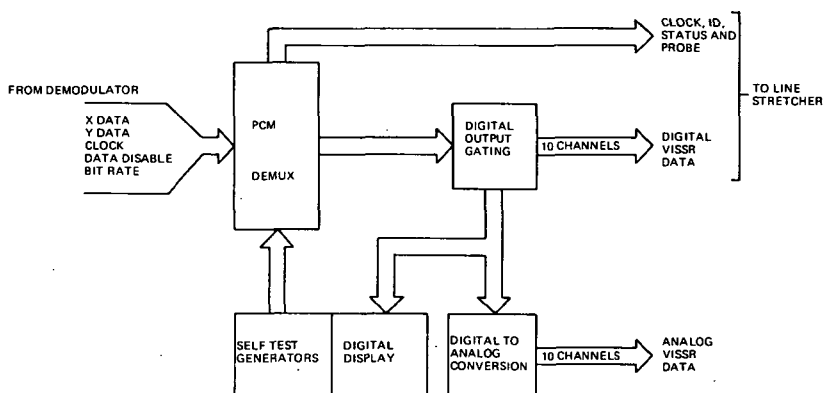


Figure 5-34. Functional Block Diagram – CDA Demultiplexer

Input signals from the demodulator consist of:

1. X data
2. Y data
3. Clock
4. Data enable
5. Bit rate.

X and Y data are two serial bit streams, which are synchronous with the clock signal, and contain VISSR channel information and synchronizing signals. The clock signal is a continuous square wave at 14 or 7 MHz. Since X and Y data are separate inputs synchronous with the clock, the effective input bit rate is twice the clock frequency – 28 or 14 megabit/sec. Data enable and bit rate are logic signals which control X and Y data input, and establish the bit processing rate.

X and Y data are “clocked” into shift registers in the PCM demux under control of signal data disable, and at bit rates established by signal bit rate. At

appropriate times, VISSR channel information is read out to the S/DB in parallel 8-bit bytes. This information is also applied to internal digital-to-analog converters which reconstruct the VISSR channel analog signals. Identification, status, and strobe signals are generated internally and along with the system clock are routed to the S/DB. The self-test generators are controlled by front panel switches and provide a means of testing the demux in the absence of valid data from the CDA demodulator. The digital display is used in conjunction with the self-test generators to monitor the digital value of each VISSR channel.

Synchronizer/Data Buffer

The VISSR video demultiplexed data is routed to the S/DB. This equipment slows down the VISSR video information, reformats and annotates the data and outputs it for retransmission to the SMS spacecraft transponder. The S/DB also can produce VISSR sensor information in various formats on an Electronic Image Systems Corporation photorecorder.

The data flow through the S/DB is discussed in this section and references Figure 5-35. The 4 phase demod demux accepts the 70-MHz signal derived from the satellite's wideband transmission. This unit demodulates the input

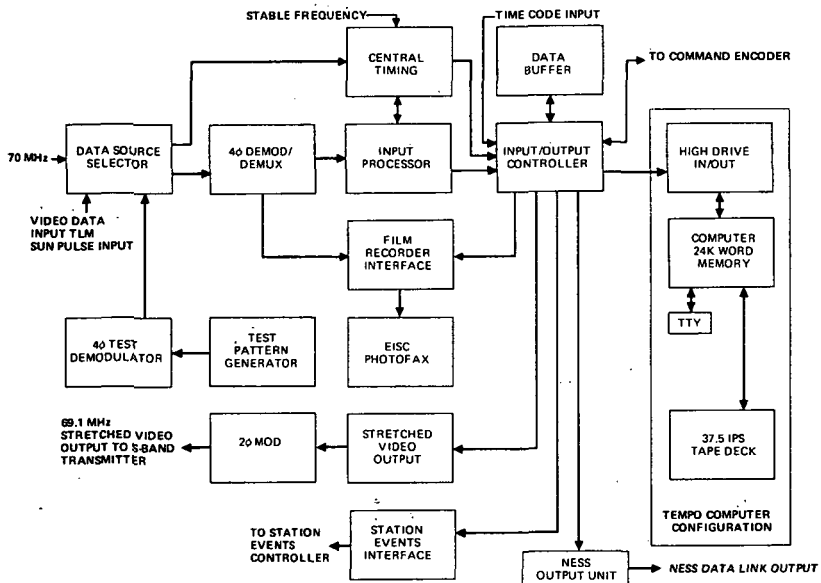


Figure 5-35. Synchronizer, Data Buffer System, Block Diagram

to form a baseband digital signal which is then bit synchronized. After bit synchronization, word synchronization is achieved; during this process the data are grouped in 8- or 6-bit groups and sent to the input processor on eight data lines. In addition to these data lines, which are provided by the demux, there are data strobes and control signals.

The central timing unit controls the operations of most of the other units in the S/DB; however, these control lines are not shown in the block diagram. The most critical function of this control is performed by the phase locked loop (PLL) subunit. The PLL divides the satellite rotation into 6289920 equal parts, regardless of spin period, referenced to a sun sensor. The time at which the satellite's sensor sweeps past the sun is sent to the Control and Data Acquisition (CDA) station as a real-time analog sun pulse and as a digital sun count. The analog sun pulse is supplied to the S/DB from the telemetry receiver after being thresholded there. The sun pulsewidth is $90 \pm 25 \mu\text{sec}$; the leading edge contains the timing information. The digital sun count is provided by the demod demux as a number representing the eight least significant bits of a counter in the spacecraft operating at a 3.5-MHz rate. This count is used to infer precisely the location of the analog sun pulse.

In operation, the PLL predicts the time at which each sun pulse arrives. The difference in time between the arrival of the actual and the predicted sun pulses is termed the PLL error, and is subsequently used to control the phase and frequency of the PLL.

The frequency is produced by a digitally-controlled synthesizer having a stable 1-MHz input. The synthesizer frequency is precisely equal to $6289920/2P$ for a spin period P . The maximum frequency achieved at 110 rpm, is 5765670 Hz.

The basic Synchronizer and Data Buffer clock frequency, termed the Voltage Controlled Oscillator (VCO) frequency, is double the synthesizer frequency.

Among the major timing signals output by central timing is the equal angle clock signal formed by dividing the VCO frequency by 21. The second set of major outputs relate to the stretched video (SV) retransmission. This includes dividing the satellite's rotation into 10 sectors; the phasing of these sectors is controlled by an offset related to the satellite's rotation angle during propagation of the satellite's signal to the CDA station. The SV bit clock is derived by dividing the VCO frequency by six in the highest resolution SV mode.

The steady state bandwidth of the PLL is adjustable in two steps to minimize the tracking error as a function of the sun pulse noise and satellite spin

acceleration. In addition, at narrow bandwidth settings, the bandwidth during mirror retrace is increased to reduce the tracking error. This bandwidth is then returned to its normal value at the beginning of each frame to minimize the effects of the step-in-mirror acceleration.

To acquire data from the earth, the sun-referenced PLL output must be offset by an angle equal to the sun-earth separation as viewed from the satellite. This offset angle, β , changes with time due mainly to the earth's rotation, to a satisfactory approximation expressed as follows:

$$S = S_0 + S_0 (t - t_0) \tag{20}$$

where

$$\beta = \beta_0 \text{ is } \beta \text{ at time } t_0.$$

The angle β need be computed only once per satellite rotation and is implemented by software in the computer.

The input processor receives the parallel digital data from the 4-phase demod/demux as indicated in Figures 5-36 and 5-37. The first 56 bits received are treated specially; the scan number and scan direction bits are stored for later transmission to the computer and the digital sun count is sent to the PLL. No check of the sync word is made, since it is assumed that this function has already been adequately performed. During the remainder of the transmission, the sync-1 and sync-2 words are checked; a count is kept of the number of times these sync words are in error. This error count is used as a measure of the bit error rate.

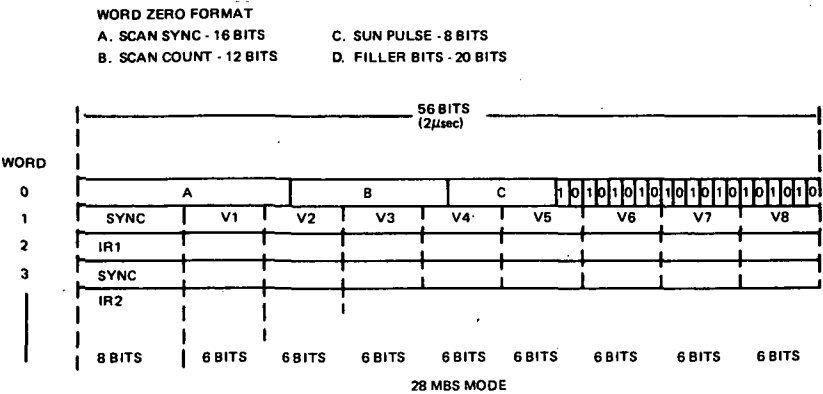


Figure 5-36. VISSR PCM Data Format, Mode 1

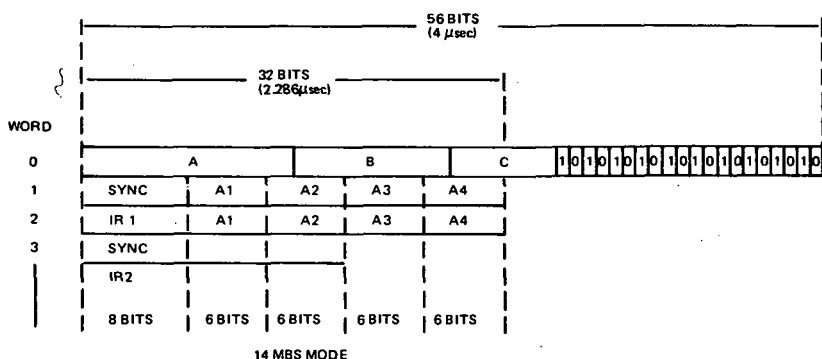


Figure 5-37. VISSR PCM Data Format, Mode 2

The visible and IR data, as well as some documentation words, are transferred to the input/output controller. In mode C (maximum stretched visible data), the visible data are averaged to reduce their resolution to that of the IR data. These visible data then replace IR-1 or IR-2 during output of the I/O controller. Virtually all data pass through the I/O controller. During data acquisition the visible data are passed to the buffer while the IR data (and in mode C, the average visible data) are passed to the computer. Other data required by the computer, such as time from the time code translator and the PLL error from central timing, are also passed to the computer.

While this data acquisition is taking place, the I/O controller is outputting visible data from the buffer. In mode B the visible data are also averaged during output to reduce its resolution. During the pre-IR period, while a random pattern is transmitted to the satellite, the PLL tracking correction is made, the sun-earth (β) angle is incremented, and time is provided to the computer. During the following sector the IR data from the computer are transmitted.

A Station Events Controller (SEC) interface is also included to route up to 64 bits of state and error indicators to the SEC for subsequent transmission to National Environmental Science Service (NESS) of NOAA.

Direct Readout Ground Station (DRGS)

The DRGS has been developed to provide ground terminal facilities for receiving, recording, and displaying the visible and infrared data collected by the very high resolution radiometer (VHRR) of the Improved Tiros Operational Satellite (ITOS) and the VISSR data of the SMS.

The DRGS is a transportable receiving station, consisting of a flatbed antenna trailer (Scientific Atlanta 3200-R18), weighing approximately 26,500 pounds, and a 30-foot instrumentation van with a maximum gross weight under 16,000 pounds.

The DRGS will be located at the Wallops CDA station for a period of time prior to and following the launch of SMS, for spacecraft/ground system evaluation tests, and in the establishment of operational and procedural steps for optimum use of the data.

The VISSR image produced by the DRGS is shown in Figure 5-38.

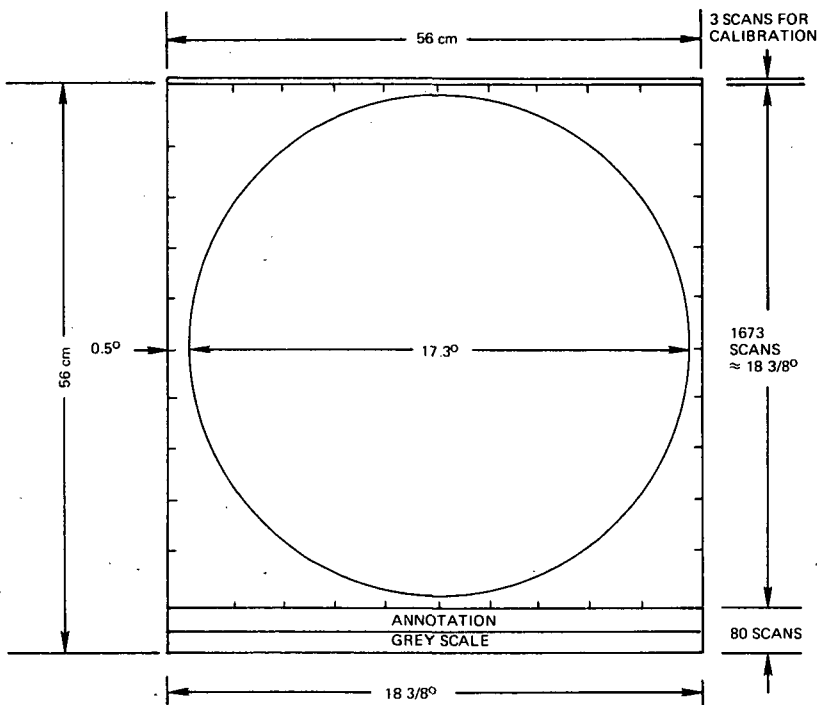


Figure 5-38. VISSR Image

The DRGS (Figure 5-39) is a versatile system designed to receive and record the stretched VISSR and VHRR data in various operational modes. The three major subsystems are:

- Antenna/pedestal assembly

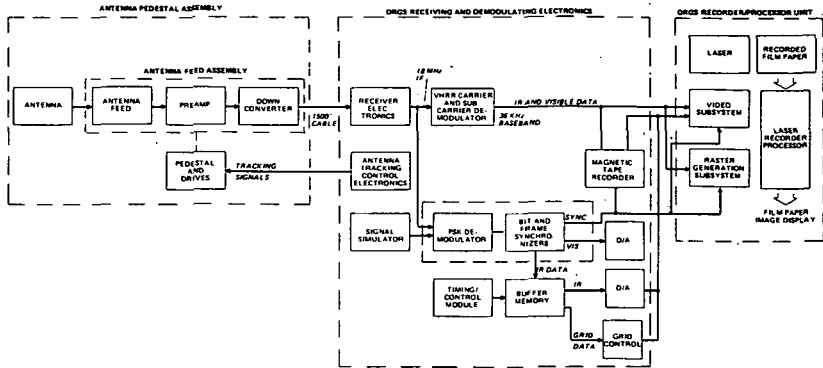


Figure 5-39. Direct Readout Ground System, Block Diagram

- Receiver and demodulating electronics
- Recorder/processor display subsystem.

Antenna/Pedestal Assembly. The antenna/pedestal assembly consists of a solid surface parabolic reflector 18 feet in diameter, a parametric amplifier and down-converter mounted in the feed assembly, and the pedestal. The antenna/pedestal assembly is designed for operation over the range of environmental conditions that are expected at remote station sites, and it can be located up to 1500 feet from the recorder/processor subsystem to facilitate site planning.

Receiving and Demodulator Processing. The receiving and demodulating electronics provides facilities for data receiving and demodulation of the stretched VISSR data that are received from SMS. The rf signal is received by the antenna and fed to a parametric amplifier by a single-channel monopulse feed assembly. The rf signal is down converted, and fed to the receiver over a coax cable. The receiver down converts the rf through two IF stages to a 10-MHz IF frequency. For SMS stretched VISSR reception, the IF signal is fed to a PSK demodulator which outputs a serial-bit stream to the bit and frame synchronizers. The IR data are directed to a core storage module and then read out for image recording purposes. The visible data are fed directly to the digital-to-analog converters, and then to the recorder/processor's video electronics. Grid data are extracted from the IR channel and used to grid both IR and visible image displays. Synchronization is extracted from the two channels of data and is used to synchronize the recorder's raster generating electronics.

VISSR Demodulation and Synchronization Electronics. The function of the VISSR demodulation and synchronization electronics is to convert the PSK/PCM signal from the receiver to an analog video signal, and to detect the transmitted sync signals for use by the recorder for synchronization. The system generates biphase PSK-NRZ-S demodulation and subsequent conversion to a word serial output accompanied by a number of synchronization signals.

The digital interface electronics system configuration is shown in Figure 5-40. It utilizes a special 10-MHz PSK demodulator, two standard Electro Mechanical Research (EMR) signal conditioners (bit synchronizers), with four standard selector modules, in conjunction with a pattern recognizer/correlator (frame synchronizer) subsystem especially designed to optimize frame synchronization for the specified formats. The system also provides a complete self-contained interface between the receiver and the recorder/processor.

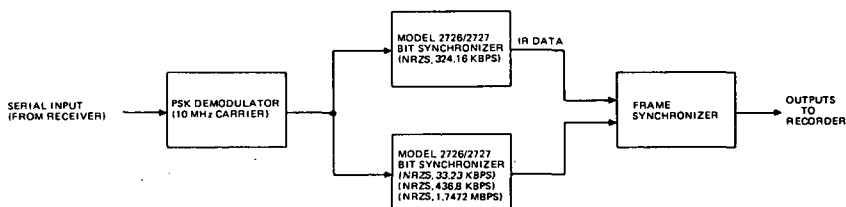


Figure 5-40. Digital Interface Electronics System Configuration

This serial, biphase, PSK, NRZS signal from the receiver is accepted by a special PSK demodulator capable of demodulating at 10 MHz PSK carrier and providing a serial PCM NRZS bit-stream output. This signal is routed to two EMR Model -2726/2727 bit synchronizers for further conditioning. One bit synchronizer is equipped with a selector module fixed at the IR data rate (524.16 kbs). A second bit synchronizer is provided which accepts one of the three visible-data selector modules. Each bit synchronizer accepts the serial NRZS signal and provides a noise-free serial NRZ-L output, accompanied by bit-rate clock pulse trains. The bit-synchronizer outputs are routed to the special frame synchronizer which performs word and frame (line) synchronization and serial-to-parallel data conversion. The frame synchronizer data and timing outputs are then routed to the recorder.

The input characteristics are:

Data transmitted	VISSR visible/IR data
Modulation	Biphase PSK NRZ-S

Carrier frequency	10 MHz
Bandwidth	6 MHz
Bit rates	Mode A - 1.7472 Mb/s (visible) 524.16 kb/s (IR) Mode B - 436.8 kb/s (visible) 524.16 kb/s (IR) Mode C - 33.28 kb/s (visible) 524.16 kb/s (IR)

Number of words per line:

1672 6-bit words sync + 512 6-bit words documentation
+ 15,288 6-bit words video: Mode A (visible)

836 6-bit words sync + 256 6-bit words documentation
+ 7,644 6-bit words video: Mode B (visible)

69 8-bit words sync + 16 8-bit words documentation
+ 1,911 8-bit words video: Mode C (visible)

418 9-bit words sync + 128 9-bit words documentation
+ 3,822 9-bit words video: All modes (IR)

A line is defined as the data interval containing sync, documentation, and video.

The above bit rates are based on a 100 rpm nominal spacecraft spin rate. The actual spin rate, however, may lie between -50 and 110 percent of the nominal value. The number of words per line remains constant but bit rates are determined by the eventual spacecraft spin rate. For example, the 1.7472 megabit/sec rate may end up to be as high as 1.92 megabit/sec or as low as 800 kilobit/sec. The digital interface electronics has the capability to cover the bit-rate ranges of all three modes. The units may consist of interchangeable modules, selected on the basis of operating modes (A, B, or C) and the actual bit rate.

Signal Simulator. A signal simulator is provided as part of the digital electronics, capable of generating selectable signals; i.e., frequency burst, 16-level gray scale, and horizontal bar patterns. The bar patterns have line groupings of 1, 2, 4, and 8 lines. The frequency bursts have provisions for data word groupings of 1, 2, 4, and 8 words. The output of the simulator is a PSK-modulated 10 MHz carrier. There is the capability of adding Gaussian noise and for accepting externally generated rf carrier and bit-rate inputs. The simulator design allows the operator to select fixed value (constant level) or 6-bit counting

sequence where each word increases counter by one. A pseudo noise (PN) generator is also provided to generate the PN sequence employed in the initial sync period.

Frame Synchronization. The initial sync interval consists of a portion of a pseudo noise sequence generated by a 15-bit feedback shift register. This register fills to 15 one's with the transmissions of the last sync bit prior to the first documentation word. This sequence is used for all formats. Feedback tapes are at bits 8 and 15 (MSB) of the shift register.

Data Randomization and Word Complementing. Documentation and video data are randomized (selectable) at the transmitting end by combining them with the output of the PN generator in an exclusive OR gate. In addition, every other word of data (documentation and video) are complemented (the first word in the documentation is sent uncomplemented). The DRGS equipment has provisions to recover the original data from the randomized and complemented data stream.

Recorder/Processor

The image recorder/processor subsystem consists of a laser drum recorder with an associated rapid-access dry processor. The raster coverage of the total drum surface is produced by coordinated indexing of an optical carriage upon which is mounted the spot-forming optics. The recorder/processor achieves recording spot size, density levels, and geometric fidelity through the combination of a precision drum-scanning and laser-light modulation system. The film processing is achieved through the controlled application of heat. The processor provides automatic transfer of the film from the recorder drum to the processor, and automatically ejects the processed image. Since the film is automatically loaded onto the recorder drum from a supply cassette, operation of the system is fully automatic at normal room temperatures. A summary of the design parameters for the recorder/processor when operating with the stretched VISSR data formats are:

Recording paper/film size	56 cm by 56 cm inches
Film type	3M Type 7869
Paper type	3M Type 774
Number of $\sqrt{2}$ density levels	16 (film) 12 (paper)
Optical spot sizes	1-1/2, 2-1/4, 3, 4-1/2, and 12 mils
Recording time/picture frame	20 minutes

Processing time/picture frame	4 minutes
Scan rate	50 to 1100 lines/minute
Resolution	14,000 elements/line
Laser source	Argon
Laser coolant	Water.

Much of the preceding information has been extracted from monthly progress reports published by Philco-Ford on Contract NAS5-21575, Westinghouse Electric Corporation on Contract NAS5-21574, Santa Barbara Research Center on Contract NAS5-21139, and Image Information, Inc., on Contract NAS5-21171.

ATTACHMENT A

ATMOSPHERIC EFFECTS IMPACTING SENSOR TECHNOLOGY

Atmospheric Limitations

Interference of the atmosphere with radiation reflected or emitted from the ground scene imposes limitations on the information from imagery collected by satellites.

For the visible spectrum the signal from a scene element arriving at the satellite is:

$$S = \frac{E\zeta}{\pi} T + P = N_o T + P$$

where E is the irradiance at the scene element, ζ is the scene element reflectance, and T and P are the atmospheric beam transmittance and path radiance, respectively. Errors in E, T, P in addition to those in the image forming system itself (S), therefore, contribute to the uncertainties in determining the reflectance ζ . The following tabular presentation gives an indication of the relative contribution of the nonimage-forming path radiance P and the residual scene radiance $N_o T$ to the received signal at the satellite:

<u>Atmosphere</u>	<u>Spectrum</u>	<u>Path Radiance/Residual Scene Radiance*</u>	<u>Contrast Transmittance**</u>
Clear	Near IR	0.8	0.25
Clear	Visible	0.5	1.00
Hazy	Visible	0.1	9.00

*Path Radiance/Residual Scene Radiance = $P/N_o T$.

**Contrast Transmittance $\tau_c = (1 + P/N_o T_d)^{-1}$, $\tau_c = c_{\text{apparent}}/c_{\text{inherent}}$.

At the present state-of-the-art predictions of atmospheric optical parameters from atmospheric models are subject to the following estimated uncertainties:

<u>Parameter</u>	<u>Estimated Uncertainty</u>
Ground Scene Irradiance Levels	5-10%
Beam Transmittance (T)	10% or less
Path Radiance or Contrast Transmittance	Approximately 10% for clear atmosphere 50% for hazy atmosphere

The errors in the mathematical algorithms in the computations are for most conditions only a few percent; the largest uncertainties derive from the atmospheric models themselves.

For reflectance ratios between two not too distant wavelength values λ_1 and λ_2 , the atmospheric effects are somewhat less critical. In this case the reflectance ratio is:

$$\frac{\xi_1}{\xi_2} = \frac{S_1 - P_1}{S_2 - P_2} \times \frac{E_2 T_2}{E_1 T_1}$$

Since, in the visible spectrum, E and T change smoothly with wavelength, the second factor will be close to one and can be estimated with reasonable accuracy. The uncertainties then are only in the path radiance determination.

IR System Limitations

Similar considerations also apply to IR systems. However much more representative atmospheric models exist for water vapor distributions than for aerosol distributions.

For a near term capability for indication and discrimination with haze and thin cirrus clouds, qualitative information can be provided by onboard near IR and thermal IR radiometer channels, in addition to visual bands. Significant improvements in atmospheric optical correction capabilities can be obtained only through simultaneous measurements of the atmospheric optical parameters. Such measurements can be conducted on the ground and from aircraft and balloons.

ATTACHMENT B

MSS CALIBRATION

The working specification for scanner gain and offset measurement was an absolute accuracy of ± 5 percent. There has been limited reporting of absolute calibration since prime importance was placed on *band-to-band relative accuracy*, the basic requirement for "signature" analysis. Band-to-band ratios are relatively insensitive to atmospheric haze, as compared with absolute signal levels.

Absolute calibration was performed, however, with traceability to NBS standards. The large integrating sphere^{1,2} was calibrated against NBS spectral radiance standards at GSFC. SBRC also ran a check comparison with a "tertiary" standard lamp. The MSS measurements against the SBRC tertiary agreed to an *average* of 2 percent with those using the GSFC sphere.

Also, field test measurements³ at Table Mtn., California were made through the MSS "sun calibrate" optics. The solar irradiance was measured at the same time by GSFC personnel with the same instrumentation used in an airborne solar measurement program⁴ (2 monochrometers and a pyrheliometer).

The measurements were repeated at several times and the measured values of MSS output voltage were extrapolated to "outside the atmosphere" values by zenith angle and extinction coefficient corrections. These values were then compared with those calculated from previous gain measurements using the GSFC "sphere."⁵

The agreement was quite good considering the long calibration chain involved which included the relation of NBS standards to the sun. The *mean* responses measured in the field agreed to within 1.5, 6, 5, and 4.5 percent of those calculated from lab measurements.

¹Mohr, E. I., "Design and Construction of a Wide Angle Diffuse Source," Research Report Grant NGR 21-023-001, Columbia Union College, June 1970.

²McCulloch, A., McLean, J., Mohr, E. D., "Evaluation and Calibration of Some Energy Sources for Visible and Near Infrared Regions of the Electromagnetic Spectrum," NASA/GSFC X-622-69-195, May 1969.

³Final Report "MSS for ERTS," Vol. 1, Hughes Aircraft NASA Contract NAS 5-11255, August 1972.

⁴Thekaekara, Kruger & Duncan, *Appl. Opt.*, 8, 1713 (1969).

⁵Lansing, J., "Sun Calibration Signals," SBRC Memo HS324-1967A. December 1971.

ATTACHMENT C

VISSR CALIBRATION

Primary Calibration

The VISSR visible and thermal channels are calibrated in a thermal/vacuum environment at five VISSR temperature plateaus.

Visible Channel Calibration

The visible channel calibration source is a quartz iodine lamp, the output of which is collimated and spectrally shaped using appropriate optical filters to be similar to the sun over the spectral band of the VISSR visible channels. The output level of the calibration source is established by eight neutral density filters to provide a calibration albedo range from 0.16 to 1.0. The absolute calibration accuracy of the VISSR visible channels is estimated to be ± 10 percent.

Thermal Channel Calibration

The VISSR thermal channels are calibrated at eight target scene temperatures between 180 K and 315 K, using a temperature controlled blackbody source. The estimated absolute calibration accuracy is $\pm 1.5^{\circ}\text{C}$, or ± 1 percent of full scale, whichever is larger.

Inflight Calibration

Visible Channels

Inflight calibration of the eight VISSR visible channels is accomplished by viewing the sun through the complete visible channel optical train via a reduced aperture, "side-looking" collecting prism. The area of the prism aperture is approximately 10^{-5} of the normal VISSR collecting aperture area to provide a signal input equal to approximately a 50 percent albedo calibration point. The prism is mounted so that its FOV leads the normal VISSR FOV in the west-east scan plane by 15 degrees to avoid any large signal recovery problems following the sun being viewed by the VISSR normal FOV. The north-south coverage of the inflight calibrator is extended to ± 26 degrees (compared to the ± 10 degree coverage of the VISSR) to assure inflight calibration capability every day of the year.

Use of the sun as the inflight calibration source assures that destripping of the ground processed picture data can be effectively accomplished even when gain changes in the eight visible channels are due to, or accompanied by, a change in channel spectral characteristics if the screen being viewed has a relatively "flat" spectral response.

Thermal Channels

The inflight calibration of the VISSR thermal channels is accomplished by means of a blackbody shutter whose temperature is monitored. The shutter is activated by command and is inserted into the optical path ahead of the thermal channel relay lens during the third scan line of a full frame.

A second method of thermal channel inflight calibration using the sun is being evaluated on the VISSR. The sun is viewed by the thermal channels through the entire optical chain and saturation of the thermal channel electronics is avoided by placing the preamplifier in a precision attenuate mode. The second section of the preamplifier is automatically attenuated by a factor of 400 immediately when the sun is sensed by the first preamplifier section. This provides a calibration signal that is approximately 50 percent of full scale.

This method, although it can provide a calibration of the complete thermal channel, is limited in operation to approximately 25 days before and after both the vernal and autumnal equinox.

ATTACHMENT D

HIGH-DATA-RATE, SPACECRAFT TAPE RECORDERS

C. Robert Thompson
RCA/Recording Systems
Camden, New Jersey 08102

and

J. M. Hayes
Systems Engineering Branch
NASA Goddard Space Flight Center

The first spacecraft tape recorder reproduced 15-kHz bandwidth data for one minute. "On Earth, peace, good will towards all men" was Dwight Eisenhower's prerecorded message — A poetic beginning to a growing science that has become invaluable to the space program.

Since that first spacecraft recorder, NASA has accumulated over 300,000 hours of in-space recorder operating time. The progress of data rate, total data capacity and recorder life is indicated by Fig. 1, 2 and 3.

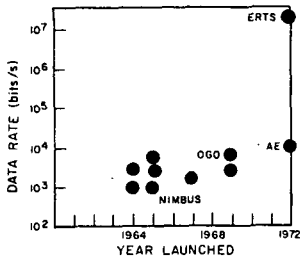


Fig. 1. Recorder data rate.

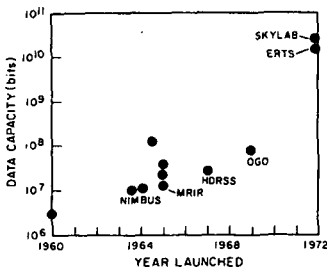


Fig. 2. Recorder capacity.

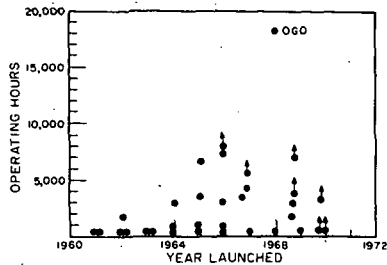


Fig. 3. Recorder life.

As technologies have matured, the capacity of spacecraft recorders has steadily increased. The 1960 Tiros Video Recorder stored 50-kHz bandwidth vidicon data for 1.5 minutes. The small endless loop recorders used on Tiros, Nimbus, Mariner and others typically stored 6×10^6 bits of binary data. In the mid-1960's, Gemini stored 1.5×10^8 bits. Of "medium sized" recorders such as these, current efforts are exemplified by the Atmospheric Explorer C&D recorder with a capacity of 10^8 bits.

In the late 1960's, the data rate and capacity requirements for spacecraft recorders took a large step increase, with capacity needs going from 10^8 bits to over 10^{10} bits. This was brought about by the development of higher data rate sensors and the initiation of the Earth Resources Technology Satellite (ERTS) program.

Current capabilities in "high rate - high capacity" recorders are exemplified by the ERTS Video Tape Recorder (VTR). This device records and reproduces for 30 minutes either analog video data at 4 MHz or digital data at 15 Megabits/s (Mb/s) — a storage capacity of 3×10^{10} bits.

Most likely, spacecraft data rate requirements will continue to increase. The magnetic tape recorder is the only approach feasible in the foreseeable future to accommodate these significantly higher rates. Other methods, including solid state memories, do not appear to be making sufficient headway to achieve the near 10^{11} - bit capacity that is, even now, required.

Magnetic tape recording technology embraces two approaches which are characterized by the geometry of the head/tape interface. They are: "rotary head" and "stationary head." The stationary head approach was utilized in all early spacecraft recorders. The number of flux reversals per unit length is limited and higher data rates therefore imply higher tape-to-magnetic-head

speeds. For instance, if we assume a density of 10,000 flux reversals per inch, a tape-to-head surface velocity of 1000 in/s would be required to store 10 Mb/s of an efficient digital code (e.g., "Double Density", "Miller", "Delay Modulation", or NRZ).

To run tape at a sufficiently high linear speed for such high rate recording would be cumbersome. Additionally, the length of tape required for suitable storage times is exorbitant. Therefore, during the 1950's, the transverse scan "rotary head" recorder was developed. Here, a very high surface speed (e.g., 1600 in/s) is achieved by moving the head at high speed while keeping the magnetic tape velocity low.

Rotary Head Recorders

Figure 4 shows the geometry of the data placement on tape of a transverse scan rotary head recorder. Typically, the tape is 2 inches wide. In transverse scan recording, four magnetic heads are placed at 90° intervals on the periphery of a nonmagnetic wheel. The tape is cupped and held against the headwheel by a tape guide, and the wheel spun at a high rate on an axis parallel to the direction of tape motion.

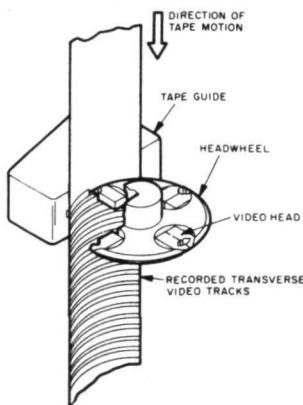


Fig. 4. Transverse scan format.

A "helical scan" recorder operates in a similar manner, but the recording is made with the headwheel at a shallow angle on the tape. Many variations in the diameter of the headwheel, the number of heads, and the tape path are possible. When a full 360° tape wrap is used, a single head is sufficient. When a 180° wrap is used,

two heads are required. The two approaches to "rotary head" recording — transverse and helical scan — both achieve bandwidths not available in contemporary longitudinal recorders.

The most appropriate example of a rotary head spacecraft recorder is the Earth Resources Technology Satellite Wide Band Video Tape Recorder (ERTS-WBVTR) shown in Fig. 5. This device will store image data from the Return Beam Vidicon (RBV) Camera or the Multi-spectral Scanner (MSS) for 30 minutes. The two systems aboard each spacecraft allow simultaneous operation of both modes. The RBV signal is analog video data with a spectrum from dc to 3.5 MHz and is reproduced with a recorder SNR of better than 42 dB. The MSS data is in the form of 15-Mb/s NRZ. This is reproduced with a recorder bit error rate of less than 1×10^{-4} (typically runs less than 1×10^{-5}). Figure 6 is a block diagram of the ERTS-WBVTR. A discussion of the signal flow is detailed in reference 1.

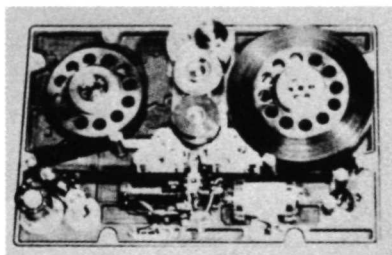


Fig. 5. ERTS Wideband Video Tape Recorder.

During playback, the magnetic head must be centered on the recorded data track. To achieve this, an auxiliary signal is recorded longitudinally, by a separate head, on the edge of the tape beyond the transverse recording area. This signal is derived from the rotational position of the headwheel, thereby establishing a relationship between the data track and this longitudinal reference track. During reproduction, this track is sensed and compared to the rotational position of the headwheel. The resultant error signal is used to servo the capstan to place the tape, and therefore the data track, directly beneath the rotating magnetic head. During record, data is usually supplied constantly to all heads (on the ERTS-WBVTR, heads not in tape contact are unpowered). This signal is transferred

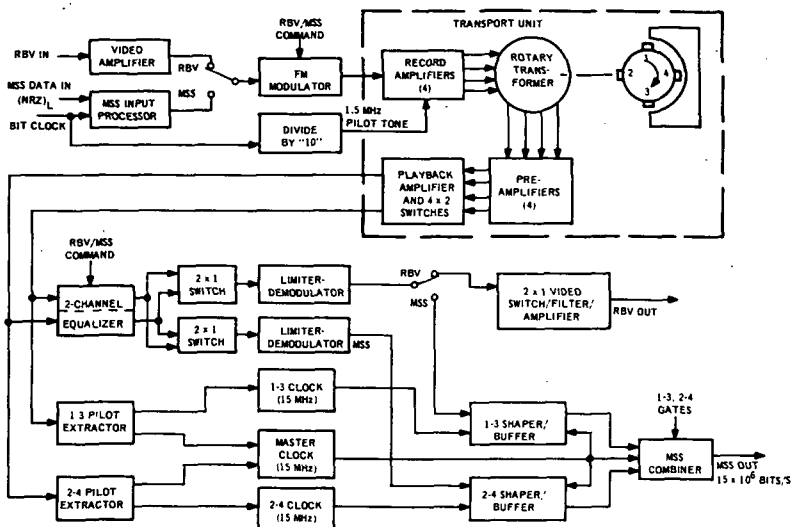


Fig. 6. ERTS-WBVTR wideband channel.

to the rotating headwheel by means of rotary transformers. Since the wrap of the tape encompasses an arc greater than the distance between adjacent heads, redundant data is recorded at the ends of the head scans. This redundancy is used to provide error free playback switching.

For a particular system, the method of switching is dependent on data characteristics. In television, and in the ERTS-RBV mode for instance, a hard rapid switch is used. The uncorrected switching discontinuity is placed in a horizontal blanking portion of the video signal which occurs during the redundant portion of the playback data. When continuous analog data is to be reproduced, the two streams of overlapping data are slowly switched during redundant overlap. This spreads the discontinuity such that the resulting amplitude transient remains below the system noise level.

Because of the high head-to-tape speeds of rotary head recorders (for transverse recorders, in excess of 1500 in/s, and for the ERTS-WBVTR, 1964 in/s), head life can be critical. Assuming that the recorder life goal of 1000 hours is met, the ERTS heads would traverse 6×10^5 feet of tape — 100 times that of most previous flight recorders. This is achieved by careful design of the head/tape interface and by the use of very hard head materials. Various alloys of aluminum,

iron and silicon are frequently used, e.g., "Alfecon" and "Alfesiil". Ferrites have also been used, but because of extreme fragility, not too successfully at transverse scan speeds. They are, however, being used on helical recorders, which generally operate at lower scan speeds.

The character of the tape itself has great effect, not only on the signal characteristic, but on life. A small change in the processing of the ERTS tape, for instance, improved the surface finish. The SNR improved 3 dB while the apparent head wear rate increased 2000 times. The 3 dB was sacrificed.

In any magnetic tape recorder, the time accuracy is much better than the amplitude accuracy, particularly in the rotary head recorders. Frequency modulation is ideally suited to that situation. Both the ERTS RBV and MSS signals modulate a carrier in the WBVTR. For the RBV video signal, normal television recording standards are satisfactory. The 3.5-Mb/s RBV signal modulates a carrier at 8 MHz. The analog bandwidth required to reproduce the 15-MHz NRZ is about 10.5 MHz. Under these conditions, a higher carrier (13 MHz) is used and a reduction in SNR results. Whereas, the SNR for the RBV mode is better than 40 dB, the MSS mode SNR is about 33 dB. This would be sufficient to achieve a bit

error rate of about 10^{-7} , although tape imperfections limit the bit error rate to about 10^{-5} .

What would be the upper limit on data rate? Significant development efforts have revealed that signals above 40 MHz may not be available for some years, if ever. Signals beyond 20 MHz would have less than 20 dB SNR. Analog recording at 6 MHz is handled easily with an SNR of 36 dB. We see that the MSS mode analog bandwidth is 10.5 MHz, which permits handling 15-Mb/s data at a BER of less than 1×10^{-5} . The use of two or more tracks (i.e., eight or more heads on the headwheel) can give higher capacities (data rate or SNR) but with added complexity. The next step for rotary recorders is clearly, in spite of poor amplitude response, direct recording. Although the FM 15-Mb/s NRZ of the ERTS-MSS data has significant spectral components to 20 MHz, a direct 30-Mb/s Double Density Code has the center of its energy spectrum at 12.5 MHz. The problems here are that there is some unreproducible dc in the Double Density Code and in addition the normal pilot tone cannot be inserted in the FM spectrum as easily as before. However, 25-Mb/s Double Density has been done and 30 Mb/s is not expected to be too difficult.

At the other end of the spectrum, how low can one go? The contact between the tape and heads at high speed is slight due to the air film, thus high speed is less feared than low speed, with regard to head and tape wear problems. The contact between heads and tape at low speed is more intimate and thus prone to wear. Some work has been done at playback-to-record speed ratios up to 250 to 1 and results have been demonstrated. Currently a 25 to 1 machine is in test and has accumulated over 1000 hours without visible degradation.

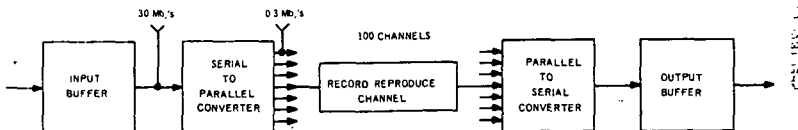
Multitrack Recorders

Concept

Multitrack Recording is another technique used to satisfy the "high rate - high capacity" spacecraft recorder requirement. The majority of existing multitrack recorders and requirements are to store digital data. An example of this technique is the SKYLAB Digital Recorder as built for NASA by Ampex to store data from Earth Resources Sensors (EREPS data). Another example is the Earth Observations Systems (EOS) proposed recorder being developed by RCA.

Spacecraft Systems Considerations

Spacecraft digital recorder data performance factors



include data capacity (bit rate/record time), timing stability and bit error rate. In many satellite applications, data is collected (recorded on tape) throughout an orbit and dumped (reproduced from tape) while passing a ground station. As the ground station access time is only a small portion of an orbit, playback must be made at a higher speed, typically 25 or 30 times faster than record.

Important recorder parameters utilized to achieve the data performance are bitpacking density, tape speed, tape load, coding technique and transport type. Each is discussed here and the authors' summary of the limitations presented.

Data capacity can be computed by multiplying record time and data rate. The SKYLAB EREPS recorder can record 10^6 bits/s on each of 28 channels simultaneously for 140 minutes, about 47×10^9 bits. The recorder designer must consider tape load and bit packing density as his criteria for satisfying a capacity requirement. The EREPS recorder packs data at about 0.6×10^6 bits/in² and utilizes a tape load of 7000 feet of 1-inch tape to obtain the 40×10^9 bits. Tape load is a function of recorder size and complexity, and rather easy to assess. Bit packing density must be assessed by considering number of tracks and number of bits per inch in each of the tracks. Tape speed is adjusted to achieve the required bit packing density and the tape transport/drive system chosen commensurate with the required tape speed and timing stability requirements.

The EREPS recorder uses 20,000 bits/in for each of 28 tracks to achieve the packing factor of 0.6×10^6 bits/in². Experience has shown that an efficient coding technique is required to achieve the 20,000 bits/in. More about that later.

In the proposed EOS recorder, a 30×10^6 -bit/s data stream is demultiplexed into 100 parallel channels across 2-inch tape. Each channel is thus recorded at a 0.3-Mb/s rate. The reproduced parallel bit streams are remultiplexed as illustrated in Fig. 7. Figure 8 shows the configuration of a recording head to accommodate 100 channels of data. Typically, 16 active components are used for each data channel. This system has a basic capacity factor of 1.25×10^6 bits/in², which for the tape load of 4000 feet results in storage of 120×10^9 total bits.

Timing stability is generally a function of tape transport design but in the sophisticated recorder described above, nearly all instabilities introduced by the transport are removed by electronic processing techniques.

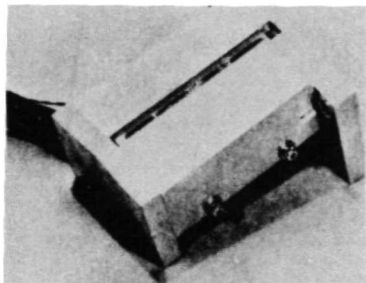


Fig. 8. Multitrack recording head.

Encoding Techniques

Most heads respond only to the change of flux density and therefore provide no dc response. In order to overcome the large concentration of low frequency energy found in an NRZ signal, many encoding techniques have been used for digital tape recording. A partial listing includes these eight: Diphase, Manchester (I, II and III), Biphasic, Enhanced NRZ, Delay Modulation (Miller Code, Wood Code), Frequency Modulation, Pulse Width Modulation and Bipolar Magnetization.

A comparison of the energy spectra of NRZ to two often used codes, delay modulation and diphase, is shown in Fig. 9. These two codes are self-clocking, an important feature to eliminate the need for an additional tape track for data clocking.

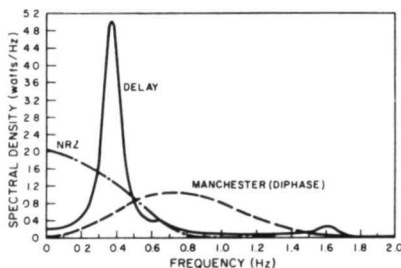


Fig. 9. Spectral density of selected coding processes.

In comparing the spectral distribution, delay modulation has a sharp peak at 3/8 data rate while diphase peaks at the data rate. Delay modulation requires better amplitude and phase linearity of the head-tape and signal processing functions, and also somewhat more complex encoding and decoding circuitry, but has the narrowest bandwidth requirement with low dc content.

Bit Error Rate

An examination of the characteristics of the playback data in its raw form (prior to processing) provides the basis for predicting data bit error rate.

Significant degradation of data bit error rate will be experienced unless adequate margin is provided for each of the following parameters: dropouts, noise, timing, crosstalk, and linearity.

An examination of the decision network (decides whether playback data is "1" or "0" for a given bit interval) is useful to pinpoint the error producing effects of the listed parameters.

Delay modulation is used as an example. Figure 10 shows the three possible recorded pulse widths ($2T_0$, $3T_0$, $4T_0$). The decision process assesses the recorded pulse width by determining if it is $<T_A$, $>T_B$, or $>T_A$ but $<T_B$ (three possibilities).

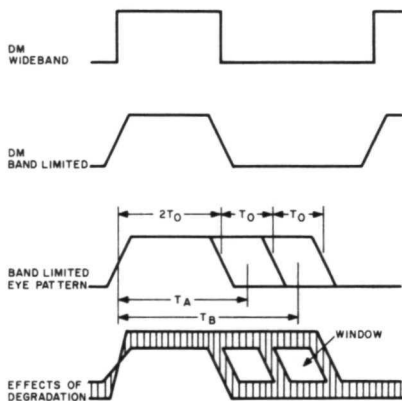


Fig. 10. Delay modulation degradation.

The cumulative effect of the latter four error producing parameters can produce a waveform as shown in Fig. 10. The resultant window can be measured and used to predict bit error rate in the absence of dropouts. The size of the window also yields margin

information for analysis of the bit error rate in the presence of tape dropouts.

Tape Transport

The key to successful operation of the parallel to serial converter (multiplexer) in a multitrack reproducer is to align the parallel data into time synchronism. Tape transport and head skew cause the parallel data to become misaligned in the reproduce mode.

Skew is defined here as the timing or tape distance instability of the longitudinal tracks across the tape relative to the center track on the tape. Flutter is considered the instability of this center track relative to an absolute time or tape distance.

Static skew is caused by gap scatter and misalignment of the recording and playback heads (when separate heads are used) and electronic circuitry timing variations between individual channels. The latter is mainly due to phase shifts at the record amplifier-head interface and group delay variations in the signal processing circuitry. Experimental tests conducted on multitrack recorders have indicated that the total peak static skew for both recording and playback is less than $100\text{ }\mu\text{in}$ for any channel compared to any other channel. Also, the skew variations within a group of five or six adjacent channels in a 100-channel head will be less than $20\text{ }\mu\text{in}$.

Dynamic skew is caused by stretching and rotation of the tape as it goes over the recording and playback heads. The effects of linear dynamic skew are shown diagrammatically in Fig. 11. Based on experimental tests of multitrack recorders, the dynamic skew is less than $200\text{ }\mu\text{in}$ across 2 inches of tape and is continuous from one channel to the next adjacent channel. That is, for 100 channels across the tape, the dynamic skew between adjacent channels will be approximately only $2\text{ }\mu\text{in}$.

An efficient method can be utilized for electronically eliminating the skew in multitrack digital recorders. The method requires no synchronization bits. For a recorder with only one recording/playback head and playback in the same direction as recording, no added timing tracks are required. The technique uses clocks derived from the data on each track to compute the skew. Each channel of data is stored in a digital buffer for an amount of time equal to the skew as computed from the clock information. See Fig. 12.

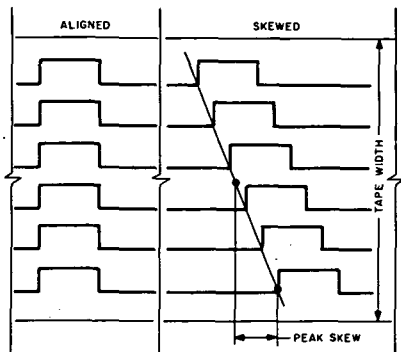


Fig. 11. Linear tape skew.

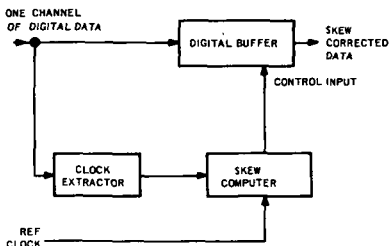


Fig. 12. Deskew technique.

Limitations

Multitrack recording technology has progressed in recent years such that it is possible to expand the scope of present designs. Some generalization of the basic limitations of multitrack recording are as follows:

Capacity. The data storage capacity is limited only by the practical limit of tape load. Further, if the physical size of the recorder is constrained (thus limiting tape load), then the limitation on capacity falls to bit packing density.

Bit Packing Density. Since bit packing densities above 2×10^6 bits/in² have been achieved in prototype hardware programs, data quality factors must be

assigned (in the form of bit error rates) when considering a large capacity recorder. The chart in Fig. 13 illustrates these parameters in existing hardware configurations. Further, bit error rate in the presence of debris (caused by particles from the tape) will seriously affect data at even very conservative packing factors (see Fig. 13).

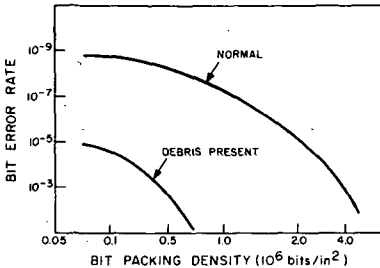


Fig. 13. Data degradation.

Bit Error Rate. With properly designed heads and signal processing circuitry and a given bit packing density, the limitation on uncorrected bit error rate is a function of the quality of the tape; particularly the size and number of tape surface imperfections (commonly called stipples). Various tape conditioning methods are commonly used to reduce stipples to a minimum prior to use on spacecraft recorders.

Data Rate. The current limit of record and reproduce data rate is constrained simply by the size complexity allowable for a given application. A data rate of 10^9 bits/s is readily achievable in a conceptual design. A quantity of 300 parallel channels (easily obtained on 4-inch-wide tape) and operating at 3.3×10^6 bits/s per channel (easily obtained running at 120 in/s at 2×10^6 -bit/in² density), yields 1-Gigabit/s record/reproduce data rate. Multiplex and skew circuitry are just beyond the state-of-the-art to accomplish this task. A 10-minute recording would utilize 6000 feet (22 pounds) of tape. A 17-minute recording would store more than 10^{12} bits of data.

The Future

Data Capacities

We've discussed the progress of capacities in the past, described current capabilities, and noted ultimate limitations. Now, what can we expect in the near future?

The EOS mission requirements of 30 Mb/s have been noted and success is likely. Further extension of the rotary head capacity appears arduous, however, and

the higher rates will probably be achieved with multitrack longitudinal machines. The next capacity step will be to pursue 60 to 100 Mb/s. It appears, however, that other factors may begin to limit data rate capabilities, such as link capacity. On-board data processing will create different requirements for tape recorders and recorder development plans include variable speeds to allow efficient storage of data from different sensors or from a varying on-board computer output.

Reliability

Conspicuously absent from this discussion is that characteristic most in need of attention — Reliability. Longer life and reliability have made only grudging progress. The emphasis has always been on meeting the higher and higher data rates.

It is only recently that comprehensive specific reliability and life programs have been undertaken. Reliability study programs recently completed have examined the head/tape interface, developed technology for very long-lived recorders (5 years), and endeavored to gain control of the design and manufacture of tape by developing a spacecraft tape. In addition to an awareness of these specific technology efforts, users must approach the procurement and application of spacecraft recorders conservatively. Time for development and life testing is probably more beneficial than merely more money spent on crash efforts.

Life

Limitations on high data rate - high capacity spacecraft recorder life have been reduced significantly through the years;

first - tape transport design was iterated and simplified in order to yield predictable results (above 20,000 transport cycles);

next - the head-to-tape interface was studied, tested and iterated to produce results acceptable for mission requirements (above 2000 hours);

now - with increasing complexity, random component failure may become the limiting life consideration on current and future design.

future - spacecraft will require extensions in performance of the recorders now available. (10^{11} -bit capacity, 10,000-hour operation)

With thoughtful planning, the reliability, life, and data capacities of tape recorders will continue to meet the needs of the world's space program.

Reference

- (1) J. M. Hayes and F. D. Keil, "Wideband image recorder for the earth resources technology satellite", 1971 National Telemetry Conference Record, Washington, D. C., April 12-15, 1971, pp. 46-53.

ATTACHMENT E

WIDEBAND IMAGE RECORDER FOR THE EARTH RESOURCES TECHNOLOGY SATELLITE

J. M. Hayes and F. D. Kell

Mr. Hayes is with the Systems Engineering Branch,
NASA Goddard Space Flight Center and Mr. Kell is with
RCA Communications Systems Division, Camden, New Jersey.

Abstract

Sensors now under development offer resolution sufficient for survey and analysis of the earth's resources. However, worldwide coverage with an orbiting satellite system requires a multiplicity of ground receiving stations, or on-board data storage. The Video Tape Recorder (VTR) which provides the latter capability for both wideband analog (4 MHz), and high rate digital (15 Megabits/sec) sensor outputs is described, together with the developmental results which predict extended orbital life.

"Development of an Earth Resources Satellite System is a project which, in my opinion, represents the largest potential return on investment of any space project to date"—Joseph E. Karth, U.S. House of Representatives.¹

The Earth Resources Technology Satellite (ERTS) is a program of NASA'S Goddard Space Flight Center, Greenbelt, Maryland. It was established as a firm project only in mid-1969 and its first launch is scheduled for Spring 1972—a very short time. The second launch is scheduled for a year after the first.

General Electric Corp. has been selected as the ERTS prime contractor and the basic spacecraft will be similar to the Nimbus, shown in Figure 1.

Efforts toward the development of the payload predate the formalization of the ERTS project. The payload consists of RCA's Return Beam Vidicon Camera (RBV), Hughes' Multispectral Scanner (MSS), RCA's Video Tape Recorder (VTR), and a Data Collection System (DCS).

As the name implies, the ERTS is directed to the collection of data for the purposes of the determination, optimal usage, and maintenance of the natural resources of the United States and the World. As the program has progressed, more and more potential applications have been suggested. The following is a listing of most of the cooperating disciplines and some of their primary areas of interest:

Agriculture	Crop distribution and vigor, disease and infestations, land use.
Forestry	Inventory and distribution—fire and disease damage.
Conservation	Land use.



Figure 1. Nimbus Spacecraft

¹Karth, Joseph E., 12/31/68, letter to Hon. George P. Miller and Hon. Olin E. Teague of the U. S. House of Representatives committee on Science and Astronautics.

Geology	petroleum and mineral detection. Prediction of volcanic activity, earthquakes, and landslides.
Hydrology	Water inventory Water conservation Water pollution Flood control Water resources.
Geography	Transportation Navigation Urban planning.
Oceanography	Shipping Sea food production Coastal geography Marine biology.
Environment	Air quality Water quality Pollution violation detection.

To be meaningful to the users, image data must be of high resolution and of particular wavelength, and repetitive. The pattern of the ERTS ground coverage is shown in Figure 2. This orbit provides the

opportunity to look at the earth's surface every 18 days.

The first item assigned to the payload and indeed about which the entire program was initially based, was the Return Beam Vidicon Camera. The RBV system consists of three return beam vidicons, each filtered and optimized to a particular spectral band.

The MSS (Multispectral Scanner) is generically a different type of device. Whereas the RBV exposes a "picture" instantaneously and reads it out at a slower rate, the MSS operates in a continuous manner. In this device, a rocking mirror (@ 15 Hz) scans horizontally (across the ground track) while the spacecraft motion provides the vertical sweep (along the track). Thus, a continuous image is formed. In the simplest of this type of scanner, only one sensing element is required.

For the ERTS application 90 scans/second are required to achieve the desired ground resolution. The high scan velocity of a mirror rocking at 90 Hz however, would not allow enough sensor dwell time to integrate enough signal to achieve a usable signal to noise ratio. Therefore, the scanner mirror is rocked at 15 Hz but six lines are scanned in parallel at once, providing the desired resolution and a

ORBIT REQUIREMENTS

- NOMINALLY CIRCULAR
- NEAR-POLAR, SUN SYNCHRONOUS
- PRESCRIBED DAY-TO-DAY ORBIT PROGRESSION

ORBIT PARAMETERS

- CIRCULAR ALTITUDE-492NM
- INCLINATION-99°

PICTURE COVERAGE

- OVERLAPPING PICTURES ALONG ORBIT TRACK
- OVERLAPPING SWATHS ON SUCCESSIVE DAYS

PICTURE OVERLAP

- 10 NM NOMINAL
- 5 NM MINIMUM

COVERAGE REPETITION INTERVAL

18 DAYS

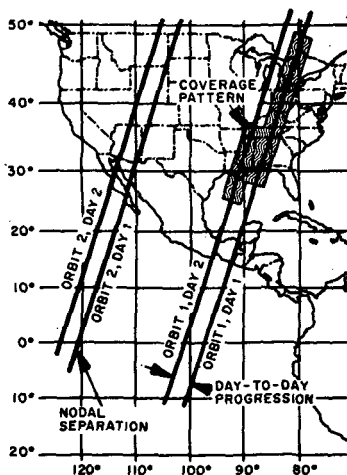


Figure 2. Orbit and Coverage Summary

satisfactory SNR. Clearly then, six sensing elements (radiometers) are required. This device however, images in four spectral bands, requiring a total of 24 elements, and resulting in 24 separate channels of data.

The purpose of sensing in different spectral channels is to permit the identification of surfaces by their unique spectral response. Although the signatures of, for example, different types of vegetation are similar, sufficient subtleties exist to allow discrimination between types and conditions as shown in Table 1.

TABLE 1²

REFLECTANCE CHARACTERISTICS OF SELECTED TARGETS IN THREE SPECTRAL BANDS

Channel	Barley vs Loam		Healthy vs Mildewed Barley		Pine vs Poplar	
Blue	.12	.07	.10	.09	.09	.09
Green	.15	.09	.11	.11	.09	.08
Red	.20	.15	.18	.15	.19	.14

The spacecraft system contains two video recorders and two transmitters. The system can record both sensors simultaneously and can transmit two channels of wideband data at once in addition to the narrowband telemetry channel. These wideband channels are located at 2229.5 MHz and 2265.5 MHz and have a data bandwidth of 20 MHz each.

Ground stations are located at Fairbanks, Alaska, Corpus Christi, Texas, and Greenbelt, Maryland. The image data from the RBV and MSS will be recorded on magnetic tape in the ground stations and physically transported to the NASA Data Processing Facility (NDPF) at the Goddard Space Flight Center.

The ultimate data output will consist of tapes, photographs, and computer printouts, having received varying degrees of processing and therefore providing varying degrees of accuracy according to the need of the user and the significance of the particular data. The NDPF will not perform "user unique" processing. The need for limiting the scope and quantity of processing becomes evident when the total numbers are considered.

The following arithmetic points out the magnitude of the task of the ERTS data systems - spacecraft and ground.

The RBV exposes a scene each 25 seconds for normally no more than 20 minutes per orbit. This gives:

$$4050 \frac{\text{orbits}}{\text{year}} \times \frac{20 \text{ minutes}}{\text{orbit}} \times \frac{2.4 \text{ exposures}}{\text{minute}} \\ = 1.94 \times 10^5 \frac{\text{exposures}}{\text{year}}$$

As the RBV exposes three spectral bands at once, the number becomes:

$$3 \frac{\text{pictures}}{\text{exposure}} \times 1.94 \times 10^5 \frac{\text{exposures}}{\text{year}} \\ = 5.82 \times 10^5 \frac{\text{pictures}}{\text{year}}$$

Now the MSS has four spectral bands and has the same "exposure" rate as the RBV, but the total number of pictures will not double as other factors tend to reduce the exposure rate, e.g., large areas of ocean that are of lesser interest. However, it is conceivable that a rate equivalent to 1,000,000 unique "pictures" per year could be achieved.

One million is a large number and these aren't just any pictures. Pursuing the math a little farther, we can calculate the quantity of data within a "picture". The RBV format is nominally 4000 lines square, resulting in a total of 16×10^8 elements per picture. If for discussion we assume a 6 bit quantization of this analog signal, each picture would represent 10^8 bits. The content of the MSS pictures is similar.

So, finally we can postulate a possible total data requirement for a year of about 10^{14} bits.

Before discussing the design and performance of the Video Tape Recorder, it is significant to examine why it is on board. Earlier in the program, a comparison was made between obtaining extra-North American data by equipping various ground stations throughout the world. Comparing the total coverage capability of the recorder versus eight ground stations gave figures of 30% for the ground stations while the recorder, of course, has ultimately 100% capability. And, it was estimated that a comparable expenditure would equip but 2 or 3 stations - not eight.

The VTR is required to record and reproduce image data from either the RBV or the MSS. Two recorders allow simultaneous operation. The RBV data is similar to commercial TV in format. The VTR accepts the RBV video baseband signal that has a bandwidth of approximately dc to 4 MHz, and the VTR must reproduce an original 33 dB signal

²Werner, E., NASA GSFC SRT Report, 1st Quarter, 1970

with a reduction of no greater than 1 dB (implies an instrument SNR of about 42 dB). The MSS output is a binary NRZ serial stream at 15 Megabits per second. The VTR must reproduce this data with a Bit Error Rate of less than one in 10^4 or one in 10^5 while disregarding dropouts.

Design Features

The basic signal recording requirements described above are generally within the capability of available ground equipment; however, the ERTS VTR has the additional requirements of long life, high reliability, minimum power consumption and minimum weight. The specifics of the implementation which have satisfied these requirements are described in the following sections.

The development of the ERTS VTR was preceded by an R&D contract with NASA's Manned Spacecraft Center which led to an extremely compact, developmental model, wideband recorder.³ Requirements for the ERTS VTR, however, particularly the extended mission life, dictated major departures from the previous design. In general, both equipments incorporate similar wideband record/reproduce electronics, and similar tape drives and reeling systems, but the ERTS equipment employs a transverse scan headwheel arrangement (see Figure 3) with a head-to-tape speed of 1964 inches/sec. This arrangement was selected in preference to the helix arrangement of the previous design because it offered longer life in a low power configuration, provided inherently faster start and stop times, and adapted conveniently to an arrangement for synchronizing the video head switching with the RBV horizontal line rate.

The final major deviation from the previous design is the division of the recording system into two discrete packages; one a hermetically sealed unit containing the tape transport and the other a housing which accommodates most of the electronics. This division of elements is a requirement of the NASA GSFC specification and is so arranged because it minimizes possibilities of tape path contamination and alleviates complications during equipment requalification or rework. With this philosophy, the recording system (VTR) has evolved into a Transport Unit which measures 21.5" x 15" x 6.5" and an Electronics Unit which measures 16.75" x 16" x 7". The complete VTR, exclusive of interconnecting cables, weighs about 72 pounds.

The tape transport for the ERTS VTR is shown in Figure 4. The transport contains 2,000 feet of

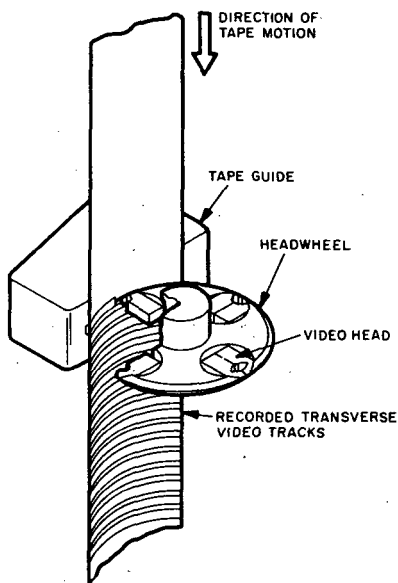


Figure 3. Transverse Scan Recording

special, two-inch wide, video recording tape. The headwheel panel ① provides the scanning motion for the four video heads and contains a shoe assembly ② which forms the tape around the headwheel. The video heads protrude above the headwheel rim and make intimate contact (0.0025 inch penetration) with the tape during recording and reproduction. The contact between the heads and tape is controlled by the shoe assembly which operates through a solenoid-driven, flexure linkage to provide about 0.010 inches of tape travel. The mechanism is arranged so that the solenoid must be powered to affect head/tape contact; thus the shoe automatically retracts with loss of power.

The tape reeling system is similarly fail safe since tape tension is always maintained through a Negator-differential mechanism ③. Two Negator springs torque an input shaft of the differential. The gear and belt ratios are such that each reel "sees" one-half the torque, or the torque of one Negator coil. The differential rotation between the two reels is exactly twice the rotation of the Negator power drum. Hence, the Negators must have sufficient turns to accommodate one-half the differential turns

³ Kell, F. D., "Video Recorder/Reproducer for Space Exploration, 1968 IEEE National Telemetering Conference Record, First Edition, April 1968, pgs. 187-192.

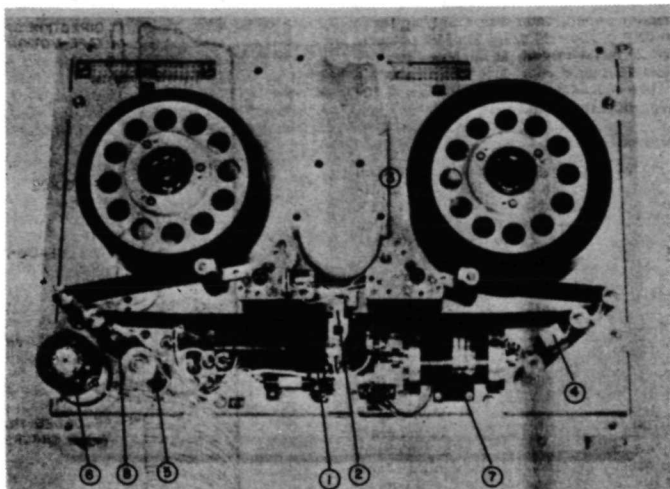


Figure 4. Front View of ERTS Feasibility Unit Transport

which occur between the supply and take-up reels when tape is transported from one reel to the other. The maximum differential turns exist when the tape is equally divided between the two reels. The mechanism is thus arranged with the Negators fully wound at the start of the transport cycle so that they may supply the necessary differential drive to the take-up sides of the reeling system. At center of tape, the Negators reach a minimum energy state and then are rewound as the direction of the differential turns reverses. Since operation of the transport involves flexing the Negator springs, care must be taken in the design of the springs to insure sufficient transport life. The springs in the ERTS transport, like the other life limiting mechanical elements, have been designed and, for the most part, experimentally verified for life in excess of 4,000 full-length, record/playback cycles (5,000 hours). The major element which has yet to be verified for this life is the head-to-tape interface which, at this writing, is approaching 2,000 hours of reliable operation during life test.

The other significant elements of the transport in Figure 4 include the ac erase head (4); the urethane coated capstan drive shaft (5); the capstan motor (6); the ω motor (7), for cancellation of the angular momentum of the headwheel assembly; and the longitudinal head assembly (8), which contains the Search and Auxiliary Channel

heads. The capstan and ω motors, like the head-wheel motor, are hysteresis synchronous units and incorporate special "start" windings for efficient, low-power, operation. The capstan motor also has separate windings for high speed tape wind and for dc braking of tape motion. The electrical drive for all motors is provided by appropriate switching of the input dc through bridge networks which supply the required two-phase, alternating current to the motor windings. The switching, for the most part, is controlled by precision time standards within the recording system. However, the supply for the capstan motor during playback derives from a VCO which is servo controlled to provide alignment of the video heads with the prerecorded video tracks. In addition, the switching for the headwheel drive is controlled in part (frequency) by a crystal standard and in part (phase) by a feedback loop. This arrangement provides a means for damping head-wheel motor oscillations and has yielded an improvement in time base stability of nearly 10:1 over undamped operation. Hence, a reproduced time stability of about 1 part in 10^4 has been attained in a low power recording system.

The wideband recording electronics are functionally similar to those used in conventional broadcast television recorders but are arranged with special circuitry to accommodate the 15 Megabit/sec. digital recording (MSS). In addition, all circuitry

has been designed with conservative component derating and employs low drift components to insure performance within specification after three years without adjustment.

The block diagram for the wideband electronics is shown in Figure 5. In the RBV mode, the incoming video signal is encoded on an fm carrier which has a quiescent frequency of about 6 MHz with the input at ground. With a full amplitude video signal, the carrier frequency is deviated to about 10 MHz. The fm signal is applied to record amplifiers which in turn drive the four video heads. The coupling of the signals into and out of the heads is performed by a four-section, rotary transformer with 1:1 turn ratios. Since each head contacts the tape for over 100° of rotation, the information is recorded redundantly for the short interval when two heads are in contact with the tape. This interval of redundancy or overlap is important to the recording operation since it provides a convenient interval for recombining the head outputs on reproduction.

During playback, the four head output signals are processed initially as four independent channels. Each output signal is applied to a preamplifier which

is located adjacent to the rotary transformer. The signals are further amplified in the playback amplifiers and equalization is applied to restore the sideband energy to a more balanced form than is received directly from the tape. At this point, the signals are recombined into two fm channels (see Figure 5) through 4 x 2 and 2 x 1 switches. These signals next receive 50 dB of hard limiting which provides immunity to noise and amplitude fluctuations. The limited fm signals are next applied to the fm demodulators which reproduce two channels of the original video waveforms. The two video channels at this point, however, have been arranged with offset switching transients as shown in Figure 6. These channels are then combined through a rapid video switch which occurs in the overlap intervals between the 1-3, 2-4 video channels. This switching results initially in a 20 nanosecond switching transient; however, the transient is essentially removed from the output by the final recorder filter.

In the MSS mode, the signal flow is essentially similar through the two limiter/demodulators since NRZ/fm recording is used. However, the video bandwidth and the fm carrier are extended to approximately 11 MHz and 13.5 MHz, respectively.

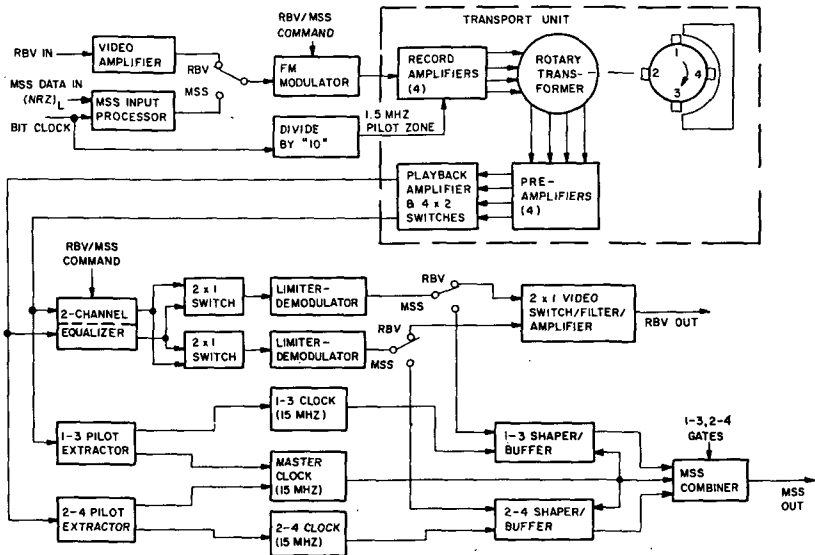


Figure 5. VTR Wideband Channel Block Diagram

With the 11 MHz bandwidth, the recorder S/N ratio is reduced to about 25 dB, pp/rms, but this is sufficiently adequate for processing the 15 Mbits/sec. data. At the outputs of the two limiter/demodulators, the NRZ signals, in addition to being noisy, contain timing errors which may approach 50 nanoseconds between adjacent head channels and 5 microseconds (at about 5 Hz rate) absolute. Hence, it is necessary to reclock the data to avoid extensive bit errors.

To understand the constraints on the data reclocking system, the nature of the recorder timing errors must be understood. The primary timing error of concern is the 50 nanosecond component which can occur between adjacent head channels. This component is caused by changes in the length of the transverse tracks which are such that the original 90° arc of recorded track contacts the head for more or less than 90° of rotation. This causes an *in-scan change in frequency and a time offset in the fm (and data) in the overlap interval of adjacent head outputs*. To negate errors from this component, two identical, 15 MHz clocks with short time constants are arranged to phase lock to the two limiter/demodulator outputs within the first third of the overlap interval. Since sufficient data transitions may not exist in a given overlap interval to permit this rapid lock-up, the recorder is provided with a 1.5 MHz pilot tone which is derived from the bit

clock and recorded (linearly added to the fm) with the NRZ data. During playback, this tone is extracted from the fm and used as a reference to lock-up the two identical 15 MHz clocks. Since the time constants of the clocks are arranged to lock-up to the data during the first third of the overlap interval, the data from each limiter/demodulator can be properly reclocked more than half the time and the two channels of reclocked data can be recombined into a single stream which is all properly reclocked. In the implementation, the two fast clocks are arranged to clock the data into separate 7 bit buffers and the data is then clocked out by a third 15 MHz clock which has a longer time constant. This Master Clock is arranged to follow the low rate time base errors (5.5 Hz), and to ignore the high rate (1250 Hz) components due to changes in the length of the transverse tracks. Hence, the output NRZ is free of high rate timing errors and the residual, low-rate component presents no problems to the ground equipment since it still represents a bit stability of about ± 1 part in 10^4 . Other performance characteristics of the MSS mode are listed below together with other VTR characteristics.

Scanning Principle	- Transverse Scan
Head-to-Tape Speed	- 1964 inches/sec.
Rec/Play Tape Speed	- 12 inches/sec.

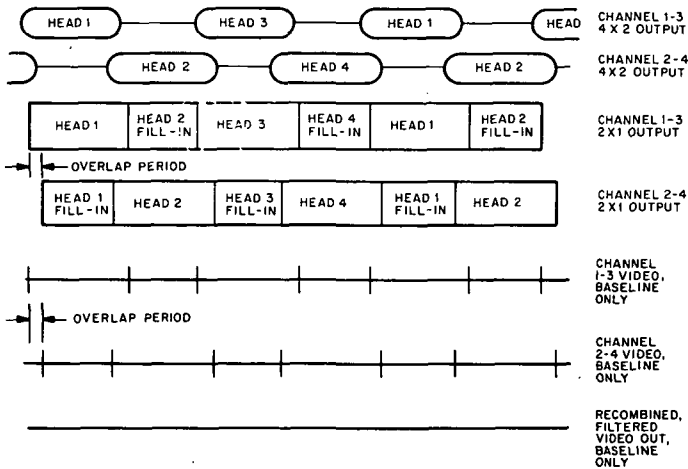


Figure 6. Wideband Channel Playback Timing

Wind Tape Speed - 48 inches/sec.
 Record Time - 30 minutes
 Power Consumption - 90 watts
 Weight - 72 pounds

RBV Mode Performance

a) Bandwidth, S/N - dc - 4 MHz, 42 dB
 b) Linearity - $\pm 3\%$
 c) Drift - $\pm 5\%$ input to output
 d) Transient Response - 5% peak overshoot

MSS Mode Performance

a) Bit Rate - 15 Megabits/sec.
 b) Format - NRZ
 c) Reproduced Accuracy - 1 in 10^4
 d) Bit Slip - No more than one in 10 Minutes

Auxiliary Channel Performance

a) Type of Channel - fm
 b) Bandwidth - dc - 5 kHz
 c) S/N Ratio - 30 dB, rms/rms

Search Track Characteristics

a) Type of Channel - Prerecorded Digital
 b) Message Format - 12 bit word every 6"

c) Code - 3 Level
 d) Bit Rate - 2.5 kbps (rec, Play)
 10 kbps (Wind)

Conclusions

The recording and reproduction of wideband analog (4 MHz) and high rate digital signals (15 Megabits/sec.) in a low-power, long-life satellite system is realizable and a storage capacity of over 30 minutes has been demonstrated. This means that in the digital mode, a storage capacity of nearly 30×10^9 bits is provided by the VTR.

The use of the VTR on ERTS will permit 100% worldwide coverage, if desired and experimental tests have indicated that the VTR operational life is more than adequate for the anticipated operation on the one-year ERTS A and ERTS B missions.

Acknowledgement

This work was supported by the National Aeronautics and Space Administration under Contract NAS5-11643.

Reprinted from:
 1971 NATIONAL TELEMETERING CONFERENCE RECORD
 Washington, D.C.
 April 12-15, 1971
 71 C10-NTC

REFERENCES

- Altshuler, T. L. *Infrared Transmission and Background Radiation by Clear Atmospheres*, G. E. Report 61 SD199, AD-401923, 1961.
- Am. Met. Soc. *Conference on Atmospheric Radiation*, Preprints, August 1972.
- American Society of Photogrammetry. *Proceedings of the Symposium on Earth Observation from Balloons* (Collection of 14 papers), February 1969.
- Anuta, P. E. and MacDonald, R. B. *Crop Surveys from Multiband Satellite Photography Using Digital Techniques, Remote Sensing of Environment*, Vol. 2, pp. 53-67, 1971.
- ASP. *American Society of Photogrammetry Seminar on Operational Remote Sensing*, Houston, Texas, February 1972.
- Bailey, H. and Mundie, L. "The Effect of Atmospheric Scattering and Absorption on the Performance of Optical Sensors," Rand Memorandum RM 5938-PR, March 1969.
- Bendix Research Laboratories. *EOS Mapping Accuracy Study*, Final Technical Report, NASA/GSFC contract NAS 5-21727, March 1973.
- Bertoni, E. *Clear Lines-of-Sight from Aircraft*, report AFCRL-67-0435, August 1967.
- Biberman, L. M., Dunkelman, L., Fickett, M. L. and Finke, R. G. *Levels of Nocturnal Illumination*, Instit. f. Def. Analysis, Research Paper P-232, 1966.
- Billingsley, F. C. "Applications of Digital Image Processing" in *Applied Optics*, Vol. 9, No. 2, pp. 289-299, February 1970.
- Billingsley, F. C. "Computer-Generated Color Image Display of Lunar Spectral Reflectance Ratios" in *Photo. Sci. and Engrg.*, Vol. 16, No. 1, pp. 51-57, 1972.
- Billingsley, F. C. "Digital Image Processing for Information Extraction," *Proceedings of Goddard Space Flight Center Conference on Parallel Image Processing for Earth Observation Systems*, GSFC X-711-72-308, pp. 41-67, March 1972.
- Billingsley, F. C. "Considerations for Digital Image Processing" in *Optical Telescope Technology*, NASA SP-233, pp. 673-692, 1970.

Billingsley, F. C. "Image Processing for Electron Microscopy II: A Digital System" in *Advances in Optical and Electron Microscopy* 4, Academic Press, pp. 127-159, 1971.

Billingsley, F. C., Goetz, A. F. H. and Lindsley, J. N. "Color Differentiation by Computer Image Processing" in *Photo. Sci. and Engrg.*, Vol. 14, No. 1, pp. 28-35, January/February 1970.

Billingsley, F. C. and Langrebe, D. A. "Computer Processing of Images in Remote Sensing Applications," to be published in *Manual of Remote Sensing*, American Photogrammetric Society, 1973.

Brown, D. R. E. *Natural Illumination Charts*, Report No. 374-1, Dept. of the Navy, Bur. of Ships, Res. Dev. Project NS 714-100, September 1952.

Churchill, S. W., Chiao-Min Chu, A. O. "Exact Solutions for Anisotropic Multiple Scattering by Parallel Plane Dispersions," Report No. 03675-1-F, Contract DA49-146-XZ-039, DASA 1257 (AD-272-325), September 1961.

Coulson, K., Dave, J. and Sekera, Z. *Tables Related to Radiation Emerging from a Planetary Atmosphere with Rayleigh Scattering*, University of California Press, 1960.

Deirmendjian, D. *Electromagnetic Scattering on Spherical Polydispersions*, American Elsevier Publishing Co., New York, 1969.

Deirmendjian, D. and Sekera, Z. "Atmospheric Turbidity and the Transmission of Ultraviolet Sunlight" in *J. Opt. Soc. Am.*, Vol. 46, p. 565, 1956.

Deirmendjian, D. and Sekera, Z. "Global Radiation Resulting from Multiple Scattering in a Rayleigh Atmosphere" in *Tellus*, Vol. 6, pp. 382-398, 1954.

Drummond, A. J. and Laue, E. C. "Solar Constant: First Direct Measurements" in *Science*, Vol. 161, pp. 888-891, 1968.

Dunne, J. A., Stromberg, W. D., Ruiz, R. M., Collins, S. A. and Thorpe, T. E. "Maximum Discriminability Versions of the Near Encounter Mariner Pictures" in *Jour. Geo. Reso.*, Vol. 76, No. 2, pp. 438-444, 1971.

Duntley, S. Q., Boileau, A. R. and Preisendorfer, R. W. "Image Transmission by the Troposphere I" in *J. Opt. Soc. Am.*, Vol. 47, No. 6, pp. 499-506, 1957.

- Efron, E. "Image Processing by Digital Systems" in *Photogrammetric Engrg.*, Vol. 34, p. 1058, 1968.
- Elterman, L. *UV, Visible, and IR Attenuation for Altitudes up to 50 Km*, 1968, Report AFCRL-68-0153.
- Elterman, L. *Vertical Attenuation Model with Eight Surface Meteorological Ranges 2 to 13 Km*, 1970, Report AFCRL-70-0200.
- Elterman, L., Toolin, R. B. and Essex, J. "Stratospheric Aerosol Measurements with Implications for Global Climate" in *Applied Optics* (scheduled for publication February 1973).
- Fried, D. *Limiting Resolution Looking Down Through the Atmosphere*, JOSA, Vol. 65, pp. 1380-1384, 1966.
- Fried, D. *Limiting Resolution Looking Down Through the Atmosphere, Appendix C*, JOSA, Vol. 55, p. 1427, 1965.
- Fried, D. "Optical Resolution through a Randomly Inhomogeneous Medium for Very Long and Short Exposures" in *J. Opt. Soc. Am.*, Vol. 56, pp. 1372-1379, 1966.
- Fuchs, A. J. and Stratella, R. A. *ERTS Orbit Selection Analysis*, NASA/GSFC X-832-70-144, April 1970.
- Gaven, J. V., Jr., Tavitian, J. and Harabedian, A. "The Informative Value of Sampled Images as a Function of the Number of Grey Levels Used in Encoding the Images" in *Photo. Sci. and Engrg.*, Vol. 14, No. 1, pp. 16-20, 1970.
- Geiger, R. *Das Klima der Bodennahen Schichten (Climate of the Boundary Layer)*, Braunschweig, 1961.
- Geist, Jon. *Optical Radiation Measurements: Fundamental Principles of Absolute Radiometry and the Philosophy of This NBS Program (1968 to 1971)*, NBS Tech. Note 594-1, June 1972.
- Geist, Jon. *Opt. Soc. Am.*, 1972 Annual Meeting Program, p. 25.
- Gillespie, A. R. and Soha, J. M. *An Orthographic Photomap of the South Pole of Mars from Mariner 7*, Icarus, Vol. 16, pp. 522-527, 1972.

- Goetz, A. F. H., Billingsley, F. C., Yost, E. and McCord, T. B. "Apollo XII Multispectral Photography Experiment, Proc. of the Second Lunar Science Conference, Suppl. 2" in *Geochim. Cosmochim. Acta.*, Vol. 3, p. 2301, 1971.
- Gordon, J. I. "Model of a Clear Atmosphere" in *J. Opt. Soc. Am.*, Vol. 59, No. 1, 1969.
- Handbook of Geophysics and Space Environment* (Edited by Shea L. Valley), Air Force Cambridge Res. Laboratories, U.S. Air Force, 1965.
- Hermann, B. M. and Browning, S. R. "A Numerical Solution to the Equation of Radiative Transfer" in *J. Atmos. Sci.*, Vol. 22, pp. 559-566, 1965.
- Hoffer, R. M., Anuta, P. E. and Phillips, T. L. "ADP, Multiband and Multi-emulsion Digitized Photos" in *Photogrammetric Engrg.*, pp. 989-1001, 1972.
- Höhn, D. "Effects of Atmospheric Turbulence on the Transmission of a LASER Beam at 6328Å, II Frequency Spectra" in *Applied Optics*, Vol. 5, p. 1433, 1966.
- Huang, T. S. "Combined Use of Digital Computers and Coherent Optics in Image Processing," *SPIE Computerized Imaging Techniques Symposium*, Washington, D.C., June 1967.
- Hufnagel, R. and Stanley, N. "Modulation Transfer Function Associated with Image Transmission through Turbulent Media" in *J. Opt. Soc. Am.*, Vol. 54, pp. 52-61, 1964.
- Jacobowitz, H. and Coulson, K. L. "The Effects of Aerosols on the Outgoing Terrestrial Radiation," in Preprints to Conference on Atmos. Radiation, Am. Meteorological Soc., Ft. Collins, Colo., Aug. 1972.
- Johnson, F. S. "The Solar Constant" in *J. Meteorolog.*, Vol. 11, No. 6, p. 431, 1954.
- Kostkowski, H. J., Erminy, D. E. and Hattenburg, A. T. *Adv. Geophys.*, 14:111, 1970.
- Landgrebe, D. *Systems Approach to the Use of Remote Sensing*, LARS Information Note 041571, Laboratory for Application of Remote Sensing, Purdue University, West Lafayette, Indiana, 1971. (See Also NASA Special Publication SP-283, Page 139 ff.)

- Lawrence, R. S., Ochs, G. R. and Clifford, S. F. "Measurements of Atmospheric Turbulence Relevant to Optical Propagation" in *J. Opt. Soc. Am.*, Vol. 60, p. 826, 1970.
- Lutomirski, R. F. and Yura, H. T. "Wave Structure Function and Mutual Coherence Function of an Optical Wave in a Turbulent Atmosphere" in *J. Opt. Soc. Am.*, Vol. 61, No. 4, April 1971.
- MacDonald, T. H. *Tables of Extraterrestrial Radiation*, Nat. Weather Records Center, U.S. Weather Bureau, Asheville, North Carolina, 1963.
- Manned Spacecraft Center. *Earth Observation Aircraft Program*, Fiscal Year 1970.
- Martin Marietta Corporation. *Formulation on Statistical Trajectory Estimation Programs*, NASA/GSFC contract NAS 1-3500, NASA CR-1462.
- McClatchey, R. A., Fenn, R. W., Selby, J. E. A., Volz, F. E. and Garing, J. S. *Optical Properties of the Atmosphere*, Report AFCRL-71-0279, May 1971.
- Michigan. *Proceedings of University of Michigan 5th Symposium of Remote Sensing of Environment*, Ann Arbor, Michigan, 1967.
- Michigan. *Proceedings of University of Michigan 6th Symposium of Remote Sensing of Environment*, Ann Arbor, Michigan, 1969.
- Michigan. *Proceedings of University of Michigan 7th Symposium of Remote Sensing of Environment*, Ann Arbor, Michigan, 1971.
- MIT Charles Stark Draper Laboratory. *Candidate Configuration Trade Study, Stellar-Inertial Measurement System (SIMS) for an Earth Observation Satellite (EOS)*, NASA/GSFC NAS 9-4085, Task Order 42. Interim Technical Reports dated 5 November 1971, 31 January 1972, 15 June 1972 and Final Report, Jan. 31, 1973.
- NASA. *Data Users Handbook, Earth Resources Technology Satellite*, NASA Goddard Space Flight Center Document No. 71SD4249, Revised 1972.
- NASA. *Earth Resources Research, Volume I*, NASA MSC-02576, July 1971.
- NASA Langley Research Center. *Remote Measurement of Pollution*, NASA SP-295, 1971.

NASA. *Remote Sensing of Earth Resources, A Literature Survey with Indexes*, NASA SP-7036, September 1970.

NASA/GSFC. *Earth Observatory Satellite (EOS) Definition Phase Report*, Draft NASA/GSFC Report, August 1971.

NASA. *Spacecraft Earth Horizon Sensors NASA Space Vehicle Design Criteria (Guidance and Control)*, NASA SP-8033, December 1969.

Nathan, R. *Image Processing for Electron Microscopy I: Enhancement Procedures, Advances in Optical and Electron Microscopy 4*, Academic Press, New York, pp. 85-125, 1971.

Norwood, V. T. *Optimization of a Multispectral Scanner for ERTS, in Michigan*, pp. 227-235, 1969.

Paulson, R., Ellis, E. and Ginsburg, N. *Atmospheric Optical Noise Measurements*, AFCRL-62-869, August 1962.

Plass, G. and Kattawar, G. "Calculations of Reflected and Transmitted Radiance for Earth's Atmosphere" in *Applied Opt.*, Vol. 7, No. 6, pp. 1129-1135, 1968.

Plass, G. and Kattawar, G. "Effect of Aerosol Variation on Radiance in the Earth's Atmosphere Ocean System" in *Applied Optics*, Vol. 11, No. 7, July 1972.

Proceedings of the Symposium on Spacecraft Attitude Determination, co-sponsored by USAF Space and Missile Systems Organization and Aerospace Corporation at Aerospace Corporation, El Segundo, California, September-October 1969.

Rindfleisch, T. C., Dunne, J. A., Frieden, H. J., Stromberg, W. D. and Ruiz, R. M. "Digital Processing of the Mariner 6 and 7 Pictures" in *Jour. Geo. Res.*, Vol. 76, No. 2, pp. 394-417, 1971.

Saunders, R. D., Jr. *Opt. Soc. Am. 1972 Annual Meeting Program*, p. 45 ff.

Schaefer, D. H. and Strong, J. P. "Parallel Image Computers," in *Proceedings of the Conference on Computer Image Processing and Recognition*, August 1972.

Schulze, R. *Strahlenklima der Erde*, D. Steinkopf Verlag, Darmstadt, 1970.

- Scott, F., Hollanda, P. A. and Harabedian, A. "The Informative Value of Sampled Images as a Function of the Number of Scans per Scene Object" in *Photo. Sci. and Engng.*, Vol. 14, No. 1, pp. 21-27, 1970.
- Siry, Joseph W. *Space Navigation*, Second Surveying and Mapping Colloquium, Alberta, Canada, May 1972.
- Smith, O. Glenn. *Manned Operation of Earth Resources Surveys from Space*, NASA Manned Spacecraft Center, AIAA paper 72-234.
- Smedes, H. W., Spencer, M. M. and Thomson, F. K. *Preprocessing of Multispectral Data and Simulation of ERTS data Channels—*, in *Michigan*, pp. 2073-2094, 1971.
- Solar Radiation* (Edited by N. Robinson), Elsevier Publishing Co., Amsterdam, London, New York, 1966.
- Syverson, C. A. and Mulholland, Donald R. *Aviation's Role in Earth Resources Surveys*, ASME Aerospace Division Conference, Los Angeles, California, 11 September 1972.
- Tanguay, M. G., Hoffer, R. M. and Miles, R. D. *Multispectral Imagery and Automatic Classification of Spectral Response for Detailed Engineering Soils Mapping*, in *Michigan*, pp. 33-63, 1969.
- Tatarski, V. I. *Wave Propagation in a Turbulent Medium*, McGraw Hill Book Comp. Inc., New York, 1961.
- Taylor, Ralph E. *Tracking and Data Acquisition for NASA Spacecraft Systems*, NASA Goddard Space Flight Center, Preprint, August 1972, to be published in a IEEE special publication.
- Thompson, B. C. and Wells, M. B. "Scattered and Reflected Light Intensities Above the Atmosphere" in *Applied Optics*, Vol. 10, No. 7, July 1971.
- TRW. *PFCS/PADS, A Collection of Papers on Precision Attitude Determination and Control*, papers presented at AIAA Guidance, Control and Flight Mechanics Conference, Hofstra University, Hemstead, New York, August 1971.
- Vincent, Robert and Thomson, Frederick J. "Rock-Type Discrimination from Ratioed Infrared Scanner Images of Pisgah Crater, California" in *Science* 175, 986 (1972).

Volz, F. E. "Infrared Absorption by Atmospheric Aerosol Substances" in *J. Geophys. Res.*, Vol. 77, No. 6, February 1972.

Weiner, M. "Atmospheric Turbulence in Optical Surveillance Systems" in *Applied Optics*, Vol. 6, No. 11, November 1967.

Wells, M. B., Collins, D. and Hopper, F. *Contrast Transmission Data for Clear and Hazy Model Tropical Atmospheres*, Report AFCRL-68-0660(I), (II), (III), December 1968.

Wilkins, L. C. and Wintz, P. A. "Bibliography on Data Compression, Picture Properties and Picture Coding" in *IEEE Transactions on Information Theory*, pp. 180-197, March 1971.

Wyngaard, J. and Cote, O. R. "The Budgets of Turbulent Kinetic Energy and Temperature Variance in the Atmospheric Surface Layer" in *J. Atm. Sci.*, Vol. 28, pp. 290-301, 1971.

Zalewski, E. F. *Opt. Soc. Am. 1972 Annual Meeting Program*, p. 45.

GLOSSARY OF ACRONYMS

ASOS	Antimony Trisulphide Oxysulphide
ATS	Applications Technology Satellite
bpi	bits per inch
B/W	Black and White (film)
CCD	Charge Coupled Devices
CDA	Control and Data Acquisition
CIR	Color Infrared (film)
CLR	Crater Lamp Recorder
CMOS	Complementary Metal Oxide Semiconductor
CRT	Cathode Ray Tube
demod	demodulation
demux	demultiplex
DRGS	Direct Readout Ground Station
EBIC	Electron Bombardment Induced Conductivity (camera tube target)
EBR	Electron Beam Recorder
EBS	Electron Bombarded Silicon (camera tube)
ECS	Electrostatic Camera System
EIFOV	Effective Instantaneous Field-of-View
EMR	Electro Mechanical Research, Inc.
EOS	Earth Observatory Satellite
EREP	Earth Resources Experiment Package (Skylab Program)
ERTS	Earth Resources Technology Satellite
FM	Frequency Modulation
FPS	Focus Projection and Scanning (Vidicon)
GPE	Ground Processing Equipment
I/O	Input/Output
IRIG	Inter Range Instrumentation Group
ITOS	Improved Tiros Operational Satellite
kbs	kilo bits per second
kHz	kilo Hertz
LBR	Laser Beam Recorder
LSA	Large Scale Array
LSI	Large Scale Integration
Mbs	Mega bits per second
MHz	Mega Hertz
MIS	Metal Insulator Semiconductor
MOCS	Multichannel Ocean Color Sensor

MOMS	Multimegabit Operation Multiplexer System
MOST	Metal Oxide Silicon Transistor
MSS	Multispectral Scanner
MTF	Modulation Transfer Function
MTTF	Mean Time To Failure
NAB	National Assoc. of Broadcasters
NEA	Negative Electron Affinity
NEP	Noise Equivalent Power
NES	Noise Equivalent Signal
NESS	National Environmental Science Service (National Oceanographic and Atmospheric Administration)
NRZ	Non Return to Zero
NRZ-S	Non Return to Zero - Space (IRIG Standard)
PCM	Pulse Code Modulation
Pixel	Picture Element
PLL	Phase Locked Loop
PMT	Photo Multiplier Tube
PN	Pseudo Noise
PSK	Phase Shift Keyed
RBV	Return Beam Vidicon
RSE	Receiving Site Equipment
SCE	Signal Conditioning Electronics
SEC	Secondary Electron Conduction (Chapter 3)
SEC	Station Events Controller (Chapter 5)
SEOS	Synchronous (altitude) Earth Observatory Satellite
SIMS	Stellar Inertial Measurement System
SIS	Scanning Imaging Spectroradiometer
SIT	Silicon Intensifier Tube
SMS	Synchronons Meteorological Satellite
S/N	Signal-to-Noise
SPDT	Single Pole Double Throw (switch)
SR	Shift Register
STADAN	NASA Tracking and Data Acquisition Network
SV	Stretched Video
TIROS	Name for the Operational Weather Satellite
USDA	United States Department of Agriculture
USGS	United States Geological Survey (U.S. Department of Interior)
UTM	Universal Transverse Mercator
VCO	Voltage Controlled Oscillator
VISSR	Visible Infrared Spin Scan Radiometer
WBVTR	Wide band Video Tape Recorder
WISP	Wide range Imaging Spectro Photometer

APPENDIX

LIST OF NAMES AND ADDRESSES

Dr. Ken J. Ando
Interplanetary Photography
Jet Propulsion Laboratory
4800 Oak Grove Drive
Pasadena, California 91103

Mr. George Barna
RCA Astro Electronics Division
Box 800
Princeton, New Jersey 08504

Dr. James Robert Biard
Spectronics Incorporated
541 Sterling Drive
Richardson, Texas 75080

Mr. Fredric C. Billingsley
MS: 168-427
Jet Propulsion Laboratory
4800 Oak Grove Drive
Pasadena, California 91103

Dr. Donald E. Bode
Santa Barbara Research Center
75 Coromar Drive
Goleta, California 93017

Mr. Joseph W. Clifton
1301 Elsinor Avenue
McLean, Virginia

Mr. Frank Cook
Columbia Broadcasting System
227 High Ridge Road
Stamford, Connecticut 06905

Dr. S. Q. Duntley, Director
Visibility Laboratory
Scripts Institution
Building 348
San Diego, California 92152

Dr. James M. Early
Fairchild Camera and Instrument Company
4001 Miranda Avenue
Palo Alto, California 94304

Mr. James Edmond
Bendix Research Labs
Bendix Center
South Field, Michigan 48075

Dr. Reinhard D. Ennulat, Director
Far Infrared Technical Area
U. S. Army Night Vision Lab.
AMSEL-NV-FIR
Fort Belvoir, Virginia 22060

Dr. Robert Fenn
A. F. Cambridge Research Lab.
Hanscom Field
Bedford, Massachusetts 01930

Mr. William Fischer, Senior Scientist
EROS Program
U. S. Geological Survey
GSA Building - Room 5209
Washington, D. C. 20244

Mr. Frank Gabron
Arthur D. Little, Inc.
16 Acorn Park
Cambridge, Massachusetts 02140

Mr. Jerry C. Glover, Special Assistant
to the Deputy Director
NESS-NOAA
Federal Office Building 4 - Room 2065
Suitland, Maryland 20023

Mr. Isodore L. Goldberg
NASA-GSFC
Code 731
Greenbelt, Maryland 20771

Mr. Olin Graham
NASA Johnson Space Center
Building 15 - Room 2332
Houston, Texas 77058

Dr. Martin Green
Westinghouse Electric Company
Elmira, New York

Dr. Arun K. Guha
NASA-GSFC
Code 732
Greenbelt, Maryland 20771

Dr. Herbert M. Gurk
RCA Astro-Electronics Division
P. O. Box 800 - Mail Stop 83
Princeton, New Jersey 08540

Mr. Jay Harnage
NASA-Johnson Space Center
Code HA
Houston, Texas 77058

Mr. Robert C. Heller
Pacific SW Forest & Range
Experiment Stations
P. O. Box 245
Berkeley, California 94701

Mr. Fred Huck
NASA-Langley Research Center
Hampton, Virginia 23365

Mr. Robert Hummer
Santa Barbara Research Center
75 Coromar Drive
Goleta, California 93017

Mr. Leonard Jaffe
Deputy Associate Administrator
National Aeronautics and Space
Administration
Office of Applications
Washington, D. C. 20546

Mr. Barry Kerne
Operations Research, Inc.
1400 Spring Street
Silver Spring, Maryland

Mr. Edward W. Koenig
ITT Aerospace/Optical Division
3700 E. Pontiac Street
Fort Wayne, Indiana 46803

Mr. Alex Koso
Honeywell Radiation Center
2 Forbes Road
Lexington, Massachusetts 02173

Dr. David Landgrebe
Director of LARS
FLEX Lab. No. 1
1220 Potter Drive
West Lafayette, Indiana 47906

Mr. Norman P. Laverty
TRW Systems
Bldg. 6 - Room 1595
One Space Park
Redondo Beach, California 90278

Mr. Frank Leccese
General Electric Company
Space Systems Department
Bldg. 100 - Room U2432
P. O. Box 8555
Philadelphia, Pennsylvania 19101

Mr. Jules Lehmann
National Aeronautics and Space
Administration
Code ERF - Room B254
Washington, D. C. 20546

Mr. Donald S. Lowe, Deputy Director
Infrared and Optics Division
Environmental Research Institute
of Michigan
Box 618
Ann Arbor, Michigan 48107

Mr. John Lowrance
Princeton University
Peyton Hall
Princeton, New Jersey 08540

Mr. Robert B. MacDonald
NASA-Johnson Space Center
Code TF
Houston, Texas 77058

Mr. Marvin Maxwell
NASA-GSFC
Code 734
Greenbelt, Maryland 20771

Dr. Robert McEwen
U. S. Geological Survey
Room 302
McLean, Virginia 22101

Mr. Joseph Mudar
ERIM-P.O. Box 618
Ann Arbor, Michigan 48107

Dr. Lloyd Mundie
RAND Corporation
1700 Main Street
Santa Monica, California

Mr. Harvey Ostrow
NASA-GSFC
Code 731
Greenbelt, Maryland 20771

Mr. Charles T. Paludan
NASA-Marshall Space Flight Center
Huntsville, Alabama 35812

Dr. Arch Park
National Aeronautics and Space
Administration
Code ERR
Washington, D. C. 20546

Mr. Roamer Predmore
NASA-GSFC
Code 731
Greenbelt, Maryland 20771

Mr. Edward Risley
EROS Program
U. S. Geological Survey
GSA Building - Room 5209
Washington, D. C. 20242

Mr. Charles Robinove
EROS Program
U. S. Geological Survey
Room 815
1717 H Street, N. W.,
Washington, D. C. 20242

Dr. Bernard Rubin
National Aeronautics and Space
Administration
Code REE - Room B607
Washington, D. C. 20546

Dr. Eugene D. Savoye
RCA Electronic Components Division
New Holland Pike
Lancaster, Pennsylvania 17604

Mr. Leo M. Schaefer, Director
Program Performance Division
Department of Agriculture
Room 4716-S
14th & Independence Avenue
Washington, D. C. 20250

Mr. Joseph R. Schulman
NASA-GSFC
Code 731
Greenbelt, Maryland 20771

Mr. Robert L. Sendall
Xerox Corporation
300 N. Halstead Street
Pasadena, California 91107

Prof. John Sherman
Department of Geography
University of Washington
Seattle, Washington 98105

Mr. John W. Sherman, III
NOAA-Spacecraft Oceanography Project
Suite 405 - Iverson Mall
3737 Branch Avenue
Hillcrest Heights, Maryland 20031

Dr. Philip N. Slater
Optical Sciences Center
University of Arizona
Tucson, Arizona 85721

Mr. Melvin St. John
Wright-Patterson AFB
Dayton, Ohio 45433

Dr. Bruce Steiner
B-312, Metrology
National Bureau of Standards
Washington, D. C. 20234

Dr. Gene Strull
Westinghouse Electric Corporation
Box No. 1521
MS-3519
Baltimore, Maryland 21203

Mr. Leslie L. Thompson
NASA-GSFC
Code 731
Greenbelt, Maryland 20771

Dr. Paul K. Weimer
RCA Labs.
Princeton, New Jersey 08540

Prof. William Wolfe
Optical Sciences Laboratory
University of Arizona
Tuscon, Arizona 85721

Mr. Oscar Weinstein
NASA-GSFC
Code 731
Greenbelt, Maryland 20771

Dr. George Zissis
Environmental Res. Inst. of Michigan
P. O. Box 618
Ann Arbor, Michigan 48107

INDEX

- Absorption, photon, 127
- Agriculture, crops, production, 43, 45; identification requirements, 46, 49; weeds, 38, 44; sensing data for, 447
- Air, pollution, 441; quality assessment, 15, 16
- Angular aberrations, 72
- Arrays, characteristics of, Charge-Coupled Devices, 352–360, photodiodes, 314–318, phototransistors, 323–327; measurement of performance, Charge-Coupled Devices, 360, photodiodes, 318, phototransistors, 326; optical design, 372; spatial frequency response—see MTF, 354
- ASOS (Antimony trisulfide oxysulfide), 197–201, 202, 203, 204
- Atmosphere, effects of, 413–415, 425, refraction effects, 491; infrared emission, 438
- ATS (Applications Technology Satellite), multispectral scanner on, 80; ATS-3, use of 1-inch image dissector, 233
- Bell Telephone, studies, 224
- Bendix Research Lab., EOS Mapping-Accuracy Study, 460, 470
- Blackbody, theory, 454
- Blooming control, (CCD), 355, 357, 359; electron beam devices, 224
- Blur circle, 104
- Brayton cycle, 142–143
- Camera, framing, 247; image dissector, 231, 237; multispectral framing system, 283; panoramic, 247, characteristics, 248, limitations, 248
- Camera Tubes, direct beam readout, 260, characteristics, 260, 263; target storage characteristics, 259; high sensitivity, 257; correctly focused image, 259
- Carbon fixation, 32
- Cassegrain, 102
- Cathode, M-type dispenser, 205
- CBS Laboratories, 250, 254, 256
- Charge-Coupled Device, in silicon detector arrays, 306, 310, 329; charge transfer, 347; implanted asymmetry CCD, 335; infrared, development of, 365, 366; power dissipation, 348, 349, 350, 368; recommended use of indium antimonide, 307; technology, 329, 340
- Cloud, particle size, 28, photography, 35
- CMOS (Complementary Metal Oxide Semiconductor), technology, 314
- Cold cathode, development, 187, 269; emitter, 276, 277, 300
- Cold shielding, 126; background noise reduction, 126
- Computers, Tse, 517
- Copernicus Observatory, 462
- Crater Lamp Recorder (CLR), 494
- Cryogenic Systems, 73, 129
- Dall Kirkham System, 102
- Dark current, 260; element-to-element variation, 311, effect of, 322; noise level variations, 327; low in photomultiplier tubes, 110; noise in, 117; sources, 338, 339
- Darlington configuration, 325
- Data, accuracy, 447; banks, 37; collection facilities, 398, 402; connection, 413; modulation loss, 497; multispectral, 30, 97, 451; processing, 26, 38, 423; rates, 418; sensor, 492; skew, two dimensional, 503; systems concepts, 418; transmission, 26, 424; user data analysis, 413
- Detector, arrays, high density, 311; arrays, quantum efficiency, 390; arrays, silicon, 311; CCD, 306, 329; cooling systems, Brayton cycle, 142, 146; cooling systems, closed

- cycle, 131, 133, 140, 144; cooling systems, cryogenic, 72, 74, 78, 130, 131, 138; 140; cooling system, design, 72; cooling systems, Gifford-McMahon, 141; cooling system, Joule-Thomson effect, 131, 136, 137; cooling systems, methane/ammonia, 139; cooling systems, open cycle, 74, 131, 132, 133, 136, 140; cooling systems, passive radiators, 131, 133, 134, 135; cooling systems, requirements, 74; cooling systems, Stirling cycle refrigerators, 74, 141, 145, 146; cooling systems, Vuilleumier cycle refrigerator, 74, 141, 142, 143, 145, 146; extrinsic silicon, development of, 365; infrared, 364, 369; photoconductors, 86, 89, 92, 94, 97; photodiodes, 86, 88, 89, 93; photomultipliers, 86, 91, 92, 97; phototransistors, 323, 328; sample coverage, 20; sensitivity, 20; silicon, 128, 305, 309
- Dielectric tape camera, 189, 193
- Digital processing, 25
- Direct beam readout vidicon, 189, 191
- Disaster prediction, 35
- Draper Laboratory, SIMS study, 469
- Earth, curvature, 491; elevation contours, 27; life cycles, 32; resources, data, 37, rotation, 491, 500; soil moisture, 28
- Earth sensing, feature identification, 240
- EBS, signal-to-noise ratios, 267, 268
- ECS (electrostatic camera system), principle of operation, 250
- Effective Instantaneous Field of View (EIFOV), definition, 20
- Electron Beam Imaging Tubes, 194
- Electron Beam Recorder (EBR), 419, 494, 505; use for ERTS, 494
- EBR, spatial frequency response, 495
- Electron multipliers, channel type, 232; venetian blind, 232
- Energy, consumption estimates, 27
- Environment, legislation, 19; monitoring, 15, 31
- EOS (Earth Observatory Satellite), spacecraft and flight acronyms, 80; study, 13, 18, 35
- Earth Resource Applications, requirements, 23; system design recommendations, 15, 16
- ERTS (Earth Resources Technology Satellite), automatic picture transmission, 26; hydrologic application, 57; MSS, 452, 527, 534; multispectral scanner, 80; orbit estimations, 416; wideband video tape recorder (WBVTR), 475
- ERTS Missions, improvements in performance, 224
- Film, material, 273; polycrystalline silicon films, 329; processing, 26, 514; quality control, 26; range limitation, 25; recorders, characteristics, 494
- Filters, development of striped, 186; function, 105; ground station operation, 287, 3-color stripe, 233
- Flicker noise ($1/f$), 122
- Forestry, detecting fires, needs, 519; inventory, 48; requirements, 44, 46, 47, 49
- Fourier analysis, 106
- Fourier transform, use of, 105, 107, 516
- FPSV (Focus Projection and Scanning Vidicon), 189, 191, 210
- Fraunhofer line, measurement, 15, 28
- Gated Charge Integrator Amplifier, 340, 341
- Gaussian output, 127
- Geohydrology, 18, 58
- Geology, requirements 51, 55; use of sensing data, 447
- Geometric registration, 487
- Gifford-McMahon Cycle, 141
- Global Irradiance, 429, 430
- Ground Processing Equipment (GPE), MSS, 537, 539, 540

- Hadamard, scanning, 75, 169, 176
- High Sensivity Direct Beam Readout Camera Tube, 189
- Hughes Aircraft, report on ERTS MSS, 539
- Hummer curves, 149
- Image Dissector Camera, 189, 191, 192, 230
- Image generation, 414
- Image processing, onboard, 506
- Image quality, 354, 404
- Image storing, 515, 522
- Imaging systems, applications groupings, 19; automatic transmission, 26; electron beam, 183; ERTS Return-Beam Vidicon (RBV), 183; frame format, 26, 488; line, 488; night, 27; phototransistor, 394; present scheduling, 13; processing, 26; solid state, 306, 307
- Infrared (IR), channels, 21; development, 369
- Infrared Vidicons, for spectral region, 228, 229
- Integrator, differential gated charge, 345; gated charge, 340, 341, 345
- ITOS (Improved TIROS Operational System), multispectral scanner, 80
- ITOS-D, Three-stage passive radiator, 136
- Jet Propulsion Lab., Optical technique development, 517; use of VICAR, 507, 509, 510
- Jitter, effect on spatial registration, 461; mechanical, 465
- Johnson noise, 120
- Joule-Thomson system, 131
- Lamp, quartz-halogen, 451
- Land use, 43
- Laser Beam Recorder (LBR), 494
- Lattice parameter, 273
- LBR, spatial frequency response, 494
- Lens, double-gauss design, 372, 374; Einzel, 212; general considerations—high resolution systems, 373; MTF, 280; Petzval-type, 372, 374
- Linear 431; field, charge in, 378
- Luminescence, mapping, 15, 28
- Mariner ('71), digital filtering, 512; two-stage J-T coolers, 137
- Measurement, Aerosol content, atmosphere, 28; crop acreage, 28, 39; distinctions between, 416; global ocean, currents, 33; global ocean, needs, 33; Langley and Norick formulas, 30; limb spectroscopy, 31; soil moisture, 28; urban growth, 31; water, chlorophyll content, 32; water, quality, 15, 17, 31; water, salinity, 31
- Mesometeorology, 19
- Meteorology, needs, 19, 35, 61
- Minority carriers, 331, 354
- Mirrors, beryllium system, 97, 98, 100; fused silica egg crate, 167; materials used, 163; reflective coatings, 165, 166; scan, 97
- MIS Capacitor, storage element, 331, 332, 333
- MOCS (Multi-Channel Ocean Color Sensor), 194, 291
- MOST (Metal Oxide Silicon Transistor), 314, 316
- Modulation Transfer Function, 352, 393, 394
- MTF, curves, 355, 356, 432; typical quality system, 235
- MSS 86, 90, 92, 93, 103, 109; crop identification, 31
- Multimegabit Operation Multiplexer System (MOMS), program development, 472, 473
- Multiplexer, Pulse Lode Modulation, 418, 549
- NEA (Negative-Electron-Affinity), Emitters, technology, 269, 270, use of GaAs, 270

- NES (Noise Equivalent Signal), definition, 320; standard measure, 337
- Nimbus, meteorological cameras, 230, 232, 247; Nimbus IV, single-stage passive radiator, 136; scanning mirrors, 150
- Nipkow Scanning Wheel, 157, 158
- Noise, amplifier, 444; atmospheric backscatter, 117; blackbody, 119, in CCD, 337; CCD array readout, 275, 276; flicker, 122, 386; generation-recombination noise, 117; thermal G-R noise, 119; in imaging arrays, 386; Johnson-Nyquist, 120; nonwhite, 123; pattern, 386; photon, 171, 172, 173, 337; shot noise, 86, 116, 234, 347; spatial, 316
- Nyquist Criteria, 106
- Ocean, chlorophyll, 34; phytoplankton content, 15; quality assessment, 15; productivity detection, 28, 32; sensor needs, 65; spectral identification, 244; thermal information, 448
- Optics, array, sensor, 372; atmospheric models, 442; effects of atmosphere, 414, 427; Hadamard, 75; materials used, 160; modified Schmidt, 207; narrow-field, optical system, 74, 149; narrow-field, Newtonian, 75, 149, narrow-field, Cassegrain, 75, 149, 150; narrow-field, Dale-Kirkham, 75, 149, 150; narrow-field, Ritchey Chretien, 75, 149, 150, 543; Nipkow scanning wheel, 157, 158; split-field, Kennedy, 152, 153; reflective, 280; refractive, 187; technology, present 72; total blur, 151; two-mirror system, 101, 102; wide-field, Bouwers Maksutov, 75, 149; wide-field, optical system, 74; wide-field, Schmidt, 75, 149, 150, 159
- Orbit, geosynchronous, 459; requirements, 459, 461, sunsynchronous, 459
- Photocathode development, 272; image dissector, spectral response decay, 234; image dissector, tube size, 235
- Photodetectors, photoconductive, extrinsic, 73, 113, 115, 121; intrinsic, 73, 113, 115, 122, 125, 129; devices, 113; material, 112; noise in, 117; values, 124; photodiode, 111, 114, values, 124, response speed, 129, germanium, 128; photodiode, 306, 313, 316; photodiode, HgCdTe, 129; photodiode, infrared, 129; photodiode, PhSiTe, 129; photomultiplier tubes, 73, 110; phototransistor, 306, 310, 311, 322, 328; silicon planar p-n junction, 73, 110, 116, noise in, 117
- Photodiode, integration mode, 314; silicon, rise time, 127
- Photo Emission, history, 271
- Photography, low altitude, 29
- Photomultiplier tubes, 110
- Pierce-type gun, 213, 215
- Pioneer, 80
- Planar configuration, 357, 358
- Platforms, 413, 425, 445; effects, 455, 456; motion, 462
- Polar, orbit 97; stereographic, 37, 38
- Polycrystalline silicon (poly-si), as gate material, 352, 360
- Pushbroom, correction, 498
- Pushbroom scan, technique illustrated, 311, 312, 314, 363, 369
- Quantum efficiency, 391
- Radiance, path, 432, 433
- Radiation, solar, 428; lunar, 428; absorption by solar particles, 431
- Radiometry, calibration, 413, 415, 416, 443, 448, 449, 478, 492; space 450
- Radiometric, requirements, 444
- RBV (Return-Beam Vidicon), 189, 191, 192, 195; camera, 462, 494

- RCA optical motion compensation, 295; photoconductive-dielectric tape camera, 246, 247-248
- Receiving Site Equipment (RSE), 533, 535, 536, 538
- Ritchey Chretien System, 102; energy from VISSR scan mirror, 543
- Satellite, coverage, 441
- Scanners, airborne, 78; angular resolution, 71, 73; conical, 487, 498, 500; coverage rate, 79; design parameters, 71, 80; electromechanical, 71, 77; geostationary, 78; image plane, 104; low altitude orbiters, 78; multichannel, 99; multispectral, 125; object plane, 104; parameters, 86, signal-to-noise ratio, 86; Pfund, 159; requirements, 72; resolution, 85, 89, 97; state-of-the-art, 71, 77, 78; techniques, Hadamard, 71; thermatic mapper, 95
- Scanning Polygon, 155
- Standard, engineering terminology, 19; requirements, 23
- Secondary Emission Conductivity Tube (SEC), 193
- SEC (Secondary Electron Conductor Tubes), spectral coverage, WX-31958, 262, 267, WX-32193, 262, 263, 267; mirror image effects, 262
- Sensor, data systems, 413, 425; frame imaging, 482, 483, 485; horizon, 464; line imaging, 485; Stellar-Inertial Measurement System (SIMS), 465
- SEOS, (Synchronous EOS Earth Observatory Satellite), multispectral scanner, 80
- Shade, O., electron optics, 278
- Shannon, criteria, 106
- Shift Register (SR), 317, 318
- Shot Noise, 86, 116, 117
- Signal-to-Noise ratio, 421, 427
- Silicon Gate Technology, 332, 352
- SIMS (Stellar-Inertial Measurement System), 465
- SIS (Scanning Imaging Spectroradiometer), land mode, 292; ocean mode, 293
- Skylab program, 141, 416, 452, 455; EREP recorder, 475
- SMS (Synchronous Meteorological Satellite), multispectral scanner, 80
- Snow, cover evaluation, 57; runoff evaluation, 58
- Solar, spectral irradiance curves, 429
- Solar Panels, 141
- Space Council, study, 13, 18
- Space Data, map, 25
- Spectral band, analysis of, 421; classification, 78; evaluation, 375; panel conclusions, 13; resolution, 78; separation, 375, 376; vegetation, 78
- Spectral Beam Splitter, 375
- Spectral, information, 446, 479; parameter relationships, 526; regions, 451; response, typical diode, 319
- Spectral Transmittance, due to surface imperfections, 280
- Stanford Research Institute, striped filter system, 287
- Stirling Cycle Refrigerator, 74
- Targets, silicon diode array, 187, 205, 217, 221; spectral response, 221, 224
- TIROS, scanning mirrors on, 150
- Tse Computers, 517, 518
- Urban, settlement, patterns, 27, 31
- User Data, analysis, 413
- UTM (Universal Transverse Mercator), 37, 38
- Van Allen Belt, 163
- VICAR, Image processing language aide, 507
- Vidicon, copper-doped-germanium, 228; image lag, 218; infrared, 229; slow scan, 228; zinc-doped-germanium, 228

- Viewer, requirement, 25
- Viking, 80, 85
- VISSR (Visible Infrared Spin Scan Radiometer), 86, 90, 91, 109, 444, 453, 540, 541, 544, 552, 555, 561
- Volcanic activity, 28
- Vuilleumier Cycle Refrigerators, 74
- Water, quality assessment, 15, 17, 31, 57
- Water Vapor, 434
- Wavelength, range, 310
- Weather, analysis, 35, 36; modification, 19; prediction 35
- Westinghouse Electronic Corp., grating target tape camera, 248, 250; high resolution tubes, 262; EBS camera tube, 266
- Whiskbroom mode, 370
- Wildlife, management, 15, 32
- Wisp (Wide-Range Imaging Spectro-Photometer), 187, 194, 257; for multispectral separated signals, 282; basic concept, 289, 294
- Woods Hole Study Report, 19